SANDIA REPORT

SAND89—2612/A • UC—132
Unlimited Release
Printed January 1990

Multiwell Experiment Final Report:
IV. The Fluvial Interval of the Mesaverde Formation

Multiwell Experiment Project Groups
at Sandia National Laboratories
and
CER Corporation

Prepared by
Sandia National Laboratories
Albuquerque, New Mexico 87185 and Livermore, California 94550
for the United States Department of Energy
under Contract DE-AC04-76DP00789

SF2900Q(8-81)

468 p.

Issued by Sandia National Laboratories, operated for the United States Department of Energy by Sandia Corporation.

Printed in the United States of America. This report has been reproduced directly from the best available copy.

Available to DOE and DOE contractors from
Office of Scientific and Technical Information
PO Box 62
Oak Ridge, TN 37831

Prices available from (615) 576-8401, FTS 626-8401

Available to the public from
National Technical Information Service
US Department of Commerce
5285 Port Royal Rd
Springfield, VA 22161

NTIS price codes
Printed copy: A99
Microfiche copy: A01

SAND89-2612/Part A
Unlimited Release
UC Category 132

MULTIWELL EXPERIMENT FINAL REPORT:
IV. THE FLUVIAL INTERVAL OF THE MESAVERDE FORMATION

Compiled by the
Multiwell Experiment Project Groups
Sandia National Laboratories
Albuquerque, NM 87185
and
CER Corporation
Las Vegas, NV 89109
for the
U.S. Department of Energy

Printed January, 1990

Abstract

The Department of Energy's Multiwell Experiment (MWX) is a field laboratory in the Piceance Basin of Colorado which has two overall objectives: to characterize the low permeability gas reservoirs in the Mesaverde Formation and to develop technology for their production. Different depositional environments have created distinctly different reservoirs in the Mesaverde, and MWX has addressed each of these in turn. This report presents a comprehensive summary of results from the fluvial interval which lies between 4400 ft and 6000 ft at the MWX site. The reservoirs consist of heterogeneous, amalgamated point-bar sequences which form broad meanderbelts which create irregular, but roughly tabular, reservoirs with widths of 1000-2500 ft. Separate sections of this report are background and summary; site descriptions and operations; geology; log analysis; core analysis; in situ stress; well testing, stimulation, fracture diagnostics, and reservoir evaluation in two separate sandstones; stress, fracture diagnostic, and stimulation experiments in an additional sandstone; supporting laboratory studies; and a bibliography. Additional detailed data, results, analyses, and data file references are presented as appendices which are included on microfiche. The results show that stimulation of fluvial reservoirs can be successful if proper care is taken to minimize damage to the natural fracture system. Both an accelerated leakoff phenomenon and the ability to alter the in situ stress were quantified. Overall, the fluvial interval offers the highest production potential of the three nonmarine intervals studied.

CONTENTS
PART A--CHAPTERS 1 THROUGH 6
(See Part B for Sections 7 through 12)

CONTENTS, PART A

CONTENTS

PART B--CHAPTERS 7 THROUGH 11 (MICROFICHE APPENDICES INSIDE BACK COVERO
(See Part A for Chapters 1 through 6)

CONTENTS, PART B

CONTENTS, PART B

CONTENTS, PART B

CONTENTS, PART B

CONTENTS, PART B

1.0 BACKGROUND AND SUMMARY

David A. Northrop
Sandia National Laboratories

1.1 INTRODUCTION

New and improved technology is required to enhance natural gas production from the low permeability reservoirs of the United States. This is a large potential resource with an estimated maximum recoverable resource of over 600 TCF.[1] The U.S. Government's efforts to stimulate production from these reservoirs began in the mid-1960s. The early work evaluated the use of nuclear explosives for fracturing, but this technique was abandoned in 1973.[2] Efforts then focused upon massive hydraulic fracturing and several government-industry projects were conducted.[3,4] The results were disappointing and did not result in either an improved technology or confident, commercial production. The basic shortcoming was that these past field tests provided insufficient data to define the critical factors affecting gas production from this resource.

The U.S. Department of Energy's Multiwell Experiment (MWX) was conceived as a field laboratory to obtain sufficient information on the geologic and technical aspects to understand this resource. A key feature of MWX was three wells spaced between 110 and 215 ft apart. Detailed core, log and well test data from wells with such close spacings provided a detailed characterization of the reservoir. Interference and tracer tests, as well as the use of fracture diagnostics in offset wells, gave additional, out-of-the-ordinary information on stimulation and production. A second key was the synergism resulting from a broad spectrum of activities: geophysical surveys, sedimentological and geological studies, core and log analyses, well testing, in situ stress determinations, stimulation, fracture diagnostics, and reservoir analyses. All these activities were further enhanced by data from the closely spaced wells. Thus, the Multiwell Experiment provided a unique opportunity for understanding the factors affecting production from tight gas reservoirs. The long-term research program at this facility was managed by DOE's Morgantown Technology Center.

Further discussion of the rationale, plans, objectives, and activities of MWX can be found in References 5-8. References 9 and 10 present summaries of the insights and contributions resulting from MWX. The intent of this report is to compile results from activities associated with one interval--the fluvial--at the MWX site. Final reports for the marine,[11] paludal,[12] and coastal[13] intervals were completed previously.

1.2 GEOLOGIC SETTING

The Multiwell Experiment's focus is the Mesaverde Formation in the Piceance basin of northwest Colorado. This thick sequence was deposited during the late Cretaceous age over a broad region of the western United States and contemporaneous formations are found in the Green River, Wind River, Uinta and San Juan basins. The great extent and thickness of these gas-containing deposits represent a significant natural gas resource.[1]

At the MWX site, the Mesaverde Formation lies at a depth of 4000 to 8250 ft, between the overlying Wasatch Formation and the underlying Mancos Shale (Figure 1.1). The Mesaverde is exposed in outcrop along the Grand Hogback and elsewhere in the Piceance Basin. These outcrops, especially those at Rifle Gap approximately 11 miles northeast of the MWX site, gave excellent insight into the subsurface geology at the site. The sandstones stand out clearly in outcrop, and sedimentological and natural fracture studies were performed on them. These studies show that the Mesaverde can be divided into five distinct intervals based upon different depositional environments and resulting sandstone morphologies.[14-16]

(1) The lowest interval, the marine, (7450-8250 ft) was formed immediately on either side of an oscillating coastline and is composed of widespread shoreline-to-marine blanket sandstones, marine shales, and paralic coals and mudstones. This interval contains the Corcoran, Cozzette, and Rollins Sandstones which are interspersed with tongues of the Mancos Shale.

(2) The paludal interval (6600-7450 ft) lies above the Rollins Sandstone and contains thick, abundant coal deposits. These are interspersed with lenticular, distributary channel and splay sandstones formed in a lower delta plain environment. The sandstone percentage in this zone is markedly lower (26%) than other intervals (40%), and channel widths are probably 250-500 ft.

(3) The coastal interval (6000-6600 ft) is characterized by distributary channel sandstones deposited in an upper delta plain environment. Most of these sandstones are probably 250-500 ft in width and are interbedded with carbonaceous mudstones and siltstones.

(4) The fluvial interval (4400-6000 ft) consists of irregularly shaped, multistory, composite sandstones which were deposited by broad meandering stream systems. These sandstones have widths on the order of 1000-2500 ft and contain abundant internal discontinuities. This interval is the focus of this report.

(5) The uppermost interval, the paralic, (4000-4400 ft) is a zone of returned marine influence with more widespread, uniform sandstones. The interval is believed to be water-saturated at the MWX site and was not investigated in detail.

Specific sandstones in the shoreline/marine, paludal, coastal and fluvial intervals have been the focus of separate MWX investigations.

1.3 MWX DESCRIPTION

The Multiwell Experiment field laboratory is located in the Rulison Field in the east central portion of the Piceance basin in northwestern Colorado. The site is in the SW 1/4, NW 1/4, Sec. 34, T6S, R94W, Garfield County, and it is seven miles southwest of Rifle and just south of the

Colorado River. Agreements on the lease and with landowners were obtained in mid-1981 and work at the site began in August of that year. A chronology of MWX activities is given in Figure 1.2.

Three wells were drilled: MWX-1 to a depth of 8350 ft in September-December 1981,[17] MWX-2 to a depth of 8300 ft in January-March 1982,[18] and MWX-3 to a depth of 7565 ft in June-August 1983.[19] Over 4100 ft of four-inch core, approximately 1135 ft of it oriented, were cut with a recovery of >99%. Numerous logging programs containing both standard and experimental logs were conducted. An overview of the coring and logging activities in all three wells in relation to the Mesaverde section at the site is given in Figure 1.3. The three wells are exceptionally straight as seen in Figure 1.4; relative separations are between 110 and 215 ft within the Mesaverde. Significant gas shows were encountered throughout the section in all three wells and mud weights as high as 15 lbs/gal were required to maintain well control. Wells were drilled as near to balanced conditions as possible to minimize invasion.

The entire Mesaverde at the MWX site, as seen by gamma ray logs in the three wells, is shown in Figure 1.5.

1.4 THE FLUVIAL INTERVAL

The fluvial interval lies between 4400 and 6000 ft and is shown in detail in Figure 1.6. It was arbitrarily subdivided into the upper (4400-4950 ft), middle (4950-5450 ft), and lower (5450-6000 ft) sections. Most activities were focused in the lower interval (Figure 1.7), where a series of continuous, distinct sandstones offered the opportunity for careful investigation. Coring, logging and in situ stress measurements were made in the upper two sections, but well tests or stimulations were not attempted due to concerns about increasing water saturation and the lack of time and funds for the project.

Activities in the lower interval were conducted between May 1986 and December 1987. These included:

- In the B sandstone: nitrogen gas breakdown, prefrac interference tests, argon injection test, nitrogen step-rate/flow-back tests, nitrogen foam minifrac, propped nitrogen foam hydraulic fracture treatment, post-frac production and interference test, winter production and a final buildup test, and borehole seismic diagnostic studies before and after the frac treatments.

- In the C sandstone: KCl water pump-in/shut-in and step-rate/flow-back tests, two separate nitrogen foam minifracs in MWX-1 to assess an accelerated leakoff phenomenon, measurement of altered stresses in MWX-2 during the minifracs, borehole seismic monitoring in MWX-3 in the sand being fraced, and a short post-frac flow test.

- In the E sandstone: nitrogen impulse breakdown, tailored pulse breakdown, prefrac interference tests, KCl water pump-in/shut-in and step-rate/flow-back tests, nitrogen foam minifrac, propped nitrogen foam hydraulic fracture treatment, borehole seismic diagnostics, post-frac production and interference test.

- Throughout the interval: in situ stress measurements.

1.5 ACTIVITY SUMMARIES

The results of MWX activities conducted in the fluvial interval of the Mesaverde are presented in separate sections of this report; each are authored by the principal investigator. Summaries of these sections are presented here.

1.5.1 Geology (Section 3.0)

The rocks of the fluvial interval are amalgamated, meander-belt sandstones deposited on a low relief alluvial plain.[16] The composite sandstones are irregular in shape but are roughly tabular with average widths of 1000-2500 ft and thicknesses from 20-50 ft. The reservoirs are very heterogeneous, consisting of point bar sandstone units which are separated or partially separated from each other by minor lithologic discontinuities, such as thin mudstone layers, which control matrix permeability distribution and the distribution of natural fractures. While these are the largest of the lenticular reservoirs in the nonmarine portion of the Mesaverde, they are also the most complex and heterogeneous.

Six sandstones in the lower fluvial interval were studied in detail. Core and log data, along with outcrop studies, were analyzed from a sedimentological standpoint and interpretations of the lithology and morphology for each sandstone were made. Reservoir widths were estimated by empirical relationships between point bar thickness, channel width, and meanderbelt width. Estimates of reservoir orientations were made from the spatial relationships in the three wells, sedimentological interpretations from slabbed core, and a high resolution dipmeter log run in MWX-3. Each of the three sandstones of primary interest, B, C and E, are meanderbelt sandstones, each composed of several partial point bar sequences. The B sandstone is one of the more uniform reservoirs. Its estimated minimum width is 1000 ft and evidence indicates a probable north-south trend. The C sandstone has an estimated minimum width on the order of 1400-1500 ft and a best estimate of its orientation is a southwest to northeast trend. It is underlain by a thin fluvial splay deposit which is shaled out in MWX-1. The E sandstone has an estimated minimum width of about 1800 ft and a possible northwest to southeast trend. It is overlain by a multilayered splay deposit which is not present in MWX-3.

Sandstone petrology (grain size, composition, and diagenetic history) is the primary control on reservoir porosity and matrix permeability. The sandstones consist of quartz, feldspar, and lithic fragments, and are dominantly lithic arkoses and feldspathic litharenites. These fluvial rocks contain significantly more unstable grains (rock fragments and feldspar) than rocks in the other Mesaverde intervals. The highest clay content is 20% in the D sandstone and illite and mixed layer illite-smectite are the dominant clay materials. The fluvial sandstones were subjected to several similar, but slightly different, paragenetic sequences. These usually begin with an early stage of authigenic clay formation, followed by alteration/dissolution of feldspars, then additional clay formation, then cementation by quartz and calcite, and finally the formation of secondary porosity by dissolution.

The fluvial sandstones contain many internal lithologic discontinuities. These include thin mudstone partings, zones of siderite and/or mudstone ripup clasts, highly carbonaceous material, thin siltstone beds, and beds of alternating sand-grain sizes. For example, core from the B sandstone in all three wells showed a total of 17 lithologic discontinuities. These discontinuities have two important effects on the reservoir. First, they create a heterogeneous matrix permeability creating internal barriers to gas flow. Second, and more important, they significantly influence the natural fracture system.

The fluvial interval contains the highest frequency of natural fractures in all the intervals studied.[20,21] The majority of these are unmineralized, irregular shear planes in mudstones which have essentially no permeability. However, over 200 vertical, calcite-and/or quartz-mineralized extension fractures were observed, with over 80% of them found in sandstones or siltstones (Figure 1.8). This type of fracture was not observed to extend more than an inch from a sandstone into a shale. Thus, shale breaks affect the natural fractures within a sandstone, which results in a permeability system which is irregular, both vertically and horizontally, and is controlled by the existing irregular sedimentologic patterns. All the fluvial reservoirs in the MWX wells contain a dominant unidirectional fracture system.[22] However, several cross fractures were observed in oriented core from the E sandstone and the overall reservoir permeability in this reservoir was less anisotropic than in other reservoirs tested. Several other types of natural fractures (e.g., low-angle shear fractures) were observed, but significantly less frequently. Thirty-five coring-induced petal fractures were also observed; these give further information on the present in situ stress state.

1.5.2 Log Analysis (Section 4.0)

Extensive logging programs were conducted during the drilling of the MWX wells. The well logs were analyzed with TITEGAS, a tight gas sandstone log interpretation model developed in conjunction with the MWX log data base.[23] This extensive data base allowed analyses, crossplotting, and verification of the results for porosity, matrix calculations, clay volume, water saturation and permeability.

Detailed log analyses were made in the lower and middle fluvial zones. A total of 10 distinct sand bodies were analyzed in the lower zone and 12 distinct zones in the middle zone. Representative results for MWX-1 are given in Table 1.1. The log analyses allowed each zone to be classified into one of six reservoir types defined in Section 4.5. Individual overall reservoir descriptions are presented based upon petrographic, geologic and the log interpretation studies.

The log analyses included the opportunity to compare several natural fracture identification logs in MWX-3 and to indicate which zones appeared to be naturally fractured. Assessments of cement bond quality, interpretation of stresses for hydraulic fracture containment, two different matrix permeability analyses, and petrophysical relationships in the fluvial interval were also part of the extensive fluvial log analysis effort.

1.5.3 Core Analysis (Section 5.0)

A total of 2010 ft of four-inch-diameter core was taken in the fluvial interval: 1600 ft of continuous core (the entire interval) in MWX-1, 190 ft in two intervals in MWX-2, and 220 ft in two intervals in MWX-3. A total of 593 ft was oriented. In addition, 36 ft of 2-1/2-inch-diameter pressure core were taken in MWX-3 to obtain a precise water saturation value. Core samples were distributed to over 20 participants in a comprehensive core analysis program.[24]

Both routine and special core analyses for reservoir properties were made at frequent intervals in the sandstones. Many analyses extended above and below the sandstones so that properties are also available for the bounding lithologies.

An example of core-derived (matrix) reservoir properties for the fluvial interval are shown in Figure 1.9 for the B sandstone in MWX-1. There are more differences in the "typical" behavior of the fluvial zones than are found in the coastal zone. Sandstone porosities are on the order of 5-8%, water saturations are around 45-60%, and dry Klinkenberg permeabilities are generally 1-20 μd measured at 2000 or 3000 psi confining stress. The permeabilities are strongly influenced by water saturation: the dry permeabilities would be reduced by about a factor of 10-50 at the observed water saturations. Also, the matrix permeabilities are far more stress sensitive than samples from the paludal zone. These effects combine to give a realistic estimate for the true in situ matrix permeability of 0.1 to 0.2 μd. Permeabilities are quite variable within a sandstone and were often measured to be enhanced along carbonaceous stringers and mineralized narrow natural fractures. In addition, capillary pressures of several hundreds of psi were found at the prevailing water saturations.

Mechanical properties show that at confining pressures around 2700 psi, Young's moduli and compressive strengths range from 3.6-7.1 x 10^6 psi and 21-45 x 10^3 psi in the sandstones and from 2.5-7.8 x 10^6 psi and 14-21 x 10^3 psi in the abutting siltstones and mudstones. In general for the fluvial zone, it appears that the moduli, compressive and tensile strengths, and fracture toughnesses are highest for the siltstones, intermediate for the sandstones, and lowest for the mudstones.

Other core analyses included directional permeabilities, capillary pressure, caprock analyses, compressibility, permeabilities to brine in preserved and oven-dried core, triaxial tests for compressive strength, tensile strength, cation exchange coefficient, formation factor, resistivity index, vitrinite reflectance, and rock evaluation pyrolysis. Core samples were also used extensively in other MWX activities such as sedimentology, mineralogy/petrology, natural fracture studies, in situ stress, and laboratory work supporting stimulation; these activities are described in their respective sections of this report. Finally, correlations were also made between stress-related core measurements and televiewer and oriented caliper logs to determine in situ stress orientations.

1.5.4 In Situ Stress Measurements and Analyses (Section 6.0)

Twenty-six cased-hole stress tests were made in sandstone and mudstone lithologies in the fluvial interval and the results are summarized in Figure 1.10. These tests consisted of repeated small volume hydraulic fractures (<100 gal) conducted through a two-foot perforated interval under conditions where the instantaneous shut-in pressure is nearly equal to the minimum in situ stress.[25] Generally, there is good correlation between rock type and in situ stresses: stress gradients in the sandstones and mudstones are typically 0.77-0.88 psi/ft and 0.82-1.11 psi/ft, respectively. Different stress conditions were observed for the fluvial compared with the other intervals. Between 5000 and 6000 ft, the stresses in the sandstones hardly change. Also, the mudstone stresses between 5000 and 5800 ft are lower than lithostatic. These give rise to varying stress contrasts between the sandstones and mudstones ranging from 1500 psi at 6000 ft to as low as 100-200 psi at 5000 to 5400 ft. Larger contrasts and regular gradients reappear above 5000 ft. Thus the expected degree of hydraulic fracture containment varies for the three reservoirs that were stimulated: good for the B sandstone and only moderate for the C and E sandstones. The reasons for these changes are unknown, but it should be noted that the interval with lower contrasts coincides with the peak in natural fracture concentration.

Anelastic strain recovery (ASR) measurements were made on oriented core from all three wells, but analyses are presented only for MWX-3, for which a much improved strain measurement system was available.[26] The primary ASR result is the direction of the maximum horizontal in situ stress, which is the azimuth of a hydraulic fracture. Three sandstone cores around 4910 ft gave an average azimuth of N75°E and five sandstone cores between 5724 and 5782 ft gave an average azimuth of N89°E. These ASR-derived azimuths suggest that there is a probable clockwise rotation of fracture azimuth with increasing depth at this site: from N75°E at 4950 ft to N115°E at 7550 ft.[26] Stress magnitudes were also calculated from ASR data and by differential strain curve analysis (DSCA). The results suggest that the difference in horizontal stress varies from 500-1200 psi. A single mudstone test indicated isotropic horizontal stresses.

1.5.5 Fluvial B Sandstone Stimulation Experiment (Section 7.0)

The first major focus of fluvial activities was a stimulation experiment conducted in the B sandstone. Usually, MWX-1 was the production and main well test well. MWX-2 and MWX-3 were also perforated in the B sandstone and served as interference/observation wells. The sequence of activities included: perforation and nitrogen gas breakdown of the three wells, prefrac production/interference tests which included an argon injection/tracer test, nitrogen gas step rate and flow back tests, a series of borehole seismic diagnostics tests, two periods of fishing in MWX-2, a nitrogen foam minifrac, a propped nitrogen foam stimulation treatment, clean-up, postfrac production/interference tests, winter shut-in, and a final month-long production and build-up test.

For the first time at MWX, nitrogen gas was used as the fracturing fluid to break down the perforations of all three wells. This was done to ensure that no liquids were introduced that might hinder cleanup in MWX-1 or cause liquid blockages that could mask or hinder small pressure transients in the vicinity of the observation wells. The prefrac tests consisted of several periods of flow and shut-in of MWX-1 with bottomhole pressures measured at MWX-2 and MWX-3 (Figure 1.11). In all cases bridge plugs below the zone and just above bottomhole closures were used to significantly reduce wellbore storage. (The anomalous pressure drop occurring at buildup pressures ~3200 psi are believed to be due to a leaky bridge plug.) The production data showed that the B sandstone in MWX-1 was capable of producing 25-30 MCFD and no evidence of interference was observed. Drawdown analyses indicated a total reservoir flow capacity of 8-12 μd; this is a 100-fold increase over the matrix value and indicates the contribution of natural fractures. Further, the natural fracture system exhibited severe permeability anisotropy (on the order of 100:1). An argon gas injection test into MWX-2 confirmed the effects of anisotropy: argon was not detected after three to four days of gas chromatographic analyses at MWX-1 and MWX-3. An additional flow and buildup test was conducted in MWX-3 and gave similar results to the tests in MWX-1, except the anomalous pressure drop didn't occur. Both a naturally fractured reservoir model and a homogeneous reservoir model containing a single hydraulic fracture (due to the breakdown) were used in the prefrac analyses.[27] Results for the two models were essentially the same: acceptable matches of the pressure data for the fluvial B sandstone were found for either a highly anisotropic (100:1), naturally fractured, tight (0.1 μd) matrix reservoir or a homogeneous, tight (0.4 μd) reservoir.

Step-rate, pump-in, and flow-back tests were conducted with nitrogen gas September 4-5, 1986. The closure stress was estimated to be 4450 psi and the frac extension pressure to be 4650 psi from the step rate test. The pump in, flow back tests with nitrogen gas are believed to be a first, but the results are equivocal due to several possible effects. The minifrac and main stimulation of the B sandstone were performed October 31 and November 1, 1986, using the same wellbore configuration, fluid system, and instrumentation. The minifrac consisted of 8000 gal of 75 quality nitrogen foam, pumped at 10 bpm (Figure 1.12). The Nolte-Smith plot was relatively flat and the Nolte pressure decline analysis gave a very low leakoff coefficient of 0.00026 ft/$\sqrt{}$min. The stimulation was designed to inject 22,000 gal of 75 quality nitrogen foam and 46,000 lb of intermediate strength proppant (Proflow) in a pad stage and three proppant stages at one, three, and four ppg, at overall slurry rates of 2.5 to 4.3 bpm. The stimulation treatment (Figure 1.13) was complicated by several operational problems: a pumper sandout (12 min shutdown), two minor sandouts (decreased sand concentration), screenout within 10-15 min after the sand entered the perfs (sharp pressure increase), two drops in pressure (attributed to movement of the bridge plug), an incorrectly calibrated densitometer (higher sand concentrations than designed, e.g., 3.5 ppg actual versus two ppg design). After treatment and cleanout of the wellbore, the bridge plug was found about 600 ft below its original position.

Several pressure-history-match calculations were performed using a pseudo-3D fracture simulator to evaluate the minifrac and the main stimulation. The analysis of the minifrac indicated that there was a sudden flattening of the pressure record above a threshold of approximately 1050 psi above the closure stress.[28] This flattening could best be matched by increasing the leak-off coefficient by a factor of 50 (Figure 1.12). This increased leakoff was attributed to either the opening of the natural fractures at pressures above the threshold level or possible height growth into thin, naturally fractured siltstones known to exist in the bounding rocks. (This phenomenon was investigated further in the fluvial C and E operations.) The accelerated leakoff was also observed in the main treatment (Fig. 1.13) and could explain the early screenout. The pressure history match was able to account for many of the features observed in the complicated main stimulation's treatment pressure record. The match gives an estimated total length of 1060 ft (but with a propped length of only 318 ft) and total height (near the wellbore) of >150 ft.

The postfrac testing was conducted in two Phases: Phase I in December 1986 immediately after stimulation and clean-up and Phase II in March 1987 after a two-month winter shut-in. Phase I (Fig. 1.14) showed very little production improvement after the treatment. Flow rates were sporadic due to irregular water production and were 20-25 MCFD, as compared with prefrac rates of around 20 MCFD at the same bottomhole pressures of 1000 psi. The Phase I pressure buildup data appeared influenced by complications associated with the treatment. The Phase II production rates were initially 110-120 MCFD and continually decreased to a range from 32-40 MCFD over the last five days of the 16-day production period (Figure 1.15). Thus only small production enhancement was observed for this treatment. The expected production rates from MWX-1 for various fracture lengths were calculated by both the reservoir models used in the prefrac analyses.[27] These results were used to qualitatively evaluate postfrac performance and are consistent with the stimulation and production data.

Borehole seismic diagnostics were used in this stimulation experiment.[29] Several improvements (including a six-channel digitizer operating at 13.3 kHz/channel, a clamp arm force indicator, and downhole geophone exciters to test operation in situ) were made to the system. A series of prefrac tests were performed where velocities along three different well-to-well paths were measured by firing perforations in one well while borehole seismic tools were set in one or both of the other two wells. The results gave formation velocities ranging from 15.5 to 18.4 ft/ms, indicating that large velocity anisotropy exists at the site. Using signals generated in MWX-1 and recorded at MWX-2 and MWX-3, a two-tool location algorithm showed that the perforation signals could be located within a 25-ft radius and within an azimuth of 4°. Over 100 microseismic events were recorded during and after the main treatment. Twenty-nine of these could be analyzed in both wells, and their locations (Fig. 1.16) yield a fracture azimuth of N68°W, and upwards growth of 50 to 80 ft. However, signal strengths in MWX-2 were approximately three times stronger than in MWX-3, and 73 signals could be mapped using just data from the one well. These locations give an azimuth of N80°W. Systematic differences between the data from the two observation wells show that dependence on data from a single observation well could result in errors in fracture azimuth for heterogeneous, anisotropic geologies.

1.5.6 Fluvial C Sandstone Activities (Section 8.0)

In late April and May 1987, experiments were conducted in the fluvial C sandstone. Two separate minifracs were conducted in MWX-1 to further examine the accelerated leakoff phenomenon observed in the fluvial B and to examine the use of 100 mesh sand to mitigate the higher leakoff.[28] Coincident with the minifracs, in situ stress measurements were made to quantify the change in stress a short distance away in MWX-2[30] and a borehole seismic tool was emplaced in the C sandstone, the first time a tool had been located at the same horizon as the frac.

The MWX-1 tests were initiated by a series of pump-in/shut-in, step-rate/flow-back, and pump-in/flow-back tests with KCl water which gave a value of 4575 psi for the closure stress. The first minifrac was conducted April 30, 1987, and consisted of 150 bbl of 75 quality nitrogen foam containing 20 lb/1000 gal gel in the liquid phase. Customary pressure decline analyses showed no indications of a pressure sensitive leakoff. However, a pressure history match showed a threshold 875 psi above closure and a factor of 70 increase in the leakoff coefficient from 0.0001 ft/$\sqrt{}$min to 0.007 ft/$\sqrt{}$min. The effect is not seen in the pressure decline analysis because the pressure falls rapidly upon shut-in and only a small fraction of the data is recorded above the threshold pressure. The second minifrac was conducted May 12, 1987, and consisted of 240 bbl of the same nitrogen foam, but was pumped as a pad plus four sand stages containing 0.25 to 1.0 lb/gal of 100 mesh sand followed by a foam stage with no sand. The pressure record for this treatment is shown in Figure 1.17 with the pressure history match for the first minifrac superimposed. The pressure history match of the second minifrac showed that the accelerated leakoff coefficient (that above the threshold) was 0.002 ft/$\sqrt{}$min, a factor of 20 increase rather than the factor of 70 observed without sand. This positive effect in controlling leakoff, plus the possibility of delaying height growth and increased permeability to the hydraulic fracture, led to a recommendation to use 100 mesh sand on subsequent stimulations at MWX.

Investigation of gas production was not an objective of activities in the C sandstone and well testing was limited to short production tests after each minifrac. Figure 1.18 shows the test period after the first minifrac where stable production rate about 60 MCFD was observed at a bottomhole pressure of 1000 psi. Clean-up after each of the minifracs was rapid and indicated the same production rate. This rate is slightly better than in the fluvial B sandstone, but, in general, the two reservoirs appear comparable.

Small volume hydraulic fracture stress measurements were conducted in MWX-2 to measure the minimum in situ stress before, during, and after each of the two minifracs in MWX-1. As hypothesized, significant stress increases of up to 300 psi were observed (Figure 1.19 and Section 8.2.5). Thus, the feasibility of locally altering the stress field has been demonstrated.[30] The minifracs were not designed to provide a large perturbing stress. However, supporting analytic and finite element calculations quantified the effects of formation modulus contrasts, fracture height, and fracture length. These results show that the stresses can be readily increased high enough (600-800 psi at the MWX site) that the minimum horizontal in situ stress will become the maximum horizontal stress, and thus the azimuth of hydraulic fracture conducted in this altered stress region will be perpendicular to the usual direction.[30] The advantages of such a altered stress fracturing concept were quantified by a series of reservoir simulations which examined the effect of a hydraulic fracture along or across the unidirectional naturally fractured reservoir model used for the fluvial B sandstone. The results show that a 100-ft fracture perpendicular to the natural fractures gives about the same production rate and cumulative volumes as a 900-ft fracture which parallels them.[30]

A single borehole seismic tool was placed in MWX-3 in the C sandstone and oriented by perforations in the other two wells. Reproducible directions (±2°) were observed for the group of perforations in each well. However, the tool orientation based on the data from MWX-1 and the tool orientation based on the data from MWX-2 differed by 9.6°, a difference presumably due to as yet not understood effects of the complex geology upon seismic signal propagation. A fracture map was derived from a total of 53 microseismic events digitized during both minifracs (Figure 1.20). The frac azimuth was N63°W, with west and east wings of at least 250 ft and 200 ft, respectively, and a fracture height of about 100 ft. Overall, the results indicate that placing the borehole seismic tool in the stimulated sandstone does not result in a significantly improved signal as compared with previous results where the tools are routinely located tens of feet above the target sandstone.

1.5.7 Fluvial E Stimulation Experiment (Section 9.0)

The final focus of fluvial activities--and the last of the Multiwell Experiment--was a stimulation experiment conducted in the E sandstone.[31] As before, MWX-1 was the production and main test well. MWX-2 and MWX-3 were also perforated in the B sandstone and served as interference/observation wells. The sequence of activities included: different breakdown procedures in each of the three wells, prefrac production and interference tests, KCl water pump-in/shut-in and step-rate/flow-back tests, nitrogen foam minifrac, propped nitrogen foam hydraulic fracture treatment, borehole seismic diagnostics, and postfrac production and interference tests.

In all sandstones studied at MWX, some form of breakdown treatment was required to connect the naturally fractured reservoir to the wellbore.[32] KCl water plus ball sealers had been used routinely for achieving this breakdown, but the introduced fluid would impair the flow of gas in the natural fractures and relatively long cleanup times were required. Pumped nitrogen gas was tried in the coastal and fluvial B sandstones, but this method did not affect all perforations equally and thus treat the entire interval effectively. Four different, nonaqueous techniques were tried in breaking down the three wells in the fluvial E sandstone. (1) MWX-2 was perforated in an underbalanced (1000 psi, surface) column of nitrogen; satisfactory connection was achieved. (2) MWX-1 was perforated under an overbalanced (6000 psi, surface) column of nitrogen (350,000 SCF). This subjected all perforations to the same high pressure, well above the 4850 psi fracture extension pressure. Flow rates through the perforations averaged 75,000 SCF/min over 45 sec. Pressures measured at MWX-2 showed an immediate poroelastic response, which was followed by a slower, continuous rise indicating pressure interference (Figure 1.21) and excellent connection of MWX-1 to the reservoir. (3) A commercial tailored pulsed technique was attempted in MWX-3. Two 12-ft tools were used to cover the 20 ft of pay and were fired two days apart under a 2000-ft column of liquid carbon dioxide which served as a nonaqueous tamp. There was no enhanced flow indicative of successful breakdown. Subsequent review indicated the most probable cause was that some original workover fluid probably covered the perforations and was then forced into the formation by the shots. (4) A nitrogen gas impulse was subsequently used to break down MWX-3 successfully. This was similar to (2) above, but since the well was already perforated, a packer with a tubing plug, fastened with shear pins designed to fail at 6500 psi, was set just above the perforations. The tubing and annulus (connected at the surface) were filled with nitrogen gas and the pressure increased until the tubing plug released at 6450 psi, creating a rapid pressure rise at the perforations. The conclusion is that alternatives to normal fluid breakdown procedures are available. The three nitrogen gas impulse methods tried in the fluvial E sandstone all provide field-executable, practical methods for effectively connecting the wellbore with a fluid-sensitive, naturally fractured reservoir. Evaluation of the tailored pulse method was compromised by the presence of residual fluid in the wellbore.

Prefrac production, buildup and interference tests in the E sandstone were conducted over a 60-day period and consisted of an initial two-week production and buildup period, two two-day production/two-day shut-in interference pulses, and a final 7-1/2-day production period followed by a final 31-day buildup (Figure 1.22).[33] Flow rates of 70 and 50 MCFD at a constant 1000 psi bottomhole pressure were observed at the beginning and end of the test period, respectively. Unlike other nonmarine intervals studied at MWX, clear, correlatable pressure interference was observed at the observation wells. Analysis of the test data by Horner, log-log pressure and pressure derivative techniques gave a kh of 0.37 md-ft, a reservoir pressure of 3200 psi, a skin of -1.7 to -2.2, and an average reservoir permeability of 13 μd. As before, the latter is much greater than the core-derived matrix permeability, indicating the presence of natural fractures. Two different models of naturally fractured reservoirs were applied. The first was a single-layer model with an isotropic natural fracture flow capacity. This model provided an excellent match of the MWX-1 flow and pressure data, especially as seen in the Horner and other pressure plots. However, matches to the pressures at the observation wells were not possible, despite introducing significant anisotropy. The second model was a three-layer, bounded model which was derived from E sandstone geologic, core, and log data and is defined in Figure 1.23. This model provided very reasonable matches with data from all three wells and was adopted as the prefrac reservoir model for the E sandstone. These results emphasize the fact that single well analyses can be ambiguous and not allow discrimination between multilayered, heterogeneous and single layer, homogeneous, naturally fractured reservoirs, a distinction which could impact stimulation design and ultimate production.

The E sandstone stimulation activities[31] began with a pump-in/shut-in, step-rate/flow-back, and three pump-in/flow-back tests which yielded a closure stress of 4550 psi and a minimum fracturing pressure of 4850 psi. A minifrac was conducted September 26, 1987, and consisted of a 2000 gal pad of foamed water, followed by 10,000 gal of 75 quality nitrogen foam containing a 20 lb/1000 gal biopolymer gel, all pumped at a bottomhole flow rate of 23 bpm. Accelerated leakoff was observed at a threshold pressure 850 psi above closure, and a pressure history match indicted a factor of 50 increase in the leakoff coefficient (to 0.04 ft/$\sqrt{}$min) above this threshold. The design for the main stimulation called for a propped hydraulic fracture with about 750 ft wing length, 75 quality nitrogen foam to minimize damage to the natural fracture system, and the use of 100 mesh sand to control leakoff. A new breaker system was also developed[34] and a special foamed water/breaker prepad was added to enhance gel degradation and return. The treatment design was complex: foamed water/breaker prepad; a two-part pad of nitrogen foam, the first part foam only and the second part containing 0.5 ppg of 100 mesh sand; and three prop stages at 1-4 ppg intermediate strength proppant, each containing 0.25 ppg of 100 mesh sand. Totals injected were 42,000 gal foam, 72,000 lbs of 20/40 mesh intermediate strength proppant, and 10,000 lbs of 100 mesh sand. The treatment was conducted September 27, 1987, with only minor problems (a two-min surface sandout at four ppg) and all instrumentation functioned properly (Figure 1.24). Postfrac temperature and gamma logs were not conclusive and indicated at least a 50 ft total height at the wellbore. Flowback occurred at two bpm and 127 bbls of 286 bbls of injected liquids were recovered within 12 hours; this fast cleanup and resultant flow (initially 300 MCFD) indicate little damage to the natural fractures. The pressure history match (Fig. 1.24) used a 115-130 ft height obtained from borehole seismic diagnostics and gave a total length of 885 ft with only 390 ft having a high prop concentration. The fine-mesh sand appeared to help retard the leakoff as the designed treatment was put away and a screen-out was avoided.

The post-frac testing consisted of a 16-day production test, two-day shut-in to create an interference pulse, 7-day production test, and a final 42-day pressure buildup test (Figure 1.25). Gas flow rate was 200-220 MCFD at the end of the 16-day production test; thus a good productivity enhancement occurred. Clear pressure interference was observed in the two observation wells. Analytical techniques indicated that the propped fracture length was short, 54-150 ft depending upon the amount of damage assumed, but the log-log and derivative data showed complexities that were not evident in the prefrac well test data and which are probably indicative of a dual or interporosity flow behavior. The initial modeling attempt to include a simple, simulated propped fracture into the multilayered prefrac model did not yield an acceptable match. Instead the model had to be altered by the inclusion of some damage to the natural fractures that abut the propped fracture and by reducing the matrix permeability in one of the three model layers. This produced an acceptable match for a 500-ft propped fracture. These analyses underscore the complexity of the in situ processes that are involved.

Borehole seismic fracture diagnostics were used during the stimulation treatment.[35,36] This system contained three further improvements: different geophones with more appropriate response characteristics, a unique four-axis, equally oriented (with respect to the tool axis) geophone configuration, and a 10 kHz/channel digitization rate with a two-sec write-to-disk capability. Seismic tool orientations were determined by firing perforations in the other wells and then the accuracy of the orientations and tool positions were assessed by locating the perforations in MWX-1. The data recorded in MWX-2 were considered accurate, but the data recorded in

MWX-3 cast serious doubts on the accuracy of locations determined by signals detected in that well. Thus the seismic map of the E sandstone treatment was based upon the analysis of signals recorded in MWX-2, and although the selected signals were seen in MWX-3, their analyses showed they contained no valid directional information. A total of 160 microseismic events were eventually analyzed: four, 72, and 84 from the pump, shut-in, and flow-back phases, respectively. These locations are plotted in Figure 1.26, and show a symmetric fracture with wings of 250 ft length, an azimuth of N60°W, and fairly well defined fracture top and bottom with a frac height of about 120 ft.

1.5.8 Laboratory Studies (Section 10.0)

Pre- and post-frac laboratory studies were performed as an integral part of fluvial zone stimulations. One focus was investigation of the damage by stimulation fluids to natural fracture permeability.[37] As core samples with natural fractures were limited, fluvial core was cracked and these artificial fractures were used for many of the measurements. Permeabilities were measured after injection and cleanup for a variety of fluids or combinations: brine, surfactants, breaker formulations, methanol, hydroxypropyl guar, hydroxethylcellulose, and xanthan biopolymer. Varying degrees of damage were observed in all cases. Leakoff parameters were also measured during these measurements and were found to be somewhat smaller than those observed in the field.

The second focus of these studies was the development of a breaker system for the xanthan biopolymer which was the gel component in the foam fluid system.[34] This biopolymer is very temperature stable, and an efficient breaker was required to minimize the amount of gel left in the reservoir. In addition, the frac design for the E sandstone included a breaker prepad with the idea of introducing breaker ahead of the gel, which would flow back over the gel during cleanup. It was felt that the new fluid system contributed to the success of the E sandstone stimulation.

A final focus was the analysis of fluids returned after the frac. These analyses measured both viscosity and organic composition and amount. Material balance showed that while only about 30% of the biopolymer was recovered after the B sandstone treatment, about 70% was recovered after the treatment of the E sandstone. This latter recovery was further evidence for the success of the new breaker system.

1.5.9 Other Activities

Three geophysics-related experiments were conducted over the Mesaverde Formation at the MWX site: a three-dimensional surface seismic survey,[38,39] vertical seismic profiles (VSP),[38-40] and cross-well acoustic surveys.[38,41] (These studies are not presented in this report, but can be found in the referenced documents.) The focus of these studies was the lenticular sandstones of the paludal, coastal, and fluvial intervals. The lithologies in the coastal and fluvial show essentially no relative impedance contrasts. Additionally, the uniform sine wave character of synthetic seismograms based on log data is indicative of an unresolved fine structure as the seismic wavelengths of the 3D and VSP surveys are significantly greater than the coastal's and fluvial's lithologic features.[38]

1.6 COMPARISON WITH OTHER MESAVERDE INTERVALS

Gas production from the various individual Mesaverde reservoirs measured during MWX testing and stimulation is given in Table 1.2; there are definite correlations with depositional environment and with degree of natural fracturing.[42] The individual marine reservoirs have the highest production potential. The coastal and paludal intervals have the same basic limited, distributary channel reservoir morphologies. However, the coastal has lower potential than the paludal due to the paludal's improved reservoir rock properties, higher pore pressures, and adjacent coal seams and organic-rich sediments. The coastal and fluvial reservoirs have similar unstimulated production, but fluvial reservoirs offer the potential of better stimulation ratios (postfrac rate/prefrac rate) due to their greater average width resulting from the broad meandering-stream depositional systems. The unstimulated production per foot of net perforated pay for the different intervals are approximately two, <2, five, and >10 MSCFD/ft for the fluvial, coastal, paludal, and marine intervals, respectively.

MWX data were used to estimate the amount of gas in place in the Mesaverde at the MWX site (Table 1.3). The data for each reservoir studied were derived from core and well test data, the estimated width of each sandstone, and an assumed mile length. The large values for the marine reservoirs are due to their blanket nature (i.e., a one-mile "width" for this calculation). The total interval values are based upon measured properties and the sandstone fraction in the interval. Fluvial reservoirs represent over a third of the gas-in-place. There is an estimated 156 BCF/section in the Mesaverde at the MWX site, and this total increases to more than 180 BCF/section if estimated contributions from coal seams are included.

1.7 SIGNIFICANT ACCOMPLISHMENTS

Three wells were drilled which penetrated the Mesaverde Formation in the Piceance basin at a site near Rifle, Colorado. These wells established the Multiwell Experiment, a field laboratory for the study of the tight gas reservoirs in this formation. The Mesaverde was subdivided into distinct intervals based on their depositional environments, which, in turn, strongly influence their reservoir characteristics. This report is the culmination of work in the fourth and last of the intervals--the fluvial. (Reports for the marine,[11] paludal,[12] and coastal[13] intervals have been published.)

The fluvial interval has been characterized with most emphasis placed upon the lower third, between 5450 ft and 6000 ft. The fluvial reservoirs are meander-belt sandstones composed of point bar sequences separated by various lithologic discontinuities. They are irregular in shape and have relatively large widths of 1000-2500 ft. A comprehensive body of core, log, stress, and geologic data has been compiled for this interval of the

Mesaverde Formation and it is available publicly as a result of the Multiwell Experiment.

The significant importance of natural fractures in gas production from these tight sandstone reservoirs has been demonstrated (Figure 1.27). While the fluvial sandstones have matrix permeabilities that are less than one microdarcy under in situ conditions of stress and water saturation, the overall permeability was found to be 10-15 μd, some two orders of magnitude higher. The effect of natural fractures was further noted in the E sandstone where a second fracture set was found to influence reservoir behavior.

In situ stress measurements and analyses indicate that the fluvial sandstones between 5000 and 6000 ft have a nearly constant stress about 4500 psi, whereas the confining siltstone and mudstone lithologies have stresses which vary with depth. Thus, the confining stress contrasts range from 1500 psi to as low as 100-200 psi, a factor which will affect hydraulic fracture growth. Anelastic strain recovery measurements on oriented fluvial core gave a range of directions from N67°E to N103°E for the maximum horizontal in situ stress, and are consistent with a clockwise rotation with increasing depth through the Mesaverde.

New breakdown procedures were demonstrated to be practical methods for connecting the wellbore with a fluid-sensitive, naturally fractured reservoir. These included simultaneous perforation in a nitrogen-filled wellbore at pressures both above (more effective) and below the fracturing pressure or, in the case of a perforated well, the use of a tubing plug designed to create a high pressure nitrogen impulse. Evaluation of a tailored pulse method was compromised by the presence of residual fluid in the wellbore.

Well tests were conducted in three fluvial reservoirs, with comprehensive pre- and post-frac tests performed in the B and E sandstones to characterize fluvial reservoir performance. Gas production from individual unstimulated fluvial sandstones was 25-70 MCFD; these correspond to values of 1.5, 2.3, and 2.3 MCFD per foot of perforated pay in the B, C, and E reservoirs, respectively. Pressure interference during production and shut-in periods was not observed in the B sandstone. However, it was observed for the first time in nonmarine reservoirs at MWX in the E sandstone and is presumably the result of the secondary fracture system and different stress regime at this particular depth.

The preservation of the permeability of the natural fracture system intersected by a hydraulic fracture is critical to production enhancement. The fractures are susceptible to damage by liquids, fracturing fluid polymers, and high fracturing pressures. Laboratory studies have provided insight into the possible damage mechanisms, in particular the damage to the narrow natural fractures. These studies led to the development of a new frac fluid/breaker system that was used successfully in the E sandstone stimulation.

Minifrac and stimulation treatments in the fluvial quantified the phenomena of a significantly increased leakoff above a threshold pressure, usually 800-1100 psi above the closure stress. This leakoff led to a screenout in the B sandstone. Subsequent studies in the C sandstone indicated that fine mesh sand mitigated the leakoff and its use during the E sandstone treatment was successful in allowing the job to be placed as designed.

The feasibility of altered stress fracturing was demonstrated when significant stress increases were measured in MWX-2 during minifracs conducted 121 ft away in MWX-1. The results show that stresses could be readily increased high enough (600-800 psi at MWX) that the minimum horizontal in situ stress will become the maximum stress, and thus the azimuth of a hydraulic fracture in this altered stress region will be perpendicular to the usual direction. A reservoir simulation showed that a 100-ft fracture perpendicular to the natural fracture direction at MWX would be as effective as a 900-ft fracture along a unidirectional, naturally fractured reservoir such as the B sandstone.

A successful hydraulic fracture stimulation was conducted in the E sandstone. The treatment was designed to control accelerated leakoff with fine-mesh sand and to minimize damage to the natural fractures system through a new fluid/breaker system. The 42,000-gal-foam, 72,000-lb-proppant treatment was conducted smoothly. Immediately after an efficient flowback, production was >300 MCFD, a rate which decreased to 200-220 MCFD at the end of a sixteen day flow period. Fracture diagnostics and analyses indicated a frac height of 120 ft, a propped frac length of 400 ft, and a frac azimuth of about N60°W.

An advanced, naturally fractured, fully transient reservoir simulator was used to successfully match pressure data from the well tests conducted before and after the stimulations. The versatility of the simulator was shown in the development of a complex, three-layer reservoir model for the E sandstone that was based upon core, log, and geologic data and provided a very good match to pressure data from all three wells. Significantly, it was shown that excellent matches to data from a single well could be made by several very different reservoir models, but that matching interference data accurately provided new insight into the complex phenomena associated with these naturally fractured reservoirs.

A pseudo-3D stimulation model was used to history match the fracturing pressure data. These matches detailed the existence of accelerated leakoff and provided good values for hydraulic fracture parameters.

Several advancements in the borehole seismic instrumentation and analyses were made. These resulted in diagnostic maps for all fluvial stimulation treatments. The complexities associated with accurate microseismic event detection and location were encountered in each case and remain a source for future research.

Overall, the fluvial interval is characterized by relatively wide (1000-2500 ft), heterogeneous, low permeability sandstones (<1 μd) which contain a complex anisotropic natural fracture system which creates an overall reservoir permeability of ~15 μd. Fluvial reservoirs offer the opportunity for good stimulation performance due to their larger widths. As such, the fluvial interval offers the highest production potential of the three non-marine intervals studied during the Multiwell Experiment.

1.8 ACKNOWLEDGMENTS

A project of this magnitude is clearly the result of the efforts of a large number of people. The principal investigators express their appreciation for the assistance received from the MWX project personnel at Sandia National Laboratories and CER Corporation. Special thanks are extended to the CER field crew for their hard work and dedication in maintaining the site and conducting the various tests, often under difficult conditions. We also acknowledge the contributions from many contractors and other participants in MWX who have helped us compile a unique, comprehensive set of data for this potential resource.

The Multiwell Experiment was the major production technology project in the U.S. Department of Energy's Western Gas Sands Subprogram. DOE personnel responsible for MWX in the past have been C. H. Atkinson, A. B. Crawley, and J. K. Westhusing. For the past six years, the Western Gas Sands Subprogram has been managed by K-H. Frohne, at DOE's Morgantown Energy Technology Center.

1.9 REFERENCES

1. National Petroleum Council, "Unconventional Gas Sources--Volume V: Tight Gas Reservoirs, Part I," Library of Congress Card Number 80-82488, December 1980.

2. Luetkehans, G. R. and J. Toman, "Status Report on Three Nuclear Experiments for Stimulation of Tight Gas Sands," Proceedings of the Symposium on Stimulation of Low Permeability Reservoirs, Golden, CO, February 16-17, 1976.

3. Fitch, J. L., W. L. Medlin, and M. K. Strubhar, "Demonstration of Massive Hydraulic Fracturing, Piceance Basin, Rio Blanco County, Colorado," Proceedings of the 5th Annual DOE Symposium on Enhanced Oil and Gas Recovery, Tulsa, OK, August 22-24, 1979.

4. Merrill, R. G., "Progress Report and Review of Natural Buttes Unit - Massive Hydraulic Fracturing Project," Proceedings of the 4th Annual DOE Symposium on Enhanced Oil and Gas Recovery, Tulsa, OK, August 29-31, 1978.

5. Atkinson, C. H., A. B. Crawley, D. A. Northrop, A. R. Sattler, R. L. Mann, and J. C. Schillo, "The Department of Energy's Western Gas Sands Project Multi-Well Experiment," SPE/DOE 9891, Proceedings of the 1981 SPE/DOE Symposium on Low Permeability Gas Reservoirs, Denver, CO, May 27-29, 1981, pp 577-582.

6. Crawley, A. B., D. A. Northrop, and A. R. Sattler, "The Department of Energy's Western Gas Sands Project Multi-Well Experiment Update," SPE 11183, the 57th Annual Society of Petroleum Engineer's Technical Conference and Exhibition, New Orleans, LA, September 26-29, 1982.

7. Northrop, D. A., A. R. Sattler, and J. K. Westhusing, "Multi-Well Experiment: A Field Laboratory for Tight Gas Sands," SPE/DOE 11646, Proceedings of the 1983 SPE/DOE Joint Symposium on Low Permeability Gas Reservoirs, Denver, CO, March 13-16, 1983, pp 393-398.

8. Northrop, D. A., A. R. Sattler, R. L. Mann, and K-H. Frohne, "Current Status of the Multiwell Experiment," SPE/DOE/GRI 12868, Proceedings of the 1984 SPE/DOE/GRI Unconventional Gas Recovery Symposium, Pittsburgh, PA, May 13-15, 1984, pp 351-358.

9. Northrop, D. A., "Insights into Natural Gas Production from Low Permeability Reservoirs," SPE 17706, Proceedings of the 1988 SPE Gas Technology Symposium, Dallas, TX, June 8-11, 1988, pp 25-34.

10. Northrop, D. A. and K-H. Frohne, "Insights and Contributions from the Multiwell Experiment: A Field Laboratory in Tight Sandstone Reservoirs," SPE 18286, Proceedings of the 63rd Annual Technical Conference and Exhibition of the Society of Petroleum Engineers of AIME, Houston, TX, October 2-5, 1988, Volume Sigma.

11. Multiwell Experiment Project Groups at Sandia National Laboratories and CER Corporation, "Multiwell Experiment Final Report: I. The Marine Interval of the Mesaverde Formation," Sandia National Laboratories Report, SAND87-0327, April 1987.

12. Multiwell Experiment Project Groups at Sandia National Laboratories and CER Corporation, "Multiwell Experiment Final Report: II. The Paludal Interval of the Mesaverde Formation," Sandia National Laboratories Report, SAND88-1008, May 1988.

13. Multiwell Experiment Project Groups at Sandia National Laboratories and CER Corporation, "Multiwell Experiment Final Report: III. The Coastal Interval of the Mesaverde Formation," Sandia National Laboratories Report, SAND88-3284, March 1989.

14. Lorenz, J. C., "Sedimentology of the Mesaverde Formation at Rifle Gap, Colorado and Implications for Gas-Bearing Intervals in the Subsurface," Sandia National Laboratories Report, SAND82-0604, March 1982.

15. Lorenz, J. C., "Reservoir Sedimentology in Mesaverde Rocks at the Multiwell Experiment Site," Sandia National Laboratories Report SAND83-1078, June 1983.

16. Lorenz, J. C., "Reservoir Sedimentology of Mesaverde Rocks at the Multiwell Experiment Site and East Central Piceance Creek Basin," Sandia National Laboratories Report, SAND87-0040, January 1987.

17. CER Corporation, "Multi-Well Experiment: MWX-1 As-Built Report," Sandia National Laboratories Contractor Report, SAND82-7201, July 1982.

18. CER Corporation, "Multi-Well Experiment: MWX-2 As-Built Report," Sandia National Laboratories Contractor Report, SAND82-7100, August 1982.

19. CER Corporation, "Multi-Well Experiment: MWX-3 As-Built Report," Sandia National Laboratories Contractor Report, SAND84-7132, February 1984.

20. Finley, S. J. and J. C. Lorenz, "Characterization of Natural Fractures in Mesaverde Core from the Multiwell Experiment," Sandia National Laboratories Report, SAND88-1800, September 1988.

21. Finley, S. J. and J. C. Lorenz, "Characterization and Significance of Natural Fractures in Mesaverde Reservoirs at the Multiwell Experiment Site," SPE 19007, Proceedings of the SPE Joint Rocky Mountain/Low Permeability Reservoirs Symposium and Exhibition, Denver, CO, March 6-8, 1989, pp 721-728.

22. Lorenz, J. C., P. Branagan, N. R. Warpinski, and A. R. Sattler, "Fracture Characteristics and Reservoir Behavior of Stress-Sensitive Fracture Systems in Flat-Lying Lenticular Formations," SPE 15244, Proceedings of the SPE Unconventional Gas Technology Symposium, Louisville, KY, May 18-21, 1986, pp 423-436.

23. Kukal, G. C., "A Systematic Approach for the Effective Log Analysis of Tight Gas Sands," SPE/DOE/GRI 12851, Proceedings of the 1984 SPE/DOE/GRI Unconventional Gas Recovery Symposium, Pittsburgh, PA, May 1984, pp 209-220.

24. Sattler, A. R., "The Multi-Well Experiment Core Program," SPE/DOE 11763, Proceedings of the 1983 SPE/DOE Joint Symposium on Low Permeability Gas Reservoirs, Denver, CO, March 13-16, 183, pp 437-444.

25. Warpinski, N. R., P. Branagan, and R. Wilmer, "In Situ Stress Measurements at U.S. DOE's Multiwell Experiment Site, Mesaverde Group, Rifle, Colorado," Journal of Petroleum Technology, 37 (3), 527-536, March 1985.

26. Warpinski, N. R. and L. W. Teufel, "In Situ Stresses in Low-Permeability, Nonmarine Rocks," SPE/DOE 16402, Proceedings of the 1987 SPE/DOE Joint Symposium on Low Permeability Reservoirs, Denver CO, May 1987, pp 125-138. Also Journal of Petroleum Technology, 41 (4), pp 404-414, April 1989.

27. Branagan, P. T., C. Cipolla, S. J. Lee, and J. Chen, "Designing and Evaluating Hydraulic Fracture Treatments in Naturally Fractured Reservoirs," SPE/DOE 16434, SPE/DOE Symposium on Low Permeability Reservoirs, Denver, Colorado, May 1987.

28. Warpinski, N. R., "Dual Leakoff Behavior in Hydraulic Fracturing of Tight Lenticular Gas Sands," SPE 18259, Proceedings of the 63rd Annual Technical Conference and Exhibition of the Society of Petroleum Engineers of AIME, Houston, TX, October 2-5, 1988.

29. Thorne, B. J. and H. E. Morris, "Advances in Borehole Seismic Fracture Diagnostics," SPE Formation Evaluation, pp 711-715, December 1988.

30. Warpinski, N. R. and P. T. Branagan, "Altered-Stress Fracturing," SPE 17533, Proceedings of Rocky Mountain Regional Meeting of the Society of Petroleum Engineers, Casper, WY, May 11-13, 1988, pp 465-476. Also Journal of Petroleum Technology, 41 (9), pp 990-997, September 1989.

31. Warpinski, N. R., P. T. Branagan, A. R. Sattler, C. Cippola, J. C. Lorenz, and B. J. Thorne, "A Case Study of a Stimulation Experiment in a Fluvial, Tight Sandstone Gas Reservoir," SPE 18258, Proceedings of the 63rd Annual Technical Conference and Exhibition of the Society of Petroleum Engineers of AIME, Houston, TX, October 2-5, 1988.

32. Branagan, P. T. and R. H. Wilmer, "Breakdown Procedures Designed to Minimize Damage to Naturally Fractured Reservoirs," SPE 17716, Proceedings of the 1988 SPE Gas Technology Symposium, Dallas, TX, June 8-11, 1988.

33. Branagan, P. T., S. J. Lee, C. L. Cippola, and R. H. Wilmer, "Pre-Frac Interference Testing of a Naturally Fractured, Tight Fluvial Reservoir," SPE 17724, Proceedings of the 1988 SPE Gas Technology Symposium, Dallas, TX, June 8-11, 1988.

34. Sattler, A. R., C. J. Raible, B. L. Gall, and P. J. Gill, "Frac Fluid Systems for Naturally Fractured Tight Gas Sandstones; A General Case Study from Multiwell Experiment Stimulations," SPE 17717, Proceedings Gas Technology Symposium, Dallas, TX, June 8-11, 1988, pp 117-130.

35. Thorne, B. J., and H. E. Morris, "Passive Seismic Monitoring of Hydraulic Fracture Experiments at the Multiwell Experiment Site," Sandia National Laboratories Report, SAND88-1284, August 1988.

36. Thorne, B. J. and H. E. Morris, "An Assessment of Borehole Seismic Fracture Diagnostics," SPE 18193, Proceedings of the 63rd Annual Technical Conference and Exhibition of the Society of Petroleum Engineers of AIME, Houston, TX, October 2-5, 1988.

37. Gall, B. L., A. R. Sattler, D. R. Maloney, and C. J. Raible, "Permeability Damage to Natural Fractures Caused by Fracturing Fluid Polymers," SPE 17542, Proceedings of the Rocky Mountain Regional Meeting of the Society of Petroleum Engineers, Casper, WY, May 11-13, 1988, pp 551-560.

38. Searls, C. A., M. W. Lee, J. J. Miller, J. N. Albright, J. Fried, and J. K. Applegate, "A Coordinated Seismic Study of the Multiwell Experiment Site," SPE/DOE 11613 Proceedings of the 1983 SPE/DOE Joint Symposium on Low Permeability Gas Reservoirs, Denver, CO, March 13-16, 1983, pp 115-120.

39. Searls, C. A., "The Multiwell Experiment Geophysics Program; Final Report," Sandia National Laboratories Report, SAND85-1013, September 1985.

40. Lee, M. W., "Detection and Delineation of Lenticular-Type Sand Bodies by the Vertical Seismic Profiling Method," United States Geological Survey Open File Report, 84-757, November 1984, pp 121-134.

41. Albright, J. N., P. A. Johnson, W. S. Phillips, C. R. Bradley, and J. T. Rutledge, "The Crosswell Acoustic Surveying Project," Los Alamos National Laboratory Report, LA-11157-MS, March 1988.

42. Lorenz, J. C. and S. J. Finley, "Differences in Fracture Characteristics and Related Production: Mesaverde Formation, Northwestern Colorado," SPE Formation Evaluation, pp 11-16, March 1989.

Table 1.1 Summary of Log-Derived Reservoir Properties, MWX-1

Zone	Depth (ft)	Pay (ft)	ϕ (%)	S_w (%)	V_{cl} (%)	kh (md-ft)	Type*
O	Missing	-	-	-	-	-	-
N_2	5001.0-5018.5	15.5	8.3	45.7	20.7	0.167	1a
N_1	5030.0-5052.0	22.0	7.8	42.1	17.1	0.292	1
M	5071.5-5086.5	15.0	9.2	41.2	16.5	0.285	1
L_2	5112.0-5116.0	4.0	6.9	61.8	22.2	0.019	3
L_1	5130.0-5139.5	9.5	8.3	76.6	11.6	0.080	3
K	Missing	-	-	-	-	-	-
J	5293.0-5301.5	8.5	4.7	99.3	5.4	0.008	4
I	5333.0-5343.5	10.5	5.1	53.9	17.9	0.015	4
H_2	5382.5-5390.5	8.0	5.5	70.7	15.0	0.014	4
H_1	5398.0-5404.0	6.0	4.2	77.8	16.8	0.004	4
G	5425.0-5429.5	4.5	5.5	76.6	13.4	0.007	4
F	5478.5-5491.5	13.5	6.0	64.9	9.2	0.039	3
E_2	5525.0-5531.5	7.0	4.5	64.6	12.6	0.009	4
E_1	5544.0-5565.0	21.5	6.0	64.0	5.6	0.072	2,3
D_2	Missing	-	-	-	-	-	-
D_1	5624.5-5635.5	11.5	6.4	60.2	8.3	0.053	2
C_2	5714.5-5737.5	23.5	7.8	63.0	7.8	0.170	1a
C_1	Missing	-	-	-	-	-	-
B	5827.0-5843.0	16.5	7.1	53.8	5.5	0.156	1a
A_2	5957.0-5971.0	14.5	4.8	47.9	10.3	0.044	3
A_1	5977.0-5983.0	7.0	6.2	62.9	10.6	0.049	4

*Zone classification defined in Section 4.5.

Table 1.2 Comparison of Mesaverde Reservoirs

Interval	Reservoir	Approx. Depth (ft)	Reservoir Pressure (ft)	Perf. Net Pay (ft)	Production*		Test Activity	Prefrac Production (MSCFD/ft)
					Prefrac (MSCFD)	Postfrac (MSCFD)		
Fluvial	E sandstone	5550	3100	30	70	240	Stimulation Experiment	2.3
	C sandstone	5725	3300	22	50	--	Unpropped Minifracs	2.3
	B sandstone	5825	3400	17	25	35	Stimulation Experiment	1.5
Coastal	Yellow sandstone	6450	4400	32	60	100	Stimulation Experiment	1.9
	Red sandstone	6525	4400	39	50	--	Interference Test	1.3
Paludal	Zones 3 and 4	7100	5300	48	250	170**	Stimulation Experiment	5.2
	Zone 2	7250	5400	28	160	--	Single Well Test	5.7
Marine	Upper Cozzette	7850	6300	37	550	--	Interference Test	15.0
	Lower Cozzette	7975	6400	14	>150	--	Single Well Test	>10.7
	Corcoren	8150	6600	65	>450	--	Single Well Test	>6.9

*Generally after 10 days production. Actual time may vary, but data reflect relative production.
**Increased to 400 MSCFD upon reentry after extended shut-in.

Table 1.3

Gas-in-Place in the Mesaverde at MWX
Using MWX Data

Interval	Reservoir	Each Lens (BCF/mile length)	Total Interval* (BCF/Section)
Fluvial	E Sandstone	1.9	54.7
	C Sandstone	1.4	
	B Sandstone	0.6	
Coastal	Yellow	0.5	31.2
	Red	1.1	
Paludal	Zones 3,4	0.6	35.0 (+23 Coals)
	Zone 2	0.7	
Marine	U. Cozzette	15.2	35.2 (+ 3 Coals)
	L. Cozzette	10.9	
	Corcoran	7.9	
			156.1 (+26 Coals)

*Based upon all sandstones penetrated and measured properties.

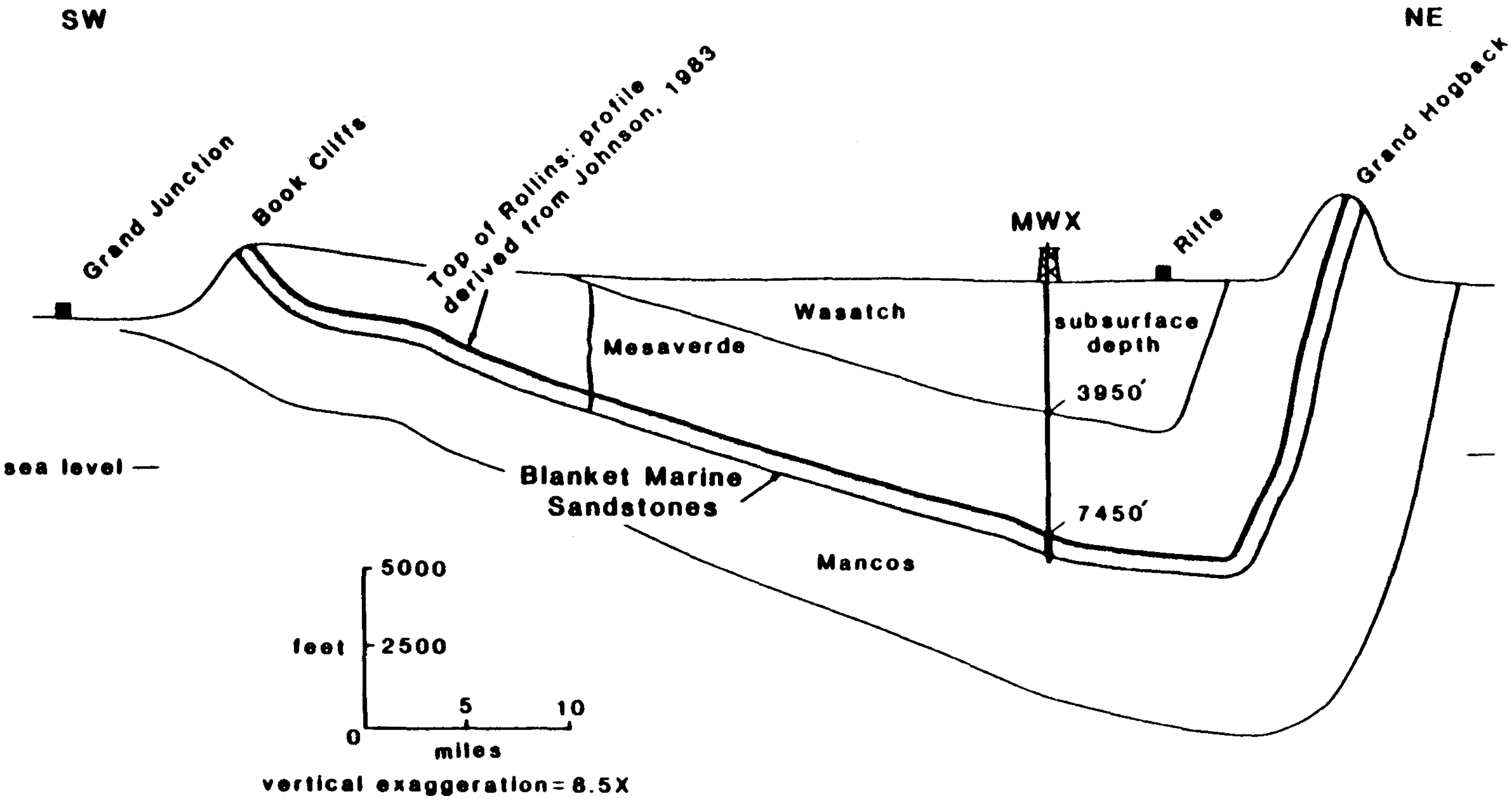

Figure 1.1 General Structure of Mesaverde Formation in Piceance Basin, NW-CO

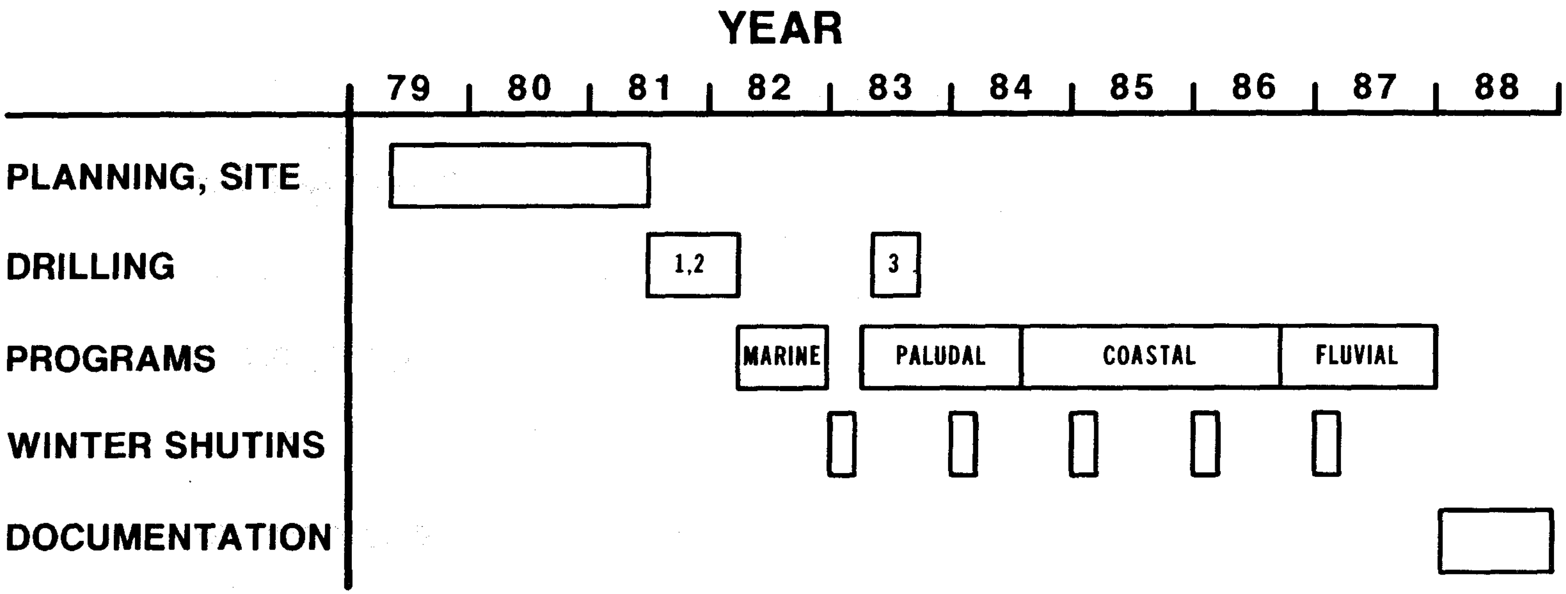

Figure 1.2 Overall Multiwell Experiment Schedule

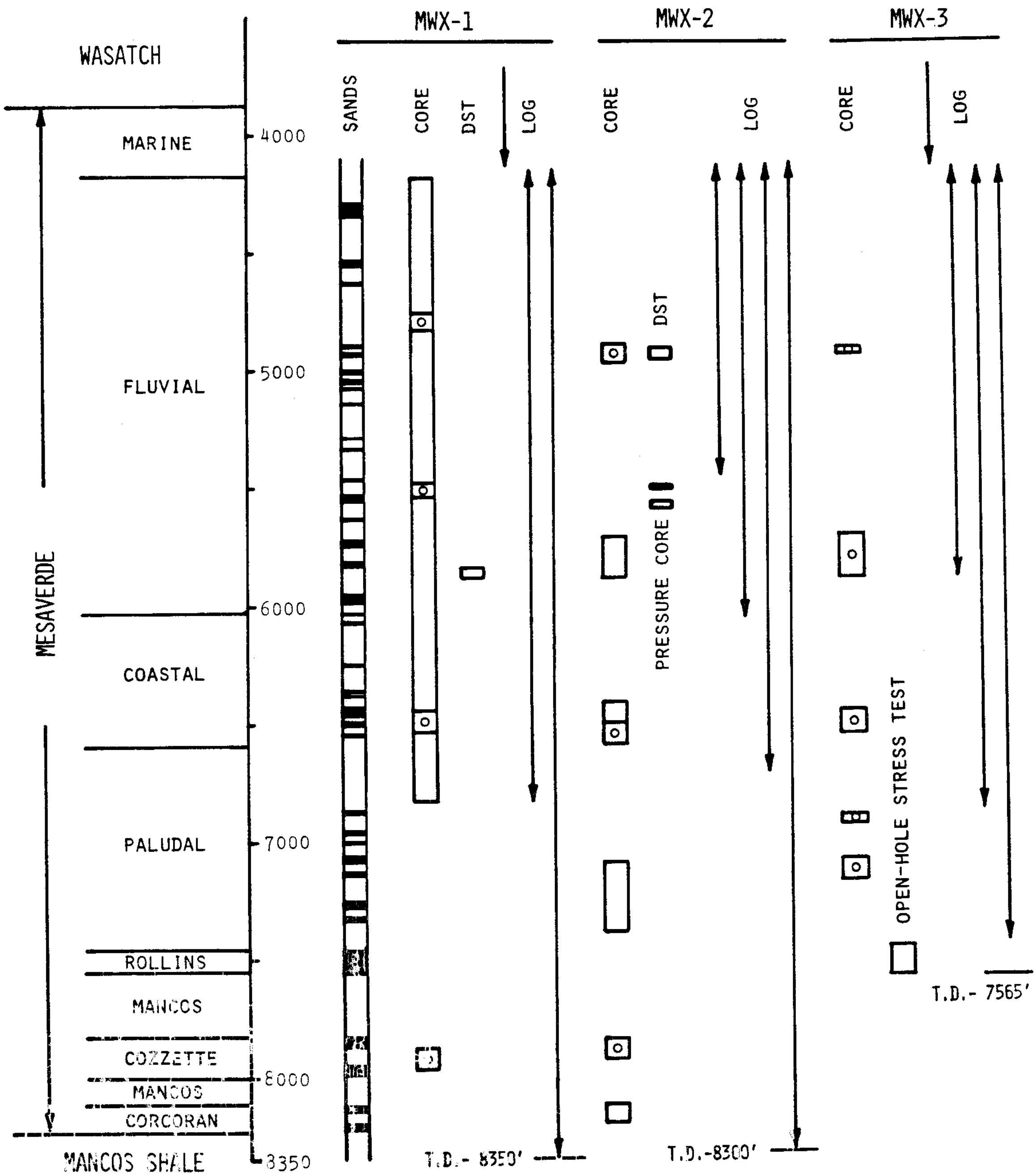

Figure 1.3 Summary of Coring and Logging Programs at MWX

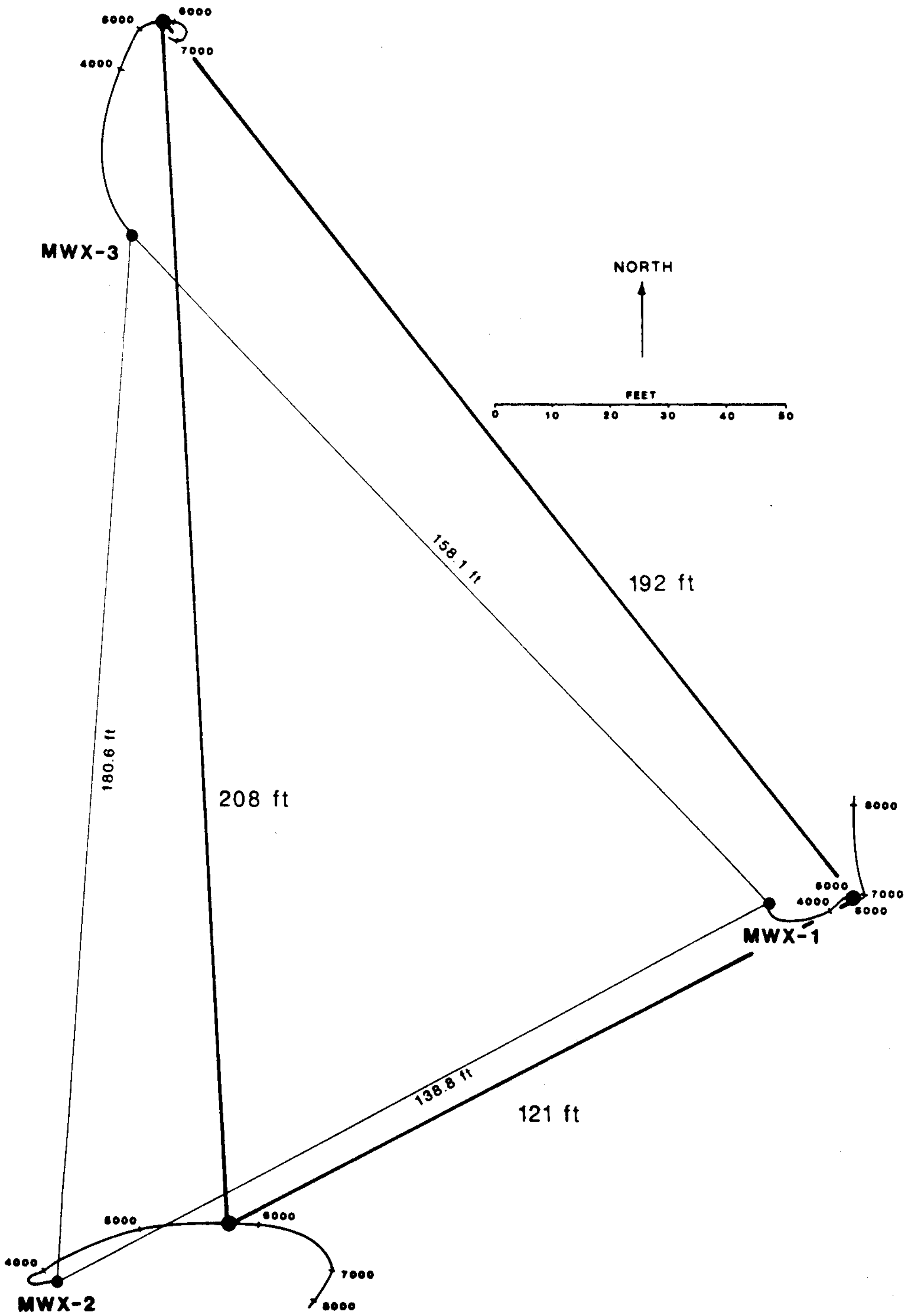

Figure 1.4 Relative Well Spacings at Surface and at 5700 ft

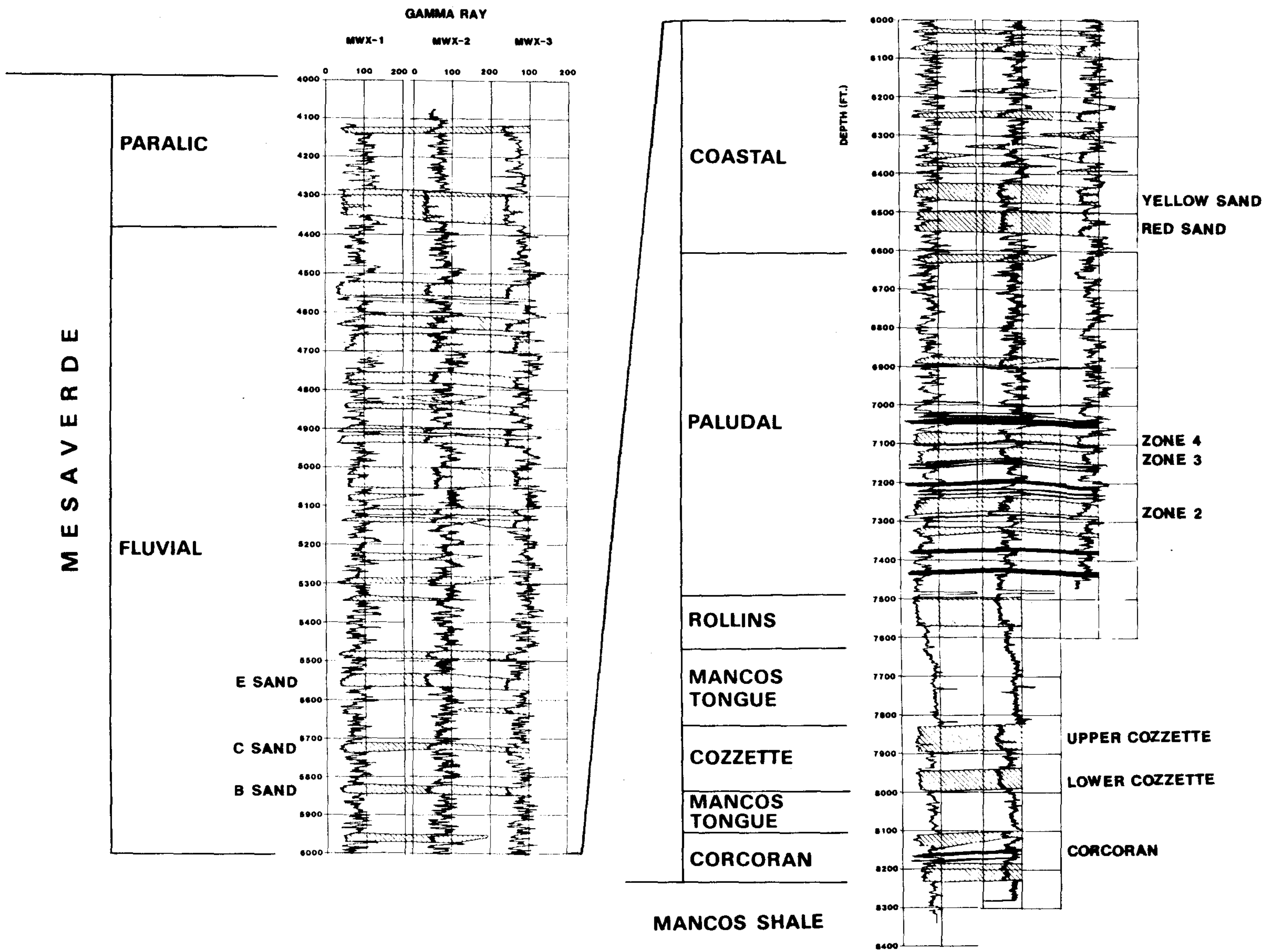

Figure 1.5 Gamma Ray Logs of the Mesaverde in the Three MWX Wells

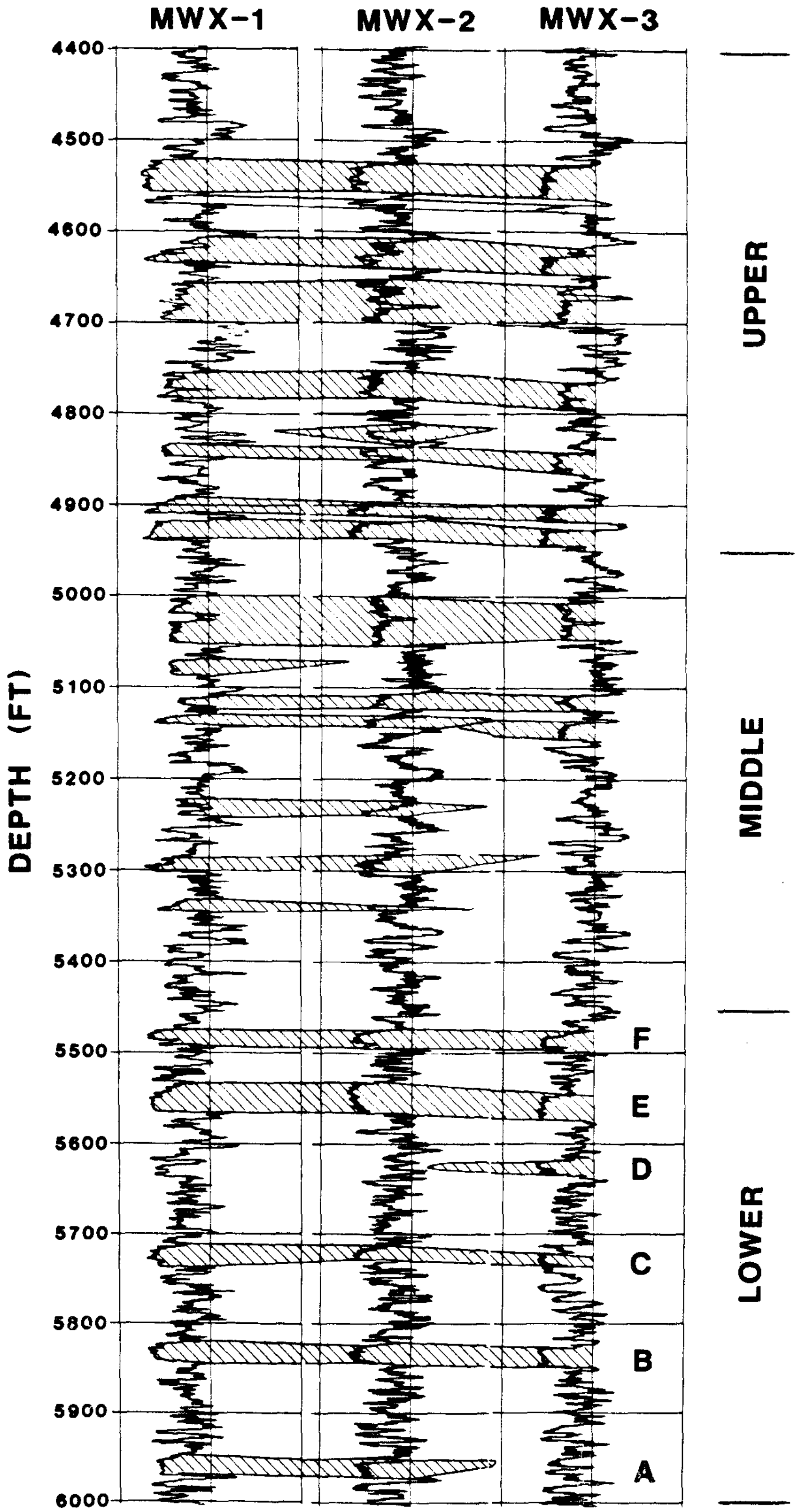

Figure 1.6 Gamma Ray Logs of the Fluvial Interval at MWX

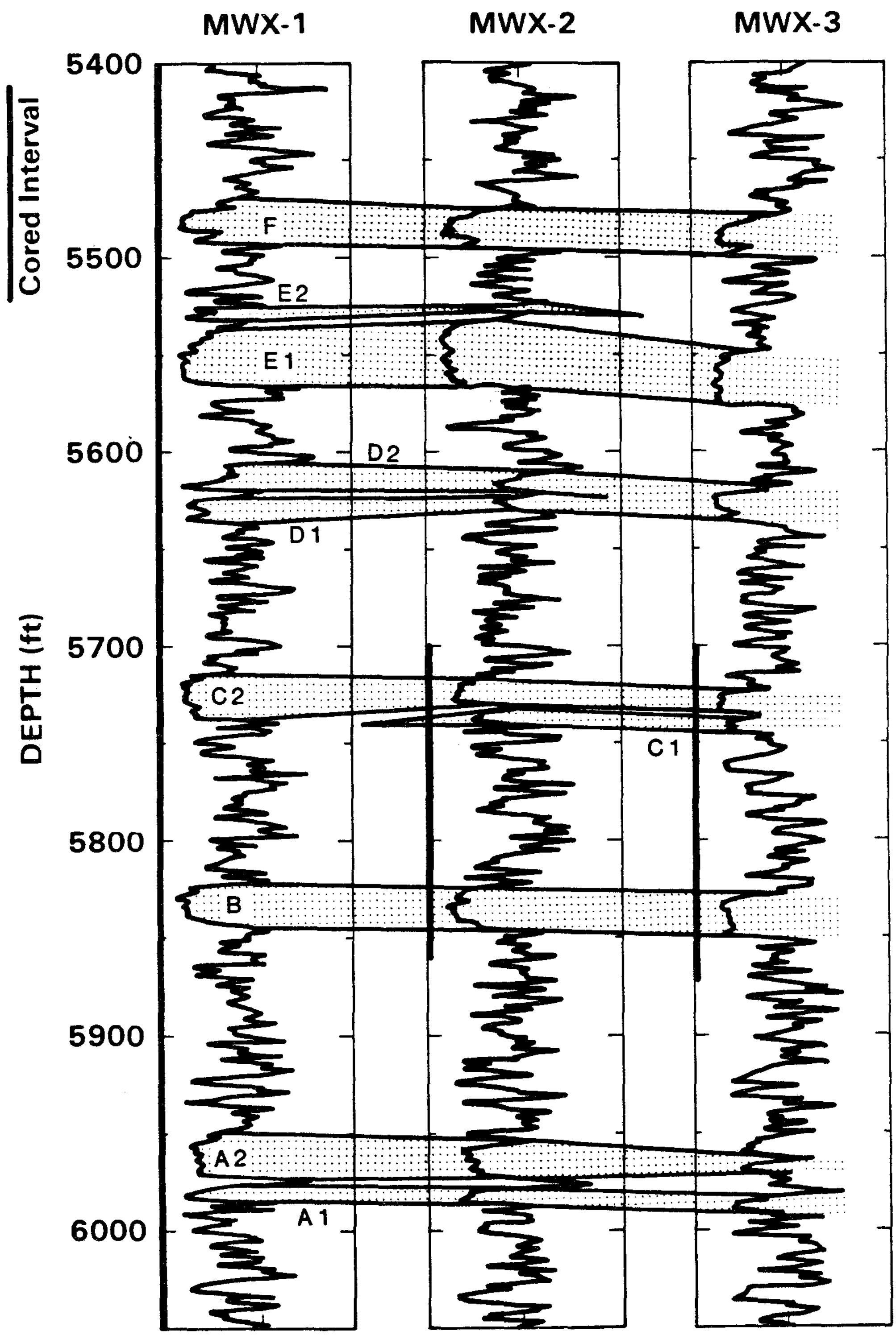

Figure 1.7 The Lower Fluvial Interval

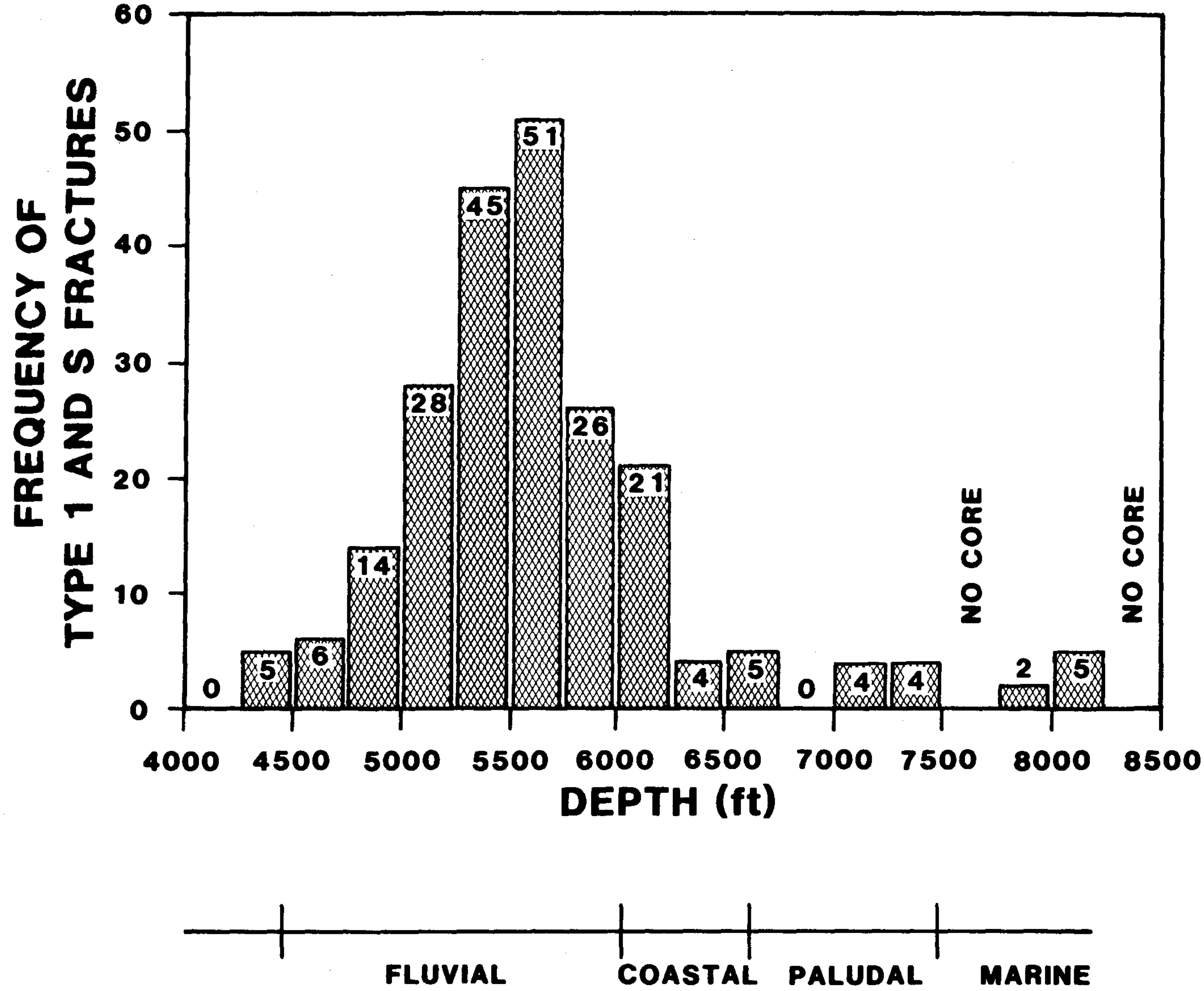

Figure 1.8 Distribution of Mineralized, Extension Natural Fractures at MWX

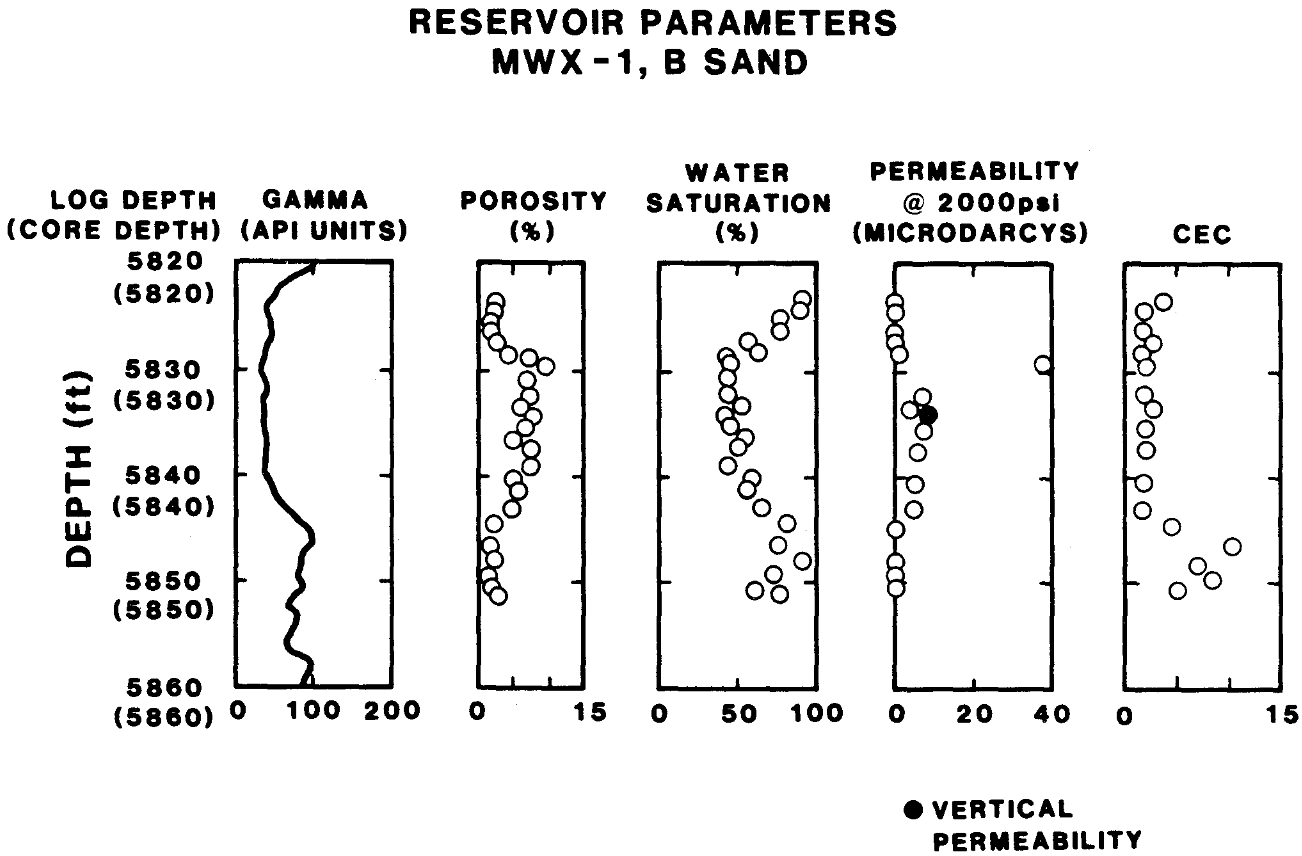

Figure 1.9 Typical Fluvial Matrix Reservoir Properties

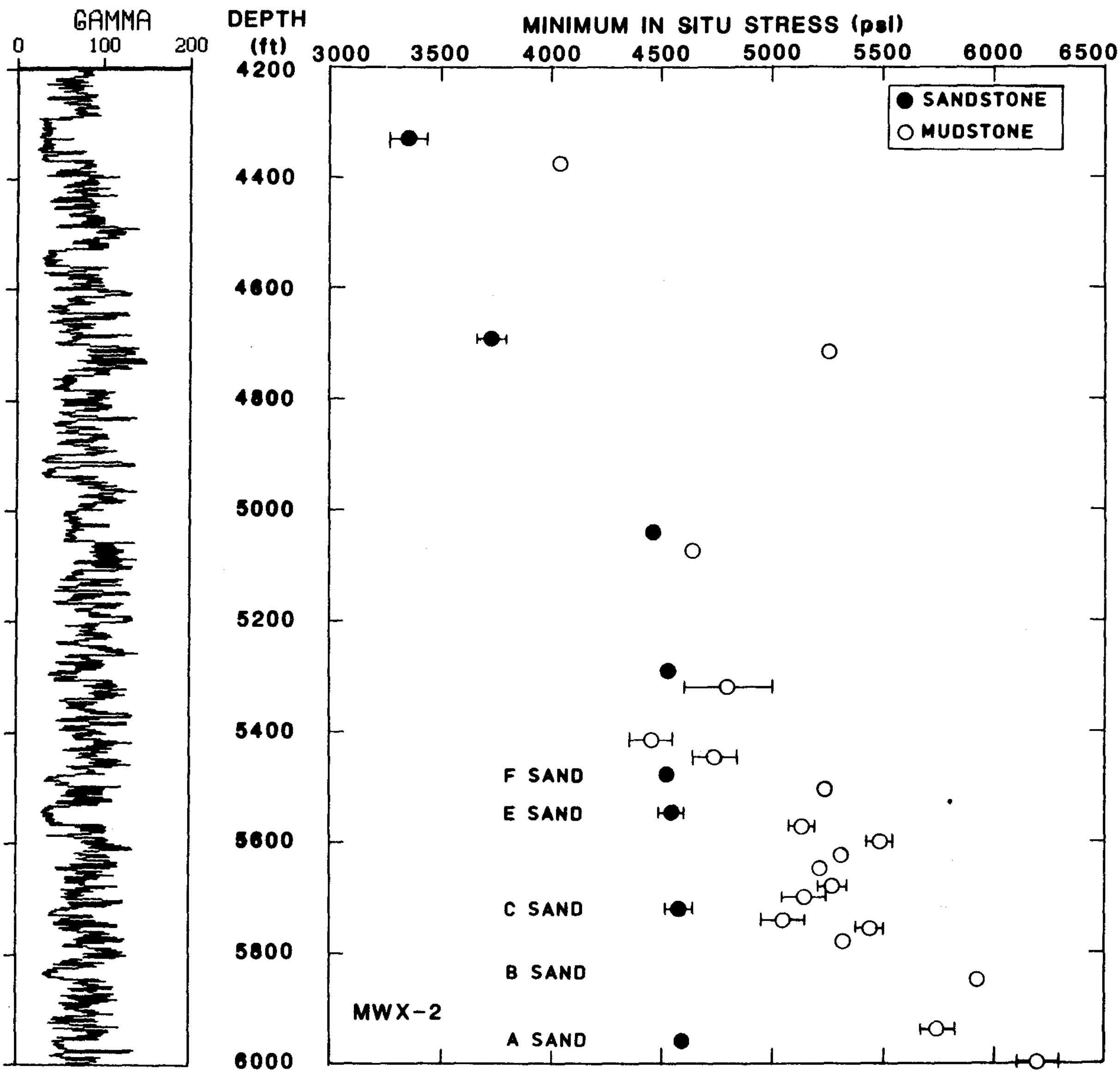

Figure 1.10 Fluvial Stress Test Results

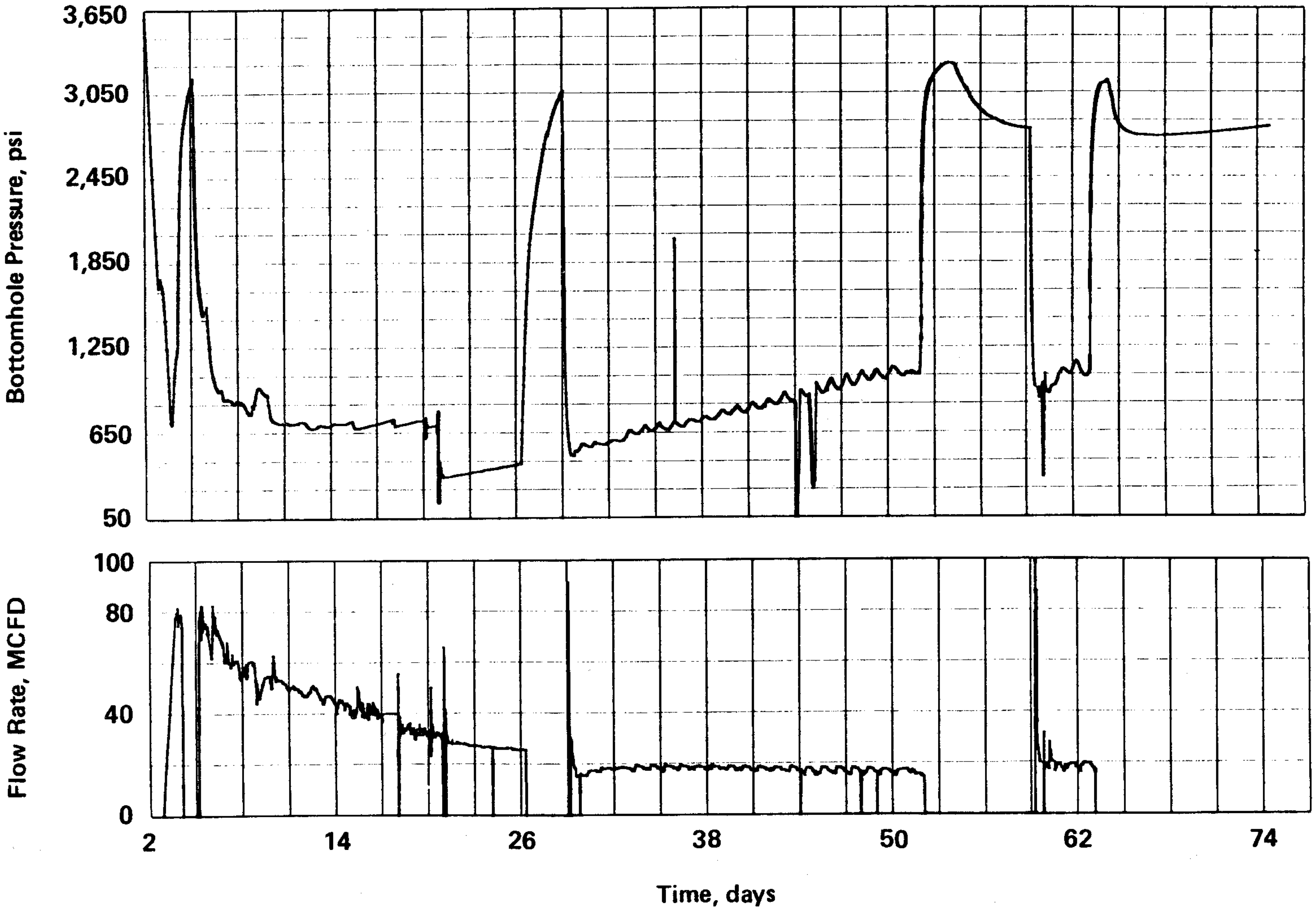

Figure 1.11 Prefac Wall Test Period, B Sandstone

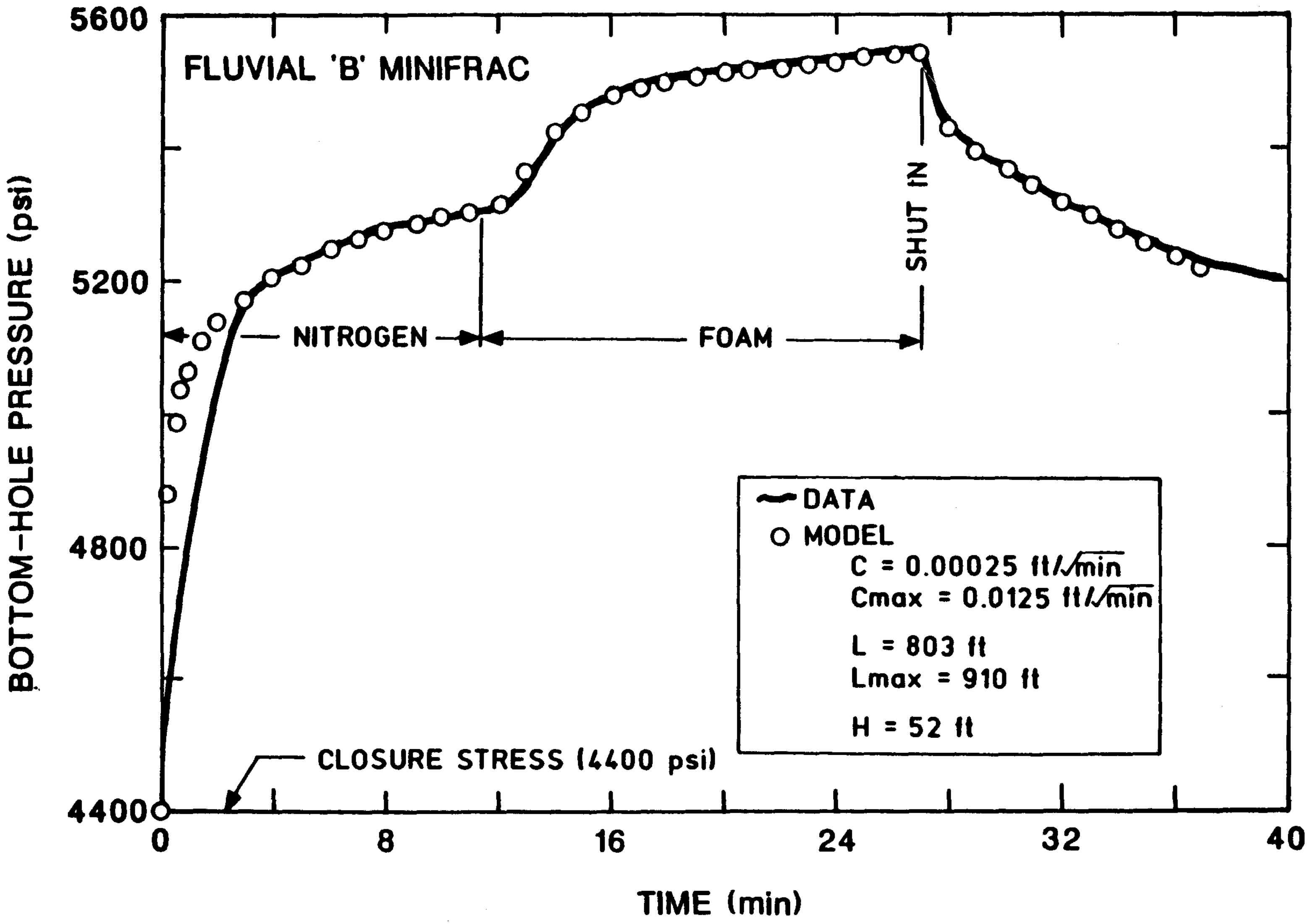

Figure 1.12 Minifrac and Pressure History Match, B Sandstone

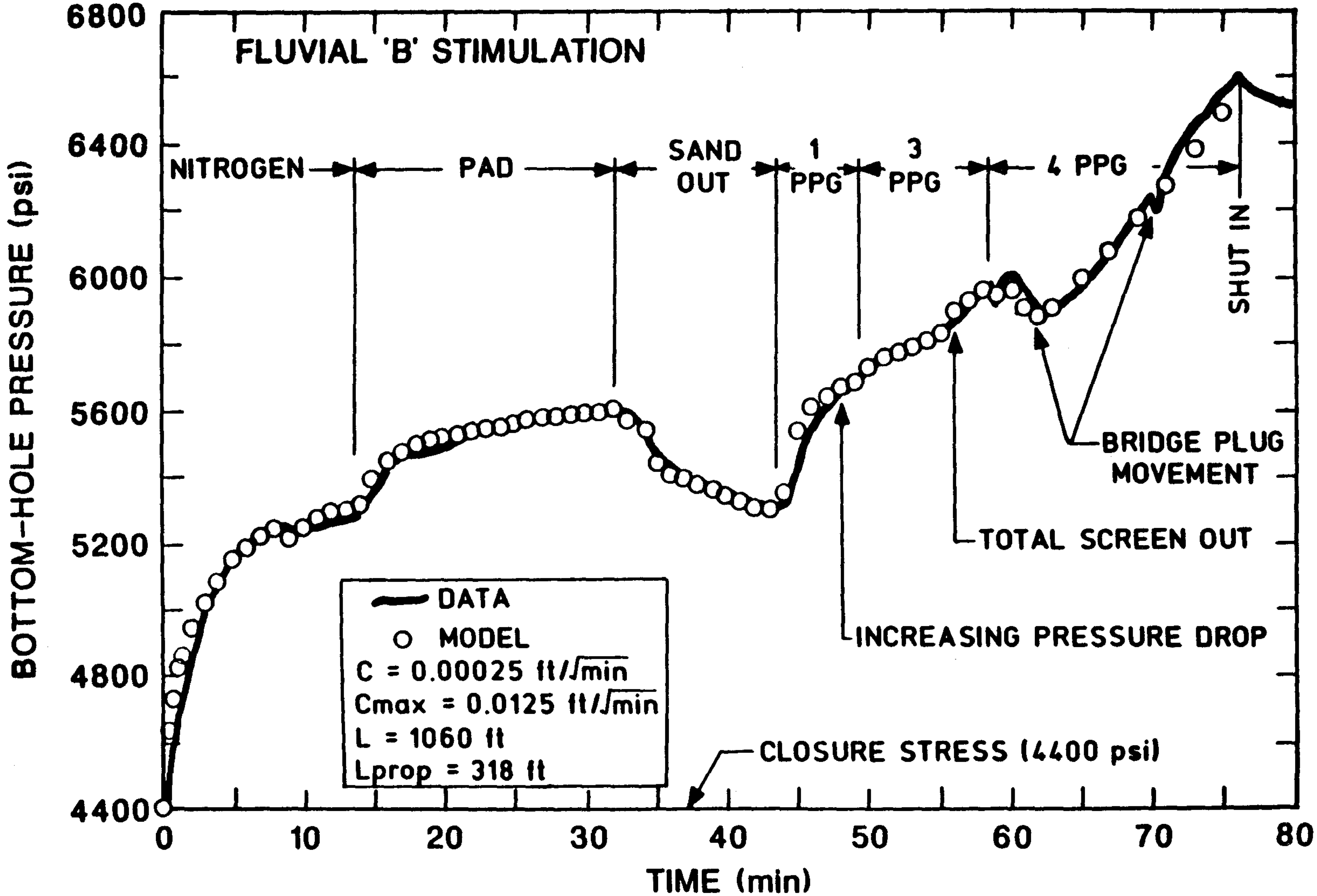

Figure 1.13 Stimulation and Pressure History Match, B Sandstone

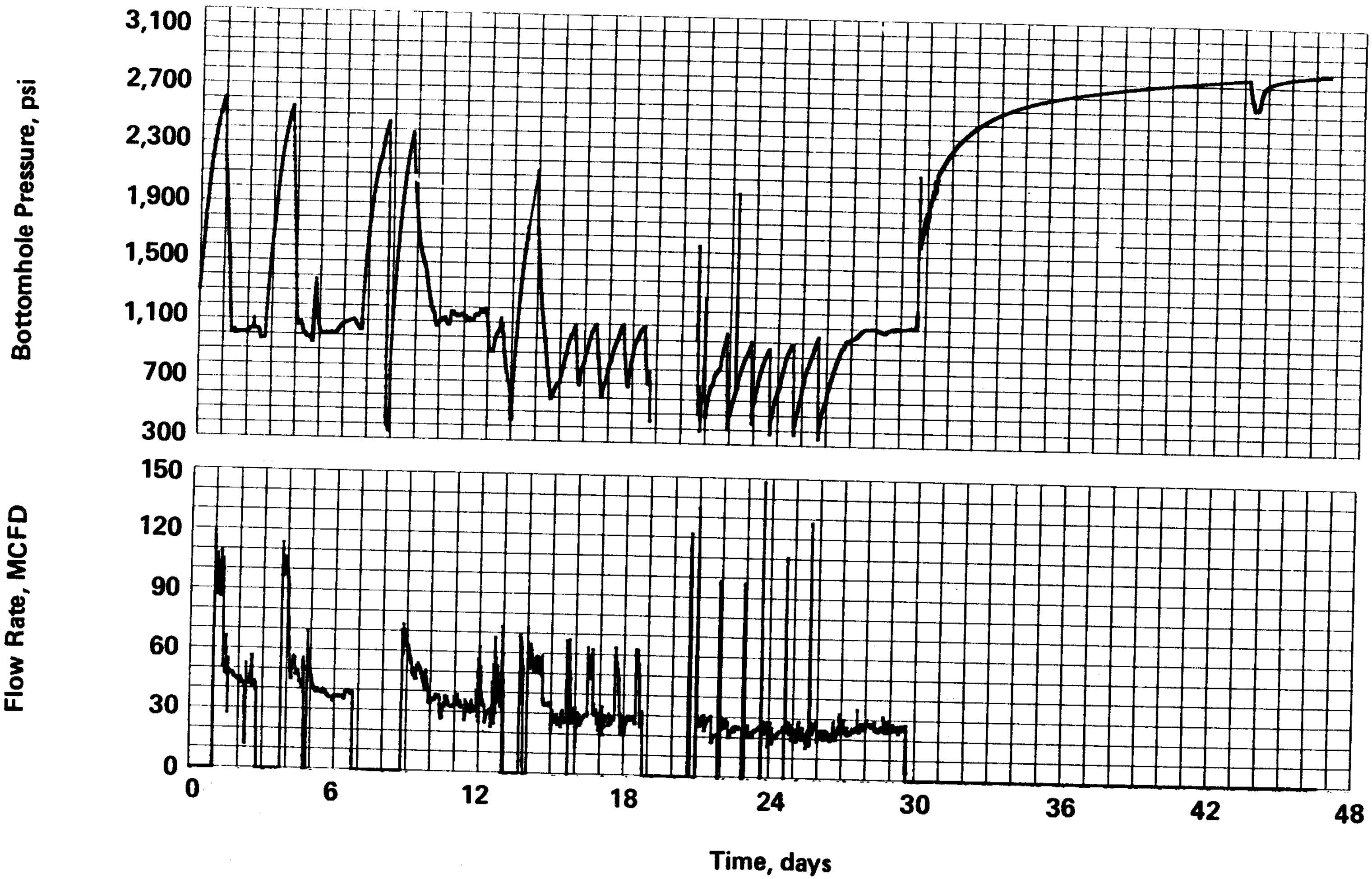

Figure 1.14 Postfrac Well Test Period, Phase I, B Sandstone

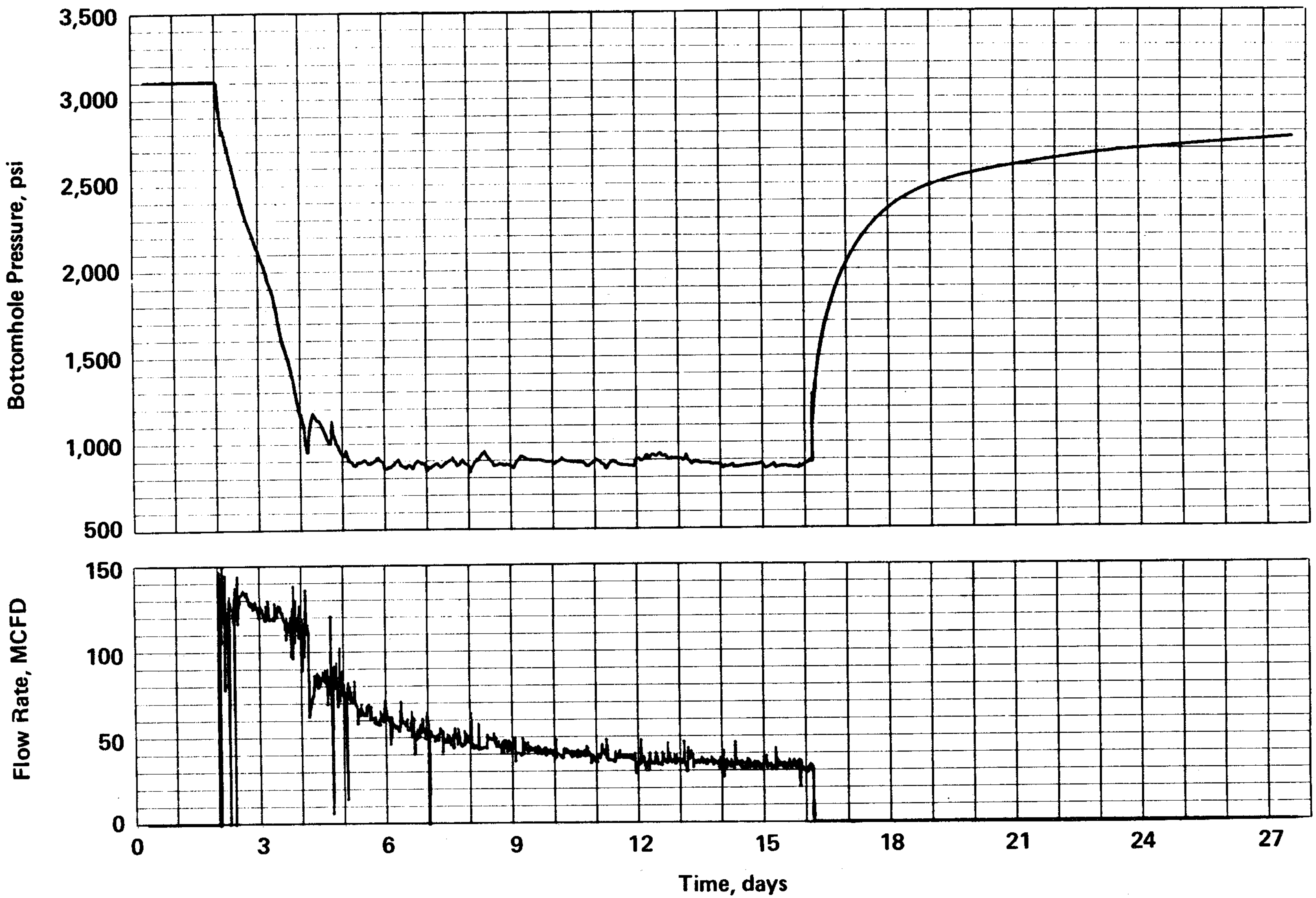

Figure 1.15 Postfrac Well Test Period, Phase II, B Sandstone

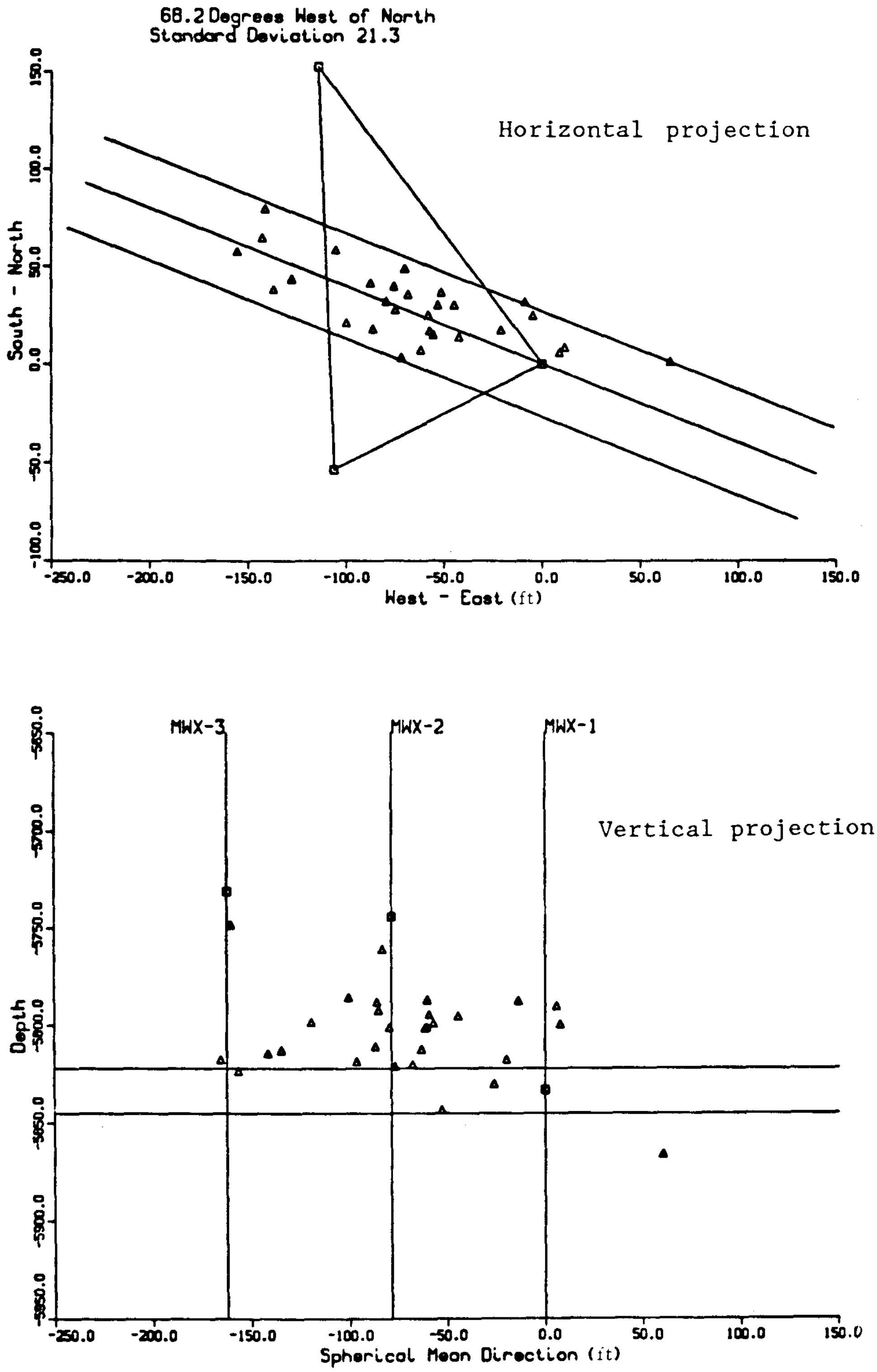

Figure 1.16 Borehole Seismic Fracture Map, B Sandstone

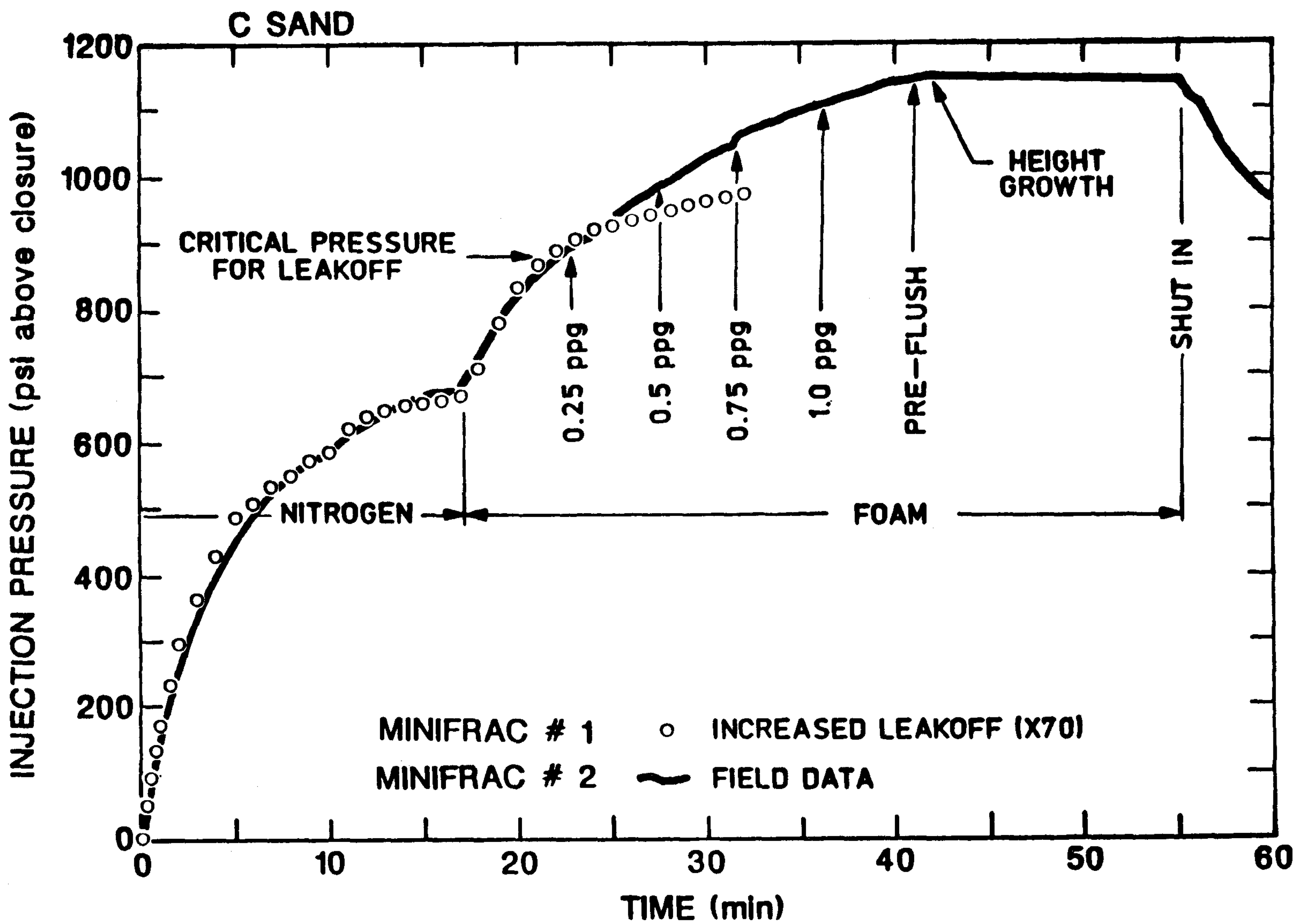

Figure 1.17 Comparison of Two Minifracs, C Sandstone

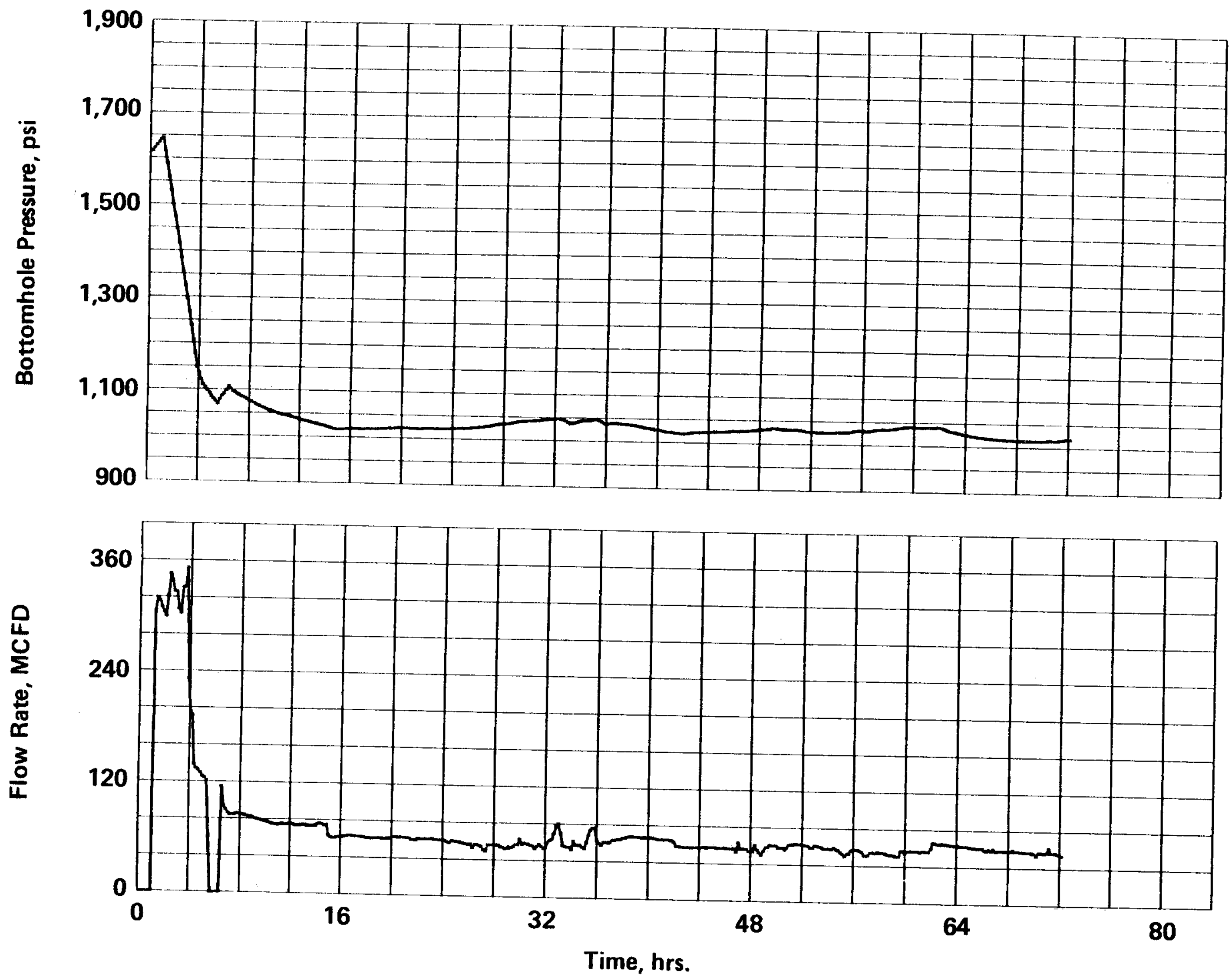

Figure 1.18 Flow Period, C Sandstone

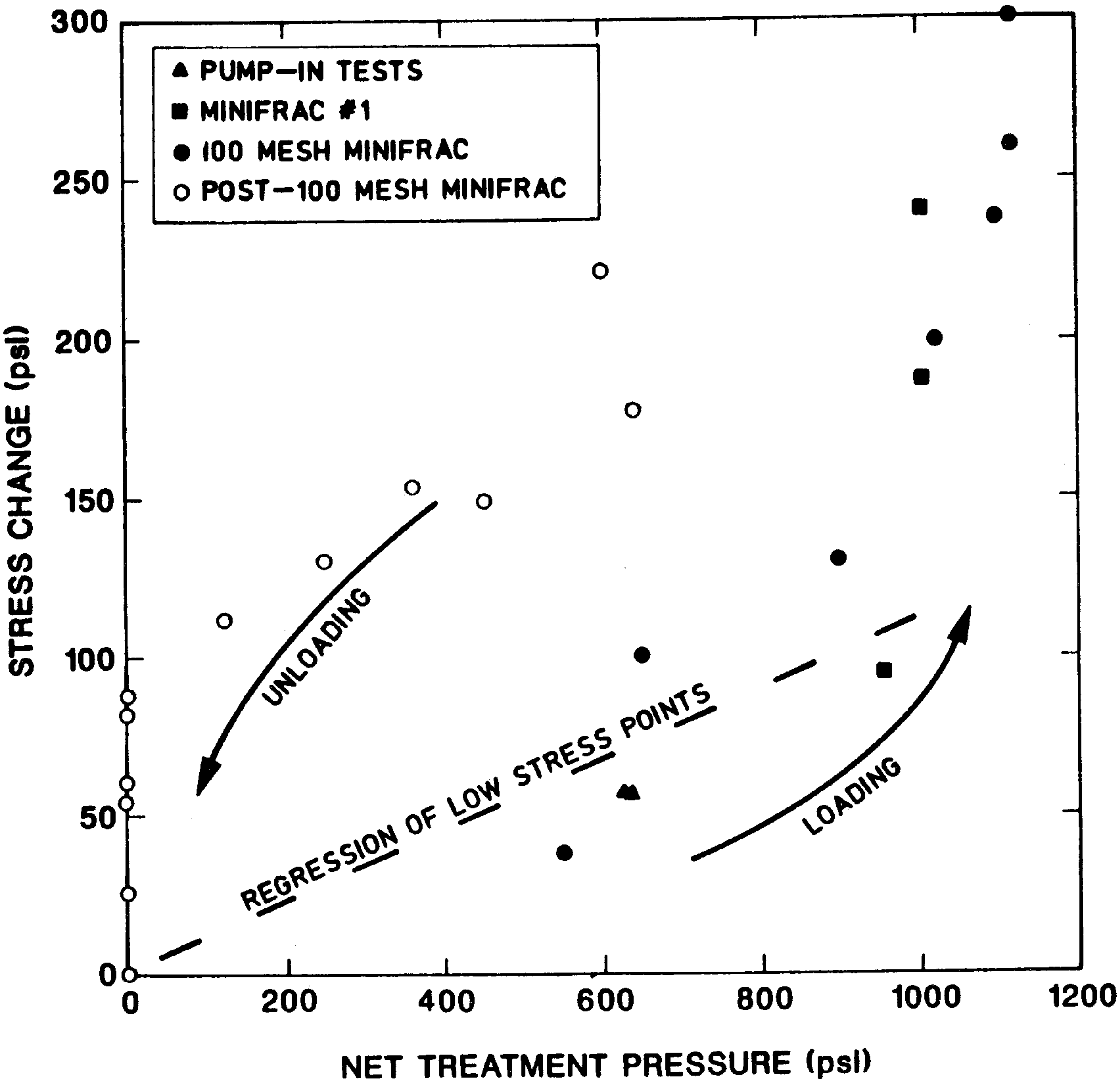

Figure 1.19 Stress Change at MWX-2, Altered Stress Concept, C Sandstone

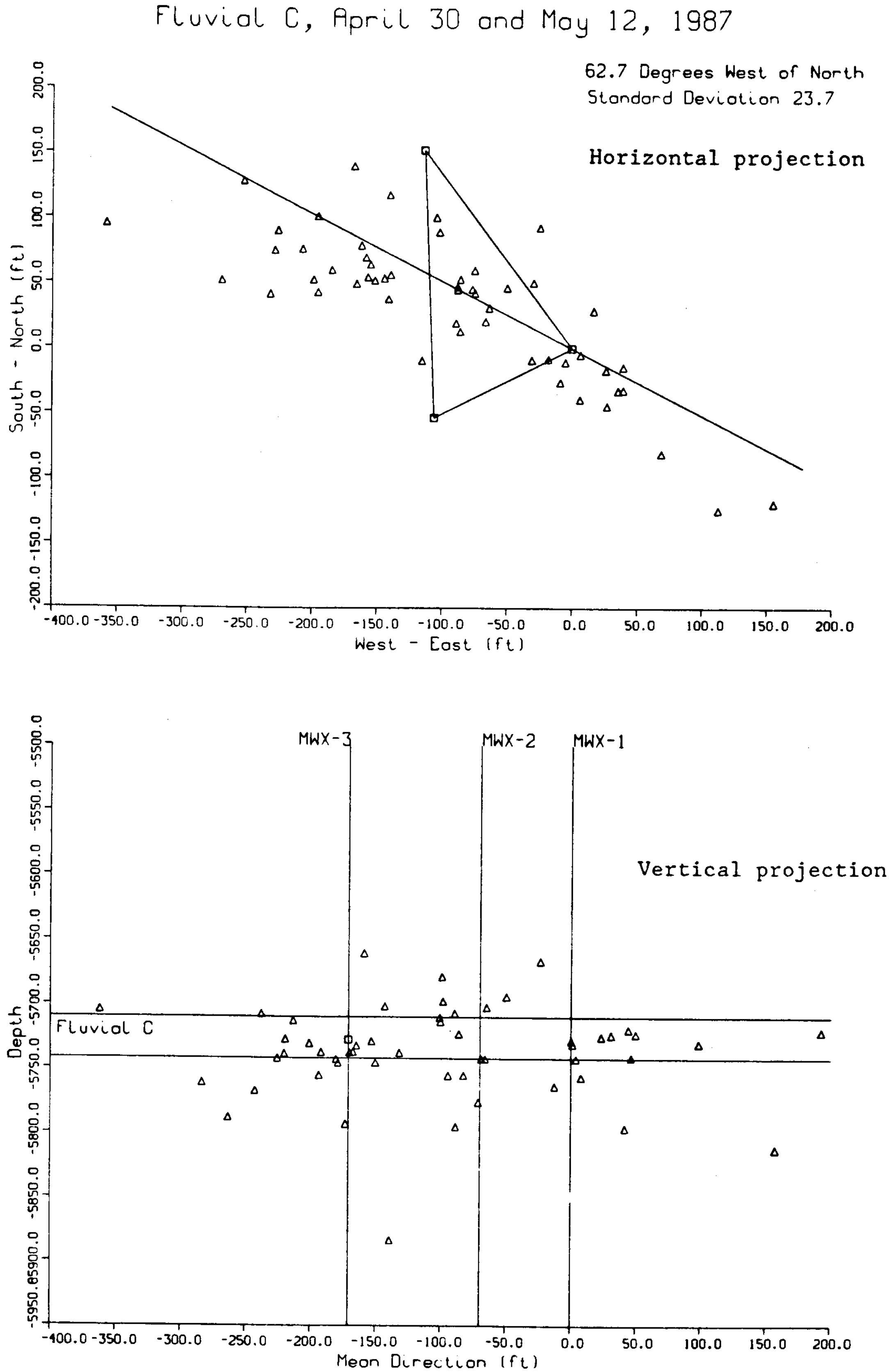

Figure 1.20 Borehole Seismic Fracture Map, C Sandstone

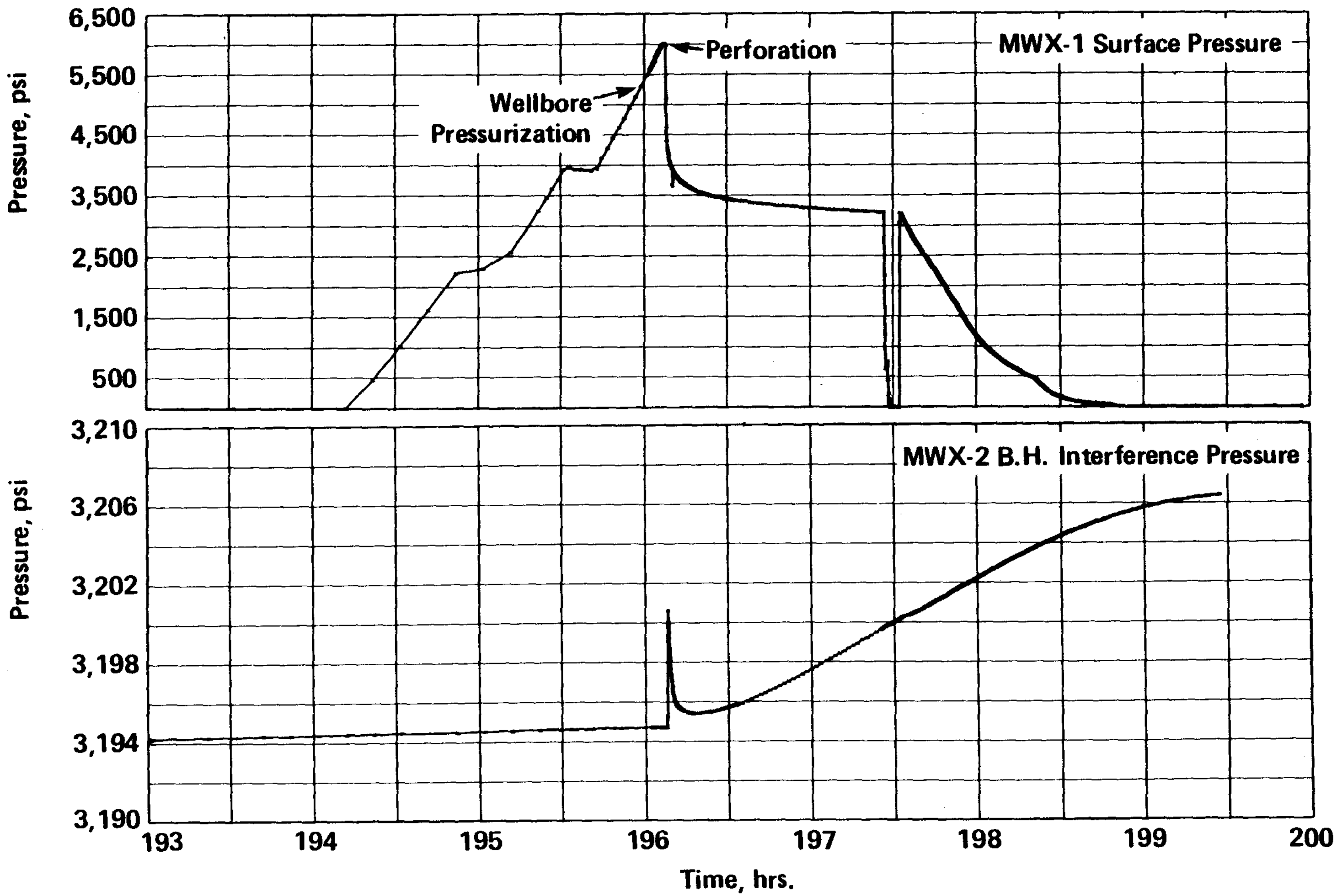

Figure 1.21 Nitrogen Impulse Fracturing and Interference, E Sandstone

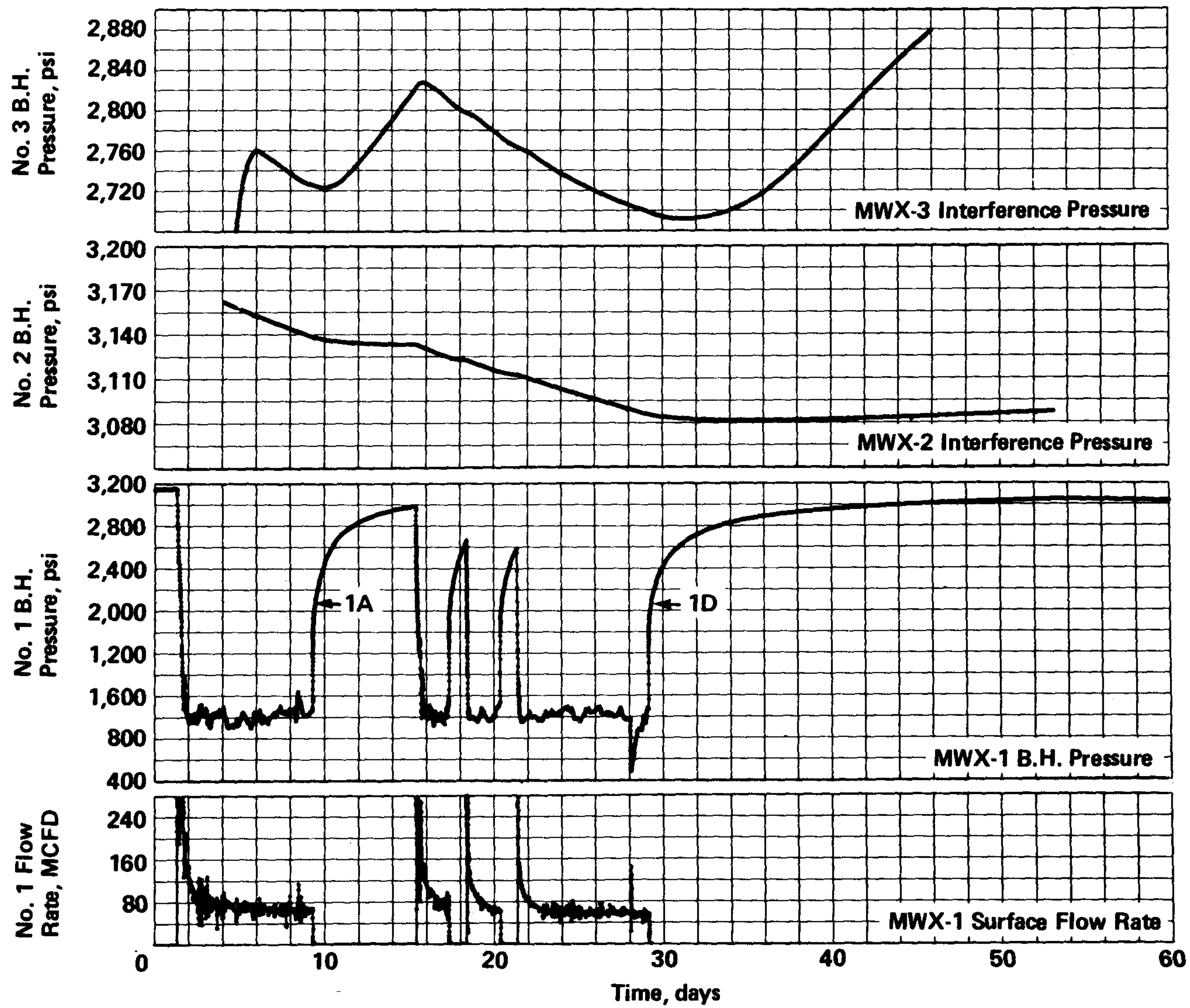

Figure 1.22 Prefac Well Test Period, E Sandstone

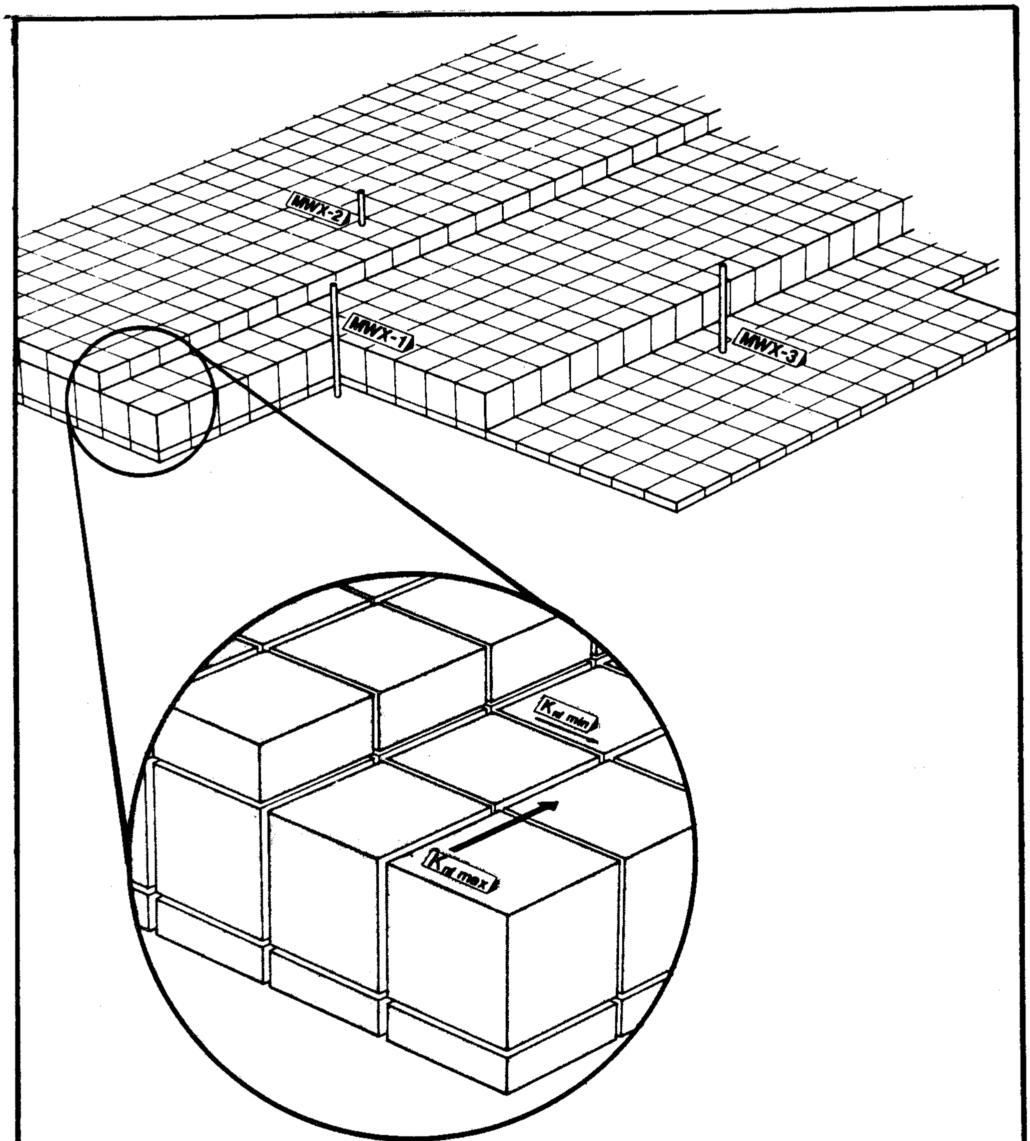

	Layer 1	Layer 2	Layer 3
k_{fmax}	165 darcy	33 darcy	80 darcy
k_{fmin}	5.5 darcy	1.1 darcy	80 darcy
w_f	0.0003 in.	0.0003 in.	0.0003 in.
ϕ_f	50%	50%	50%
k_{matrix}	2 μd	2 μd	2 μd
Spacing	20 ft	20 ft	20 ft
ϕ_m	2.4%	2.4%	2.4%
height	7 ft	24 ft	1 ft
p_i	3,200 psi	3,200 psi	3,200 psi

Figure 1.23 Three-Layer Reservoir Model Derived for E Sandstone

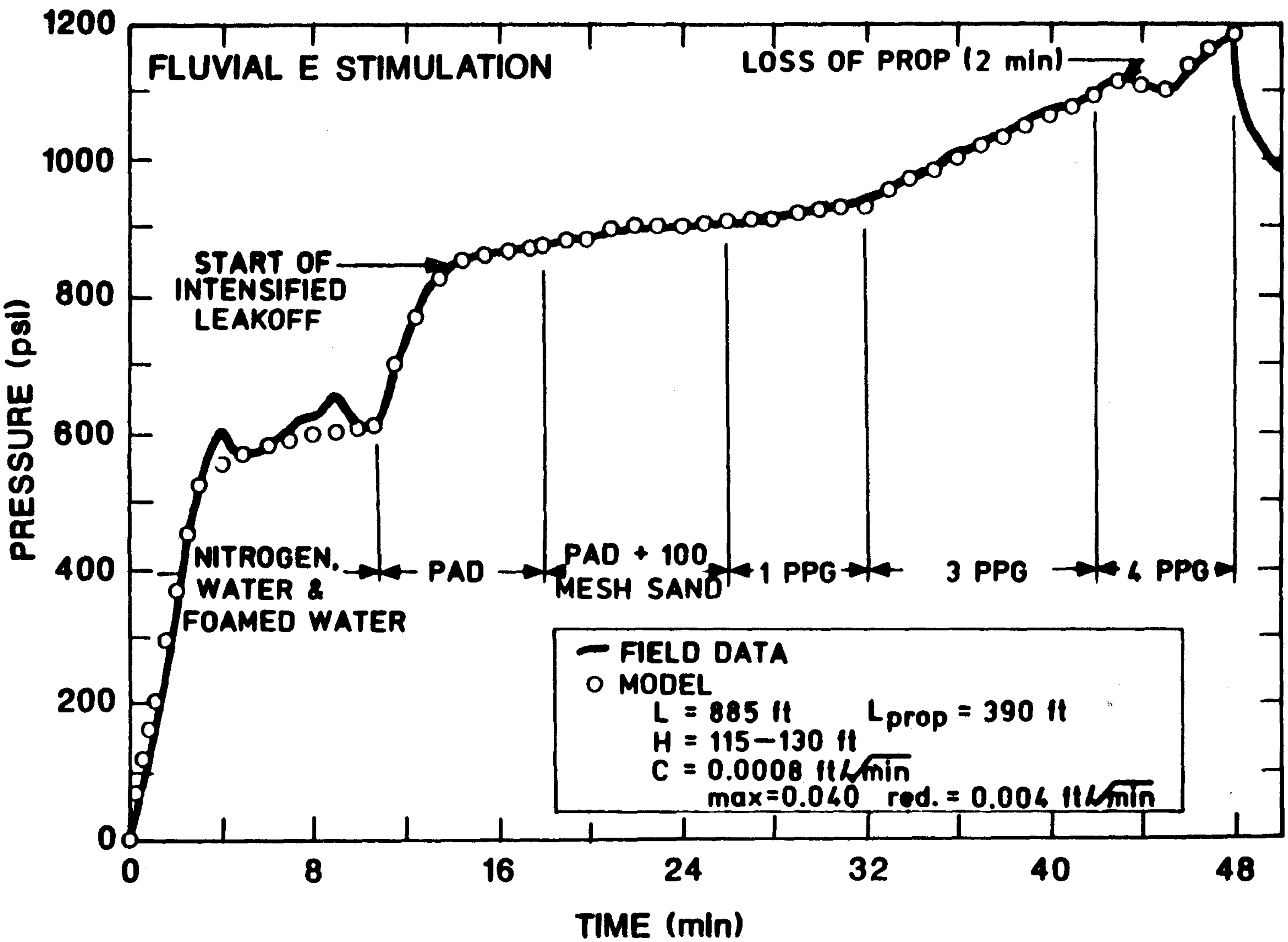

Figure 1.24 Stimulation and Pressure History Match, E Sandstone

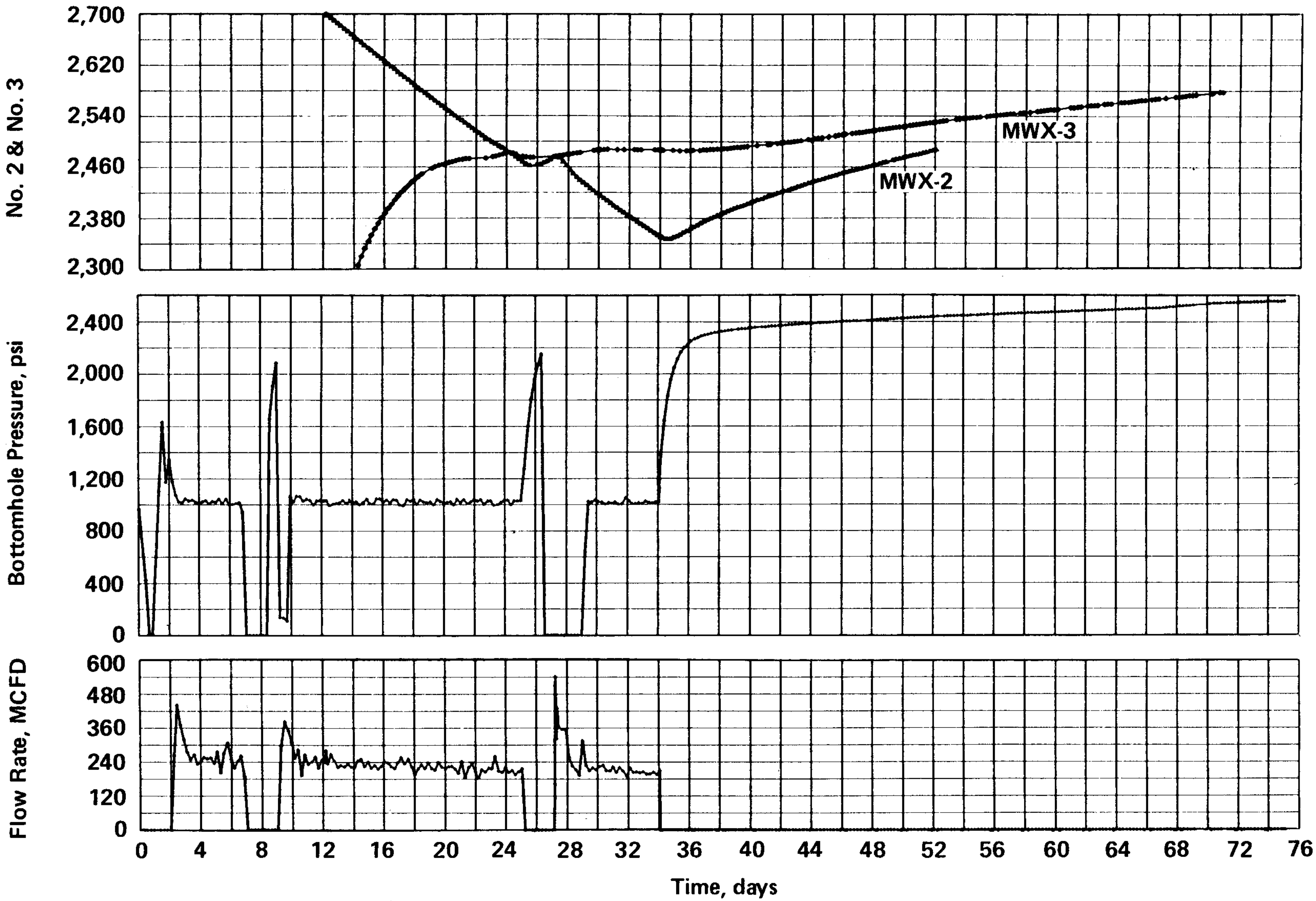

Figure 1.25 Postfrac Well Test Period, E Sandstone

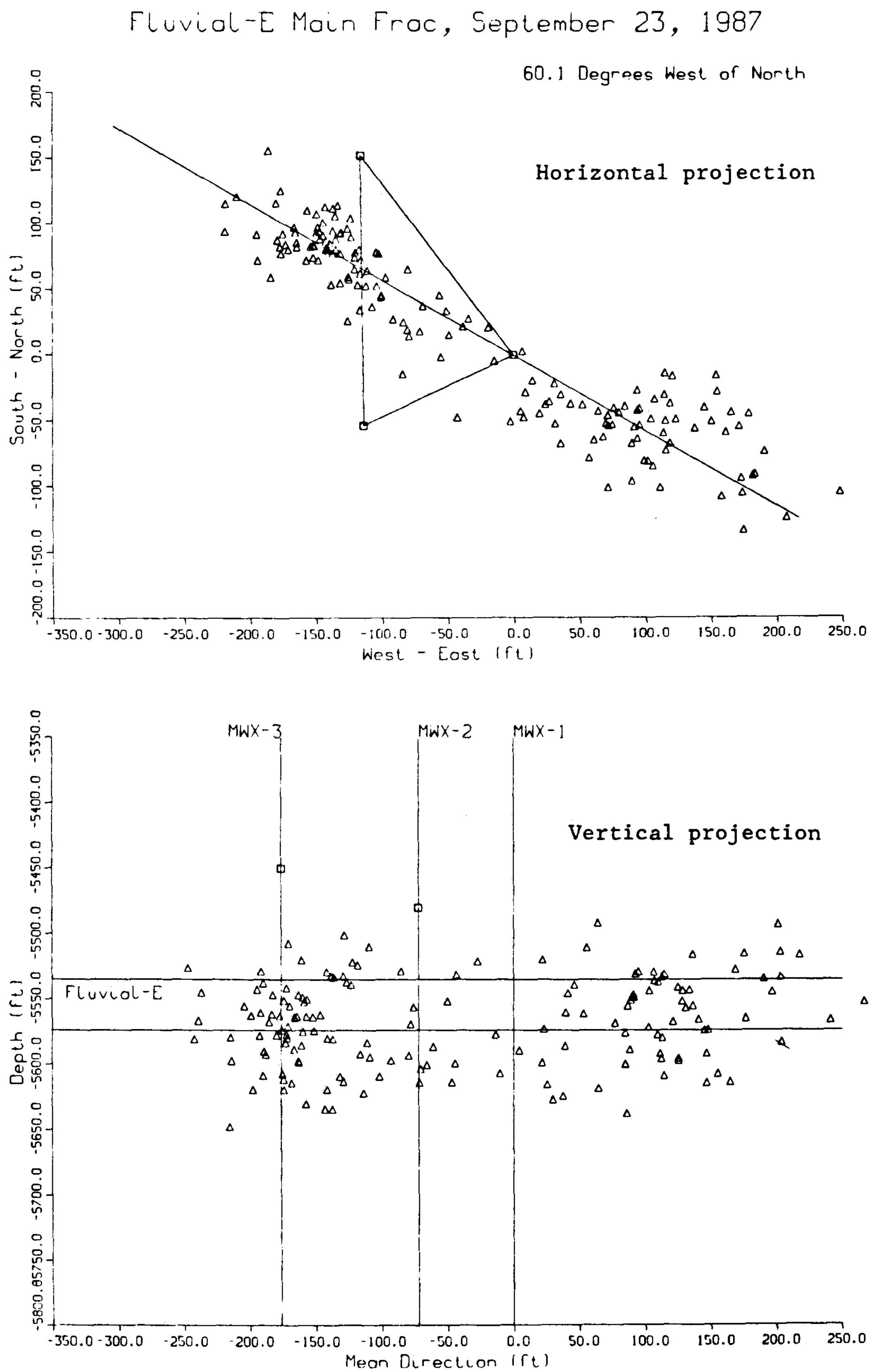

Figure 1.26 Borehole Seismic Fracture Map, E Sandstone

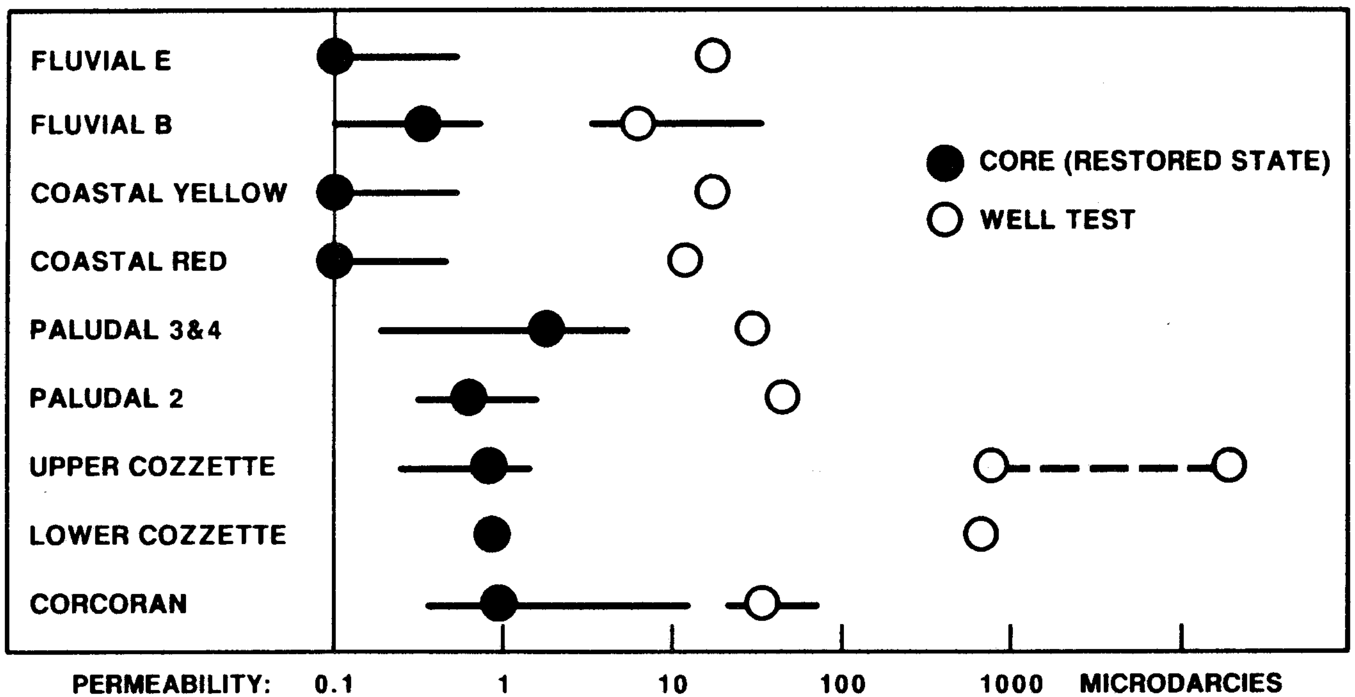

Figure 1.27 Matrix vs. Reservoir Permeabilities; Effect of Natural Fractures

2.0 SITE DESCRIPTION AND OPERATIONS

F. Richard Myal
CER Corporation

2.1 WELL DRILLING AND WELL DESCRIPTIONS

As shown in Figure 2.1, the Multiwell Experiment (MWX) is located in the Rulison Field in the southeastern portion of the Piceance Basin in Colorado. The site is located in the SW1/4 NW1/4 Section 34, T6S, R94W, Garfield County, and is about 7 miles southwest of Rifle.

An agreement was reached with Superior Oil Company in mid-1981, and all necessary drilling and operating permits were acquired. Drilling of MWX-1 began in mid-September 1981, achieving total depth at 8350 ft. The well was drilled through the blanket marine Mesaverde sections and 7-in., 29-lb/ft N80 casing was run and cemented. As shown in Figure 2.2, a total of 2747 ft of the Mesaverde group was cored and recovered, including 470 ft of oriented core.

The rig was moved to the adjoining location and the second well was spudded on December 31, 1981. MWX-2 was also drilled through the blanket marine Mesaverde to a depth of 8300 ft with 915 ft of formation cored and recovered, as shown in Figure 2.3. The MWX-2 casing program was similar to the first well. The casing was run and cemented and the rig released on March 30, 1982.

The third well, MWX-3, was spudded on June 7, 1983, and was drilled to a depth of 7564 ft. As shown in Figure 2.4, it penetrated the Rollins Formation but not the Corcoran/Cozzette. "As-built" reports were published on all three wells. An approximate geologic section and the formation tops in MWX-1 are shown in Figure 2.5.

During the drilling of the three MWX wells, it was noted that a gradual increase of formation pressure was encountered starting at approximately

5600 ft. Mud weight had to be continually increased with depth from 9.0 lb/gal at 5600 ft to over 15.0 lb/gal at 8350 ft, as shown in Figure 2.6. The Cozzette required a pressure gradient of 0.71 psi/ft and the Corcoran 0.75 psi/ft to control the formation pressure during drilling. From these data and subsequent test data, it is apparent that the lower formations in the Mesaverde Group are substantially overpressured.

Detailed directional surveys were also run in the wells to determine the relative well spacing at various depths, as well as at the surface. The wells were drilled with very little directional deviation so the relative spacing with depth does not change significantly. Figure 2.7 shows the relative locations of the three wells at the surface and at 7300 ft.

Complete logging suites were run on all three wells and the logs and analyses for the fluvial interval are given in Section 4.0. A temperature log for MWX-1 is shown in Figure 2.8.

2.2 CHRONOLOGY OF FLUVIAL OPERATIONS

The chronology of events presented is a topical account of all fluvial activities undertaken at the Multiwell Experiment. This section is an abridged version of a detailed operational record given in Appendix A. The chronology is presented graphically in Figure 2.9.

2.2.1 Fluvial B Sandstone Operations

Stress Tests Below The B Sandstone, MWX-2
(May 2-9, 1986)

May 2, a service unit was moved on the well, the wellhead removed, and the BOP's were installed (no tubing is in the well). Dresser Atlas set a bridge plug at 6390 ft to abandon the coastal interval. Dresser then perforated the following five intervals for stress testing below the B sandstone with four 13.5-gram bullet holes per foot (0.47-in. hole diameter):

6006 ft to 6008 ft
5962 ft to 5964 ft
5940 ft to 5942 ft
5896 ft to 5898 ft
5850 ft to 5852 ft

On May 5, a stress test assembly was run in the well on 198 joints of 2-7/8-in. tubing. Communication was established behind pipe with the perforations from 5962 ft to 5964 ft while straddling and attempting to stress test the perforations from 6006 ft to 6008 ft. The next day, questions about the integrity of the trump valve resulted in pulling the stress test assembly. The trump valve seals were found to be leaking and the trump valve was laid down.

May 7 and 8, the stress test assembly was rerun in the well and the remaining three intervals were stress tested, but communication to the annulus occurred in all cases. The next day, the stress test assembly was unseated and lowered three joints, the circulating valve was opened, and Dowell displaced the 3% KCl water from the well with 151,000 SCF of N_2. The stress test assembly was pulled from the well and laid down. Dynajet then set a bridge plug at 5846 ft and tubing was run in the well open-ended, the BOP's were removed, the wellhead was installed, and the service unit was moved off the well.

Perforate, Nitrogen Breakdown and Test the B Sandstone, MWX-1 (June 13-15, 1986)

On June 13, the B sandstone was perforated from 5822 ft to 5845 ft with two 14-gram jet shots per foot (JSPF) (0.36-in. hole diameter). A tubing string, downhole shut-in tool (DHSIN), and packer were run in the well, and the packer was set at 5797 ft. The wellhead was then installed and successfully pressure tested to 7000 psi.

On June 15, a N_2 step-rate test was conducted on the B sandstone. N_2 was pumped down the tubing at a rate of 1000 SCFM for 9 min and 1500 SCFM for 12 min. Pumping was then shut down to allow the bottomhole pressure to drop below closure pressure. N_2 pumping was then resumed at rates of

1000 SCFM for 9 min, 2000 SCFM for 5 min, 4000 SCFM for 5 min, 6000 SCFM for 6 min, 8000 SCFM for 5 min, and then the rate was decreased to 6000 SCFM for 5 min. The HP gauge was seated in the downhole shut-in tool and N_2 pumping was terminated. The maximum treating pressure was 5000 psi, and the total N_2 used was 159,000 SCF. The well then flowed back N_2 for 4-1/2 hrs before natural gas appeared.

Perforate, Nitrogen Breakdown and Test the B Sandstone, MWX-2
(June 3, 1986)

June 3, Dynajet perforated the B sandstone from 5822 ft to 5842 ft with two 14-gram JSPF (0.342-in. hole diameter). A tubing string, DHSIN tool, and packer were run in the well. The tubing tail was landed at 5822 ft and the packer was set at 5786 ft. The BOP's were removed, and the wellhead installed and successfully pressure tested to 7000 psi. The service unit was then moved off the well.

On June 5, efforts to pressure the 2-7/8-in. tubing with N_2 to seat the HP gauge in the DHSIN tool were unsuccessful. On June 6, a service unit was moved on the well, the wellhead was removed, BOP's were installed, the packer was unseated and the downhole assembly was pulled from the well. Chunks of iron were recovered on top of the packer and in-between the packer rubbers. The next day, the bottom 120 ft of casing were brushed and scraped to ensure a clean packer seat. The downhole assembly was then rerun in the well on the 2-7/8-in. tubing. The tubing tail was landed at 5979 ft and the packer was set at 5758 ft. The BOP's were removed, and the wellhead was installed and successfully pressure tested to 7000 psi. The lubricator was then installed.

June 8, the HP gauge was seated downhole and the tubing was successfully pressure tested with N_2 to 1,100 psi. However, once the N_2 pressure in the casing-tubing annulus reached 1,000 psi, the tubing pressure and casing pressure started tracking, indicating a leak around the packer element. After various attempts to set the packer, it was replaced with another type and was finally set at 5786 ft on June 10. The BOP's were removed, the wellhead was installed and successfully pressure tested to 6000 psi, and the service unit was released and moved off the well. The next day, the HP gauge was seated and the tubing was successfully pressure tested with N_2 to 3800 psi. The casing-tubing annulus was also successfully pressured to 3800 psi with N_2.

June 15, a N_2 step-rate test was conducted on the B sandstone. N_2 was pumped down the tubing at a rate of 3000 SCFM for 8 min, 5000 SCFM for 3 min, 7000 SCFM for 5 min, and then the rate was decreased to 5000 SCFM for 5 min. The HP gauge was seated in the downhole shut-in tool and N_2 pumping was terminated. The maximum treating pressure was 4300 psi, and the total N_2 used was 97,000 SCF.

Perforate, Nitrogen Breakdown and Test the B Sandstone, MWX-3
(June 4-15, 1986)

June 4, Dynajet perforated the B sandstone from 5828 ft to 5848 ft with two 19-gram JSPF (0.48-in. hole diameter). A tubing string, DHSIN tool, and packer were run in the well. The tubing tail was landed at 5847 ft and the packer was set at 5809 ft. The BOP's were removed, the wellhead was installed and was successfully pressure tested to 7000 psi. The service unit was then released and moved off the well.

On June 15, a N_2 step-rate test was conducted on the B sandstone. N_2 was pumped down the tubing at a rate of 4000 SCFM for 4 min, increased to 8000 SCFM for 5 min, then decreased to 6000 SCFM for 2 min, and shut down to allow bottomhole pressure to drop below closure pressure. To achieve rapid closure, the well was flowed back at a rate of 100 MCFD to 150 MCFD for 15 minutes. Pumping was then resumed at 6000 SCFM for 10 min, the HP gauge was seated in the DHSIN tool, and N_2 pumping was terminated. The maximum treating pressure was 4050 psi, and the total N_2 used was 128,000 SCF.

Prefrac Interference Testing, B Sandstone, MWX-1 Producer
(June 15-August 28, 1986)

Prefrac interference testing was initiated June 15, with MWX-1 the production well, and MWX-2 and MWX-3 equipped with HP gauges bottomhole to measure pressure interference. MWX-1 was flow tested from June 15 to July 10 through the test separator to the flare pit. The well was then shut in at 8:30 p.m., July 10, for a 3-day pressure buildup. Flow testing was resumed at 2 p.m., July 13, and continued to 3:30 p.m., August 5. The HP gauge was seated in the DHSIN tool with N_2, and a pressure buildup was undertaken and continued from 3:30 p.m., August 5, to 6 p.m., August 12. A second flow period was undertaken from 6 p.m., August 12, to 3 p.m., August 16. A second shut-in was initiated at 3 p.m., August 16, and terminated at 1 p.m., August 28.

Argon Injection Test, B Sandstone, MWX-2 Injector
(July 30, 1986)

July 30, an argon injection experiment was performed in the B sandstone in MWX-2 in an attempt to establish that communication existed between MWX-1, MWX-2, and MWX-3. Argon was injected into MWX-2 above fracturing pressure to achieve a reasonable injection rate and volume. MWX-1 and MWX-3 were flowed during the injection into MWX-2, and the produced gas was monitored with a gas chromatograph for argon content. Dowell pumped approximately 253,700 SCF of argon into MWX-2 at rates varying from 750 SCFM to 3500 SCFM. The maximum injection pressure was 4350 psi, the minimum injection pressure was 3000 psi, and the final injection pressure was 4000 psi. Chromatographic monitoring of the gas produced from MWX-3 was terminated at 7:30 a.m., August 2, while monitoring of the gas produced from MWX-1 continued until 3:30 p.m., August 5.

Prepare MWX-1 For Nitrogen Step-Rate/Flow-Back Tests
(August 29-September 2, 1986)

August 29, a service unit was moved on the well, the wellhead was removed, two joints of 2-3/8-in. tubing were pulled, one additional joint of tubing was run in the string, and the packer was reset at 5753 ft, with the tubing tail at 5792 ft. The BOP's were removed, the wellhead was installed and successfully pressure tested to 6500 psi, and the service unit was moved off the well.

Nitrogen Step-Rate/Flow-Back And Pump-In/Flow-Back Tests, MWX-1 (September 3-5, 1986)

On September 3, Dowell arrived on location with the necessary pumping equipment, the treatment monitor vehicle (TMV), and N_2 and proceeded to install all injection lines, meters, electronic equipment and supporting gear. The next day, all the flow meters and lines were successfully pressure tested to 6000 psi. The tubing was loaded with 30 BBL of 3% KCl water. Ninety-two ball sealers were dropped over a period of 46 min (10 every 2 min). The ball sealers were followed with N_2 down the tubing at rates of 3000 to 5000 SCFM at pressures from 2950 psi to 4600 psi. No ball action was observed. N_2 injection was initiated at 1000 to 3000 SCFM at pressures to 4200 psi for testing prior to the actual step-rate/flow-back tests.

The N_2 step-rate test was conducted at rates ranging from 800 SCFM at 3200 psi to 10,000 SCFM at 5700 psi, in eight increments. A N_2 volume of 198,000 SCF was used during the step-rate test. An additional 120,000 SCF of N_2 was pumped at 10,000 SCFM and at pressures from 3800 psi to 5650 psi during the N_2 pump-in test. On September 5, Dowell injected 165,500 SCF of N_2 down the tubing at 10,000 to 11,000 SCFM at pressures from 3500 to 5300 psi. The MAG meter did not work properly during the N_2 pump-in test and the decision was made to cancel the N_2 foam injection for perforation breakdown.

KCl Water Breakdown, B Sandstone, MWX-1 (September 5, 1986)

On September 5, the B sandstone perforations were broken down with 52 BBL of 3% KCl water injected down 2-3/8-in. tubing at 5 BPM at 3500 to 6500 psi. The HP gauge was pumped off the end of the wireline and seated in the DHSIN tool while attempting to shut in the well downhole following perforation breakdown.

Prepare MWX-3 For Sandia Borehole Seismic Activities (September 6 and 19, 1986)

On September 6, a service unit was moved on the well, the wellhead removed, BOP's installed, the packer was released, and the packer and 2-7/8-in. tubing was pulled from the well and laid down. Dynajet then set a retrievable bridge plug at 5806 ft to isolate the B sandstone perforations from the remainder of the wellbore. The BOP's were removed, a 7-in. full open valve was installed on the casing, and the service unit was moved off the well.

On September 19, a service unit was moved on the well, the Orbit valve was removed, BOP's were installed, and a retrieving head was run in the well on the 2-7/8-in. tubing to the retrievable bridge plug at 5806 ft. The bridge plug was released, pulled from the well on the 2-7/8-in. tubing, and laid down. MWX-3 was now ready for the Sandia borehole seismic activities.

Fishing Operations While Preparing MWX-2 For Sandia Borehole Seismic Activities (September 8-18, 1986)

September 8, a service unit was moved on the well, the wellhead removed, BOP's installed, and the packer was released with difficulty. After pulling three joints of the 2-7/8-in. tubing, the packer stuck completely.

Between September 9 and 17 various fishing operations (Appendix A) were unsuccessful at removing the fish. Finally, on September 18, Dynajet ran in the well with a retrievable bridge plug, tagged the fish at 5636 ft, and then set the bridge plug at 5623 ft. The BOP's were removed, the 7-in. full open valve was installed on the casing, the service unit was moved off the well, and the well was turned to Sandia for the borehole seismic activities.

Sandia Borehole Seismic Operations: MWX-1, 2, and 3
(September 20-October 7, 1986)

September 20, the Sandia borehole seismic package was run in MWX-2 and landed at 5620 ft. MWX-1 and MWX-3 were both equipped with a BOP and a lubricator to facilitate running a perforating gun as a source of seismic energy in the B sandstones. Sandia borehole seismic activities were initiated September 20 and were concluded October 4, when it was concluded that the fish in MWX-2 would not allow a seismic tool close enough to the B sandstone for good event location.

Fishing Operations, MWX-2
(October 5-21, 1986)

On October 5, a service unit was moved on the well, the BOP's were installed, a retrieving head was run in the well, and the bridge plug at 5623 ft was released, pulled from the well on the 2-7/8-in. tubing, and laid down.

Extensive fishing operations were conducted between October 6 and 19 (Appendix A). Various fishing and milling steps were unsuccessful in removing the fish. However, in the end, the fish was freed and it moved downhole to 6028 ft, approximately 186 ft below the B perforations. After smoothing the casing, a bridge plug was set on October 21 at 5900 ft, isolating the fish below the B sandstone perforations. This fish, isolated between a bridge plug at 6390 ft abandoning the coastal interval, and the bridge plug at 5900 ft, consists of one joint of 4-1/2-in. 11.6-lb N80 casing, a 4-1/2-in. x 2-7/8-in. crossover, DHSIN tool, a packer, a 2-7/8-in. coupling, one joint of 2-7/8-in. tubing, and a pinned 2-7/8-in. coupling.

A 7-in. casing scraper and a steel brush were run to 5884 ft and the hole was circulated for 75 min to remove solids. Dowell reverse circulated the 3% KCl water from the well with 160,000 SCF N_2. On October 22, the scraper, brush, and tubing were pulled from the well and laid down in preparation for Sandia borehole seismic activities. The BOP's remained installed on the 7-in. casing during seismic activities while the service unit was moved off the well.

Sandia Borehole Seismic Operations: MWX-1, MWX-2, and MWX-3
(October 22-28, 1986)

Sandia borehole seismic activities resumed October 22 with the firing of perforations in the B sandstone in each of the three MWX wells to select the best position for monitoring seismic activity during stimulation, and to orient the borehole seismic packages in MWX-2 and MWX-3 for monitoring the upcoming foam fracture treatment of the B sandstone in MWX-1.

On October 23, Dynajet ran a retrievable bridge plug in MWX-2 with a Squire-Whitehouse instrument attached below in a perforated sub. The retrievable bridge plug was set at 5800 ft to isolate the wellbore for seismic monitoring operations, while the Squire-Whitehouse records pressure response in the B sandstone during stimulation in MWX-1.

On October 28, Dynajet ran retrievable bridge plug in MWX-3 with a Squire-Whitehouse instrument attached below in a perforated sub. The retrievable bridge plug was set at 5790 ft to isolate the wellbore for seismic monitoring operations while the Squire-Whitehouse records pressure response in the B sandstone during stimulation operations in MWX-1. Seismic tool positioning and orientation were also concluded the same day, with the borehole seismic tool in MWX-2 clamped at 5720 ft, and the tool in MWX-3 clamped at 5730 ft.

Prepare MWX-1 For B Sandstone Stimulation
(October 30, 1986)

October 30, a service unit was moved on the well, and 184 joints of 2-3/8-in. tubing was run in the well with the tubing landed at 5703 ft. The BOP's were removed, the wellhead was installed and successfully pressure tested to 7000 psi, and the service unit was moved off the well. Dowell premixed all the frac liquids for both the minifrac and the main frac in a

500 BBL frac tank. All injection lines and metering equipment was tested at this time with clear water, KCl water, N_2, and foam.

B Sandstone Minifrac, MWX-1
(October 31, 1986)

On October 31, the casing-tubing annulus was filled with N_2, and the temperature sonde was run in the tubing on a wireline. The B sandstone mini foam frac was initiated at 11:30 a.m. down the casing-tubing annulus with the N_2 based foam frac fluid containing 48 BBL of 2.75% KCl water, 20-lb J-312 gelling agent, 0.5 gal of M-76 bacteriacide, 2 lb of CNA (cyanuric acid), 16 gals of F-81 foamer, 30 gals of sodium hypochlorite (breaker), and 248,757 SCF of N_2. The frac was then flushed with the same amount of identical fluid. A total of 89 BBL of liquid and 520,000 SCF of N_2 was used in the minifrac. No proppant was used. The average treating rate was 10 BPM at a maximum treating pressure of 5000 psi, average treating pressure of 4900 psi, and a final treating pressure of 5000 psi. The well was shut in for 1 hr for a temperature survey prior to initiating flowback operations. Forty of the 89 BBL of load fluid were recovered October 31.

B Sandstone Main Frac, MWX-1
(November 1, 1986)

On November 1, Dowell conducted the main foam frac operation in the B sandstone interval. The temperature sonde was run in the tubing to approximately 5670 ft prior to starting the fracturing treatment.

The foam frac treatment was conducted down the casing-tubing annulus. The wellbore was pressurized with N_2 injected at a rate of 12,000 SCFM. This was followed by an 8000-gal 75% quality foam pad, 14,000 gal of 75% quality foam containing 32,500 lb 20/40 Proflow intermediate strength prop, and flushed to the top perforation with 7770 gal of 75% quality foam. The Proflow was introduced at 1 PPG and increased in two stages to 4 PPG. Screen-out began to occur when the 1 PPG sand hit the perforations. The job was completed at 2:59 p.m. The average injection rate was 3 BPM liquid and

12,000 SCFM N_2 at a maximum treating pressure of 5790 psi, an average treating pressure of 4800 psi, and an ISIP of 5400 psi. The foam frac liquid phase consisted of 179 BBL of 2.75% KCl water, 20 lb of J-312 gelling agent, 0.5 gal of M-76 bacteriacide, 3 lb of CNA (cyanuric acid), 61 gal of F-81 foamer, and 114 gal of sodium hypochlorite breaker. A N_2 volume of 1,096,000 SCF was used during the B sandstone stimulation.

The temperature log run immediately after the stimulation was concluded encountered sand fill at 5813 ft, 9 ft above the B sandstone perforations at 5822 ft to 5845 ft. Flowback operations were initiated at 5:30 p.m. and 84 BBL of liquid were recovered during the first 14 hrs following stimulation.

Post-Frac Cleanout Operations, MWX-1
(November 3-11, 1986)

On November 3, 1986, a service unit was moved on the well, the wellhead was removed, BOP's installed, and 205 BBL of KCl water were pumped into the well to fill the hole. As insufficient water was available due to a water well failure, it was decided to displace the water in the wellbore to the flat tank with N_2. A total of 175 BBL of load water was recovered following displacement of the wellbore with 56,000 SCF of N_2. The top of the sand fill was encountered at 5797 ft and sand was circulated out with 3% KCl water and N_2 to 6042 ft without encountering the permanent bridge plug previously set at 5950 ft.

On November 5, the post-frac gamma ray log was run from 6071 ft to 5650 ft to define the fracture height near the wellbore. Perforations were shot in MWX-1 to verify the orientation of Sandia's borehole seismic packages in MWX-2 and MWX-3.

On November 6, sand cleanout operations resumed. The hole was filled with 226 BBL of KCl water and Proflow was circulated out to a depth of 6388 ft. Halliburton displaced the KCl water with 75,000 SCF of N_2 at 2700 psi. The next day, the hole was loaded with 230 BBL KCl water and sand was circulated out to the bridge plug, now at 6530 ft in the coastal perforations. Halliburton again displaced the KCl water with 70,000 SCF of N_2. Sand cleanout operations were then terminated. A total of 12,190 lb of Proflow intermediate strength proppant was recovered during wellbore cleanout operations following the B sandstone stimulation.

November 11, following a second post-frac gamma ray log, the 2-3/8-in. tubing was pulled from the well. Dynajet set a bridge plug at 6490 ft between the coastal Red and Yellow sandstones and then set a retrievable bridge plug at 5900 ft, above the coastal Yellow sandstone perforations. A tubing string, DHSIN tool, and packer were run in the well. The tubing was landed at 5713 ft and the packer was set at 5672 ft. The BOP's were removed, the wellhead was installed and successfully pressure tested to 6500 psi, and the service unit was moved off the well. The mast pole and the lubricator were installed and the well was ready for post-frac production testing.

Prepare MWX-3 For Post-Frac Interference Testing
(November 6 and 13 1986)

On November 6, a service unit was moved on the well, and the bridge plug at 5790 ft and Squire-Whitehouse instrument were pulled from the well and laid down. A tubing string, DHSIN tool, and packer were run in the well with the tubing landed at 5732 ft and the packer was set at 5692 ft. The BOP's were removed, the wellhead was installed and successfully pressure tested to 6500 psi, and the service unit was moved off the well. A week later the HP gauge was run in MWX-3 and seated in the DHSIN tool at 5691 ft in preparation for post-frac interference testing.

Prepare MWX-2 For Post-Frac Interference Testing
(November 10, 1986)

On November 10, a service unit was moved on the well, the 7-in. valve was removed, and the BOP's installed. A retrieving head was run in the well and the retrievable bridge plug at 5800 ft and the Squire-Whitehouse instrument were pulled from the well and laid down. A tubing string, DHSIN tool, and packer were run in the well. The tubing was landed at 5711 ft, and the packer was set at 5674 ft. The BOP's were removed, the wellhead installed and successfully pressure tested to 6600 psi, and the service unit was moved off the well. An HP gauge was subsequently run in MWX-2 and seated in the DHSIN tool in preparation for post-frac interference testing.

Post-Frac Production Testing, B Sandstone, MWX-1 Producer
(November 13-December 1, 1986)

At 5 p.m., November 13, B sandstone pressure drawdown testing was initiated in MWX-1. This test was terminated at 12 noon, November 19. The well was then alternately shut in for pressure buildup and produced to unload accumulated liquids, through December 1.

Prepare MWX-1 For B Sandstone Post-Frac Interference Test
(December 2, 1986)

On December 2, the wellhead was removed, BOP's installed, and the packer was released and pulled from the well. A tubing string, DHSIN tool and packer were run in the well. The packer was set at 5788 ft. The BOP's were removed, the wellhead installed and successfully pressure tested to 6500 psi, and the service unit was moved off the well.

Post-Frac Interference Test, B Sandstone, MWX-1 Producer
(December 3-26, 1986)

Post-frac interference testing in the B sandstone was initiated December 3. Flow testing MWX-1 was initiated at 30 MCFD and 830 psi FBHP, and was terminated at 9:45 a.m., December 13, when the pressure buildup portion of the flow test was initiated. The pressure buildup portion of the post-frac interference test was terminated December 26, when the HP gauge became unseated downhole.

Winter Shutdown
(December 26, 1986-March 6, 1987)

On December 26, the B sandstone post-frac interference test was terminated and site winterization was essentially complete. The HP gauges were retrieved from MWX-2 and MWX-3 on January 5. Preparations to ship the test trailer to Las Vegas for routine winter maintenance were completed January 7 and the trailer left the site on January 12.

B Sandstone Production Test, MWX-1
(March 6-April 2, 1987)

Flow testing MWX-1 was initiated March 6, at a rate of 125 MCFD and a flowing bottom hole pressure of approximately 1250 psi. Following the first 24-hr production, the rate was stabilized at approximately 80 MCFD and 900 psi FBHP. The flow test was terminated at 12 noon, March 20, when the well was shut in bottomhole for a pressure buildup. The pressure buildup test was terminated April 2.

Abandon B Sandstone, MWX-3
(March 31-April 2, 1987)

March 31, a well service unit was moved on the well, the wellhead was removed, BOP's installed, the packer was released, pulled from the well, and was laid down. A retrieving head and hydrostatic bailer were run in the well on the 2-7/8-in. tubing to the sand fill on top of the retrievable bridge plug at 5896 ft. The sand was circulated off the plug, the plug was released and the tubing was pulled from the well, minus the retrievable bridge plug, and laid down.

On April 1, Dynajet ran in the well with a sinker bar on a wireline and tagged the plug at 5900 ft. Further attempts to recover the bridge plug were terminated at this time. Dynajet then set a bridge plug at 5800 ft with two sacks of cement on top to permanently abandon the fluvial B perforations. The BOP's remained on the well for use during the Sandia borehole seismic operations in the C sandstone. The well service unit was moved off the well, on April 2.

Abandon B Sandstone, MWX-1
(April 2-7, 1987)

On April 2, the wellhead was removed, BOP's installed, the packer was released and pulled from the well. A retrieving head was then run in the well to the top of the sand plug back, the hole was filled with 205 BBL of 3% KCl water, and the tubing was circulated down to the bridge plug at 5900 ft. The bridge plug was released, pulled from the well, and laid down. Dynajet then set a bridge plug at 6410 ft with two sacks of cement on top. Plugback total depth (PBTD) was 6400 ft. The well was then scraped and circulated to clean the hole.

On April 4, Dia-Log ran a casing inspection log to 6400 ft PBTD. April 6, Schlumberger ran the CET from 6393 ft to 5800 ft with the wellbore pressured to 3000 psi to ensure that the tool functioned properly. Dynajet then set a bridge plug at 5800 ft and dumped two sacks of cement on top to permanently abandon the B sandstone. PBTD was 5790 ft. The tubing was then run in the well to 5790 ft, and gas was reverse circulated out of the hole prior to Schlumberger completing the CET log from 5790 ft to 4100 ft. The next day, a tubing string and packer were run in the well and the packer set at 5503 ft. The wellhead was installed and the service unit was moved off the well.

2.2.2 Fluvial C Sandstone Operations

Stress Test Up To C Sandstone, MWX-2
(April 8-16, 1987)

April 8, a service unit was moved on the well, the wellhead removed, BOP's installed, and the packer was unseated and pulled from the well. Dynajet then set a bridge plug at 5800 ft and placed two sacks of cement on top to permanently abandon the B sandstone. The next day the well was scraped and circulated to clean the hole. On April 10, Dynajet ran in the well and perforated the following four stress test intervals with four 14-gram JSPF (0.38-in. hole diameter):

5788 ft to 5790 ft
5778 ft to 5780 ft
5757 ft to 5759 ft
5744 ft to 5746 ft

The Sandia borehole seismic package in MWX-3 monitored clearly the perforating in MWX-2. Dynajet then ran a smaller perforating gun, rigged for select fire operation, and perforated the same four stress test intervals with five 10-gram JSPF for borehole seismic orientation purposes. The seismic package in MWX-3 clearly recorded the 10 gram select fire perforating charges in MWX-2.

April 13, a tubing string, DHSIN tool, and packer were run in the well to stress test the perforations at 5788 ft to 5790 ft. Three separate, unsuccessful attempts were made to stress test the perforations at 5788 ft to 5790 ft. The perforations at 5778 ft to 5780 ft were successfully stress tested twice. After performing water hammer tests, the packer was released, pulled from the well, and laid down.

April 14, a straddle packer with a 13-ft spacer between packers, and a DHSIN tool were run in the well. The stress test assembly was successfully seated over each perforated interval, but were unable to breakdown the perforations at 5744 ft to 5746 ft, 5757 ft to 5759 ft, and 5788 ft to 5790 ft at surface injection pressures of 6300 psi. The stress test assembly was released and was pulled from the well.

April 15, Gearhart reperforated the intervals 5744 ft to 5746 ft and 5757 ft to 5759 ft with four 23-gram JSPF (0.43-in. hole diameter). The stress test assembly was again run in the well and both intervals were successfully stress tested. Following stress testing, the packers, DHSIN tool, and tubing was pulled from the well and laid down. The BOP's remained installed on the 7-in. casing during seismic activities, but the service unit was moved off the well.

Perforate C Sandstone For Altered Stress Experiment, MWX-2
(April 21, 1987)

April 21, Dynajet perforated the C sandstone from 5721 ft to 5723 ft with four 23-gram JSPF (0.43-in. hole diameter) for stress testing during the altered stress experiment. In addition, Dynajet ran a casing gun, rigged for select fire operation, and perforated the same interval with five 10-gram JSPF for seismic orientation purposes. The Sandia borehole seismic package, downhole in MWX-3, clearly monitored the 10-gram charges select fired in MWX-2.

Stress Test C Sandstone Prior To Altered Stress Experiment MWX-2
(April 22, 1987)

April 22, a straddle packer assembly with a 13-ft spacer between packers and a DHSIN tool was run in the well and set over the C sandstone perforations at 5721 ft to 5723 ft. Ten separate stress tests were conducted on this interval as a base case, against which the results of the altered stress experiment would be compared. The HP gauge was pulled from the well and the service unit was moved off the well. The stress test assembly remained in the well and the BOP's remained installed on the well. All preparations were now complete at MWX-2 for the altered stress experiment.

Seismic Orientation Shots, MWX-1
(April 24, 1987)

On April 24, the wellhead was removed, BOP's installed, and the packer at 5510 ft was unseated and pulled from the well. Dynajet then ran in the well with a casing gun loaded with 10-gram charges. Sandia positioned the perforating gun at 5720 ft to 5738 ft and perforated 1 JSPF to orient the borehole seismic tool in MWX-3.

Perforate, Breakdown The C Sandstone, MWX-1
(April 24-29, 1987)

On April 24, Dynajet perforated the C sandstone with one 23-gram JSPF (0.43-in. hole diameter) from 5720 ft to 5738 ft (18 holes). A tubing string was run in the well with the tubing tail at 5669 ft. The BOP's were removed, and the wellhead was installed and successfully pressure tested to 7000 psi. Three days later, a temperature sonde was run to 5600 ft, and the well was logged in preparation for the altered stress experiment.

April 29, the C sandstone perforations were broken down by Dowell with 26 BBL of 3% KCl water pumped down the tubing at 3 BPM. Eighty ball sealers were dropped throughout the job to ensure the majority of the perforations were open. Fair to good ball action was observed. The well was surged three times to remove ball sealers from the perforations. The perforation breakdown was followed with a pump-in test in which 71 BBL of 3% KCl was pumped at a rate of 7.2 BPM at a treating pressure of 2625 psi. The well was then shut in for 40 min to monitor pressure decline.

Altered Stress Experiments, MWX-1
(April 28-May 23, 1987)

On April 28, Dowell tested all lines, flow meters, and instrumentation for the step-rate/pump-in tests and for the minifrac portion of the altered stress experiment.

April 29, a step-rate/pump-in test was conducted in the C sandstone perforations at rates of 1.0, 1.5, 2.0, 3.0, 4.0, 5.0, and 7.0 BPM. A total of 71 BBL of 3% KCl water was pumped at a maximum bottom hole pressure of 5200 psi. Flowback began immediately at 1 BPM.

Following a temperature log, a second pump-in/flowback test was conducted at 7 BPM for 10 min at a maximum bottomhole pressure of 5250 psi. Flowback began immediately at 1-1/2 BPM for 15 min. A third pump-in/flowback test was conducted at 7 BPM for 11 min at a maximum bottom hole pressure of 5300 psi. Flowback began immediately at 3/4 BPM. A temperature log was run at the end of the flowback test. A total of 77 BBL of 3% KCl water was pumped during this testing.

The first altered stress experiment was conducted April 30 in the C sandstone. No fluid loss control additive was used in the minifrac portion of the altered stress experiments. The KCl water in the wellbore was displaced with 160,000 SCF of N_2. The HP gauge and the temperature sondes were run inside the 2-3/8-in. tubing to 5650 ft. N_2 injection was established down the casing-tubing annulus at 2:10 p.m. at a rate of 11,200 SCFM to pressurize the wellbore. Injection of 75% quality foam was initiated at 2:17 p.m. at a rate of 2.5 BPM liquid rate and 11,200 SCFM N_2 (10 BPM bottom hole rate) for 46 min. The last 18 min was essentially a "flush" of 75% quality foam. Pumping operations were completed at 3:03 p.m with about 675,000 SCF of N_2 and 115 BBL of gelled liquid pumped. A total of 280 BBL of 75% quality foam was injected at a maximum bottom hole treating pressure of 5590 psi, and a surface treating pressure of 5050 psi. Concurrent with foam fracturing the C sandstone in MWX-1, repetitive stress tests were undertaken in the C sandstone in MWX-2 to determine the resulting stress alteration.

Following a 1-1/2-hr shut-in to ensure fracture closure, post frac temperature logs were conducted. The well remained shut in until 1 p.m., May 4, when flow testing was initiated at 80 MCFD and 1000 psi FBHP. The flow test was terminated at 6 a.m., May 8.

The second altered stress experiment was conducted May 12, in the C sandstone using 100 mesh sand as a fluid loss control additive in the minifrac portion of the altered stress experiment. The HP gauge and the temperature sonde were run inside the 2-3/8-in. tubing to 5650 ft. N_2 injection was initiated at 1:09 p.m. down the casing-tubing annulus at a rate of 11,200 SCFM to pressure the wellbore. This was followed by a 2000-gal, 75% quality foam pad, and 8000 gal of 75% quality foam containing 5000 lb of 100 mesh sand in increments ranging from 0.25 PPG to 1.0 PPG, pumped at 2.5 BPM liquid rate and 11,200 SCFM N_2 (10 BPM bottom hole rate). This was followed by an additional 5000 gal of 75% quality foam carrying no sand, to observe any differences in fluid leak-off rate with the foam containing 100 mesh sand. The foam minifrac was then flushed to the top of the C perforations with 7600 gal of 75% quality foam. The maximum treating pressure was 4460 psi, the average treating pressure was 4000 psi, and the ISIP was 3950 psi. The minifrac was completed at 2:12 p.m., May 12. Approximately 700,000 SCF of N_2, 150 BBL of gelled liquid, and 580 BBL of 75% quality foam was pumped during the 100 mesh sand treatment. Along with the foam fracturing operations in the C sandstone in MWX-1, repetitive stress tests were undertaken in the C sandstone in MWX-2 to determine the resulting stress alteration.

Following a 2-hr shut-in to ensure fracture closure, post-frac temperature logs were conducted. On May 13, frac liquid recovery was initiated and continued until 7 a.m., May 23, when the well was shut in for pressure buildup. Pressure buildup operations in the C sandstone were terminated June 3.

Altered Stress Experiment, MWX-2
(April 28-May 12, 1987)

April 28, a service unit was moved in, lubricator installed, and the HP gauges run in the well to 5709 ft. The C sandstone was then stress tested twice during the 26 BBL KCl water perforation breakdown and ballout operations in MWX-1, and three times during the 71 BBL KCl water pump-in test in MWX-1. The next day, four separate stress tests were conducted in MWX-2 while step-rate, pump-in, and flowback testing was being undertaken in MWX-1.

On April 30, three separate stress tests were conducted in MWX-2 during the foam minifrac in MWX-1. Following a 1-1/2-hr shut-in and a post-frac temperature survey in MWX-1, two additional stress tests were conducted in MWX-2. The well was then shut-in with the stress test assembly downhole.

May 11, the HP gauge was rerun in the well to the downhole shut-in at 5709 ft and four stress tests were conducted in the C sandstone to serve as a base case for the altered stress experiment. On May 12, twelve separate stress tests were conducted in the C sandstone perforations in MWX-2, during and after the foam minifrac (containing 100 mesh sand) was conducted in MWX-1. Following stress testing, the packers were released and the stress test assembly was pulled from the well and laid down.

2.2.3 Fluvial E Sandstone Operations

Stress Test Up To E Sandstone, MWX-2
(May 13-18, 1987)

May 13, Dynajet perforated the following six intervals with four 23-gram JSPF (0.43-in. hole diameter) for stress testing.

5700 ft to 5702 ft
5680 ft to 5682 ft
5649 ft to 5651 ft
5620 ft to 5622 ft
5600 ft to 5602 ft
5575 ft to 5577 ft

A straddle packer assembly with a 12-ft spacer between the packer elements, a DHSIN tool, and tubing string were run in the well. The perforations at 5700 ft to 5702 ft, 5680 ft to 5682 ft, and 5649 ft to 5651 ft were successfully stress tested. The remaining three intervals 5620 ft to 5622 ft, 5600 ft to 5602 ft, and 5575 ft to 5577 ft were also successfully stress tested the next day.

May 18, the straddle packer assembly was released, pulled from the well, and was laid down. Dynajet then set a bridge plug at 5580 ft and placed two sacks of cement on top to permanently abandon the stress test perforations below the E sandstone. The 2-7/8-in. tubing was run in the well to within 5 ft of the plug, the hole was loaded with 3% KCl water containing corrosion inhibitor, and reverse circulated for 1-1/4 hrs. The tubing tail was then landed at 5565 ft and the service unit was moved off the well.

Perforate E Sandstone and Prepare For Interference Test, MWX-2
(May 20-30, 1987)

May 20, Dowell displaced the 3% KCl water from the well with 80,000 SCF of N_2. Three days later, a service unit was moved on the well, and the tubing was pulled from the well and laid down.

May 26, Gearhart perforated the E sandstone with eight 20-gram JSPF (0.73-in. hole diameter) from 5532 ft to 5566 ft for a total of 272 holes. The well was then shut in pending Stress-Frac operations, and the service unit was moved off the well.

May 29, a service unit was moved on the well. A tubing string, DHSIN tool, and packer were run in the well. The next day, the tubing was landed at 5528 ft, and the packer was set at 5511 ft. The BOP's were removed, the wellhead was installed and successfully pressure tested to 6000 psi, and the service unit was moved off the well.

Perforate E Sandstone And Stress-Frac, MWX-3
(May 19-30, 1987)

On May 19, a service unit was moved on the well, and 2-7/8-in. tubing was run in the well and landed at 5784 ft 5 ft. The next day Dowell displaced the 3% KCl water from the well with 65,000 SCF of N_2. On May 21, the tubing was pulled from the well and laid down, and the well service unit was moved off the well.

May 26, Gearhart perforated the E sandstone with eight 20-gram JSPF (0.73-in. hole diameter) from 5550 ft to 5574 ft for a total of 192 holes.

May 27, the 7-in. 32-lb casing was pressured to 1100 psi with 89,100 SCF of N_2 followed by 89 BBL (330,000 SCF) of liquid CO_2 to serve as a liquid free tamp for the Servo-Dynamics stress-frac tool. This dynamic fracturing technique was being used to connect the perforations and wellbore to the natural fracture system in the E sandstone (Section 9.1.3). The first 12-ft stress-frac carrier, containing 38 lb of propellant, was run in the well and positioned at 5562 ft to 5574 ft, but failed to fire because of an open circuit. When the device was pulled from the well, a wire was found to have broken in the bridle. A second stress-frac tool containing 38 lb of propellant was run in the well, positioned from 5562 ft to 5574 ft, and successfully ignited. However, the 12-ft steel carrier and the collar locator tool were lost in the well. The CO_2 was vented from the well to 1100 psi to limit any pressure increase due to liquid CO_2 vaporization overnight. The next day, fishing operations recovered both the casing collar locator and the stress-frac carrier on the first attempt. The Gearhart forty arm caliper was run from 5650 ft to 5450 ft with one tight spot noted at 5572 ft.

May 29, natural gas was transferred from MWX-1 and MWX-2 to MWX-3 to pressure the well to 1100 psi prior to loading the well with 82 BBL (304,000 SCF) of liquid CO_2. This liquid CO_2 provided a 2000 ft liquid tamp for the stress-frac tool at a wellhead pressure of 1370 psi. A third stress-frac tool, also containing 38 lb of propellant, was positioned at 5550 ft to 5562 ft and ignited without incident. A second caliper survey, run following the stress-frac, also indicated damage to the 7-in. 32-lb casing at 5572 ft. Flow tests and pressure buildup tests of the C sandstone following stress-frac, were disappointing.

May 30, a service unit was moved on the well, and preparations were undertaken to roll out the "burr" in the 7-in. casing indicated on the caliper logs at 5572 ft. Two days later a bottom hole assembly consisting of a 6.010-in. OD casing swage, four drill collars, and bumper and hydraulic jars were run in the well on tubing to the "burr" at 5572 ft. The "burr" took 12,000 lb of weight before the bottom hole assembly worked through the tight spot. The bottom hole assembly was run 100 ft below the tight spot at 5572 ft, and then was pulled from the well and laid down. The presence of liquid standing at 5000 ft in the wellbore was indicated on the tubing when the bottom hole assembly was pulled from the well. A pressure gradient run following the casing roll-out operations confirmed the presence of water in the wellbore. Analysis of a water sample obtained June 5, indicated the water was completion fluid (3% KCl water) that had not been reverse circulated from the well with N_2 prior to perforating for the stress-frac.

Prepare MWX-3 For E Sandstone Interference Test
(June 2-16, 1987)

June 2, Dynajet set a bridge plug at 5620 ft and placed two sacks of cement on top to limit the wellbore storage below the E sandstone to 36 ft. A tubing string, DHSIN tool, and packer were run in the well. The tubing was landed at 5548 ft, and the packer was set at 5530 ft. The BOP's were removed, the wellhead installed and successfully pressure tested to 6200 psi, and the service unit was moved off the well. The shut-in tubing pressure at 7 a.m. the next day, was 68 psi. On June 6, a pressure gradient conducted with the HP gauge indicated liquid standing at 4940 ft.

June 8, a service unit was moved on the well, the wellhead was removed, BOP's installed, the packer released and the tubing tail was lowered to 5609 ft. Several days of intermittent swabbing recovered 11.46 BBL water. Two days later the downhole assembly was pulled from the well.

June 11, a packer fitted with a 2-7/8-in. pump-out plug (pump-out pressure 7000 psi BHP, 5700 psi WHP) was run in the well on the 2-7/8-in. tubing and the packer was set at 5521 ft. The casing-tubing annulus and the tubing were each pressured in stages to 4200 psi. Tubing pressure was increased gradually to a maximum of 5700 psi where the pump-out plug released and the N_2 pressure "dynamically" broke down the E sandstone perforations (Section 9.1.3). A total of 232,000 SCF of N_2 was used in this breakdown procedure.

June 12, the HP gauge was run in the well to 5500 ft, and the well was shut in for pressure buildup at 7:00 p.m. At 8 a.m., the next day, following a 13-hr shut-in, the shut-in tubing pressure was 937 psi.

June 16, the packer was unseated, and the packer and tubing were pulled from the well. A tubing string, DHSIN tool, and packer were run in the well. The tubing was landed at 5548 ft, and the packer was set at 5530 ft. The BOP's were removed, and the wellhead installed and successfully pressure tested to 6000 psi. The service unit was then moved off the well.

Perforate, Breakdown E Sandstone, MWX-1
(June 3-5, 1987)

June 3, a service unit was moved on the well, the wellhead was removed, the BOP's installed, and the tubing was pulled from the well. Dynajet set a bridge plug at 5710 ft with two sacks of cement on top to permanently abandon the C sandstone perforations. The ring joint seal in the wellhead was then replaced to ensure pressure integrity during the N_2 breakdown operations to follow.

June 4, Dynajet ran in the well with a 30-ft-long perforating gun, containing two 19-gram JSPF and positioned it opposite the E sandstone from 5535 ft to 5565 ft. The intent was to create a dynamic nitrogen frac by simultaneously perforating the casing under a high pressure of nitrogen (Section 9.1.3). Dowell pressure tested their lines to 7000 psi and then initiated pumping N_2 downhole. At 4454 psi, a leak developed in the wellhead assembly, and operations were shut down at 3 p.m. to repair the leak. The Dynajet perforating gun was pulled from the well and laid down as additional N_2 was transported to the site overnight.

June 5, the perforating gun was rerun in the well and positioned opposite the E sandstone from 5535 ft to 5565 ft. Dowell pressured the 7-in. casing to 6000 psi WHP with N_2, the perforating gun was fired, and the perforations were "dynamically" broken down with the N_2 with approximately a 3000 psi pressure differential toward the formation. Approximately 779,900 SCF of N_2 were used during this perforation breakdown procedure. Following a 1-hr shut-in for pressure stabilization, the well was depressured and Dynajet set retrievable bridge plug at 5610 ft with two sacks of sand placed on top to minimize wellbore storage during pre-frac interference tests.

Prepare MWX-1 For E Sandstone Interference Test
(June 6-8, 1987)

June 6, a tubing string, DHSIN tool, and packer were run in the well. The tubing tail was landed at 5531 ft and the packer was set at 5512 ft. The BOP's were removed, the wellhead was installed and successfully pressure tested to 6000 psi, and the service unit was moved off the well. The next day, the HP gauge and the temperature tool were run in the well. The well was shut in at the surface for pressure buildup at 10 a.m.

E Sandstone Pre-Frac Interference Testing
(June 17-August 20, 1987)

June 17, the HP gauges were seated in the DHSIN tool in MWX-2 and MWX-3 with N_2. Flow testing MWX-1 was initiated at 7 a.m. through the separator to the flare pit at 77 MCFD, 1024 psi FBHP, and 804 psi FTP. The flow test was terminated at 7 a.m., June 24, and the HP gauge was seated in the DHSIN tool, initiating the pressure buildup. The pressure buildup was terminated at 5 p.m., June 29, when the second flow test was initiated. The second flow test was terminated at 10:15 a.m., July 13, when the HP gauge was seated in the DHSIN tool, initiating the second pressure buildup.

At 8:30 a.m., July 29, flow testing of MWX-3 was initiated at 12 MCFD, 531 psi FBHP, and 452 psi FTP. MWX-1 and MWX-2 remained shut-in bottomhole. Flow testing MWX-3 was terminated on August 1, due to the poor production performance of MWX-3.

On August 7, flow testing of MWX-2 was initiated at 65 MCFD, 1022 psi FBHP, and 668 psi FTP. MWX-1 and MWX-3 remained shut-in bottomhole. Flow testing MWX-2 was terminated on August 18 and all E sandstone pre-frac interference testing was terminated August 20.

Prepare Wells For Borehole Seismic Activities
(August 20-22, 1987)

August 20, a service unit was moved on MWX-1, the wellhead was removed, BOP's installed, and the packer was released, pulled from the well, and laid down. The BOP's remained on the well for use during the borehole seismic activities, while the service unit was moved off the well.

On August 20, a service unit was moved on MWX-3, the wellhead was removed, and the BOP's installed. The packer was released, it and the tubing were pulled from the well and laid down. The next day, a magnet was used to recover the cast iron pump-out plug left on bottom as a result of the "dynamic" breakdown on June 11. Dynajet next set a retrievable bridge plug at 5540 ft with two sacks of sand on top to isolate the E sandstone perforations from the wellbore during the seismic activities.

August 22, a service unit was moved on MWX-2, the wellhead removed and the BOP's were installed. The packer was released, and it and the tubing were pulled from the well and laid down. The BOP's remained on the well for use during the borehole seismic activities, while the service unit was moved off the well.

Sandia Borehole Seismic Operations: MWX-1, MWX-2, And MWX-3
(August 25-September 5, 1987)

August 25, the Sandia borehole seismic tool was run in MWX-3 and landed at 5490 ft opposite the F sandstone. MWX-1 and MWX-3 were both equipped with a BOP to facilitate running a perforating gun for seismic shots. All seismic shots were conducted in existing E perforations.

August 26, Dynajet set retrievable bridge plug, with a Squire-Whitehouse instrument beneath, in MWX-2 at 5500 ft. The retrievable bridge plug was necessary to isolate the E sandstone perforations to eliminate gas flow noise in the well from interfering with borehole seismic activities.

August 31, a service unit was moved on MWX-3 and the sand fill at 5532 ft was reverse-circulated off the bridge plug with 3% KCl water. Dowell then displaced the KCl water to the pit with 170,000 SCF of N_2. A large quantity of grease was recovered with the KCl water circulated from the well. The bridge plug was released, pulled from the well, and laid down. Two days later the wellbore was scraped clean and the well was shut in at the surface with the perforations open to the wellbore and no tubing in the well. On September 5, Dynajet set a retrievable bridge plug, with a Squire-Whitehouse instrument beneath, at 5540 ft. The retrievable bridge plug was necessary to isolate the E sandstone perforations and eliminate noise from gas flow in the well from interfering with borehole seismic activities.

September 2, Dynajet set a retrievable bridge plug at 5520 ft in MWX-1 to isolate the E sandstone perforations and eliminate noise from gas flow from interfering with borehole seismic activities.

Prepare MWX-1 For E Sandstone, Minifrac
(September 8-10, 1987)

On September 8, a service unit was moved on the well. The bridge plug at 5520 ft was recovered on the second trip into the well, after changing out the retrieving head. The next day, Dynajet ran in a well with a wireline retrieving tool and recovered a perforating gun centralizer lost August 27 during perforations in conjuction with borehole seismic activities. On September 10, a 2-3/8-in. tubing string was run in the well to 5452 ft. The BOP's were removed, the wellhead was installed and successfully pressure tested to 6000 psi, and the service unit was moved off the well.

E Sandstone Minifrac, MWX-1
(September 10-17, 1987)

September 10, Dowell pumped N_2 at different rates to check meters and instrument calibration, and displaced the gas in the wellbore with 2.75% KCl water. The CER pressure and temperature sonde were run in the well and the injection lines were pressure tested with KCl water to 6000 psi. The next day, a series of pump-in/flowback and step-rate/flowback tests were conducted in the E sandstone allowing 30 min to 1 hr for equilibration after each test.

On September 12, the 2.75% KCl water was displaced from the well with N_2. The foam frac liquid phase, 2.75% KCl water, was gelled and pre-mixed with additives in a 500 BBL frac tank. The E sandstone minifrac was initiated at 12 noon. Dowell pressurized the wellbore with N_2 followed by 2000 gals of foamed-water breaker prepad. This was followed with 10,000 gals of 75% quality N_2 foam containing no proppant which, in turn, was flushed with 7750 gals of 75% quality N_2 foam. The job was completed at 12:35 p.m. Following a 75-min shut-in, a post-frac temperature log was obtained across the E sandstone. The well was flowed intermittently to recover 249 BBL of load fluid. Dowell reverse-circulated the wellbore liquids to the pit with N_2, but could not get the well to flow.

September 17, a service unit was moved on the well, the wellhead was removed, and the tubing was lowered to 5585 ft. Dowell then reverse-circulated approximately 10 BBL of 2.75% KCl water from the well with 89,600 SCF of N_2.

E Sandstone Main Foam-Frac, MWX-1
(September 21-23, 1987)

September 21, a service unit was again moved on the well, the wellhead was removed, four joints of 2-3/8-in.tubing were laid down, a blast joint was picked up, and the tubing tail was landed at 5452 ft. The wellhead was installed and successfully pressure tested to 7200 psi, and the service unit was moved off the well. The next day, Dowell moved in the stimulation equipment, transferred KCl water to the frac tank, laid and tested the injection lines to the wellhead, hooked up meters, and installed all instrumentation to the TMV.

At 11:36 a.m., September 23, 1987, the main E sandstone frac was initiated by pumping N_2 down the casing-tubing annulus to establish a rate of 25,000 SCFM. This was, in turn, followed by 44,600 gal of 75% quality foam containing 9500 lb of 100 mesh sand, 72,000 lb of 20/40 mesh intermediate strength proppant (Proflow), 1,660,868 SCF of N_2, and 290 BBL of gelled 2.75% KCl water. The 20/40 mesh proppant concentrations ranged from 1-4 PPG and contained from 0.5-0.25 PPG of 100 mesh sand for fluid leak-off control. The propped fracture treatment was designed to be pumped at a rate of 23 BPM, bottomhole. The N_2 rate was planned to be 25,000 SCFM and the gel (liquid) rate was set at 5.8 BPM. The maximum treating pressure was 6520 psi, average treating pressure was 6100 psi, and the final treating pressure was 5940 psi. The job was completed at 1:12 p.m. The ISIP was 5000 psi. Flowback was initiated at 4:30 p.m. following a post-frac temperature survey.

E Sandstone Post-Frac Cleanup, MWX-1
(September 23-29, 1987)

Flowback operations were initiated at 4:30 p.m., September 23. The well was flowed to the 400 BBL tank until 10 p.m. when the well was turned through the separator to the flare pit. A post-frac gamma ray log was run early on the next day to delineate the propped fracture height near the wellbore. Flowback proceeded very well with the well testing at rates in excess of 280 MCFD within two days of the stimulation at 987 psi FBHP and 642 psi FTP. Flowback continued until 4 a.m., September 29, when post-frac cleanup was terminated.

Prepare MWX-2 For Post-Frac Interference Test
(September 25-28, 1987)

On September 25, a service unit was moved on the well, a tool was run in the well on the 2-7/8-in. tubing to the top of the sand fill at 5492 ft to recover a neoprene centralizer lost from the Sandia shear wave source tool. The tubing, fishing tool, and neoprene centralizer were pulled from the well and the centralizer and fishing tool were laid down.

September 26, a retrieving head was run on tubing to the top of the sand fill at 5492 ft, and the sand was reverse circulated off the retrievable bridge plug with 3% KCl water. Dowell reverse-circulated the KCl water from the well with 150,651 SCF of N_2. The bridge plug was then released, and it and the Squire-Whitehouse instrument package (beneath the bridge plug) were pulled from the well and were laid down. Two days later, a tubing string, DHSIN tool, and packer were run in the well. The tubing was landed at 5528 ft and the packer was set at 5511 ft. The BOP's were removed, the wellhead installed and successfully pressure tested to 6000 psi, and the service unit was moved off the well. MWX-2 was now equipped for the post-frac interference test.

Prepare MWX-3 For Post-Frac Interference Test
(September 28-29, 1987)

September 28, a service unit was moved on the well, and the retrievable bridge plug at 5540 ft was released, and it and the Squire-Whitehouse instrument package (beneath the bridge plug) were pulled from the well and were laid down. The next day, a tubing string, DHSIN tool, and packer were run in the well. The tubing was landed at 5548 ft and the packer was set at 5530 ft in 23,000 lb compression. The BOP's were removed, the wellhead was installed and successfully pressure tested to 6000 psi, and the service unit was moved off the well. MWX-3 was now equipped for the post-frac interference test.

Prepare MWX-1 For Post-Frac Interference Test
(September 30, 1987)

On September 30, a service unit was moved on the well, the wellhead was removed, BOP's installed, and the 2-3/8-in. tubing was pulled from the well. A DHSIN tool and packer were added to the end of the tubing, and the string was run in the well. The packer was set at 5513 ft, and the tubing tail was landed at 5583 ft, below the E perforations from 5535 ft to 5565 ft. The BOP's were removed, the wellhead was installed and successfully pressure tested to 6200 psi, and the service unit was moved off the well. MWX-1 was now equipped for the post-frac interference test.

E Sandstone Post-Frac Interference Test
(October 3-December 6, 1987)

Post-frac interference testing was initiated October 3, at 285 MCFD and 1017 psi FBHP. This testing consisted of a 16-day flow period, a 2-day pressure buildup/pulse, a 7-day flow test, and a 7-week pressure buildup. The final flow rates were 200 to 220 MCFD, compared to 65 MCFD prefrac. The pressure buildup test was terminated on December 6.

MWX-1 has remained shut in since December 6, 1987 (through winter, 1989), pending negotiation of a gas sales.

Permanently Abandon The E Sandstone, MWX-2
(November 16, 1987)

November 16, a service unit was moved on the well, the wellhead was removed, BOP's installed, and the packer was unseated, pulled from the well, and was laid down. Western Atlas then set a bridge plug at 5528 ft to permanently abandon the E sandstone perforations at 5535 ft to 5565 ft. Due to mechanical problems, no cement was placed on the bridge plug at that time.

2.2.4 Subsequent Operations

Stress Tests Above E Sandstone, MWX-2
(November 17-December 4, 1987)

On November 17, Dresser Atlas perforated the following six intervals, each with four 13.5-gram bullets per foot (0.47-in. hole diameter):

5506 ft to 5508 ft
5480 ft to 5482 ft
5450 ft to 5452 ft
5414 ft to 5416 ft
5320 ft to 5322 ft
5294 ft to 5296 ft

The same day, the stress test assembly was run in the well on the 2-7/8-

in. tubing to isolate the perforations at 5506 ft to 5508 ft. These perforations, in a mudstone, were isolated but could not be broken down and stress tested. The stress test assembly was then moved up hole to isolate the perforations in a sandstone at 5480 ft to 5482 ft. These perforations were successfully broken down and stress tested. On November 18, the next two intervals, 5450 ft to 5452 ft, and 5414 ft to 5416 ft, both in mudstones, were successfully stress tested. A third attempt to stress test the perforations at 5506 ft to 5508 ft was unsuccessful. On November 19, the intervals at 5320 ft to 5322 ft, and from 5294 ft to 5296 ft were successfully stress tested. The stress test assembly was pulled from the well and was laid down.

November 24, Dynajet perforated the following seven intervals with four 19-gram JSPF (0.46-in. hole diameter).

5502 ft to 5504 ft
5074 ft to 5076 ft
5044 ft to 5046 ft
4714 ft to 4716 ft
4692 ft to 4694 ft
4376 ft to 4378 ft
4330 ft to 4332 ft

Dynajet then placed 1-1/2 sacks of cement on the bridge plug at 5528 ft. The stress test assembly was then run in the well and operations were then shut down until after Thanksgiving.

November 30, stress test operations were resumed. The perforations at 5502 ft to 5504 ft were isolated with the stress test assembly and successfully stress tested. The next day, the perforated intervals at 5074 ft to 5076 ft, 5044 ft to 5046 ft, 4714 ft to 4716 ft, and 4692 ft to 4694 ft were all successfully stress tested. On December 2, the remaining two intervals from 4376 ft to 4378 ft, and from 4330 ft to 4332 ft were successfully stress tested. This completed stress testing over the entire Mesaverde interval at the Multiwell site.

Mothball MWX-2
(December 2-3, 1987)

December 2, Dynajet set a bridge plug at 4310 ft and placed two sacks of cement on top to permanently abandon the stress test perforations. PBTD is now 4300 ft. The next day, 2-7/8-in. tubing was run in the well open ended and landed at 4284 ft. Dowell then displaced the 3% KCl water from the well with 97,000 SCF of N_2. The BOP's were removed, the wellhead was installed, and the service unit was moved off the well. Preparations were now complete for long term shut-in of MWX-2 with no perforations open to the wellbore.

Mothball MWX-3
(December 4-5, 1987)

On December 4, a service unit was moved on the well, the wellhead was removed, BOP's were installed, the packer was released, and the downhole assembly was pulled from the well. Dynajet set a bridge plug at 5540 ft and placed two sacks of cement on top to permanently abandon the E sandstone perforations. The next day, 2-7/8-in. tubing was run in the well open ended and landed at 5498 ft. Dowell then displaced the 3% KCl water from the well with N_2. The BOP's were removed, the wellhead was installed, and the service unit was moved off the well. Preparations were now complete for long term shut-in of MWX-3 with no perforations open to the wellbore.

2.3 REFERENCES

1. CER Corporation, "Multi-Well Experiment: MWX-1 As-Built Report," Sandia National Laboratories Contractor Report, SAND82-7201, July 1982.

2. CER Corporation, "Multi-Well Experiment: MWX-2 As-Built Report," Sandia National Laboratories Contractor Report, SAND82-7100, August 1982.

3. CER Corporation, "Multi-Well Experiment: MWX-3 As-Built Report," Sandia National Laboratories Contractor Report, SAND82-7132, February 1984.

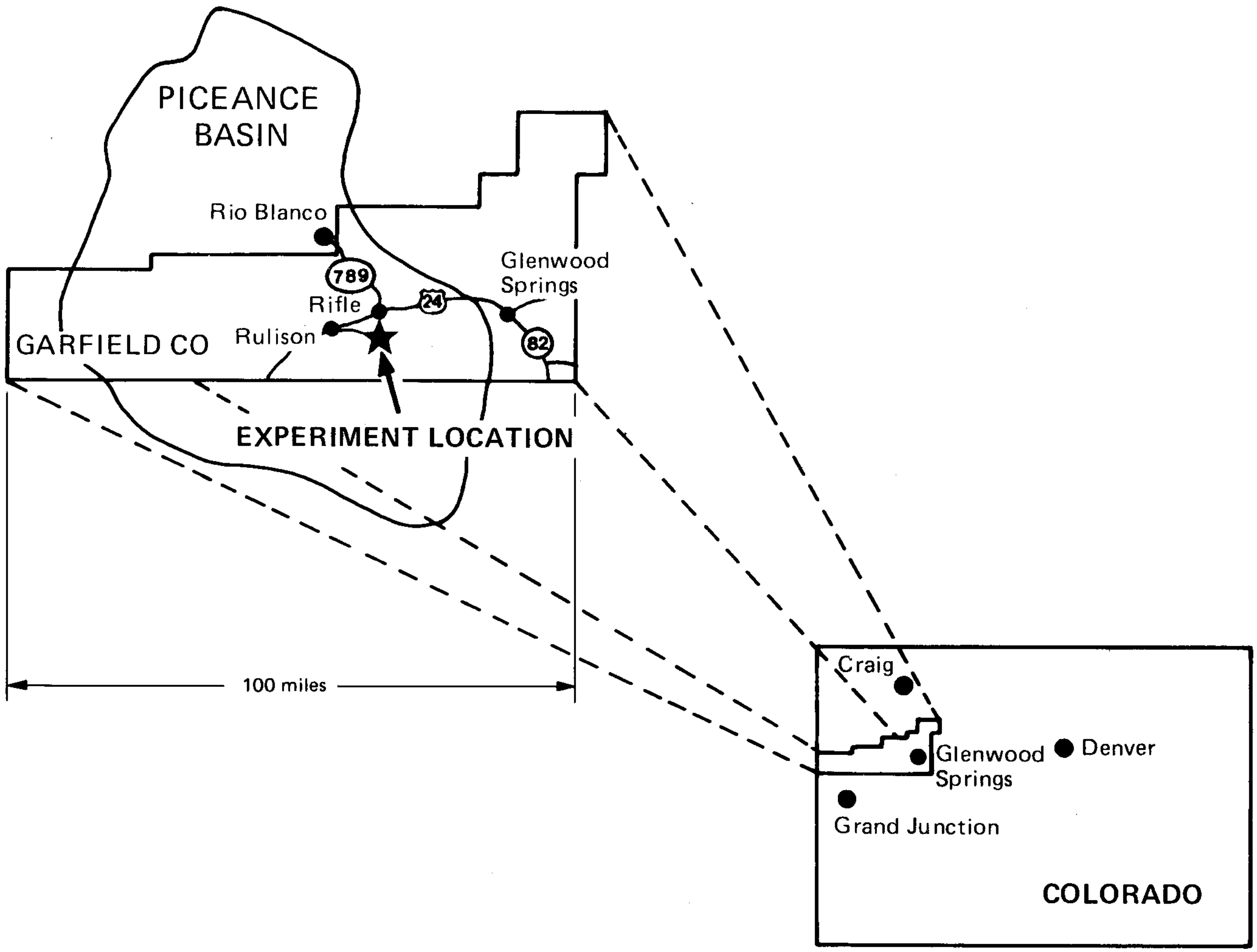

Fig. 2.1 Multiwell Experiment Location

MWX-1

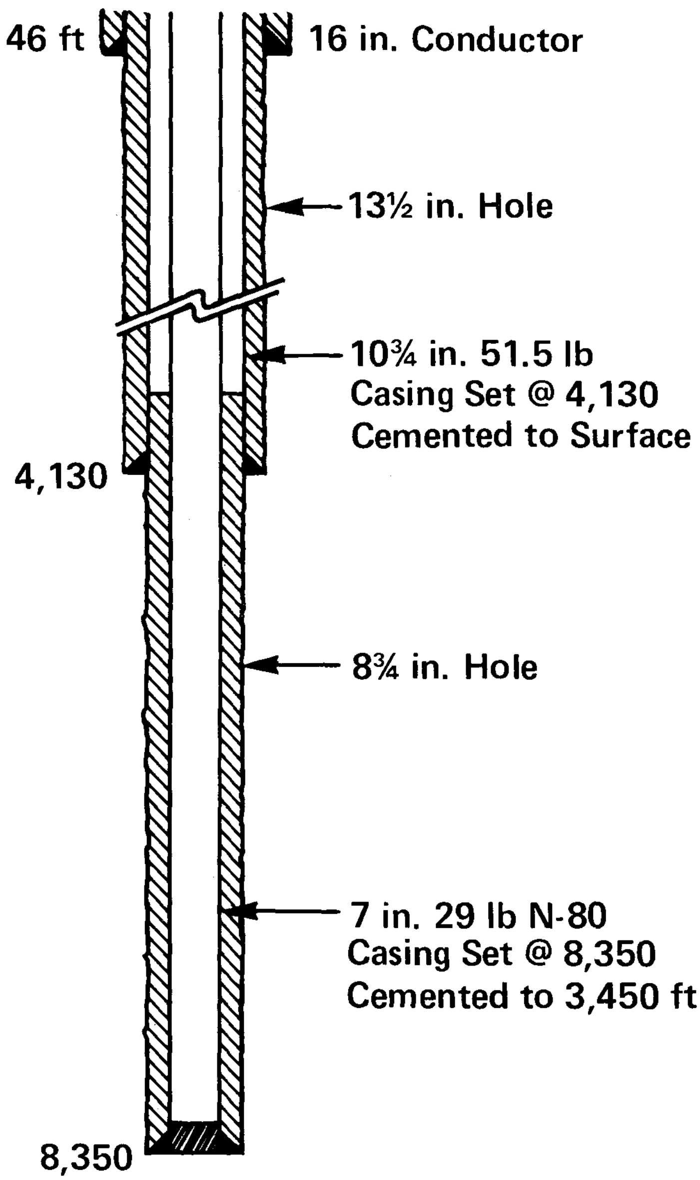

CORES	
4,170 - 6,827 ft	2,657 ft
7,870 - 7,960	90 ft
Total	2,747 ft
Oriented	470 ft

LOGS

4,130 - Surface
4 Logs - comb.

6,827 - 4,130 ft
11 logs - comb.

8,350 - 4,130 ft
18 logs - comb.

DSTs

5,885 - 5,830 ft

RFTs

8,135 -4,535 ft
12 tests

Spud Date:	Sept. 13, 1981
Rig Released:	Dec. 21, 1981

Fig. 2.2 MWX-1 Well Information

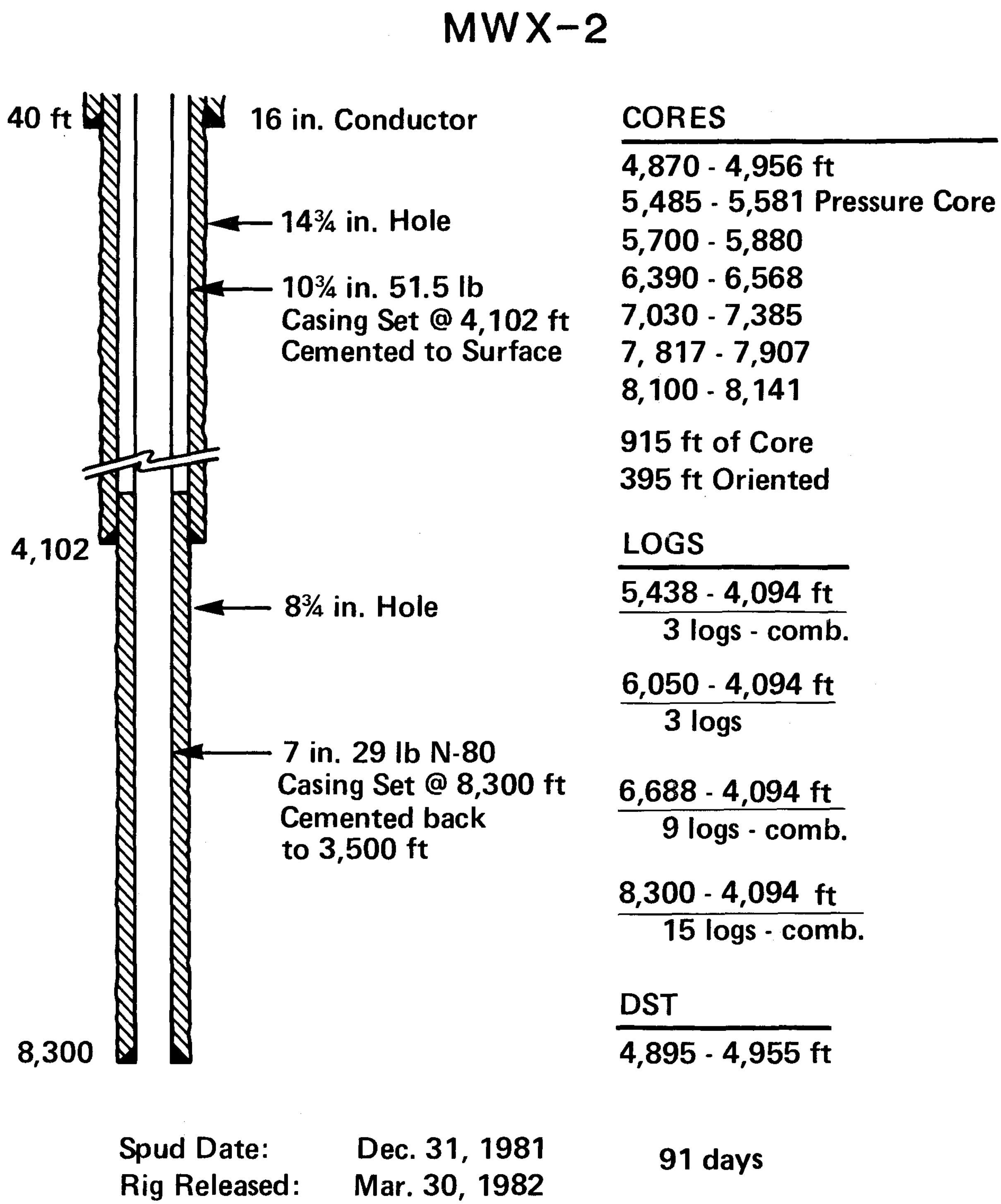

Fig. 2.3 MWX-2 Well Information

MWX-3

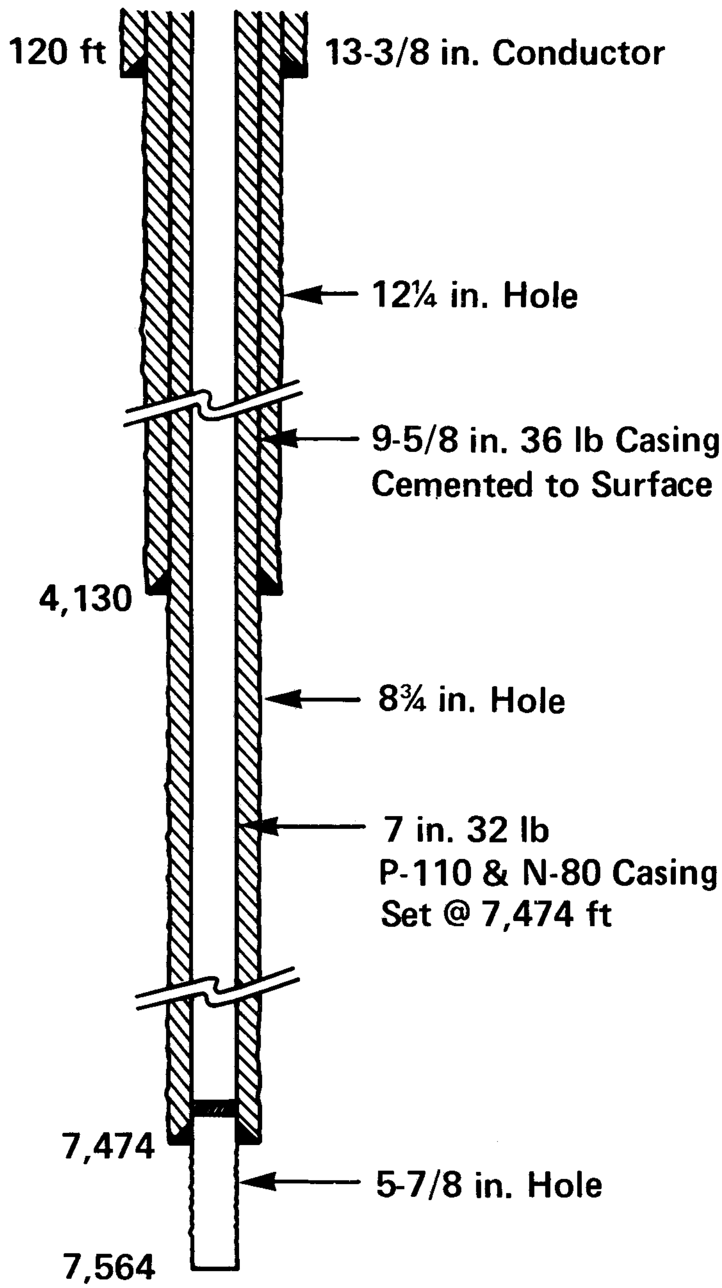

CORES

4,887 - 4,928 ft
5,690 - 5,870
6,431 -- 6,528
6,875 - 6,910
7,071 - 7,160
7,536 - 7,564

435 ft of Core
All Oriented

LOGS

4,134 - Surface
4 logs - comb.

5,875 -4,129 ft
5 logs - comb.

6,875 - 4,130 ft
7 logs - comb.

7,463 - 4,129 ft
28 logs - comb.

Spud Date: June 7, 1983
Rig Released: Aug. 17, 1983

72 days

Fig. 2.4 MWX-3 Well Information

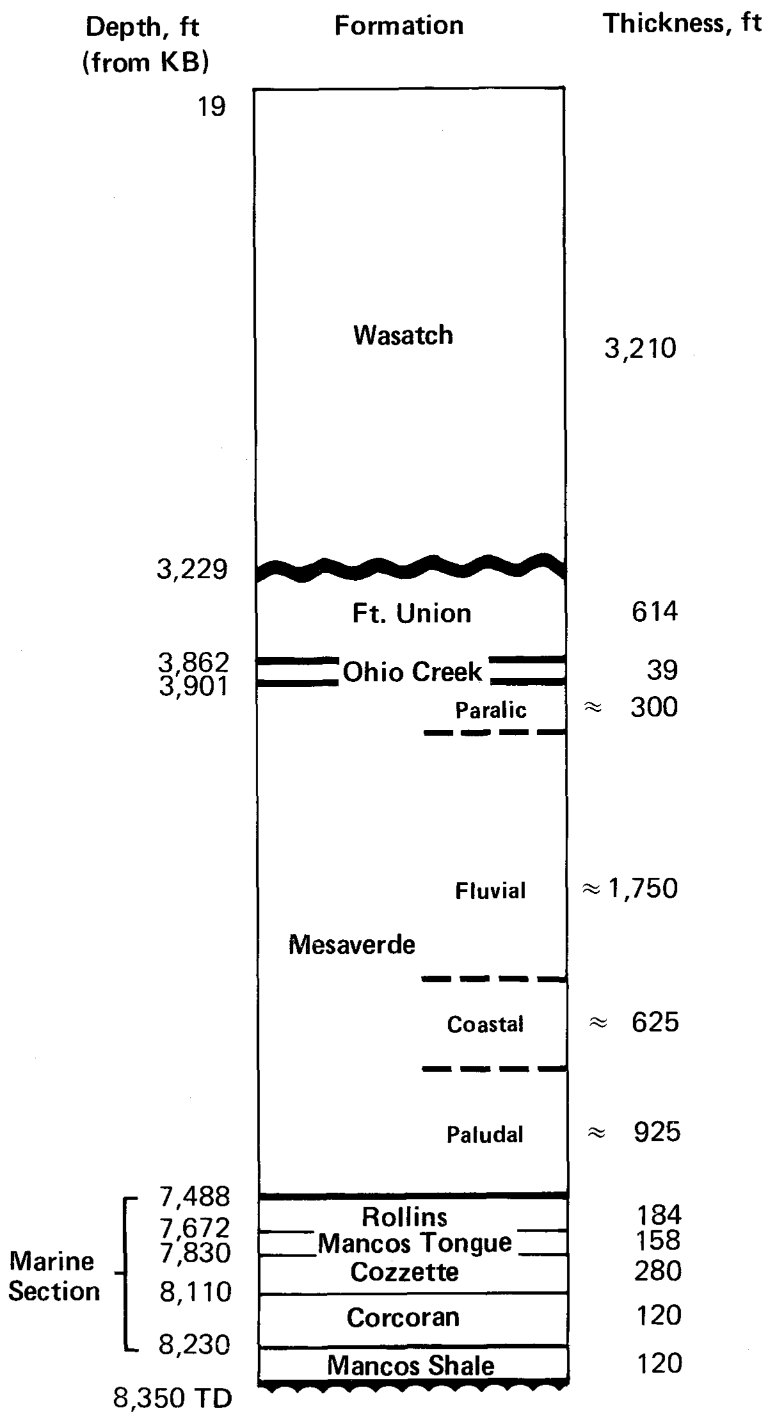

Fig. 2.5 Geologic Cross-section of MWX-1

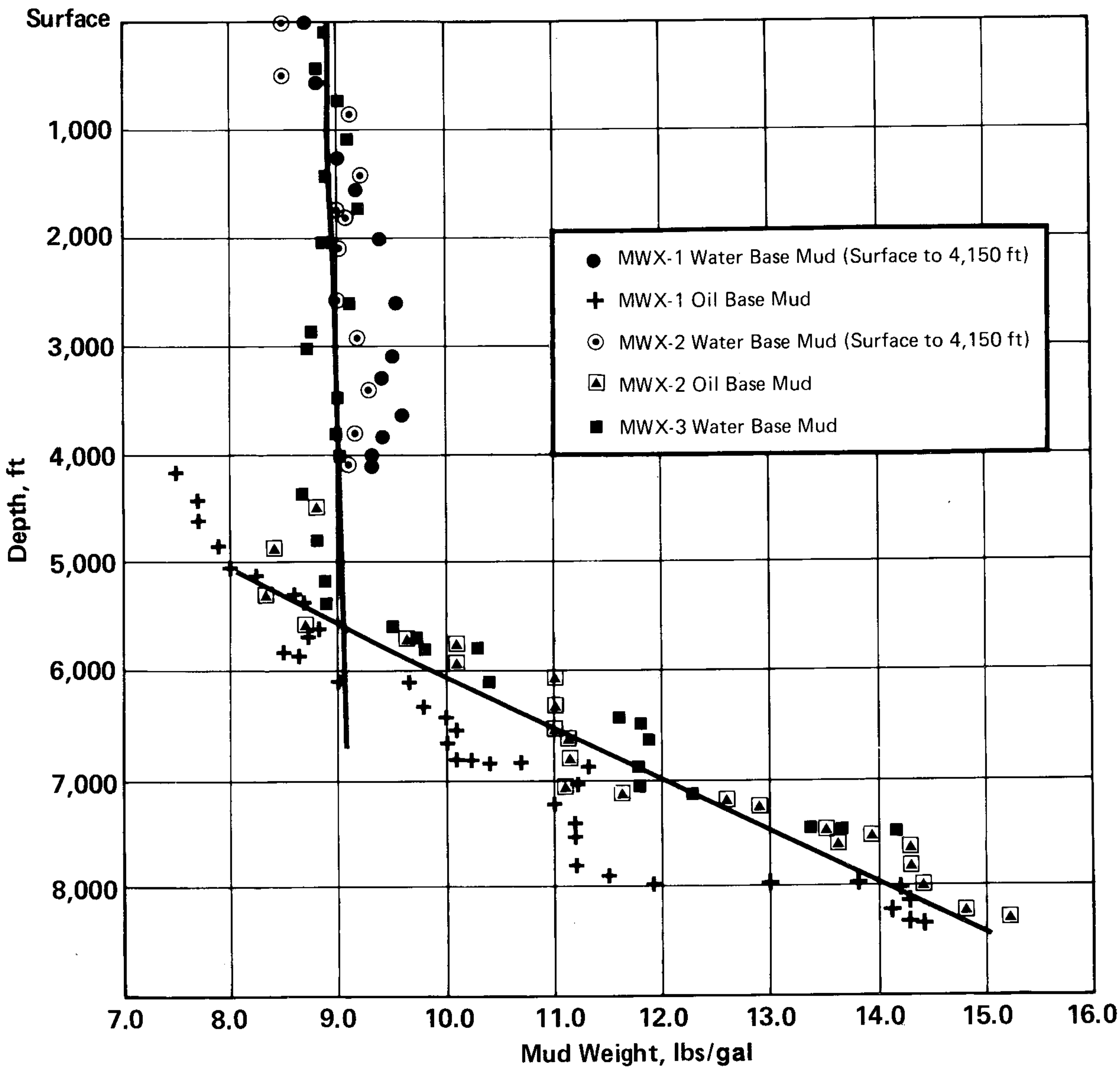

Fig. 2.6 Mud Weight Versus Depth

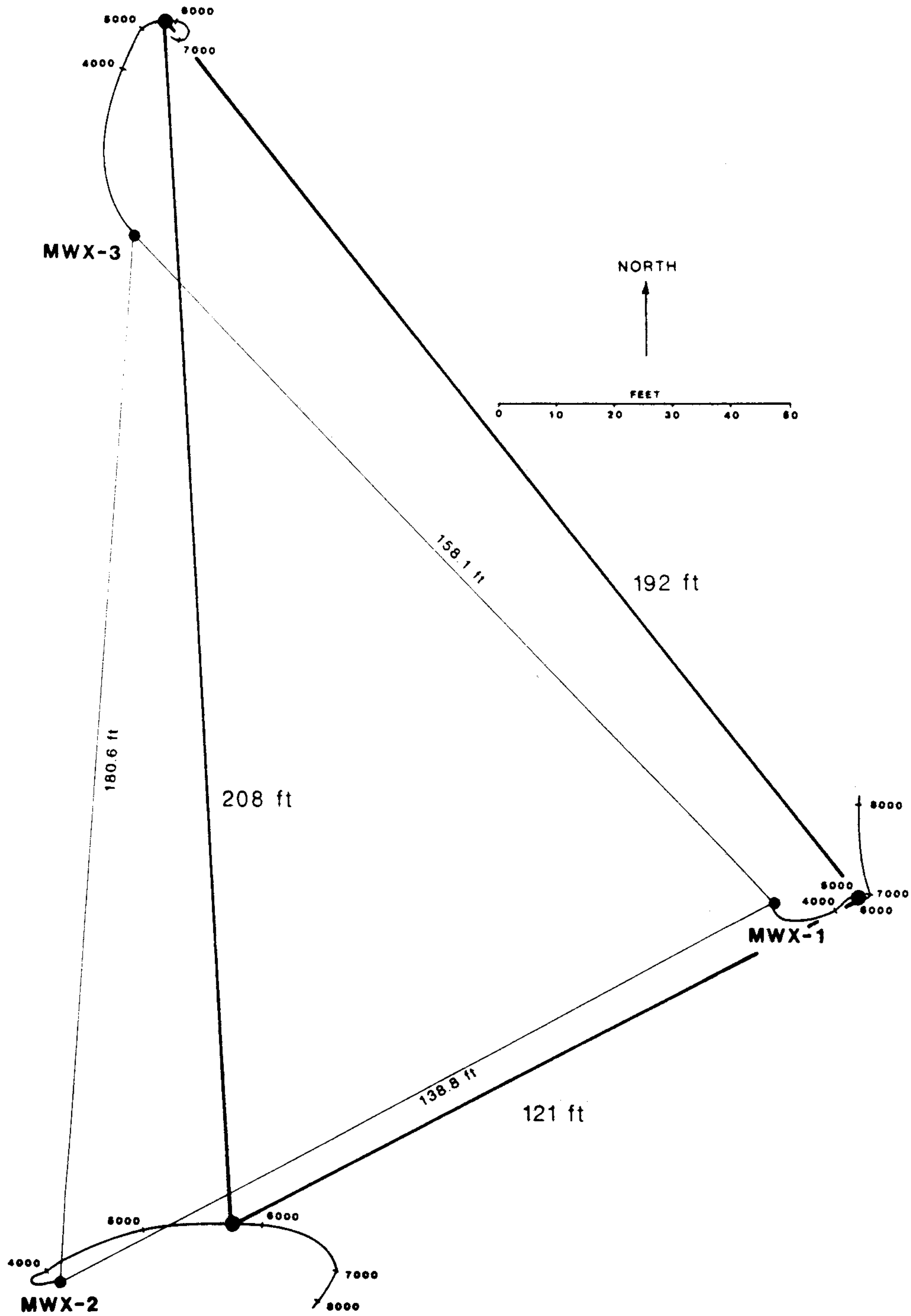

Figure 2.7 Relative Well Spacings at Surface and 5500 ft

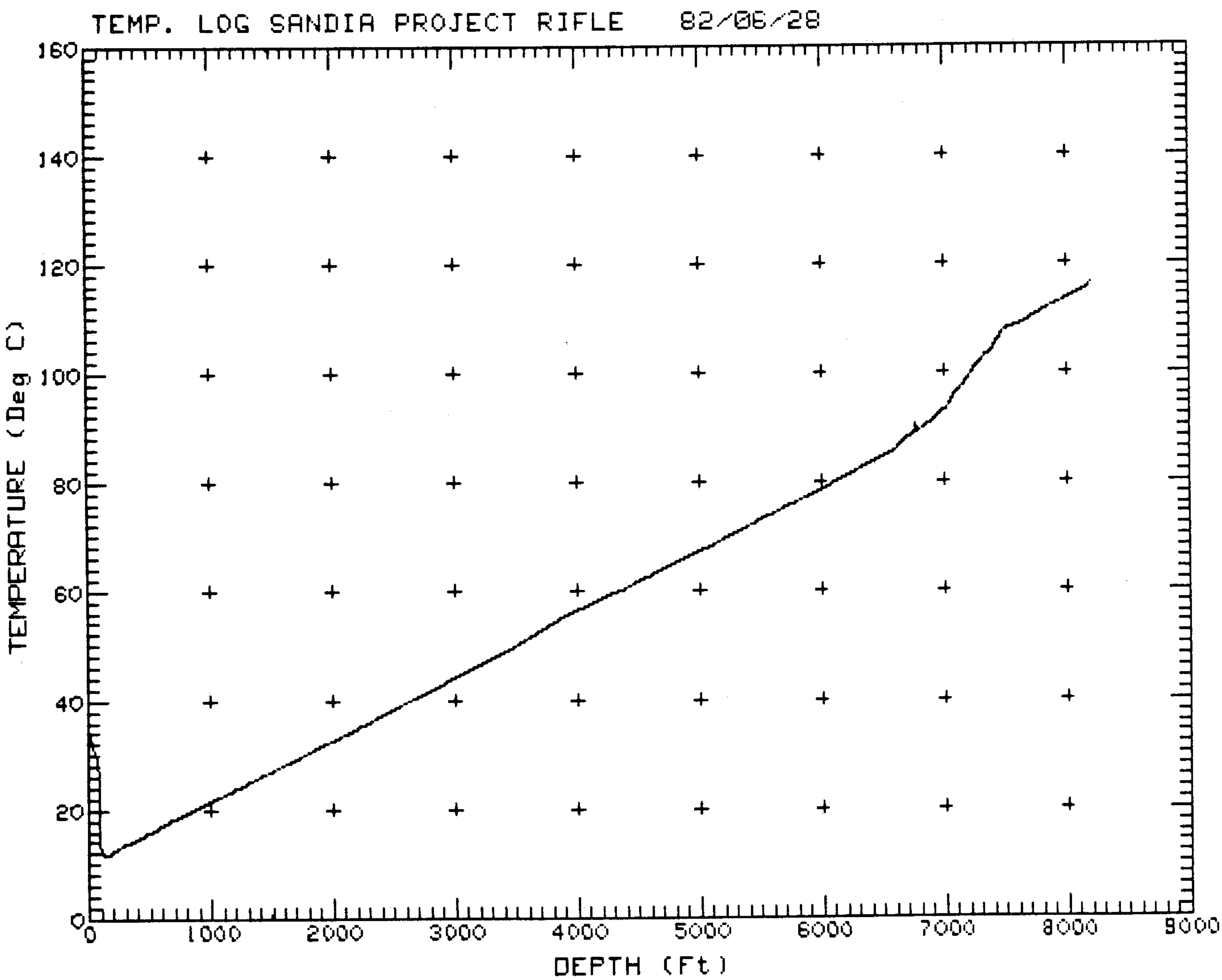

Figure 2.8 Temperature Log of MWX-1.

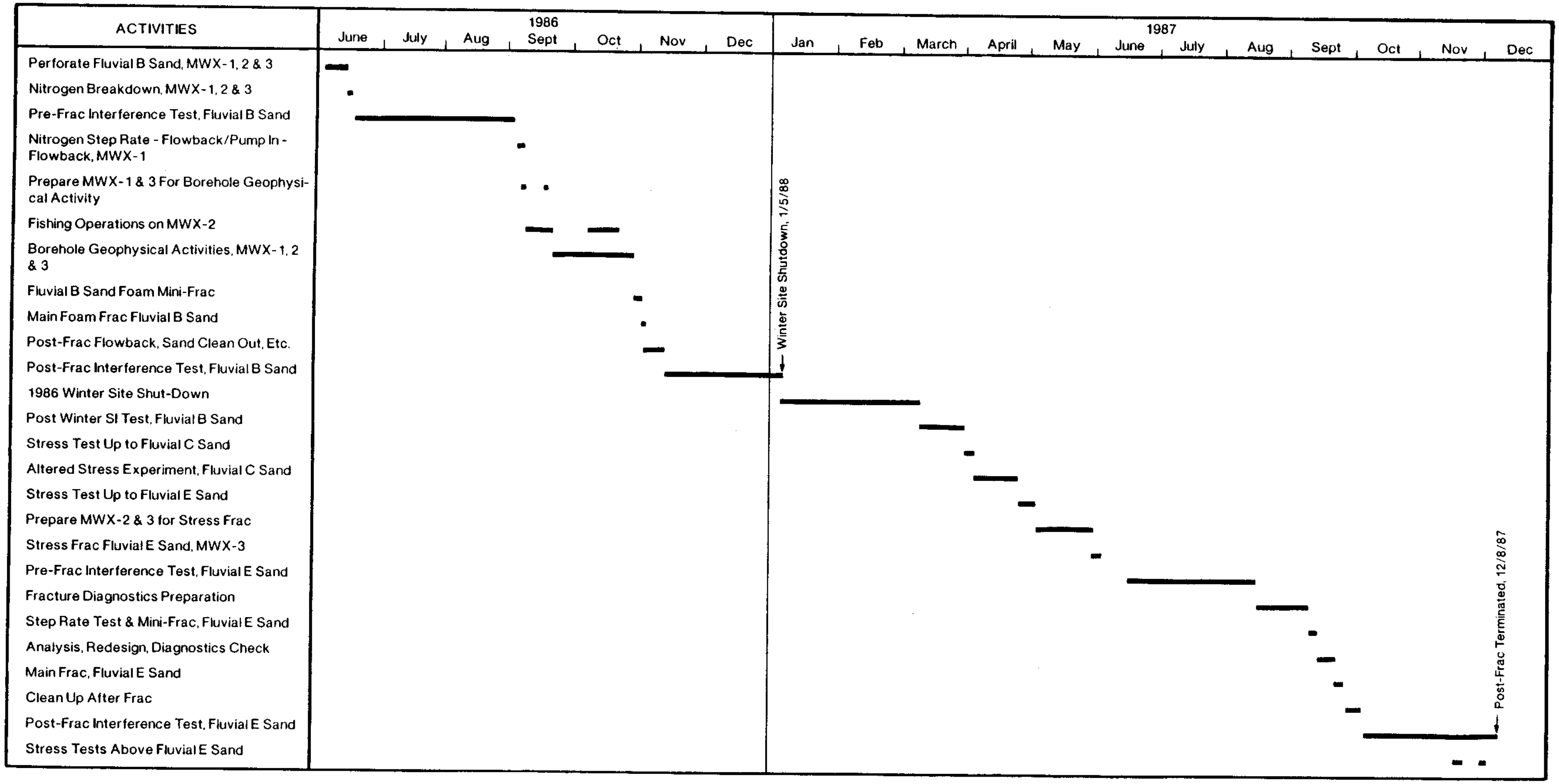

Figure 2.9 Chronology of Fluvial Operations

3.0 GEOLOGY

John C. Lorenz
Sandia National Laboratories

3.1 INTRODUCTION

The fluvial interval of the Mesaverde Formation is found between the depths of about 4300 ft and 6000 ft in the MWX wells. The strata in this interval were deposited on a low-relief alluvial plain, between delta-plain deposits (the coastal and paludal intervals) to the east (seaward), and braided stream deposits, closer to the sediment sources in the active overthrust belt to the west.

Sandstones were deposited principally in fluvial meander-belts, but also as locally extensive flood deposits, and as more restricted levee and splay deposits. These sandy units are intimately interbedded with heterogeneous mudstones, sandstones, siltstones, and carbonaceous shales that are the products of lacustrine, paludal, and broad interfluve environments.[1] The meander-belt sandstones form the reservoirs of interest in the fluvial interval at MWX, and most of the natural gas may have derived from the organic material in the interbedded fine-grained rocks. Sandy flood deposits are known only from the outcrop; none were encountered in MWX core.

The meander-belt sandstone reservoirs are irregular in shape, but broadly speaking they are elongate and tabular. Average reservoir widths are on the order of 1000 to 2500 ft,[2] and reservoir thicknesses range from 20 to 50 ft. Reservoir lengths are effectively unbounded with respect to stimulation fracture lengths and the radius of wellbore drainage.

These reservoirs are not homogeneous, but rather are composed of point-bar sandstones that are generally arcuate in plan view. The point-bar units are separated or partially separated from each other by minor lithologic discontinuities (thin mudstone layers, thin zones of carbonaceous sandstone, etc.) that control the matrix permeability distribution as well as the distribution of fractures, and, therefore, the fracture permeability.

The interval of fluvial meander-belts thins to the north and south of the MWX site, as coal-bearing delta-plain deposits thicken, probably in response to a closer proximity to the Cretaceous Interior Seaway to the north and south. The zone overlying the fluvial zone at the MWX site is a paralic interval that may be correlative to the transgression of the Lewis Shale,[3] indicating a transgression of the seaway from the embayment to the north. To the west, the entire Mesaverde Group thins (due to diminished rates of contemporaneous subsidence of the basin), to about half of the thickness at the MWX site. The fluvial interval in the west-central part of the basin is commensurately thinner, and consists of wide, extensive sand bodies deposited in both meandering and braided environments. The changes in environment and in subsidence rates produced an interval with considerably greater sandstone content (about 80 percent, as opposed to the 40 percent sandstone content in the fluvial at MWX).

The regional geography seems to have been rearranged during this time, probably in response to the early tectonism of the Laramide orogeny. Whereas the paleoshoreline trended north-northeast and the paleoslope of the coastal plain trended east-southeast during the initial phases of deposition of the Mesaverde,[4] the paleodrainage seems to have been diverted, probably toward the north (but also, possibly, to the south) by incipient elevation of the White River Uplift and Sawatch Mountains directly east of the Piceance basin. Therefore the trends of the rivers that laid down the meander-belt reservoirs (and thus the trends of the reservoirs) are not constrained at the MWX site, as it is located just west of the uplift that created the drainage diversion. Probable axial trends for six reservoirs, reconstructed from minimal subsurface data at MWX, range from east (1) to northeast (3) to north (1) to northwest (1) (see below).

As with the other Mesaverde strata at MWX, the fluvial is essentially flat-lying (Figs. 3.1, 3.2). A large horst block can be recognized on seismic lines in the basement rocks near the MWX site,[5] but these same seismic lines indicate no deformation at the level of the Mesaverde, considerably higher in the stratigraphic section. This is somewhat surprising, as elsewhere in the basin, other structures of a similar scale to this horst were reactivated and elevated during the Laramide orogeny.

3.2 LITHOLOGY

3.2.1 Introduction

The entire 1700-ft-thick fluvial interval was cored in MWX-1. Only the intervals from about 5700 ft to about 5870 ft were cored in MWX-2 and MWX-3, although 55 ft of two-inch diameter pressure core was also taken between 5485 ft and 5581 ft in MWX-2 (Fig. 3.3). Correlation of the wide, tabular, meander-belt sand bodies across the 135 to 200 ft that separate the MWX wells is very good. The correlation of the associated splays and finer-grained lithologies is much poorer, as these units are much less widespread.

Only the six reservoirs in the lower 550 ft of the fluvial interval have been fully described, as the reservoirs uphole were not tested or stimulated. These six reservoirs were designated (from the base up), A, B, C, D, E, and F (Fig. 3.3).

3.2.2 Outcrop Description

Outcrops of the Mesaverde Group that are equivalent to those penetrated by the MWX wells occur along the Grand Hogback, especially at the Rifle Gap, 12 miles northeast of the MWX site. These outcrops are principally sandstones, as most of the other strata are less erosion resistant and are eroded or covered with talus and vegetation. The Mesaverde Group at Rifle Gap has been structurally rotated about a horizontal east-west axis, and now dips between 80° to 90° to the south. Large flatirons of sandstones protrude from the hillslope, locally exposing gross sand-body morphology and plan-view (before structural rotation) surface features. The standard edge-on sections through the reservoir sandstones are less well exposed, and are commonly inaccessible as well, but from distant vantage points, lateral-accretion (point-bar) bedding planes can be seen to cut diagonally through many of the sandstones.[6]

The sandstones of the fluvial interval can be traced along the outcrop for up to 7000 ft, but statistical analysis suggests that many of the sandstones are on the order of 1000 ft wide.[2] Internally, most of these sandstones are highly heterogeneous, with superimposed beds of different grain sizes as well as major lithologic discontinuities caused by mudstone partings (from one inch to 30 ft thick) along point bar surfaces. Mud rip-up clasts are common.

Most of the sandstones were probably originally crossbedded, but syndepositional soft-sediment deformation was common, and because it is combined with abundant lichen cover at present, the measurement of paleoflow vectors (related to paleogeography and lens trends) is difficult. No statistically valid data population of crossbeds was measurable from any individual sandstone lens.

One sandstone at Rifle Gap appears to have had a history of vertical as well as lateral accretion,[6] and a sand body at Estes Gulch, one mile west of Rifle Gap, was probably deposited during a series of floods.[1] However, many of the sandstones of the fluvial interval along the Grand Hogback adjacent to Rifle Gap display point-bar accretion surfaces and are interbedded with significant volumes of overbank material, and most are therefore thought to have been deposited as meander-belt sandstones.

The interbedded overbank material consists of siltstone, mudstone, claystone, and carbonaceous shale. Fossil plant impressions and invertebrate tracks and trails are common on bedding planes, indicating subaqueous deposition, probably in well-drained swamp environments adjacent to and between meander-belts. A thin, restricted coal bed is present in the mid-fluvial interval at Rifle Gap,[7] but elsewhere coals are absent.

Fresh-water invertebrate fossils occur in some beds, but in general, both vertebrate and invertebrate fossils are rare to absent.

3.2.3 Mineralogy-Petrology

The sandstones of the fluvial interval (Fig. 3.4) consist of quartz, feldspar, and lithic fragments, and are dominantly lithic arkoses and feldspathic litharenites.[8] (Data sheets for all the mineralogy-petrology analyses are given in Appendix B.) They contain significantly more unstable grains (rock fragments and feldspar) than reservoirs in the coastal, paludal, or marine zones. Petrology studies[9] show that the E and F reservoirs (see Table 3.1) have the largest grain size (average 0.24 and 0.31 mm), whereas the B and C reservoirs have the highest porosity (eight and 14 percent, respectively). In general, the fluvial reservoirs average six to eight percent porosity, and 0.1 to 2.0 microdarcys permeability.

The D reservoir has the highest clay content at 20 percent (Table 3.1). Most of the pores observed in this section are clay-filled. Illite and mixed-layer illite-smectite are the dominant clay minerals, although chlorite and iron-bearing chlorite are locally abundant. Kaolinite is present in trace amounts in some samples. The mixed-layer clays and illite are typically fibrous, and occur as residual pore fillings and as coatings on framework grains.[8]

A few intervals of sandstone showed slightly higher than normal gamma-ray readings on the downhole gamma-ray log. Detailed petrographic analysis of one such zone[9i] showed slightly higher than usual amounts of sand grains composed of thorium- and uranium-bearing monazite, thorium-bearing xenotime, uranothorite, and zircon.

The fluvial sandstones were subjected to a complex diagenetic history. The Bendix petrology reports[9] cover five specific fluvial zones, each with a similar but slightly different paragenetic sequence. This sequence usually began with a very early stage of authigenic clay formation, although locally an even earlier phase of calcite cementation took place.

Both of these stages took place prior to significant compaction of the sediments. The next phases included the alteration/dissolution of feldspars and a second stage of authigenic clay formation, followed by cementation of the grains by both quartz and calcite. The final phase in most samples was the formation of secondary porosity by dissolution, although locally, later stages of cementation and clay formation, and even of dolomitization of calcite, took place. Much of the present porosity in these sandstones is due to the dissolution of carbonates and other unstable grains during diagenesis. The overall low porosity values are due to "abundant deformed lithic fragments which destroyed original porosity, to the extensive development of authigenic clay, or to widespread carbonate cement."[8]

3.3 RESERVOIR MORPHOLOGY

3.3.1 Introduction

The estimation of reservoir widths and orientations from four-inch diameter core is difficult, even when data from three closely spaced wells are available. The data consist primarily of sedimentological interpretations of slabbed core, supplemented by gamma ray logs in both cored and uncored intervals, and Schlumberger's SHDT (dipmeter) log in MWX-3.

Interpretations of reservoir width are made using the formulae

(1) $W_c = 6.8\ h^{1.54}$ (metric units)

(2) $W_m = 7.44\ W_c^{1.01}$ (English units)

as described in Lorenz et al.,[2] where W_c is channel width, h is bankfull channel depth (approximated by point bar thickness) and W_m is meander-belt width (taken to be approximately equivalent to reservoir width). Point bars can usually be recognized in core where sufficient core remains after sampling, although care must be used to define complete, individual sequences rather than truncated and/or amalgamated deposits.

Meander-belt reservoirs are composite both vertically and laterally, and are therefore complex. They differ from the more classically lenticular reservoirs of the paludal and coastal in that:

(1) There are more internal lithologic discontinuities, thus gross reservoir permeability and fracture patterns will be more complex.

(2) The edges of the reservoir and the internal distribution of sedimentary structures are highly irregular, therefore interpretations of reservoir position, made using spatial distributions of lithologies, are tenuous.

(3) Because of channel migration, the width of the reservoir is significantly wider than the width of the channel that deposited it, and there is a corresponding increase in the width to thickness ratio of these sandstones.

(4) Because of the high sinuosity of the rivers, local crossbedding derived from oriented core or dipmeters are indicative only of local paleoflow directions, and not necessarily of the orientation of the axis of the reservoir.

Despite all of these ambiguities, some estimate is better than none. The following interpretations are made, however, with the caveat that they represent a best estimate only.

3.3.2 Reservoir A (Figs. 3.5a and 3.5b)

Bed A_1 probably represents a single sweep of a point bar/channel system across the MWX area. It is of uniform thickness (eight ft) and has similar fining-upward gamma ray profiles in all three wells. Core from MWX-1 (Fig.3.5a) shows an uninterrupted lower point bar sequence of crossbedded sandstone grading into an upper point bar/overbank sequence of 6- to 12-inch-thick beds of rippled, rooted, and disrupted sandstone. Similar gamma ray profiles suggest that similar lithologic sequences are present in MWX-2 and MWX-3. (Note that the horizontal dimensions of the core lithology logs in Figs. 3.5 through 3.10 are exaggerated on the order of 10 times relative to these vertical dimensions, whereas the vertical dimensions of the entire figures are exaggerated on the order of five times: four-inch core does not provide as much information on lateral variability as might be suggested in these figures.)

Orientation of the sandstone body is indeterminate: no oriented core or SHDT data are available for this interval, but the reservoir is probably arcuate in shape. The sedimentary structures suggest a bankfull channel depth (point bar thickness) of seven ft, which can be converted to a meander-belt width of 550 ft. However, this small river apparently did not develop a full meander-belt, thus the isolated point-bar sequence may be only on the order of 300 ft wide, and perhaps up to twice as long. The MWX wells must be centered fairly well on this lens, in order for all three to have penetrated it.

The A_2 sandstone is well developed in MWX-1 and MWX-2, but thins significantly in MWX-3. There is in fact no guarantee that the thin sandstones in MWX-3 are correlative with those designated as A_2 in the other wells. Lens A_2 in core from MWX-1 consists of a basal, fining-upward, apparently structureless, incomplete, point bar sandstone seven to eight ft thick, overlain by several thinner units of crossbedded sandstone (also lower point bar deposits) totaling another seven to eight ft in thickness. These, in turn, grade up into rippled and distorted sandstones and siltstones of probable upper point-bar and overbank origin. Thus, lens A_2 is an amalgamated meander-belt/point-bar sandstone.

The original thickness of the point bars is unknown, but the preserved portion is the same thickness as the complete sequence in A_1, and therefore the fluvial system and its meander-belt deposits were probably larger, although by how much is moot. The poor or nondevelopment of lens A_2 in MWX-3 suggests that the bulk of the reservoir is located south of MWX-3, and that MWX-1 and MWX-2 penetrate only the edge of it. No oriented core or reliable dipmeter patterns occur in this interval.

3.3.3 Reservoir B (Figs. 3.6a and 3.6b)

On a gross scale, the B sandstone is one of the more uniform reservoirs in the fluvial zone at MWX. However, internal bedding in the core (available in all three wells) shows that the reservoir is in fact heterogeneous in detail, each well containing multiple partial point-bar sequences. The thickest point-bar sequence, that in the basal part of MWX-2, is about 10 ft thick, and seems to be relatively complete. This figure can be used to reconstruct a minimum meander-belt width of 1000 ft. Dipmeter and oriented core data from MWX-3 provide two instances of northerly paleoflow from two different point bars, while crossbeds in MWX-2 core, oriented by paleomagnetics, indicate northwesterly paleoflow. The base of the sandstone in MWX-1 seems to be about five ft lower than in the other two wells, suggesting that the original location of the channel was in that area, and perhaps subparallel to the MWX-2/MWX-3 trend, also generally north-south, where its absence restricts possible orientations. Thus, it is probable that the axis of the B reservoir trends north-south, although data are insufficient to be certain.

3.3.4 Reservoir C (Figs. 3.7a and 3.7b)

Lens C_1 appears to be a fluvial splay deposit. It is best defined in MWX-3, where several thinner beds constitute a total of six ft of rippled, fine-grained sandstone with rooting and carbonaceous material. Although there is a reasonable gamma ray response in MWX-2, core from that well shows that C_1 contains only a single foot-thick bed of sandstone, the rest of the interval consisting of thin shales and siltstones that probably originated as the splay entered a lake.

Bed C_1 does not exist in MWX-1, due either to nondeposition or to erosional scour by the base of the overlying C_2 sandstone (which is seven ft lower on MWX-1 than in the other two wells). Another distinct possibility is that C_1 is a splay derived from the basal C_2 channel, and is therefore in hydraulic communication with the basal parts of C_2 in MWX-1.

Reservoir C_2 is an amalgamated point-bar/meander-belt sequence. Seven partial point bars are recorded in MWX-1 core, the top one seeming to be a complete sequence about 13 ft thick. Insufficient core remains to draw conclusions regarding point-bar thicknesses from the other two wells. A 13-ft-thick point bar can be extrapolated to a probable meander-belt width on the order of 1400 to 1500 ft. As with bed B, deeper scour in MWX-1 suggests a northerly trend. However, limited oriented core and dipmeter data in MWX-3 indicate local northeasterly paleoflow in a lower point bar, and southeasterly paleoflow in an upper point bar, thus meander-belt orientation is not constrained. A best estimate might be a northeasterly axial trend.

3.3.5 Reservoir D (Figs. 3.8a and 3.8b)

Reservoir D seems to bifurcate from a 12-ft-thick sandstone in MWX-3 into two thinner sandstones in the other two wells. Core shows D_1 to be composed of crossbedded sandstone with coaly partings and soft-sediment deformation, with no definitive point bar-on-point bar scoured contacts. The upper two feet of this sequence becomes finer grained, rippled, and burrowed. This entire sequence is probably a single though irregular point bar 14 ft thick, which can be used to calculate a meander-belt width of 1600 to 1700 ft. D_2 is a double sandstone of ambiguous origin, with a crossbedded lower zone, and a dark, organic-rich, massive (but fining-upward) upper part.

No oriented core or definite dipmeter patterns exist through this area in either D_1 or D_2. It is possible that the channel system originated along the east-west MWX-2/MWX-1 axis, subsequently migrated laterally northward to the MWX-3 area where it deposited a thick sandstone, and then migrated back to the south where it deposited sandstone on the silts and muds that accumulated there while the river was active to the north. This interpretation would suggest an east-west meander-belt orientation.

3.3.6 Reservoir E (Figs. 3.9a and 3.9b)

E_1 is another meander-belt sandstone. In MWX-1, both gamma-ray logs and core lithology indicate a general fining-upward trend, but extensive sampling has precluded measurement of point-bar thickness. A gross estimate of 15 ft yields a meander-belt width of about 1800 ft. Two dipmeter pattern groups from MWX-3 suggest northwesterly paleoflow, but estimates of reservoir width and orientation for this zone are tenuous.

E_2 is apparently present only in MWX-1 and MWX-2, and core from MWX-1 suggests that it is a splay deposit. It contains multiple foot-thick beds of rippled sandstone, occasional 2-1/2-ft-thick crossbedded sandstone beds, and common rooting, burrowing, and soft-sediment deformation. No directional data are available for this zone, but it is thickest in MWX-1, thins toward MWX-2, and is not present in MWX-3, suggesting that the splay was derived from a southeastern source and that it was probably unrelated to lens E_1 in origin.

3.3.7 Reservoir F (Figs. 3.10a and 3.10b)

MWX-1 core from bed F is heavily sampled and was badly rubblized during removal from the core barrel, and thus an estimate of point-bar thickness (11 ft, indicating a meander-belt 1100 ft wide) is of marginal validity. Dipmeter patterns from MWX-3 show three diffuse pattern groups with northerly and northeasterly paleoflow orientations in the upper part of Bed F. The bed seems to be composite in all three wells, however, with significant intervals of mudstone separating the lower third from the upper two thirds, and it is possible that a larger meander-belt overlies the deposits of a small system, with the two reservoirs having different and unrelated orientations.

The lower sequence may be on the order of only 230 ft wide based on a possible point-bar thickness of four ft, although it seems to be present in all three wells. The orientation of this meander belt is poorly constrained.

3.3.8 Reservoir Breaks

Numerous lithologic discontinuities occur within the fluvial sandstone reservoirs. These include thin mudstone partings, zones of siderite and/or mudstone rip-up clasts, zones with a high content of carbonaceous material, thin siltstone beds, and beds of alternating sand-grain sizes. The latter type is most common, occurring throughout the reservoirs, but it probably affects reservoir permeability the least. The other types are more likely to occur nearer to the tops and bases of the reservoirs, although they are known to occur in all positions.

The B reservoir sandstone was examined, as a base-case (because it is relatively simple) representative unit for reservoir breaks. The core in this unit from all three wells shows 17 lithologic discontinuities, about half of which are grain size changes across a bedding plane (Table 3.2, Fig. 3.11). (Additional discontinuities may have been present in the 20 percent of the core that has been sampled.) No siderite rip-up zones occur in the core from this reservoir, but they are present in other fluvial reservoirs. At least one of the discontinuities in the B sandstone is composite, being a combination of both carbonaceous material and mudstone rip-up clasts.

These types of lithologic discontinuities or reservoir breaks have an important effect on the reservoir. They create a heterogeneous matrix-permeability system, wherein gas flow will be diverted along these relatively low permeability discontinuities, despite the orientation of pressure gradients, toward areas where the permeability discontinuities have been cut out by syndepositional erosion, or to where they were never deposited.

The matrix permeability system, however, is less important (by several orders of magnitude) than the permeability created by natural fractures in the sandstone. Here also the reservoir breaks play an important role, as the natural fractures commonly do not cut across these discontinuities. Thus the distribution of the natural-fracture permeability system is irregular, both vertically and horizontally, being controlled by the pre-existing irregular sedimentologic patterns, that is, by the distribution of the lithologic discontinuities.[10]

3.4 NATURAL FRACTURES

3.4.1 Mudstone Fractures

Numerous natural fractures occur in the fluvial interval.[11] By far the most common (slightly over 1000 noted, Fig. 3.12) are unmineralized, irregular, 30° to 60° shear planes in the mudstones, designated as "Type 3" fractures (see Reference 11 for definition of Types). These locally occur immediately below soft-sediment dewatering conduits in sandstones, both in outcrop[12] and in MWX core. They are most likely the result of dewatering and compaction of the mudstones. Although they are planes of weakness in the core, they do not contribute to the overall permeability of the Mesaverde, nor do they allow communication between reservoirs separated by thick mudstone intervals. In contrast to the low-stress, anisotropic sandstones, the mudstones are presently at an isotropic and lithostatic stress state,[13] suggesting that they are sufficiently plastic to close off all permeability along these perfectly mated shear planes. The absence of mineralization in all but two instances indicates that this has been true in the past as well as at present, i.e., that fluids which could have precipitated minerals never flowed along these planes after the early dewatering and compaction phases. Moreover, they commonly intersect, and are randomly oriented. Most of these planes are of limited extent (a few feet at most), even where fully exposed on outcrop.

3.4.2 Vertical Extension Fractures

The next most common type of fracture (213 noted) is a vertical, calcite- and/or quartz-filled extension fracture (Type 1, Table 3.3). One hundred seventy three of these are single, closely-spaced multiple, or en echelon fractures, the rest occur as fracture "swarms," each containing three or more adjacent fractures spaced about 0.1 ft apart. Eighty three percent of the Type 1 fractures are found in sandstone or siltstone, only two percent occur in mudstones, and the rest are found in various laminated or mixed combinations of sandstone, mudstone, and siltstone. Only a fourth of the single fractures, and none of the swarms, are located in sandstones greater than 10 ft thick.

Instances of this type of fracture extending from the sandstone reservoir into an adjacent mudstone or shale more than a fraction of an inch are unknown, and most often the fractures become narrower as they approach the contact, terminating at or just before the lithologic discontinuity. Of the known types of fracture termination (i.e., excluding categories such as "beyond the edge of the core" or "within missing core"), 44 percent of the terminations of Type 1 fractures, including swarms, are at reservoir-bounding mudstones. Thirty-four percent terminate within the sandstone, in zones of no apparent lithologic discontinuity, but four percent terminate at gradational lithology changes, and six percent are at marked grain-size changes within the sandstone. Although many thin ($\leq$ one inch) mudstone partings in the reservoirs are cut across by Type 1 fractures, the remaining 12 percent of the known terminations in core occur at such partings within the reservoir sandstones.

These fractures are important, but irregularly distributed, permeability enhancement mechanisms in the Mesaverde reservoirs.[10,14] Although permeability along the fractures as measured in the laboratory (restored-state conditions) is only of the order of hundreds of microdarcys,[15] it is still several orders of magnitude greater than the measured permeability (submicrodarcy) of the unfractured matrix sandstone. Only the tighter, well-cemented fractures could be plugged and measured in the laboratory, and the more open, wider fractures undoubtedly account for the even higher (millidarcy-scale) system permeabilities[14] measured during reservoir production tests.

All reservoirs in the MWX wells contain a dominant unidirectional fracture system, trending west-northwest.[14] This accounts for the highly anisotropic (between 10:1 and 100:1) Mesaverde reservoir permeabilities, and the minimal interference seen between the closely spaced wells at the MWX site. This unidirectional system is present in most of the fluvial reservoirs (Fig. 3.13). However, a departure from the norm occurs in the E sandstone (and possibly in the C sandstone) where several cross fractures were measured in oriented core (see Table 3.3), and where the system permeability is not nearly so anisotropic as in other reservoirs.[16] This possible set of cross fractures is located near the maximum frequency of the fracture distribution curve (Fig. 3.14). The significance of the uneven distribution is poorly understood at present, but other anomalies occur in this interval, including irregular formation stresses, anomalous fluid inclusion and isotope data from fracture mineralization, and several small thrust fractures (described below).

Even in the anisotropic systems, however, a fair degree of variation in fracture strike is present (Fig. 3.13). Outcrop studies of nearby Mesaverde fractures show that a ± 25° variation in strike is common in the regional fracture set.[10] Although a ± 40° variation is apparent in the strikes of subsurface fractures, much of the greater variability may be due to errors in the multishot techniques.

3.4.3 Other Natural Fractures

Several other types of fractures are present in core from the fluvial interval (Table 3.4). Nineteen mineralized to partially mineralized, low-angle, Type 2 fractures are present (Fig. 3.15) following thin mudstone partings within sandstone units. Slickensides and rare slickencrysts on the fracture surfaces indicate shear motion, although offset is minimal, and the motion indicated by slickensides is often oblique to the dip azimuth. These fractures may represent lateral readjustments of different layers of the sandstone during different phases of subsidence and uplift. Only one such fracture occurs in oriented core, striking east-southeast (113°).

Possibly related to the Type 2 fractures are the Type 4 fractures, which consist of slickensided low-angle shear planes, commonly mineralized with calcite slickencrysts, and which also occur in sandstones, but not along mudstone partings. Only three of these fractures are found. The offset is minimal (< one inch) but it occurred in a reverse sense of motion (thrust). Two Type 4 fractures occur in oriented core, and have strikes of 110° and 140°. This strike and the thrust motion suggest local compression from the north-northeast, most probably related to uplift and thrusting of the east-west segment of the Grand Hogback 12 miles to the north-northwest.

The rarity of these fractures suggests that they are not important to the permeability systems of most reservoirs. One of these fractures, however, occurs in the E sandstone, where other cross fractures and interwell communication exist; the other two are located in the F sandstone, which has not been tested.

One additional shear fracture of unknown affinities (Type 5) occurs in a nonreservoir sandstone (Table 3.4), and two moderate-angle shear fractures (Type 6) are found in mudstones between reservoirs. The latter differ from dewatering fractures (Type 3) in that they are more planar, and are post-compaction/post lithification in origin.

The final fracture type (Type 7) is a horizontal to subhorizontal fracture without offset. Thirteen such fractures occur, nine of them in sandstone or siltstone, and seven in sandstones more than 10 ft thick. These are usually mineralized with calcite, although quartz is also present locally. The significance of these to reservoir permeability is unknown, but five of these fractures are found in the productive E sandstone.

3.4.4 Induced Fractures

Thirty-five petal fractures and one scribe-line fracture were logged in the fluvial zone. Three-fourths of the petal fractures occur in sandstone or siltstone, and none were found in mudstones. They strike between 80°

and 130° (except for two between 40° and 50°), indicating that their orientation is controlled by the present in situ stresses.[17]

3.5 REFERENCES

1. J. C. Lorenz, "Reservoir Sedimentology of Mesaverde Rocks at the Multiwell Experiment Site and East Central Piceance Creek Basin," Sandia National Laboratories Report SAND87-0040, 1987, 42 pp.

2. J. C. Lorenz, D. M. Heinze, J. A. Clark, and C. A. Searls, "Determination of Widths of Meander-Belt Sandstones From Vertical Downhole Data, Mesaverde Group, Piceance Creek Basin," Am. Assoc. Petrol. Geol. Bull., Vol. 69, 1985, pp. 710-721.

3. J. S. Lorenz, and A. K. Rutledge, "Facies Relationships and Reservoir Potential of Ohio Creek Interval Across the Piceance Creek Basin, Oil and Gas Journal," Vol. 83, 1985, pp. 91-96.

4. D. L. Warner, Mancos-Mesaverde (Upper Cretaceous) Intertonguing Relations, Southeast Piceance Basin, Colorado, Am. Assoc. Petrol. Geol. Bull.; Vol. 48, 1964, pp. 1091-1107.

5. N. B. Waechter, and W. E. Johnson, "Seismic Interpretation in the Piceance Basin, Northwest Colorado," in R. R. Gries and R. C. Dyer (eds.), Seismic Exploration of the Rocky Mountain Region, Rocky Mountain Assoc. Geol., 1985, pp. 247-258.

6. J. C. Lorenz, and A. K. Rutledge, "Late Cretaceous Mesaverde Group Outcrops at Rifle Gap, Piceance Creek Basin, Northwestern Colorado," in S. S. Beus (ed.), Rocky Mountain Section of the Geological Soc. Am., Centennial Field Guide, Vol. 2, 1987, pp. 307-310.

7. G. H. Horn, and W. C. Gere, "Geology of the Rifle Gap District, Garfield County, Colorado," U.S. Geol. Survey Open File Report, 1954, 13 pp., 1 plate.

8. J. K. Pitman, and C. W. Spencer, "Petrology of Selected Sandstones in the MWX Wells (Northwest Colorado) and Its Relationship to Borehole Geophysical-Log Analysis and Reservoir Quality," in C. W. Spencer and C. W. Keighin (eds.), Geologic Studies in Support of the U.S. Department of Energy Multiwell Experiment, Garfield County, Colorado, U.S. Geol. Survey Open-File Report 84-757, 1984, pp. 33-66.

9. Petrology Reports Prepared by Bendix Field Engineering Corp., Grand Junction, Colorado, for Sandia National Laboratories.

   a. M. L. Dixon, D. R. Allen, and M. O. Eatough, "Preliminary Results of Mineralogy and Petrology of the High Fluvial II Interval (Depth 4490 to 4840 ft) Drill Core MWX-1," July 19, 1983, 91 pp.

b. L. M. Fukui, and R. D. Dayvault, "Preliminary Results of Mineralogic and Petrographic Analyses of the High Fluvial I Interval, MWX-2 and MWX-3, and the Fracture Zone Interval, MWX-3," July 30, 1984, 40 pp.

c. M. D. Eatough, M. L. Dixon, and M. J. Eatough, "Preliminary Results of Mineralogy and Petrology of the High Fluvial I Interval (Depth 4840 to 4960 ft) Drill Core MWX-1, March 29, 1983," 47 pp.

d. R. D. Dayvault, L. M. Fukui, and R. B. Hopping, "Preliminary Results of Mineralogic and Petrographic Analyses of the Mid-Fluvial II Interval (Depth 5300 to 5690 ft), Drill Core MWX-1," December 22, 1983, 97 pp.

e. L. M. Fukui, and R. D. Dayvault, "Preliminary Results of Mineralogy and Petrology of the Mid-Fluvial I Interval (Depth 4960 to 5300 ft), Drill Core MWX-1," September 30, 1983, 86 pp.

f. M. D. Eatough, "Preliminary Results of Mineralogy and Petrology of the Fracture Zone Interval (Depth 5700 to 5870 ft), Drill Core MWX-1," October 18, 1982, 88 pp.

g. M. D. Eatough, "Preliminary Results of Mineralogy and Petrology of the Fracture Zone Interval (Depth 5690 to 5870 ft), Drill Core MWX-2," May 26, 1983, 43 pp.

h. R. D. Dayvault, "Preliminary Results of Mineralogic and Petrographic Analysis for the Low Fluvial Interval (Depth 5873 to 6331 ft) Drill Core MWX-1," May 23, 1984, 84 pp.

i. L. M. Fukui, "SEM/EDS Analysis of an Anomalously Radioactive Sample From the High Fluvial Interval, Drill Core MWX-3," April 26, 1984, 3 pp.

10. J. C. Lorenz, P. T. Branagan, N. R. Warpinski, and A. R. Sattler, "Fracture Characteristics and Reservoir Behavior of Stress-Sensitive Fracture Systems in Flat-Lying Lenticular Formations," SPE 15244, Proceedings, Soc. Petrol. Eng. Unconventional Gas Technology Symposium, May 18-21, 1986, Louisville, Kentucky, 1986, pp. 423-436. Also in J. Petrol. Tech. 41, 615-623, June 1989.

11. S. J. Finley and J. C. Lorenz, "Characterization of Natural Fractures in Mesaverde Core from the Multiwell Experiment," Sandia National Laboratories Report, SAND88-1800, September 1988. Also, in part as SPE 19007, Proceedings of the 1989 Joint Rocky Mountain Regional Low Permeability Reservoir Symposium, Denver, CO, March 6-8, 1989, pp 721-728.

12. E. R. Verbeek, and M. A. Grout, "Fracture Studies in Cretaceous and Paleocene Strata In and Around the Piceance Basin, Colorado, Preliminary Results and Their Bearing on Fracture-Controlled Natural-Gas Reservoirs at the MWX Site," U.S. Geol. Survey Open File Report 84-156, 1984, 30 pp.

13. N. R. Warpinski, and L. W. Teufel, "In Situ Stresses in Low-Permeability, Nonmarine Rocks," SPE/DOE 16402, Proceedings, 1987 SPE/DOE Joint Symposium on Low Permeability Reservoirs, May 18-19, 1987, Dallas, Texas, pp. 125-138.

14. J. C. Lorenz, and S. J. Finley, "Differences in Fracture Characteristics and Related Production of Natural Gas in Different Zones of the Mesaverde Formation, Northwestern Colorado," SPE 16809, Proceedings, Soc. Petrol. Eng. 62nd Annual Technical Conference and Exhibition, September 27-30, 1987, Dallas, Texas, 1987, pp. 589-596. Also in SPE Formation Evaluation, 11-16, March 1989.

15. J. C. Lorenz, A. R. Sattler, and C. L. Stein, "The Effects of Depositional Environment on Petrophysical Properties of Mesaverde Reservoirs, Northwestern Colorado," SPE 19583. Proceedings of the 64th Annual Technical Conference and Exhibition of the Society of Petroleum Engineers, San Antonio, TX, October 1989.

16. P. T. Branagan, Personal Communication.

17. J. C. Lorenz and S. J. Finley, "Significance of Drilling- and Coring-Induced Fractures in Mesaverde Core, Northwestern Colorado," Sandia National Laboratories Report SAND88-1623, May, 1988.

Table 3.1

Summary of Petrology Characteristics of the Fluvial Sandstone Reservoirs*
(from the Bendix Petrology Reports[9])

Reservoir	Grain size (mm)	pore space (%)	% pore space filled with clay	Calcite (%)	Dolomite (%)	Quartz (%)	K-Feldspar (%)	Plagioclase (%)	Lithics (%)	Chert (%)	Silica overgrowths (%)	Clay not in voids (%)
A	0.19	3	97	6	10	46	1	4	9	8	0.7	4.5
B	0.17	8	99	9	2	44	tr	6	18	8	4	2
C	0.20	10	97	4	tr	50	1	8	12	6	3	5
D	0.16	2	100	7	4.5	40	2	7	9	7	1	20
E	0.24	5	99	8	2	50	3.5	9	11	7	1	3
F	0.31	3	100	9	tr	48	6	7	-	7	1.5	5

*Only average values listed for all categories

Table 3.2

Reservoir Breaks in the B sandstone

	A mudstone partings	B siderite rip-ups	C mudstone rip-ups	D carbonaceous zones	E siltstone zones	F sandstone grain-size changes	Totals
MWX-1	0	0	0	0	1	4	5
MWX-2	2	0	1	1	0	2	6
MWX-3	2	0	0	2	0	3	7
	4	0	1	3	1	9	18

Table 3.3

Vertical Extension (Type 1) Fractures, Fluvial Zone

Depth (ft) (top of fracture)	No. of* fractures	Height (ft)	Maximum width**	Strike	Dip angle	Mineral-ization phase***	Mineral-ization amount+	Top termination++	Bottom termination++	Rock type+++	Comments
MWX-1											
4271.0	1	2.6	0.8	-	90	C	C	1	1	3	en echelon
4333.7	1	1.5	0.2	-	90	C	C	3	3	2	
4341.9	1	1.1	0.2	-	90	C	C	3	3	1	
4444.5	1	0.9	0.1	-	90	C	C	1	2	3	
4491.9	1	1.7	0.4	-	90	C	C	3	1	3	
4571.4	1	2.6	0.2	-	90	C	C	3	3	3	en echelon
4581.7	1	0.4	0.1	-	90	C	C	3	3	3	en echelon
4630.3	1	0.5	0.2	-	90	C	C	5	5	3	
4705.6	1	0.2	0.2	279	90	C	C	2	2	3	
4734.8	1	1.0	0.3	-	90	C	C	1	5	6	en echelon parallel to petal fracs
4736.6	1	0.5	0.1	-	90	C	C	3	4	6	
4759.1	1	0.4	0.1	-	90	C	C	3	3	6	
4796.0	1	0.6	0.5	278	90	C	C	6	1	3	
4843.8	1	0.9	0.2	-	90	C	C	3	7	2	
4846.4	1	1.2	0.1	-	90	Q,C	C	3	6	2	
4853.6	1	1.0	0.3	-	90	C	C	3	1	2	
4877.3	1	1.0	10.3	-	90	C	PS	1	3	3	
4881.2	1	0.6	0.2	-	90	C	C	8	3	3	
4901.6	1	1.0	0.4	-	90	Q,C	C	7	6	2	

Table 3.3

Vertical Extension (Type 1) Fractures, Fluvial Zone (continued)

Depth (ft) (top of fracture)	No. of* fractures	Height (ft)	Maximum width**	Strike	Dip angle	Mineral-ization phase***	Mineral-ization amount+	Top termination++	Bottom termination++	Rock type+++	Comments
4904.6	1	1.6	1.4	-	90	Q,C	P,S	5	2	2	
4908.0	1	1.0	10.0	-	90	Q	P,S	5	7	2	
4919.7	1	0.5	0.2	-	90	C	C	5	7	6	
4983.2	1	0.4	0.1	-	85	C	C	3	3	3	en echelon
4985.2	1	5.7	1.5	-	90	C	C	1	1	3	en echelon
4999.1	1	0.1	0.1	-	90	C	C	3	3	4	
5001.4	1	0.4	0.4	-	90	C	C	5	7	3	
5014.4	2	1.0	0.3	-	90	C	C	3	6	3	2 fracs separated by 0.2 ft
5016.4	1	3.5	10.0	-	85	Q,C	P,S	2	1	3	
5034.0	1	3.1	1.4	-	90	C	C	5	6	2	
5041.2	1	0.2	0.1	-	90	C	C	5	3	2	
5067.1	1	0.3	0.3	-	50	C	C	2	2	7	
5074.9	1	0.2	0.2	-	90	C	C	5	4	2	
5078.5	1	0.4	1.0	-	80	C	C	3	1	2	irregular plane
5080.8	1	1.0	0.1	-	90	C	C	1	1	2	en echelon
5083.3	1	0.3	0.3	-	90	C	C	2	4	2	
5094.2	1	0.3	0.2	-	90	C	C	3	1	2	
5124.8	1	4.2	1.2	-	85	C	C	6	2	2	strike 25° oblique to fracture below
5124.8	1	1.6	0.3	-	90	C	C	6	3	2	
5131.9	1	2.1	1.2	-	85	C	C	2	6	2	

Table 3.3

Vertical Extension (Type 1) Fractures, Fluvial Zone (continued)

Depth (ft) (top of fracture)	No. of* fractures	Height (ft)	Maximum width**	Strike	Dip angle	Mineral-ization phase***	Mineral-ization amount+	Top termination++	Bottom termination++	Rock type+++	Comments
5140.0	1	1.0	0.4	-	90	C	C	2	2	3	
5144.4	1	2.0	0.2	-	90	C	C	1	3	2	
5152.1	1	2.7	0.5	-	85	C	C	2	2	1	en echelon
5157.9	1	0.5	0.3	-	90	C	C	1	5	6	
5199.2	1	0.5	0.2	-	85	C	C	2	1	6	
5223.8	1	1.0	0.2	-	90	C	C	1	6	3	
5227.2	1	0.3	0.2	-	90	C	C	1	3	6	
5232.0	2	0.6	0.3	-	90	C	C	5	1	3	1.5" separation of 2 fracs
5239.7	1	1.2	0.2	-	90	C	C	5	5	3	
5249.1	2	0.5	0.2	-	85	C	C	1	1	3	
5251.4	1	0.4	0.4	-	85	C	C	1	1	2	
5255.8	1	0.4	0.4	-	65	C	C	6	2	7	
5268.3	1	0.7	0.2	-	90	C	C	6	3	3	
5269.6	1	3.0	0.4	-	90	C	C	3	1	3	
5274.3	1	0.4	0.2	-	90	C	C	1	1	5	
5302.8	1	1.4	0.2	-	90	C	C	1	2	3	
5319.6	1	1.8	0.5	-	90	C	C	1	4	3	
5321.8	1	0.4	0.5	-	90	C	C	3	1	4	
5324.6	1	0.3	0.1	-	90	C	C	4	4	4	
5334.1	1	1.1	0.4	-	90	C	C	1	1	3	

Table 3.3

Vertical Extension (Type 1) Fractures, Fluvial Zone (continued)

Depth (ft) (top of fracture)	No. of* fractures	Height (ft)	Maximum width**	Strike	Dip angle	Mineral-ization phase***	Mineral-ization amount+	Top termination++	Bottom termination++	Rock type+++	Comments
5341.4	1	1.6	1.0	-	90	C	C	1	2	3	
5347.4	1	0.3	0.1	-	90	C	C	3	3	2	
5358.6	1	1.4	0.5	-	90	C	C	2	1	2	en echelon
5360.9	1	0.8	0.4	-	90	C	C	3	3	4	en echelon
5368.1	1	1.3	0.3	-	90	C	C	6	1	2	
5373.4	1	0.7	0.2	-	90	C	C	1	1	2	en echelon
5375.3	1	0.7	0.4	-	85	C	C	2	1	4	
5388.3	1	0.1	-	-	90	C	C	3	3	3	
5389.6	1	0.4	0.1	-	90	C	C	5	5	6	
5398.6	1	0.5	0.1	-	90	C	C	3	5	2	
5399.3	1	0.4	0.2	-	90	C	C	5	5	2	
5406.0	1	1.0	0.8	-	90	C	C	3	5	2	
5409.2	1	1.1	0.8	-	90	C	C	4	2	3	
5431.6	1	2.2	0.3	-	90	C	C	1	3	3	
5438.4	3	0.2	1.5	-	70	C	C	3	3	6	
5439.5	1	0.1	0.2	-	90	C	C	6	6	6	
5431.1	2	0.3	0.2	273	90	C	C	1	1	6	
5433.9	3	1.2	0.5	285	90	C	C	1	3	3	
5440.6	1	0.6	0.3	270	90	C	C	3	1	3	
5442.2	1	1.0	0.3	330	90	C	C	1	5	6	
5447.4	2	0.2	0.5	310	90	C	C	1	1	6	

Table 3.3

Vertical Extension (Type 1) Fractures, Fluvial Zone (continued)

Depth (ft) (top of fracture)	No. of* fractures	Height (ft)	Maximum width**	Strike	Dip angle	Mineral-ization phase***	Mineral-ization amount+	Top termination++	Bottom termination++	Rock type+++	Comments
5455.0	1	1.1	1.0	260	90	C	C	1	1	3	
5474.0	1	0.1	0.2	280	90	C	C	3	1	3	
5488.0	1	0.1	0.5	-	90	C	C	5	5	3	
5493.9	3	1.4	1.0	280	90	C	C	1	5	6	
5495.4	3	0.9	1.0	280	90	Q,C	C	5	1	6	
5498.4	1	0.5	0.5	290	70	C	C	1	3	6	
5503.7	3	0.9	1.0	43	90	Q,C	C	1	1	3	
5506.0	1	1.0	0.5	43	80	C	C	1	2	3	
5520.6	1	1.7	0.5	295	85	C	C	3	1	3	
5531.8	3	0.5	0.2	285	80	Q,C	C	1	1	6	
5532.1	1	0.2	0.2	325	80	C	C	2	1	6	
5541.4	1	2.2	0.2	-	90	C	C	3	3	3	
5555.5	1	0.7	0.8	-	90	C	C	3	3	3	
5557.9	1	4.0	1.0	-	90	C	C	3	3	3	
5567.1	1	0.4	0.2	-	90	C	C	7	7	6	
5578.8	1	1.9	0.2	-	90	C	C	1	3	3	
5596.9	3	0.6	0.5	-	75	C	C	1	1	6	
5606.2	3	0.3	0.4	-	90	C	C	6	6	3	
5607.9	1	0.9	0.4	-	90	C	C	1	1	3	cuts across horiz. frac
5609.7	1	0.4	0.2	-	80	C	C	1	1	3	cut by horiz. frac

Table 3.3

Vertical Extension (Type 1) Fractures, Fluvial Zone (continued)

Depth (ft) (top of fracture)	No. of* fractures	Height (ft)	Maximum width**	Strike	Dip angle	Mineral-ization phase***	Mineral-ization amount+	Top termination++	Bottom termination++	Rock type+++	Comments
5611.2	1	0.4	0.3	-	90	C	C	1	1	3	
5615.5	1	0.9	0.5	-	90	C	C	3	2	4	strike parallel to slicks on type 2
5617.8	1	0.7	0.5	-	90	C	C	2	2	3	
5628.3	1	1.2	0.6	-	90	C	C	5	3	3	
5633.0	1	1.4	0.6	-	90	C	C	7	3	3	
5634.8	1	1.2	0.2	-	90	C	C	3	1	3	
5644.8	3	0.5	0.1	-	80	C	C	1	1	6	
5648.3	1	0.9	0.2	-	90	C	C	3	3	6	
5650.0	3	0.4	0.1	-	90	C	C	1	1	6	
5652.1	3	0.6	0.1	-	90	C	C	1	1	6	
5655.8	1	0.1	0.1	-	90	C	C	3	3	4	
5661.0	1	0.6	0.4	-	90	C	C	1	1	6	
5677.2	3	1.5	0.2	-	90	C	C	1	1	6	
5692.0	1	1.6	0.6	-	90	C	C	3	5	4	
5704.0	1	1.6	0.4	-	90	C	C	3	3	3	
5707.0	1	0.1	0.1	-	90	C	C	3	3	3	
5710.4	1	0.8	0.8	-	90	C	C	3	1	3	
5712.0	1	0.1	0.1	-	90	C	C	1	1	3	
5730.4	1	6.0	3.6	-	90	C	P,S	3	1	3	
5739.7	2	1.2	0.4	-	90	C	C	3	1	6	

Table 3.3

Vertical Extension (Type 1) Fractures, Fluvial Zone (continued)

Depth (ft) (top of fracture)	No. of* fractures	Height (ft)	Maximum width**	Strike	Dip angle	Mineral-ization phase***	Mineral-ization amount+	Top termination++	Bottom termination++	Rock type+++	Comments
5774.3	1	0.7	0.1	-	90	C	C	1	1	6	parallel to petal
5777.0	1	0.8	0.2	-	90	C	C	4	5	3	
5794.0	1	0.2	0.1	-	90	C	C	1	1	6	
5811.4	1	1.5	0.2	-	90	C	C	5	3	4	
5817.2	2	1.0	0.1	-	90	C	C	1	1	3	parallel to petal
5841.7	1	0.8	0.5	-	80	C	C	3	3	3	
5845.0	1	0.1	0.1	-	90	C	C	3	3	7	
5863.9	1	1.8	7.0	-	90	C	P,S	1	2	3	possibly 2 calcite phases
5866.6	1	4.2	7.0	-	90	C	P,S	7	1	3	
5871.7	3	0.2	0.2	-	90	C	C	1	1	3	
5872.7	1	0.6	1.0	-	85	C	C	1	1	3	
5875.0	1	0.9	0.2	-	90	C	C	3	3	3	this and 3 fracs listed above all parallel (core continuous and lockable)
5887.3	1	0.4	0.5	-	90	C	C	2	1	4	
5888.6	1	1.0	0.1	-	90	C	C	3	3	5	
5890.4	1	1.0	5.0	-	85	C	P,S	3	2	5	
5892.4	1	1.4	0.2	-	90	C	C	3	1	5	
5896.9	1	0.5	1.2	-	75	C	P,S	2	6	3	this and 2 fracs listed above all parallel

Table 3.3

Vertical Extension (Type 1) Fractures, Fluvial Zone (continued)

Depth (ft) (top of fracture)	No. of* fractures	Height (ft)	Maximum width**	Strike	Dip angle	Mineral-ization phase***	Mineral-ization amount+	Top termination++	Bottom termination++	Rock type+++	Comments
5900.3	1	0.7	0.2	-	90	C	C	3	5	4	
5904.4	1	0.3	0.1	-	90	C	C	5	3	2	
5937.6	1	0.4	0.2	-	90	C	C	5	5	2	
5988.3	1	0.2	0.1	-	85	D	C	3	3	5	
5991.4	1	1.9	4.0	-	90	C	P,S	1	3	1	
5996.0	1	1.5	0.4	-	90	D	C	1	1	3	
MWX-2											
4917.4	1	0.3	0.5	-	80	C	C	2	5	3	
5567.0	1	0.6	10.2	-	85	Q,C	P,S	2	3	2	
5568.0	1	4.0	10.0	-	90	Q,C	P,S	7	7	2	
5705.4	1	0.3	0.4	-	80	C	C	1	2	3	
5718.2	3	1.4	0.6	-	90	C	C	1	1	3	
5721.2	1	0.3	0.6	-	80	C	C	3	2	3	
5741.5	1	0.5	1.0	-	90	C	P	3	4	4	
5743.3	1	3.5	7.0	-	90	Q,C	P,S	5	2	3	
5750.4	1	1.8	1.2	-	90	C	P,S	1	1	3	
5761.5	1	3.5	8.0	300	90	Q,C	P,S	1	1	3	
5775.9	1	0.8	1.0	-	90	C	C	1	1	3	
5779.6	1	2.7	2.0	-	90	C	P,S	1	1	3	
5793.6	1	2.1	1.4	-	85	C	P,S	2	4	3	

Table 3.3

Vertical Extension (Type 1) Fractures, Fluvial Zone (continued)

Depth (ft) (top of fracture)	No. of* fractures	Height (ft)	Maximum width**	Strike	Dip angle	Mineral-ization phase***	Mineral-ization amount+	Top termination++	Bottom termination++	Rock type+++	Comments
5806.4	1	0.8	0.2	-	90	C	C	1	1	6	
5814.1	1	0.5	0.4	-	90	C	P	1	1	3	
5817.8	1	0.4	0.2	-	90	C	C	3	3	3	
5826.2	1	2.7	1.5	-	85	C	P,S	1	6	3	
5832.9	1	0.4	0.3	-	90	C	C	6	1	3	
5852.5	1	0.4	0.2	-	90	C	C	3	1	0	
5858.8	1	0.8	0.2	-	90	C	C	3	3	0	
MWX-3											
4903.7	1	0.4	0.2	140	90	C	C	5	3	0	
5707.3	2	3.0	1.0	260	90	C	C	3	1	4	
5712.6	1	0.4	1.0	275	90	C	C	3	2	4	
5713.4	1	0.6	0.5	290	90	C	C	3	3	4	
5714.9	1	0.1	0.2	-	90	C	C	7	3	6	
5749.4	1	0.8	0.5	280	90	C	C	1	3	4	
5760.3	1	0.5	0.5	80	90	C	C	1	3	6	
5767.2	2	0.4	0.2	90	90	C	C	3	2	6	
5769.5	1	0.4	0.3	280	90	C	C	1	1	3	
5780.0	1	0.8	1.0	295	90	C	C	7	2	3	
5783.3	1	0.3	0.2	290	90	C	C	7	1	4	
5788.8	3	0.2	0.2	280	90	C	C	7	3	6	

Table 3.3

Vertical Extension (Type 1) Fractures, Fluvial Zone (continued)

Depth (ft) (top of fracture)	No. of* fractures	Height (ft)	Maximum width**	Strike	Dip angle	Mineral-ization phase***	Mineral-ization amount+	Top termination++	Bottom termination++	Rock type+++	Comments
5787.7	1	0.4	0.2	90	90	C	C	7	7	6	
5800.1	1	0.5	0.2	-	90	C	C	5	5	0	
5803.7	1	0.7	0.3	-	90	C	C	3	3	5	
5807.3	1	2.5	0.3	305	90	C	C	4	1	3	
5809.5	1	0.3	10.0	310	90	Q,C	P,S	2	2	3	en echelon
5820.9	1	0.8	1.0	290	90	C	C	1	4	3	
5845.2	1	0.2	0.1	-	90	C	C	7	1	2	
5850.1	1	0.3	0.2	-	90	C	C	1	1	6	
5850.7	1	0.8	1.0	-	90	C	C	1	1	5	
5851.8	2	0.1	0.5	-	90	C	C	1	1	6	
5854.6	1	0.4	0.3	-	80	C	C	1	1	6	

*Number of fractures: multi-stranded fractures where strands are closer than 0.1 ft are counted as 1 fracture
**Fracture width is the separation of the sandstone walls, not the opening within the mineralization
***Mineralization phase: C = calcite, Q = quartz, D = dickite
+Mineralization amount: C = complete, P = partial, S = subhedral crystals (note that much "complete" fill looks patchy and incomplete on split fractures)
++Termination codes for top and bottom of fracture

1. at contact with bounding mudstone
2. out of core (unknown)
3. within the same lithology
4. at a gradational lithology change
5. at a mudstone parting
6. at a sandstone grainsize change
7. sampled (unknown)

+++Rock type code

0. thinly laminated mudstone and siltstone
1. coarse sandstone
2. medium sandstone
3. fine sandstone
4. fine sandstone with mudstone laminations
5. mixed siltstone and mudstone
6. siltstone
7. mudstone
8. coal
9. unknown

Table 3.4

Other Natural Fractures, Fluvial Zone

Type of* fractures	Depth (ft) (top of fracture)	Height (ft)	Maximum width**	Strike	Dip angle	Dip azimuth	Slickenside bearing	Mineral-ization phase***	Mineral-ization amount+	Top termination++	Bottom termination++	Rock type+++	Comments
	MWX-1												
7	4543.6	-	-	-	10	-	-	-	-	-	-	-	
5	4909.1	0.9	-	-	80	-	-	Q,C	P,S	7	5	2	strike-slip motion
2	5035.6	0.2	-	-	35	-	-	-	-	2	2	4	
2	5036.2	-	-	-	20	-	-	-	-	2	2	4	
2	5304.8	0.1	-	-	30	-	-	C	P	2	2	4	
2	5429.9	-	-	-	30	200	200	-	-	2	2	4	
7	5438.5	-	-	-	15	70	220	C	P,S	2	2	4	
4	5474.0	-	-	290	15	20	230	C	P,S	2	2	3	slickencrysts, reverse motion
4	5475.0	-	-	230	15	230	60	C	P,S	2	2	3	slickencrysts, reverse motion
7	5475.3	-	3.0	-	15	-	-	C	C	2	3	3	
2	5491.2	-	-	-	10	210	20	-	-	2	2	4	
2	5527.8	0.1	-	310	30	45	255	C	P,S	2	2	4	slickencrysts, reverse motion
2	5528.0	0.2	-	-	35	55	255	-	-	2	2	4	
2	5528.2	0.3	-	-	50	235	215	-	-	2	2	4	
7	5529.8	0.1	1.4	-	20	-	-	C	P,S	2	3	3	
7	5530.4	0.1	1.0	230	20	-	-	Q,C	P,S	2	2	3	
4	5530.9	-	-	-	10	-	265	Q,C	P,S	2	2	3	reverse motion
2	5543.2	-	-	-	-	-	-	-	-	2	2	4	

Table 3.4

Other Natural Fractures, Fluvial Zone (continued)

Type of* fractures	Depth (ft) (top of fracture)	Height (ft)	Maximum width**	Strike	Dip angle	Dip Azimuth	Slickenside Bearing	Mineral-ization phase***	Mineral-ization amount+	Top termination++	Bottom termination++	Rock type+++	Comments
7	5562.6	-	-	-	10	-	-	C	P	2	2	4	
6	5602.0	-	-	-	45	-	-	-	-	2	2	7	
7	5608.6	-	0.2	-	10	-	-	C	P	2	2	3	
7	5610.0	-	0.5	-	10	-	-	C	P	2	2	4	
2	5611.0	-	-	-	10	-	-	C	P,S	2	2	4	
7	5611.7	-	0.2	-	10	-	-	C	P	2	2	3	
2	5616.2	-	-	-	30	-	-	-	-	2	3	4	
2	5624.7	-	-	-	50	-	-	-	-	2	2	4	
2	5745.8	-	-	-	60	-	-	-	-	2	2	6	
2	5752.3	0.1	-	-	15	-	-	C	P,S	2	2	4	
7	5754.1	-	1.0	-	10	-	-	C	C	2	2	3	
2	5810.4	-	-	-	30	-	-	-	-	2	2	4	
2	5811.7	-	-	-	-	-	-	C	P,S	2	2	5	
2	5826.2	-	-	-	30	-	-	-	-	-	-	4	follows soft-sediment swirl
	MWX-2												
7	5566.6	0.2	2.0	-	40	-	-	C	C	2	2	2	
7	5567.6	0.1	-	-	30	-	-	Q	P,S	2	2	2	
2	5701.0	0.3	-	-	45	-	-	-	-	2	2	4	
2	5705.3	0.1	-	-	30	-	-	-	-	2	2	4	
6	5748.5	0.3	-	-	50	-	-	-	-	2	2	7	

Other Natural Fractures, Fluvial Zone (concluded)

Type of* fractures	Depth (ft) (top of fracture)	Height (ft)	Maximum width**	Strike	Dip angle	Dip azimuth	Slickenside bearing	Mineral-ization phase***	Mineral-ization amount+	Top termination++	Bottom termination++	Rock type+++	Comments
2	5849.6	-	-	-	25	-	-	-	-	2	2	5	slicks 45° oblique to dip
2	5850.8	-	-	-	15	-	-	-	-	2	2	5	slicks 20° oblique to slicks of above frac
	MWX-3												
2	5728.5	-	-	-	10	160	-	-	-	-	-	4	
2	5740.4	-	-	-	10	55	55	-	-	2	2	4	
2	5740.9	-	-	-	10	35	345	-	-	-	-	4	
2	5778.2	-	-	-	15	0	0	-	-	-	-	4	
2	5805.0	-	-	-	65	310	290	-	-	-	-	4	
7	5855.6	-	0.3	-	10	-	-	C	C	3	3	6	

*Type of fracture:
2. shear along mudstone parting within sandstone
4. shear showing motion, cuts across bedding
5. miscellaneous shear
6. planar fracture (shear?) in mudstone
7. subhorizontal, no shear apparent

**Fracture width is the separation of the sandstone walls, not the opening within the mineralization

***Mineralization phase: C = calcite, Q = quartz

+Mineralization amount: C=complete, P = partial, S = subhedral crystals

++Termination codes for top and bottom of fracture:
2. out of core (unknown)
3. within same lithology
5. at mudstone parting
7. sampled (unknown)

+++Rock type:
2. medium sandstone
3. fine sandstone
4. fine sandstone with mudstone laminations
5. mixed sandstone and mudstone
6. siltstone
7. mudstone

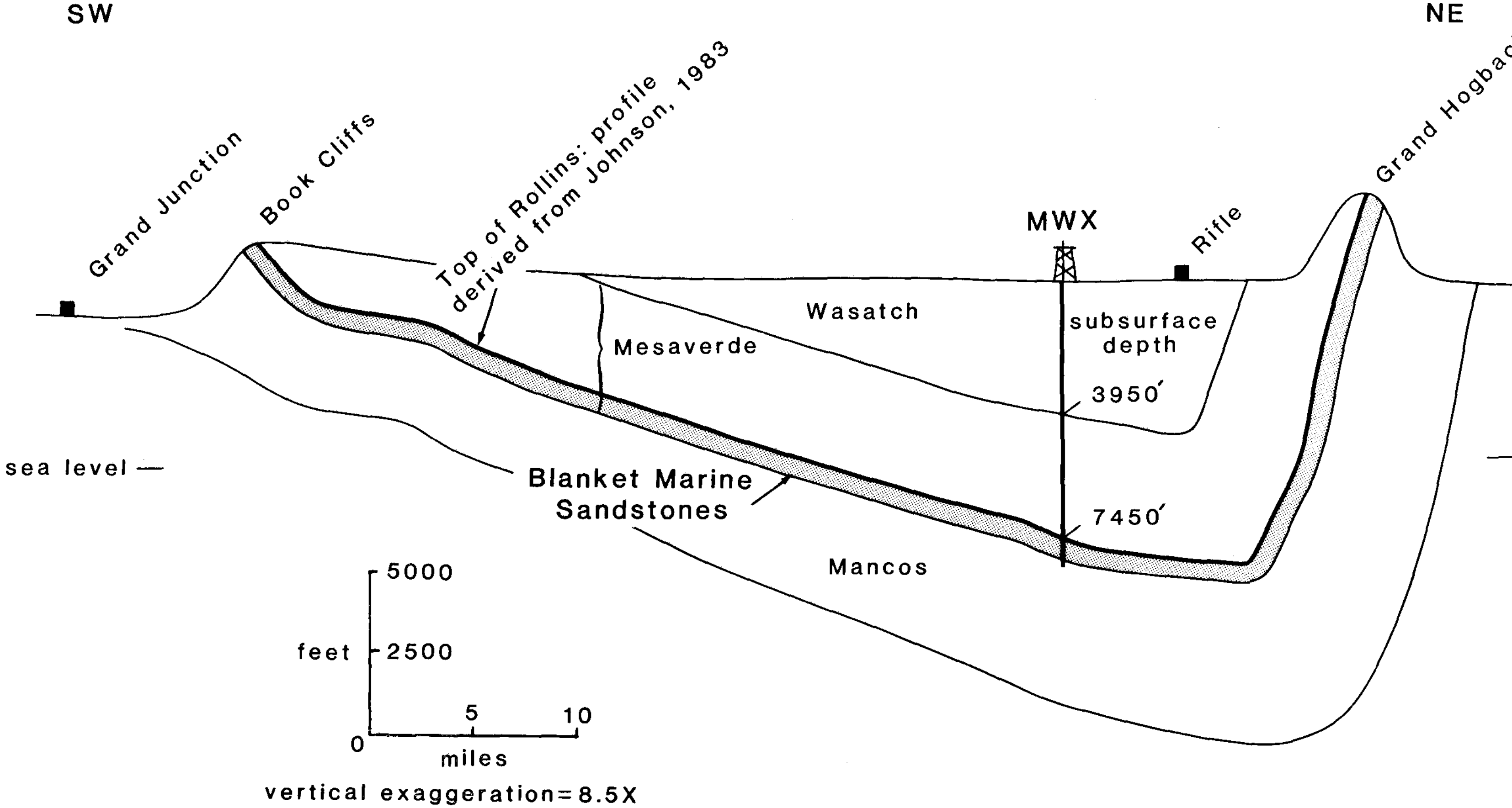

Figure 3.1 General Structure of the Mesaverde Formation in the Piceance Creek Basin

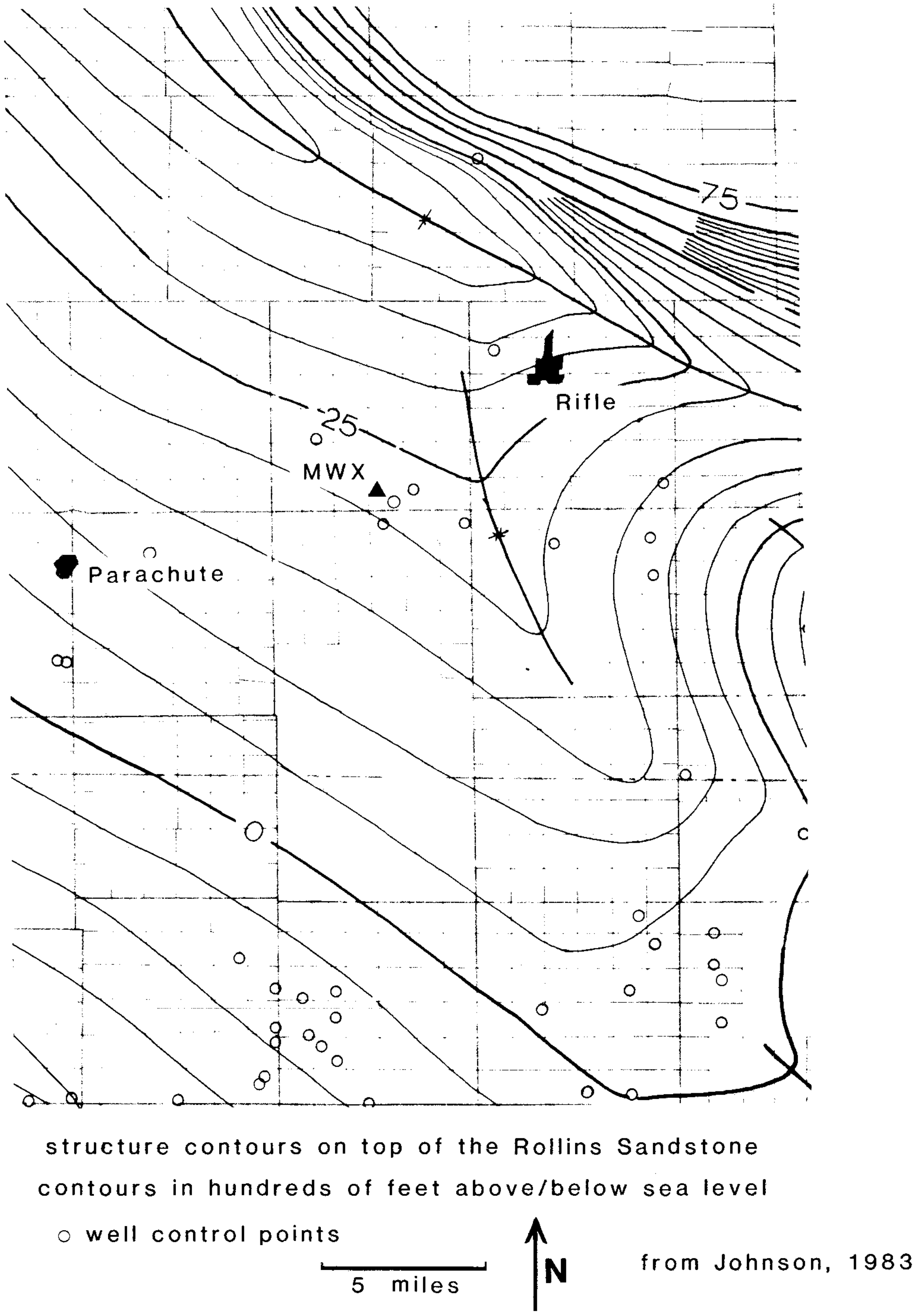

3.2 Structure Contours on Top of the Rollins Sandstone: Contours in Hundreds of Feet Above/Below Sea Level (from Johnson[12])

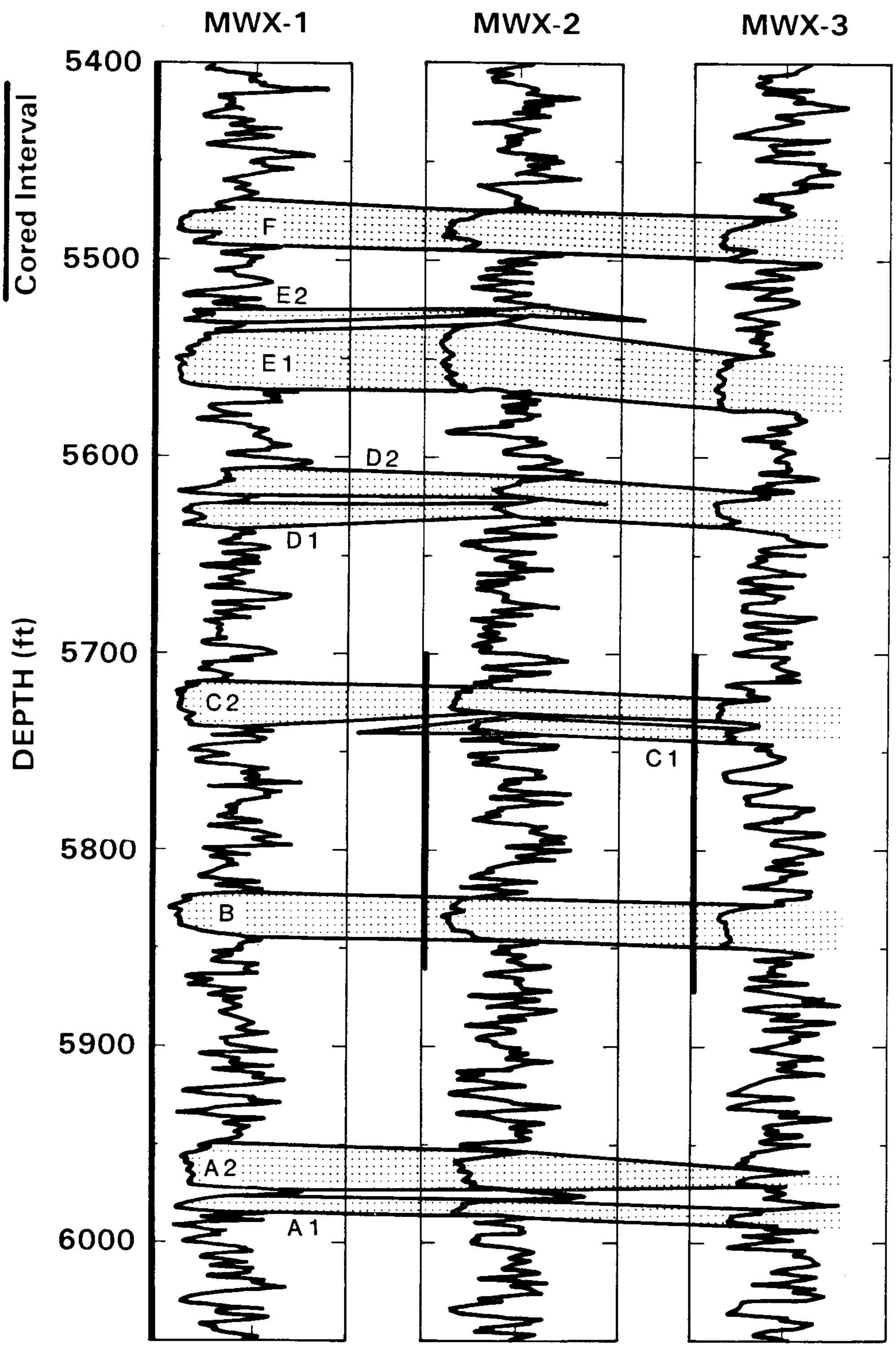

Figure 3.3 Correlated Gamma-Ray Logs and Reservoir Nomenclature for the Lower Fluvial Interval

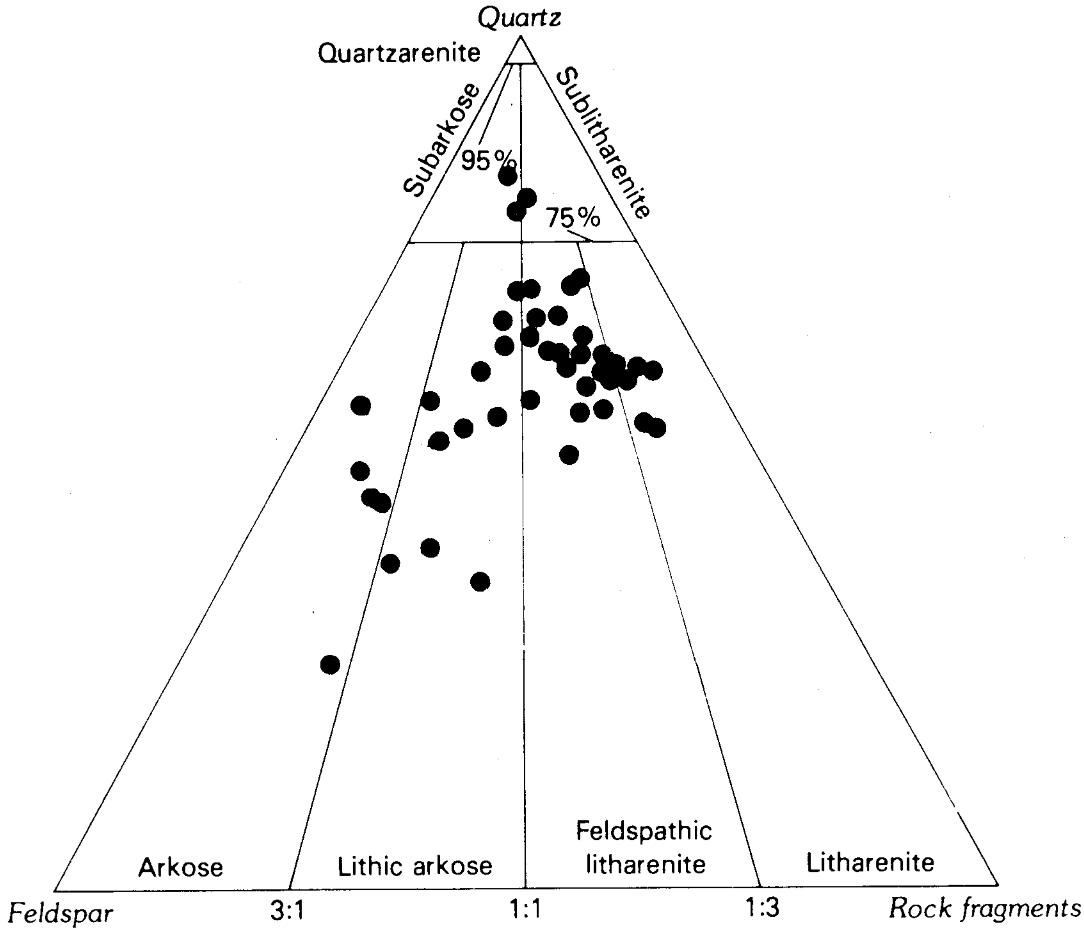

Figure 3.4 Ternary Diagram of Mineralogic Composition of Sandstones in the Fluvial Interval (from Pitman and Spencer[8])

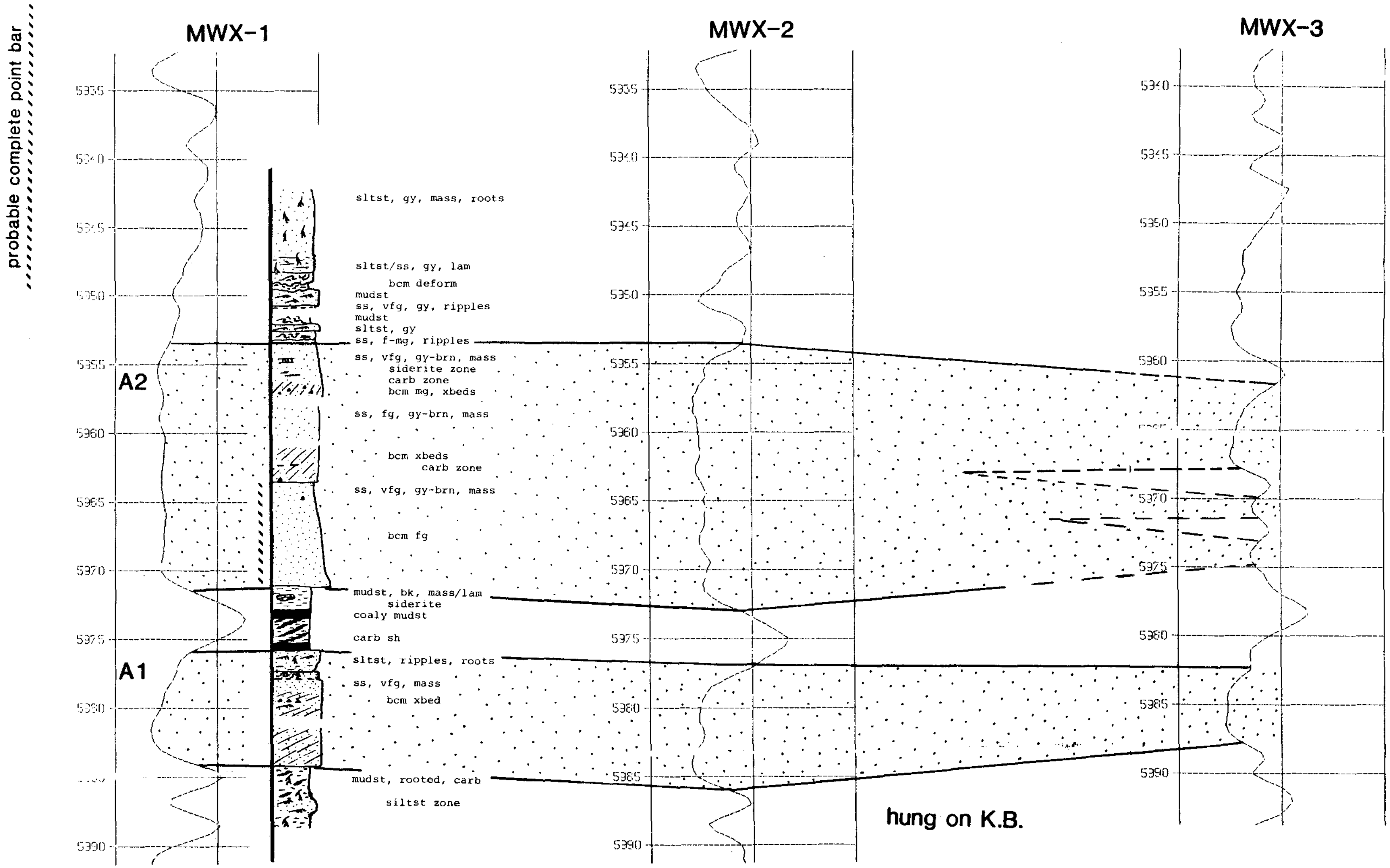

Figure 3.5a Core Lithology, Gamma-Ray Logs, and Correlation of the A Reservoirs

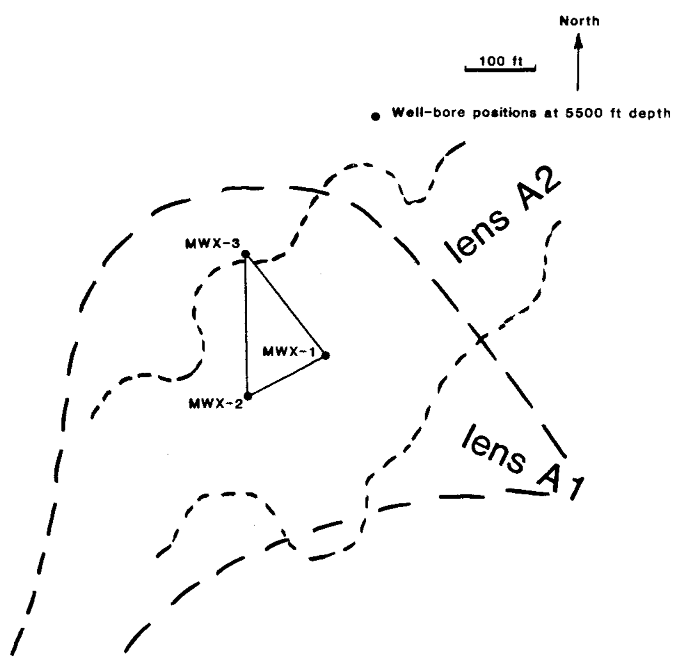

Figure 3.5b Reconstructed Size and Trend for the A Reservoirs

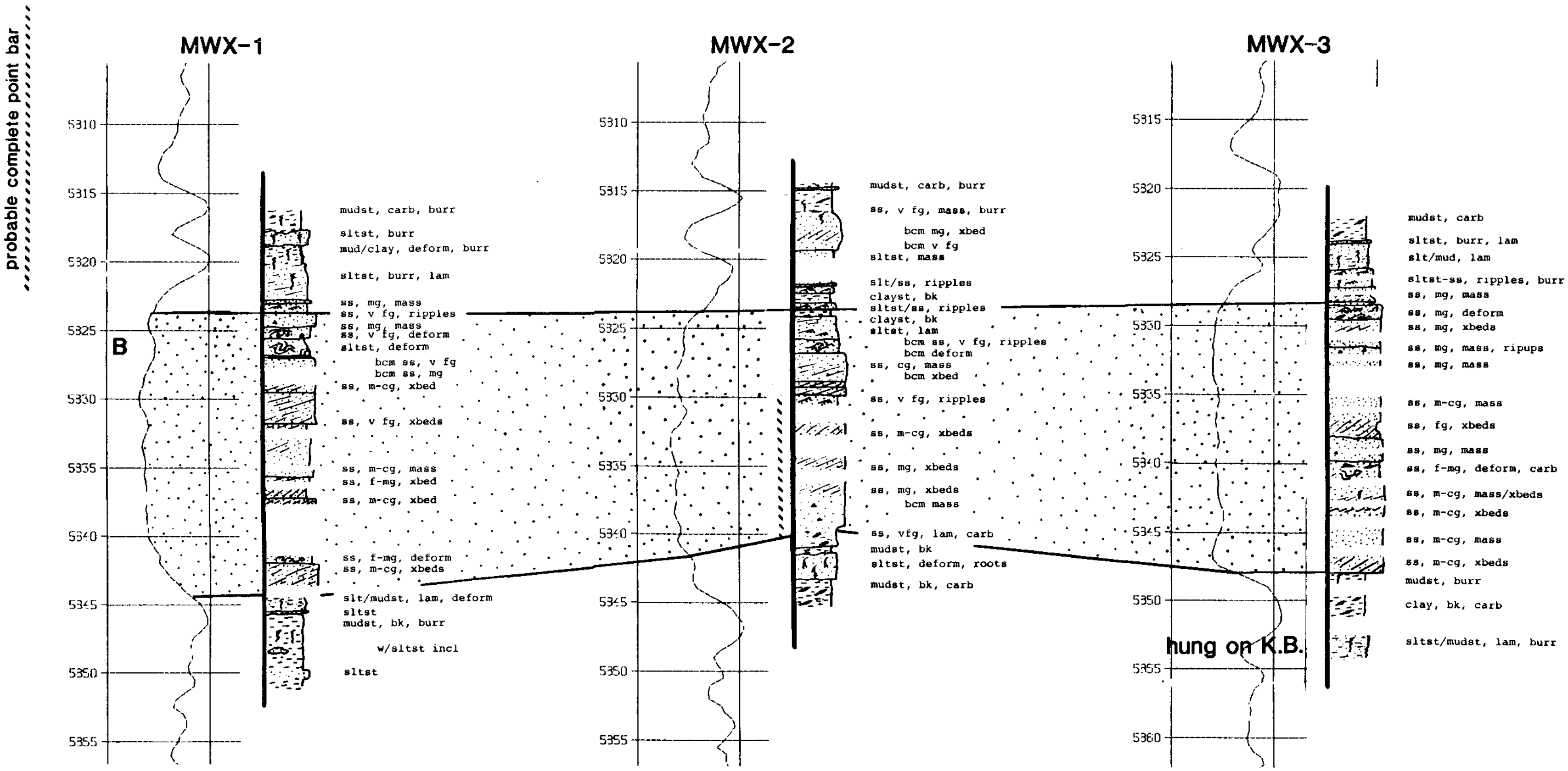

Figure 3.6a Core Lithology, Gamma-Ray Logs, and Correlation of the B Reservoir

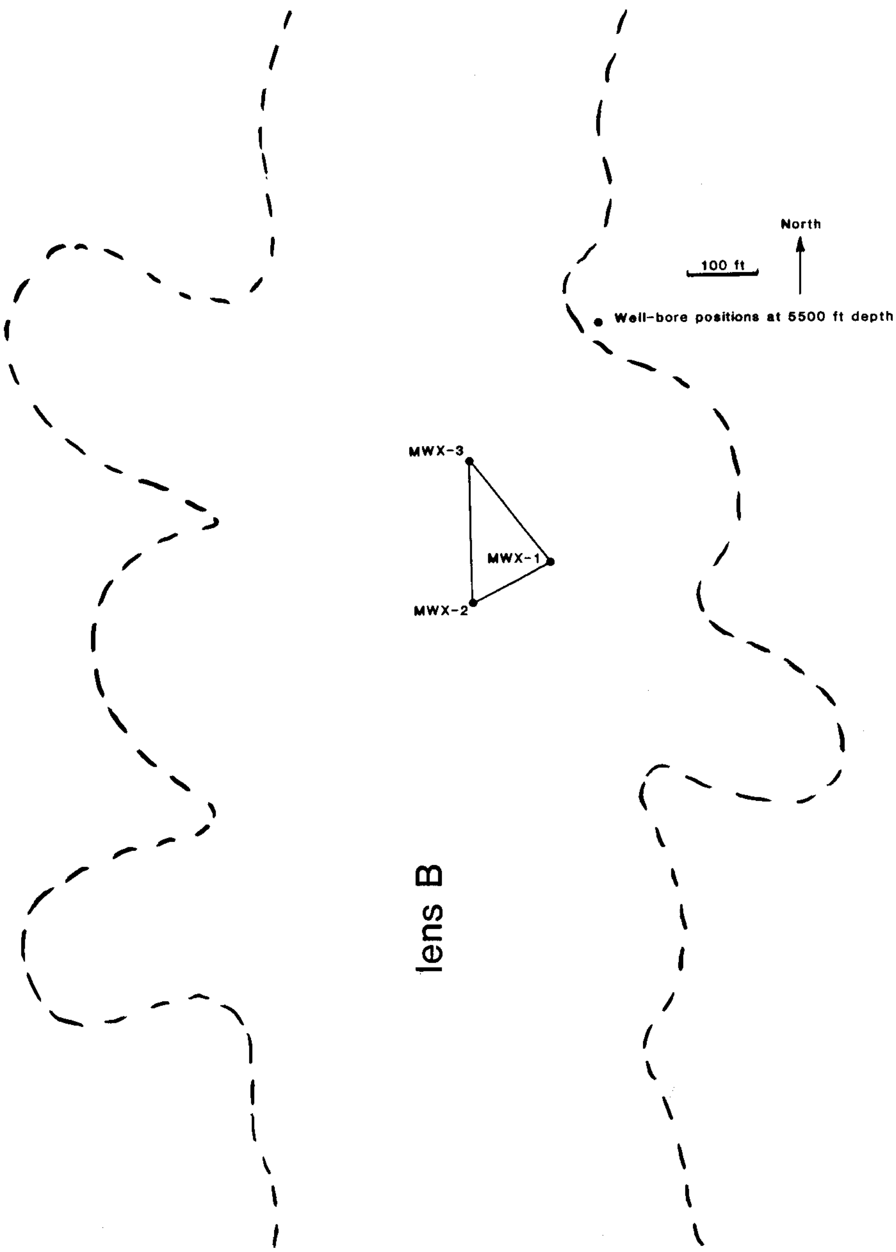

Figure 3.6b Reconstructed Size and Trend of the B Reservoir

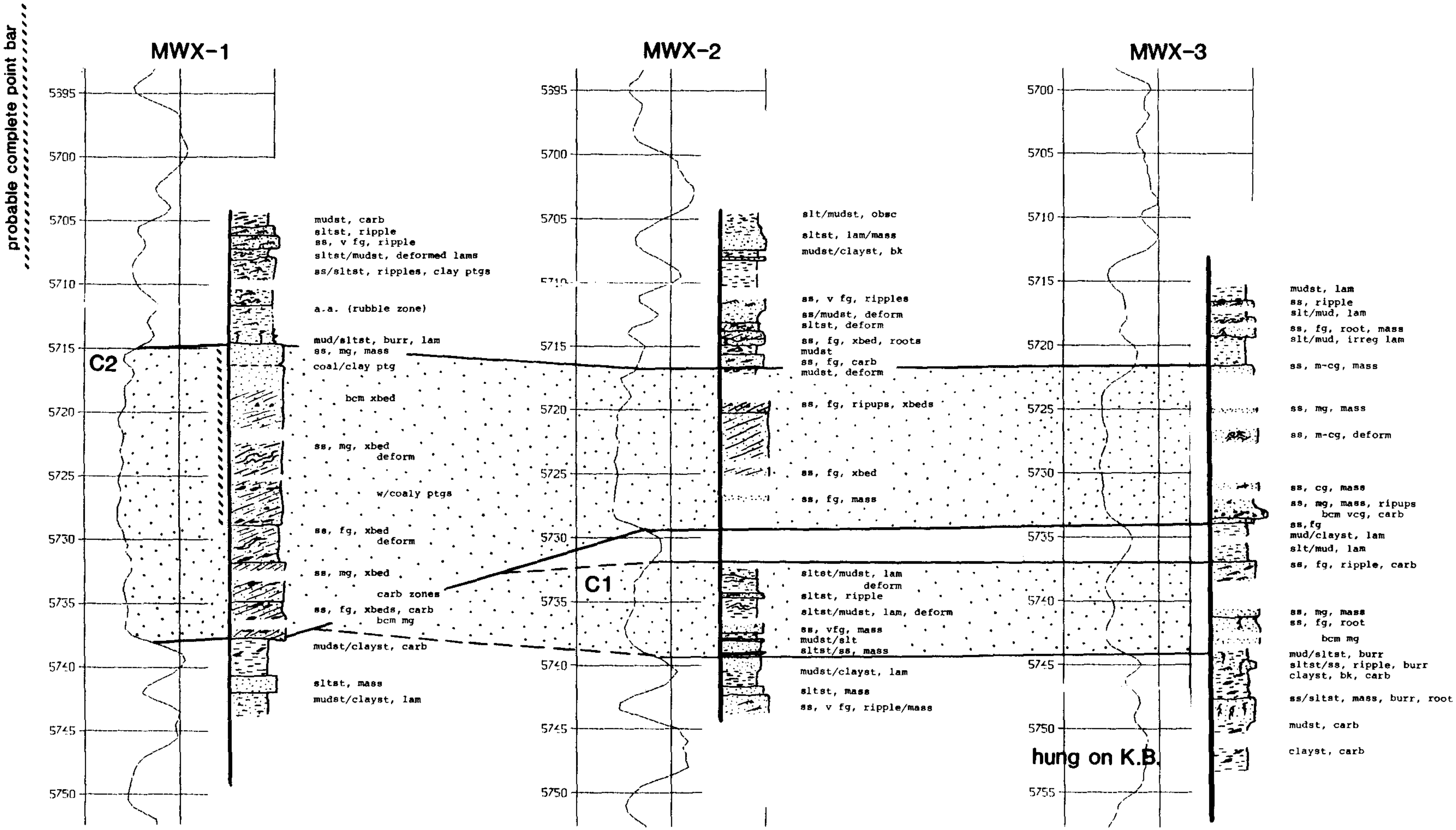

Figure 3.7a Core Lithology, Gamma-Ray Logs, and Correlation of the C Reservoirs

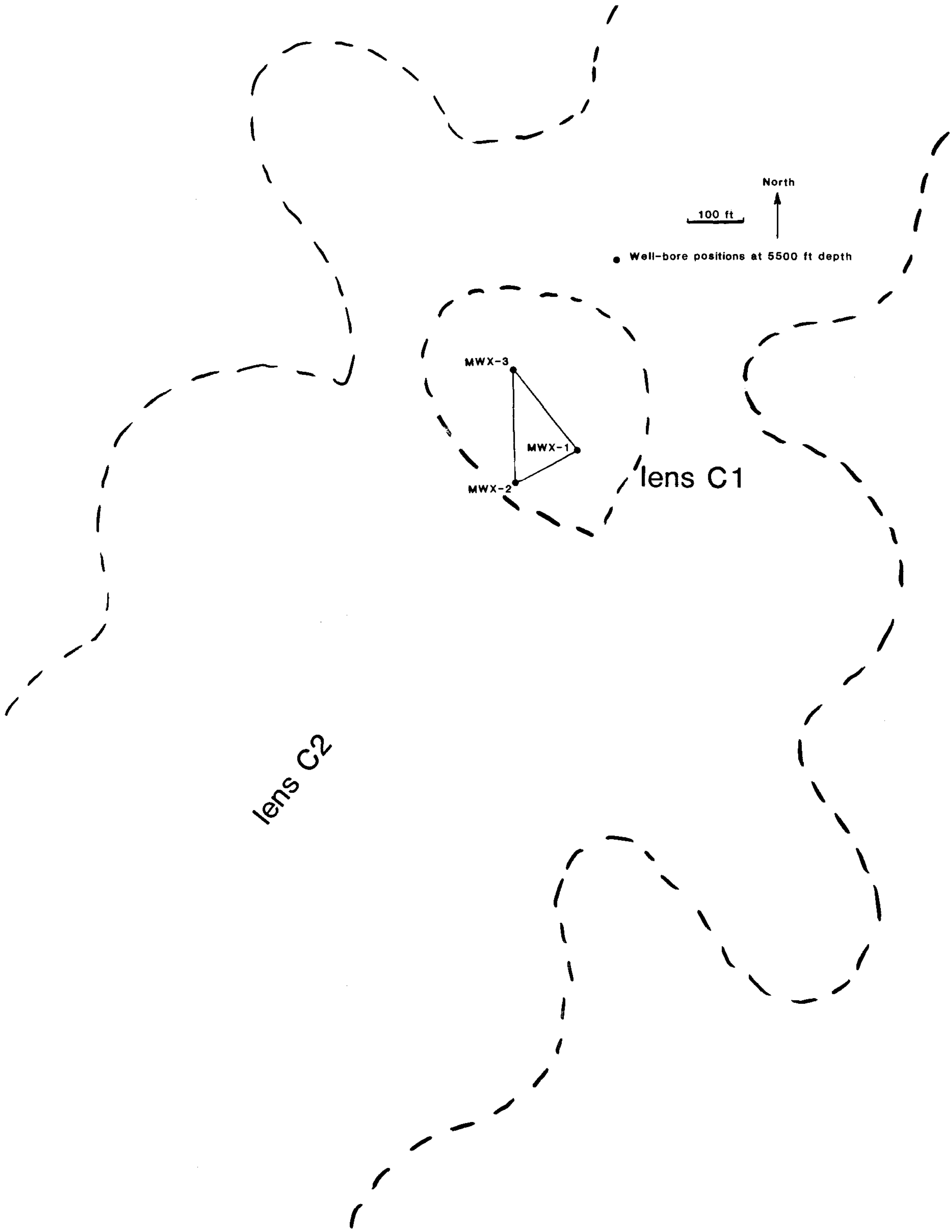

Figure 3.7b Reconstructed Size and Trend of the C Reservoirs

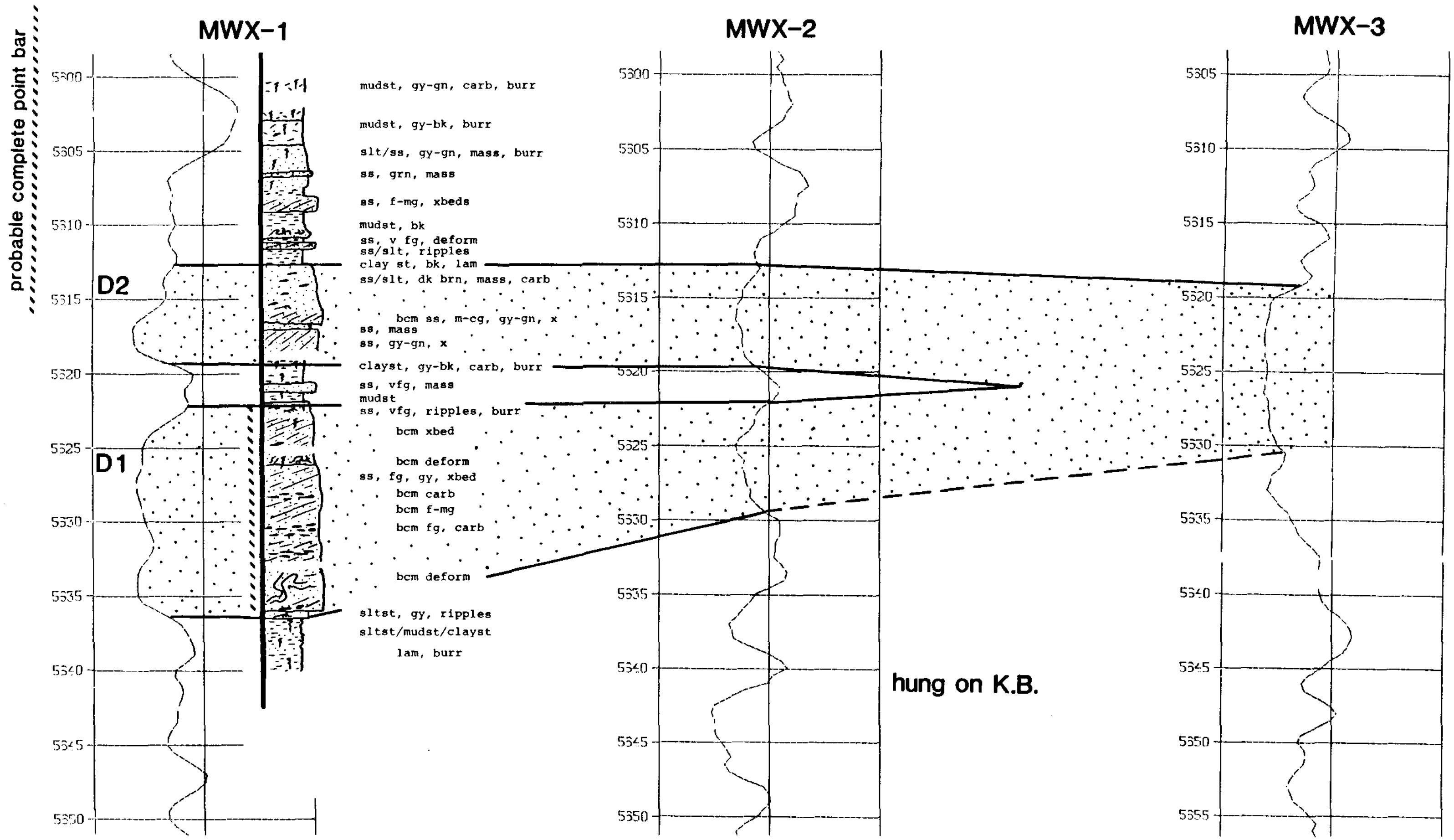

Figure 3.8a Core Lithology, Gamma-Ray Logs, and Correlation of the D Reservoir

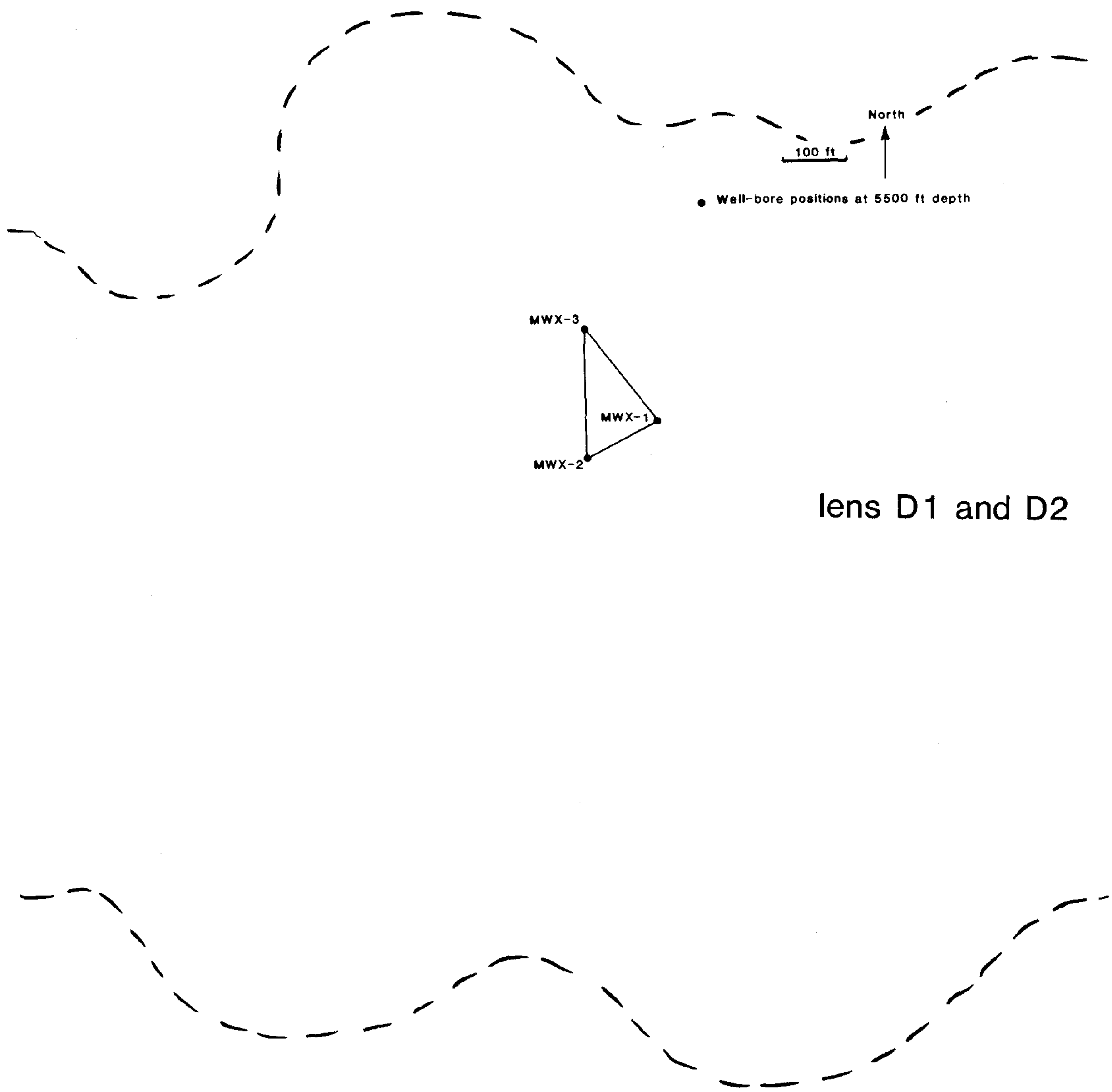

Figure 3.8b Reconstructed Size and Trend of the D Reservoir

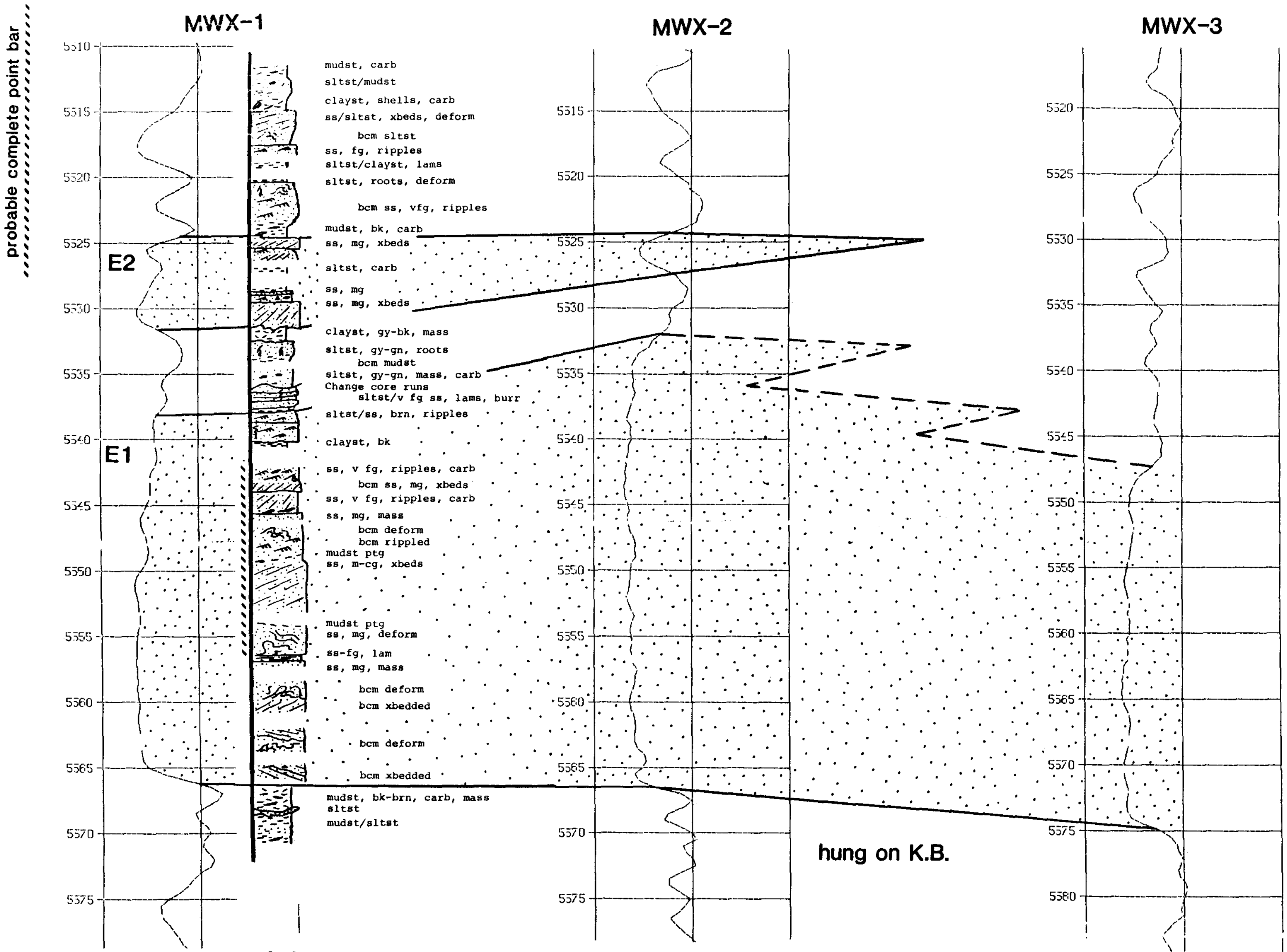

3.9a. Core Lithology, Gamma-Ray Logs, and Correlation of the E Reservoirs

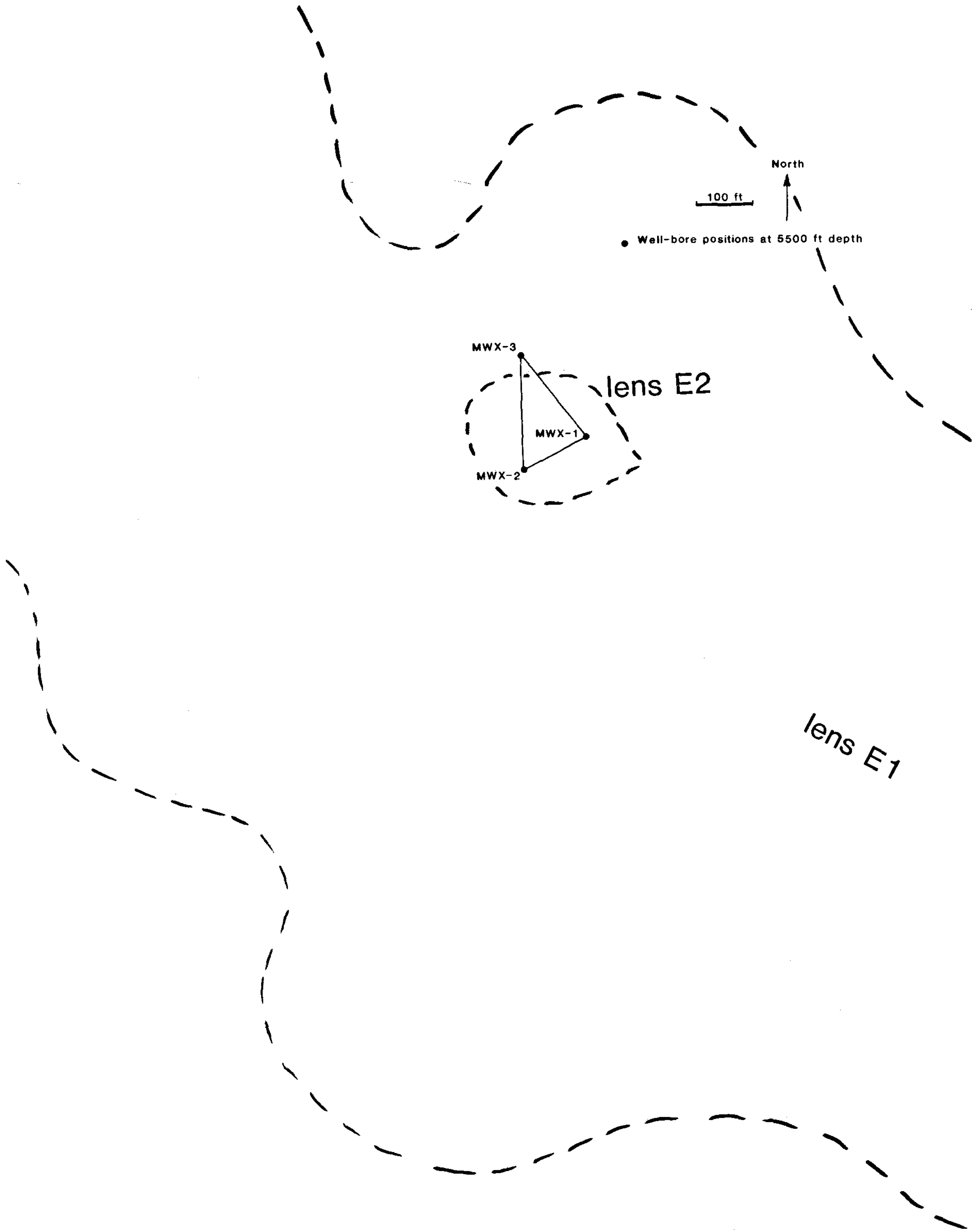

Figure 3.9b Reconstructed Size and Trend of the E Reservoirs

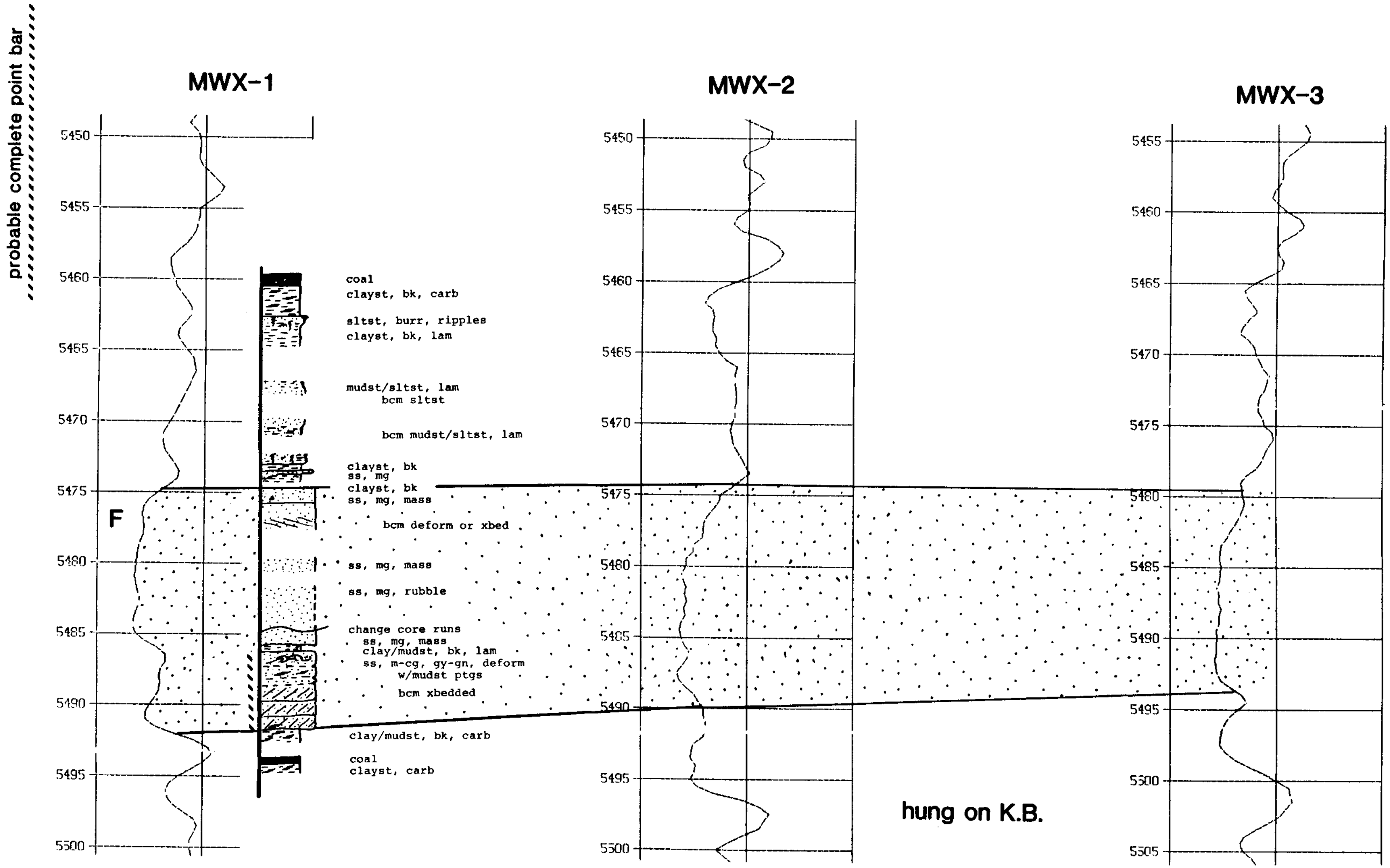

Figure 3.10a Core Lithology, Gamma-Ray Logs, and Correlation of the F Reservoirs

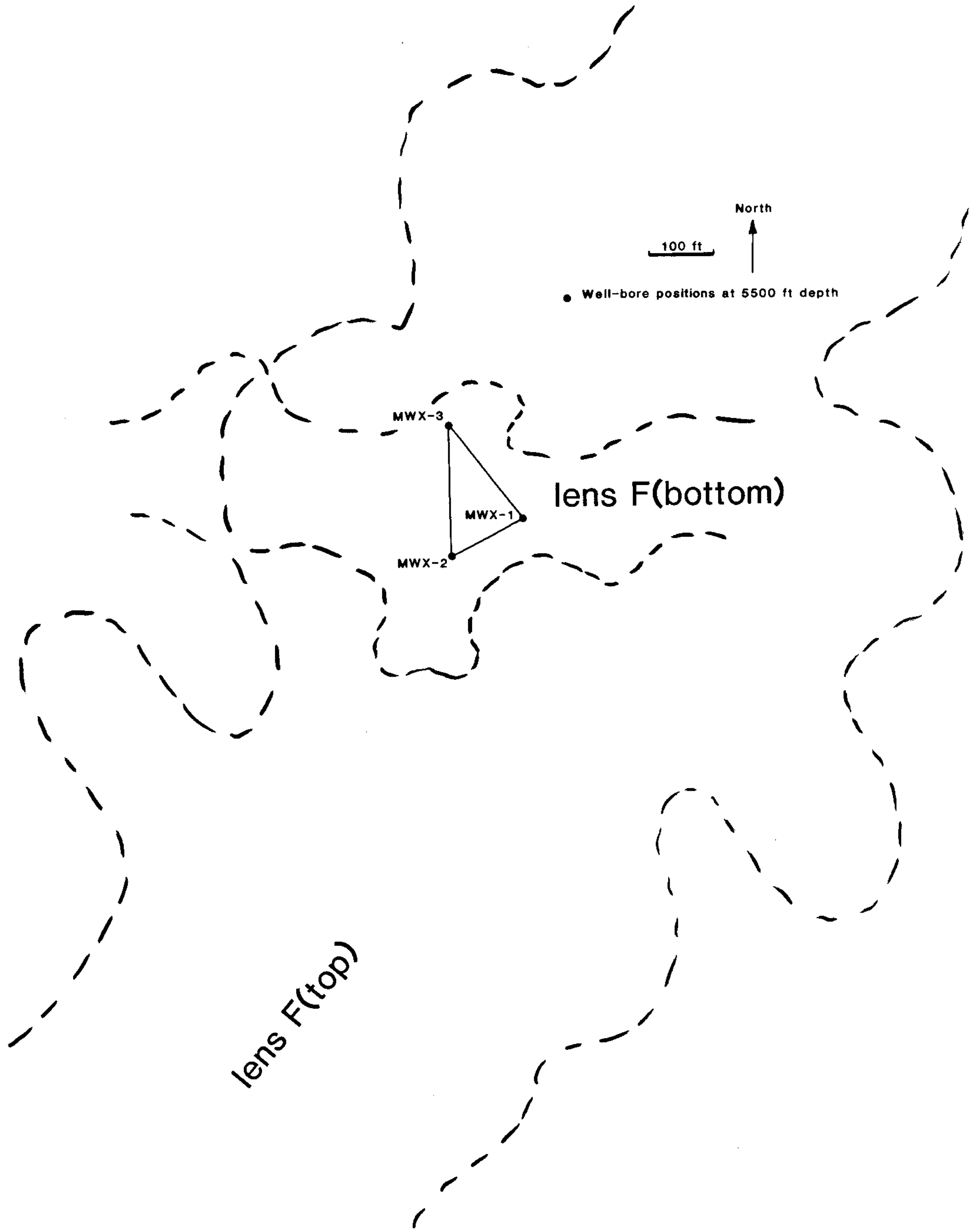

Figure 3.10b Reconstructed Size and Trend of the F Reservoirs

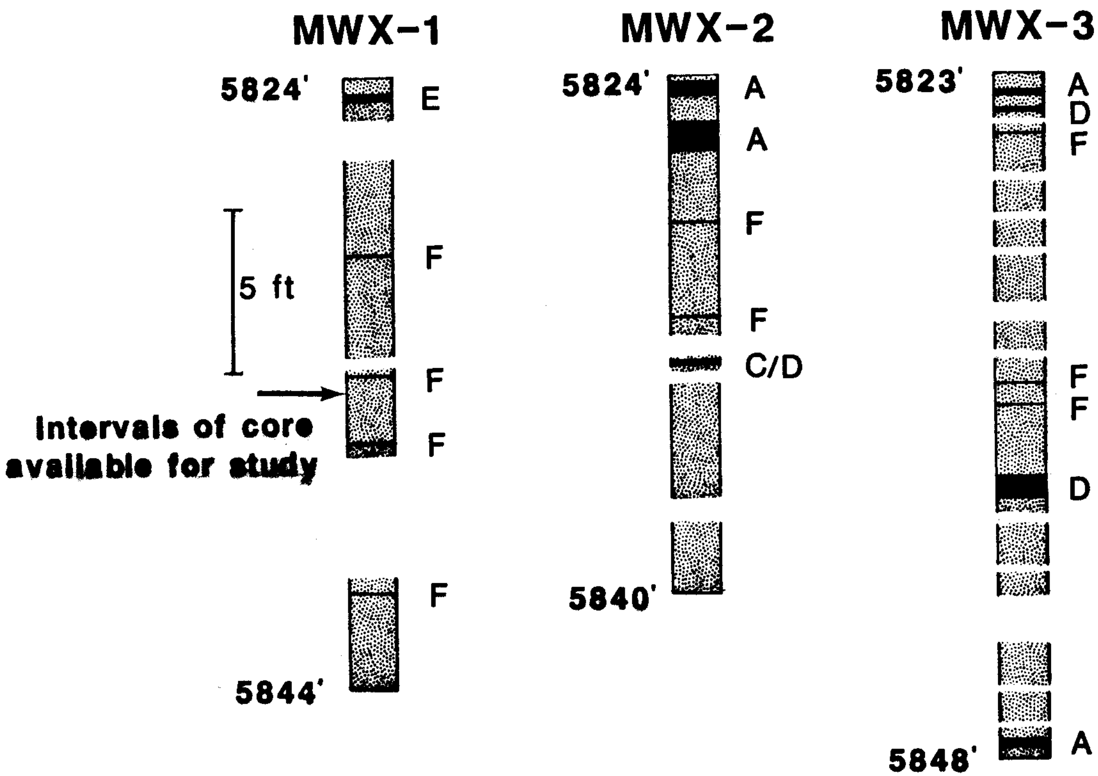

Figure 3.11 Reservoir Breaks/Lithologic Discontinuities Present in the B Reservoir (Letter Code Keyed to Table 3.2)

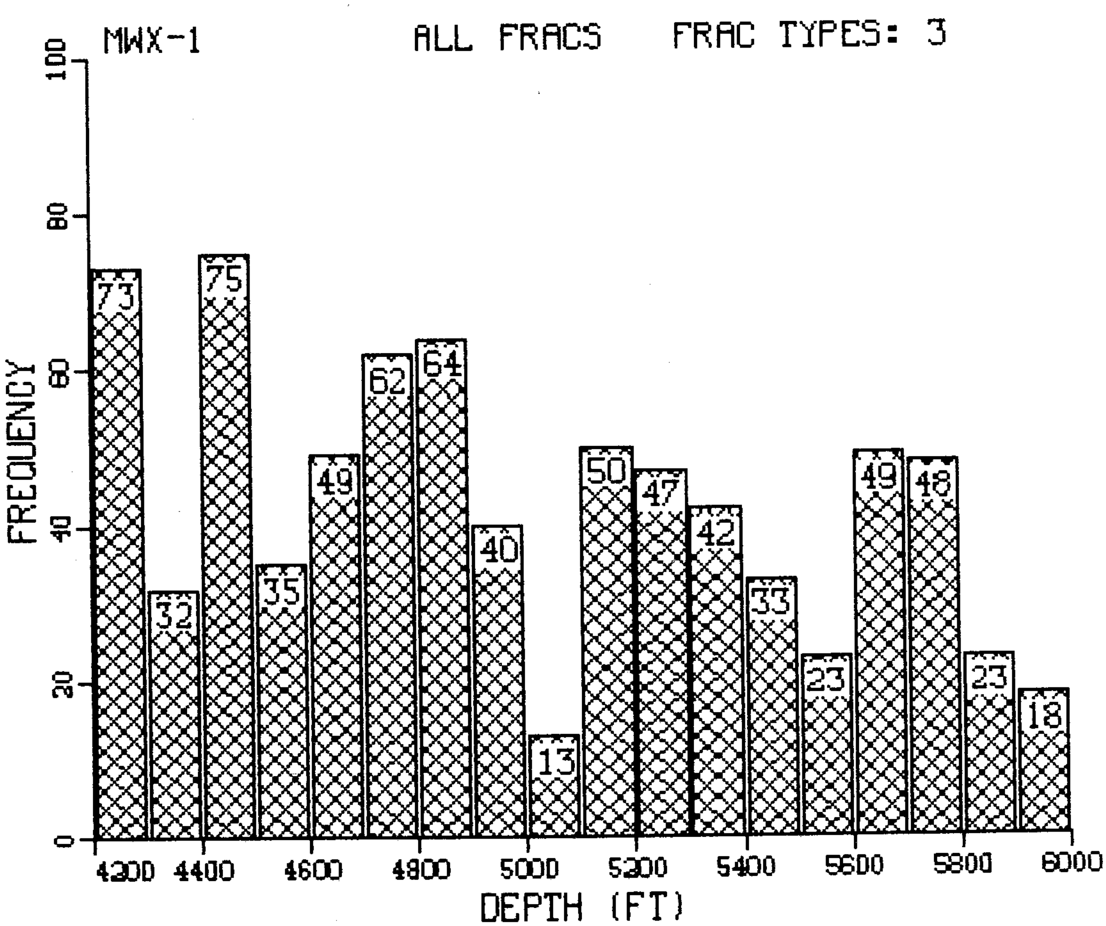

Figure 3.12 Frequency With Depth of Dewatering (Type 3) "Fracture" Planes in Mudstones (in MWX-1 Only)

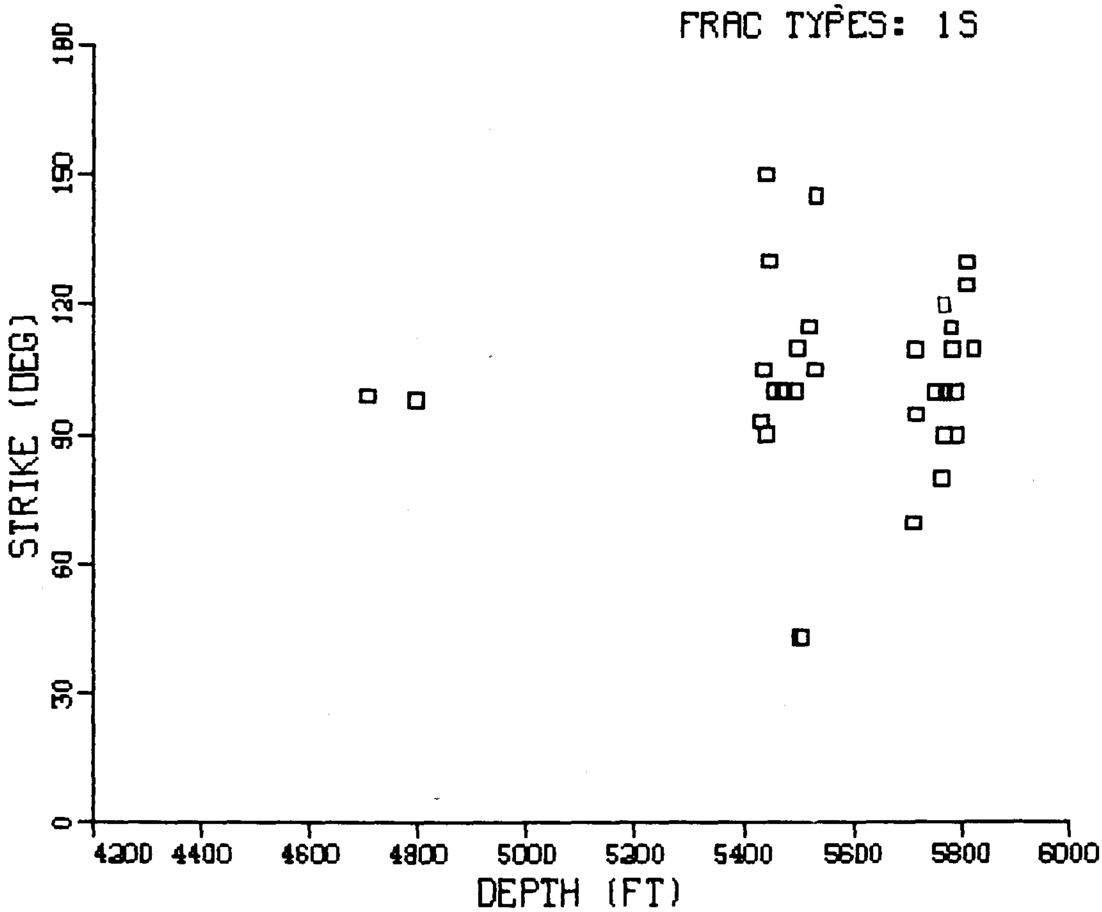

Figure 3.13 Scatterplot of Strikes of Types 1 and S, Vertical Extension Fractures in All Wells.

(A)

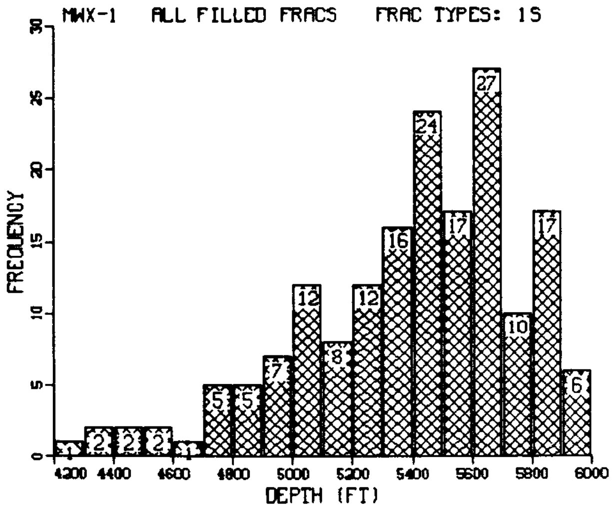

(B)

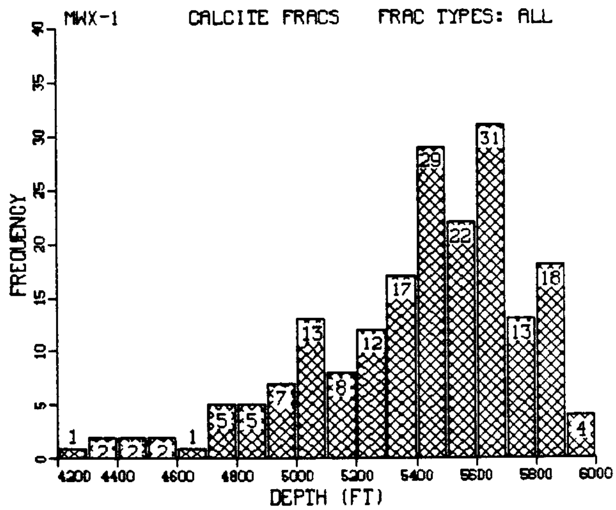

(C)

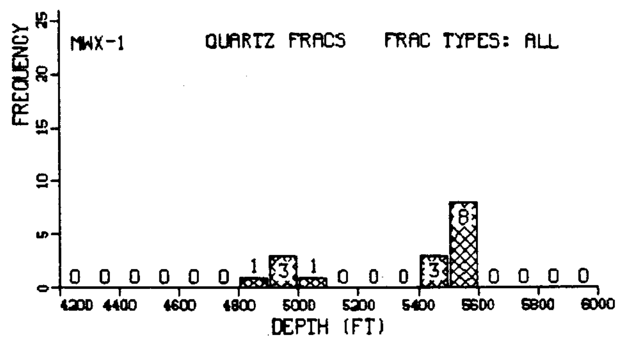

Figure 3.14 Fracture Frequency with Depth. A. All Types 1 and S Fractures (MWX-1 only); B. All Fractures with Calcite Mineralization (MWX-1 only); C. All Fractures with Quartz Mineralization (MWX-1 only).

(A)

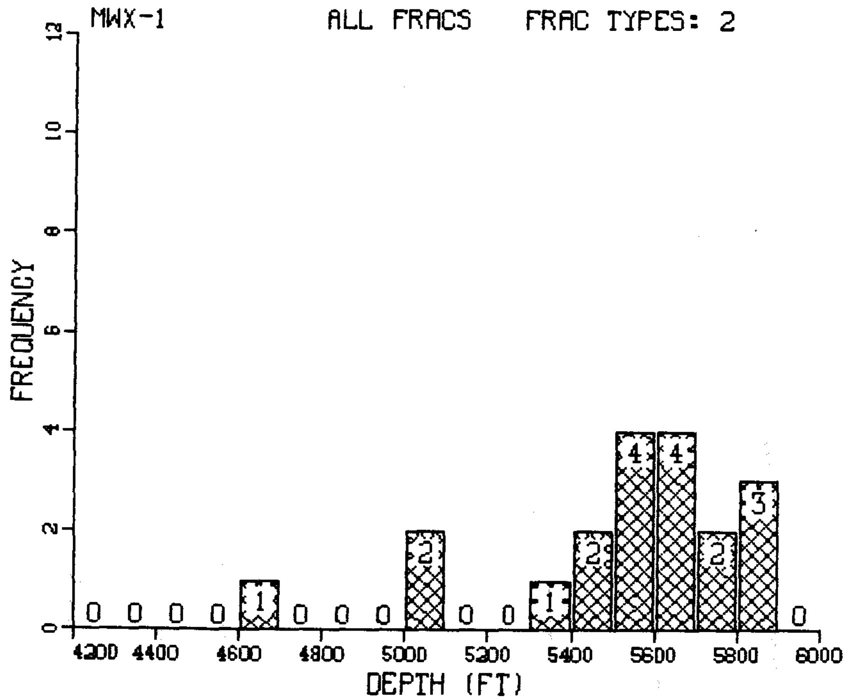

(B)

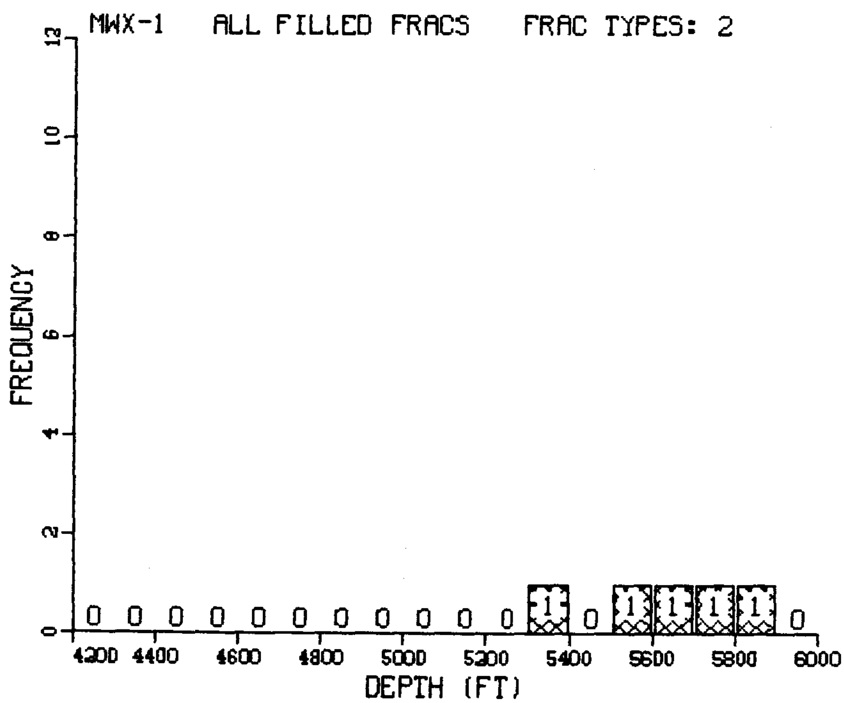

Figure 3.15 Fracture Frequency With Depth. A. All Type 2 Fractures (MWX-1 Only); B. Type 2 Fractures With Mineralization (MWX-1 Only).

4.0 LOG ANALYSIS

G. C. KUKAL
CER CORPORATION

4.1 INTRODUCTION

Extensive log analysis of the Mesaverde Group has been undertaken as part of the Department of Energy's Multiwell Experiment (MWX), a research effort aimed at developing new and improved technology to enhance natural gas production from low-permeability reservoirs. The Mesaverde Group of Western Colorado's Piceance Basin typifies low-permeability lenticular sandstone reservoirs which contain a large resource of natural gas but are difficult to characterize and produce. A log interpretation system developed specifically to deal with such tight, shaly reservoirs has been applied to the three wells drilled for the Multiwell Experiment.

Experimental wells MWX-1, MWX-2, and MWX-3 are located in Section 34 of Township 6 South, Range 94 West in the Rulison Gas Field, Garfield County, Colorado. The wells are closely spaced, 140 to 180 ft apart at the surface, and form a triangle with MWX-3 to the north and MWX-1 to the east.

This report is a synopsis of more comprehensive reports presented previously.[1,2] It presents the results of the analysis of the low fluvial interval (5450-6000 ft) and the middle fluvial interval (4950-5450 ft). There is no depositional reason to break the fluvial sequence into two analysis intervals. However, the lower interval required a more detailed analysis since some of these sands were targeted for various stimulation experiments. This report therefore contains much more detail for the lower interval.

4.2 GENERAL CHARACTERISTICS OF THE RESERVOIR ROCK

The interval described in this report consists of a 1050 ft section of siltstones and mudstones with isolated sand lenses up to 33 ft thick. Figures 4.1 and 4.2 show the correlation of sand units within the lower section (5450-6000 ft) and middle section (4950-5450 ft) respectively. The units are designated alphabetically from bottom to top, A through O. Detailed sedimentological studies by Lorenz in the lower interval characterized most of the reservoirs as being complete, truncated and amalgamated point bar sandstones deposited in meander belts up to 1700 feet wide.[3] The point bar sand contains internal discontinuities as a result of both lateral and vertical deposition.

Detailed petrographic studies show that the dominant lithology is feldspathic litharenite. Authigenic minerals present include illite/smectite, illite, chlorite, calcite and dolomite. Chlorite and dolomite are dominant through the middle of the interval, and illite/smectite and calcite are dominant above and below.[4-7] Clay and carbonate content each range from 5 to 20 percent within the reservoir sands. The mean grain density is 2.667 gm/cc and is increased by the presence of clay and carbonate minerals. The distribution of core grain density values for the low fluvial interval of MWX-1 is illustrated by the histogram in Figure 4.3.

The permeability of low fluvial reservoirs is in the microdarcy range. The extremely "tight" nature of these rocks is caused by quartz overgrowths and the authigenic clay minerals.

Porosity rarely exceeds 10 percent. Figure 4.4 shows the range of core porosity within the low fluvial interval. The distribution is bimodal with peaks at 2.5 and 5.5 percent porosity. Because core sampling was relatively continuous through this interval, mudstones, siltstones and sandstones are all represented. Plotting only the samples which were described as sandstones, as shown in Figure 4.5 reduces the number of low porosity samples. However, sandstone porosities still range from less than 2 to over 10 percent. The low porosities probably resulted from diagenetic alteration. The majority of pore space is of secondary origin.

Natural fractures are pervasive through the low fluvial interval. Thirty-eight fractures were described in the MWX-1 core. Fracture detection logs run in MWX-3 also indicated fractures throughout the interval. Because matrix permeability is low, the natural fractures or induced fractures are required to obtain significant gas production. Natural fractures are less common in the middle fluvial interval.

4.3 FLUVIAL INTERVAL DATABASE

The extensive MWX log and core database is listed in Tables 4.1 and 4.2. The database is completely digitized. All log curves are depth shifted to the primary resistivity log for each well. Core analyses have been depth shifted and are stored at log depth. Additional data utilized in the low fluvial log analysis include core descriptions (digitized using a lithology code), the core gamma ray log, thin-section point count, x-ray diffraction analyses, and mud logs. Several visual fracture detection type logs which do not lend themselves to digitizing were analyzed manually. In MWX-1, the entire fluvial interval was cored. MWX-2 was cored from 5485-5500 ft, 5551-5581 ft, and 5700-5880 ft; MWX-3 was cored from 5690-5870 ft. The two upper cored intervals in MWX-2 were pressure cored in an effort to provide reliable water saturation data for comparison with conventional core data.

Intermediate run log data was used to analyze the fluvial interval. This is because the intermediate log data was run in better borehole conditions and there was less time for invasion of drilling mud into the formation. Prior to analysis, density and neutron histograms were compared between runs in each well and between wells. The histograms were overlaid to discern discrepancies of data distribution. Several log quality problems were observed and adjusted. The following normalizations were performed on intermediate run log data:

- MWX-1 compensated neutron data was normalized by -1.5 porosity units.

- MWX-1 bulk density data was normalized by -0.01 gm/cc.

- MWX-2 compensated neutron data was normalized by -0.5 porosity units.

The MWX fluvial interval basic logs are presented in Figures 4.6-4.20 according to the following format:

	MWX-1	MWX-2	MWX-3
Resistivity	Figure 4.6	Figure 4.11	Figure 4.16
Density-Neutron Porosity	4.7	4.12	4.17
Bulk Density-Photoelectric	4.8	4.13	4.18
Spectral Gamma	4.9	4.14	4.19
Long-Spaced Sonic	4.10	4.15	4.20

4.4 ANALYSIS TECHNIQUES AND VERIFICATION OF RESULTS

Analysis of the fluvial interval was performed using TITEGAS, a sandstone log analysis model developed by CER Corporation which is documented in detail elsewhere.[8] Great effort has gone into utilizing all of the extensive log data available. The log data was first corrected for environmental influences and then used to determine lithologic and critical reservoir characteristics. The calculated model results include:

- clay volume (V_{cl});
- carbonate volume (VCO_3);
- matrix density (ρ_{ma});
- total porosity (ϕ);
- shallow zone saturation (S_{xo});
- water saturation (S_w);

- formation water resistivity (R_w); and
- absolute permeability (corrected for net stress) referred to as log calculated permeability (k)

The lower fluvial interval and middle fluvial interval were analyzed separately for each well. Clay constants and matrix constants were systematically determined using crossplot techniques as described by recent CER publications.[9,10] The results of the TITEGAS program are graphically displayed in traceplots and crossplots as well as in tabular form.

4.4.1 Porosity

In the low fluvial interval, porosity analysis is in excellent agreement with core data. TITEGAS model (log) porosity is compared to core porosity in Figures 4.21, 4.22, and 4.23 for MWX-1, MWX-2, and MWX-3, respectively. Correlations are high in all three wells with the difference in mean porosity within ±0.004 (0.4 percent). Similar results were achieved for the middle fluvial interval as shown in Figure 4.24. Core data was not available for the middle fluvial interval of MWX-2 and MWX-3. Log porosity and core porosity are also presented on the trace plots in Sections 4.5 and 4.6.

The porosity results were achieved by using both a variable fluid density and a variable matrix density. A three-component system is used to compute matrix density. The model uses three equations and three unknowns to solve for sand (quartz) volume, clay volume and carbonate volume. Two measurements are required: gamma ray and photoelectric absorption cross section index (P_e). Using a procedure outlined elsewhere,[10] clay volume is solved using the gamma ray log and then clay effects are stripped from the P_e response. This leads to a volume percent for three components - quartz, clay and a specified third component. In the case of the low fluvial interval, petrographic data establishes that the principal accessory components are the carbonate minerals calcite and dolomite. Once volumes are established, the neutron log matrix is corrected and matrix density is computed using material balance and assumed density of 2.64 for quartz, 2.73 for clay and 2.77 for carbonate.

The matrix density analysis has been hampered by the complex mineralogy of the low fluvial interval. The dolomite/calcite ratio is quite variable and the dominant clay type varies between chlorite and illite/smectite. Correlation coefficients for log calculated matrix density versus core grain density are 0.49, 0.49, and 0.53 for MWX-1, MWX-2, and MWX-3, respectively. Differences in means for log calculated matrix density and core grain density are less than 0.01 for each well.

Crossplots of gamma ray computed clay volumes versus clay volumes based upon density and neutron logs show that despite variable chlorite content, the gamma ray is a very good clay indicator for this interval[1,2] and can therefore be used to strip the density and neutron responses of clay effects. This results in reliable fluid densities used in the calculation of porosity. Further discussions of clay volume verification and the impact of accurate clay volume analysis has been reported previously.[9]

4.4.2 Water Saturation

Figure 4.25, 4.26, and 4.27 compare log interpreted water saturations to core water saturations for the low fluvial interval. Figure 4.28 shows similar results for the MWX-1 middle fluvial interval. No core data is available for the MWX-2 and MWX-3 middle fluvial interval. The plots indicate that a reasonably good estimate of water saturation is being obtained from logs.

There are several factors that affect core water saturations, including coring conditions, sampling procedures, core preservation and laboratory analytical techniques.

For MWX-1 and MWX-2, there are several reasons why core water saturations may be too low:

- The core may become partially flushed with diesel during coring, plugging, and storage (plugs were stored immersed in diesel). It is not known if the diesel displaced a fraction of the water present or only gas; however, some oil saturations are greater than 75 percent and the original oil saturation was probably zero.

- When the core was brought to surface, the gas within the pore space expanded and forced some water out of the core. Small bubbles were frequently noted coming from a core laid out for examination.

- Within the laboratory, core is at lower net stress than in situ and pores expand. The resulting water saturation is less. As a typical example, assume that porosity in situ is 8 percent, while in the laboratory it is measured 8.3 percent. If water saturation is measured 67.5 percent in the lab, it would actually be 70 percent with the smaller in situ pore volume.

- Sattler et al., presented data[11] which point out substantial discrepancy between Dean-Stark saturations and saturations measured by vacuum drying for tight sand core.

Water resistivity (R_w) used in the saturation analysis has been explained in previous discussions.[12,13] Interpreted R_w through the low fluvial interval averages 0.15 Ω-m while R_w through the middle fluvial interval averages 0.22 Ω-m.

4.4.3 Permeability

An equation developed for log interpretation of net stress corrected absolute permeability in low permeability sandstone reservoirs[14] was utilized in the fluvial interval. The results for the low fluvial interval are illustrated in Figures 4.29 and 4.30. Correlations between log calculated permeability and core permeability are fairly strong and the best fit lines indicate good one-to-one agreement. There is insufficient core data for the low fluvial interval of MWX-2 and insufficient or no core data for the middle fluvial interval.

4.5 ANALYSIS OF LOW FLUVIAL RESERVOIRS

The format and description of TITEGAS computed log output is presented in Figure 4.31. The output includes both curves from log analysis computations and plotted core data. The computed logs for MWX-1, MWX-2, and MWX-3 low fluvial interval are presented in Figures 4.32, 4.33, and 4.34, respectively.

Ten distinct sand bodies are identified as potential reservoirs in the low fluvial interval. Using model results from the TITEGAS log analysis program, each sand or zone is classified and labeled on the computed log as being one of the following types:

Type 1: These reservoirs have the best matrix reservoir quality. This type of zone is interpreted as capable of gas flow from matrix after a perforation breakdown and does not necessarily depend upon natural fractures for flow. A stimulation candidate.

Type 1a: Matrix permeability is developed as in Type 1 and the unit is also naturally fractured.

Type 2: These reservoirs are naturally fractured but generally do not have good matrix permeability.

Type 3: Marginal matrix permeability; secondary stimulation candidate.

Type 4: These reservoirs are too tight for significant production.

Type 5: These reservoirs are very marginal gas zones. Water saturation is very high and completion could possibly cause water production problems.

Type 6: These reservoirs are sands which have very high water saturation. This type of zone will contribute substantial water production.

The logs in Figures 4.32 to 4.34 are labelled with the reservoir type classification of each zone. Table 4.3 provides a summary of zone classifications and Tables 4.4, 4.5, and 4.6 summarize the zone averaged characteristics of the low fluvial interval reservoirs for each well.

For a fluvial sandstone to be considered a potentially productive individual reservoir in this analysis, it must meet these requirements:

- have porosity greater than 3 percent;
- have a clay volume less than 25 percent;
- be more than 4 ft thick; and
- be more than 3 ft from an adjacent reservoir.

However, no requirement on water saturation was imposed for this selection.

In addition to the information presented in the tables, a brief synthesis of petrographic, geologic, and log interpretation studies is presented below.

Zone A

The sandstones in this interval are discontinuous and usually have fining-upward log characters. The A2 sand in MWX-2 may be the best zone in the low fluvial interval. The very low water saturation of A2 within the MWX-2 may be the result of extensive natural fractures within the zone. The A2 sand thins from about 15 ft in MWX-1 and MWX-2 to just 5 ft in MWX-3. This illustrates the lateral variability of these reservoirs. Petrographic analysis described rocks from this interval as very fine-grained lith-sublitharenites with illite-smectite being the dominant clay mineral present.[7]

Zone B

Zone B has a very consistent thickness in all three wells of about 17 ft. The serrated gamma ray profiles of these sands reflect the shaly laminae which were described in the core.[3] Core fractures were described in MWX-2 and MWX-3, and MWX-1 had core fractures immediately above and below this zone. Fracture logs run in MWX-3 also indicated fractures in the zone.

Although this zone has a uniform thickness in the three wells, the zone is not internally homogeneous and each well contains numerous partial point bar sequences. The high carbonate peaks below this zone in MWX-1 are substantiated by the petrographic description which describes calcite and barite partially filling an open microfracture.[5]

Zone C

The C1 zone is about 6 ft thick and only present in MWX-2 and MWX-3. The zone is interpreted as a splay deposit.[3]

The C2 sand is present in each well and thins from 23 ft in MWX-1 to 11 ft in MWX-3. MWX-2 has a well-developed fining-upward profile with apparent shale interbeds. The core description identifies C2 as an amalgamated point bar/meander belt sequence.[3] Petrographic data identifies sandstone in this interval to be feldspathic litharenite, fine-grained, well sorted with extensive calcite cement which diminishes and then disappears at 5772 ft (log depth). Calcite is then described again at 5731 ft.[4] The computed log of carbonate volume documents this variation fairly well.

Zone D

This zone does not meet the reservoir limits in MWX-2 although the sandstone can be correlated through the zone. The zone is one 15-ft sand in MWX-3 but is two thinner sands in the other wells. MWX-1 core analysis describes this interval as a crossbedded sandstone with coaly partings and soft-sediment deformation.[3] The coal partings are too thin to be detected by logs. Petrographic data reveals a high carbonate content for this interval in MWX-1 which is seen on the computed log as well. The rocks are calcitic and dolomitic feldspathic litharenites, and the clays present are both illite/smectite and chlorite.[6]

Zone E

Zone E1 is the thickest zone in the low fluvial interval. In MWX-2, the zone is 33 ft thick and is about 20 ft thick in MWX-1 and MWX-3. MWX-1 has the classic point bar fining-upward character and the irregularities of the gamma ray log probably indicate shaly interbeds.

Resistivity logs run through the MWX-2 E1 zone show a step profile of invasion. The profile changed with time as evidenced by a later resistivity run. Since these reservoirs do not tend to be deeply invaded, the resistivity anomaly within the interval is interpreted to be due to the presence of natural fractures. Other evidence of natural fractures include a log interpreted porosity which is higher than core porosity and a relatively high carbonate content.

Petrographic data from MWX-1 identifies chlorite as the dominant mineral in the fine-to-medium-grained lithic arkoses and feldspathic litharenites of this zone.[6]

E2 is 7 ft thick in MWX-1 and thins to less than 4 ft (below reservoir limit) in MWX-2. The sand is not correlated to MWX-3.

Zone F

This zone is about 14 ft thick in MWX-1 and MWX-2 but is only 8.5 ft thick in MWX-3. The zone has a sharp base at the bottom, fines upward to become about 20 percent clay and then has another sharp base with gradual finding-upward profile. The lower sequence is about 6 ft thick.

Petrographic analysis describes this zone as a medium-grained feldspathic litharenite. Dolomite cement and chlorite are the dominant authigenic minerals.[6]

4.6 ANALYSIS OF MIDDLE FLUVIAL RESERVOIRS

The computed logs for MWX-1, MWX-2, and MWX-3 middle fluvial interval are presented in Figures 4.35, 4.36, and 4.37, respectively. The output includes both curves from log analysis computations and plotted core data.

Twelve distinct sand bodies are identified as potential reservoirs in the middle fluvial interval. Using results from the log analysis program, each sand or zone is classified according to the various reservoir types described in Section 4.5. These classifications are labelled on the computed logs. Tables 4.7, 4.8, and 4.9 summarize the zone averaged characteristics of the middle fluvial interval reservoirs for each well.

Some general statements can be made about the relative quality of the middle fluvial units:

- Reservoir quality varies between the three wells. MWX-2 overall has the best quality reservoirs and MWX-3, the worst.

- In all three wells, the most significant reservoirs are the N1 and N2 sandstones. They are comparatively thick, with relatively low water saturations and relatively good matrix permeability and porosity development. Log and core data for MWX-1 and MWX-3 shown these units to be fractured.

- Most of the other sand bodies have marginal to tight matrix permeability. Exceptions are Zone M in MWX-1, Zone L2 in MWX-2, and Zone L1 in MWX-3 which have fair matrix permeability.

4.7 MATRIX PERMEABILITY ANALYSIS

Two methods are available in TITEGAS for determining matrix permeability. The first is a qualitative estimate based on the difference between near-zone water saturation (S_{xo}) and deep formation water saturation (S_w). If the saturation curves are separate but track each other, the discrepancy is attributable to a local water resistivity variation. If the curves travel oppositely, then a permeable interval is interpreted. If the curves stack, then the zone is tight and uninvaded. The TITEGAS computed logs show the S_w difference, or ΔS_w.

The second method is a direct simulation of net stress corrected absolute permeability shown on the TITEGAS logs as the curve labeled k. When k, or the permeability index, is corrected for formation water saturation, the resultant effective gas permeability will be one to two orders of magnitude lower.

Visual analysis of the two permeability indicators allows reliable estimation of matrix permeability. Generally when ΔS_w is larger and the saturation curves are swinging in an opposite direction, the calculated k is high. When thickness of zone is factored in, the permeability-feet parameter (kh on the log) becomes a useful tool to judge zone merit.

4.8 NATURAL FRACTURE DETECTION

There was a major natural fracture interpretation effort for the low fluvial interval whereas the middle fluvial interval was less thoroughly characterized. This in part had to do with a great interest in the open fractures noted in MWX-1 low fluvial interval core and in part to the greater operational interest placed upon the low fluvial interval.

Several natural fracture indicators are available in the MWX database. Fractures observed in cores are the most direct method of indication. A second method relies on various so-called fracture logs, e.g., borehole televiewer (BHTV), circumferential acoustilog (CMA), fracture identification log (FIL), borehole compensated variable density log (BHC-VDL), and the fracture probability log (FPL). This log suite was run in MWX-3. The oil-base mud used in MWX-1 and MWX-2 prevented the majority of fracture log measurements from being useful in those wells; only the VDL logs were available.

Figure 4.38 is a digitized interpretation of each fracture log for the low fluvial interval of MWX-3, combined into a single trace plot. Cross-hatching indicates a log-interpreted fracture. Zones where most or all of the fracture logs exhibit a fracture response can reliably be assumed to be naturally fractured. The log indicates that every zone in the low fluvial interval may be naturally fractured in MWX-3. E1 and A1 are the only zones in which the presence of fractures is questionable.

Figure 4.39, 4.40, and 4.41 are composite illustrations for each well which include natural fracture and mud log data for the low fluvial interval. Cored intervals and core fractures are depicted. Also, fractures identified via fracture logs are shown. For MWX-1 and MWX-2, the variable density log (VDL) was the primary indicator. For MWX-3, all fracture logs described above were used. The mud log portions of the figures show total units of gas and mud weight.

Other methods have been investigated for natural fracture detection. One method utilizes various logs with different depths of investigation, such as the density-neutron, electromagnetic propagation, micro-SFL, dielectric constant and deep induction log. Water saturations are calculated from each curve and pairs of curves are plotted. When an anomalous relationship occurs, a fracture is suspected. By displaying numerous such pairs of curves, a tool for identifying fractures is created. An example of the saturation curve method (known as NATUFRAC) is shown in Figure 4.42. A description of the reasoning behind the interpretation of the saturation curves for natural fractures is given in another report.[1] Differences between saturation pairs which may indicate fractures are crosshatched in Figure 4.42. Every zone in the low fluvial interval of MWX-3 is interpreted to be naturally fractured.

Another fracture detection method based on curve comparisons is the multiple density pass (MDP) method. All available bulk density data for an interval, including different log runs and repeat run data, are compared for differences in the readings. If a density tool pad passes over a fracture, the measurement can be significantly different than from a run where the pad missed the fracture (it is possible to miss a fracture in the borehole in the case of a vertical fracture). Also, in different log runs, a lower density on a later run indicates fracture presence since this is opposite to the effect of additional invasion with time.

Figure 4.43 presents a trace plot of all density data on MWX-1 in the low fluvial interval. To the left, fractures are flagged in three columns: those anomalies detected on the same run, those detected between runs, and core-identified fractures (right most column).

The MDP fracture identification technique is supplementary to other fracture identification techniques. The MDP technique can overlook a fracture present in the borehole and can also indicate a fracture when none is present. There are several reasons why the technique is not reliable by itself. Fractures may be overlooked because pad tools tend to "channel" along the borehole, causing multiple passes to traverse the same paths. Also complex infiltration conditions may mask fractures on the early-late run comparisons. Fractures may be erroneously indicated due to various mechanical reasons associated with logging pad-borehole contact. There is a poor correlation between MDP interpreted fractures and fractures observed in cores for the low fluvial interval.

A technique similar to the previous technique and also resulting from density anomalies is a comparison of log interpreted porosity to core porosity. Fractures are suspected when core porosity is significantly lower than log porosity. Fractures in the low fluvial interval indicated by this method are Zone B in MWX-1, Zone C in MWX-2, Zone D1 in MWX-1, and Zone E1 in MWX-1 and MWX-2.

Special core analyses performed by Core Laboratories Inc. show that fracture permeability may be over two order of magnitude greater than matrix permeability. This demonstrates the importance of natural fractures to gas productivity.

4.9 CEMENT BOND QUALITY

CBL/VDL and cement evaluation logs (CEL) were examined to interpret zone isolation. The criteria for determining zone isolation for 7-in. casing is an 80% bond index over at least 10 vertical feet.[15]

The composite mud logs (Figures 4.39, 4.40, and 4.41) show the cement bond log interpretation for each well in the left column. A shaded interval indicates adequate cement bonding.

Due to the extensive testing performed in MWX-1, the cement evaluation log (CEL) was rerun in April, 1987 over the interval 4100-6390 ft with 3000 psi at the casing head. The following interpretations of MWX-1 cement bonding are based on this latest log. The interval 4870-5790 ft exhibits good bonding except at 5686-5708 ft. Gas cutting during logging affected the data at 5790-5850 ft rendering it uninterpretable. Good bonding is present between 5850-6390 ft except at 5954-5972 ft.

In MWX-2, A2 is not isolated above until 5946 ft where good bonding begins. Zones A1 and A2 as well as C1 and C2 are not isolated from each other since they are not separated by 10 or more feet. All other zones exhibit good bonding.

In MWX-3, A1 is not isolated below, and A1 and A2 are not isolated from each other. Good bonding is not present below A3 until 5934 ft. Above Zone B, communication will continue upwards to 5824 ft. Zone C sands are not isolated from each other, as they are not separated by 10 ft. All other zones exhibit good bonding.

It should be noted that the interpretations of zone isolation are consistent with those used for normal completion operations. However, empirical data has shown that when hydraulic fracturing operations are performed, the footage required for isolation is tripled.[16]

4.10 HYDRAULIC FRACTURE BARRIER INTERPRETATION

Closure stress logs were computed for the low fluvial interval of each well to interpret vertical barriers to contain hydraulic fracture treatments. The index for closure stress (CSI) logs are presented in Figures 4.39, 4.40, and 4.41. CSI is a dimensionless number defined by the equation:

$$CSI = \frac{\mu}{1 - \mu}$$

where

$$\mu = 0.5 \left[\frac{1 - 2\left(\frac{\Delta tc}{\Delta ts}\right)^2}{1 - \left(\frac{\Delta tc}{\Delta ts}\right)^2} \right]$$

where Δtc = compressional wave travel time (μsec/ft); and
Δts = shear wave travel time (μsec/ft).

Generally the CSI calculates higher for shales than for the less elastic reservoir rocks. When a sand unit having a low CSI is bounded by a unit having a high CSI, vertical fracture containment can be expected. This is supported by comparison to stress test data. A strong correlation was observed between CSI and MWX-3 low fluvial interval stress test data (least squares correlation coefficient 0.95).

CSI logs were analyzed to provide the following fracture containment evaluation. There is good fracture containment below Zone A1. Fractures may not be contained between A1 and A2 but good barriers exist above A2 except in MWX-1. Good barriers exist below Zone B in all three wells; however, an upper barrier is only 4 ft thick in MWX-3 and is not present in MWX-2 until 5800 ft. Fracture barriers are present above Zone C but not between C1 and C2. Below this zone, the fracture barriers are thin and may not contain large fracture treatments. All other zones have good fracture barriers except for between E1 and E2 in MWX-1.

4.11 PETROPHYSICAL RELATIONSHIPS IN THE LOW FLUVIAL INTERVAL

Two-dimensional crossplots offer an excellent opportunity to observe pertinent petrophysical relationships in a specified interval. Log, core and petrographic data are crossplotted and the resultant trends are significant descriptors of the reservoirs. A way to measure the relatedness of two crossplotted parameters is by a numerical correlation coefficient ranging from -1.0 to 1.0. A value of zero indicates no correlation whatsoever, while values of 1.0 or -1.0 indicate perfect correlation between the two parameters. Negative coefficients indicate inverse relationships, i.e., as one parameter increases, the other decreases.

Since hundreds of two-dimensional crossplots of log, core and thin section data can be constructed, a data reduction effort termed a crossplot matrix is presented here. This matrix consists of the correlation coefficients of various crossplots with shading intensity representing degree of correlation between the two parameters. Figure 4.44 is a matrix for the low fluvial interval in MWX-1. An explanation of crossplot variable names is given in Table 4.10.

4.12 REFERENCES

1. Kukal, G. C. and R. E. Hill: "Multiwell Experiment, Well Log Analysis of Low Fluvial Interval, MWX-1, MWX-2, and MWX-3," CER Corporation Report, May 23, 1986.

2. Kukal, G. C. and K. E. Simons: "Multiwell Experiment Well Log Analysis of Middle Fluvial Interval, MWX-1, MWX-2, and MWX-3," CER Corporation Report, June 9, 1986.

3. Lorenz, J. C.: "Sedimentology of the Low Fluvial Lenses at MWX," unpublished memorandum, January 31, 1986.

4. Eatough, M. O.: "Preliminary Results of Mineralogy and Petrology of the Fracture Zone Interval (Depth 5700-5870 ft) Drill Core MWX-1," Bendix Field Engineering Corp., October 18, 1982, 88 pp.

5. Eatough, M. O.: "Preliminary Results of Mineralogy and Petrology of the Fracture Zone Interval (Depth 5690-5870 ft) Drill Core MWX-2," Bendix Field Engineering Corp., May 26, 1983, 43 pp.

6. Dayvault, R. D., L. M. Fukui and R. B. Hopping: "Preliminary Results of Mineralogic and Petrographic Analyses of the Mid-Fluvial Interval (Depth 5300-5690 ft) Drill core MWX-1," Bendix Field Engineering Corp., December 22, 1983, 97 pp.

7. Dayvault, R. D.: "Preliminary Results of Mineralogic and Petrographic Analyses of the Low Fluvial Interval (Depth 5873-6331 ft) Drill Core MWX-1," Bendix Field Engineering Corp., May 23, 1984, 84 pp.

8. Kukal, G. C.: "A Systematic Approach for the Effective Log Analysis of Tight Gas Sands," SPE 12851, Proceedings of the 1984 SPE/DOE/GRI Unconventional Gas Recovery Symposium, Pittsburgh, PA, May 1984, pp. 209-220.

9. Kukal, G. C. and R. E. Hill: "Log Analysis of Clay Volume: An Evaluation of Techniques and Assumptions Used in an Upper Cretaceous Sand-Shale Sequence," Paper RR, Transactions of the SPWLA 27th Annual Logging Symposium, Houston, TX, June 9-12, 1986.

10. Kukal, G. C. and R. E. Hill: Improved Shaly Sand Analysis in Heavy Drilling Muds: A Simple Technique for Using the Photoelectric Measurement," Paper U, Transactions of the SPWLA 26th Annual Logging Symposium, Dallas, TX, June 1985.

11. Sattler, A. R., A. A. Heckes, and J. A. Clark: "Pressure Core Measurements in Tight Sandstone Lenses During the Multiwell Experiment," SPE 12853 Proceedings of the 1984 SPE/DOE/GRI Unconventional Gas Recovery Symposium, Pittsburgh, PA, May 1984, pp. 229-234.

12. Kukal, G. C.: "Log Analysis in Low-Permeability Gas Sand Sequences-Correcting for Variable Unflushed Gas Saturation," Paper F, Transactions of the SPWLA 24th Annual Logging Symposium, Calgary, Canada, June 1983.

13. Law, B. E., J. R. Hatch, G. C. Kukal, and C. W. Keighin: "Geologic Implications of Coal Dewatering," AAPG Bulletin, Vol. 67, No. 12, December 1983, pp. 2255-2260.

14. Kukal, G. C. and K. E. Simons: "Log Analysis Techniques for quantifying the Permeability of Sub-Millidarcy Sandstone Reservoirs," SPE Formation Evaluation. December 1986, pp. 609-622.

15. Schlumberger, Ltd. Cased Hole Applications, 1975, p. 50.

16. Fitzgerald, D. D., B. F. McGhee, and J. A. McGuire: "Guidelines for 90% Accuracy in Zone-Isolted Decisions," Journal of Petroleum Technology, November 1985, pp. 2013-2022.

Table 4.1 MWX Log Database

MWX-1 LOGS

4,130 ft to Surface

Borehole Compensated Sonic/Gamma Ray/
  Caliper/Dual Induction

6,827 to 4,130 ft

Dual Induction/Gamma Ray
Lithodensity/Caliper
Compensated Formation Density
Compensated Neutron/Gamma Ray/Caliper
Natural Gamma Spectroscopy
Long Spaced Sonic
Repeat Formation Tester

8,350 to 4,130 ft

Dual Induction/Gamma Ray/SP
Lithodensity/Compensated Neutron/Gamma
  Ray/Caliper
Long Spaced Sonic
Sidewall Neutron Porosity/Gamma Ray/
  Caliper
Electromagnetic Propagation/Gamma Ray/
  Caliper
Amoco Sonic Tool
Dipmeter - Structural and Stratigraphic
Computed Logs
  Geo Dip
  Standard Cluster
  Directional Survey
Fracture Identification Log
Repeat Formation Tester (12 tests)

MWX-2 LOGS

5,438 to 4,094 ft

Formation Density/Compensated Neutron/
  GR/Caliper

6,692 to 4,094 ft

Dual Induction/GR/SP
Formation Density/Compensated Neutron/
  GR/Caliper
Litho density/GR/Caliper
Sidewall Neutron Porosity/GR/Caliper
Natural Gamma Spectroscopy

8,291 to 4,094 ft

Dual Induction/GR/SP
Circumferential Micro Sonic/GR
  Digitized Waveforms
Formaton Density/Compensated Neutron/
  Natural Gamma Spectroscopy/Caliper
Long Spaced Sonic
  Digitized LS Waveforms
Amoco Multiple Spaced Sonic/Waveforms
Sidewall Neutron Porosity/GR/Caliper
Dipmeter

8,230 to 4,294 ft

Fracture Identification Log

Table 4.1, Continued

MWX-3 LOGS

4,134 ft to Surface

Borehole Compensated Sonic/Gamma Ray/Caliper
Formation Density/Compensated Neutron/Gamma Ray/Caliper

5,875 to 4,129 ft

Lithodensity/Compensated Neutron Log/Gamma Ray/Caliper

5,840 to 4,900 ft

Borehole Televiewer

6,875 to 4,130 ft

Lithodensity/Compensated Neutron Log/Gamma Ray/Caliper
Micro SFL/SP/Caliper

7,474 to 4,129 ft

Dual Induction Log/Gamma Ray/SP
Lithodensity/Compensated Neutron Log/Natural Gamma Spectroscopy/Caliper
Sidewall Neutron Porosity/Gamma Ray/Caliper
High Resolution Dipmeter/Gamma Ray/Caliper
Fracture Identification Log/Gamma Ray/Caliper
Borehole Compensated Sonic (Digital Sonic) Shear and Compressional Travel Times
Variable Density Log (3 ft spacing)
Mechanical Properties Quick Look (Computed Log)
Dual Laterolog/Microspherically Focused Log/Gamma Ray/Caliper
Electromagnetic Propagation Tool/Gamma Ray/Caliper
Dual Porosity Compensated Neutron Log (CNT-G)/Gamma Ray/Micro Log
Formation Density Compensated/Gamma Ray/Caliper
Amoco Multiple Spaced Sonic
Mobil Multiple Spaced Sonic
Mobil Borehole Televiewer
Spectralog
Borehole Compensated Acoustilog/Gamma Ray/Caliper
BHC Acoustic Fraclog/Gamma Ray/Caliper
Sonic Waveforms Digitized
Dielectric Constant Log
Circumferential Acoustilog

7,300 to 4,130 ft

Cement Bond Log/Variable Density Log/Gamma Ray/Casing Collar Locator
Cement Evaluation Log/Gamma Ray
Compensated Neutron Log
Thermal Decay Tool/Gamma Ray/Casing Collar Locator

Table 4.2 MWX Core Database

CORED INTERVALS

MWX-1	MWX-2	MWX-3
4,170 - 6,827	4,870 - 4,956	4,887 - 4,928
7,810 - 7,960	5,485 - 5,500[1]	5,690 - 5,870
	5,551 - 5,581[1]	6,431 - 6,530
Total: 2,807 ft	5,700 - 5,880	6,875 - 6,910
	6,390 - 6,568	7,071 - 7,160
	7,080 - 7,388	7,536 - 7,564[2]
	7,817 - 7,907	
	8,100 - 8,141	Total: 500 ft
	Total: 928 ft	

STANDARD ANALYSES

Permeability, Porosity, Water Saturation, Oil Saturation, Grain Density, Cation Exchange Capacity[3]

SPECIAL ANALYSES

Stressed Permeability,[3] Petrographic Thin Section Analysis[3]

[1] Pressure Core
[2] 2 in. diameter core
[3] Not on all samples

Table 4.3 Zone Type Classification Low Fluvial Interval

Unit	MWX-1	MWX-2	MWX-3
F	3	2	2
E_2	4	—	—
E_1	2/3	1a	4
D	2	—	2
C_2	1a	1a	1a
C_1	—	2	4
B	1a	1a	2
A_3	—	—	2
A_2	3	1a	2
A_1	4	3	4

Table 4.4 MWX-1 Low Fluvial Reservoir Characteristics

Zone	Zone Depth, ft	Pay Sand (h),* ft	Porosity (ϕ), fraction	Porosity-feet (ϕ x h), ft	Water Saturation (S_w), fraction	Hydrocarbon-feet, (ϕ x (1-S_w) x h), ft	Sxo - Sw (Δ S_w), fraction	Permeability-feet (kh), md-ft	Volume Clay (V cl), fraction	Volume Carbonate (VCO3), fraction	Core Porosity, fraction	Stressed Core Permeability, md	Core Water Saturation, fraction	Core Grain Density, gm/cc	Cation Exchange Capacity, meq/100 gm
F	5,478.5-5,491.5	13.5	.060	.81	.649	.29	.136	.0388	.092	.080	.062	.0050	.512	2.64	1.72
E_2	5,525.0-5,531.5	7.0	.045	.32	.646	.11	.045	.0085	.126	.151	.043	–	.725	2.66	–
E_1	5,544.0-5,565.0	21.5	.060	1.30	.640	.47	.109	.0723	.056	.100	.064	.0041	.519	2.64	2.00
D_1*	5,624.5-5,635.5	11.5	.064	.73	.602	.30	.104	.0534	.083	.148	.056	–	.516	2.66	–
C_2	5,714.5-5,737.5	23.5	.078	1.83	.630	.69	.034	.1701	.078	.071	.081	.0073	.436	2.66	3.02
B	5,827.0-5,843.0	16.5	.071	1.18	.538	.56	.170	.1555	.055	.188	.061	.0071	.505	2.65	2.07
A_2	5,957.0-5,971.0	14.5	.048	.70	.479	.37	.153	.0439	.103	.122	.050	.0017	.527	2.66	–
A_1	5,977.0-5,983.5	7.0	.062	.44	.629	.17	-.023	.0489	.106	.116	.056	.0020	.477	2.66	–

* D_2 only 4 ft thick

Table 4.5 MWX-2 Low Fluvial Reservoir Characteristics

Zone	Zone Depth, ft	Pay Sand (h),* ft	Porosity (ϕ), fraction	Porosity-feet (ϕ x h), ft	Water Saturation (S_w), fraction	Hydrocarbon-feet, (ϕ x (1-S_w) x h), ft	S_{xo} - S_w (Δ S_w), fraction	Permeability-feet (kh), md-ft	Volume Clay (V_{cl}), fraction	Volume Carbonate (VCO_3), fraction	Core Porosity, fraction	Stressed Core Permeability, md	Core Water Saturation, fraction	Core Grain Density, gm/cc	Cation Exchange Capacity, meq/100 gm
F	5,481.0-5,495.0	14.5	.046	.67	.499	.33	.276	.0306	.117	.097	.054	–	.672	2.69	–
E_1	5,534.0-5,566.5	33.0	.077	2.53	.583	1.10	.061	.3168	.060	.125	.082	–	.545	2.68	–
D*															
C_2	5,714.0-5,729.0	15.5	.072	1.12	.625	.44	.052	.0965	.111	.071	.064	.006**	.461	2.64	–
C_1	5,733.0-5,738.5	6.0	.043	.26	.705	.08	.218	.0044	.166	.160	.031**	–	.806**	2.66**	–
B	5,826.5-5,843.0	17.0	.065	1.10	.530	.52	.251	.1036	.072	.056	.058	–	.447	2.66	–
A_2	5,955.0-5,972.0	17.5	.053	.93	.246	.71	.430	.2914	.126	.088	–	–	–	–	–
A_1	5,978.5-5,985.5	7.5	.061	.46	.553	.21	.161	.0305	.120	.121	–	–	–	–	–

* D sands do not meet reservoir limits

** 1 data point

Table 4.6 MWX-3 Low Fluvial Reservoir Characteristics

Zone	Zone Depth, ft	Pay Sand (h),* ft	Porosity (ϕ), fraction	Porosity-feet (ϕ x h), ft	Water Saturation (S_w), fraction	Hydrocarbon-feet, (ϕ x (1-S_w) x h), ft	S_{xo} - S_w (ΔS_w), fraction	Permeability-feet (kh), md-ft	Volume Clay (V_{cl}), fraction	Volume Carbonate (VCO3), fraction	Core Porosity, fraction	Stressed Core Permeability, md	Core Water Saturation, fraction	Core Grain Density, gm/cc	Cation Exchange Capacity, meq/100 gm
F	5,486.0-5,494.0	8.5	.053	.45	.513	.22	-.038	.0238	.111	.046	–	–	–	–	–
E_1	5,555.0-5,574.5	20.0	.059	1.18	.585	.49	-.046	.0627	.094	.046	–	–	–	–	–
D	5,620.5-5,635.0	15.0	.072	1.08	.547	.49	-.038	.0970	.106	.082	–	–	–	–	–
C_2	5,724.0-5,735.0	11.5	.072	.83	.628	.34	-.025	.0799	.089	.058	.074	.0083	.477	2.64	–
C_1	5,738.0-5,744.0	6.5	.052	.34	.622	.13	.118	.0121	.143	.087	.058	.0004	.541	2.65	–
B	5,832.0-5,849.0	17.5	.064	1.12	.464	.60	.133	.1065	.094	.087	.073	.0054	.430	2.66	–
A_3	5,916.5-5,923.5	7.5	.068	.51	.388	.31	-.184	.0676	.183	.004	–	–	–	–	–
A_2	5,964.5-5,969.0	5.0	.048	.24	.560	.11	-.162	.0114	.158	.127	–	–	–	–	–
A_1	5,984.0-5,989.0	5.5	.058	.32	.509	.16	.083	.0266	.137	.179	–	–	–	–	–

Table 4.7 MWX-1 Middle Fluvial Reservoir Characteristics

Unit	Zone Depth, ft	Pay Sand (h),* ft	Porosity (ϕ), fraction	Porosity-feet (ϕ x h), ft	Water Saturation (S_w), fraction	Hydrocarbon-feet, (ϕ x (1-S_w) x h), ft	S_{xo} - S_w (Δ S_w), fraction	Permeability-feet (kh), md-ft	Volume Clay (V_{cl}), fraction	Volume Carbonate (VCO_3), fraction	Core Porosity, fraction	Stressed Core Permeability, md	Core Water Saturation, fraction	Core Grain Density, gm/cc	Cation Exchange Capacity, meq/100 gm
G	5,425.0-5,429.5	4.5	.055	0.249	.766	0.078	.093	.0068	.134	.126	.047	–	.671	2.65	–
H_1	5,398.0-5,404.0	6.0	.042	0.249	.778	0.072	.042	.0035	.168	.098	.041	–	.743	2.65	–
H_2	5,382.5-5,390.5	8.0	.055	0.443	.707	0.147	.080	.0144	.150	.097	.048	–	.611	2.64	–
I	5,333.0-5,343.5	10.5	.051	0.539	.653	0.209	.003	.0145	.179	.070	.057	–	.612	2.65	–
J	5,293.0-5,301.5	8.5	.047	0.398	.993	0.031	.053	.0077	.054	.107	.045	–	.715	2.65	–
K	–	–	–	–	–	–	–	–	–	–	–	–	–	–	–
L_1	5,130.0-5,139.5	9.5	.083	0.788	.766	0.250	.074	.0801	.116	.073	.080	.0120	.558	2.63	–
L_2	5,112.0-5,116.0	4.0	.069	0.276	.618	0.133	.060	.0191	.222	.111	.067	–	.503	2.65	–
M	5,071.5-5,086.5	15.0	.092	1.381	.412	.0835	.022	.2851	.165	.071	.079	–	.486	2.63	–
N_1	5,030.0-5,052.0	22.0	.078	1.723	.421	1.029	.088	.2916	.170	.081	.079	–	.520	2.64	–
N_2	5,001.0-5,018.5	15.5	.083	1.282	.457	0.739	.050	.1666	.207	.063	.088	–	.504	2.64	–
O	–	–	–	–	–	–	–	–	–	–	–	–	–	–	–

* Sand in zone with less than 25% clay and greater than 3% porosity. Zone averages computed using these footages.

Table 4.8 MWX-2 Middle Fluvial Reservoir Characteristics

Unit	Zone Depth, ft	Pay Sand (h),* ft	Porosity (ϕ), fraction	Porosity-feet (ϕ x h), ft	Water Saturation (S_w), fraction	Hydrocarbon-feet, (ϕ x (1-S_w) x h), ft	Sxo - Sw (ΔS_w), fraction	Permeability-feet (kh), md-ft	Volume Clay (V_{cl}), fraction	Volume Carbonate (V_{CO3}), fraction	Core Porosity, fraction	Stressed Core Permeability, md	Core Water Saturation, fraction	Core Grain Density, gm/cc	Cation Exchange Capacity, meq/100 gm
G	–	–	–	–	–	–	–	–	–	–	–	–	–	–	–
H_1	–	–	–	–	–	–	–	–	–	–	–	–	–	–	–
H_2	–	–	–	–	–	–	–	–	–	–	–	–	–	–	–
I	5,339.0-5,344.0	5.0	.064	0.320	.453	0.189	.290	.0280	.171	.021	–	–	–	–	–
J	5,298.0-5,302.0	4.0	.048	0.191	.661	0.079	.371	.0059	.093	.199	–	–	–	–	–
K	5,234.0-5,240.0	6.0	.073	0.440	.556	0.214	.267	.0376	.119	.066	–	–	–	–	–
L_1	5,135.0-5,143.0	8.0	.105	0.839	.656	.0326	.120	.1029	.109	.036	–	–	–	–	–
L_2	5,108.0-5,123.0	15.0	.078	1.170	.583	0.536	.001	.1183	.167	.059	–	–	–	–	–
M	–	–	–	–	–	–	–	–	–	–	–	–	–	–	–
N_1	5,028.0-5,054.0	26.0	.084	2.194	.431	1.282	.156	.3638	.171	.034	–	–	–	–	–
N_2	4,999.0-5.022.0	23.0	.092	2.126	.474	1.146	.120	.3206	.160	.016	–	–	–	–	–
O	–	–	–	–	–	–	–	–	–	–	–	–	–	–	–

* Sand in zone with less than 25% clay and greater than 3% porosity. Zone averages computed using the footages.

Table 4.9 MWX-3 Middle Fluvial Reservoir Characteristics

Unit	Zone Depth, ft	Pay Sand (h),* ft	Porosity (ϕ), fraction	Porosity-feet ($\phi \times h$), ft	Water Saturation (S_w), fraction	Hydrocarbon-feet, ($\phi \times (1-S_w) \times h$), ft	$S_{xo} - S_w$ (ΔS_w), fraction	Permeability-feet (kh), md-ft	Volume Clay (V_{cl}), fraction	Volume Carbonate (V_{CO3}), fraction	Core Porosity, fraction	Stressed Core Permeability, md	Core Water Saturation, fraction	Core Grain Density, gm/cc	Cation Exchange Capacity, meq/100 gm
G	5,432.0-5,437.0	5.0	.062	0.309	.765	.093	.061	.0104	.125	.024	–	–	–	–	–
H_1	–	–	–	–	–	–	–	–	–	–	–	–	–	–	–
H_2	–	–	–	–	–	–	–	–	–	–	–	–	–	–	–
I	–	–	–	–	–	–	–	–	–	–	–	–	–	–	–
J	–	–	–	–	–	–	–	–	–	–	–	–	–	–	–
K	5,241.0-5,246.0	5.0	.049	0.244	.724	.087	.126	.0060	.176	.038	–	–	–	–	–
L_1	5,140.0-5,157.0	17.0	.094	1.595	.585	.687	.046	.1796	.137	.027	–	–	–	–	–
L_2	5,110.0-5,123.0	13.0	.067	0.872	.625	.361	0	.0540	.171	.013	–	–	–	–	–
M	–	–	–	–	–	–	–	–	–	–	–	–	–	–	–
N_1	5,034.0-5,047.0	13.0	.074	0.966	.412	.597	.053	.1674	.169	.017	–	–	–	–	–
N_2	5,007.0-5,027.0	20.0	.083	1.655	.492	.875	.052	.2336	.162	.045	–	–	–	–	–
O	4,980.0-4,984.0	4.0	.095	0.380	.706	.142	.077	.0252	.220	.016	–	–	–	–	–

* Sand in zone with less than 25% clay and greater than 3% porosity. Zone averages computed using these footages.

Table 4.10 Explanation of Crossplot Variables

CARB	:	carbonaceous material, fraction
CEC	:	cation exchange capacity, meq/100 gm
CO3	:	dolomite + calcite (thin-section), fraction
CORESO	:	core oil saturation, fraction
CORESW	:	core water saturation, fraction
CORPHI	:	core porosity, fraction
DLT	:	sonic interval transit time, microseconds/ft
DOLO	:	dolomite (thin-section), fraction
GRRUN	:	gamma ray, borehole corrected, API units
KMAX	:	dry core permeability, uncorrected, md
KPFM	:	dry core Klinkenberg permeability, corrected to in situ net stress, md
LITHIC	:	rock fragments (thin-section), fraction
PEFR	:	photoelectric effect, barns/electron
PHINC	:	neutron porosity, borehole corrected, fraction
POTAR	:	spectral gamma ray potassium, fraction
QUARTZ	:	quartz (thin-section), fraction
RHOBRC	:	bulk density, borehole corrected, gm/cc
RHOGD	:	core grain density, gm/cc
RT	:	formation resistivity (deep), ohm-m
SNPR	:	sidewall neutron porosity, uncorrected, fraction
TKRAT	:	thorium/potassium ratio
VPVSRA	:	compressional wave velocity/shear wave velocity, dimensionless
XGRSZE	:	mean grain size (thin-section), mm

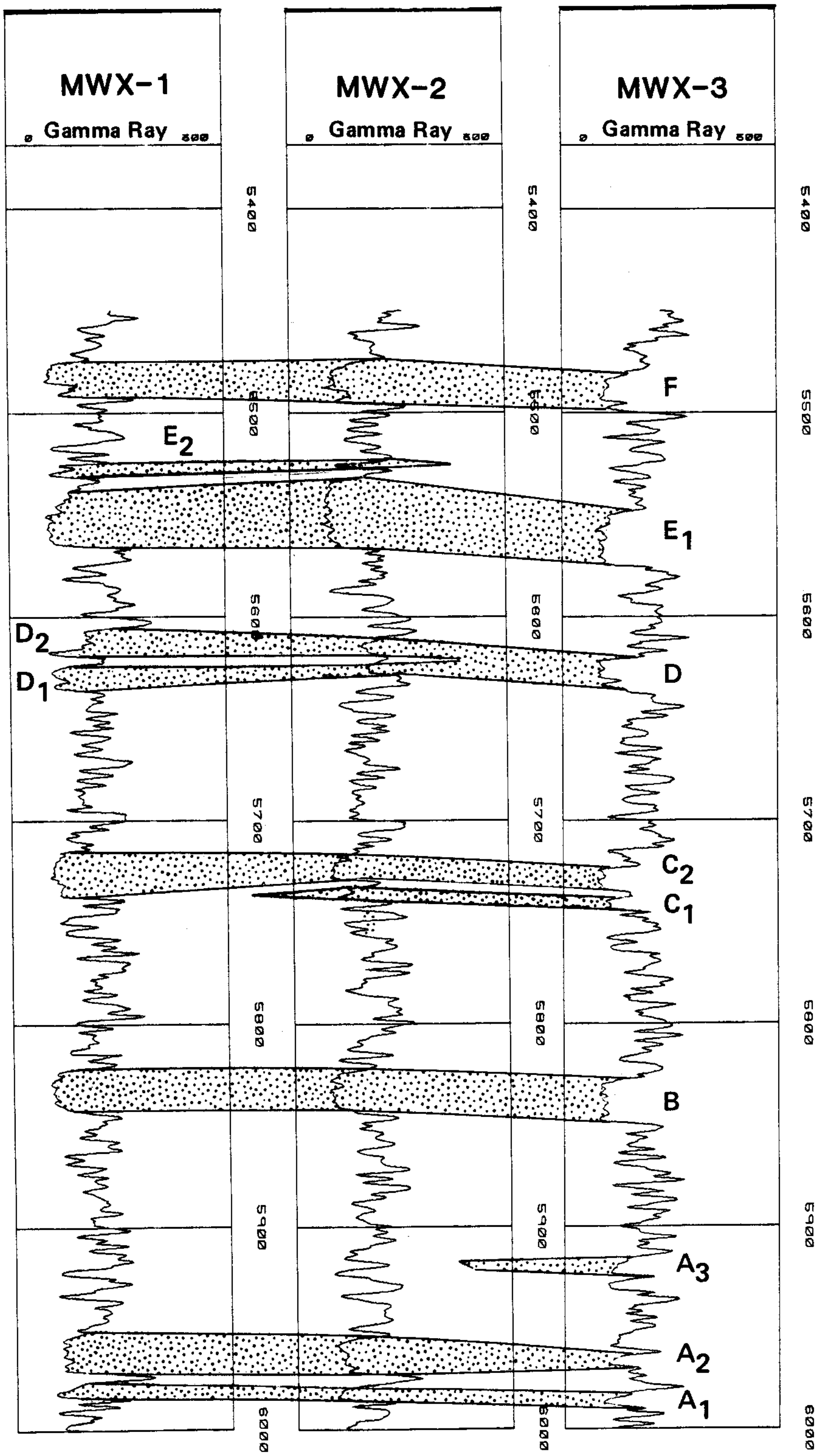

Figure 4.1 Correlation of Units Within the MWX Low Fluvial Interval

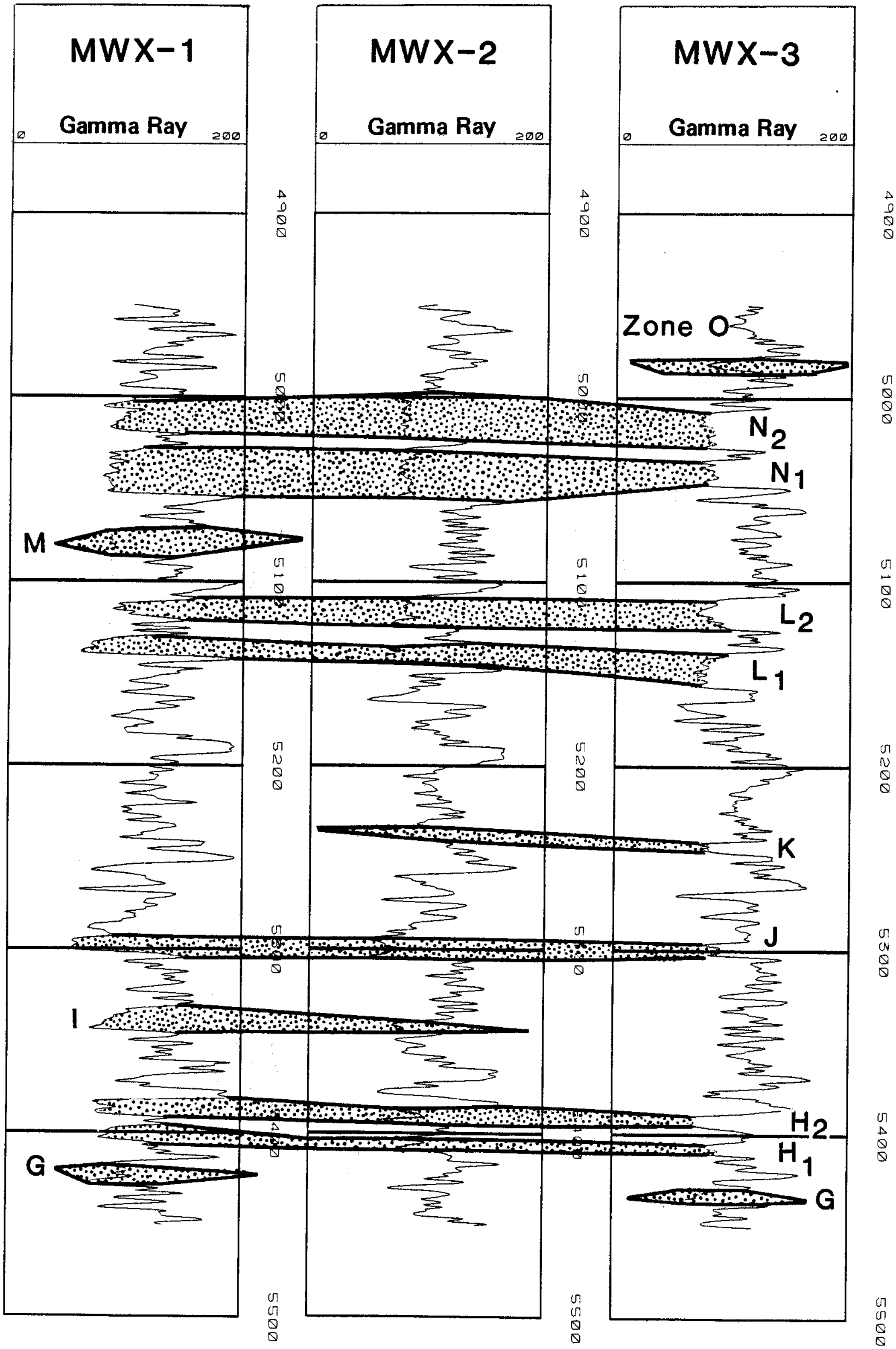

Figure 4.2 Correlation of Units Within the MWX Middle Fluvial Interval

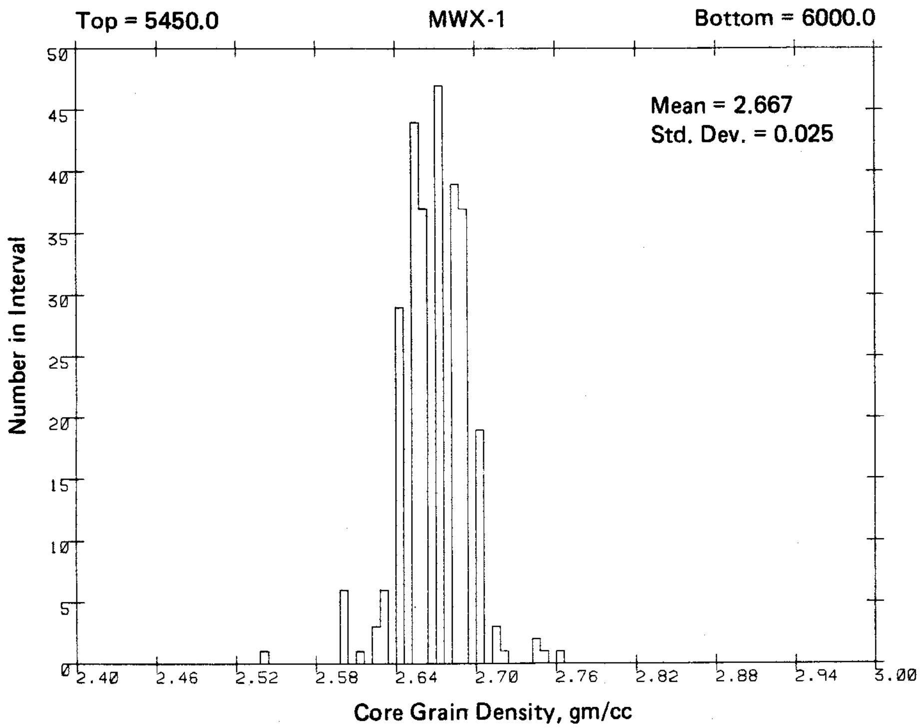

Figure 4.3 Range in Core Grain Density, MWX-1 Low Fluvial Interval

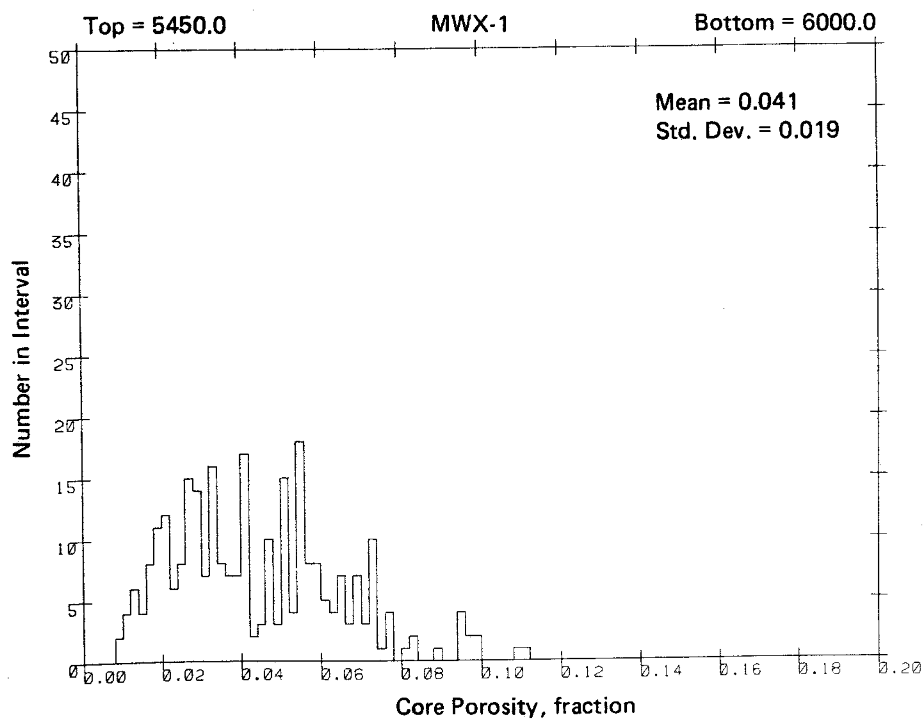

Figure 4.4 Range in Core Porosity, MWX-1 Low Fluvial Interval

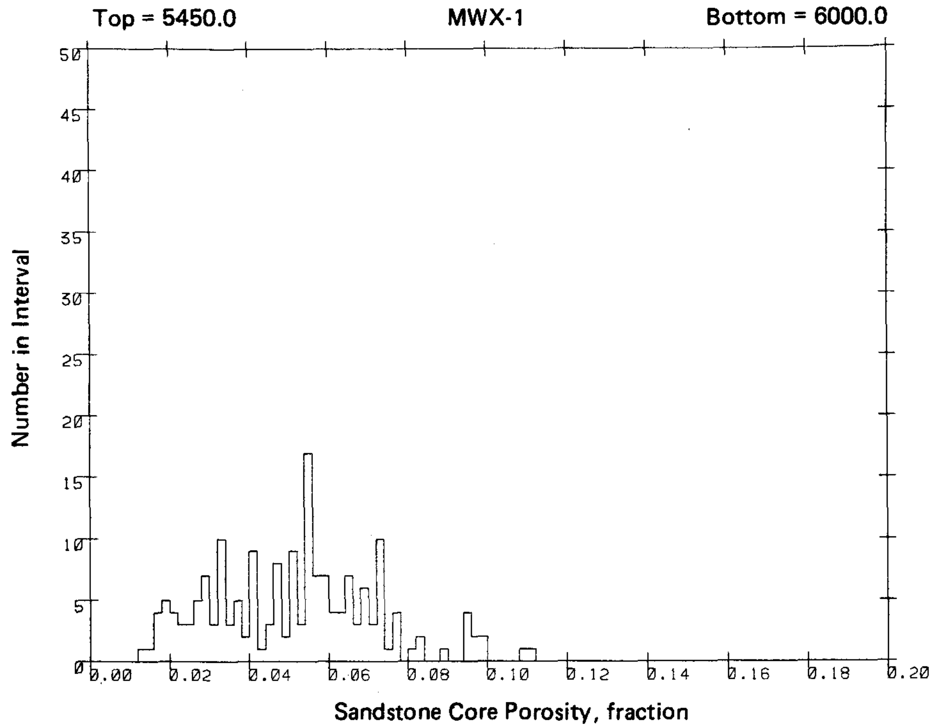

Figure 4.5 Range in Sandstone Core Porosity, MWX-1 Low Fluvial Interval

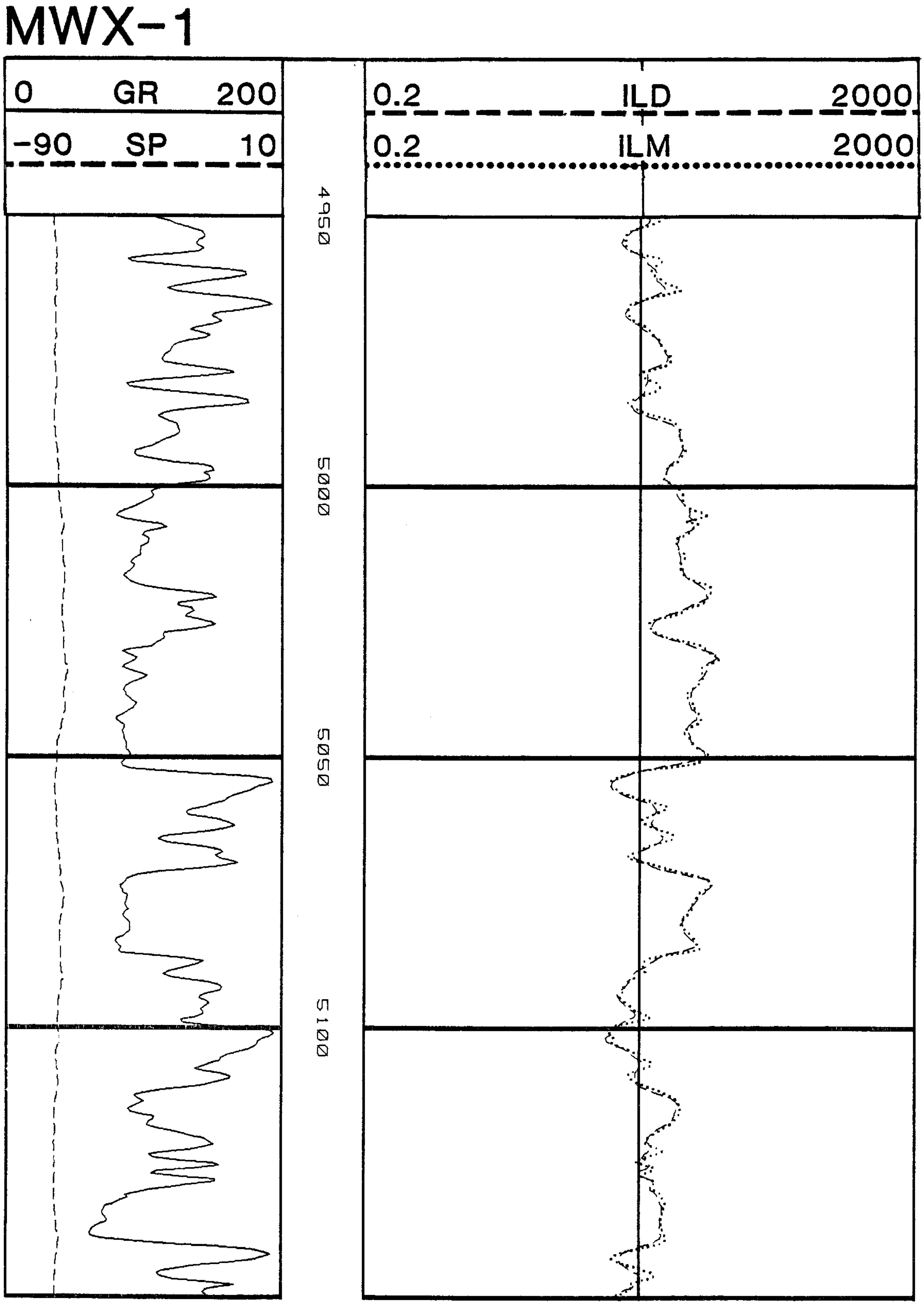

Figure 4.6 MWX-1 Resistivity Log

MWX-1

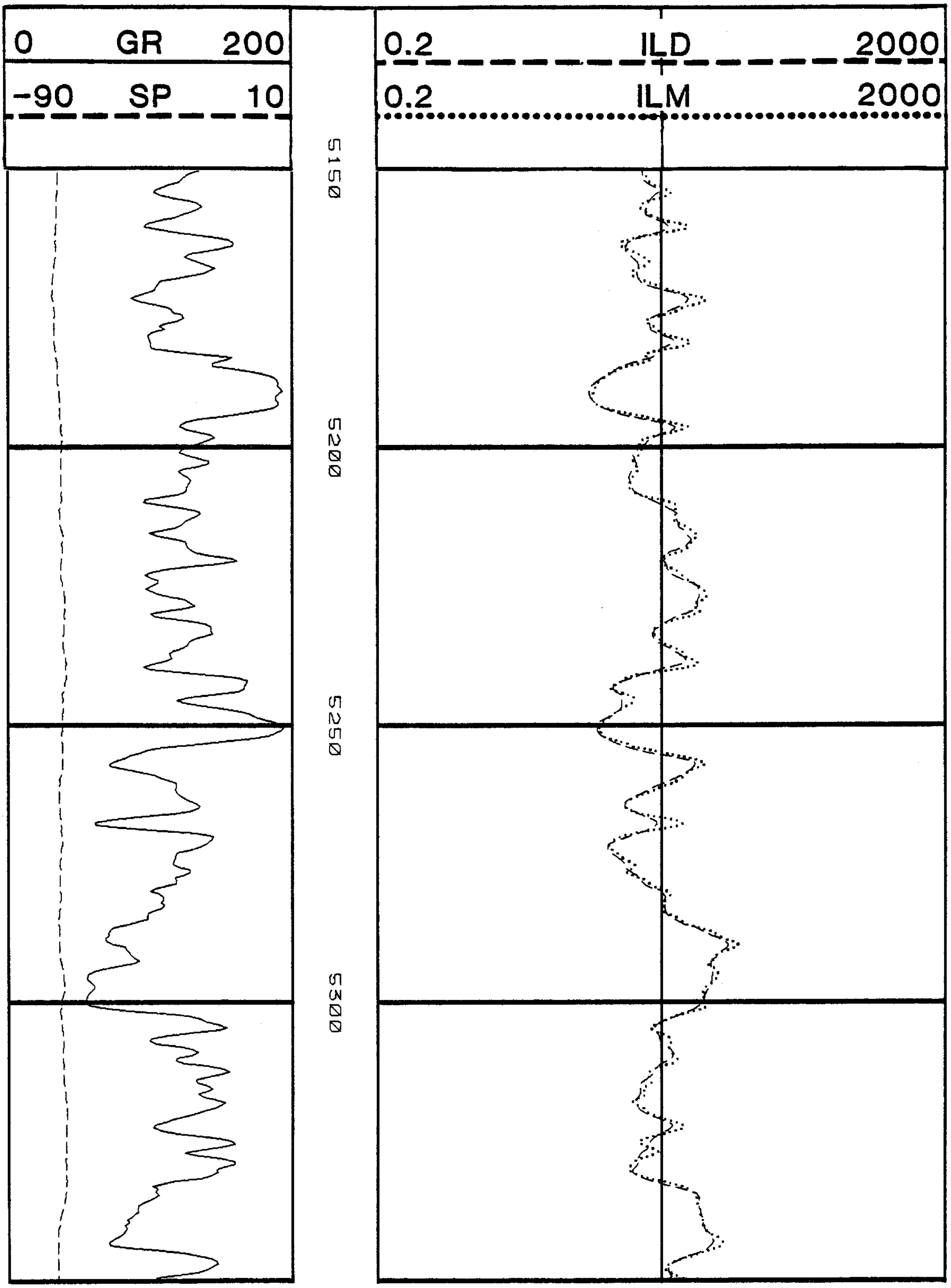

Figure 4.6, Continued

MWX-1

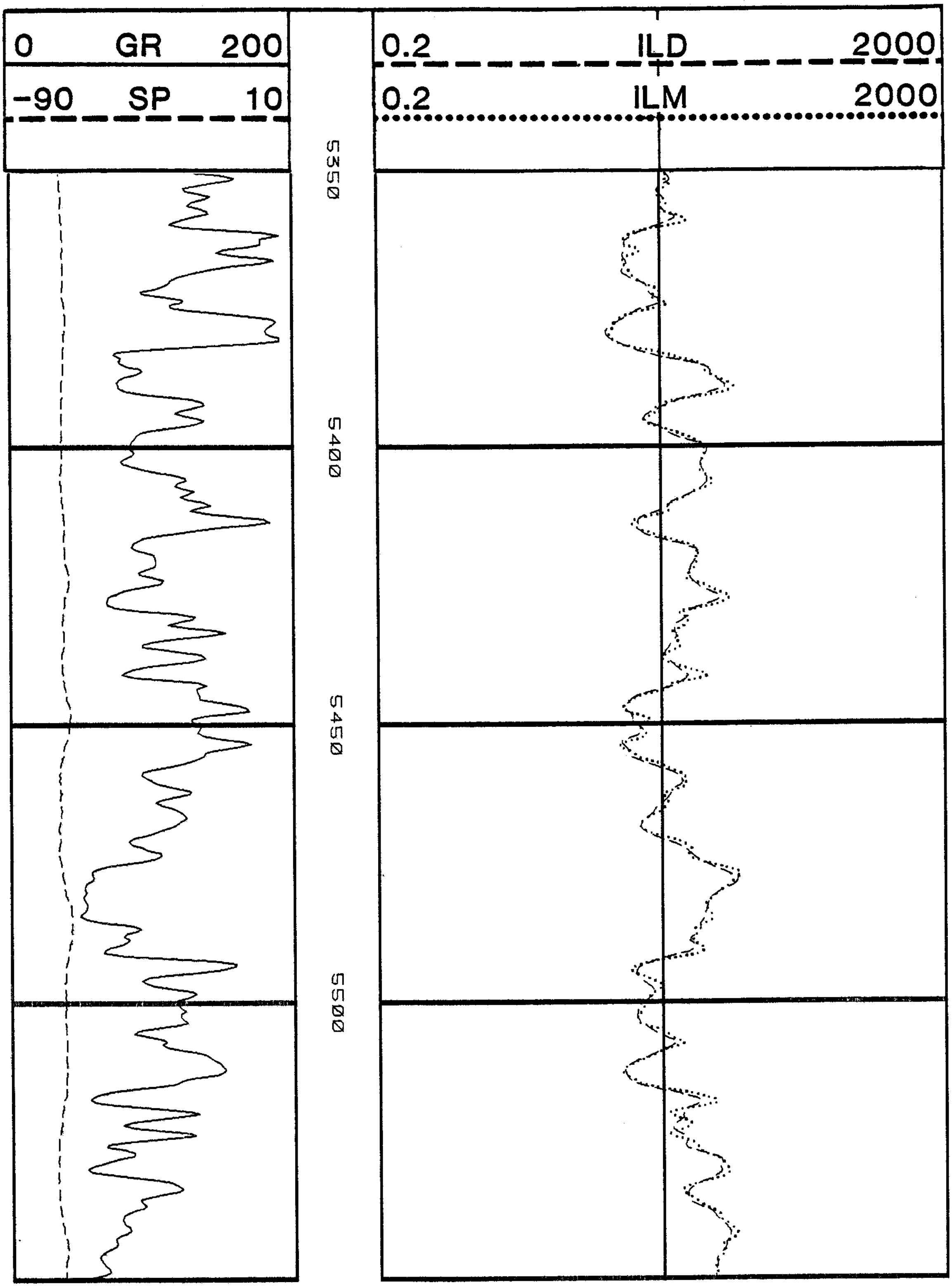

Figure 4.6, Continued

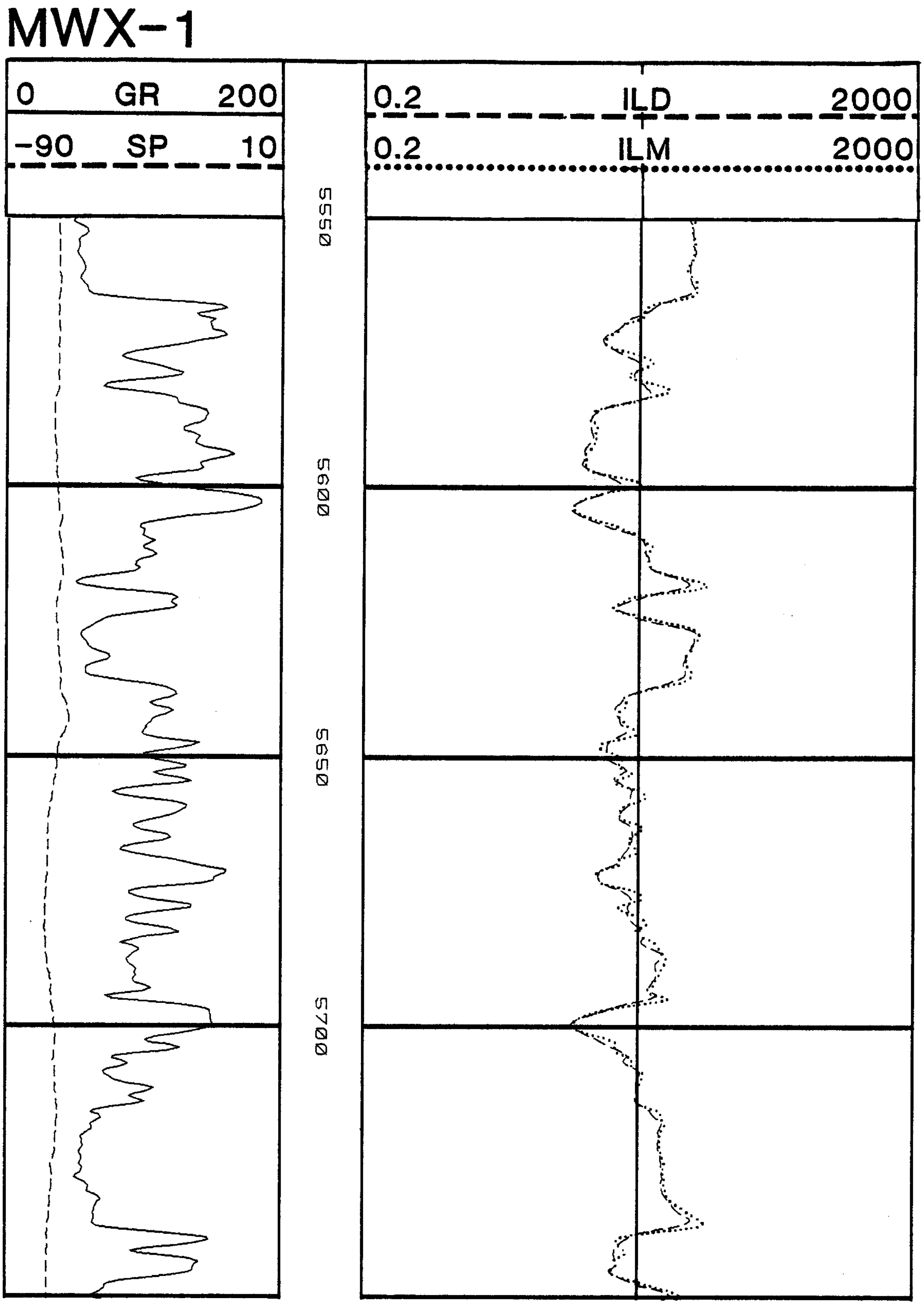

Figure 4.6, Continued

MWX-1

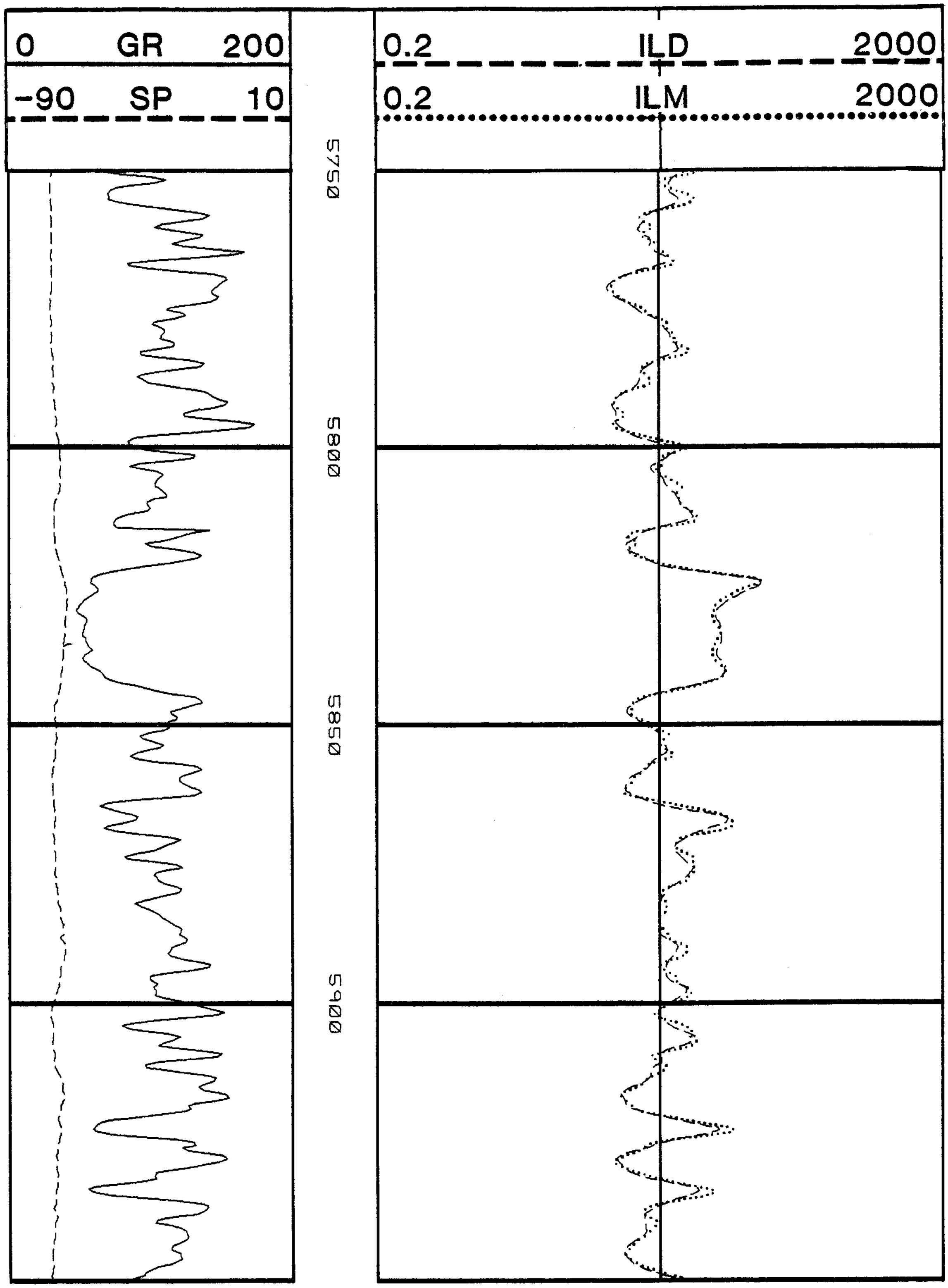

Figure 4.6, Continued

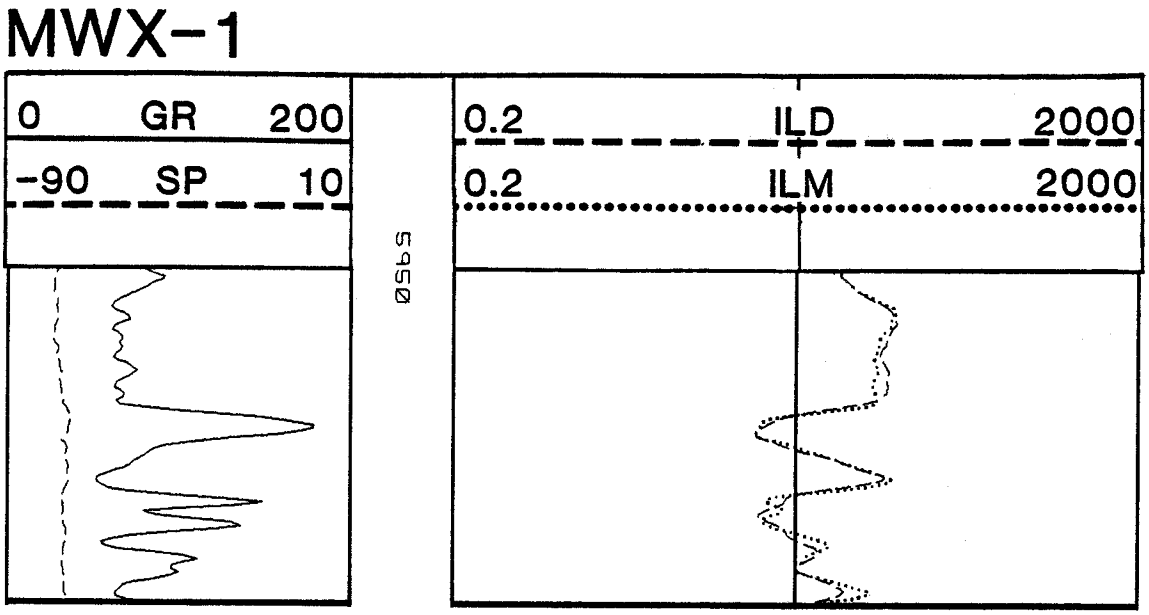

Figure 4.6, Continued

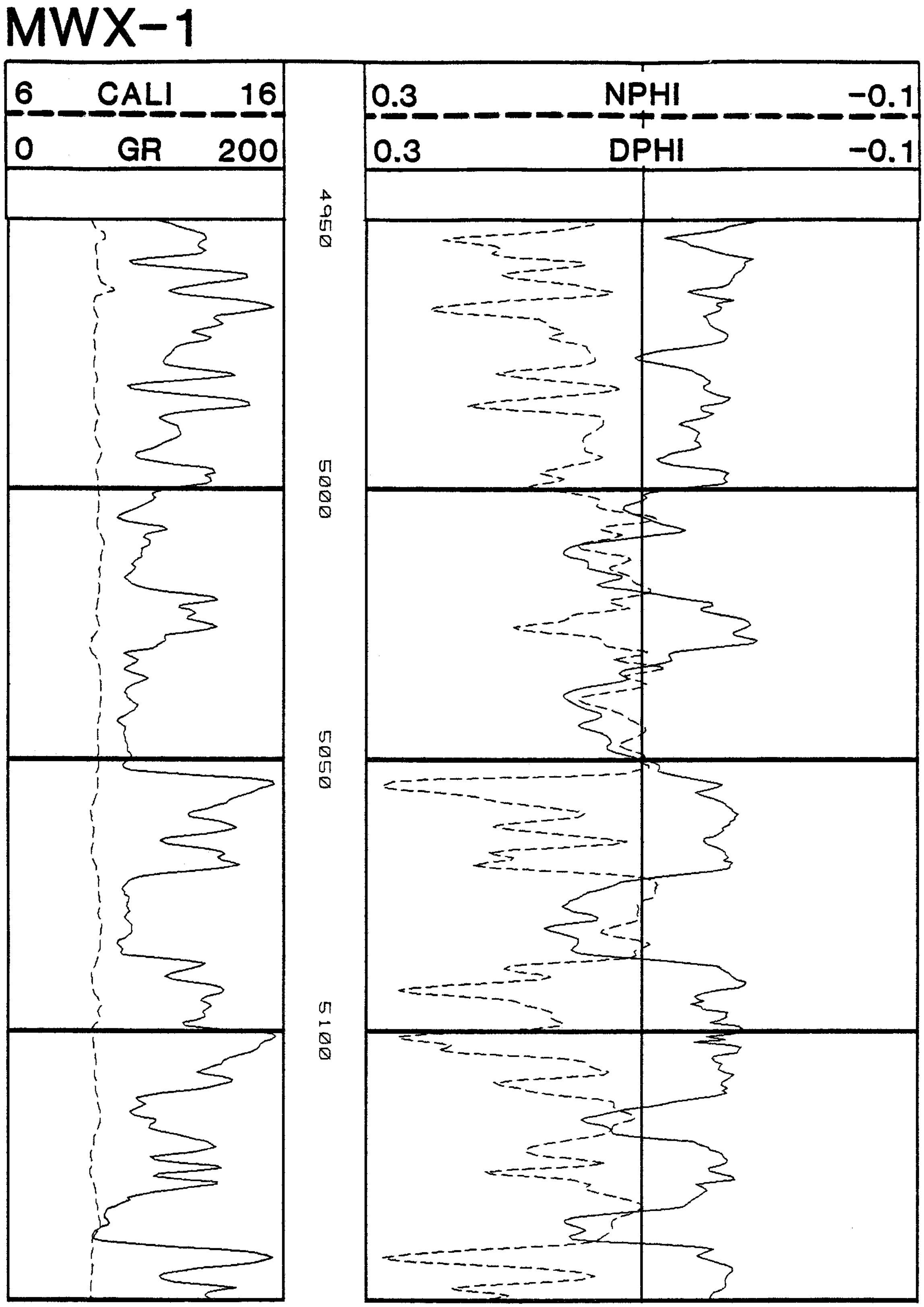

Figure 4.7 MWX-1 Density and Neutron Porosity Logs

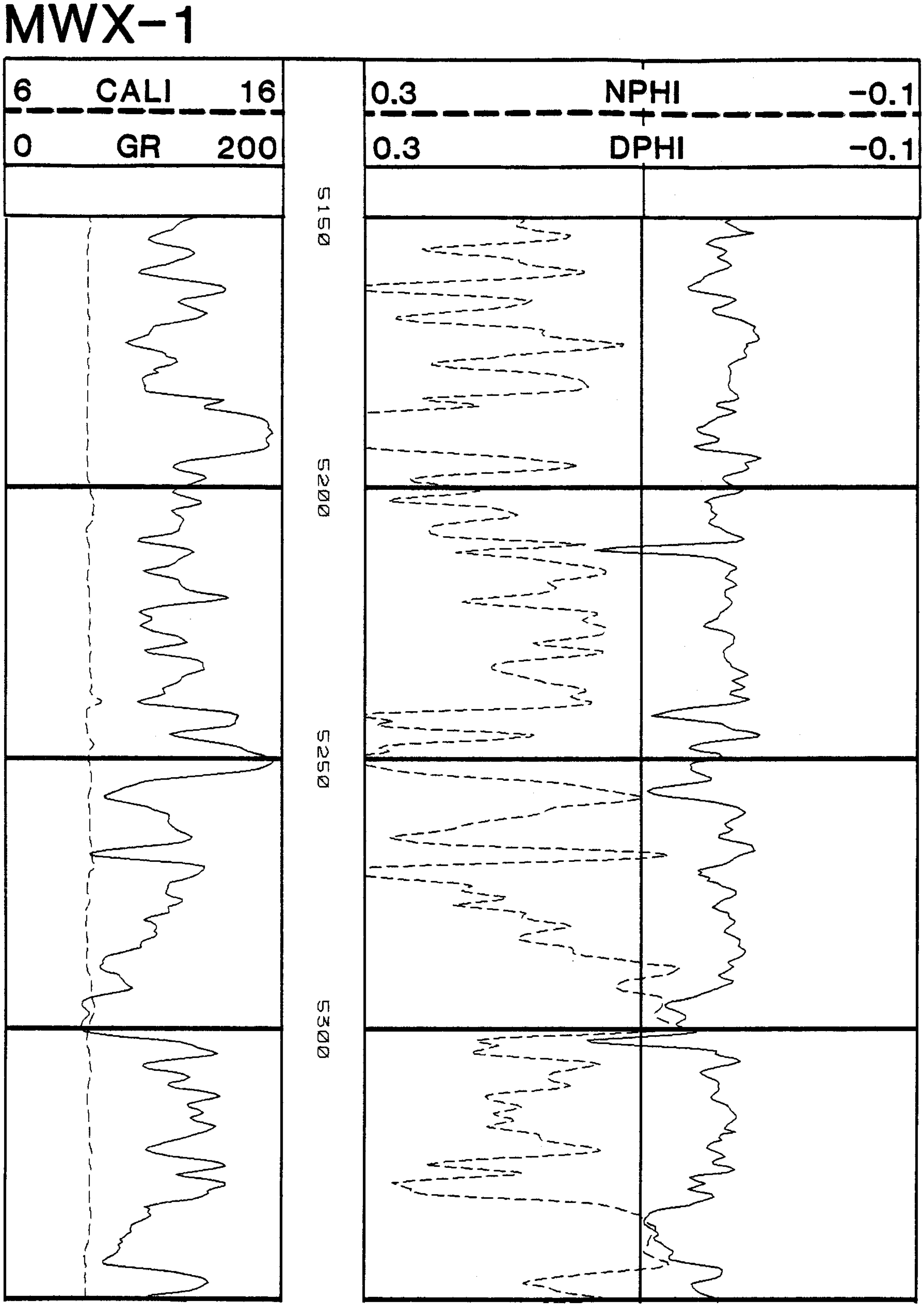

Figure 4.7, Continued

MWX-1

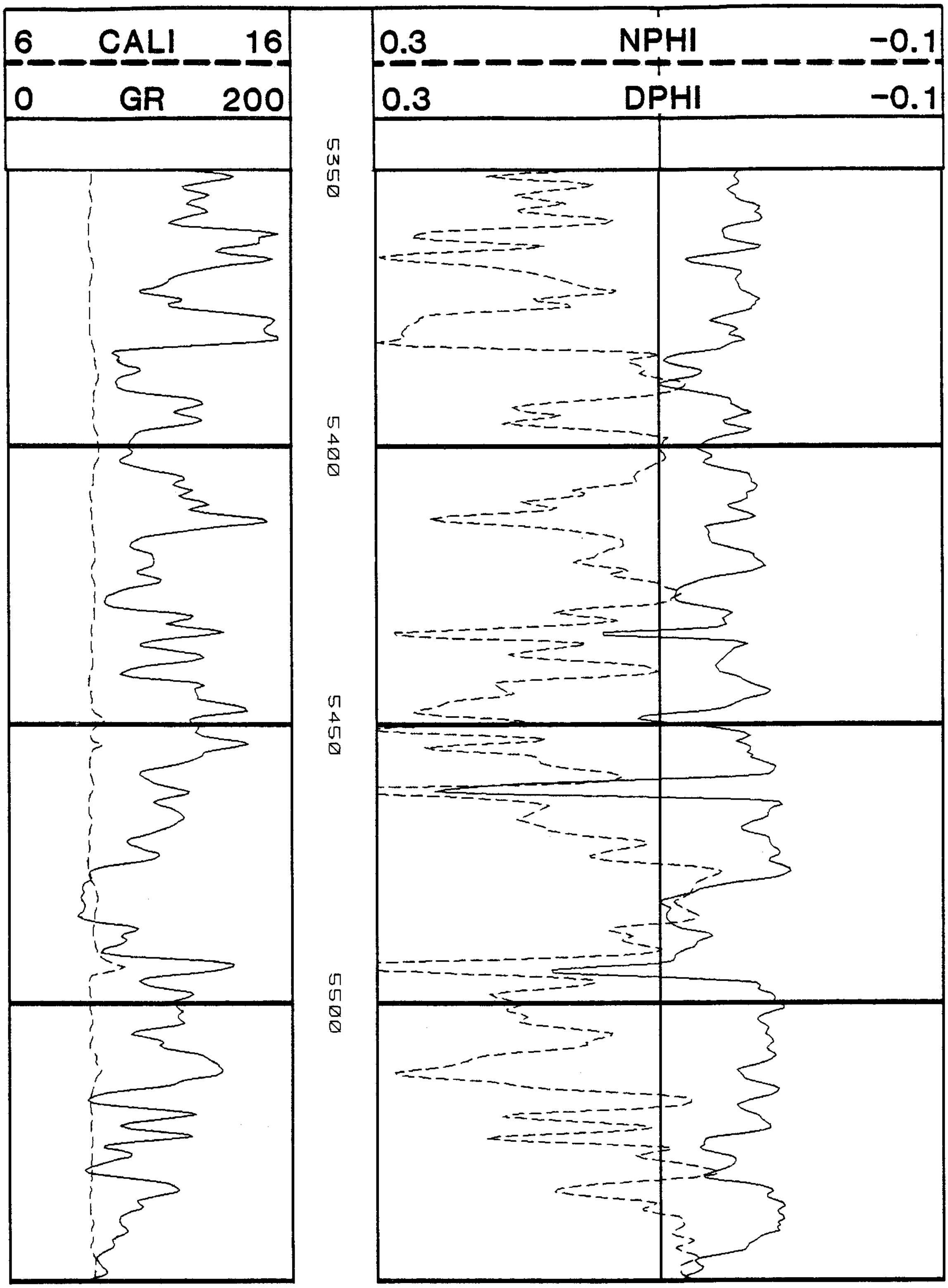

Figure 4.7, Continued

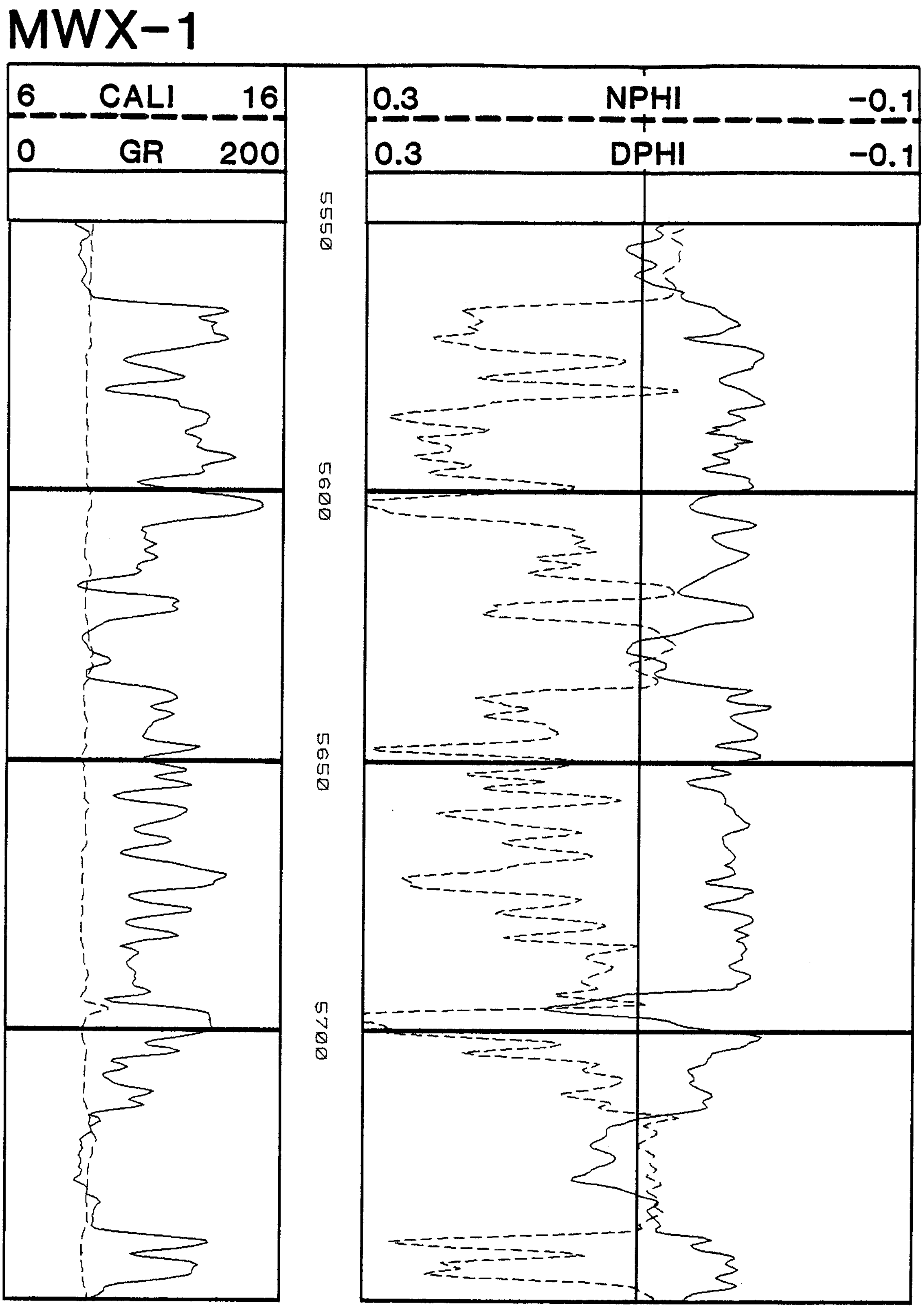

Figure 4.7, Continued

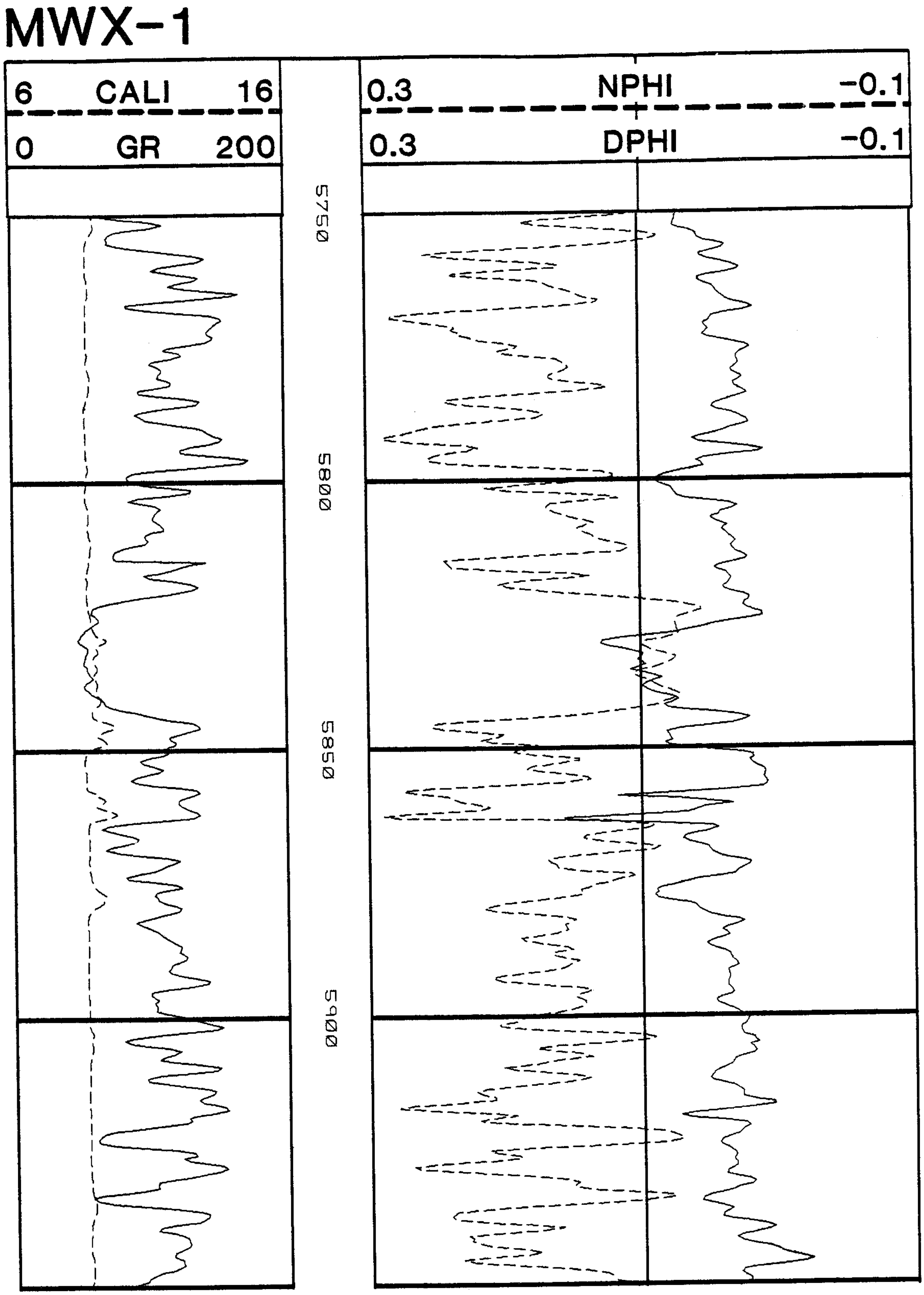

Figure 4.7, Continued

MWX-1

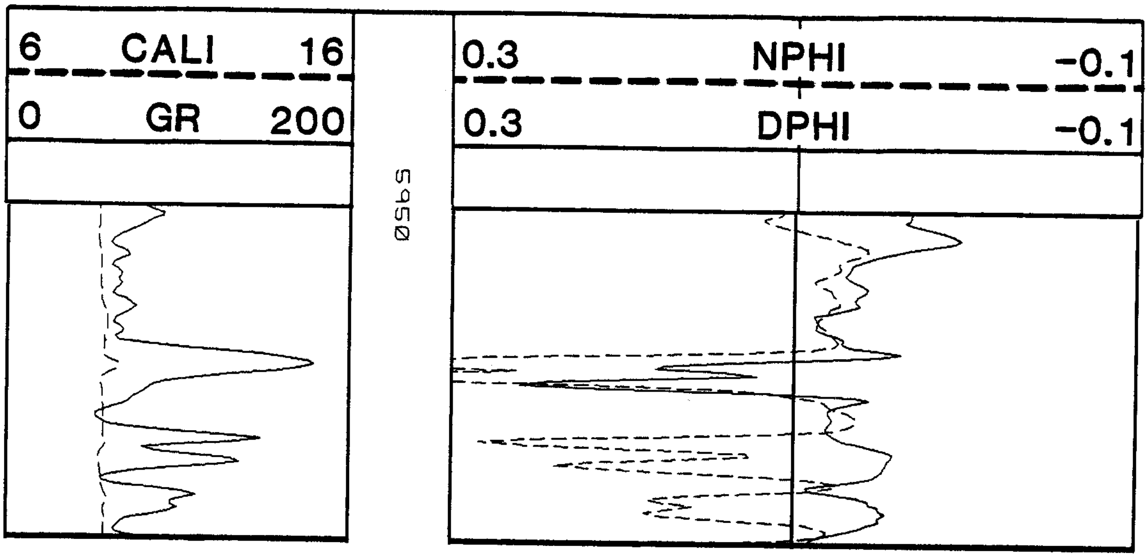

Figure 4.7, Continued

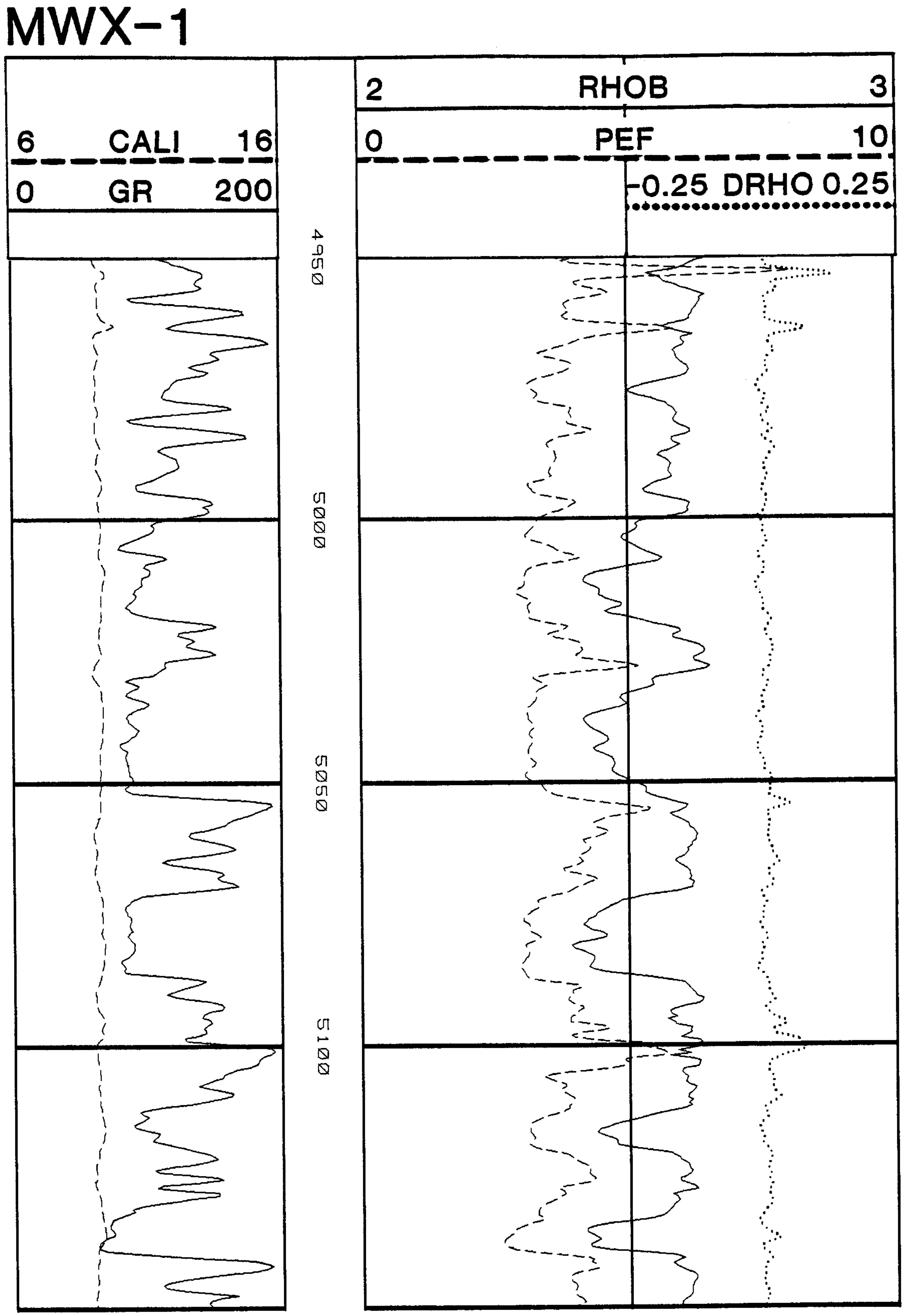

Figure 4.8 MWX-1 Bulk Density and Photoelectric Absorption Logs

MWX-1

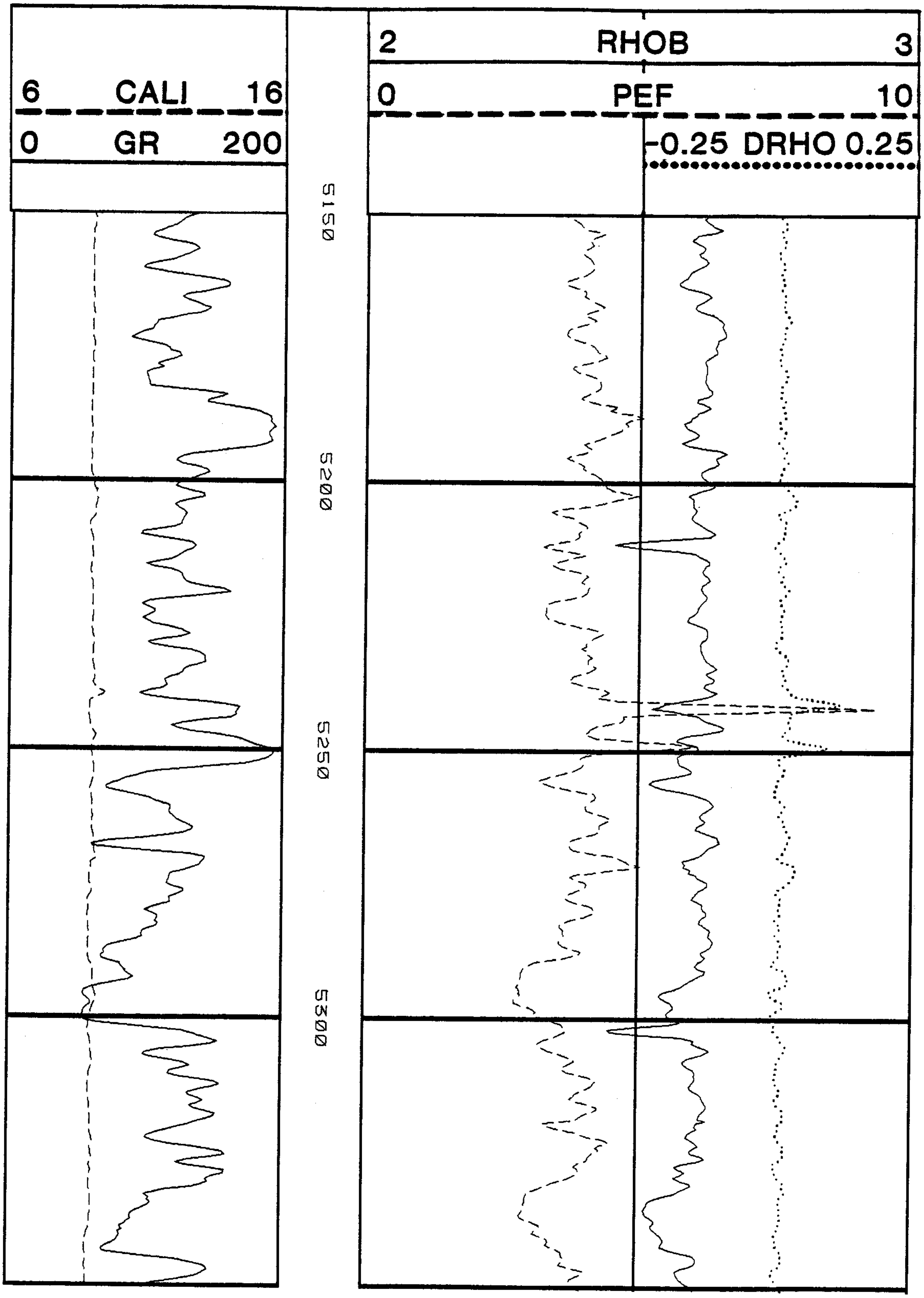

Figure 4.8, Continued

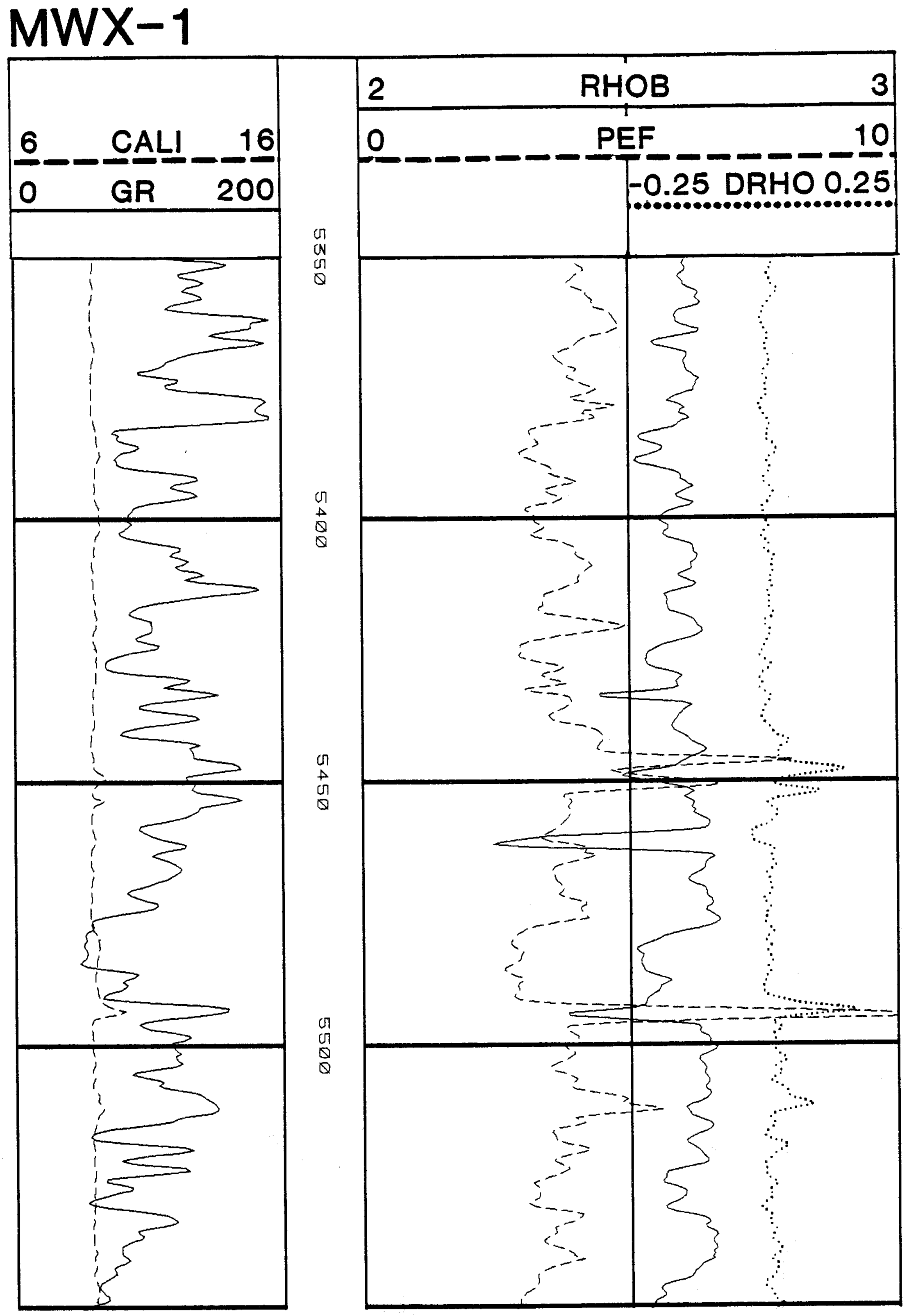

Figure 4.8, Continued

MWX-1

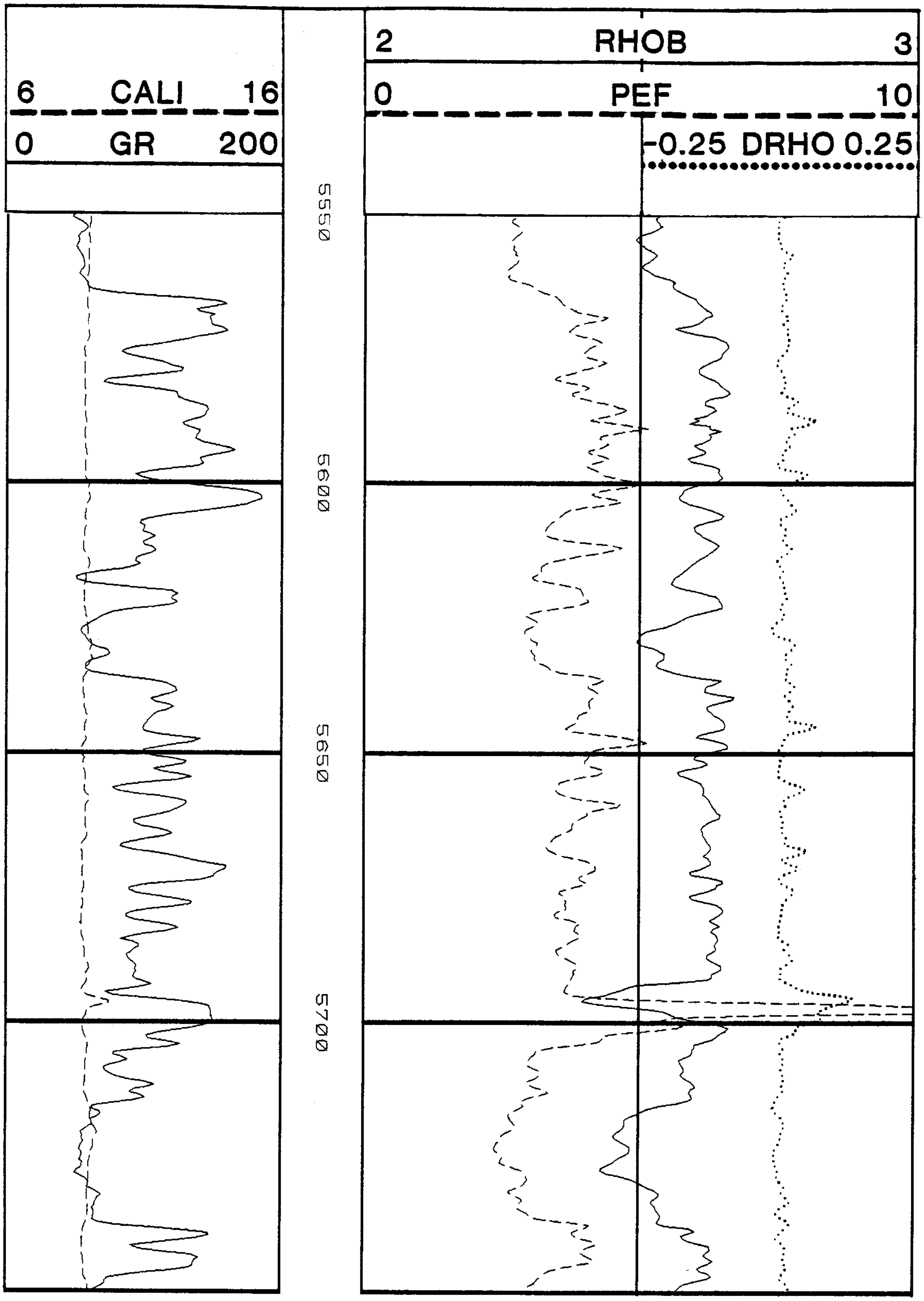

Figure 4.8, Continued

MWX-1

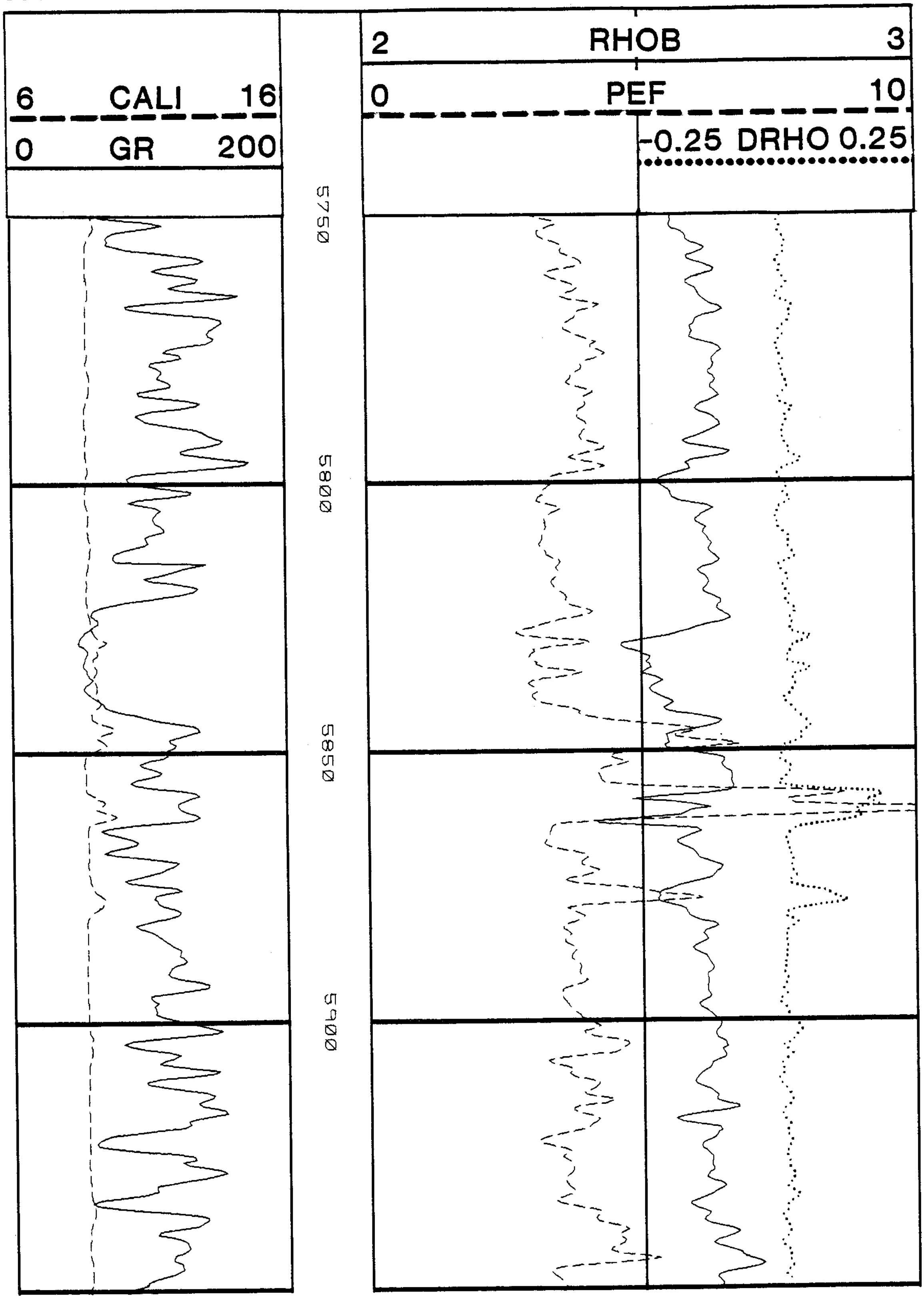

Figure 4.8, Continued

MWX-1

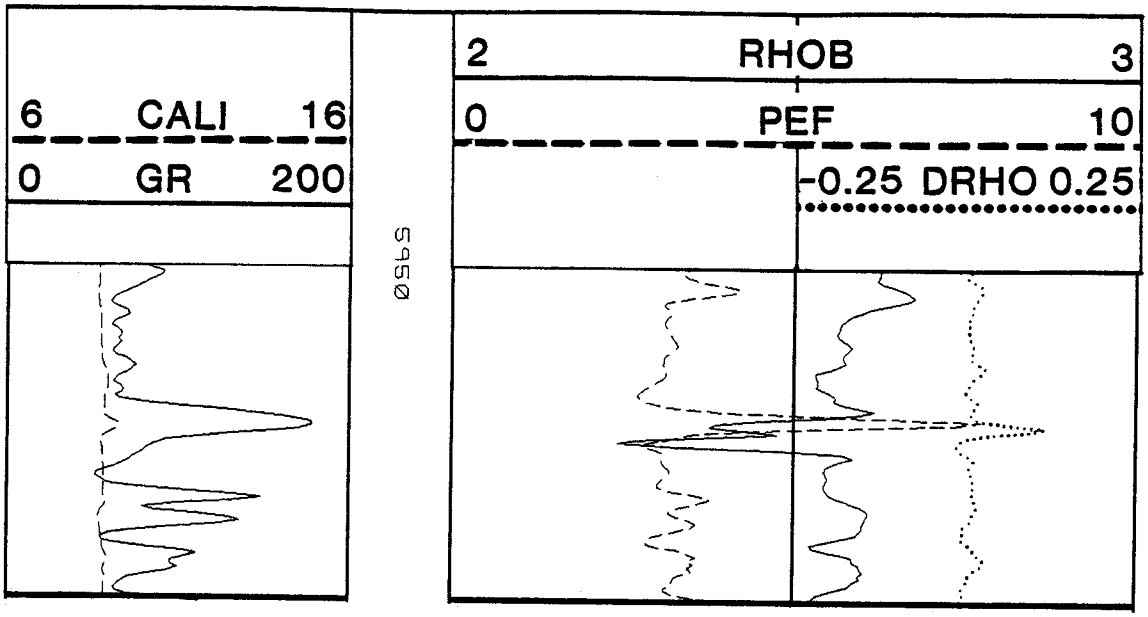

Figure 4.8, Continued

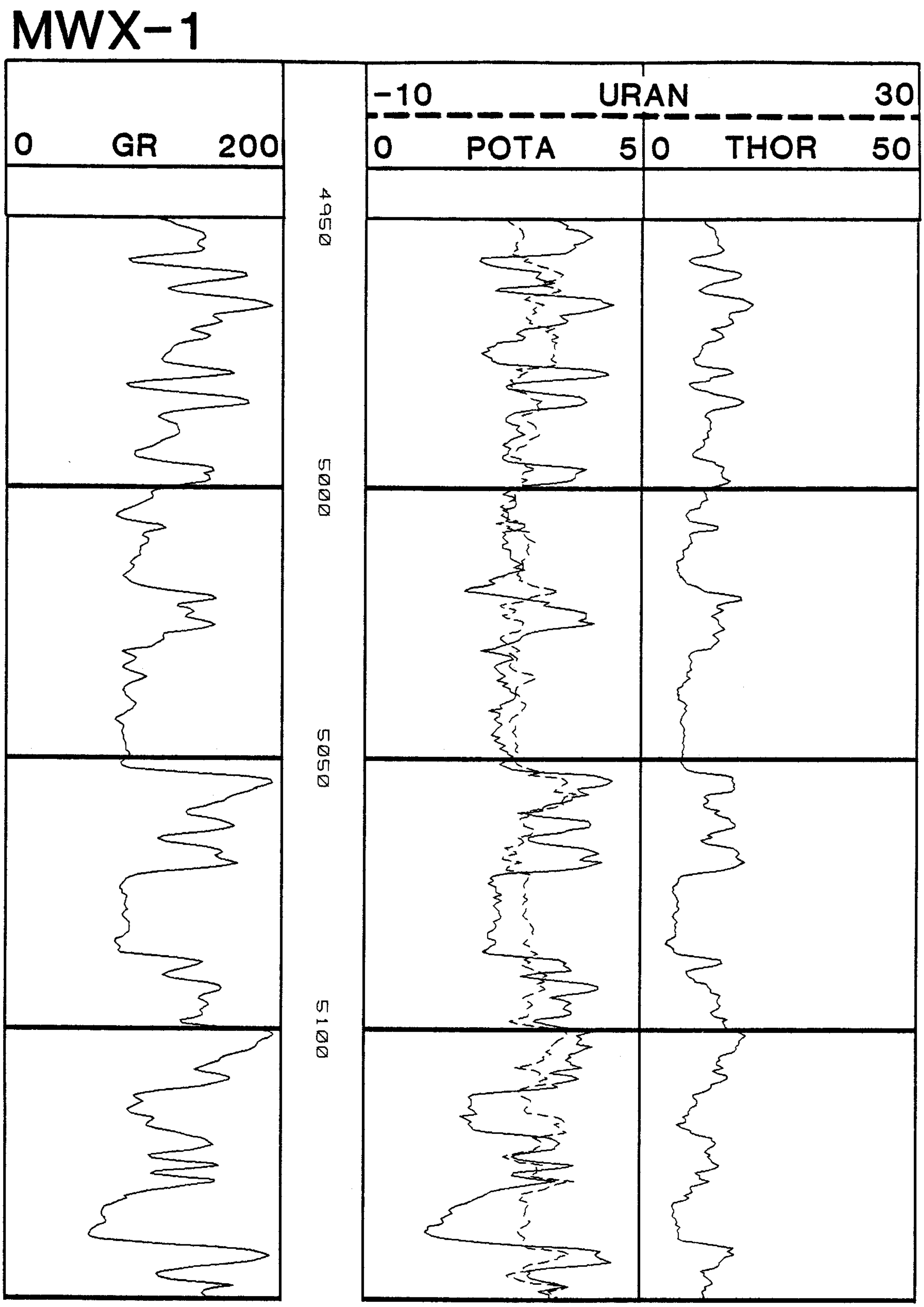

Figure 4.9 MWX-1 Spectral Gamma Log

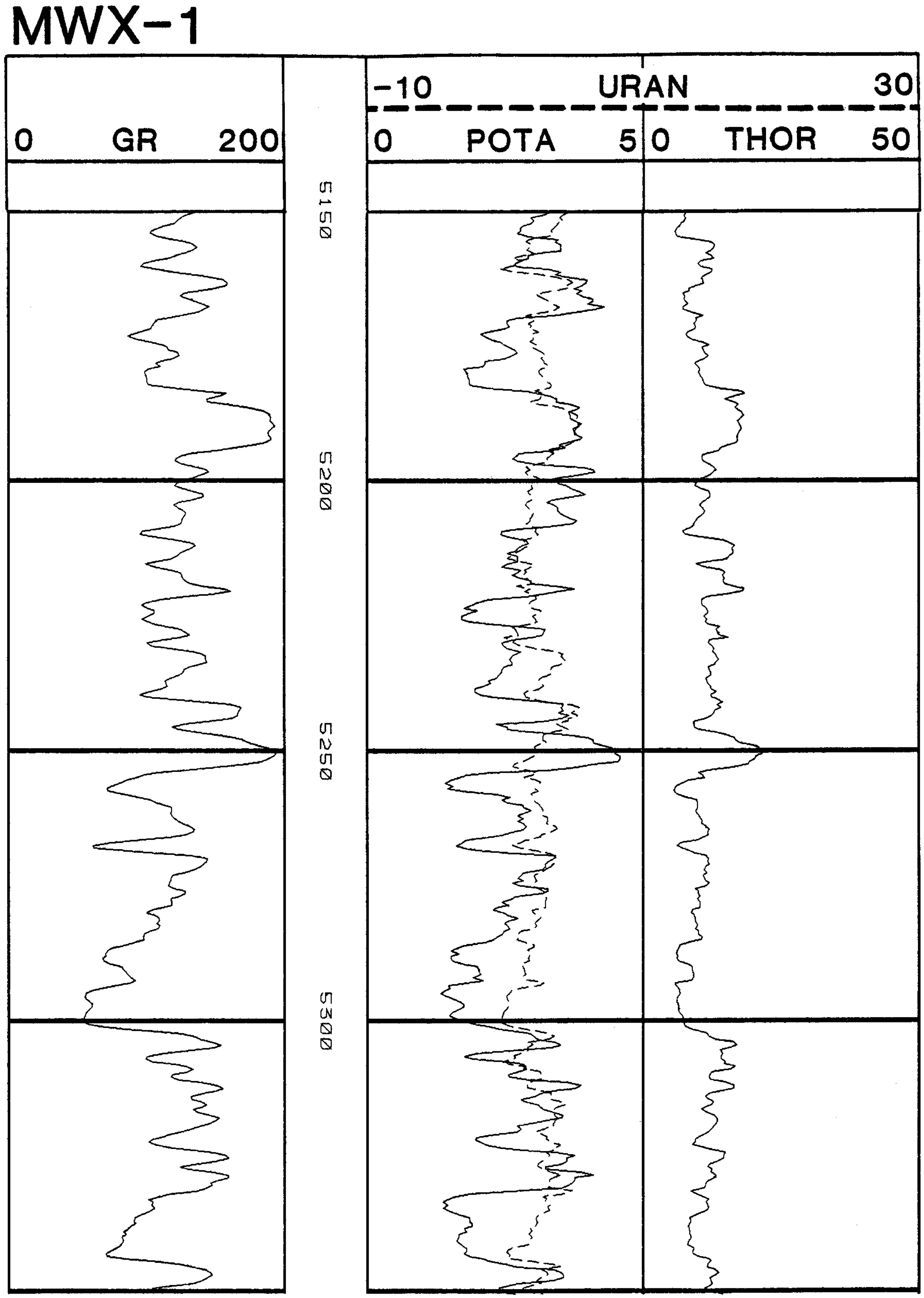

Figure 4.9, Continued

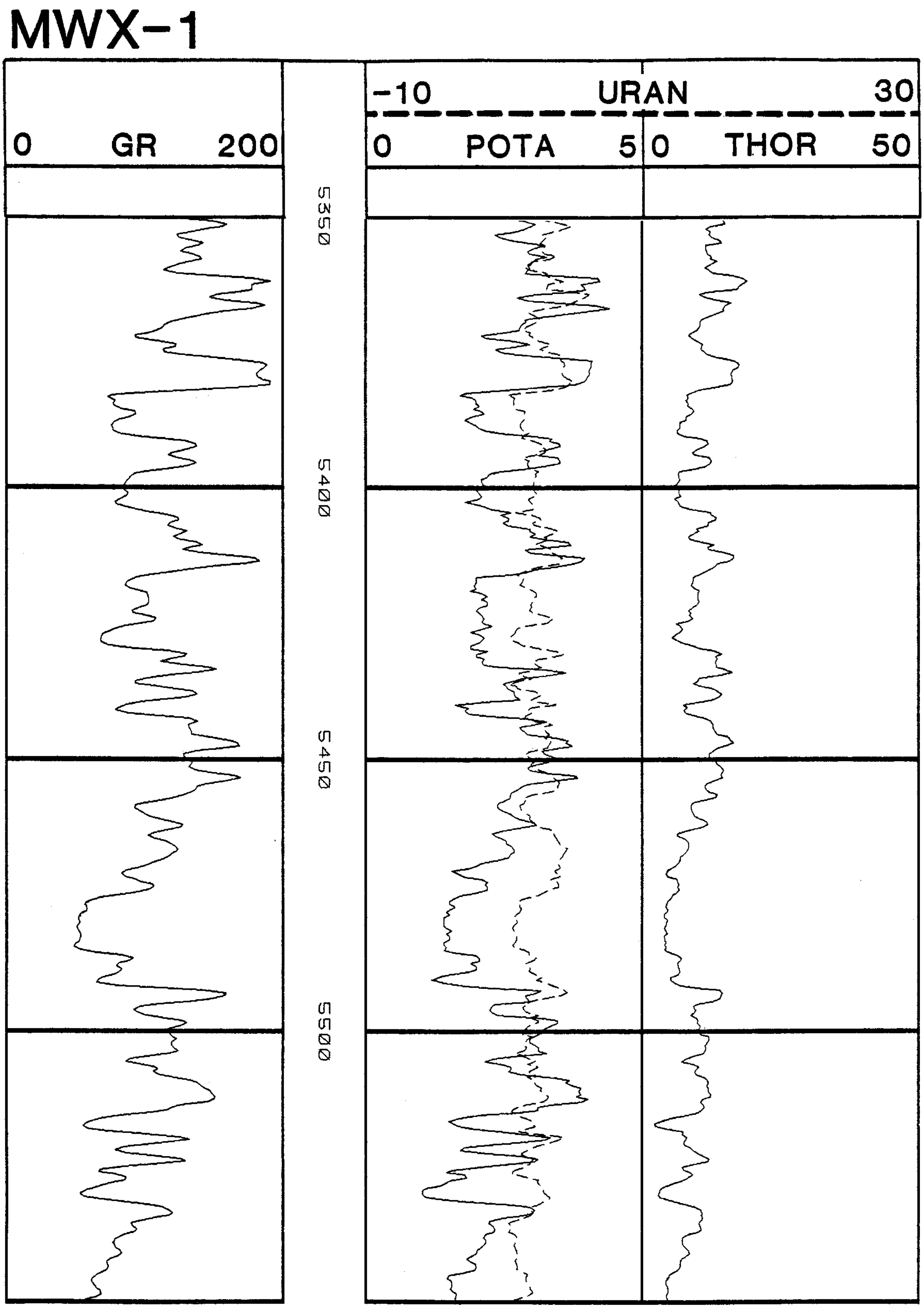

Figure 4.9, Continued

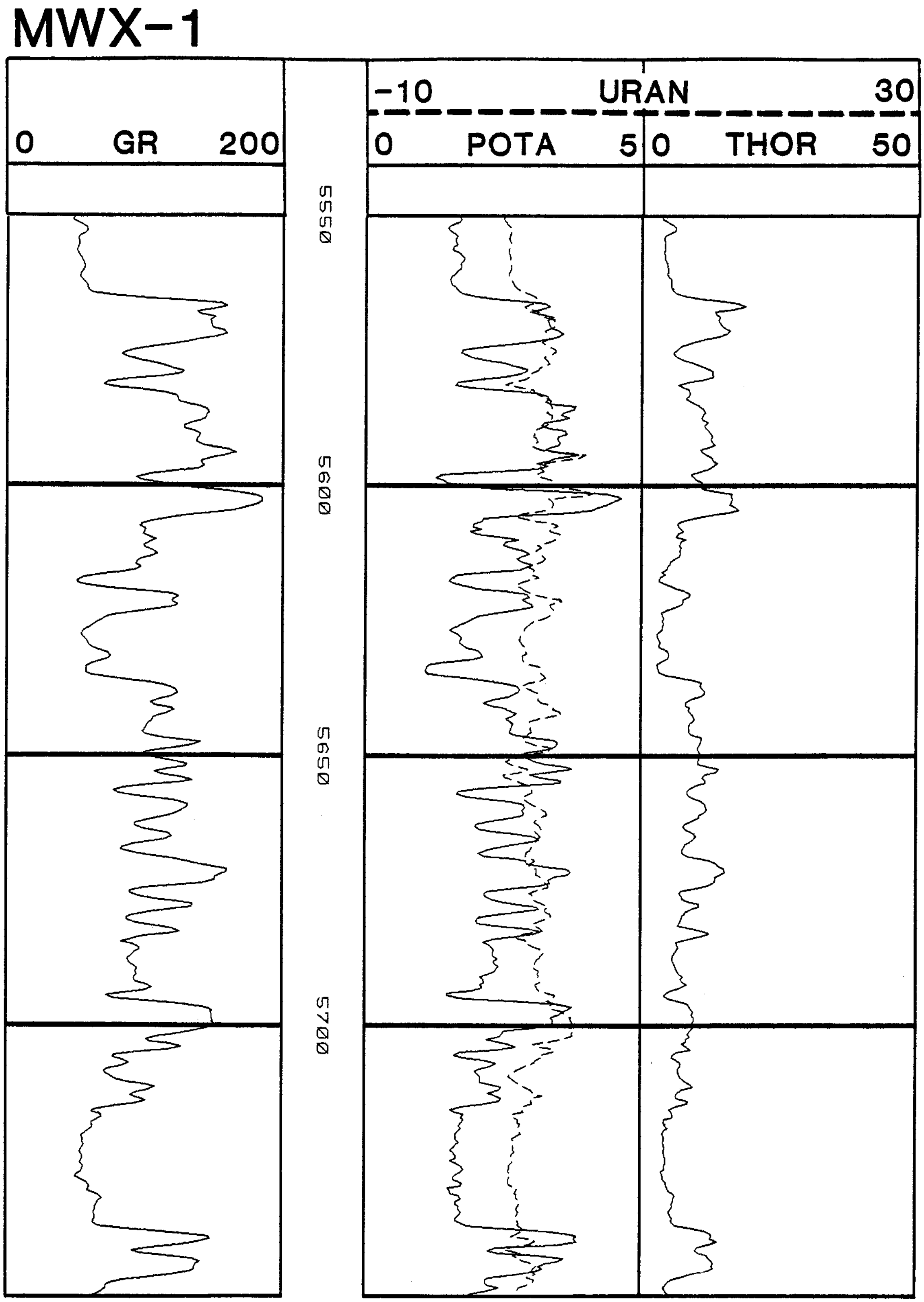

Figure 4.9, Continued

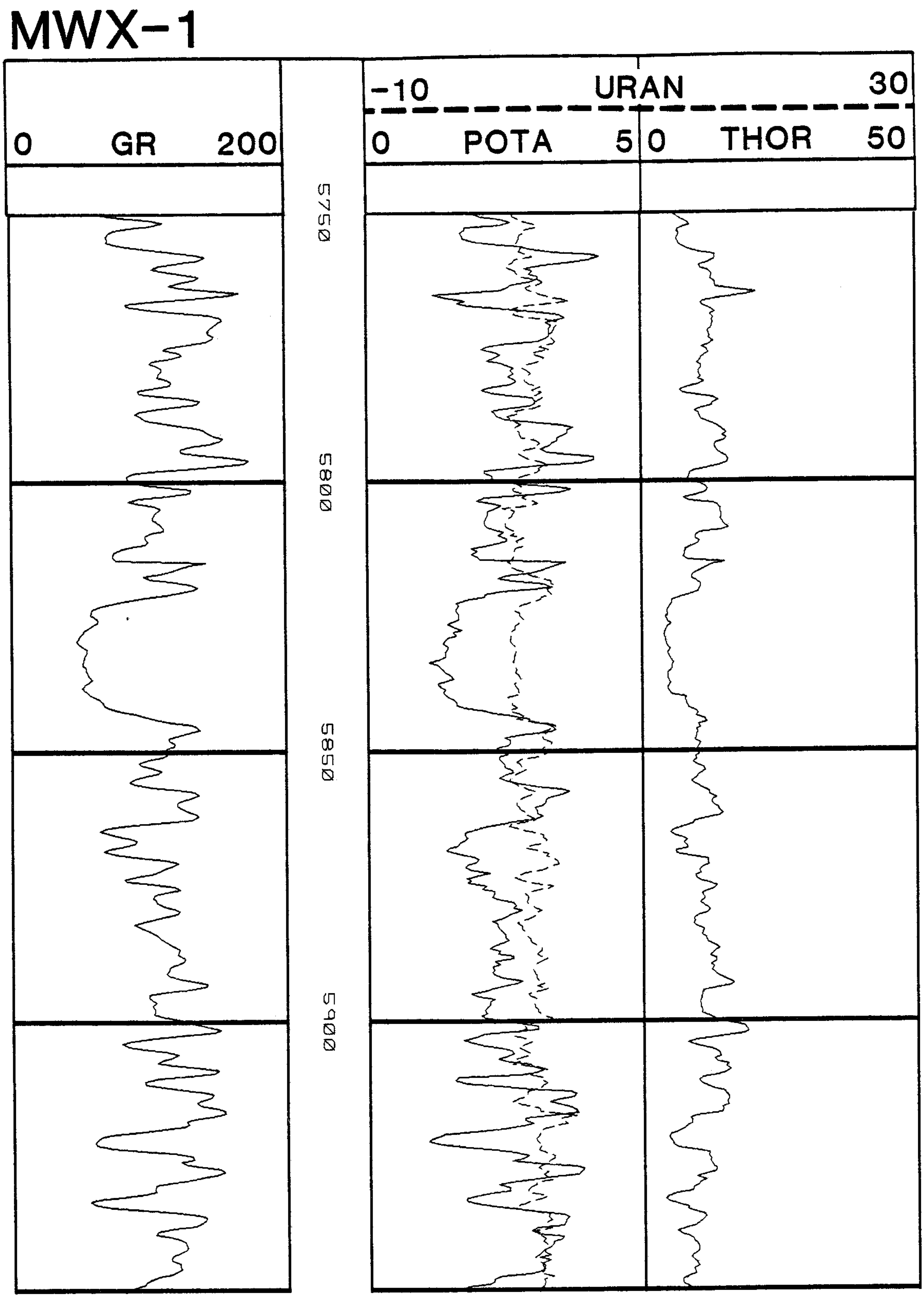

Figure 4.9, Continued

MWX-1

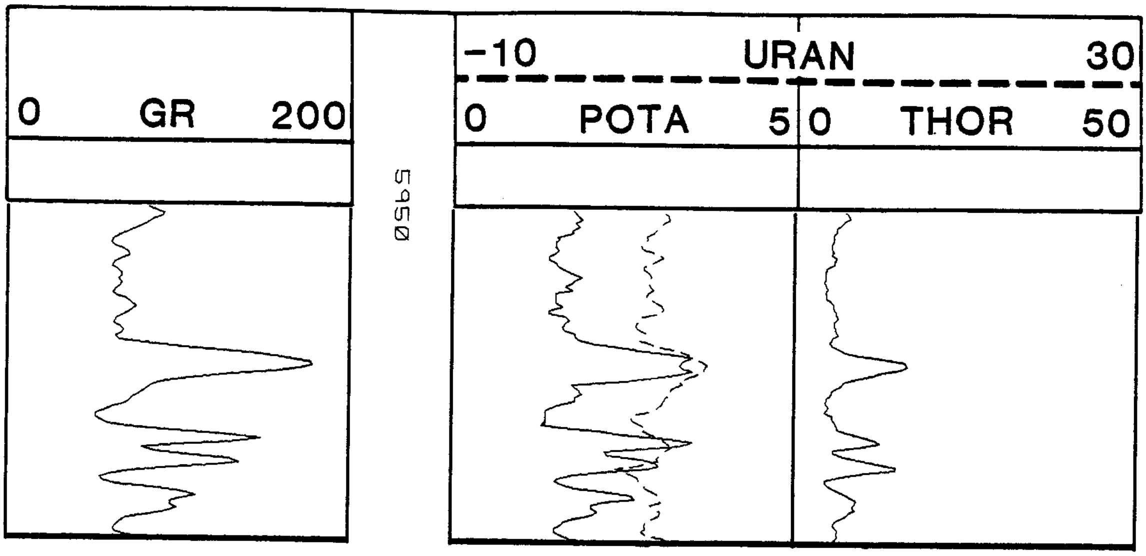

Figure 4.9, Continued

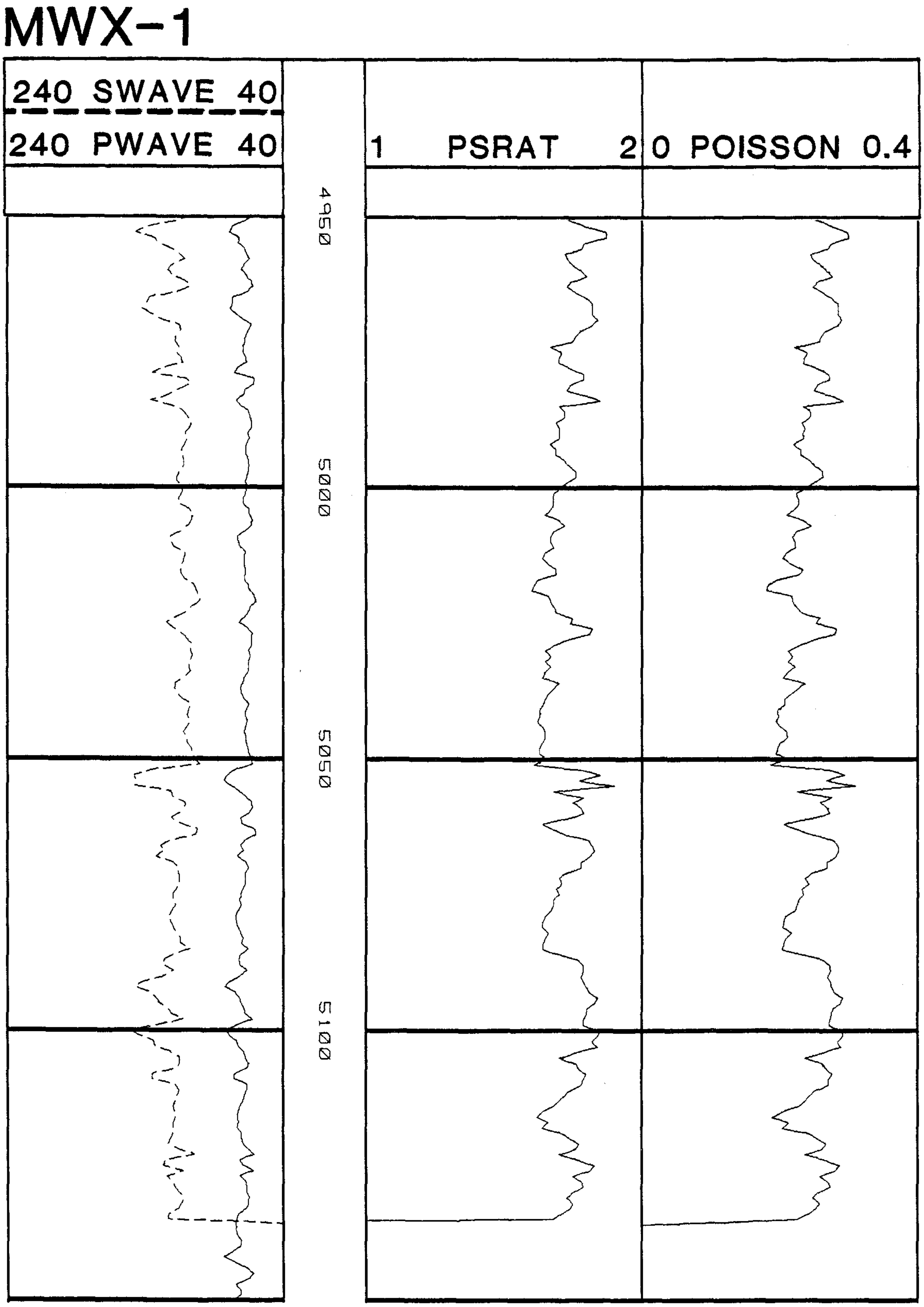

Figure 4.10 MWX-1 Long-Spaced Sonic Log

MWX-1

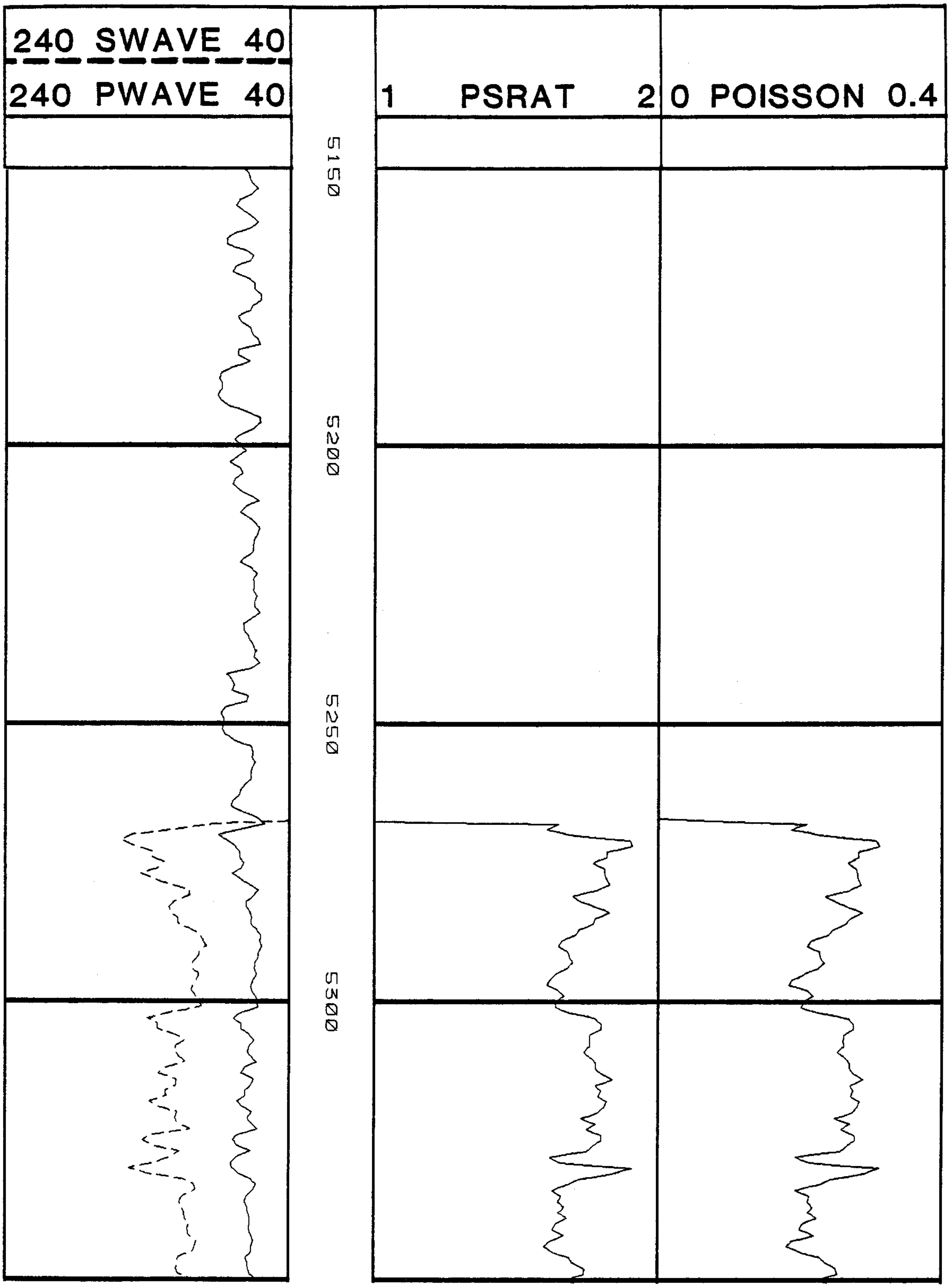

Figure 4.10, Continued

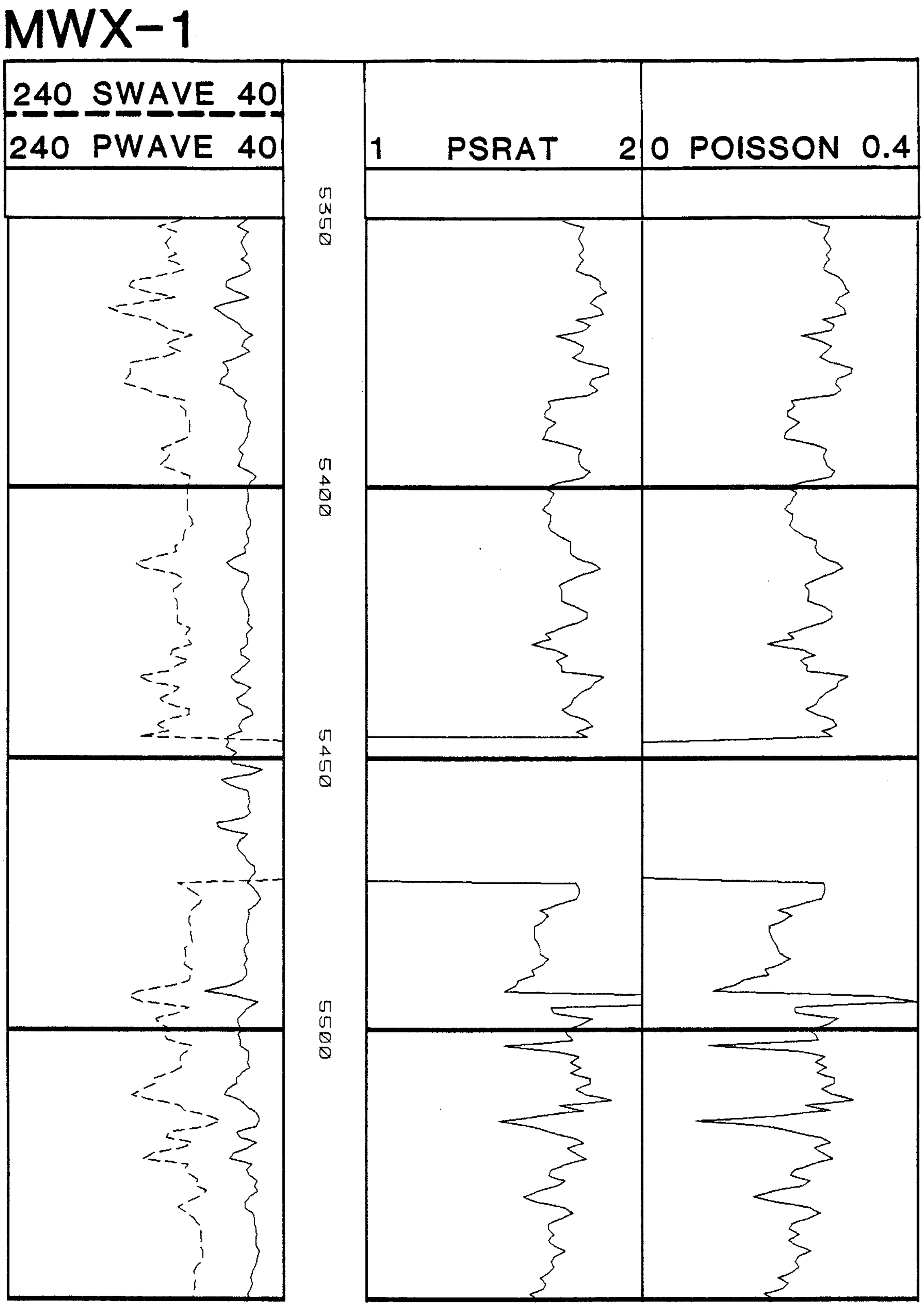

Figure 4.10, Continued

MWX-1

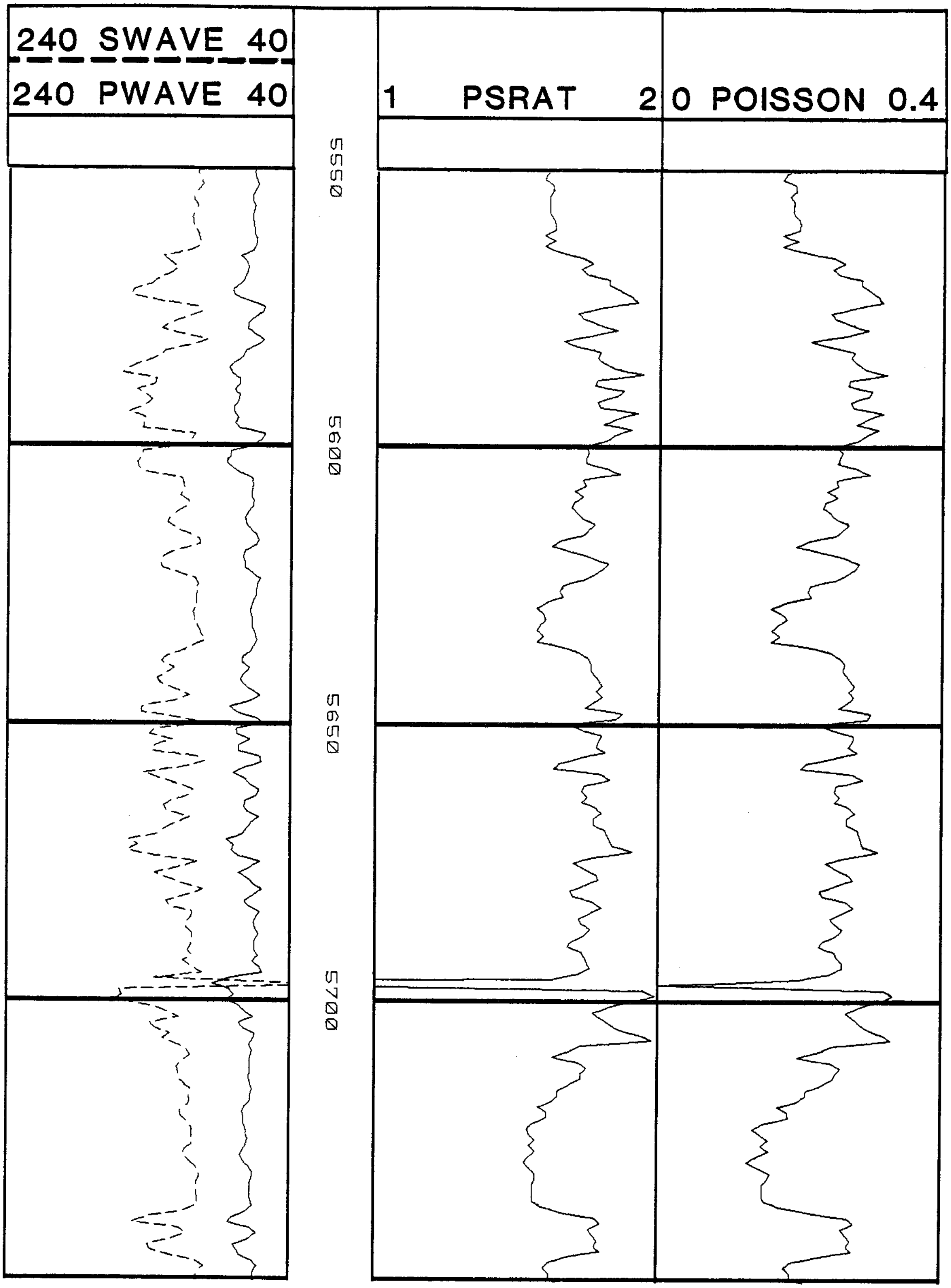

Figure 4.10, Continued

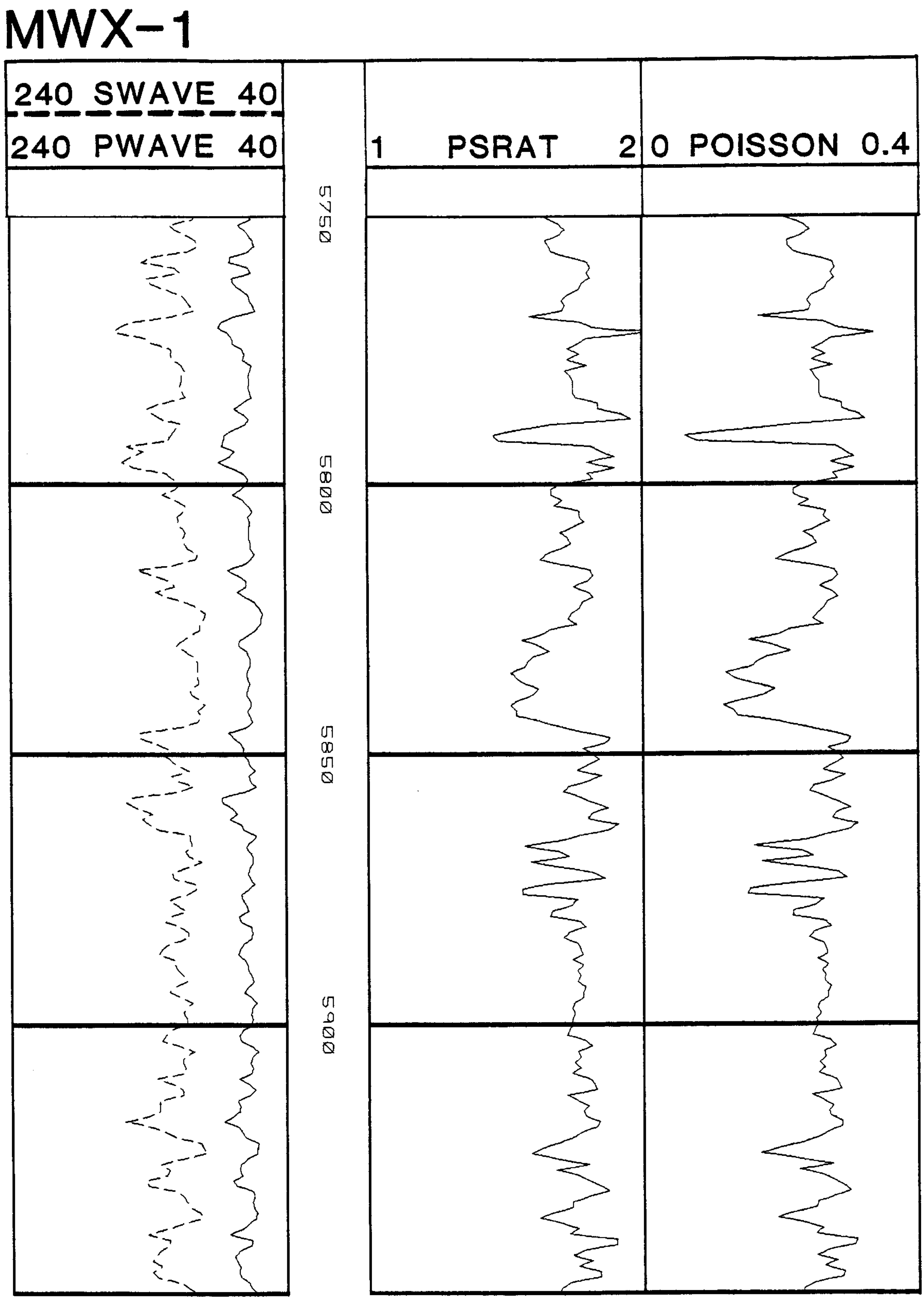

Figure 4.10, Continued

MWX-1

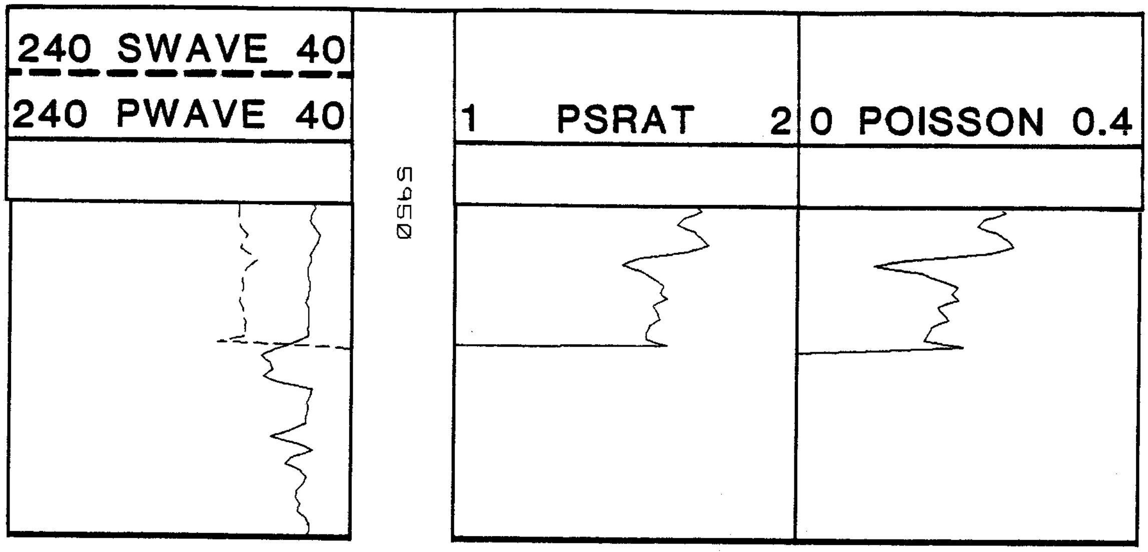

Figure 4.10, Continued

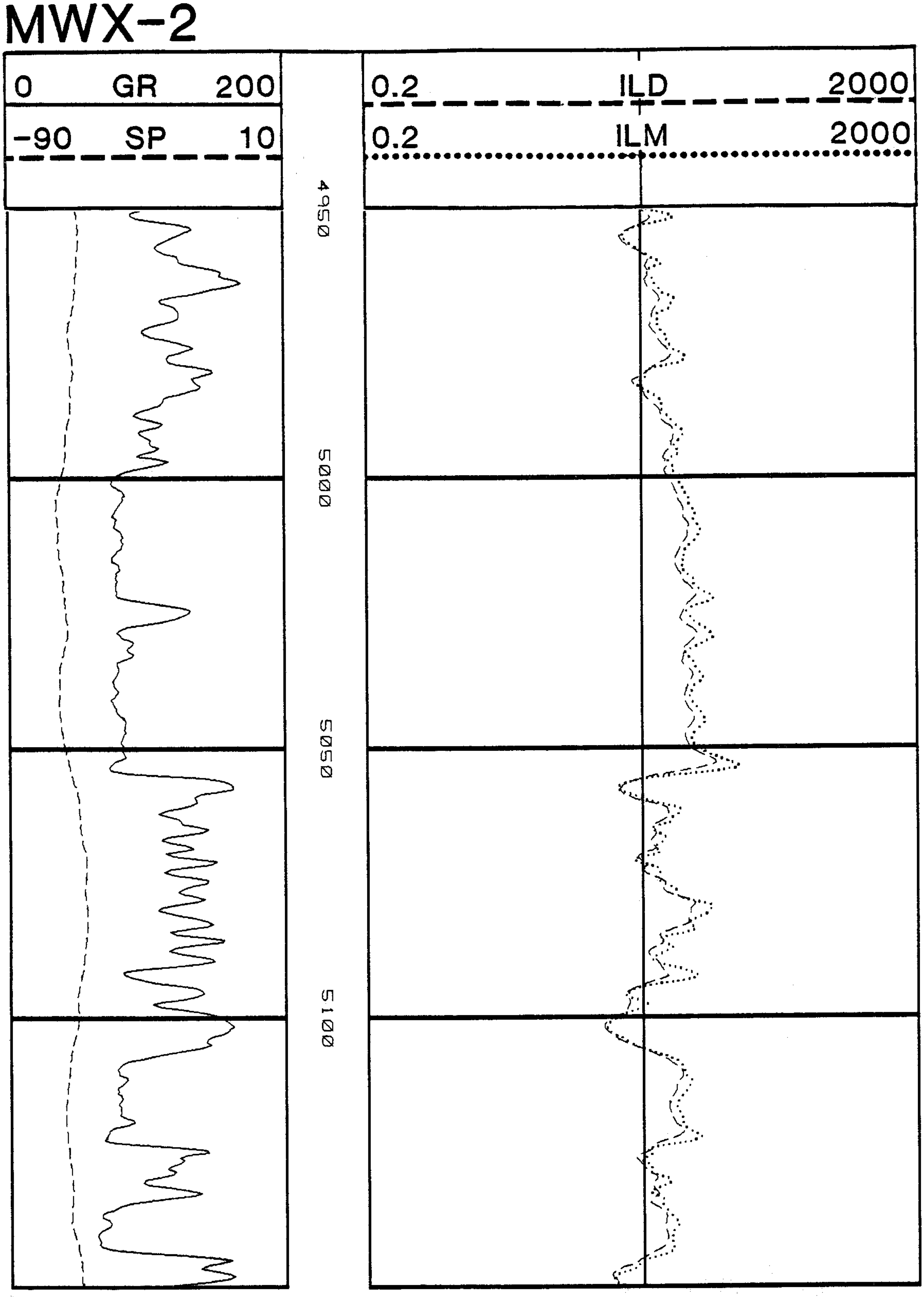

Figure 4.11 MWX-2 Resistivity Log

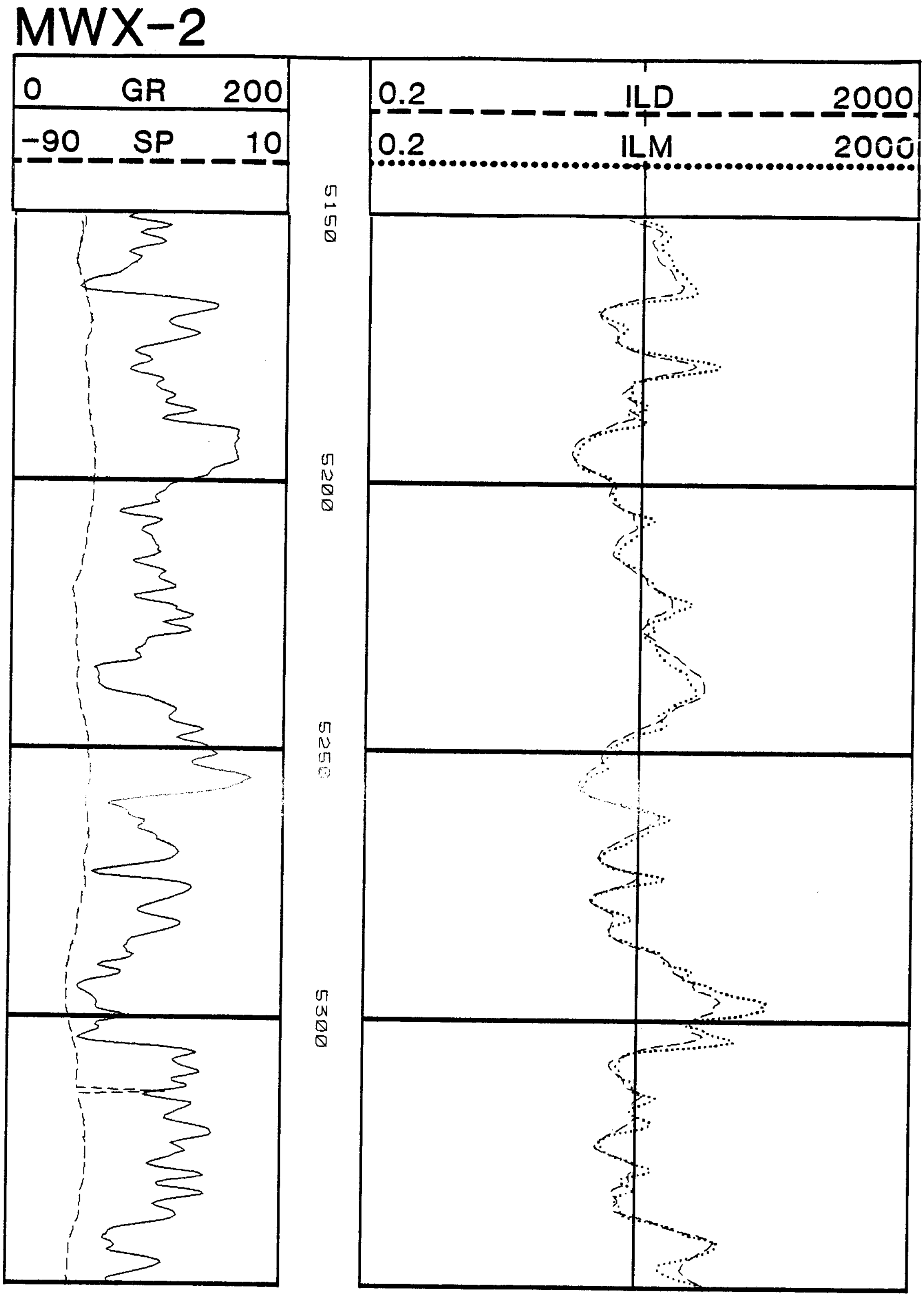

Figure 4.11, Continued

MWX-2

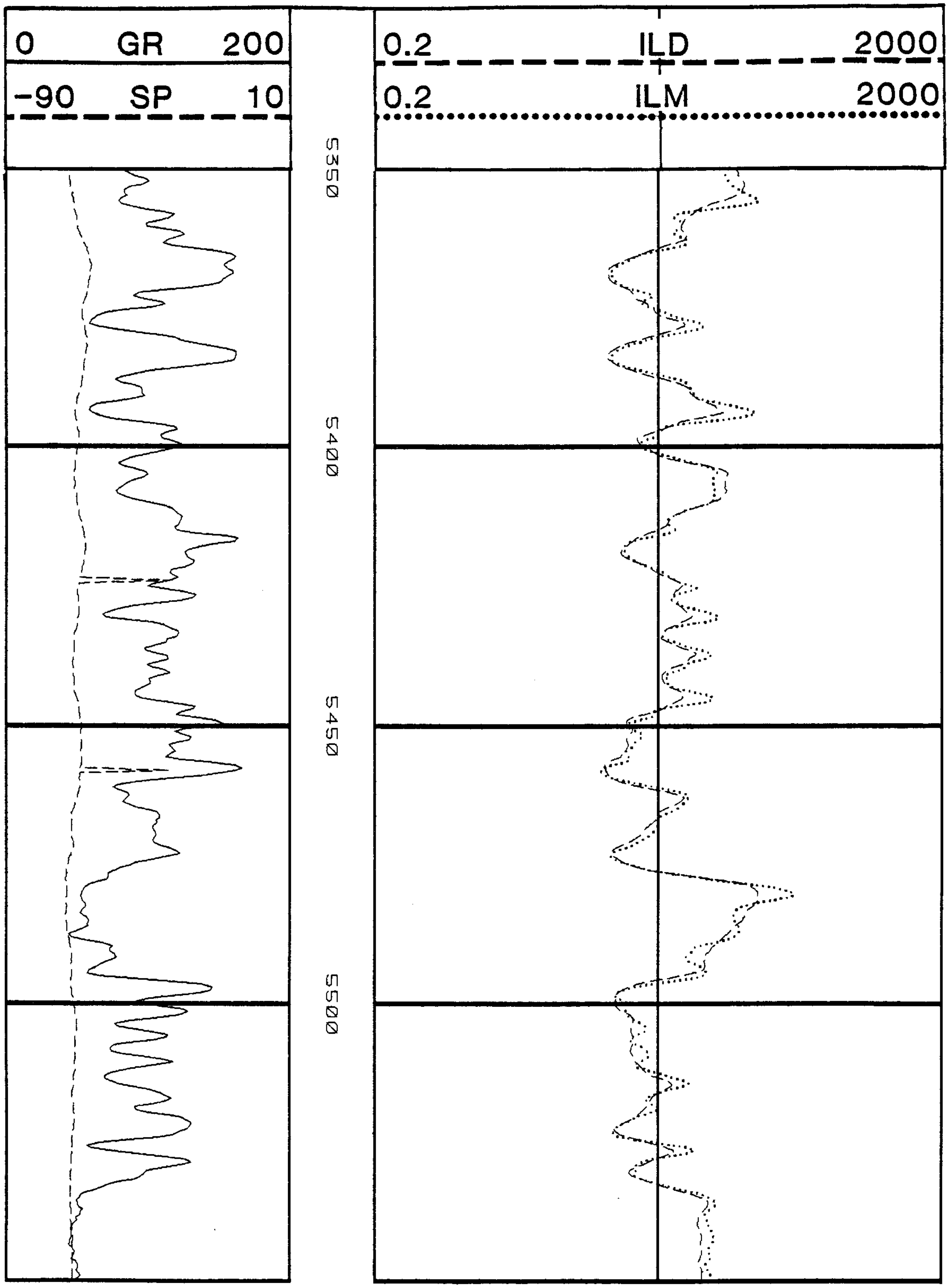

Figure 4.11, Continued

MWX-2

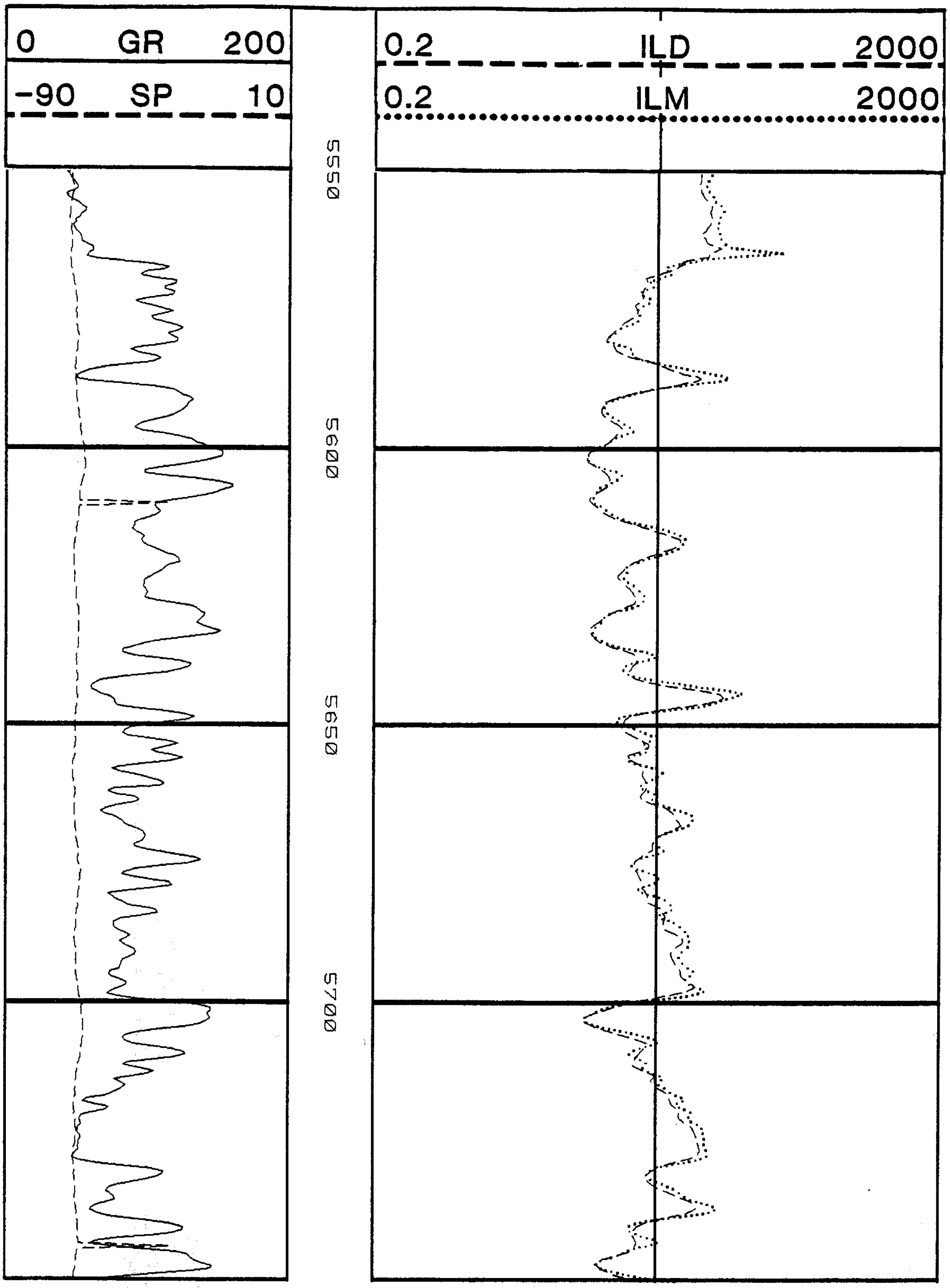

Figure 4.11, Continued

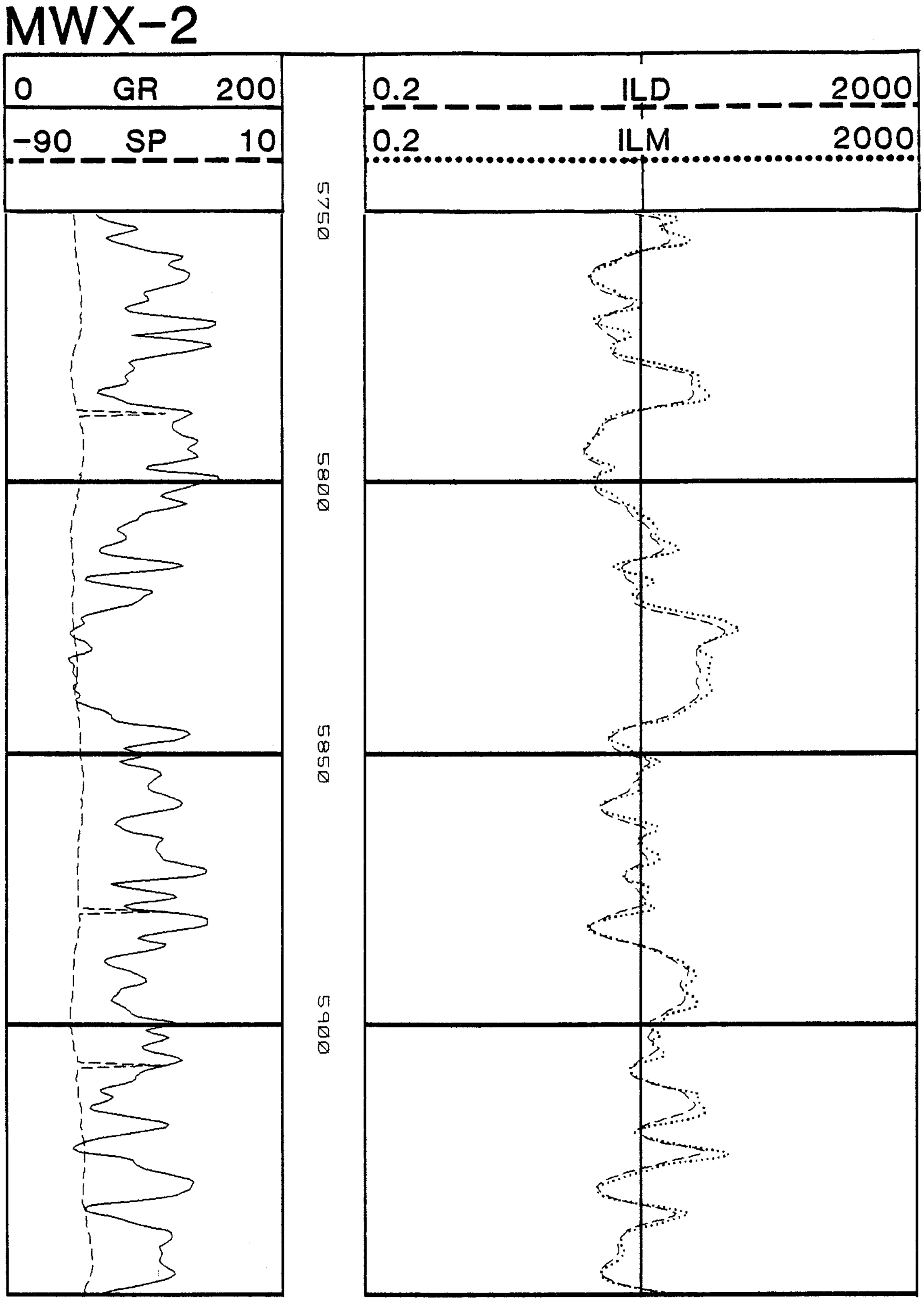

Figure 4.11, Continued

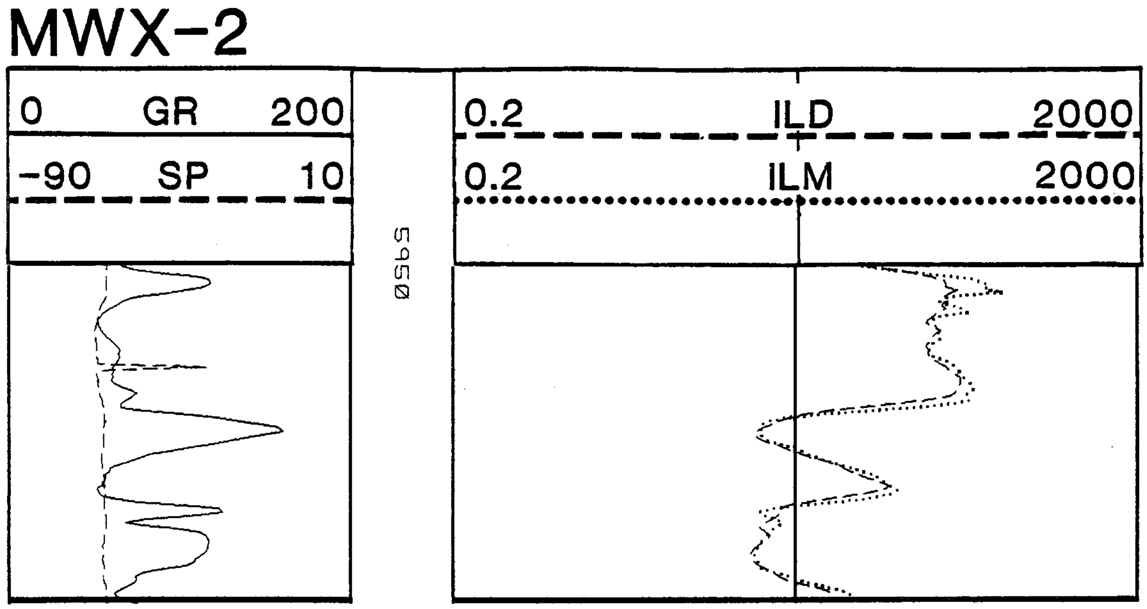

Figure 4.11, Continued

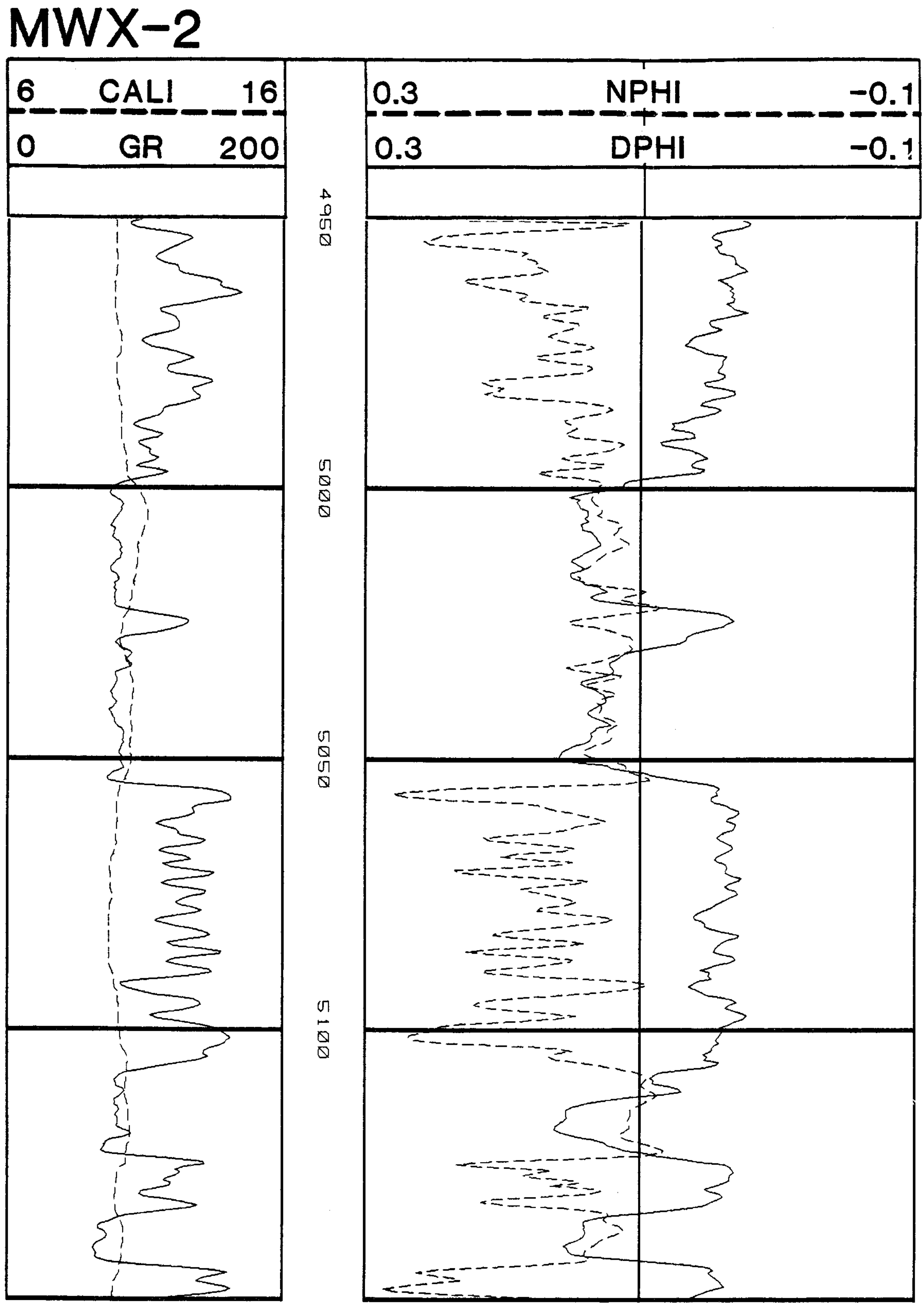

Figure 4.12 MWX-2 Density and Neutron Porosity Logs

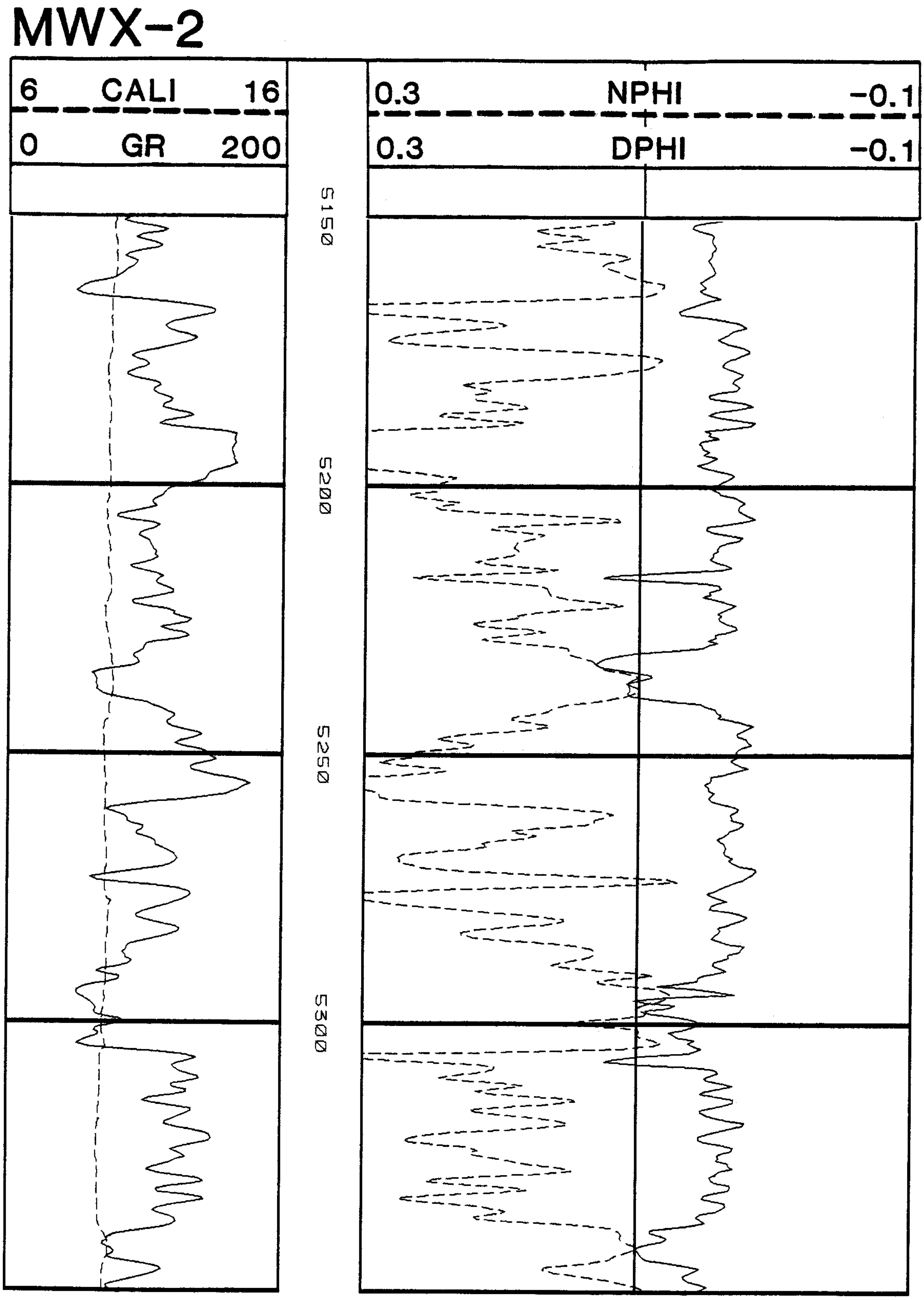

Figure 4.12, Continued

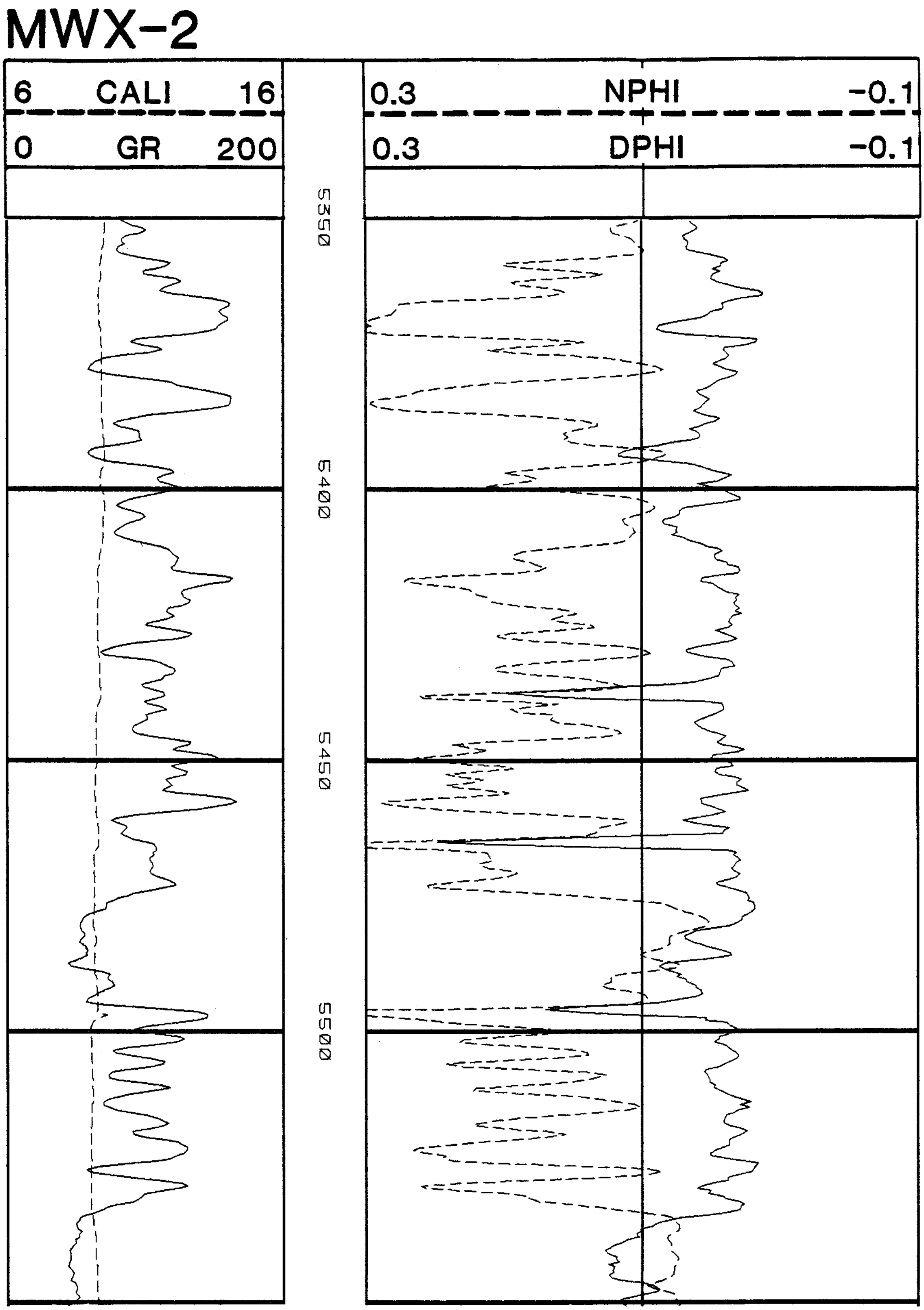

Figure 4.12, Continued

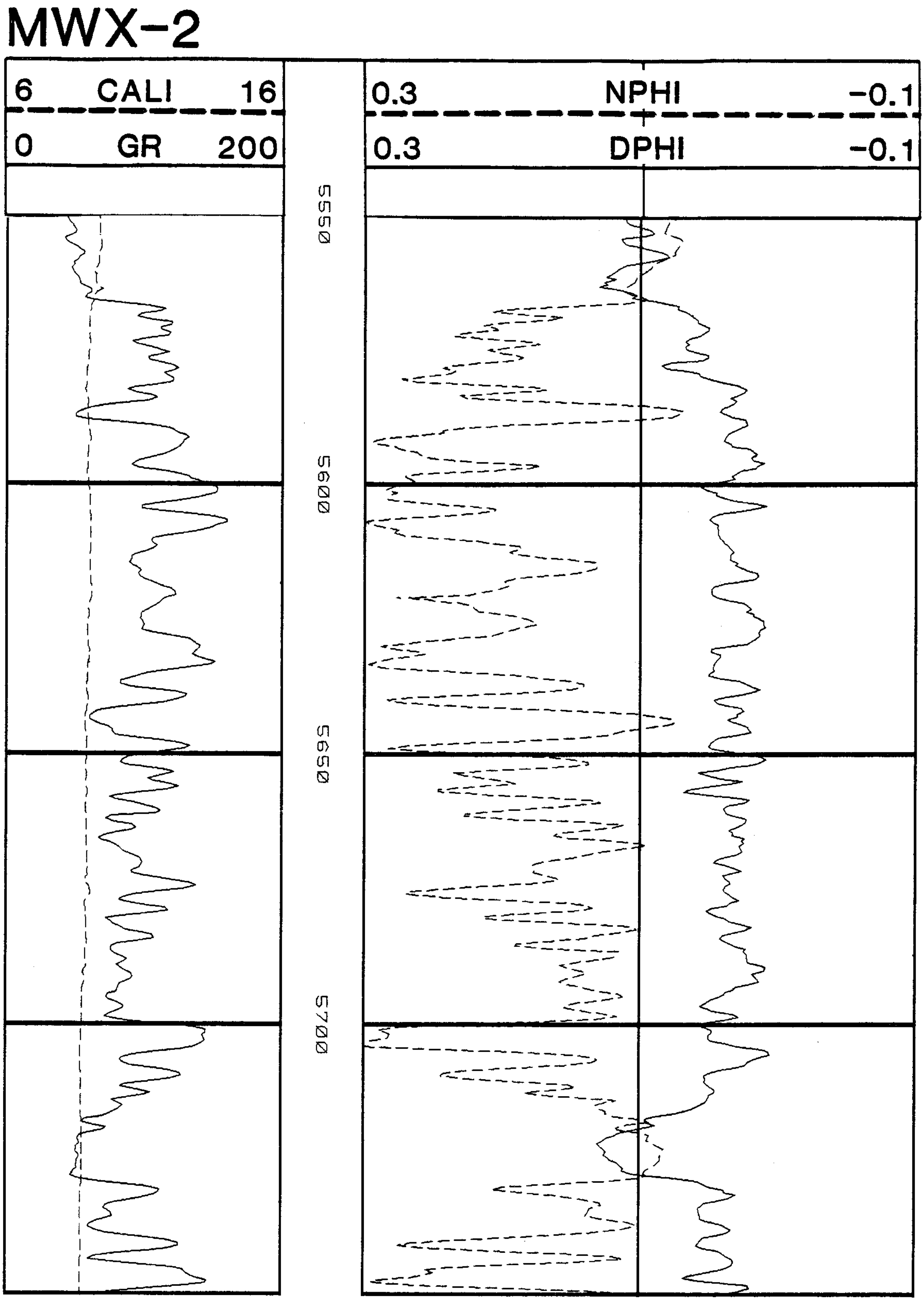

Figure 4.12, Continued

MWX-2

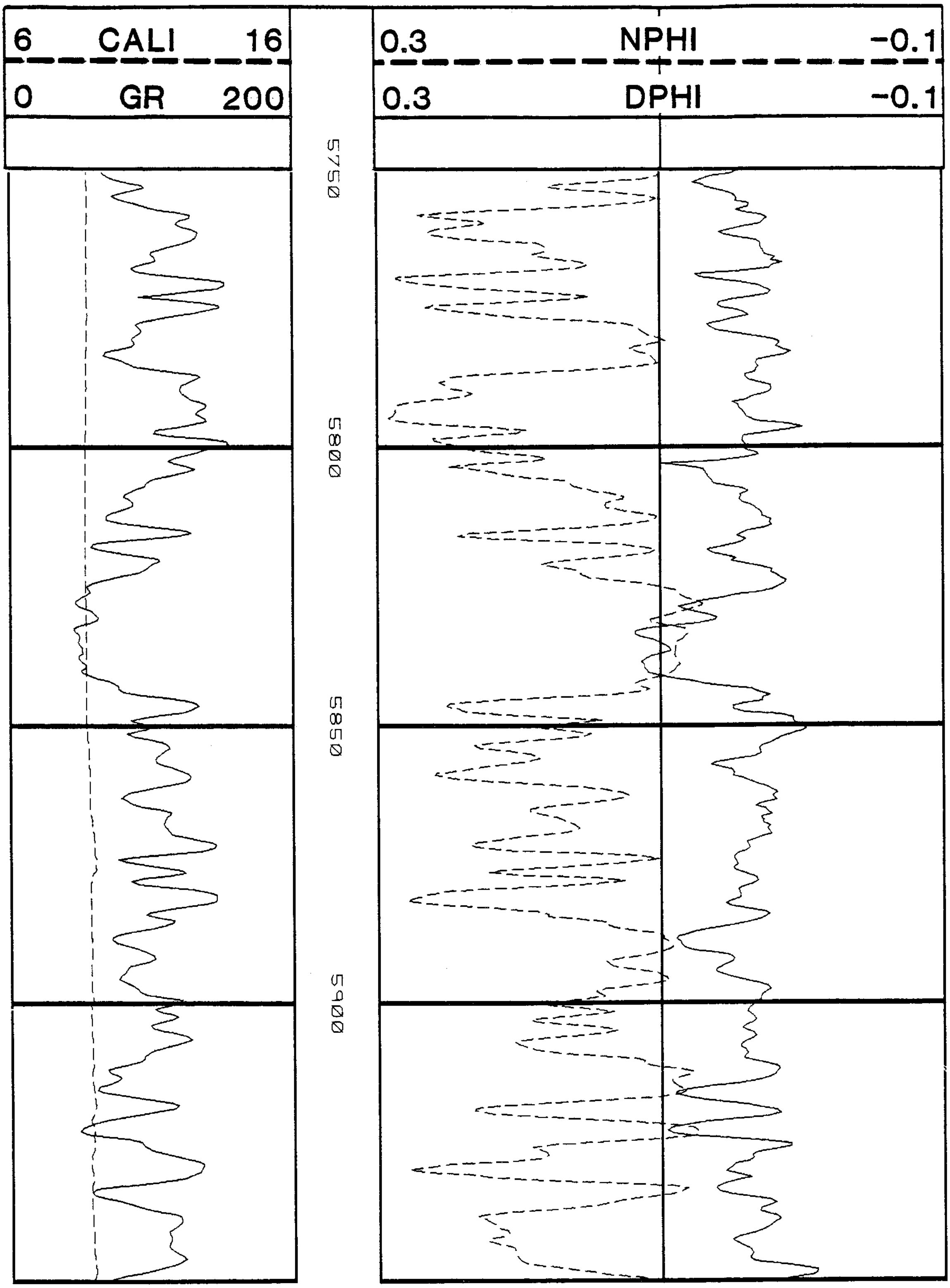

Figure 4.12, Continued

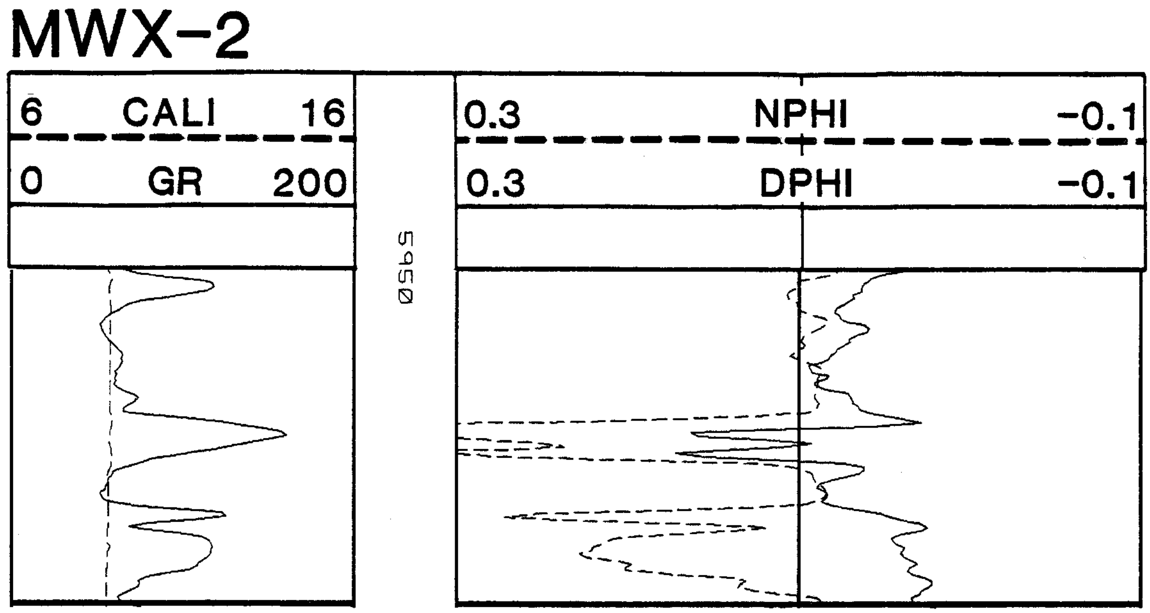

Figure 4.12, Continued

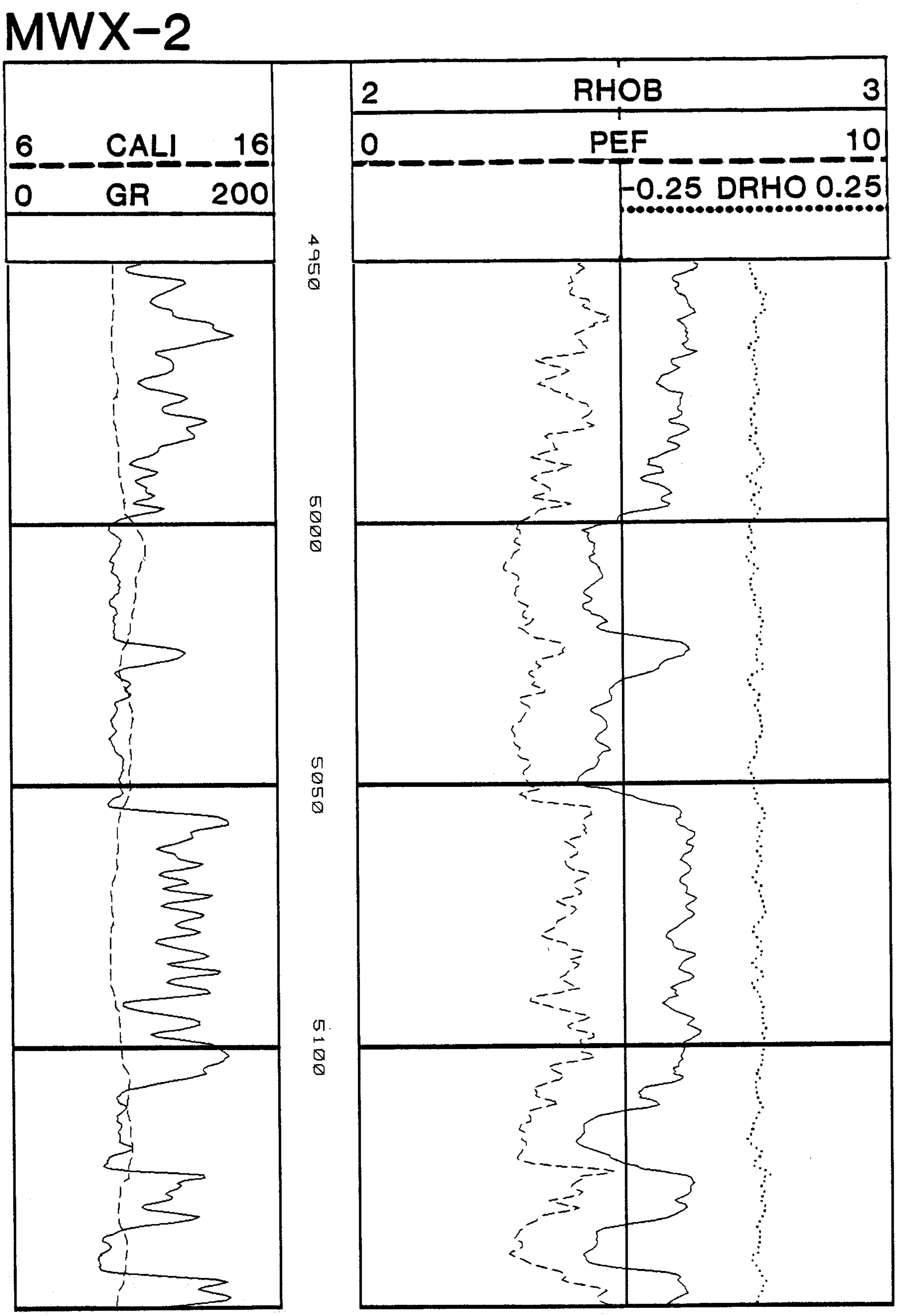

Figure 4.13 MWX-2 Bulk Density and Photoelectric Absorption Logs

MWX-2

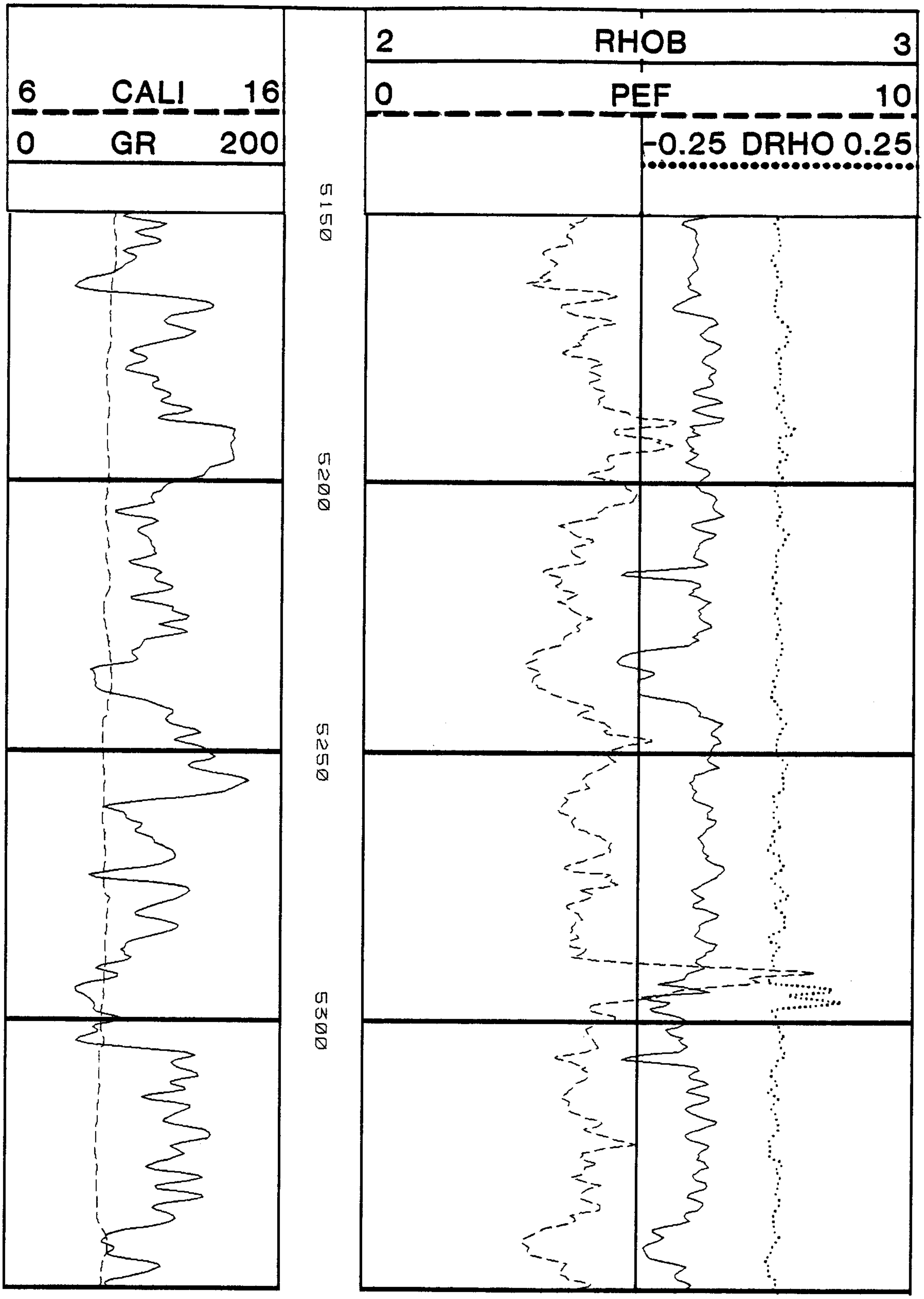

Figure 4.13, Continued

MWX-2

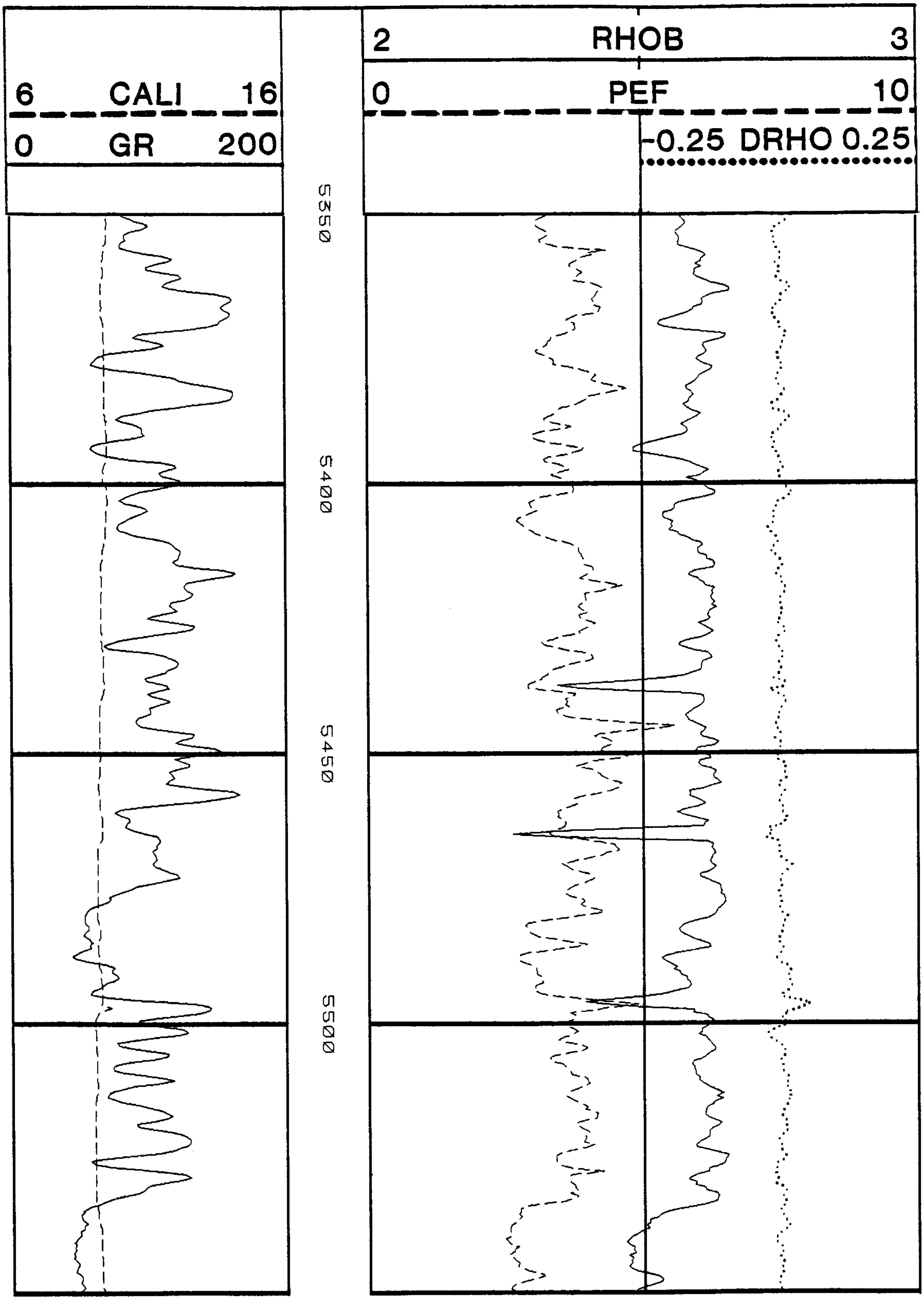

Figure 4.13, Continued

MWX-2

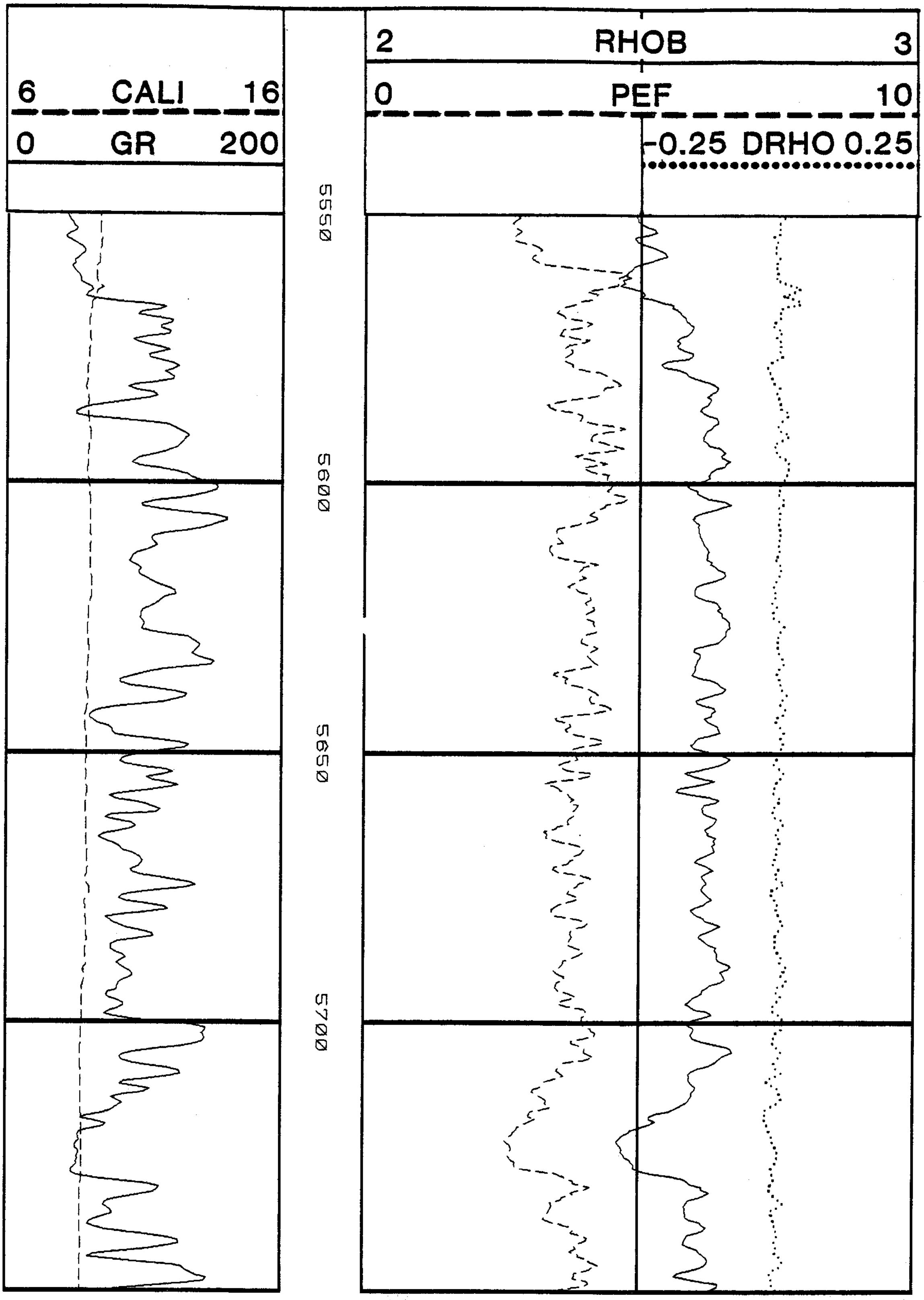

Figure 4.13, Continued

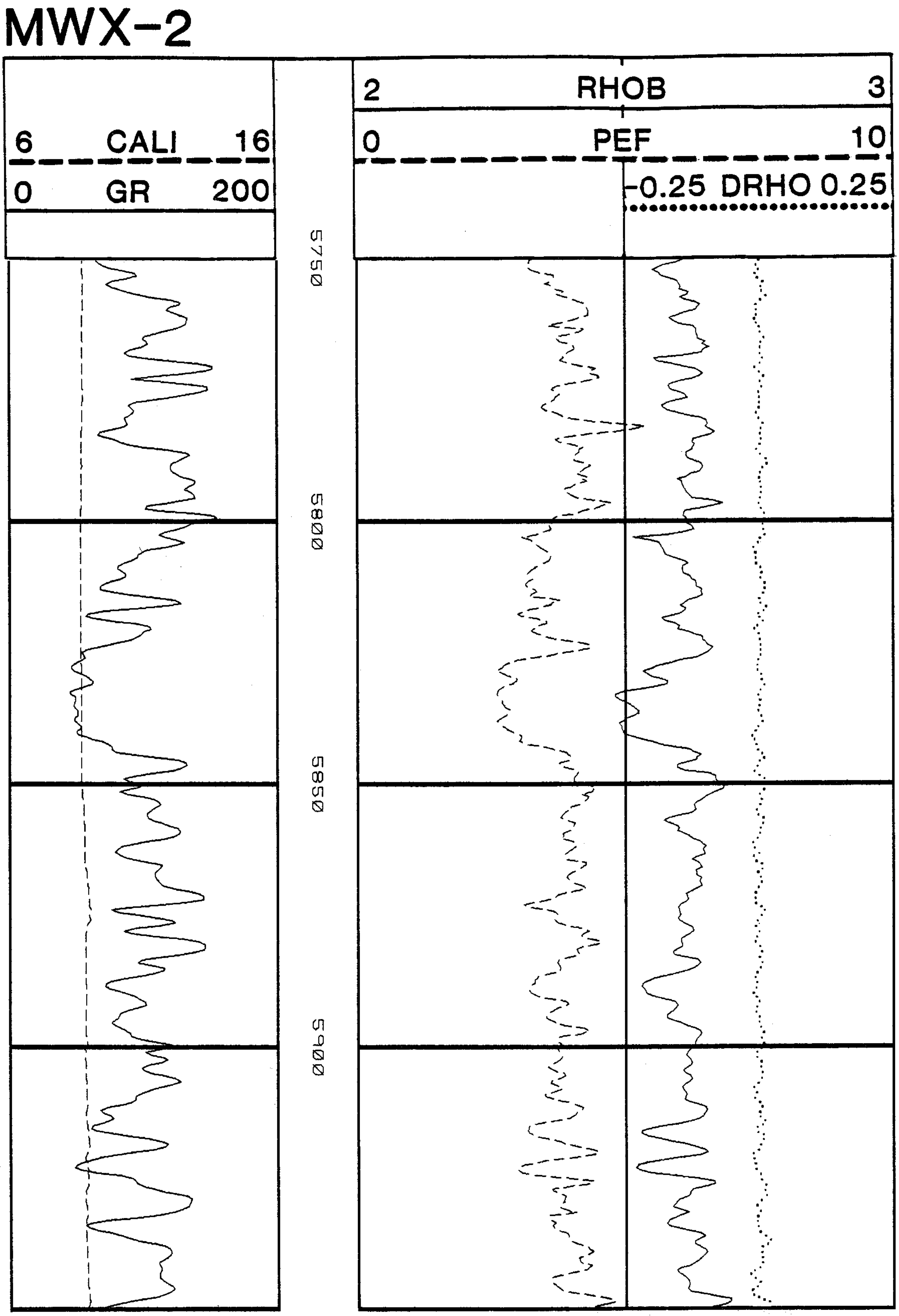

Figure 4.13, Continued

MWX-2

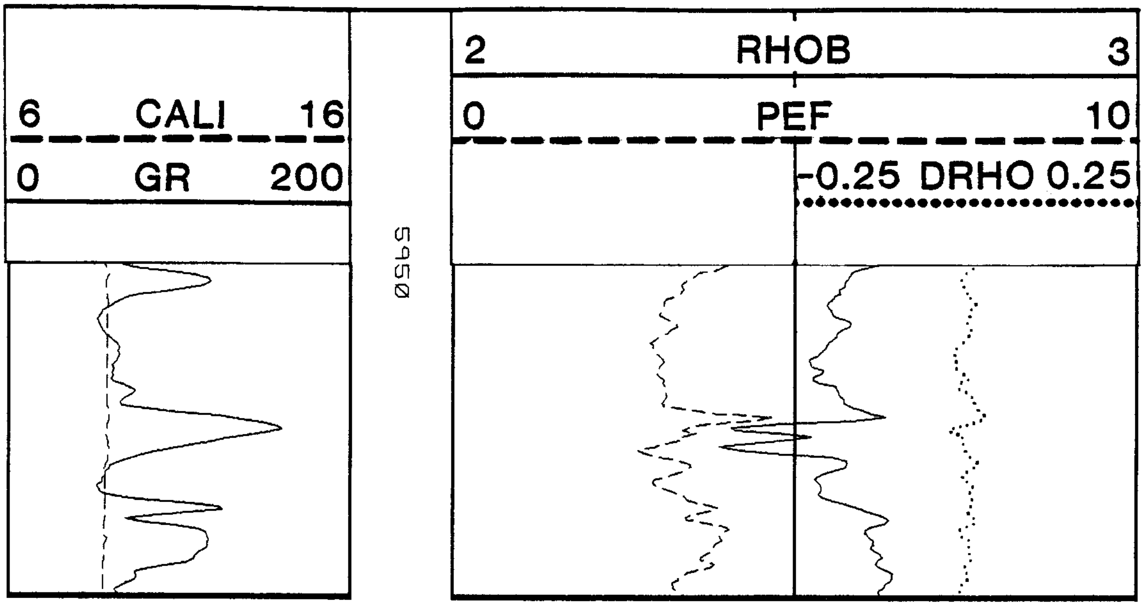

Figure 4.13, Continued

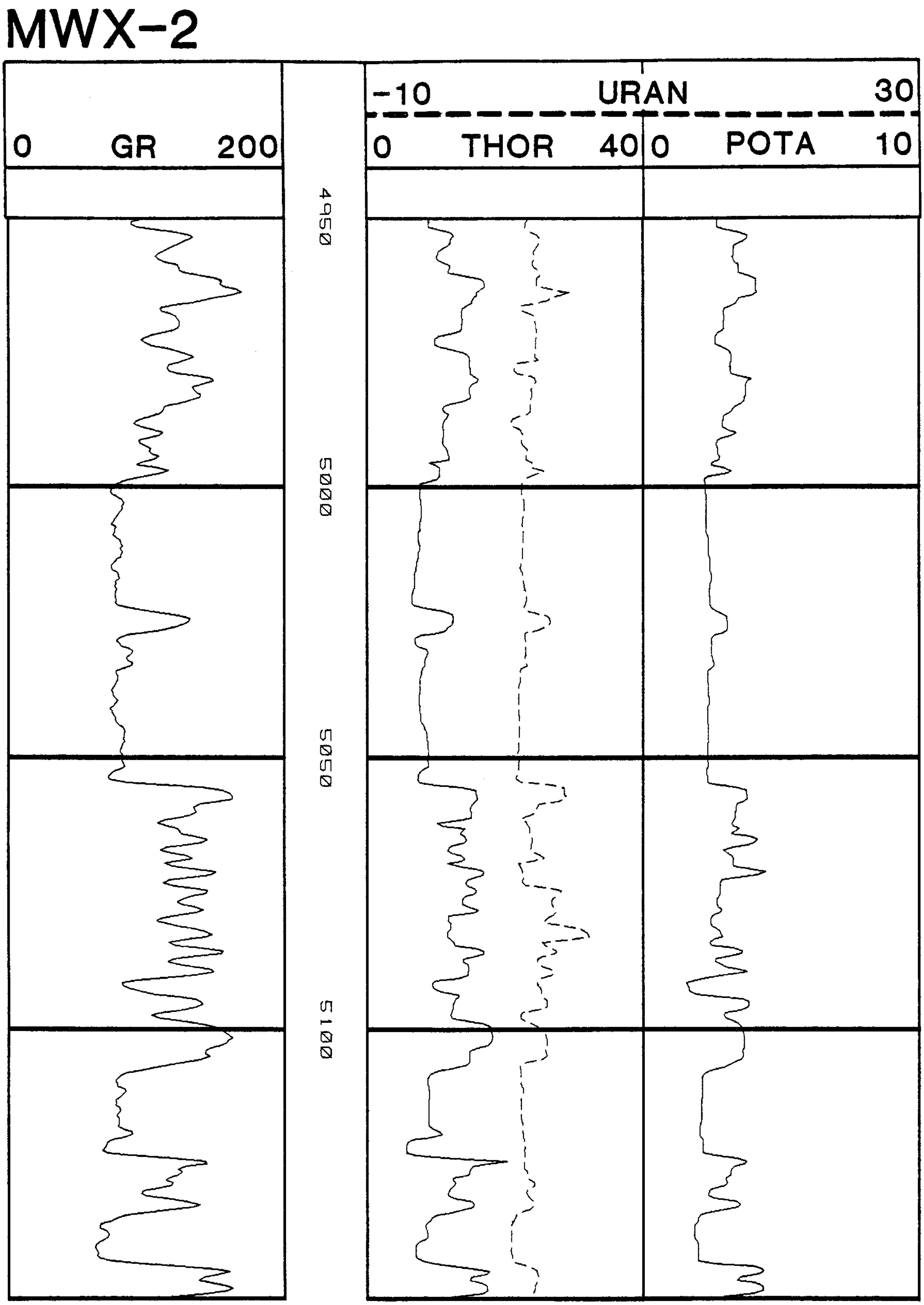

Figure 4.14 MWX-2 Spectral Gamma Log

MWX-2

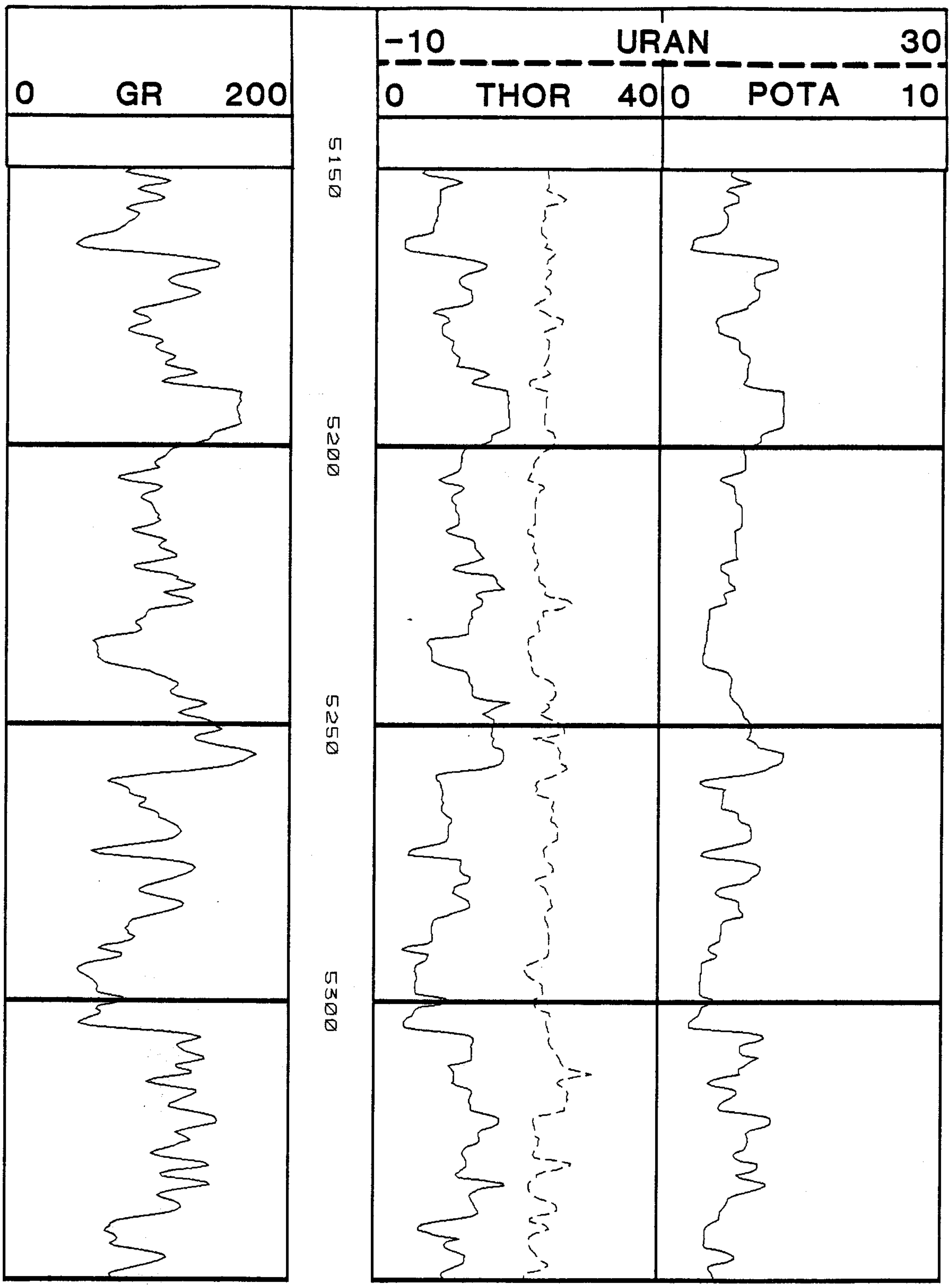

Figure 4.14, Continued

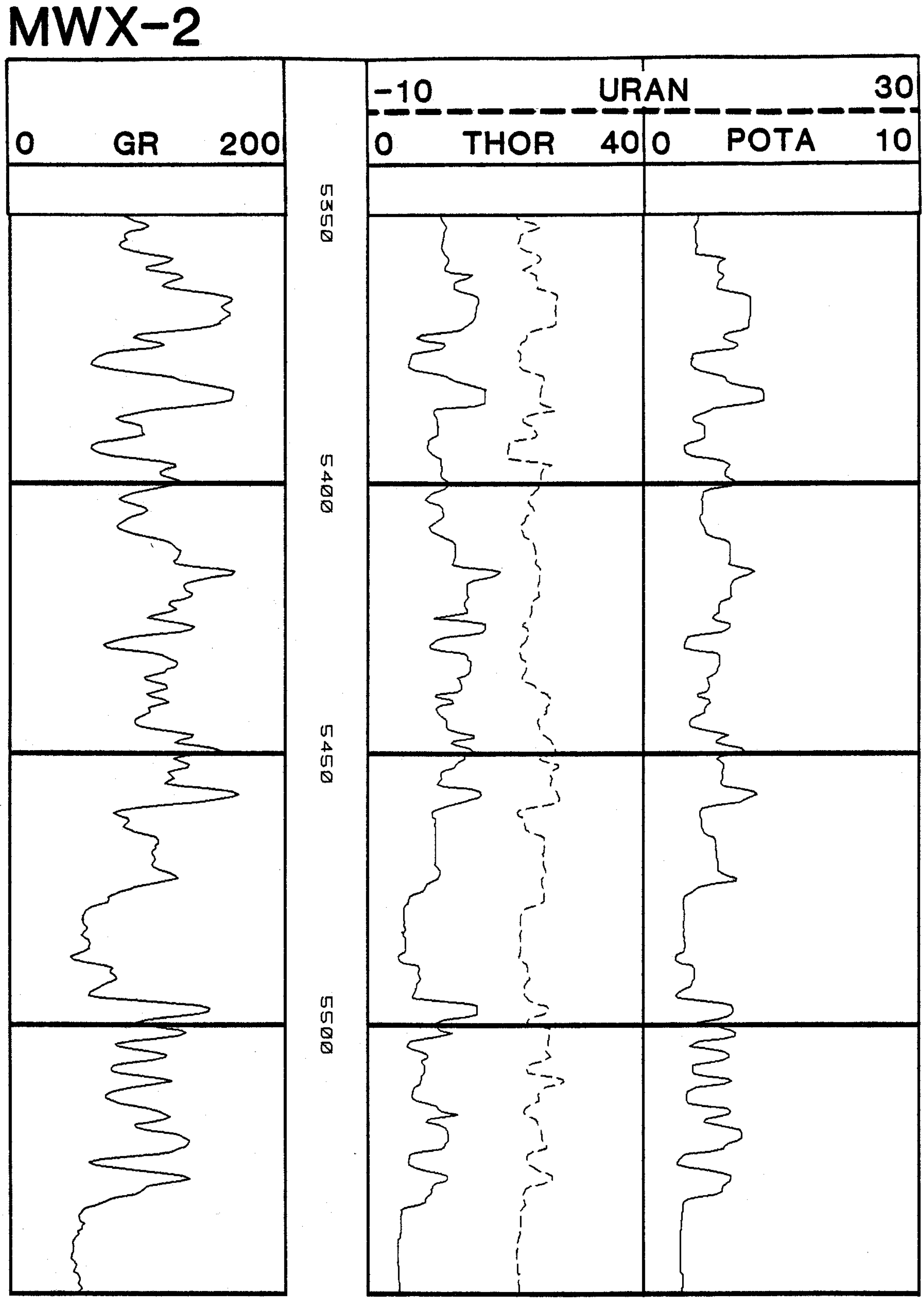

Figure 4.14, Continued

MWX-2

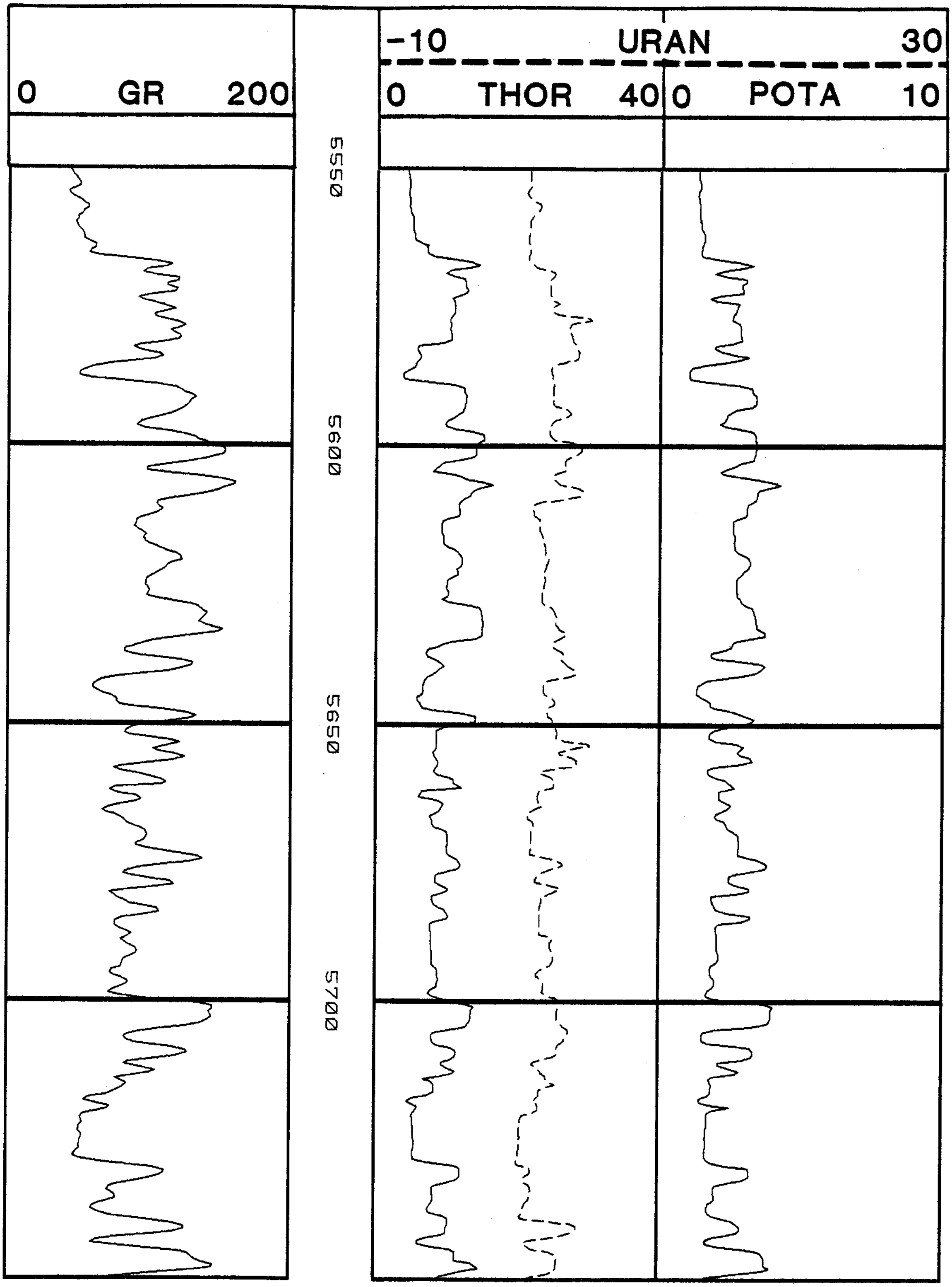

Figure 4.14, Continued

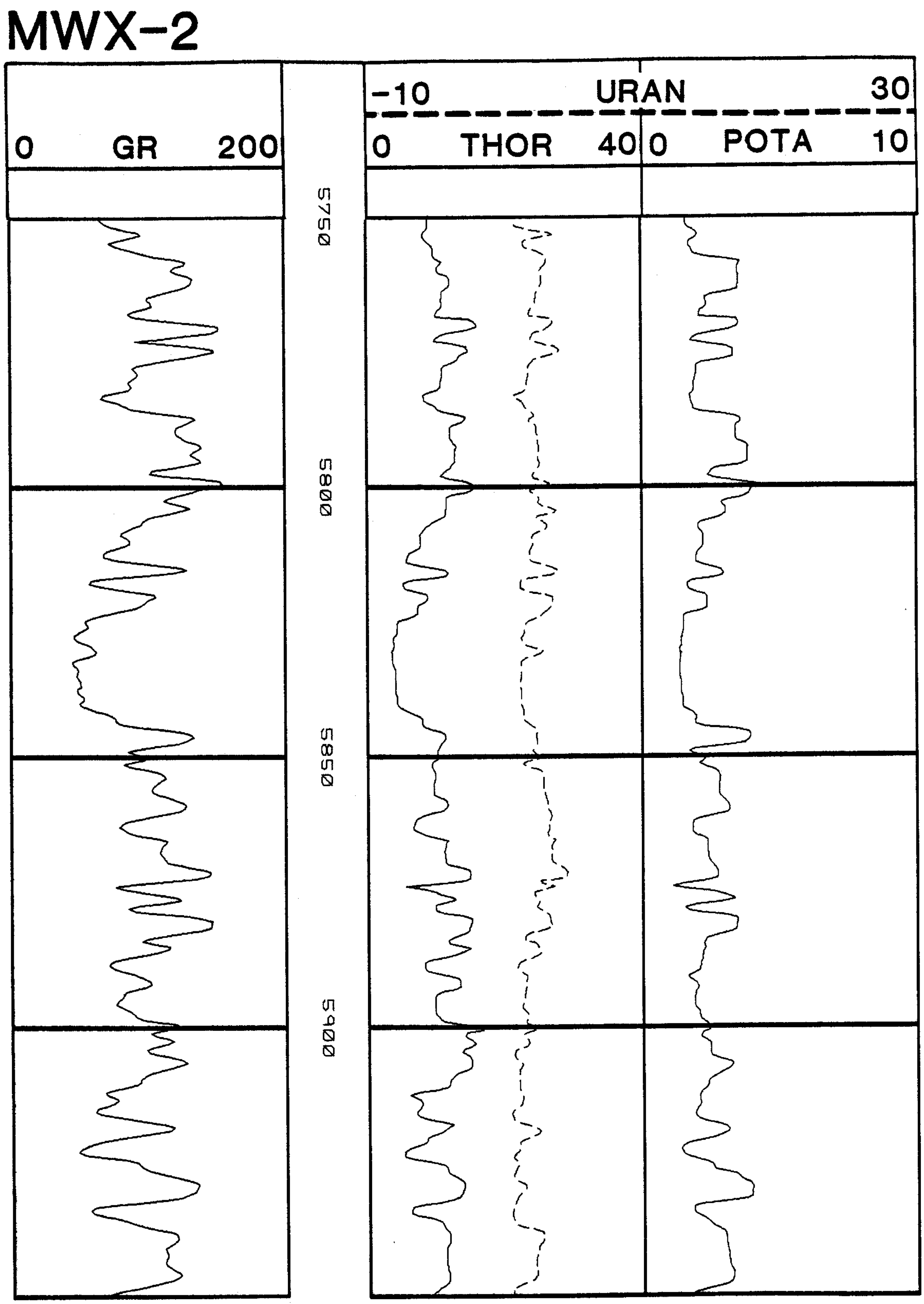

Figure 4.14, Continued

MWX-2

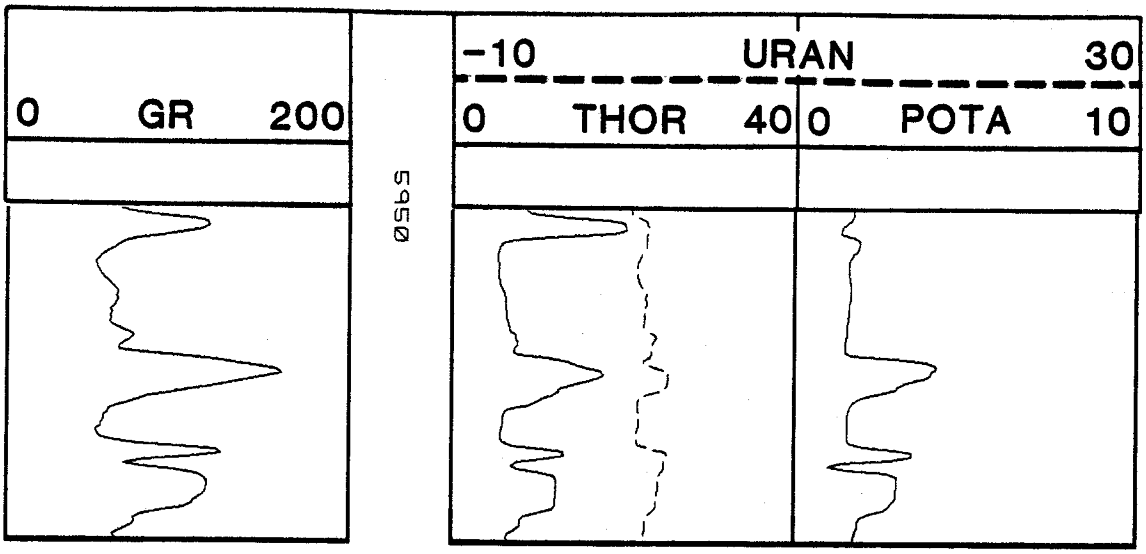

Figure 4.14, Continued

MWX-2

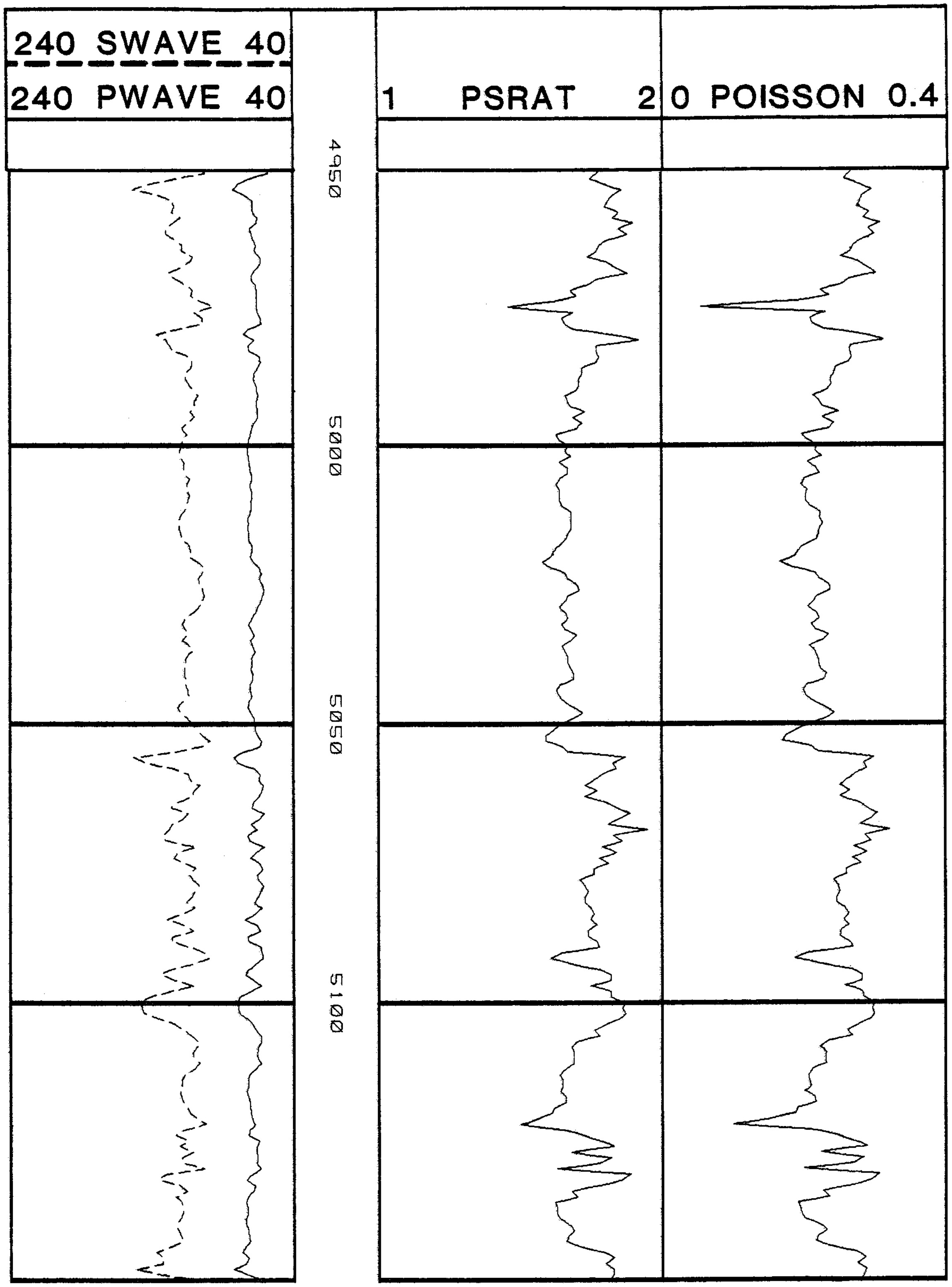

Figure 4.15 MWX-2 Long-Spaced Sonic Log

MWX-2

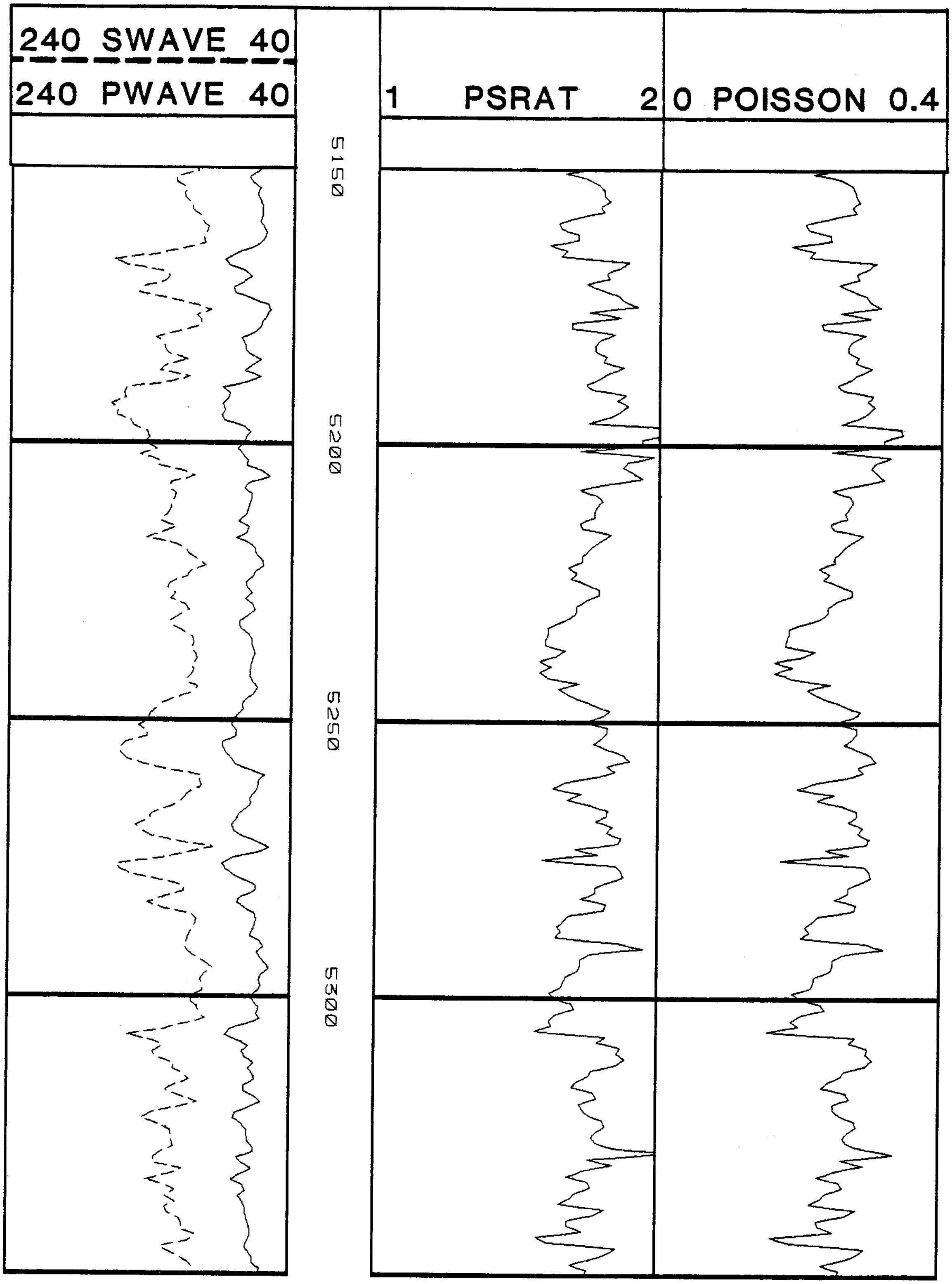

Figure 4.15, Continued

MWX-2

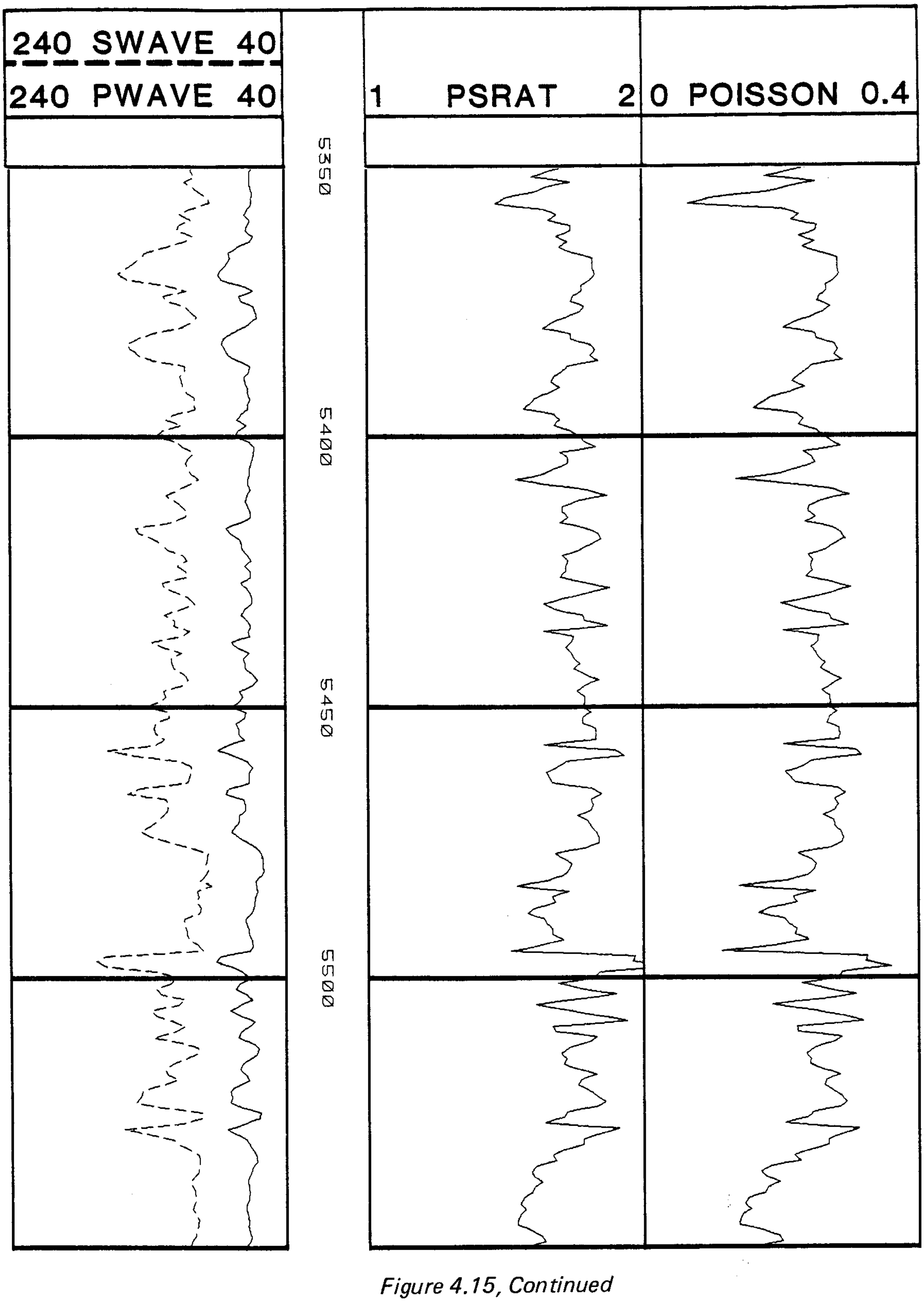

Figure 4.15, Continued

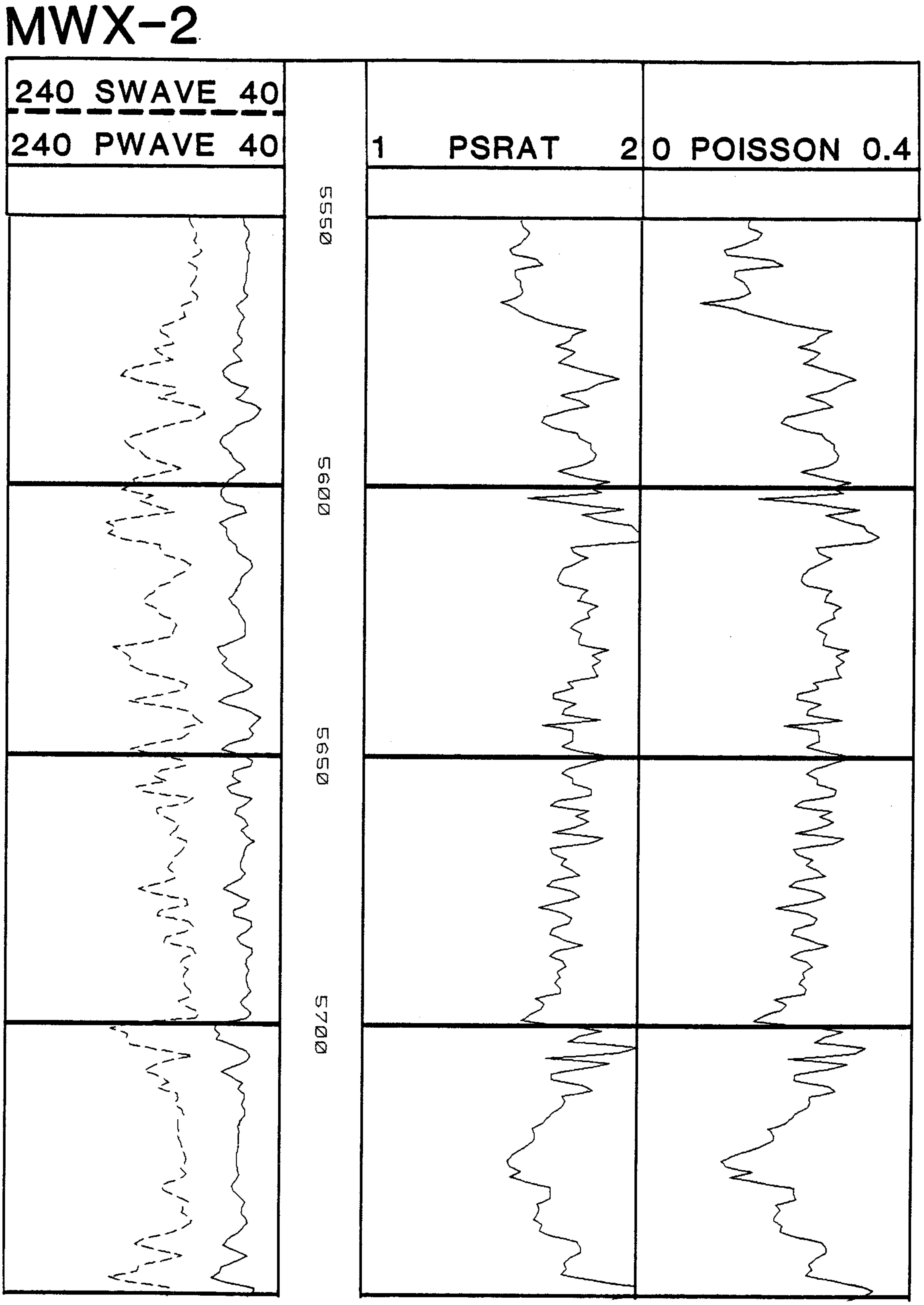

Figure 4.15, Continued

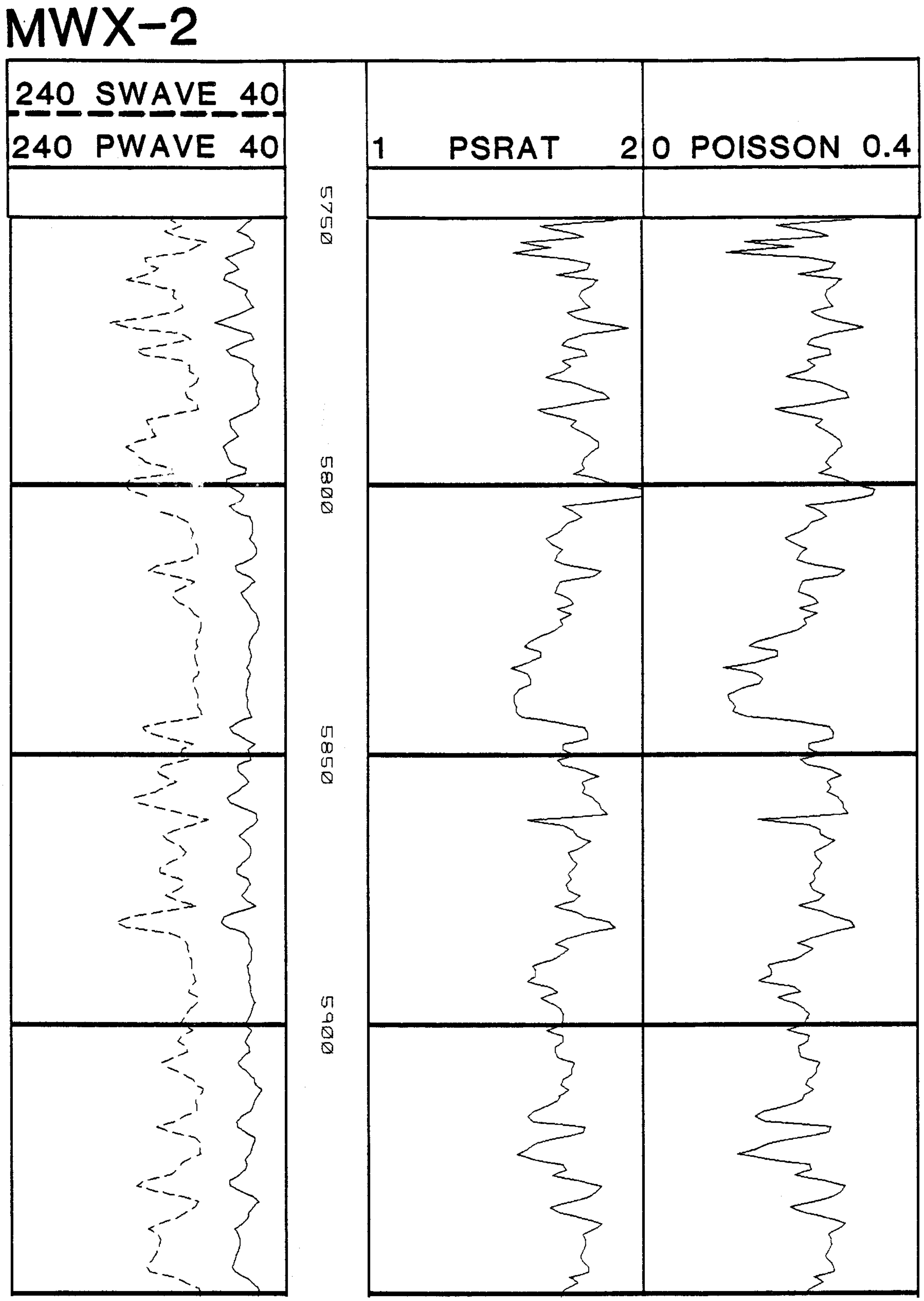

Figure 4.15, Continued

MWX-2

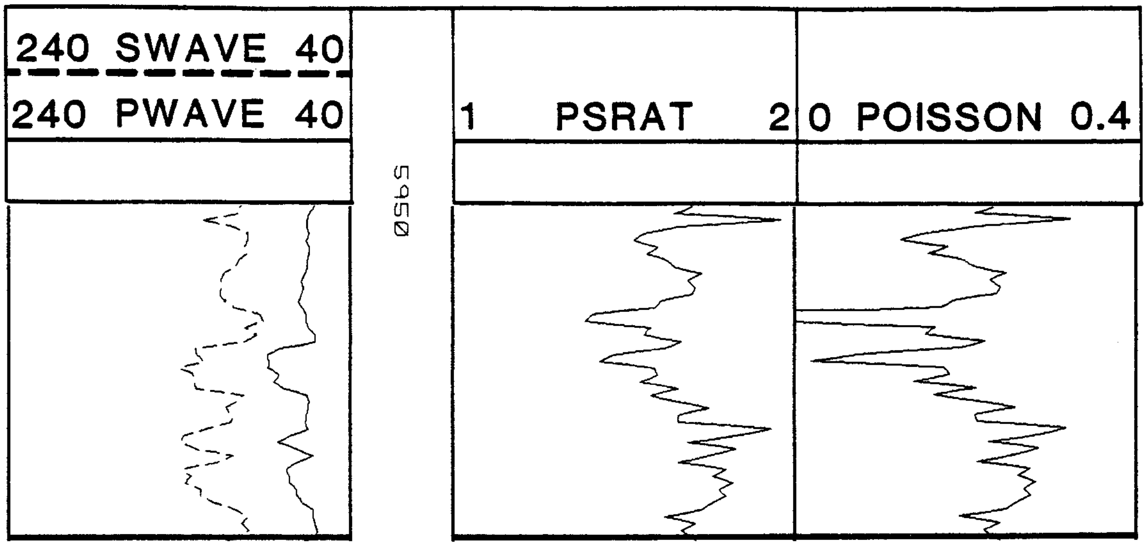

Figure 4.15, Continued

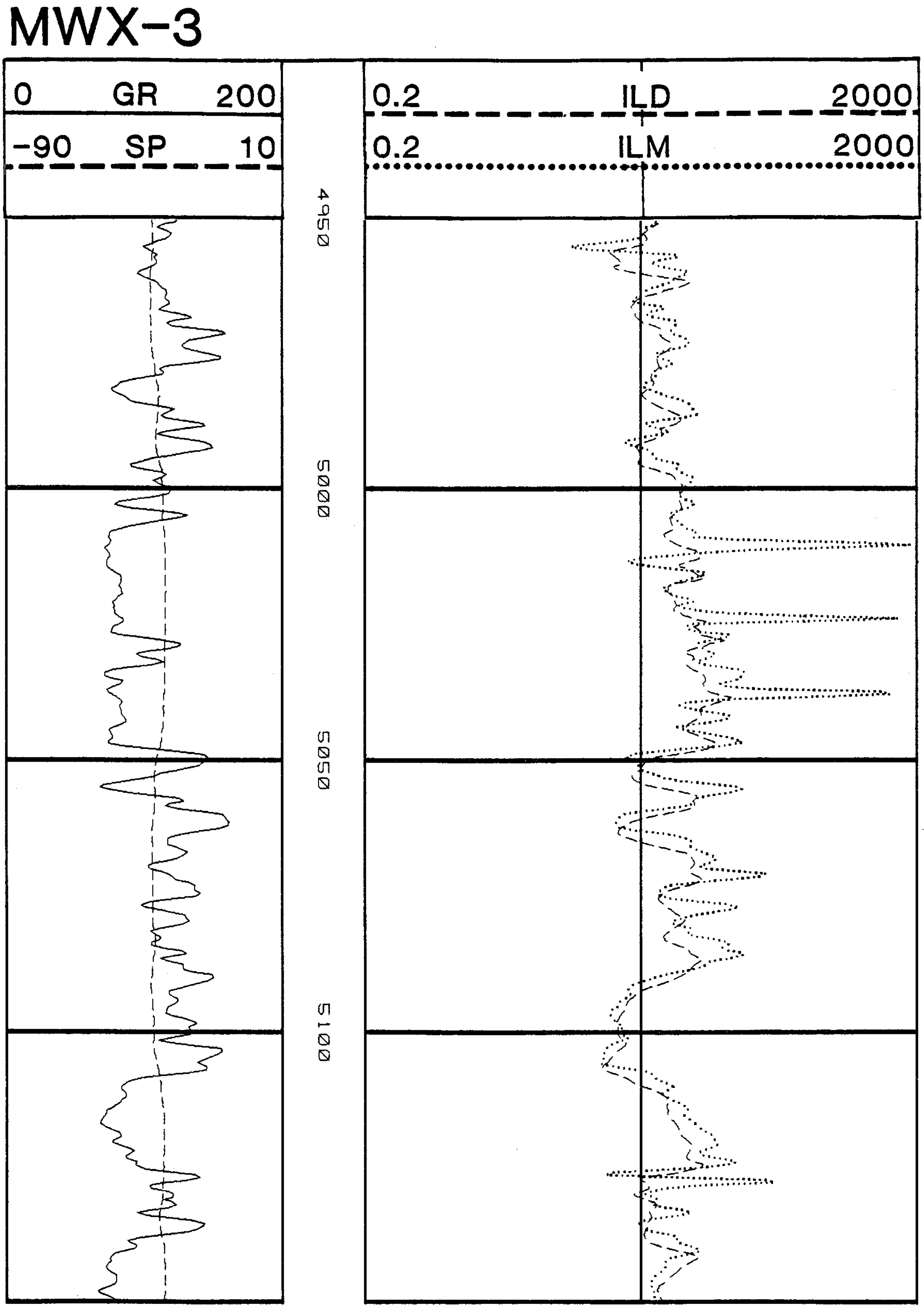

Figure 4.16 MWX-3 Resistivity Log

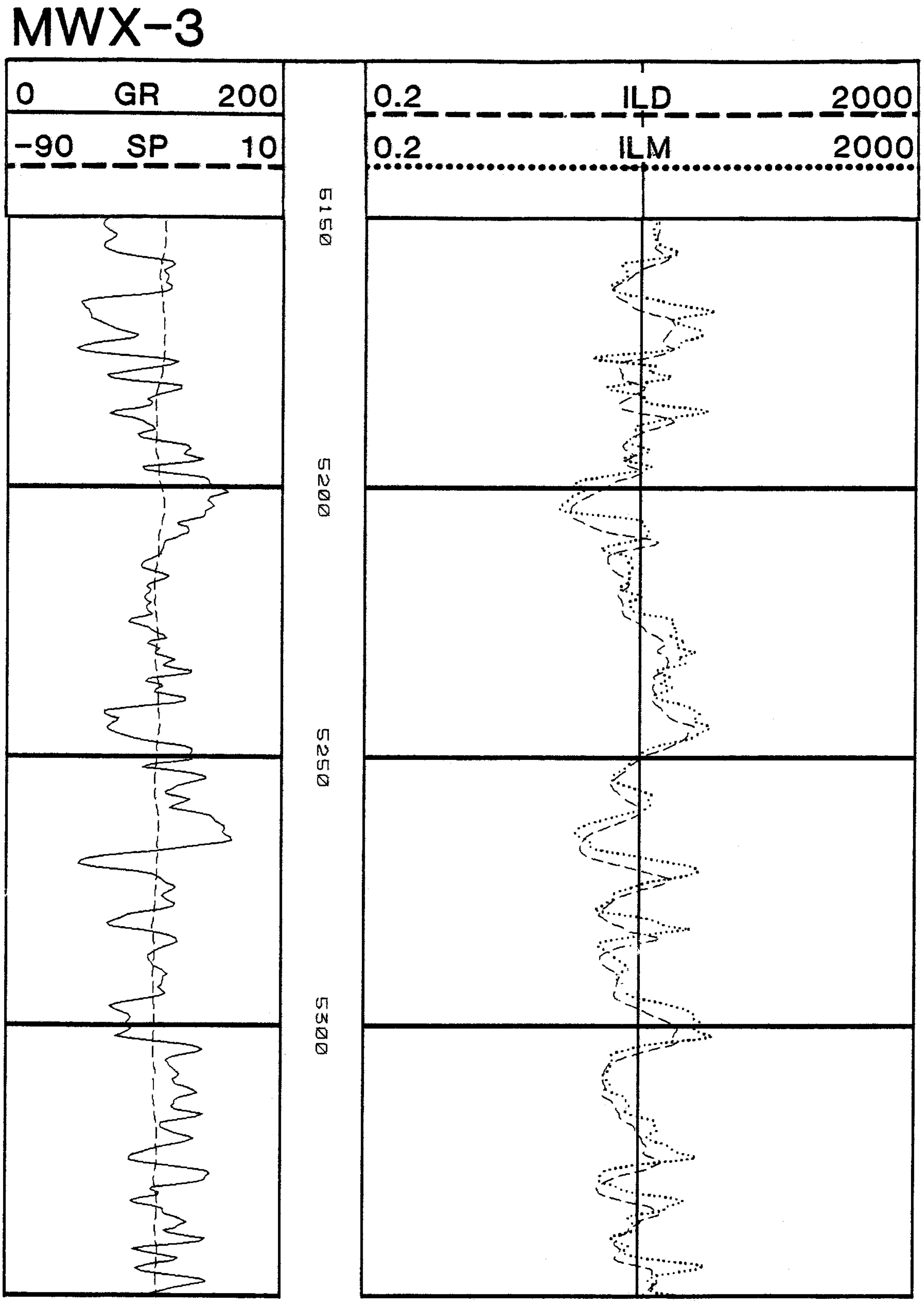

Figure 4.16, Continued

MWX-3

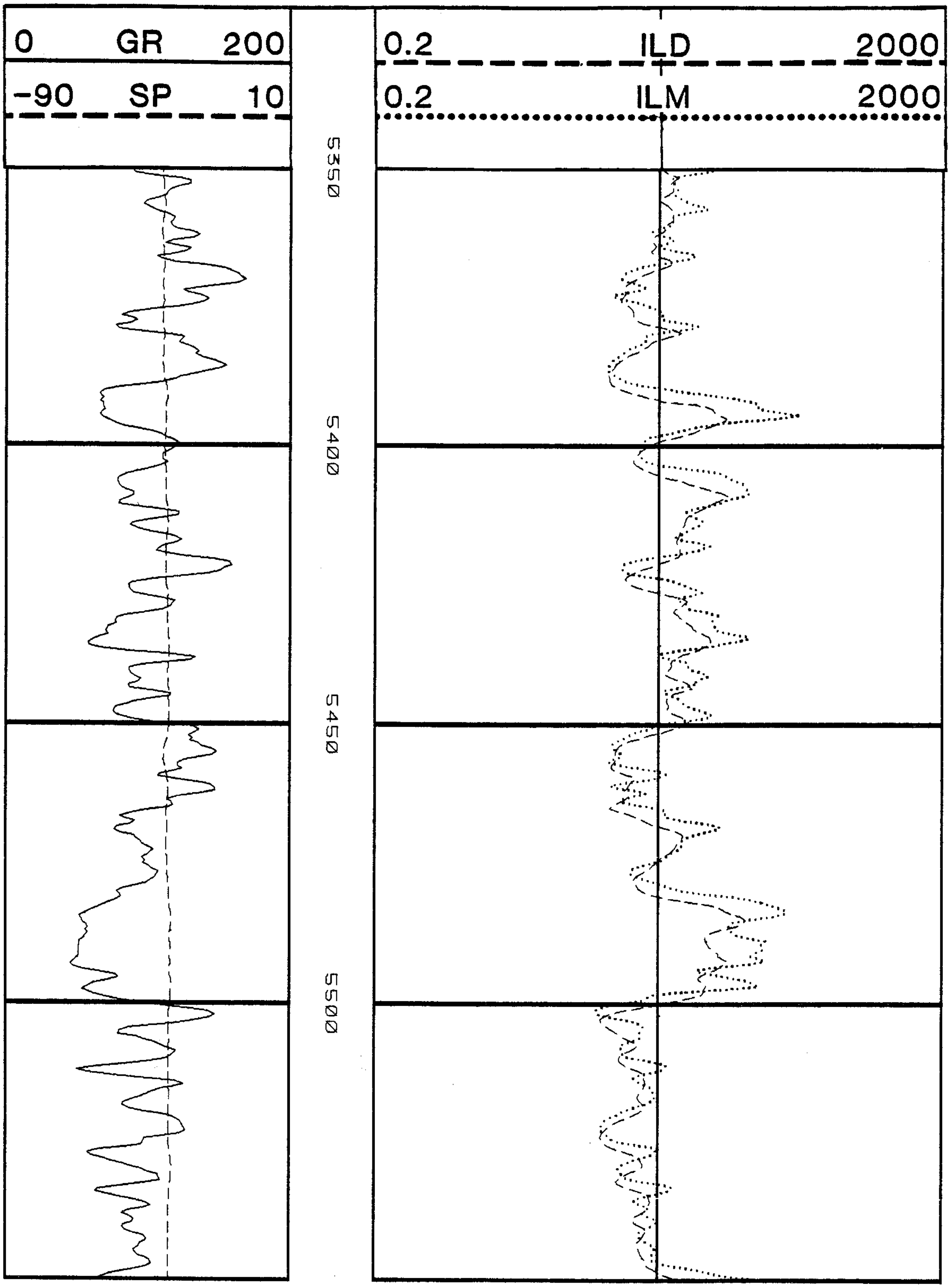

Figure 4.16, Continued

MWX-3

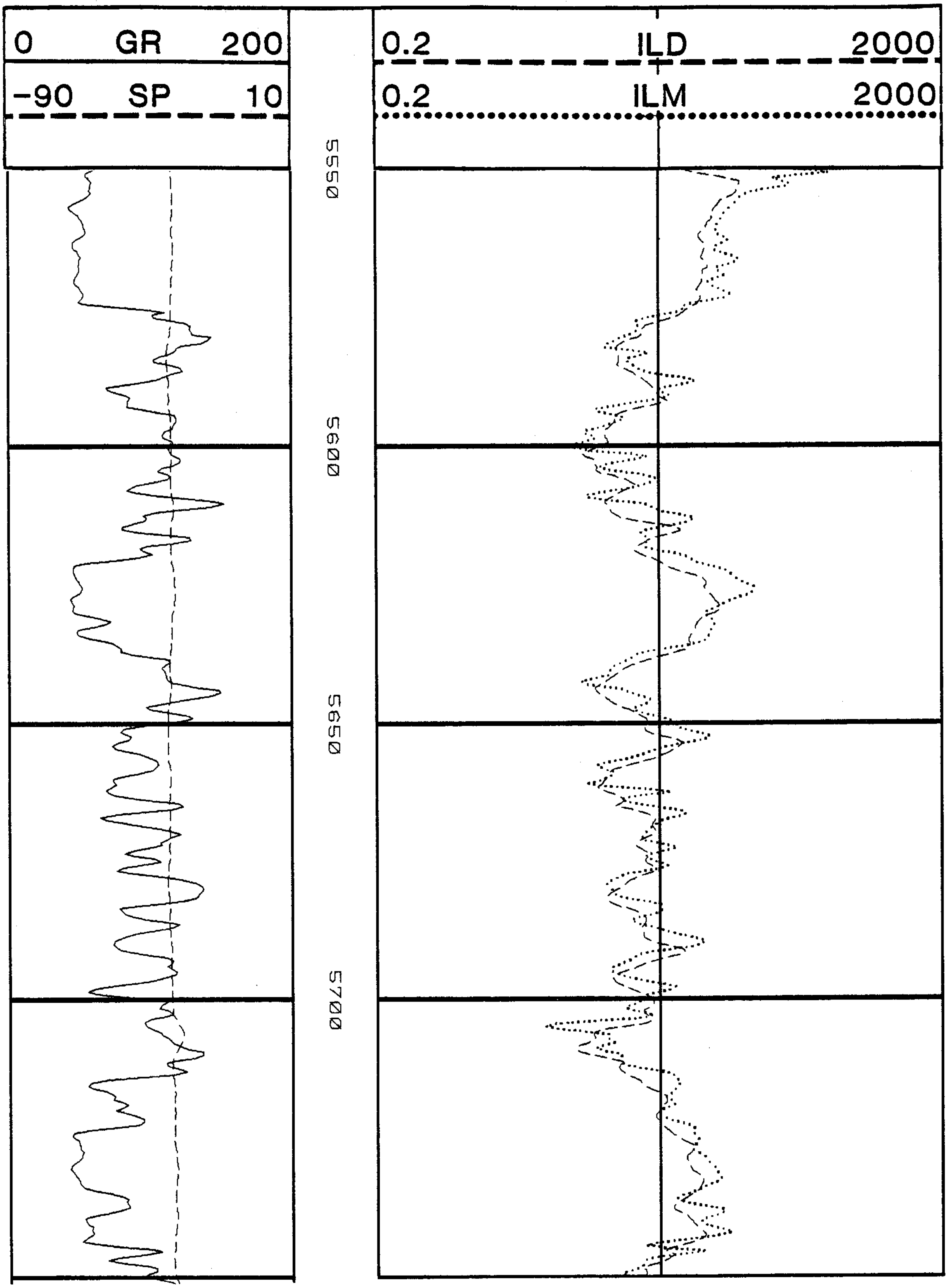

Figure 4.16, Continued

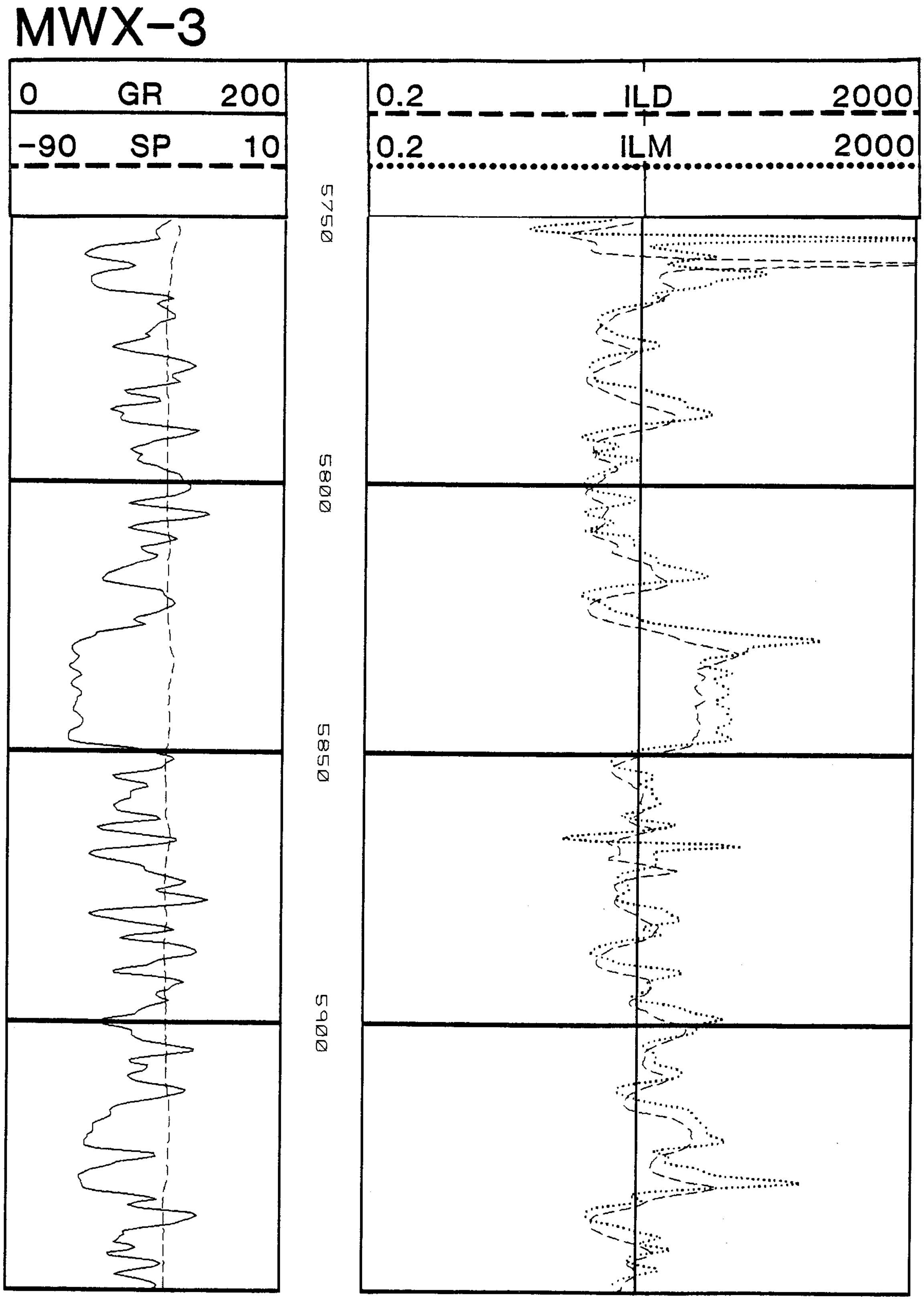

Figure 4.16, Continued

MWX-3

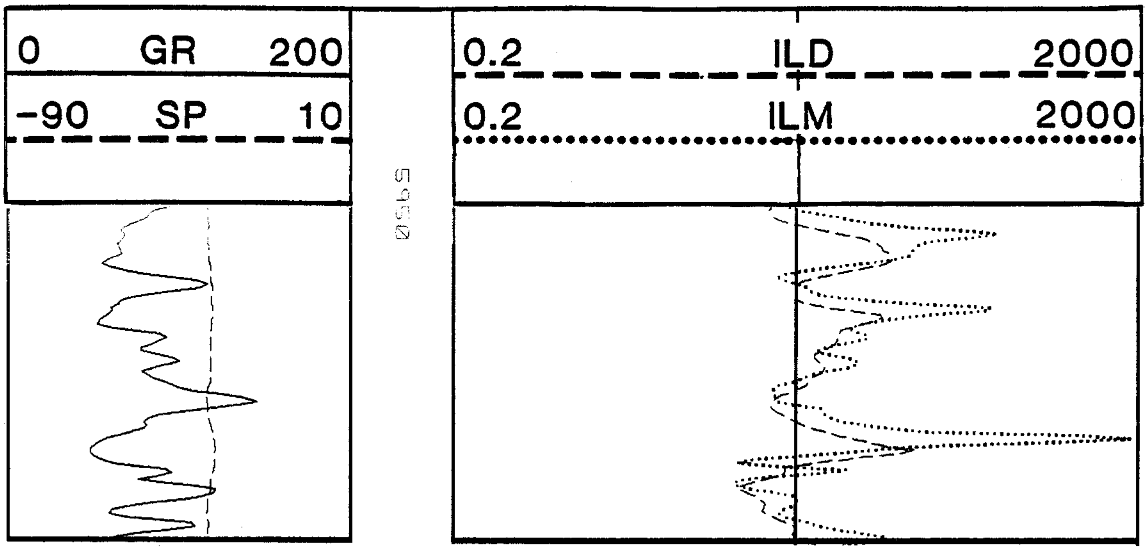

Figure 4.16, Continued

MWX-3

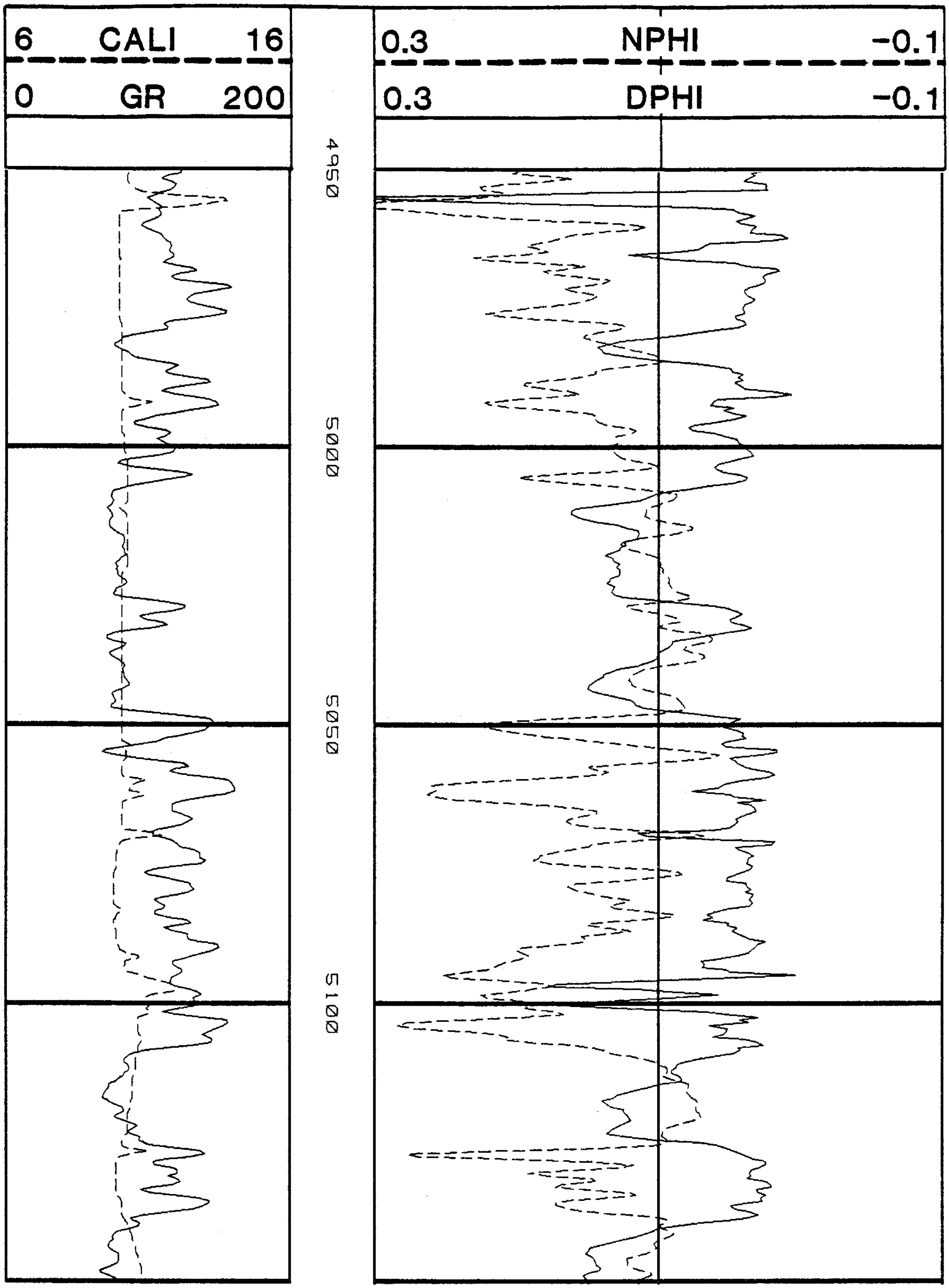

Figure 4.17 *MWX-3 Density and Neutron Porosity Logs*

MWX-3

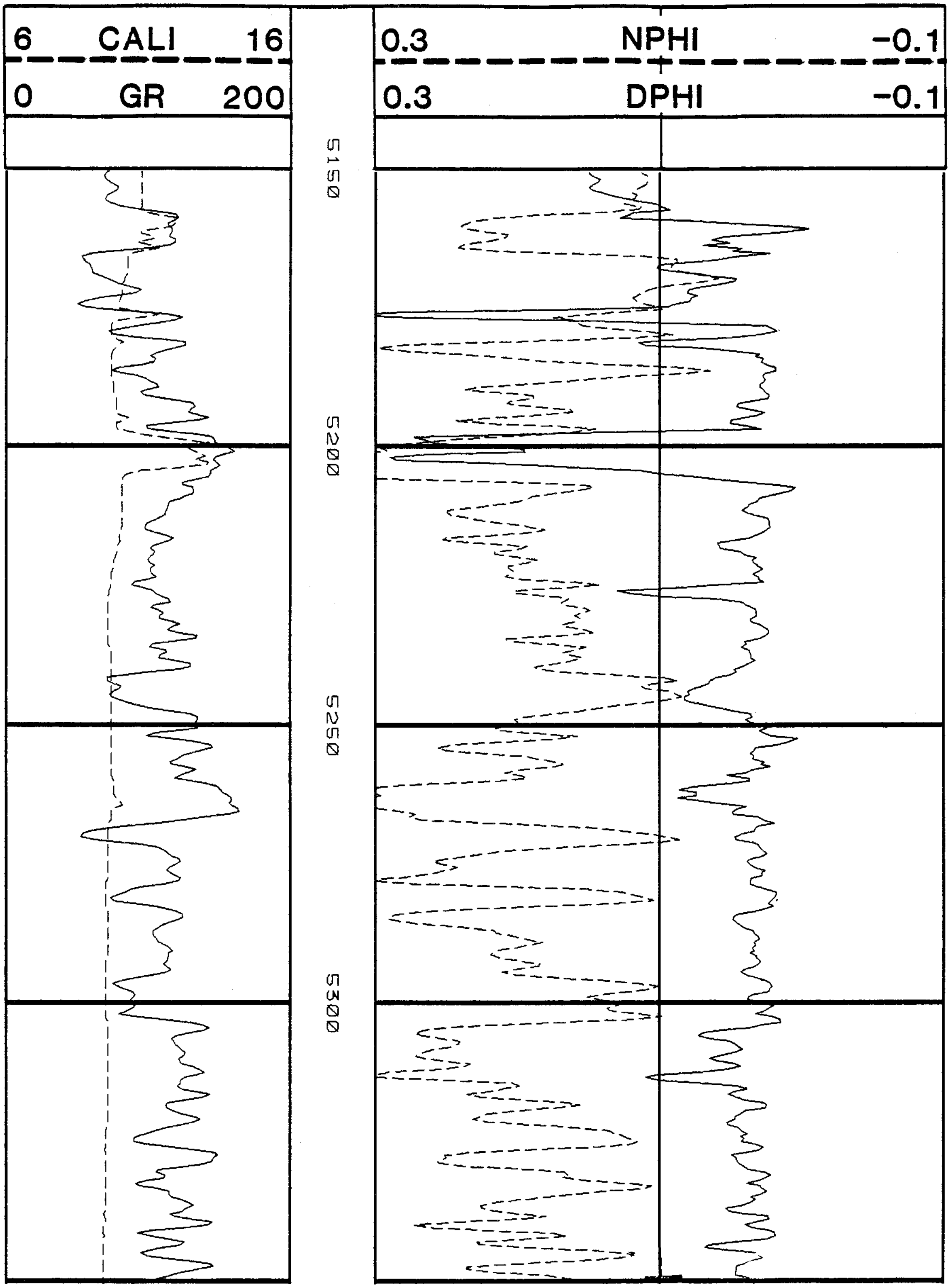

Figure 4.17, Continued

MWX-3

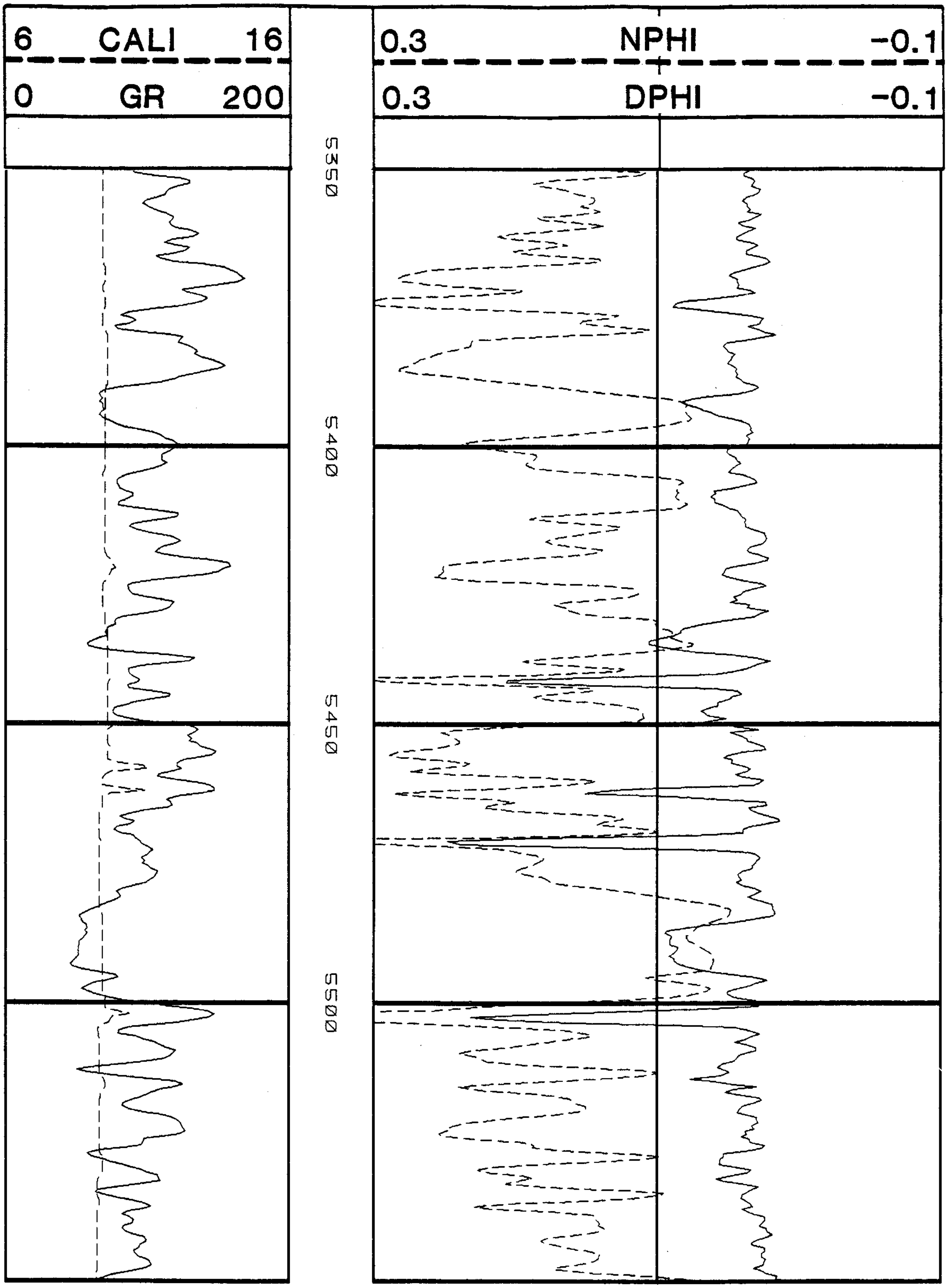

Figure 4.17, Continued

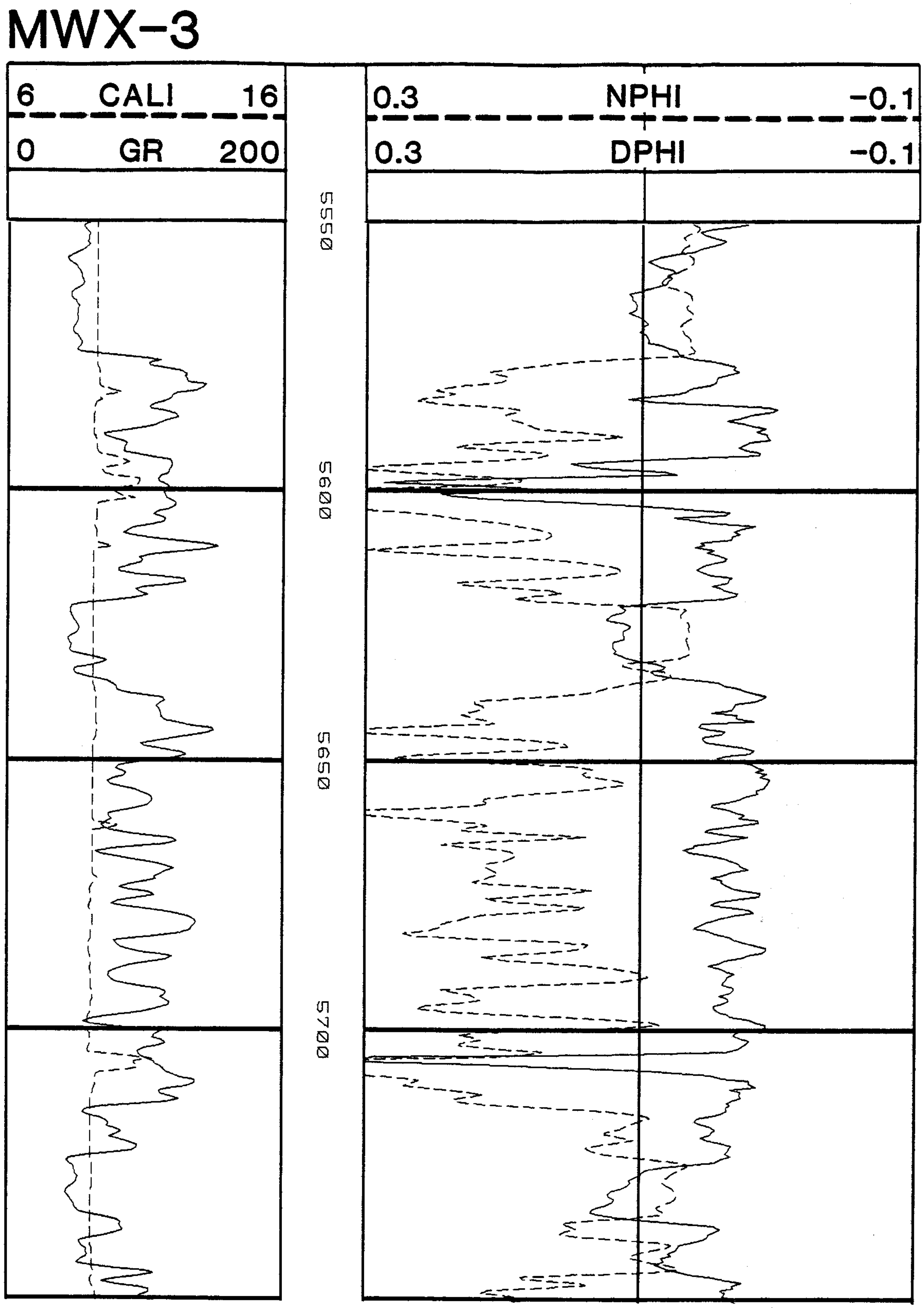

Figure 4.17, Continued

MWX-3

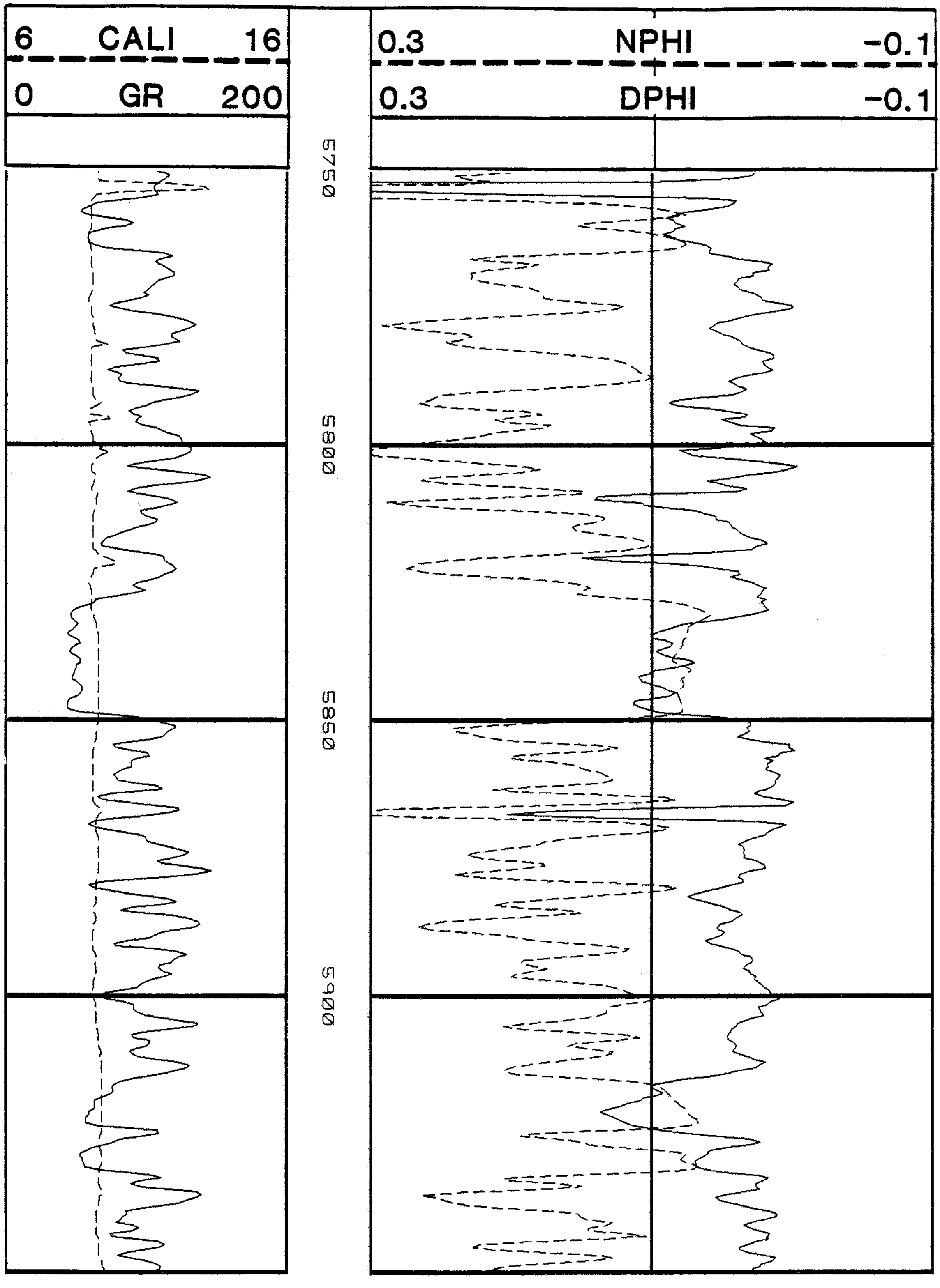

Figure 4.17, Continued

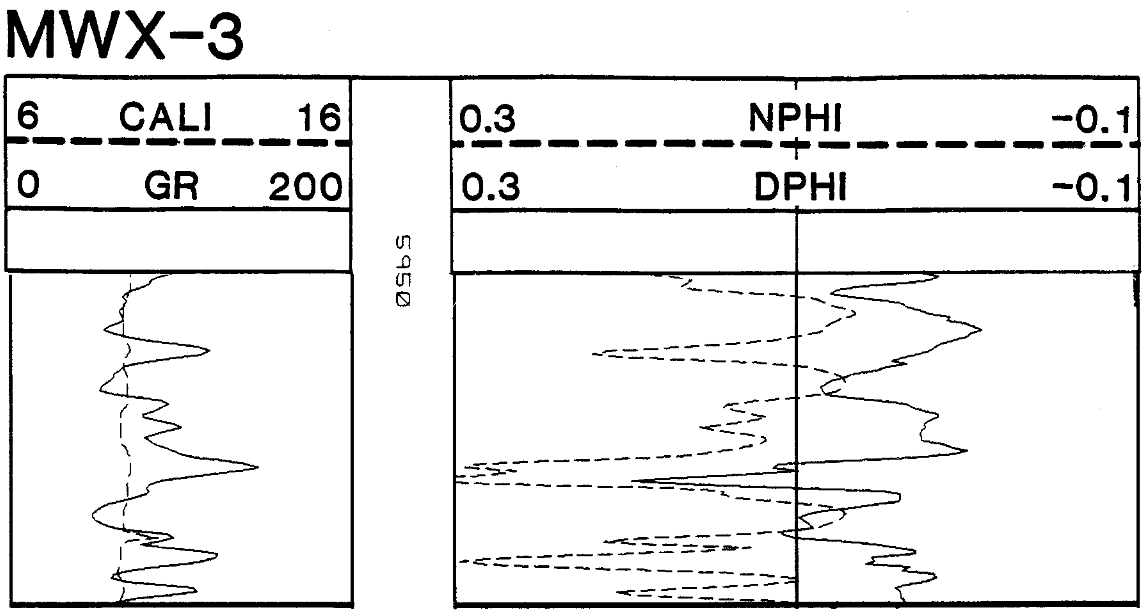

Figure 4.17, Continued

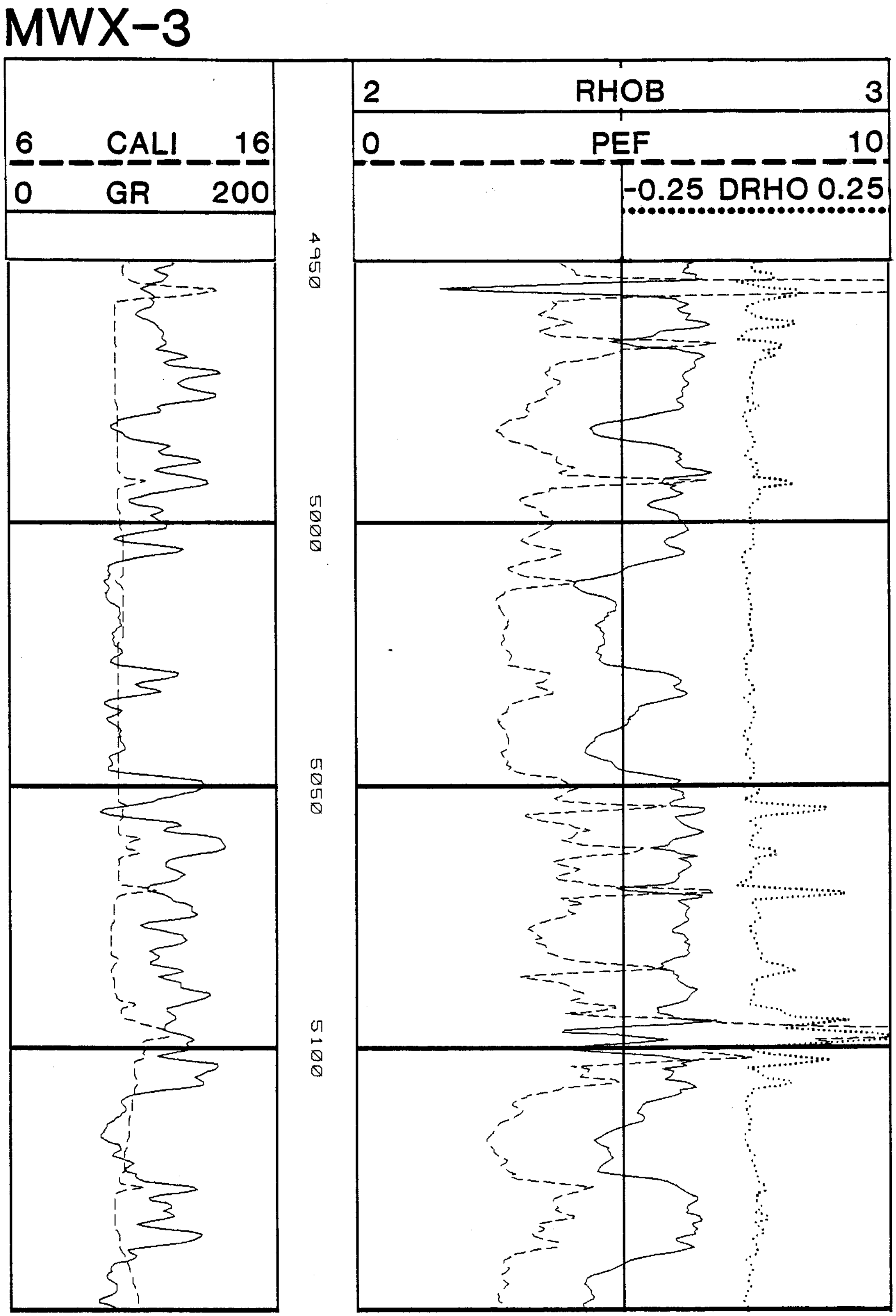

Figure 4.18 MWX-3 Bulk Density and Photoelectric Absorption Logs

MWX-3

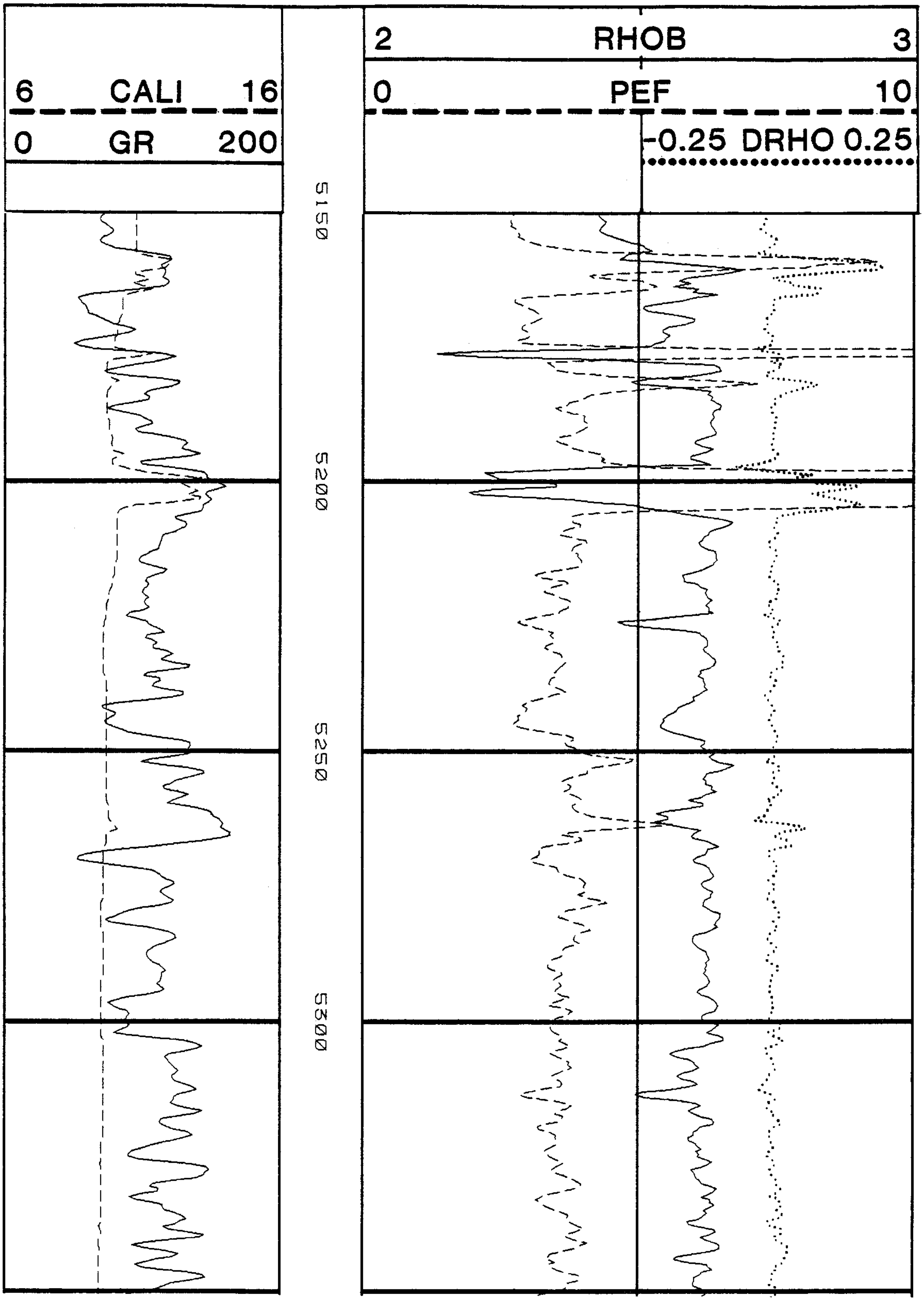

Figure 4.18, Continued

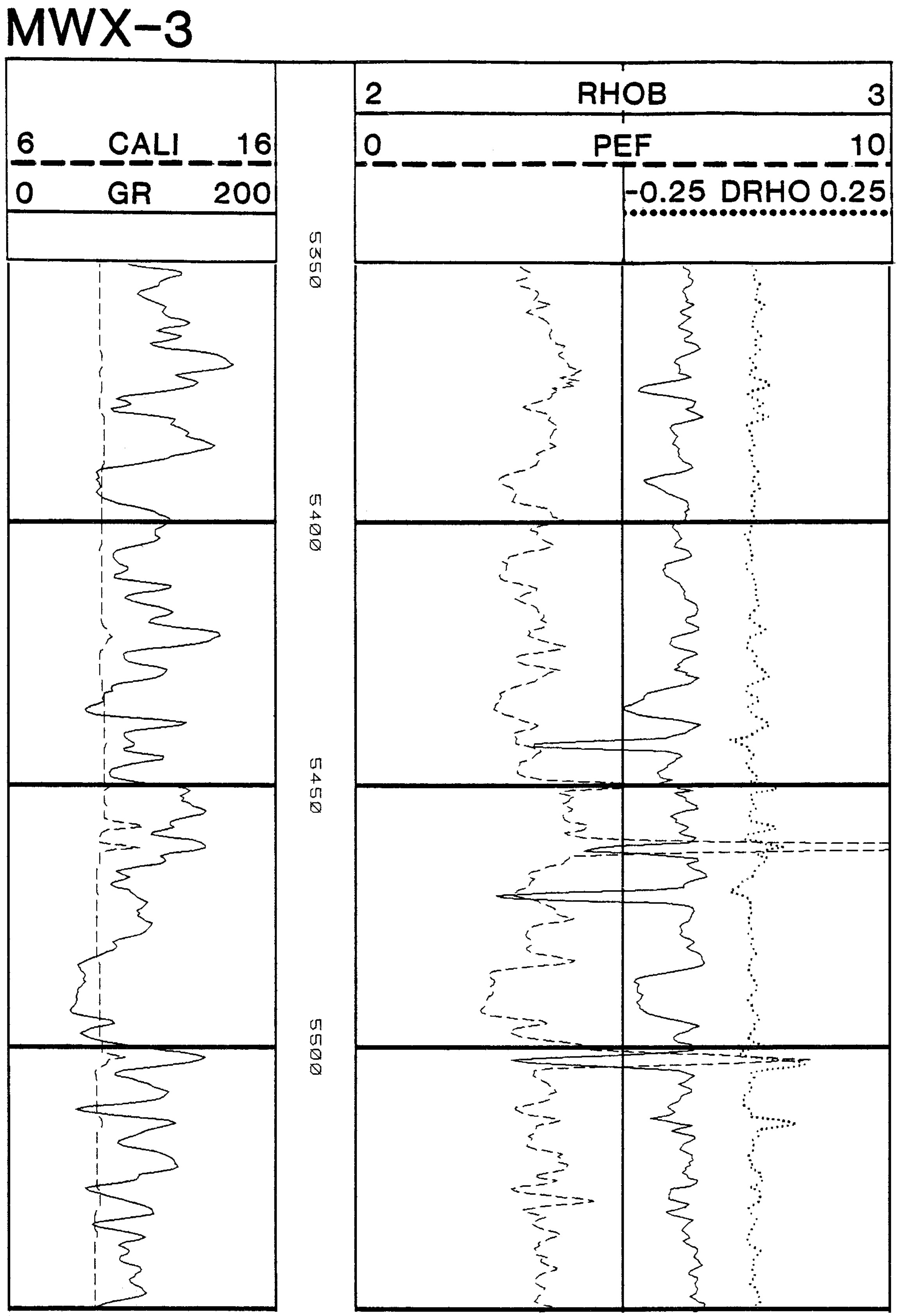

Figure 4.18, Continued

MWX-3

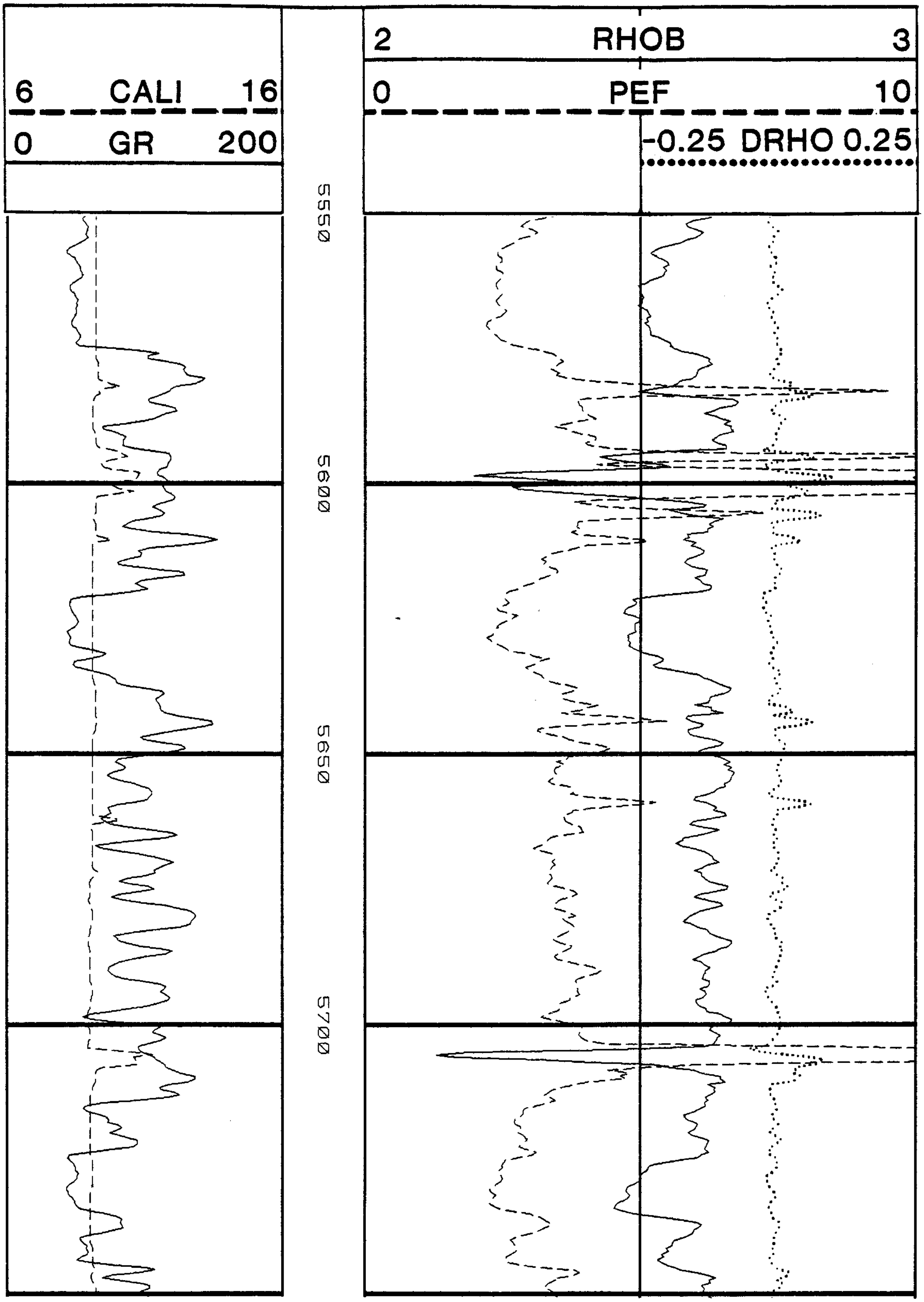

Figure 4.18, Continued

MWX-3

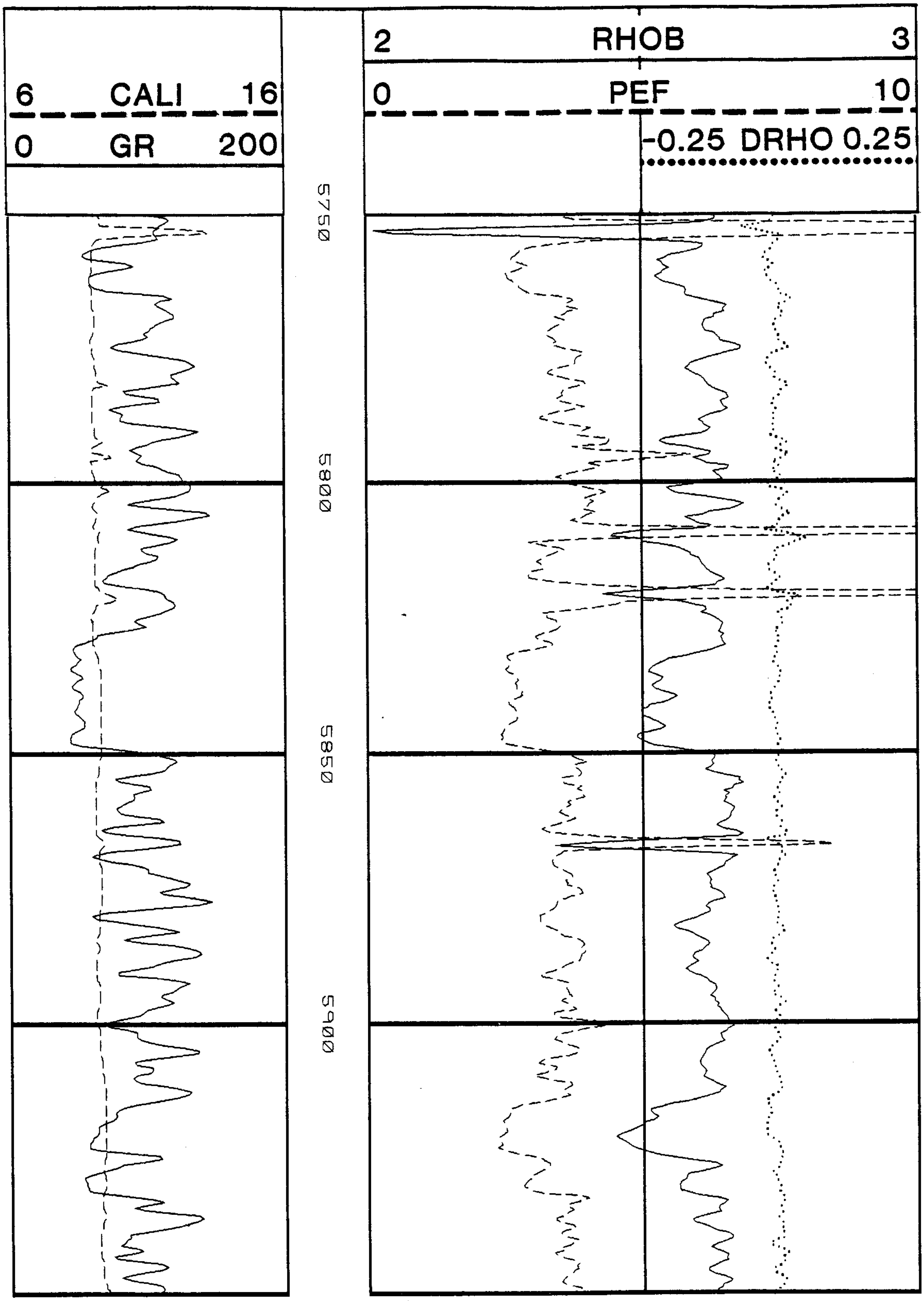

Figure 4.18, Continued

MWX-3

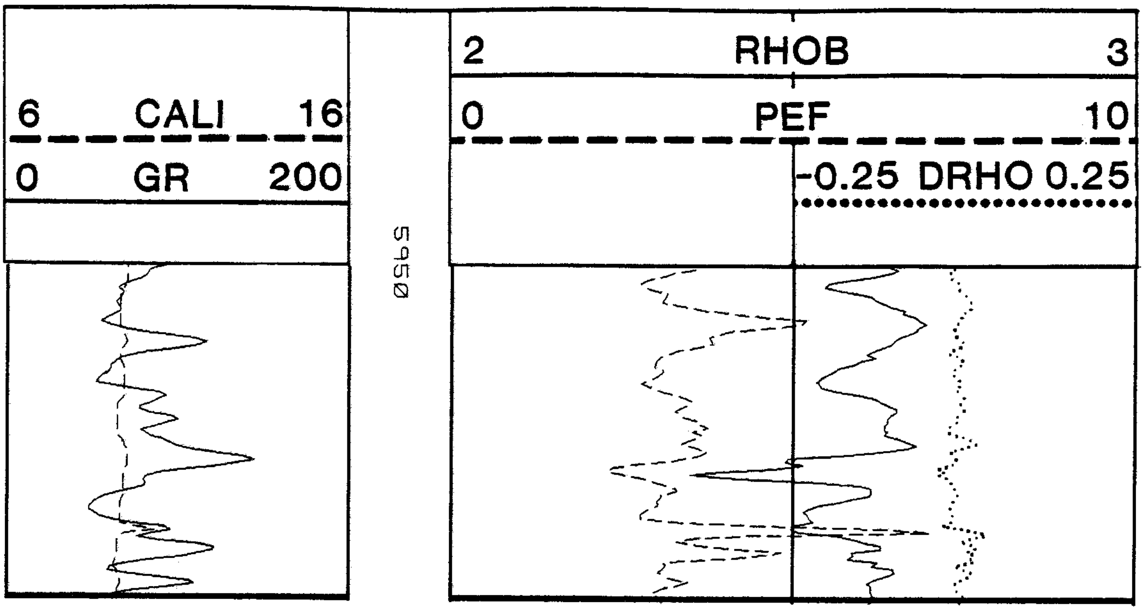

Figure 4.18, Continued

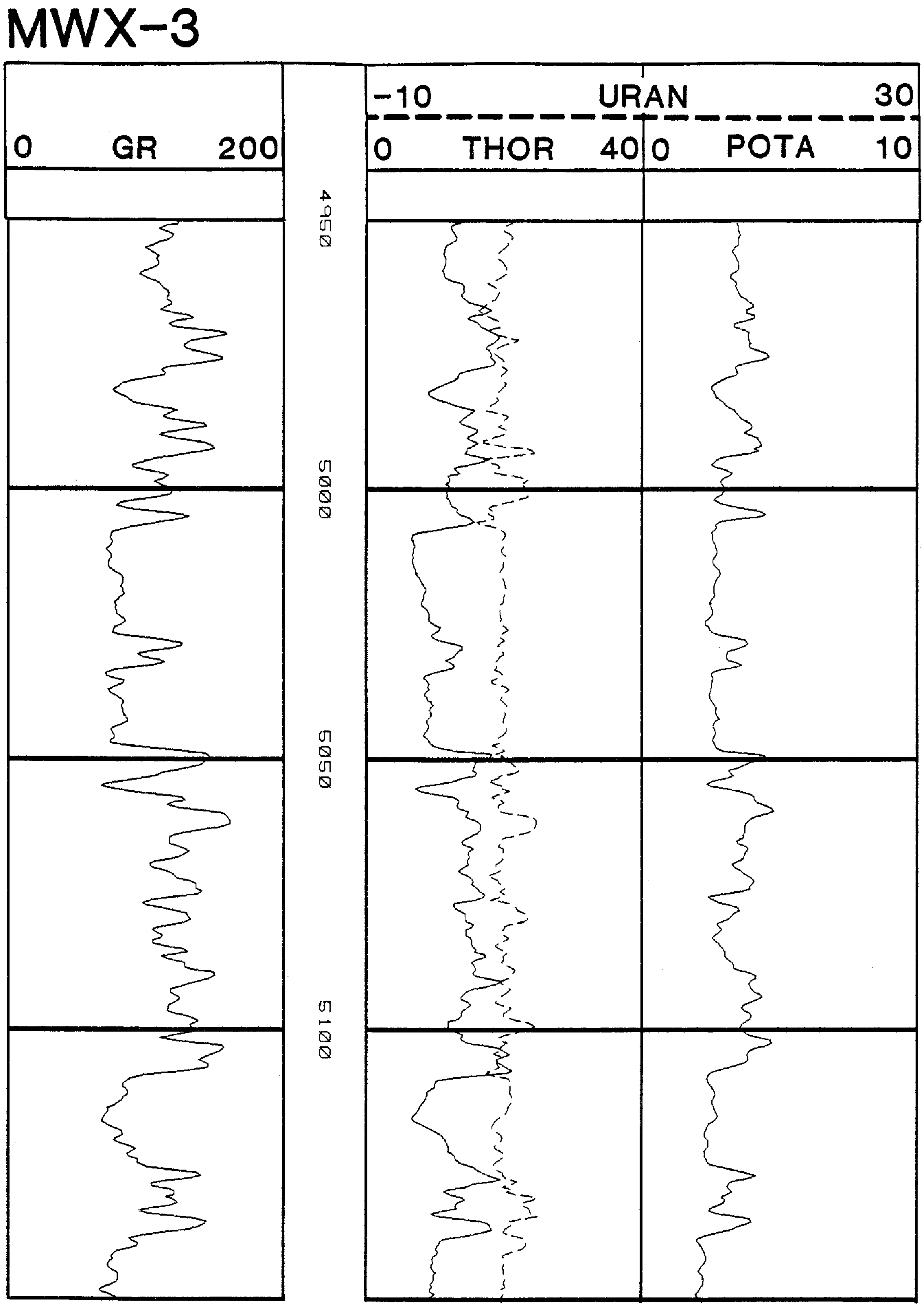

Figure 4.19 MWX-3 Spectral Gamma Log

MWX-3

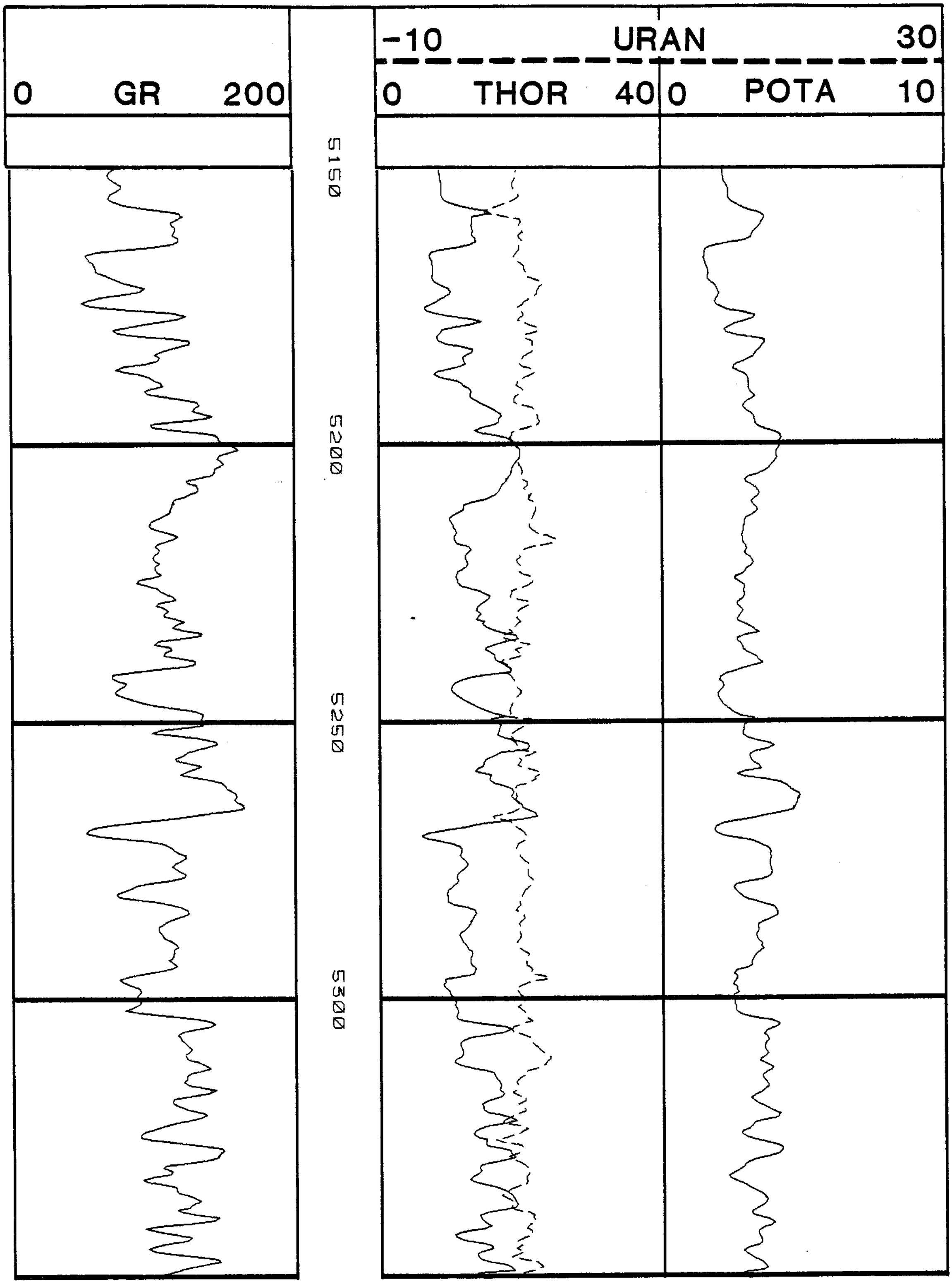

Figure 4.19, Continued

MWX-3

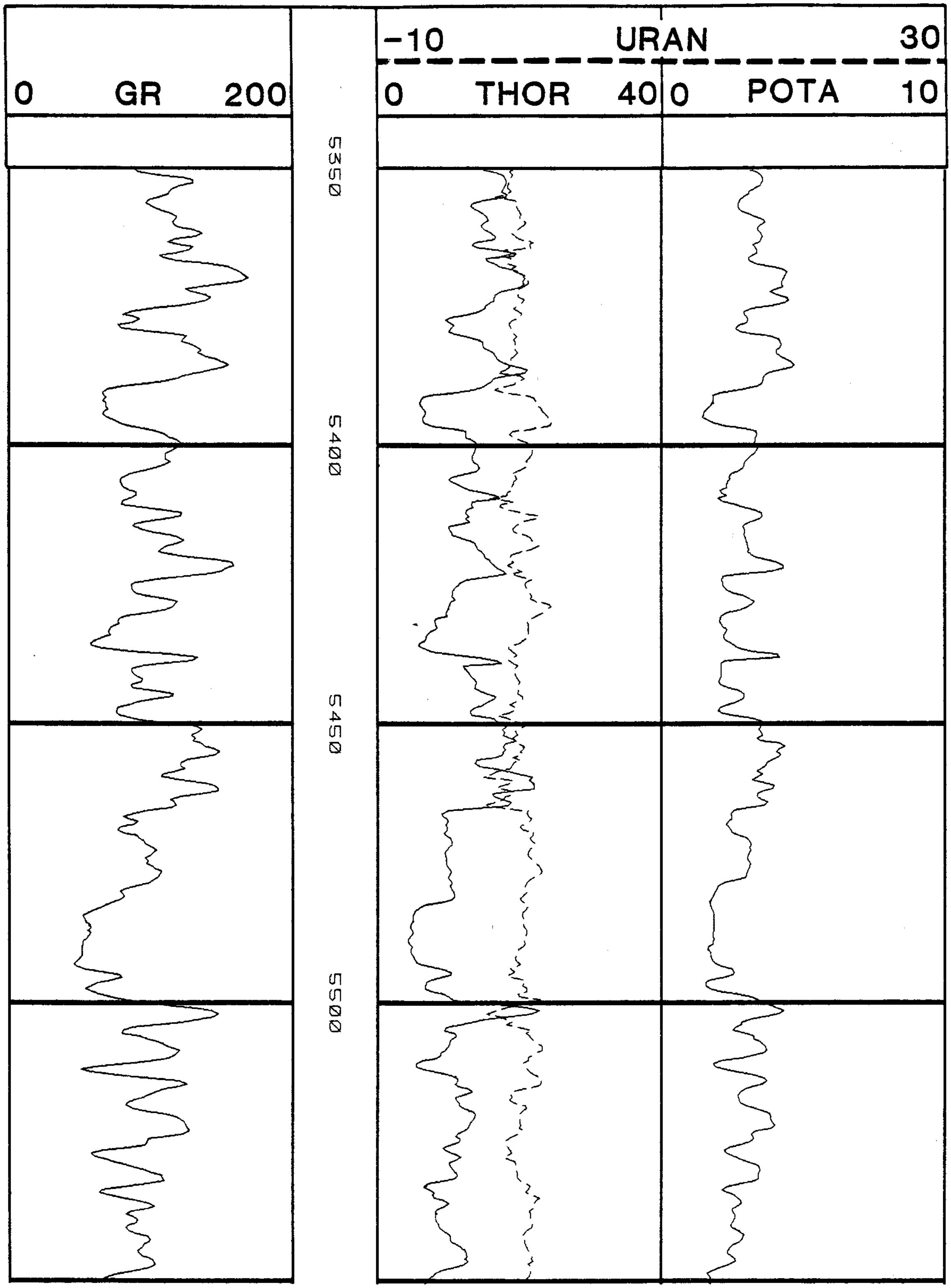

Figure 4.19, Continued

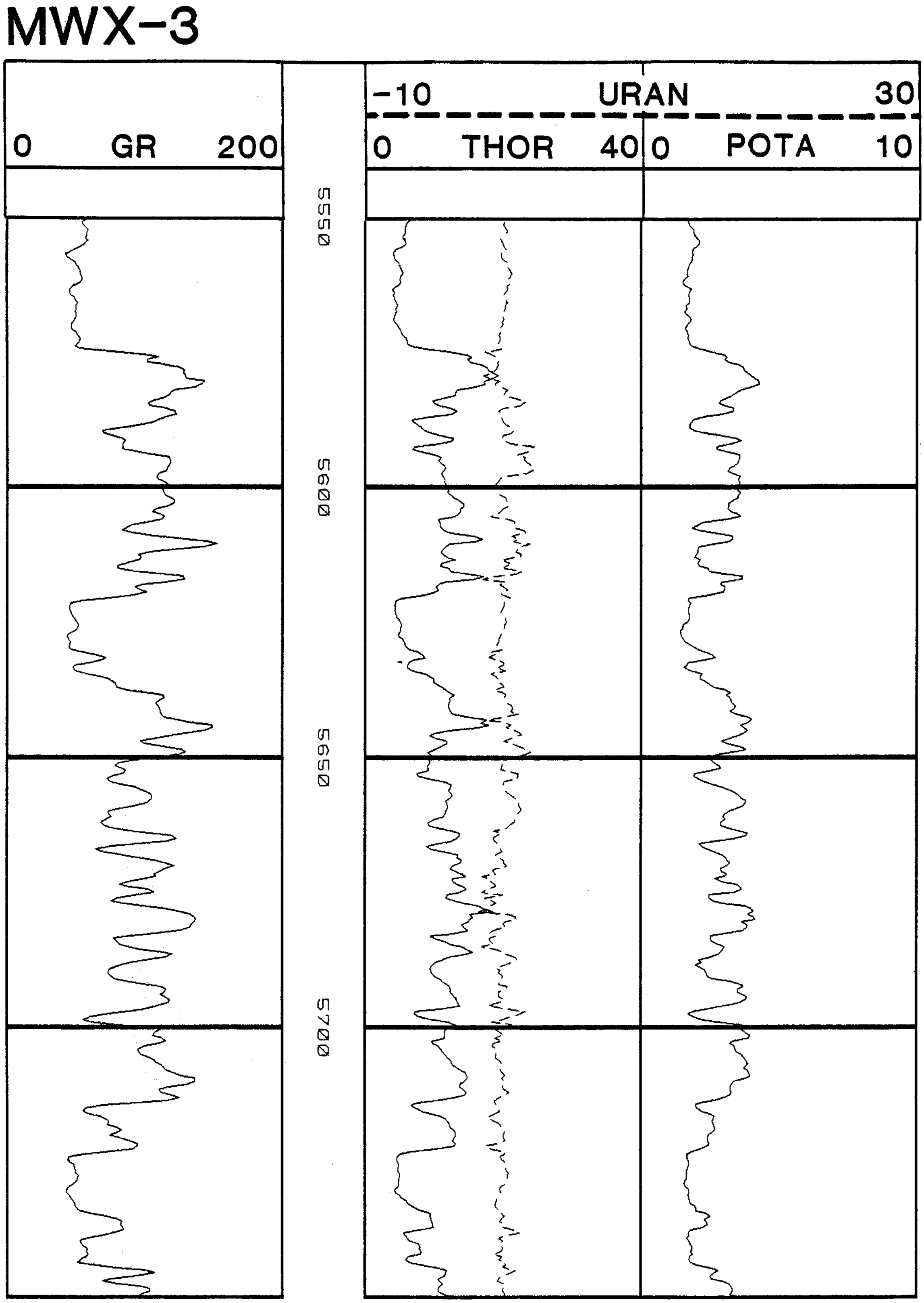

Figure 4.19, Continued

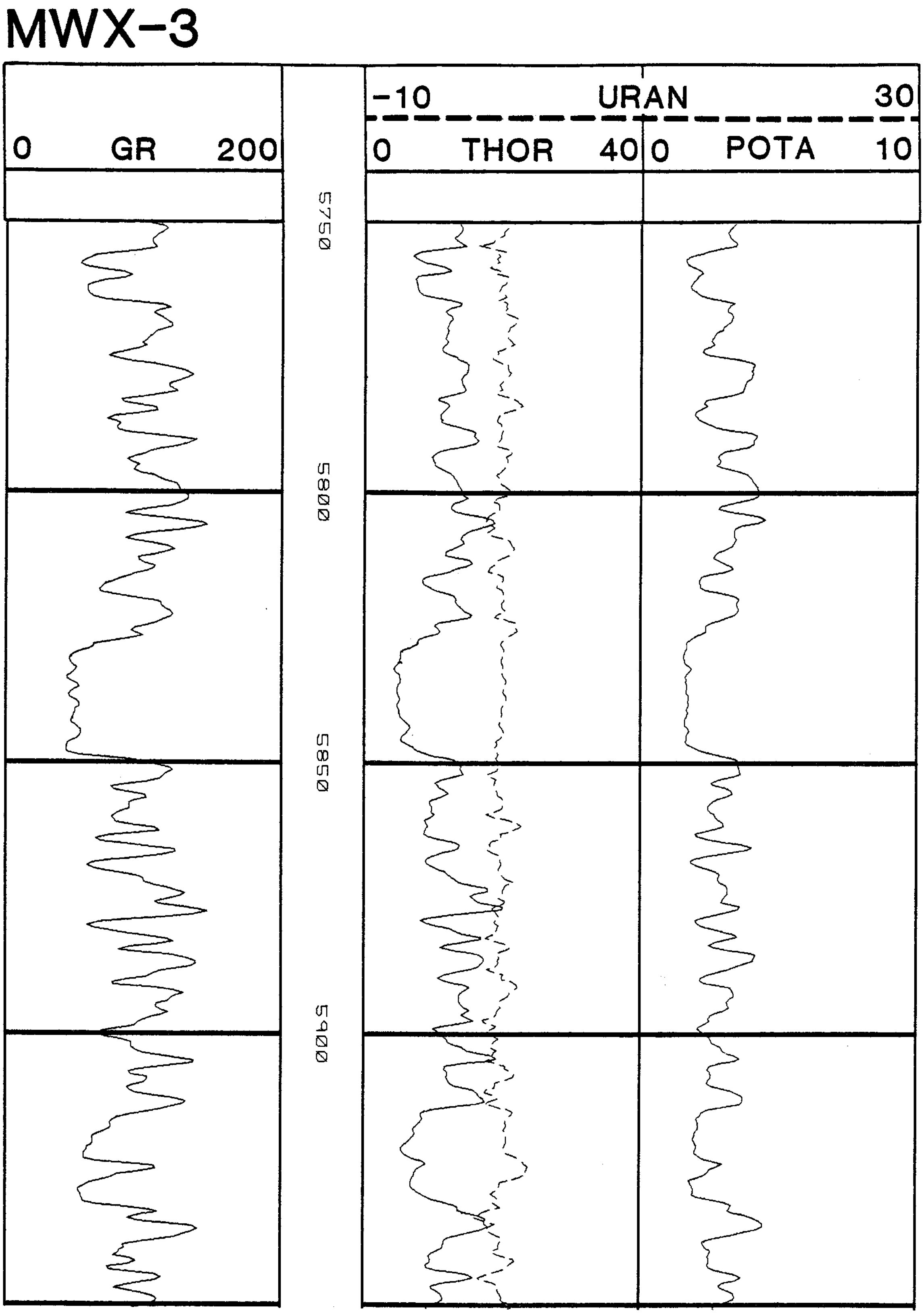

Figure 4.19, Continued

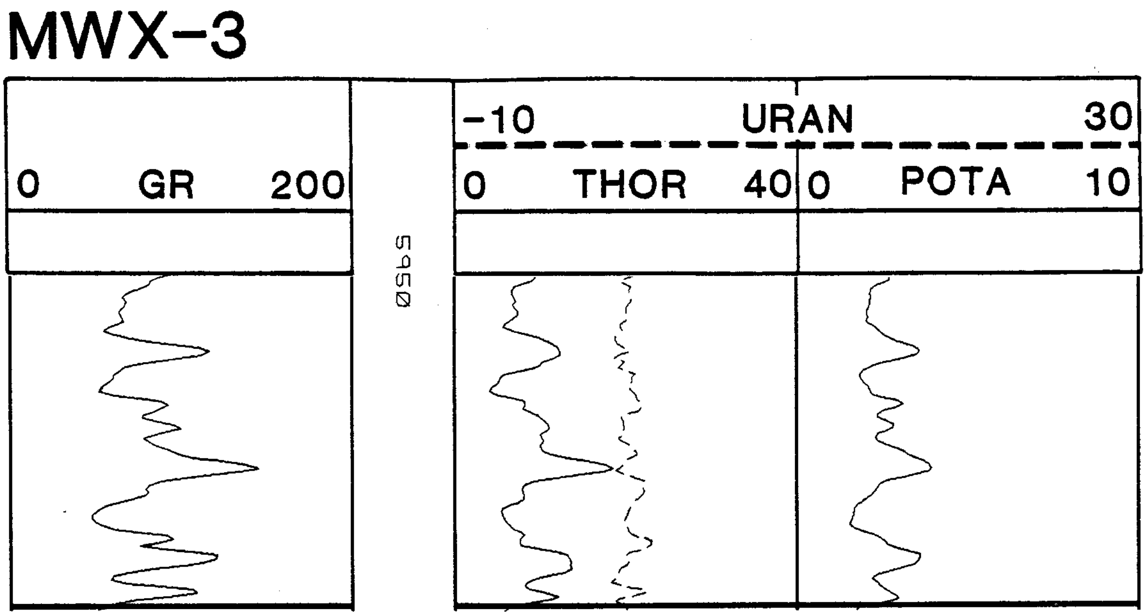

Figure 4.19, Continued

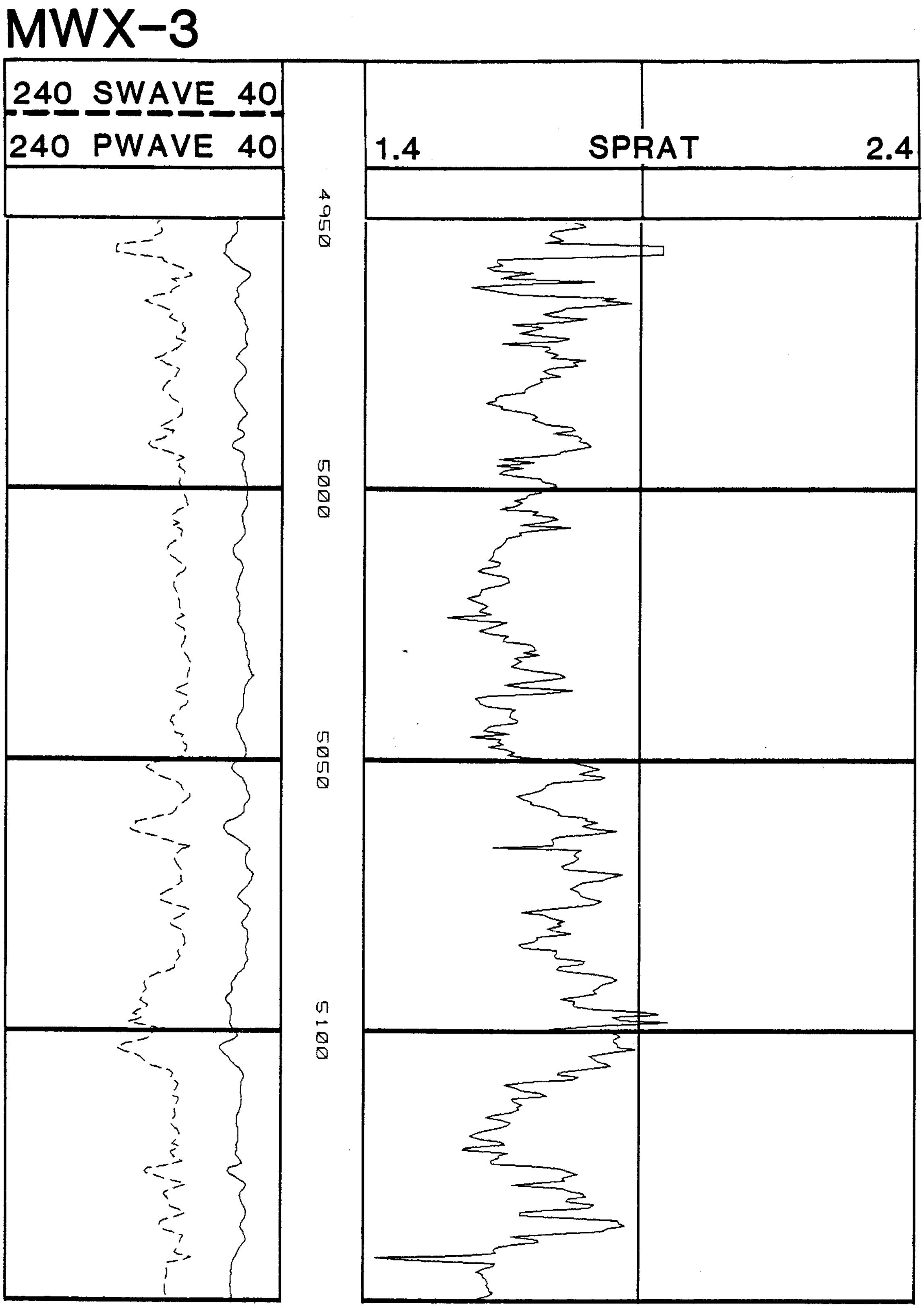

Figure 4.20 MWX-3 Long-Spaced Sonic Log

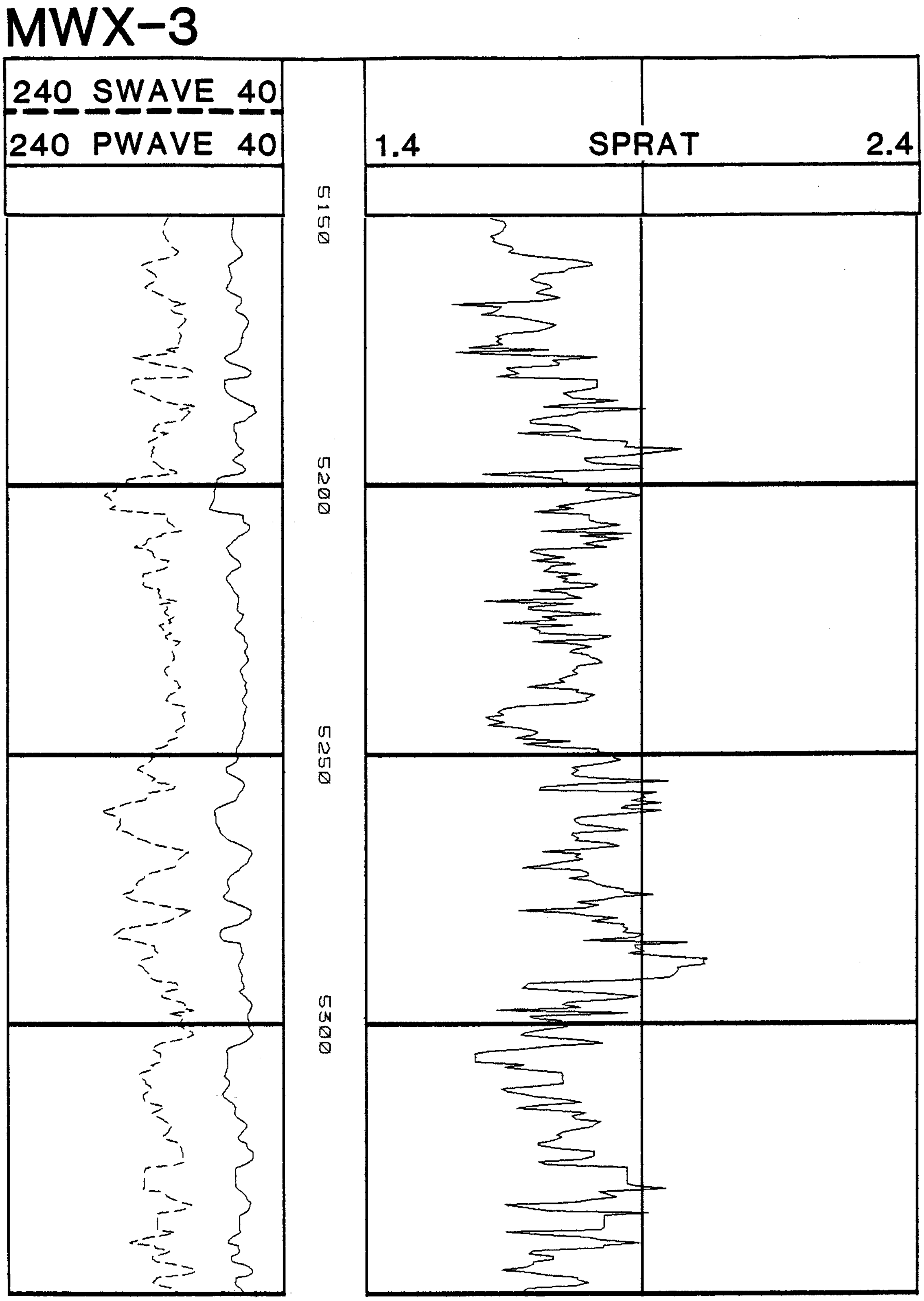

Figure 4.20, Continued

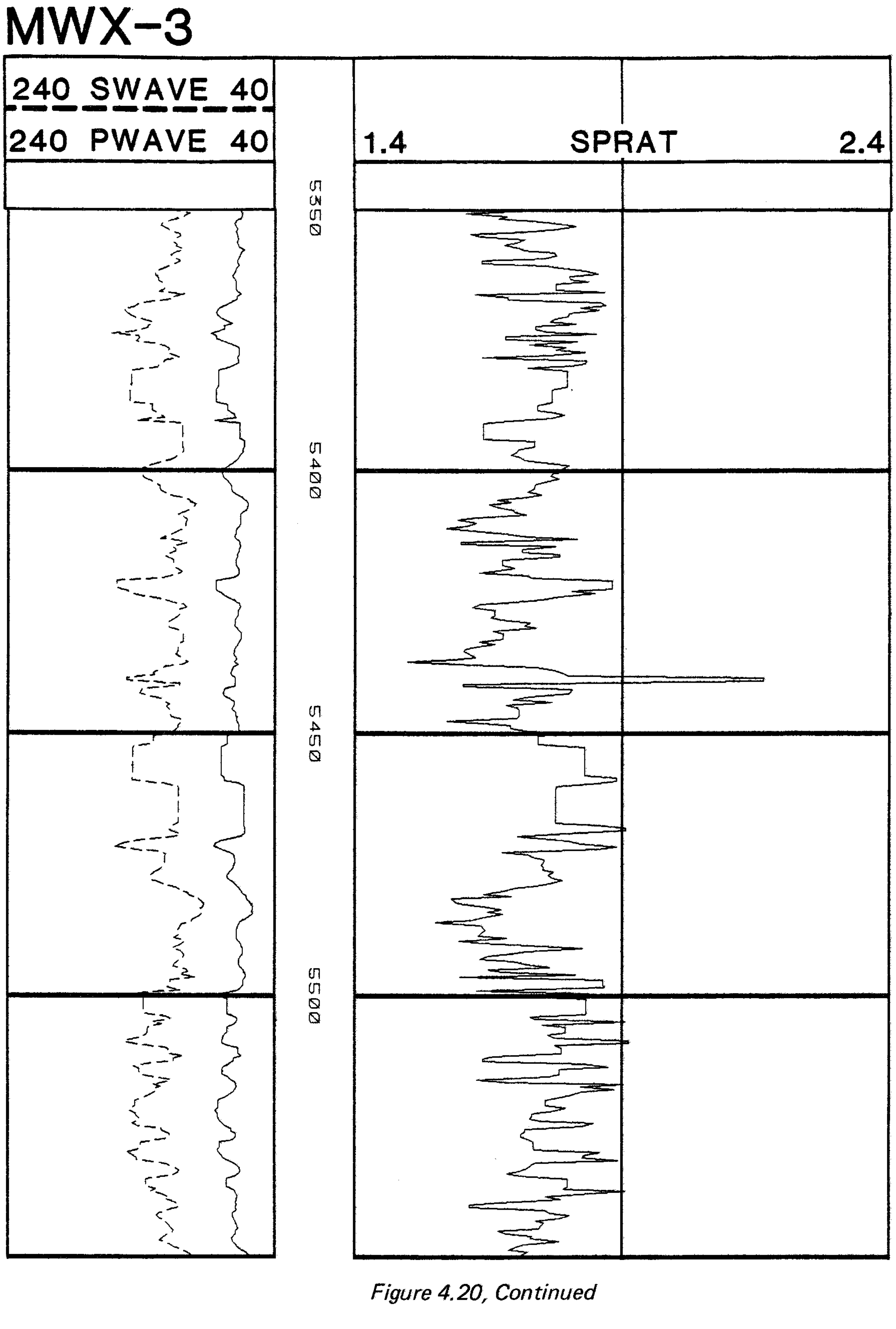

Figure 4.20, Continued

MWX-3

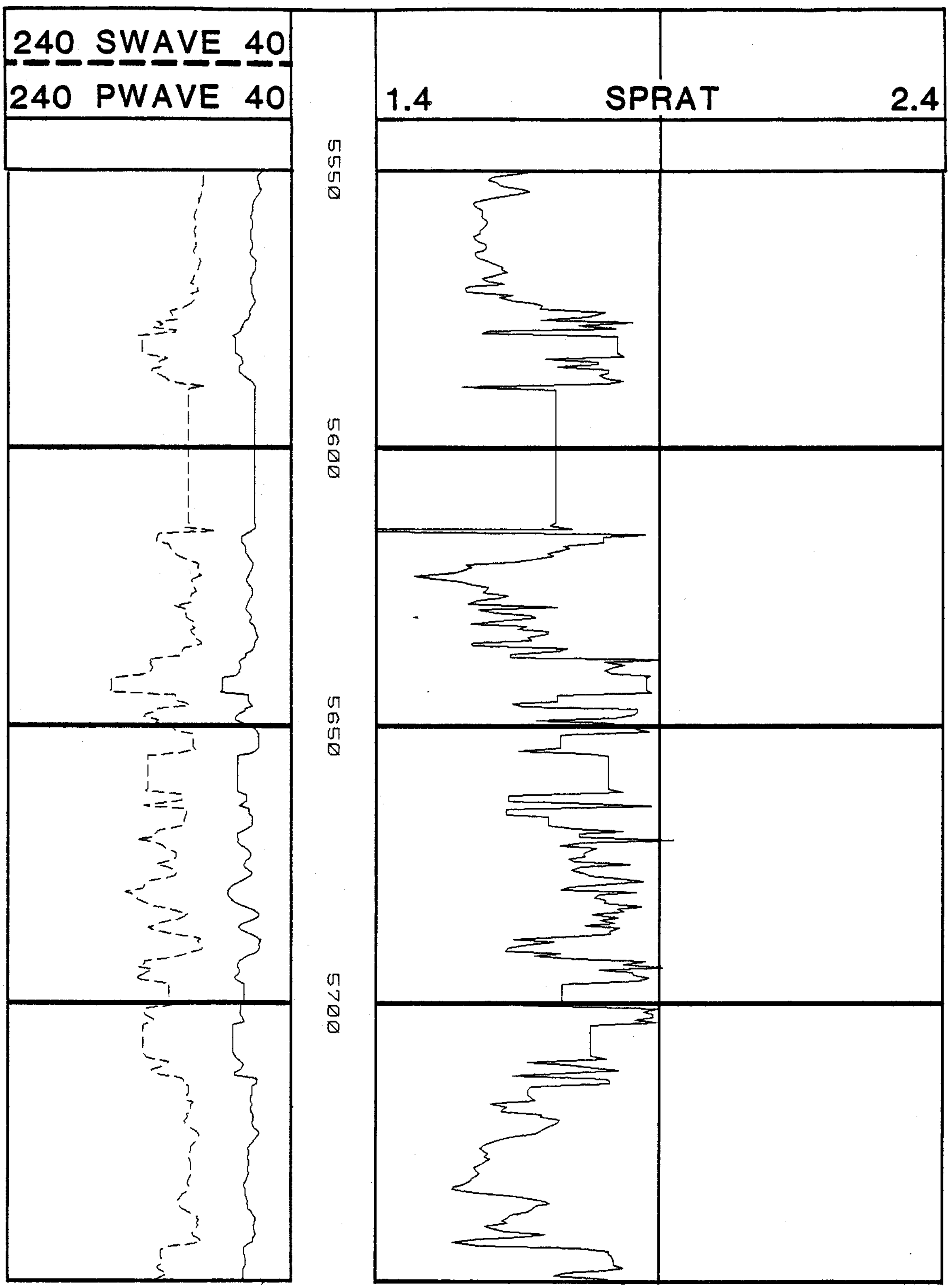

Figure 4.20, Continued

MWX-3

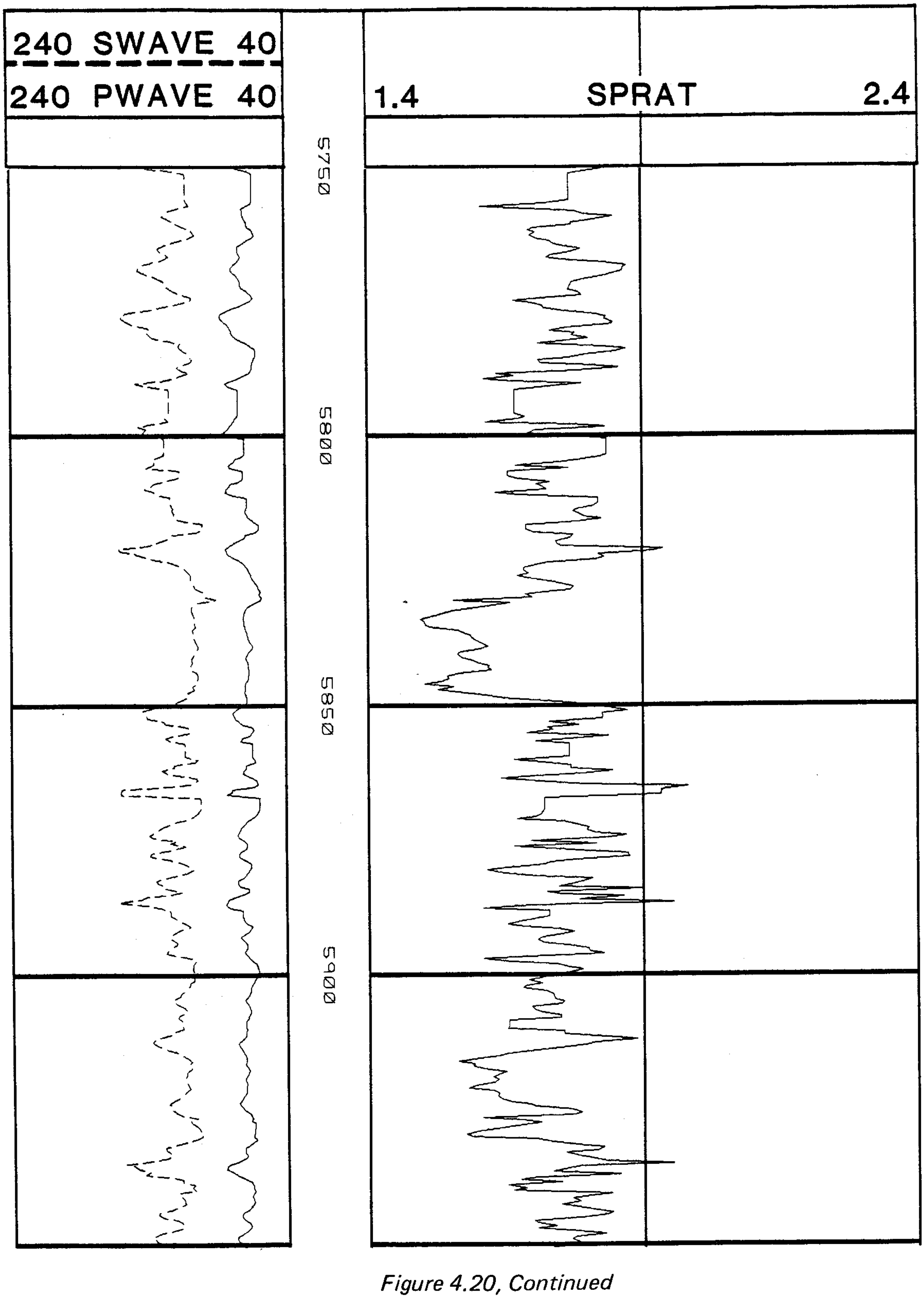

Figure 4.20, Continued

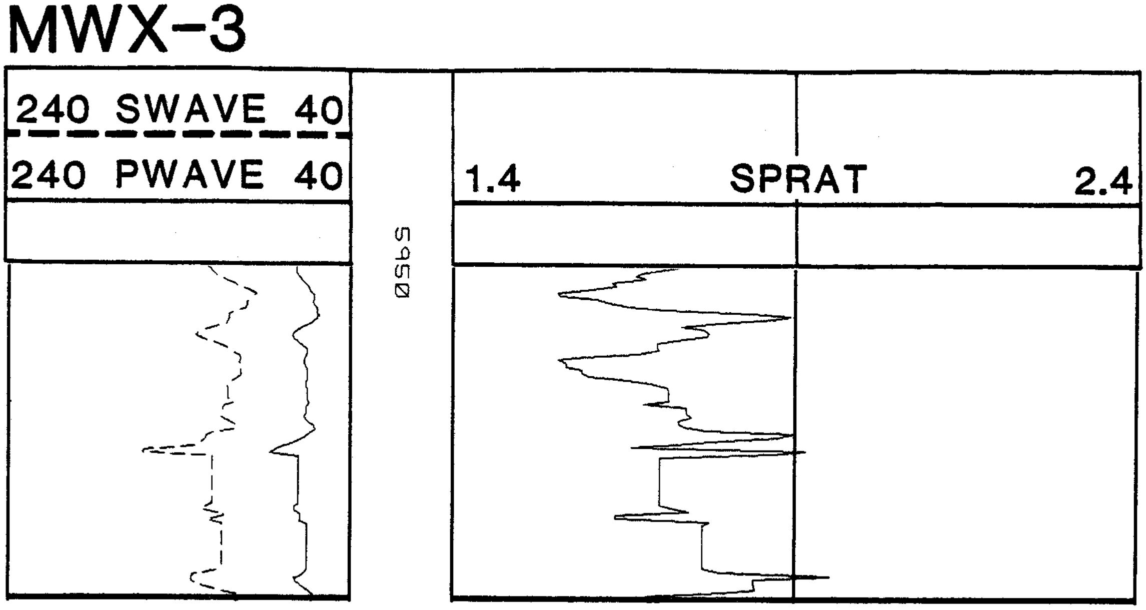

Figure 4.20, Continued

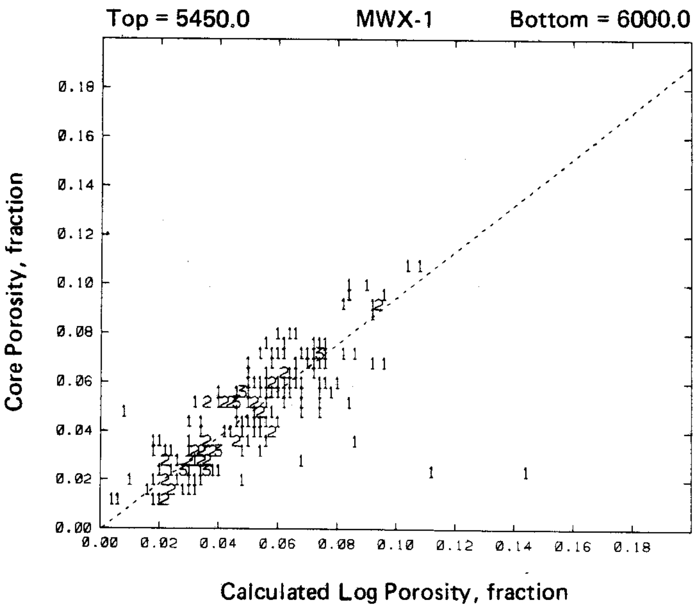

Points Plotted	192
Frequency Drop	0
Offscale X Values	0
Offscale Y Values	0
Offscale X and Y	0
Null X or Y	909
Discriminated Out	0
On Full Spots	0
Beyond Overflow	0
Total Points	1101
X Axis Mean	.0516
X Axis Std. Dev.	.0225
Y Axis Mean	.0484
Y Axis Std. Dev.	.0214
Correlation Coef.	.7474

Figure 4.21 Calculated Porosity Vs. Core Porosity, MWX-1 Low Fluvial Interval

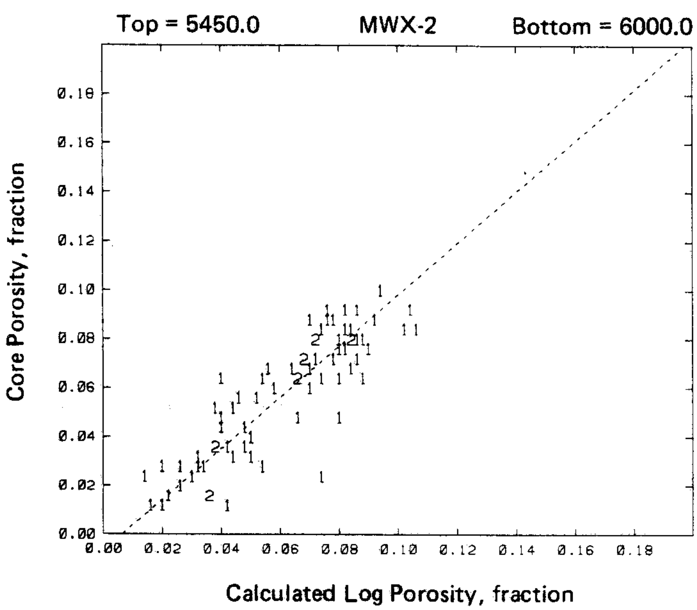

Points Plotted	74
Frequency Drop	0
Offscale X Values	0
Offscale Y Values	0
Offscale X and Y	0
Null X or Y	1027
Discriminated Out	0
On Full Spots	0
Beyond Overflow	0
Total Points	1101
X Axis Mean	.0614
X Axis Std. Dev.	.0236
Y Axis Mean	.0576
Y Axis Std. Dev.	.0247
Correlation Coef.	.8668

Figure 4.22 Calculated Porosity Vs. Core Porosity, MWX-2 Low Fluvial Interval

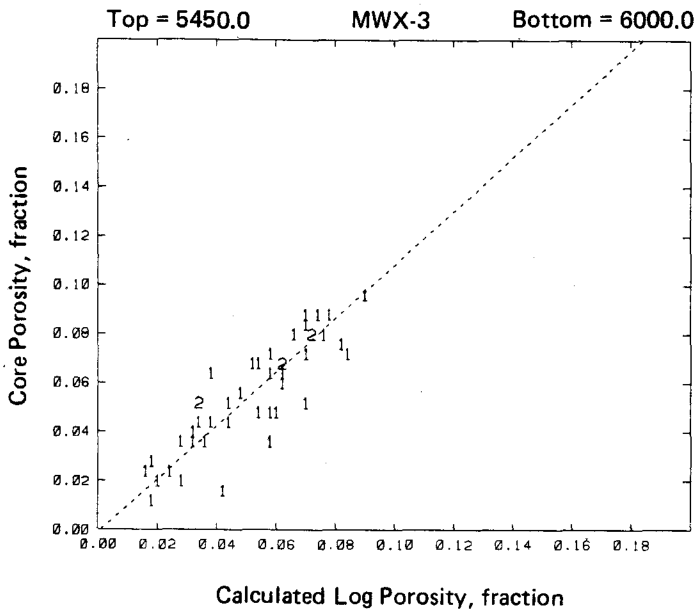

Points Plotted	44
Frequency Drop	0
Offscale X Values	0
Offscale Y Values	0
Offscale X and Y	0
Null X or Y	1057
Discriminated Out	0
On Full Spots	0
Beyond Overflow	0
Total Points	1101
X Axis Mean	.0519
X Axis Std. Dev.	.0198
Y Axis Mean	.0556
Y Axis Std. Dev.	.0217
Correlation Coef.	.8673

Figure 4.23 Calculated Porosity Vs. Core Porosity, MWX-3 Low Fluvial Interval

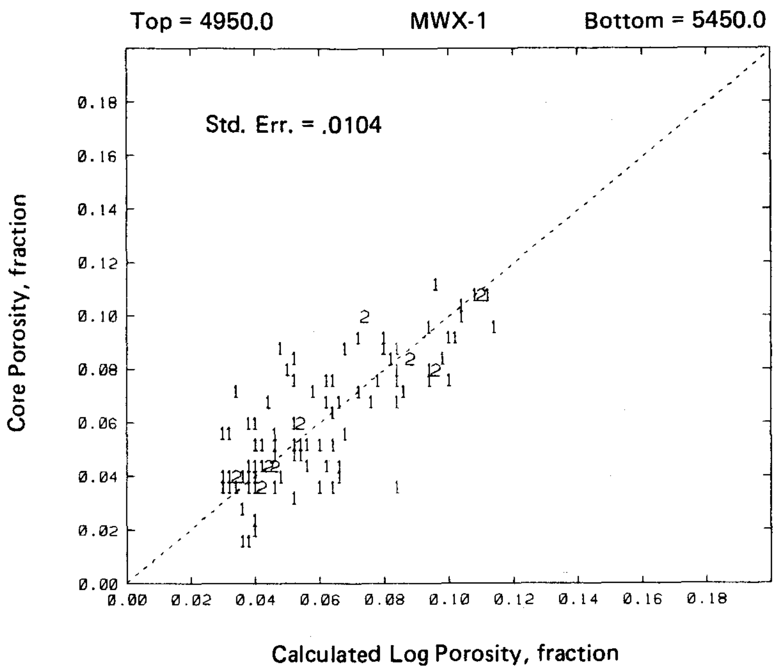

Points Plotted	102
X Axis Mean	.0619
X Axis Std. Dev.	.0237
Y Axis Mean	.0618
Y Axis Std. Dev.	.0235
Correlation Coef.	.8015

Figure 4.24 Calculated Porosity Vs. Core Porosity, MWX-1 Middle Fluvial Interval

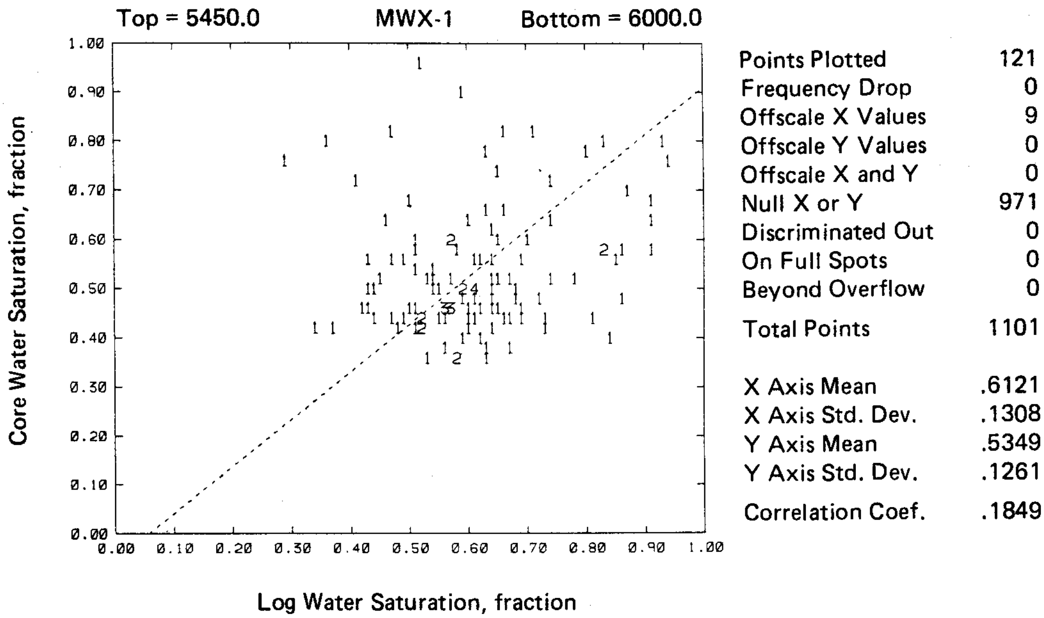

Figure 4.25 *Calculated Water Saturation Vs. Core Water Saturation, MWX-1 Low Fluvial Interval*

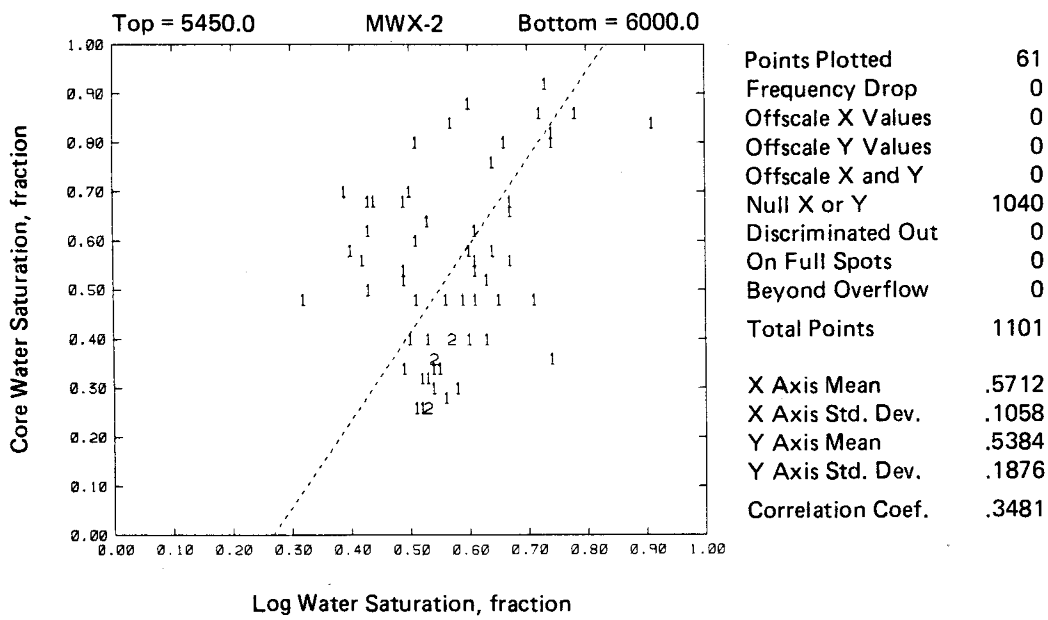

Figure 4.26 *Calculated Water Saturation Vs. Core Water Saturation, MWX-2 Low Fluvial Interval*

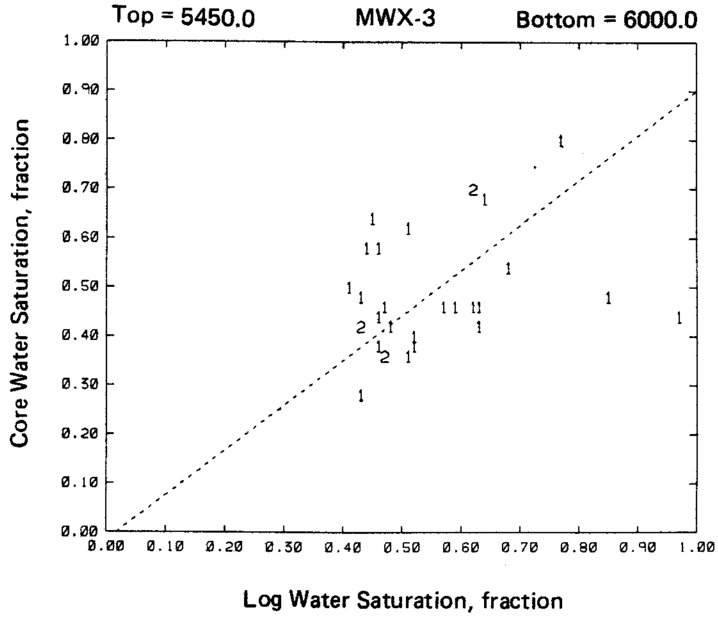

Points Plotted	30
Frequency Drop	0
Offscale X Values	4
Offscale Y Values	0
Offscale X and Y	0
Null X or Y	1067
Discriminated Out	0
On Full Spots	0
Beyond Overflow	0
Total Points	1101
X Axis Mean	.5513
X Axis Std. Dev.	.1345
Y Axis Mean	.4896
Y Axis Std. Dev.	.1233
Correlation Coef.	.3072

Figure 4.27 Calculated Water Saturation Vs. Core Water Saturation, MWX-3 Low Fluvial Interval

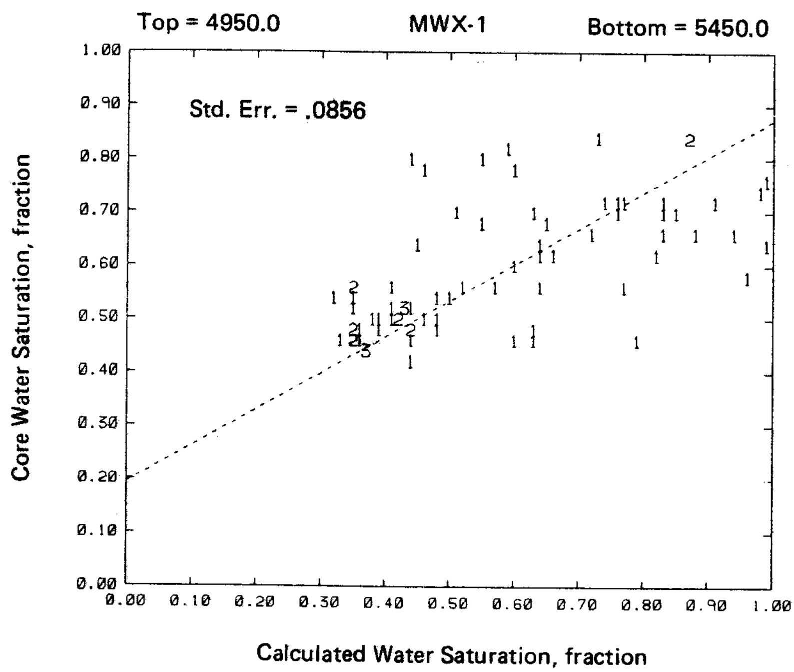

Points Plotted	79
X Axis Mean	.5700
X Axis Std. Dev.	.1978
Y Axis Mean	.5814
Y Axis Std. Dev.	.1344
Correlation Coef.	.5893

Figure 4.28 Calculated Water Saturation Vs. Core Water Saturation, MWX-1 Middle Fluvial Interval

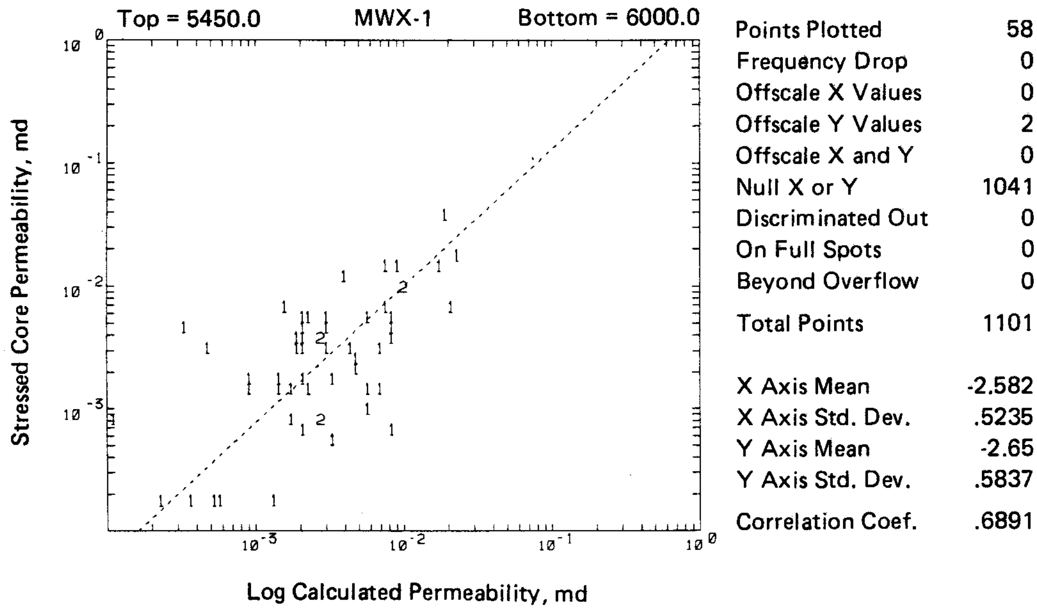

Figure 4.29 Log Calculated Net Stress Corrected Absolute Permeability Vs. Stressed Klinkenberg Core Permeability, MWX-1 Low Fluvial Interval

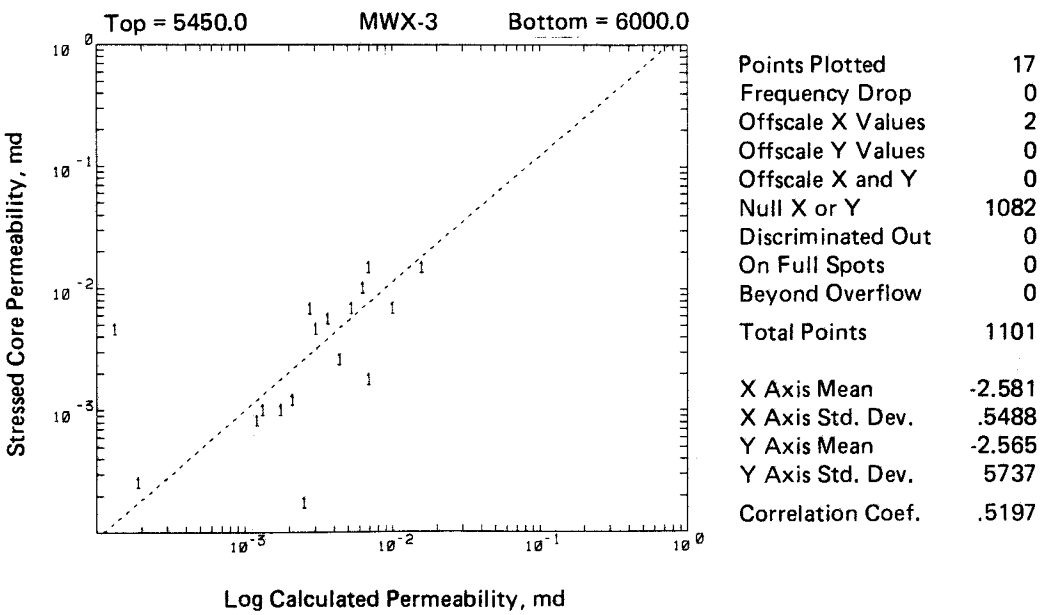

Figure 4.30 Log Calculated Net Stress Corrected Absolute Permeability Vs. Stressed Klinkenberg Core Permeability, MWX-3 Low Fluvial Interval

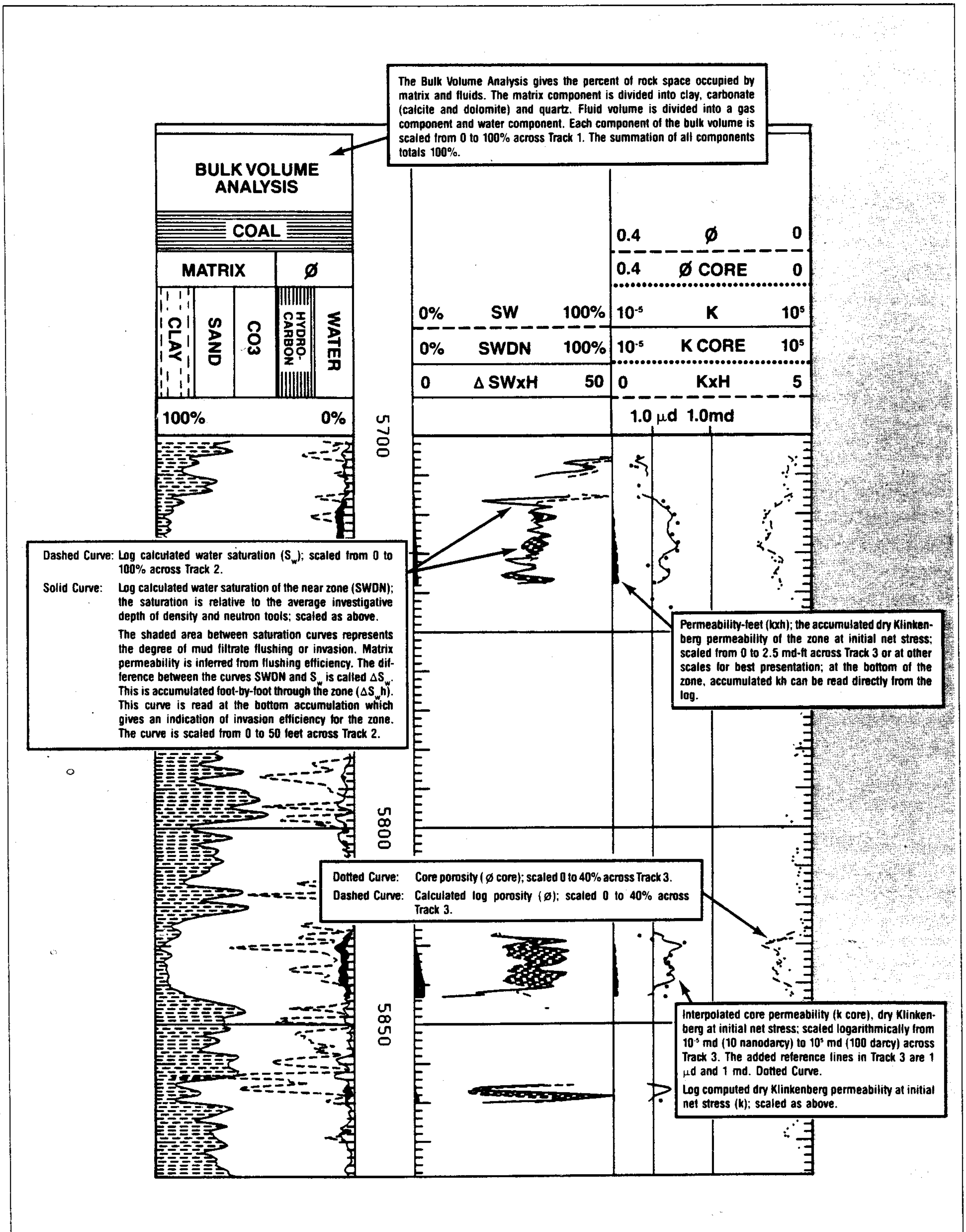

Figure 4.31 Format for TITEGAS Traceplot Output

CER COMPUTER PROCESSED ANALYSIS

CER TIGHT GAS SANDSTONE ANALYSIS

A COMPREHENSIVE MODEL FOR THE LOG INTERPRETATION OF LOW-PERMEABILITY GAS RESERVOIRS

CER Corp. Post Office Box 15090 Las Vegas, Nevada 89114 Phone (702) 735-7136

COMPANY CER Corporation

WELL MWX-1

FIELD Rulison

COUNTY Garfield STATE CO

DATE 3/26/86	LOCATION SW/NW	ELEVATION
		5374.0 KB
		— DF
ANALYST R.E. Hill	SEC. 34 TWP. 6S RGE. 94W	5355.0 GL

Figure 4.32 MWX-1 Low Fluvial Computer Processed Analysis

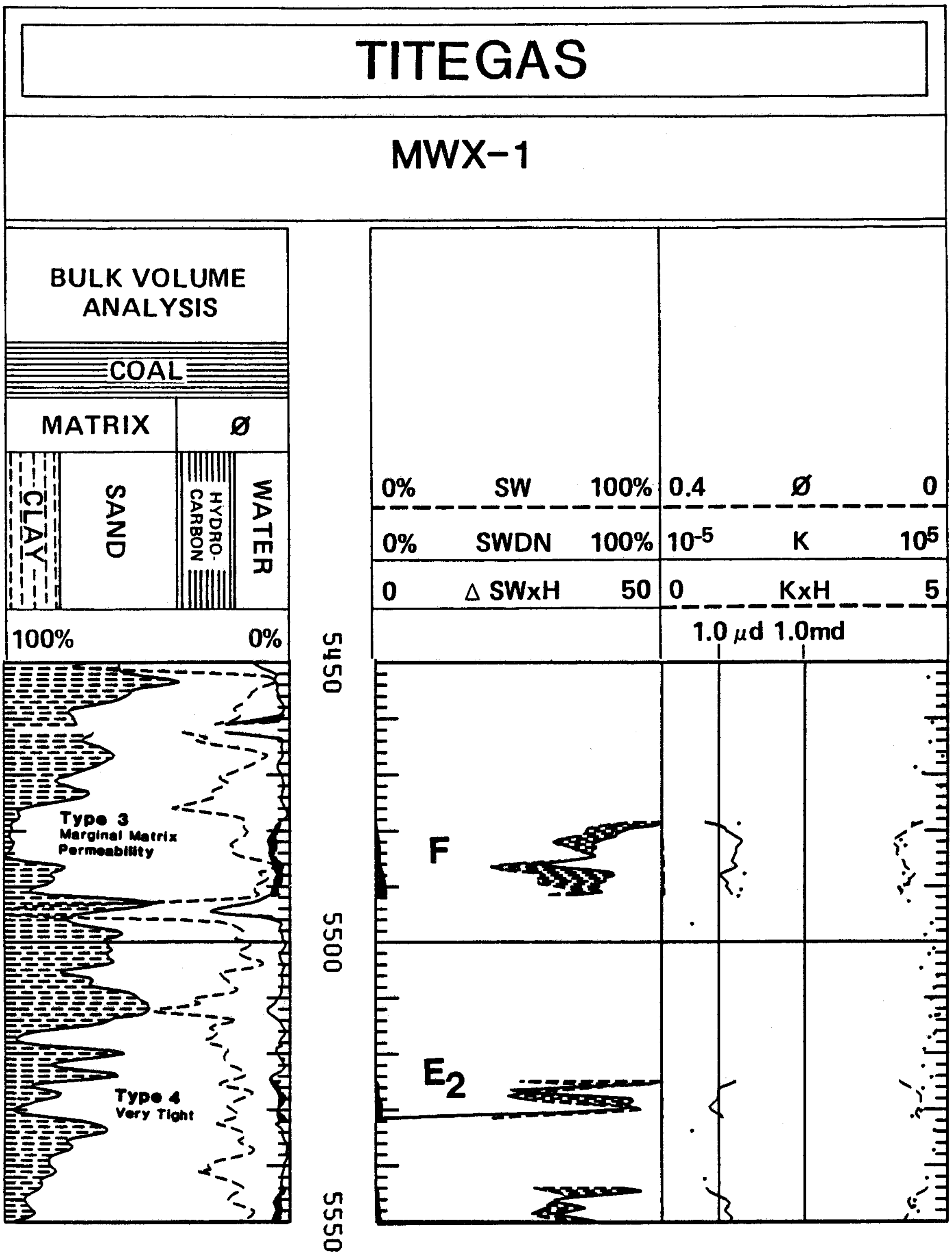

Figure 4.32, Continued

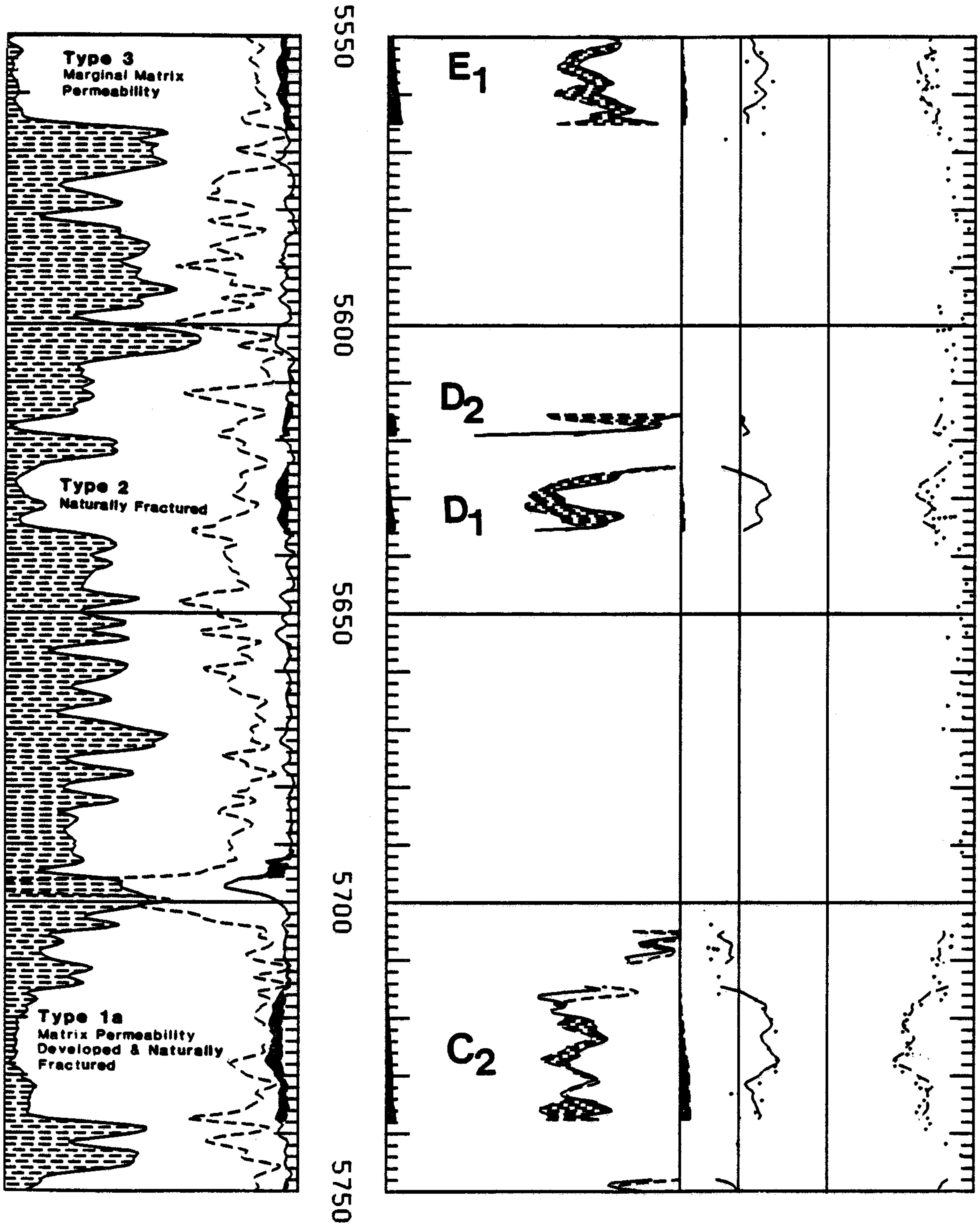

Figure 4.32, Continued

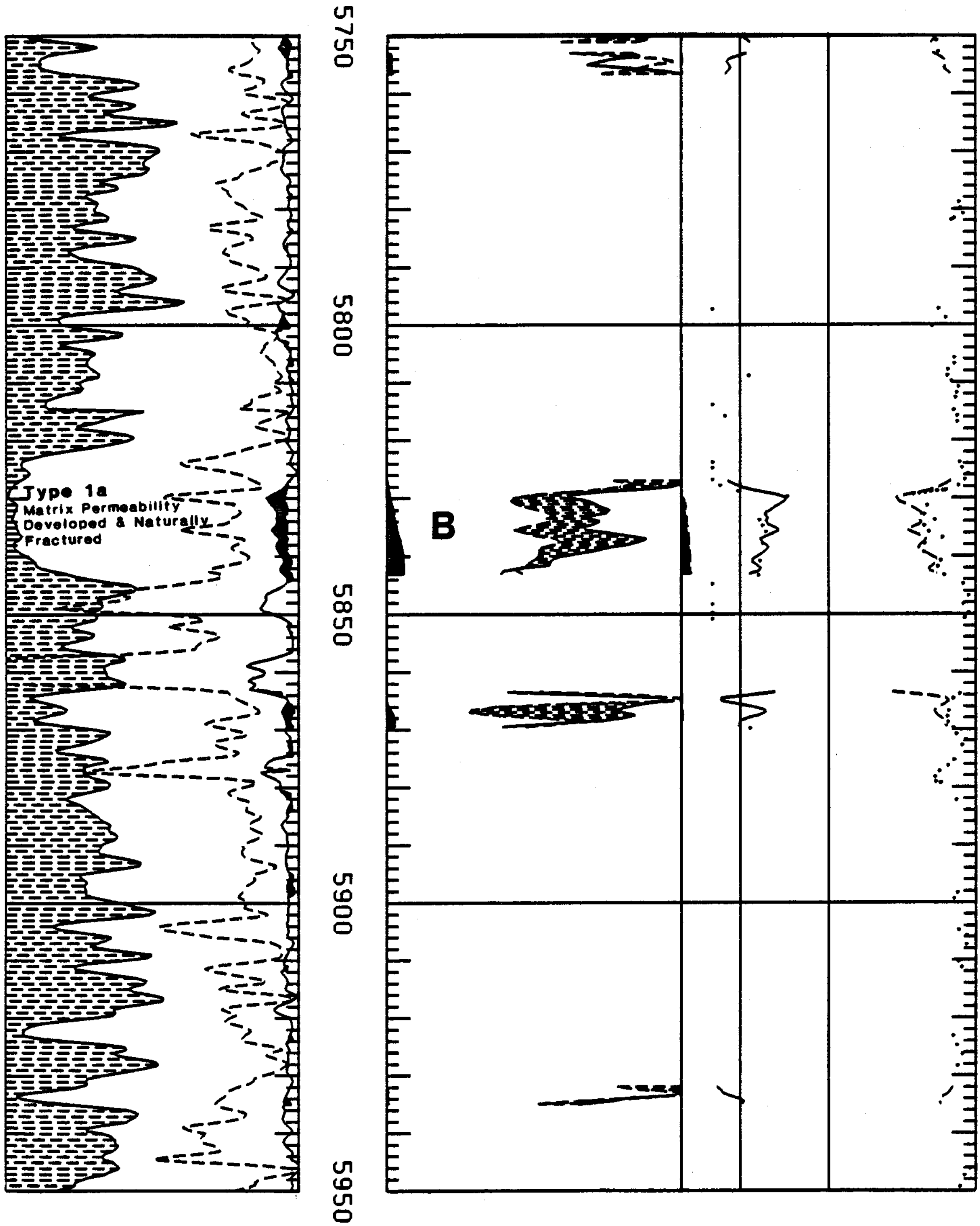

Figure 4.32, Continued

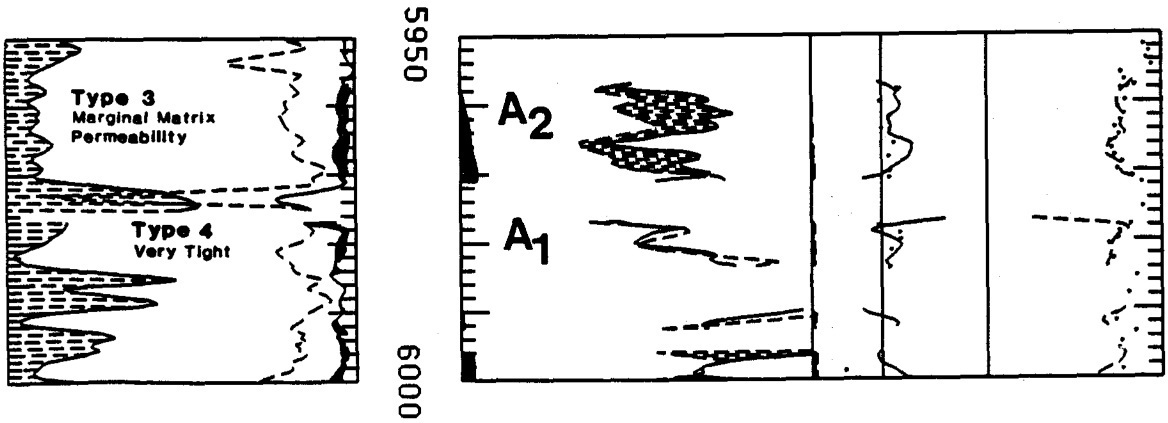

Figure 4.32, Continued

CER COMPUTER PROCESSED ANALYSIS

CER TIGHT GAS SANDSTONE ANALYSIS

A COMPREHENSIVE MODEL FOR THE LOG INTERPRETATION OF LOW-PERMEABILITY GAS RESERVOIRS

CER Corp. Post Office Box 15090 Las Vegas, Nevada 89114 Phone (702) 735-7136

COMPANY CER Corporation

WELL MWX-2

FIELD Rulison

COUNTY Garfield STATE CO

DATE 3/26/86

ANALYST R.E. Hill

LOCATION SW/NW

SEC. 34 TWP. 6S RGE. 94W

ELEVATION

5374.0 KB

5372.5 DF

5355.0 GL

Figure 4.33 MWX-2 Low Fluvial Computer Processed Analysis

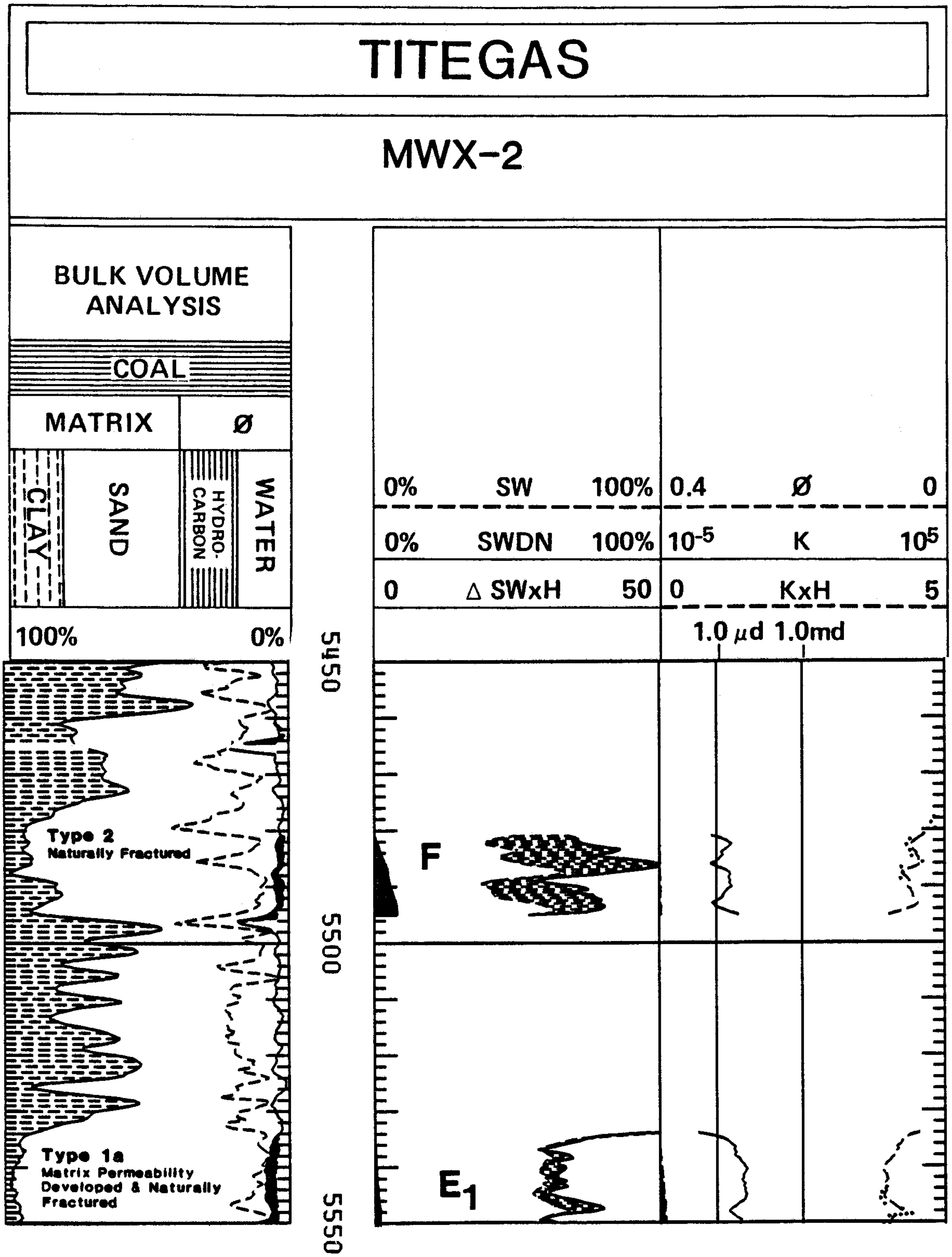

Figure 4.33, Continued

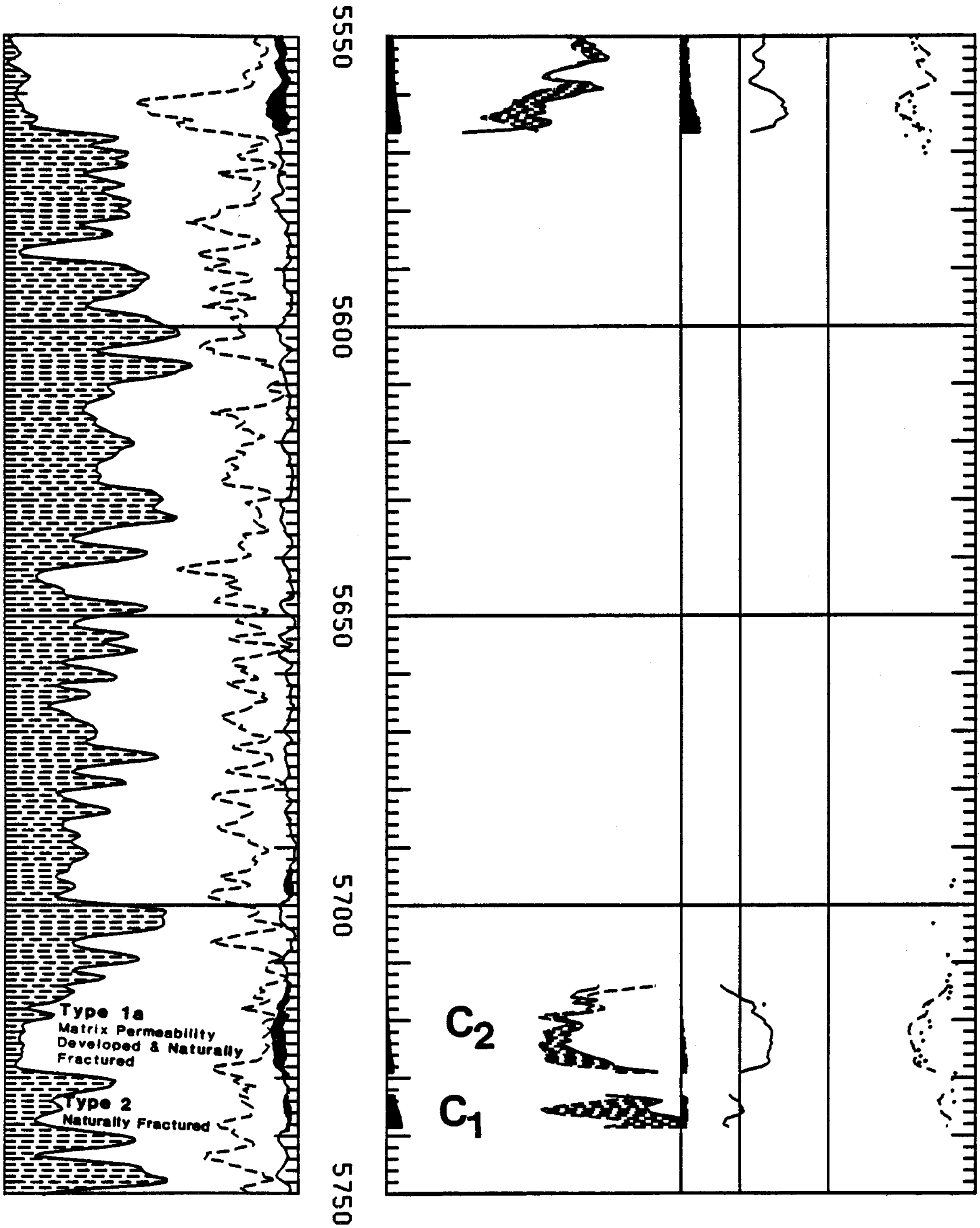

Figure 4.33, Continued

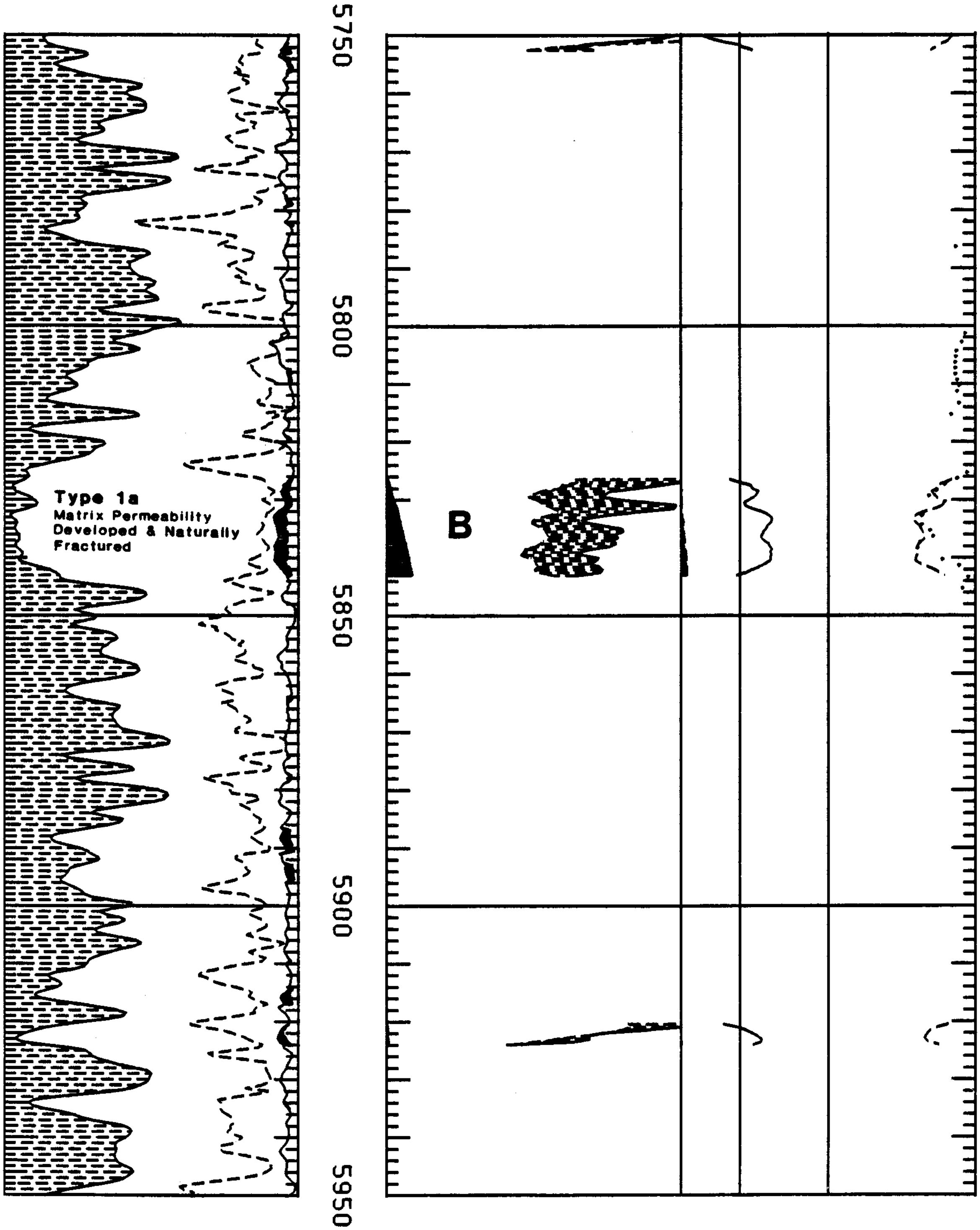

Figure 4.33, Continued

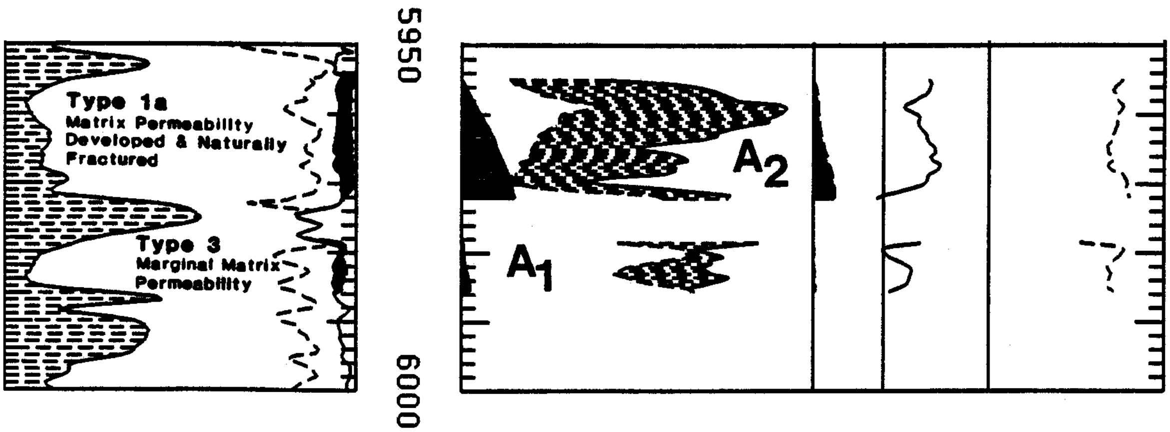

Figure 4.33, Continued

CER COMPUTER PROCESSED ANALYSIS

CER TIGHT GAS SANDSTONE ANALYSIS

A COMPREHENSIVE MODEL FOR THE LOG INTERPRETATION
OF LOW-PERMEABILITY GAS RESERVOIRS

CER Corp. Post Office Box 15090 Las Vegas, Nevada 89114 Phone (702) 735-7136

COMPANY CER Corporation

WELL MWX-3

FIELD Rulison

COUNTY Garfield STATE CO

DATE 3/26/86

ANALYST R.E. Hill

LOCATION SW/NW

SEC. 34 TWP. 6S RGE. 94W

ELEVATION
5379.0 KB
5378.0 DF
5359.5 GL

Figure 4.34 MWX-3 Low Fluvial Computer Processed Analysis

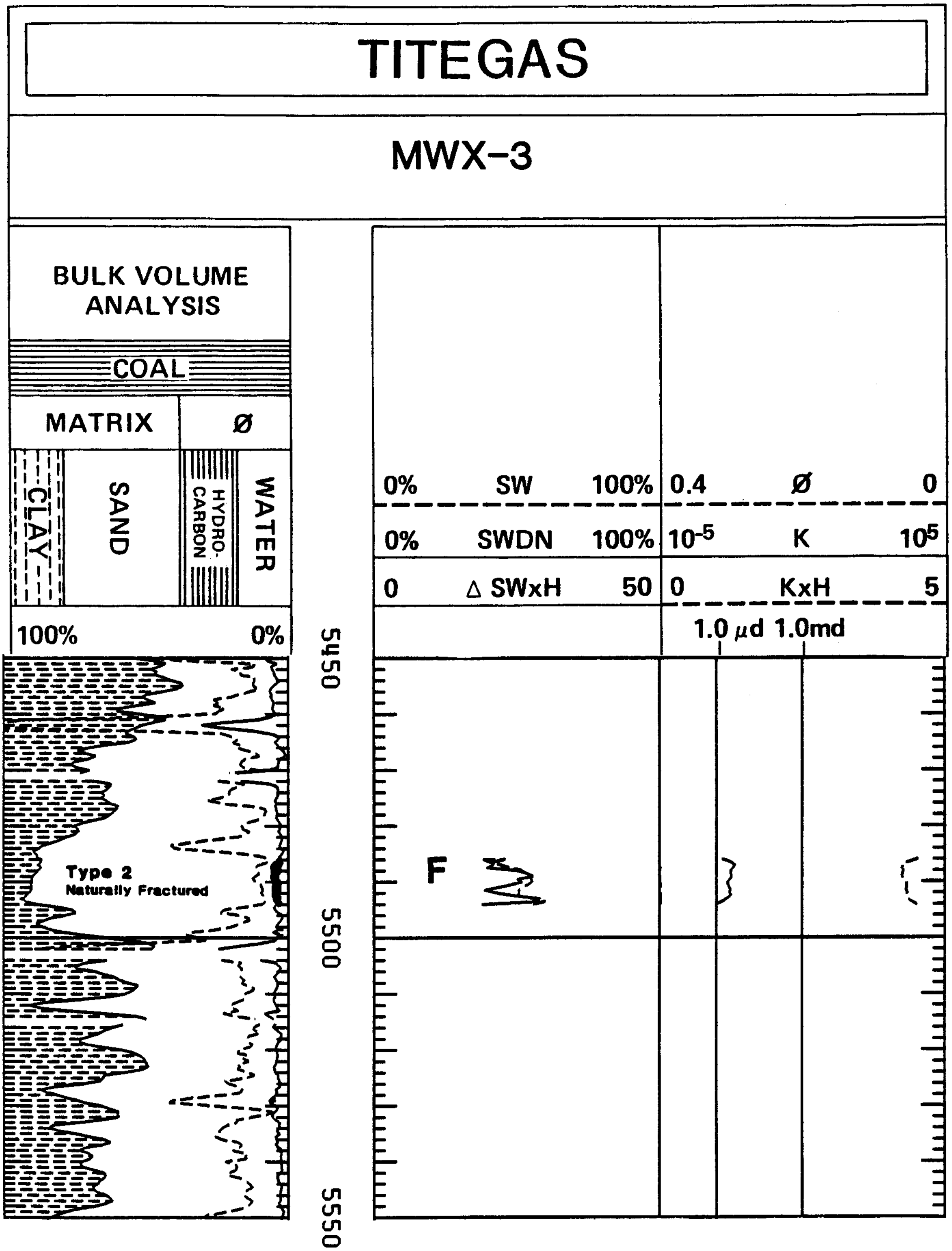

Figure 4.34, Continued

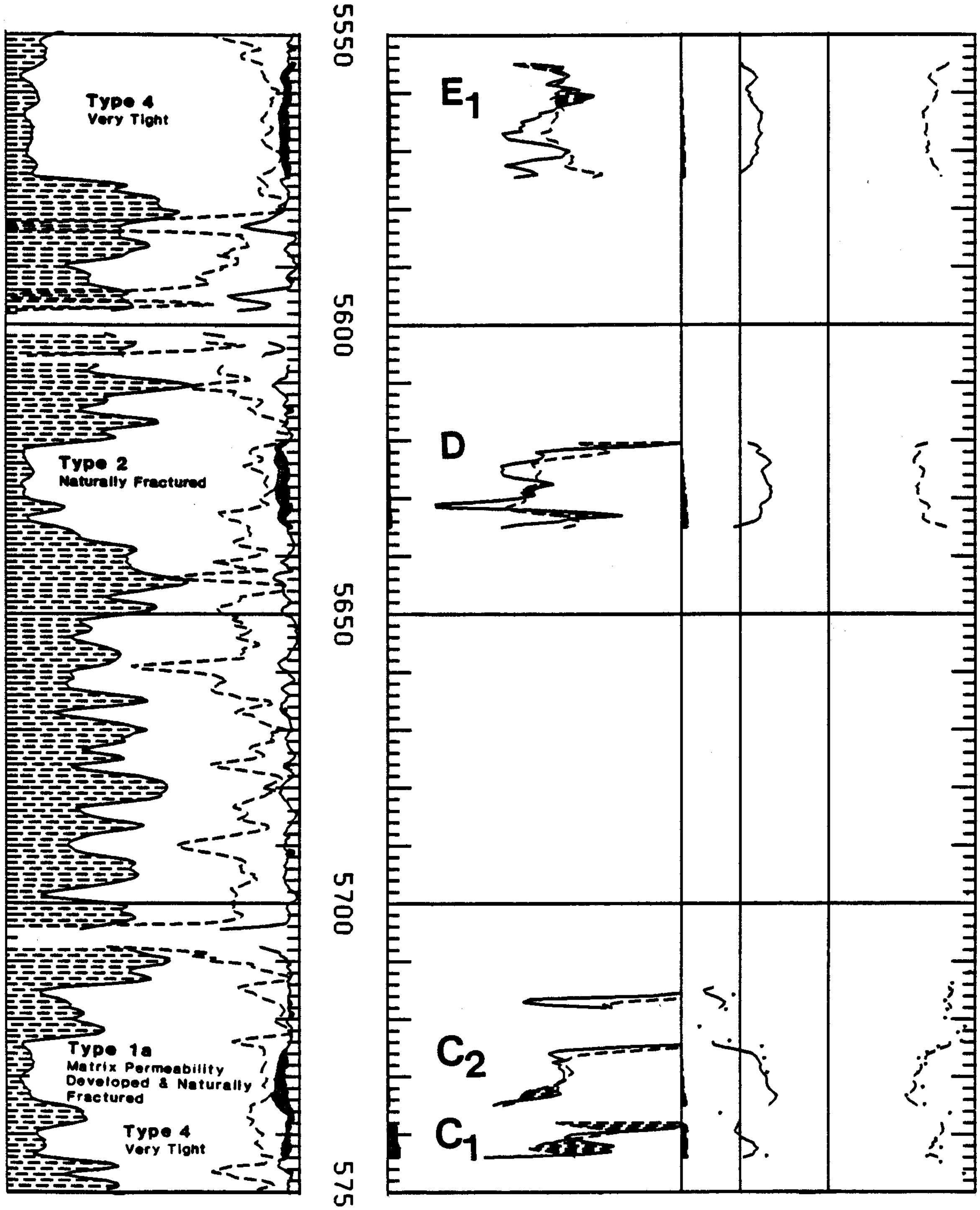

Figure 4.34, Continued

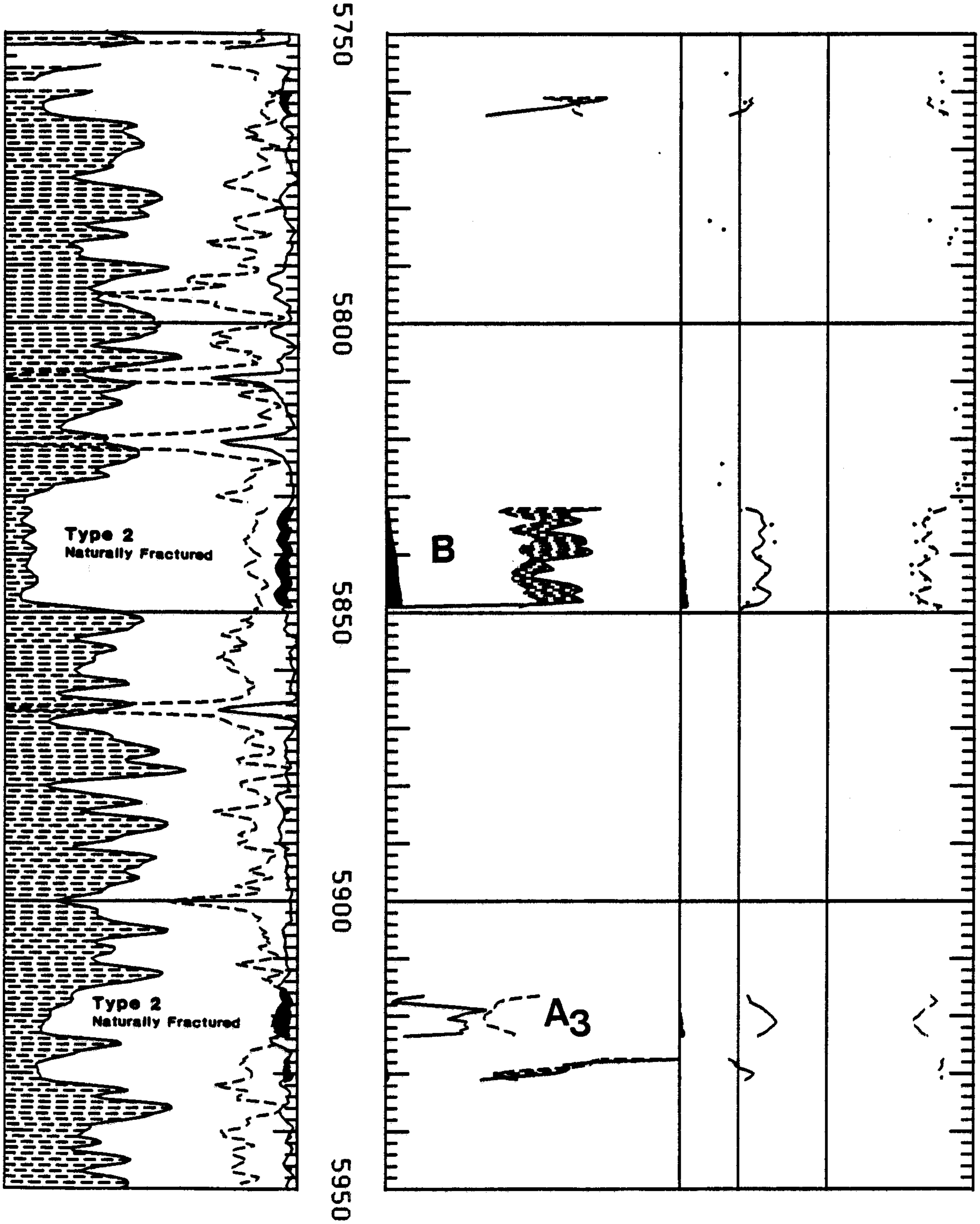

Figure 4.34, Continued

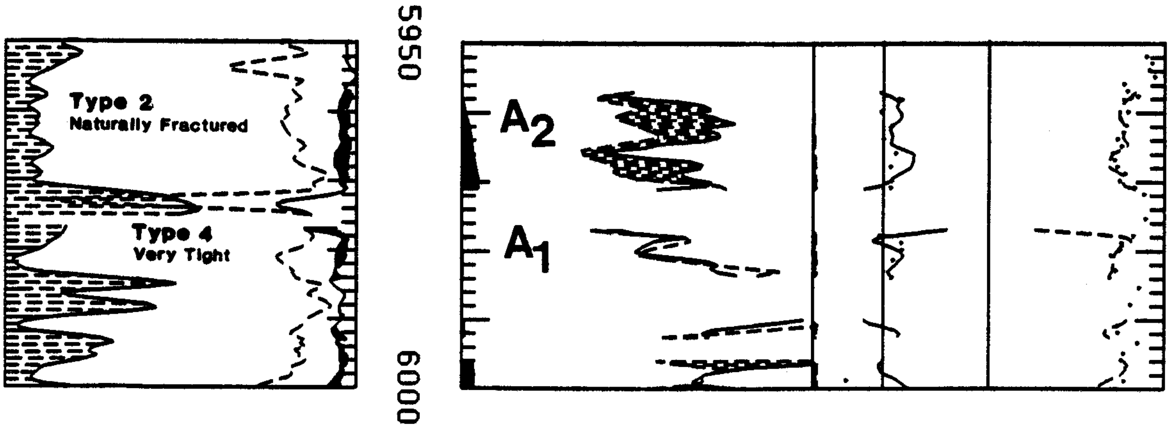

Figure 4.34, Continued

CER COMPUTER PROCESSED ANALYSIS

CER TIGHT GAS SANDSTONE ANALYSIS

A COMPREHENSIVE MODEL FOR THE LOG INTERPRETATION OF LOW-PERMEABILITY GAS RESERVOIRS

CER Corp. Post Office Box 15090 Las Vegas, Nevada 89114 Phone (702) 735-7136

COMPANY CER Corporation

WELL MWX-1

FIELD Rulison

COUNTY Garfield STATE CO

DATE 3/31/86

ANALYST K.E. Simons

LOCATION SW/NW

SEC. 34 TWP. 6S RGE. 94W

ELEVATION
5374.0 KB
– DF
5355.0 GL

Figure 4.35 MWX-1 Middle Fluvial Computer Processed Analysis

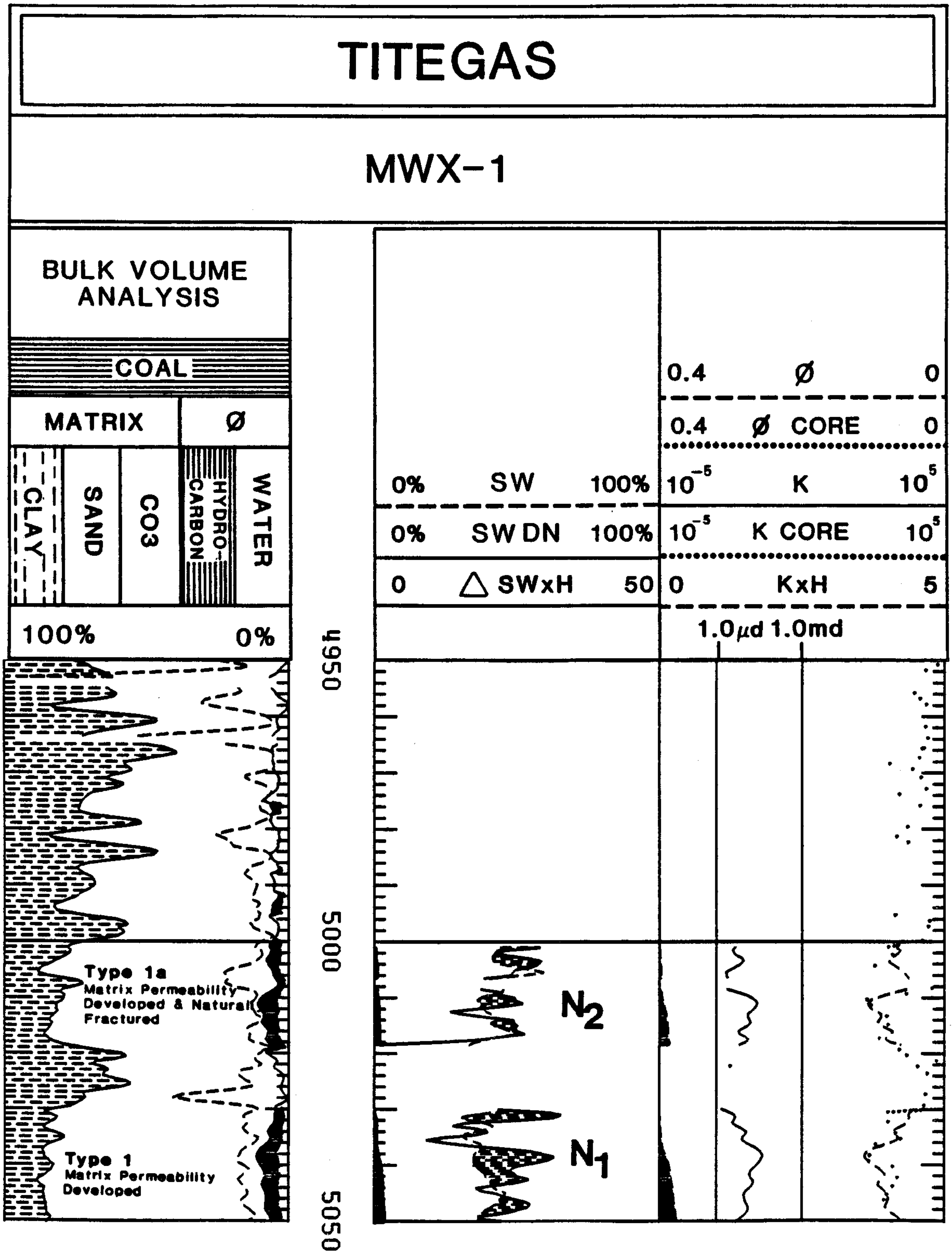

Figure 4.35, Continued

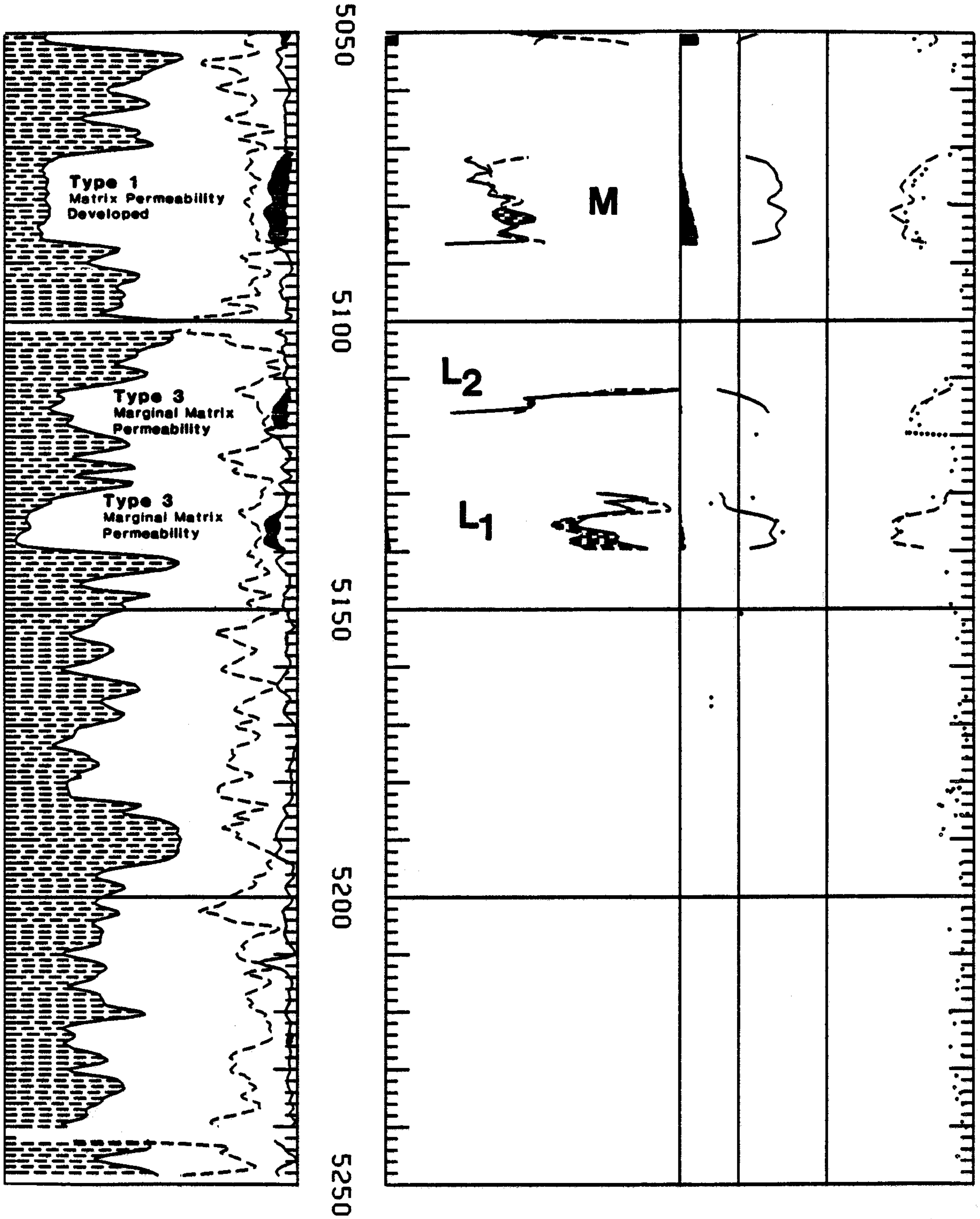

Figure 4.35, Continued

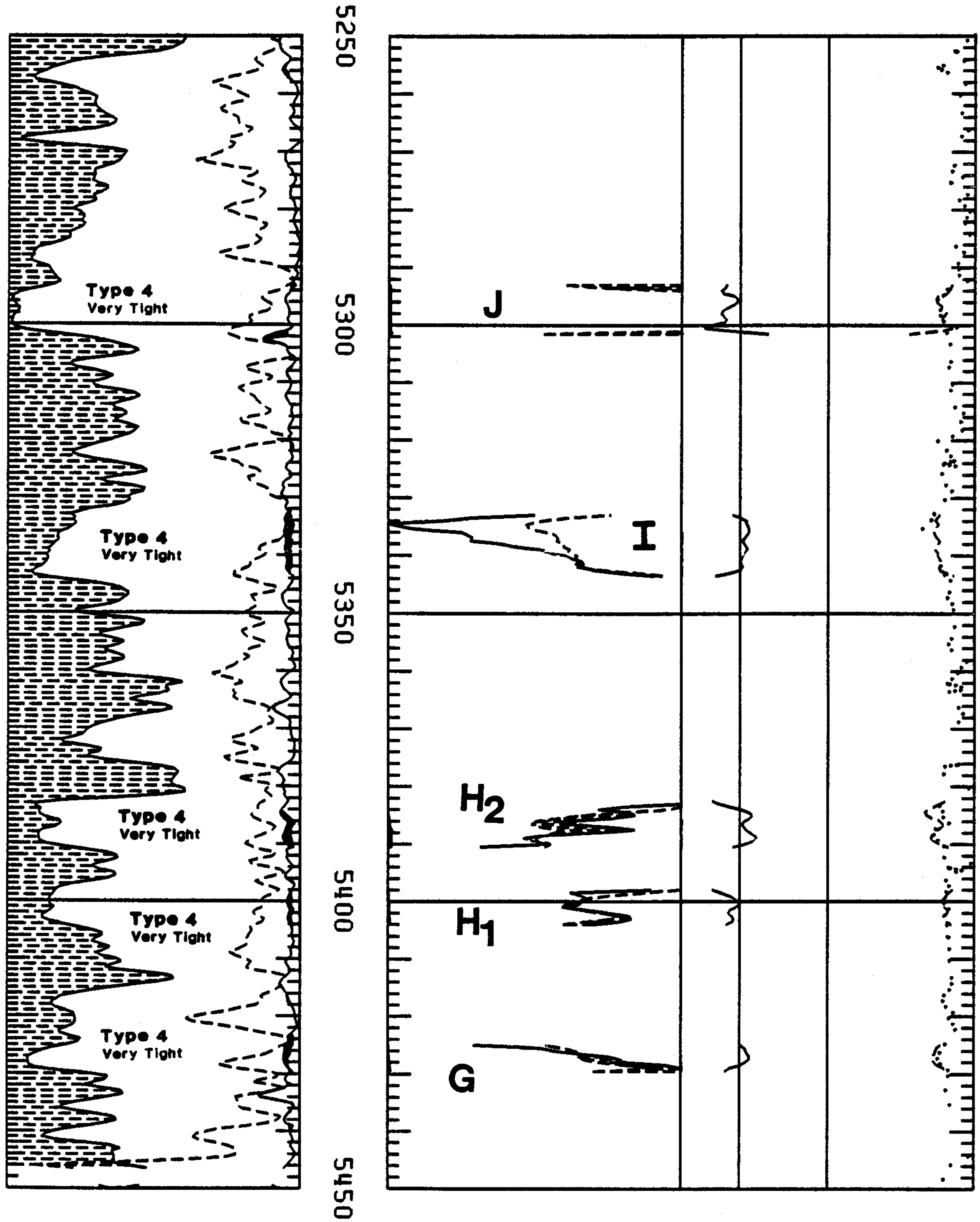

Figure 4.35, Continued

CER COMPUTER PROCESSED ANALYSIS

CER TIGHT GAS SANDSTONE ANALYSIS

A COMPREHENSIVE MODEL FOR THE LOG INTERPRETATION OF LOW-PERMEABILITY GAS RESERVOIRS

CER Corp. Post Office Box 15090 Las Vegas, Nevada 89114 Phone (702) 735-7136

COMPANY CER Corporation

WELL MWX-2

FIELD Rulison

COUNTY Garfield STATE CO

DATE 3/31/86

ANALYST K.E. Simons

LOCATION SW/NW

SEC. 34 TWP. 6S RGE. 94W

ELEVATION

5374.0 KB

5372.5 DF

5355.0 GL

Figure 4.36 MWX-2 Middle Fluvial Computer Processed Analysis

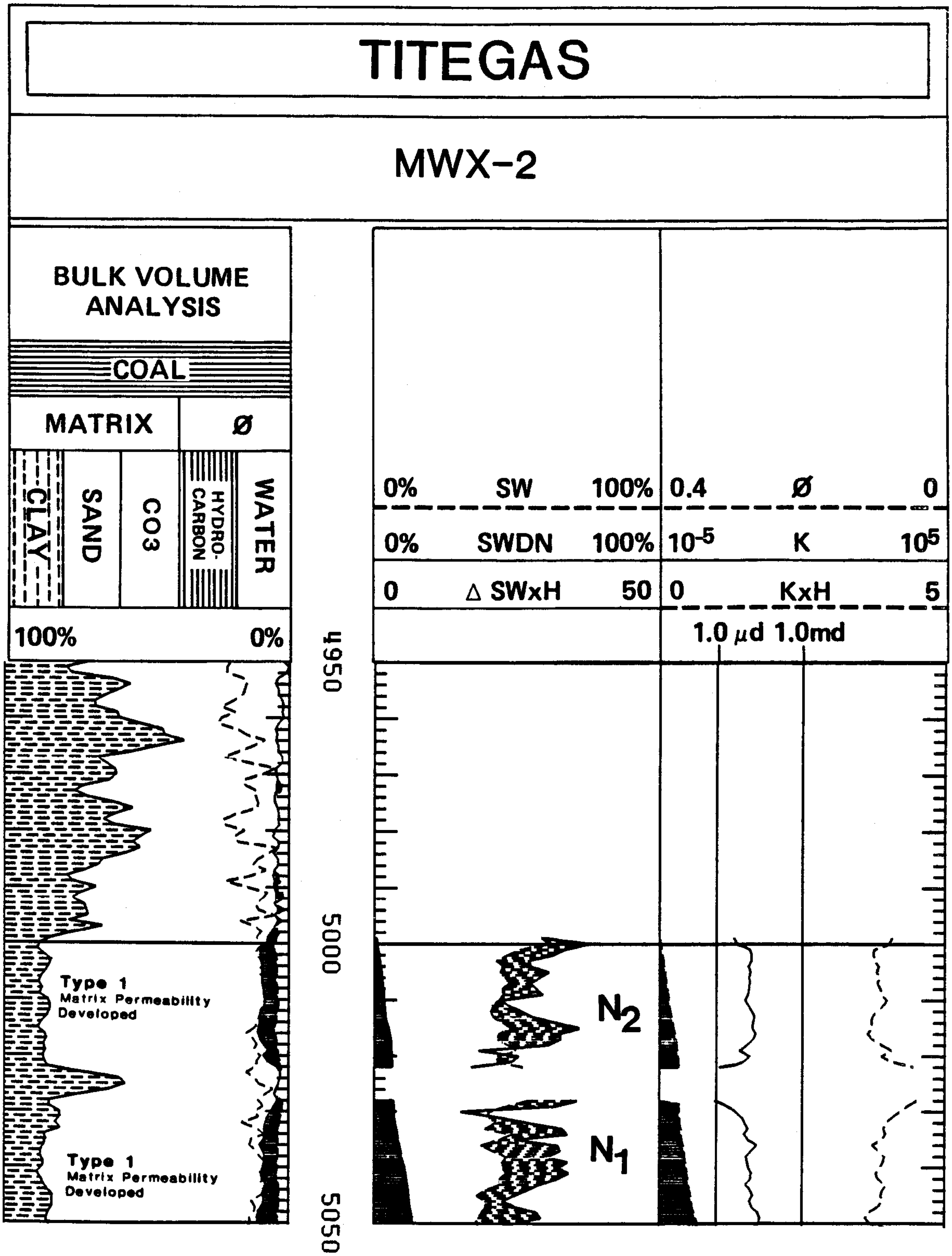

Figure 4.36, Continued

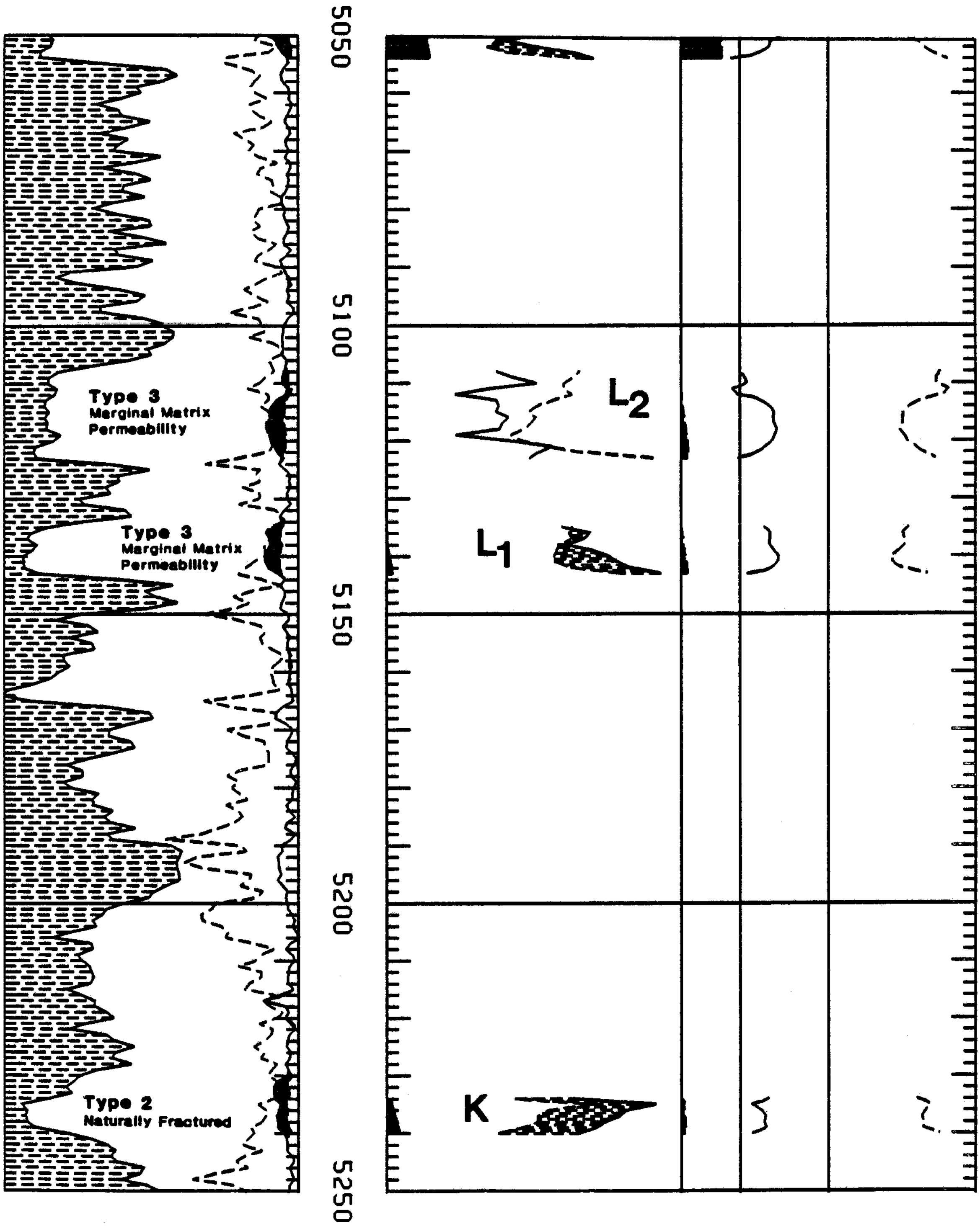

Figure 4.36, Continued

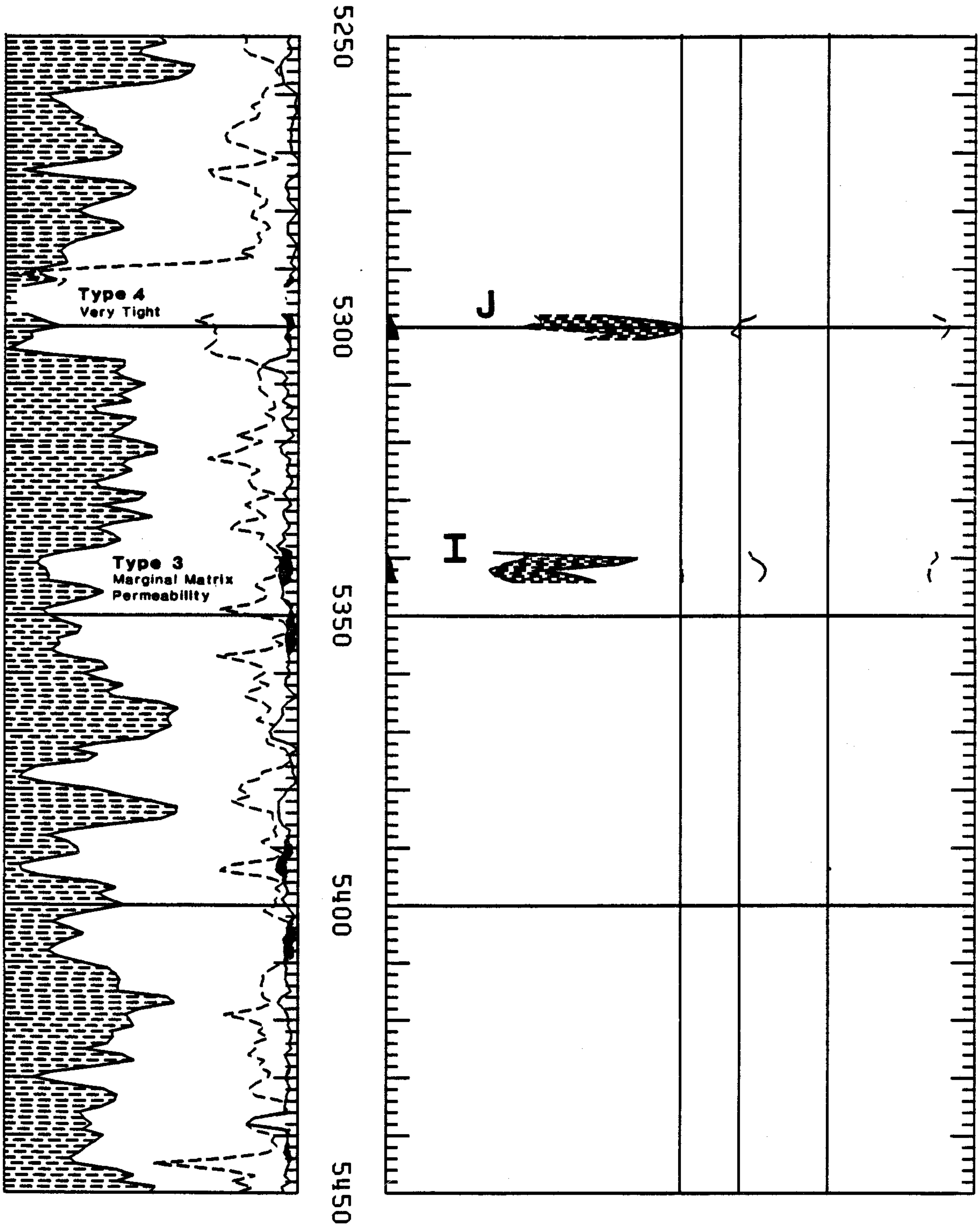

Figure 4.36, Continued

CER

COMPUTER PROCESSED ANALYSIS

CER TIGHT GAS SANDSTONE ANALYSIS

A COMPREHENSIVE MODEL FOR THE LOG INTERPRETATION OF LOW-PERMEABILITY GAS RESERVOIRS

CER Corp. Post Office Box 15090 Las Vegas, Nevada 89114 Phone (702) 735-7136

COMPANY CER Corporation

WELL MWX-3

FIELD Rulison

COUNTY Garfield STATE CO

DATE 3/31/86	LOCATION SW/NW	ELEVATION 5379.0 KB 5378.0 DF
ANALYST K.E. Simons	SEC. 34 TWP. 6S RGE. 94W	5359.5 GL

Figure 4.37 MWX-3 Middle Fluvial Computer Processed Analysis

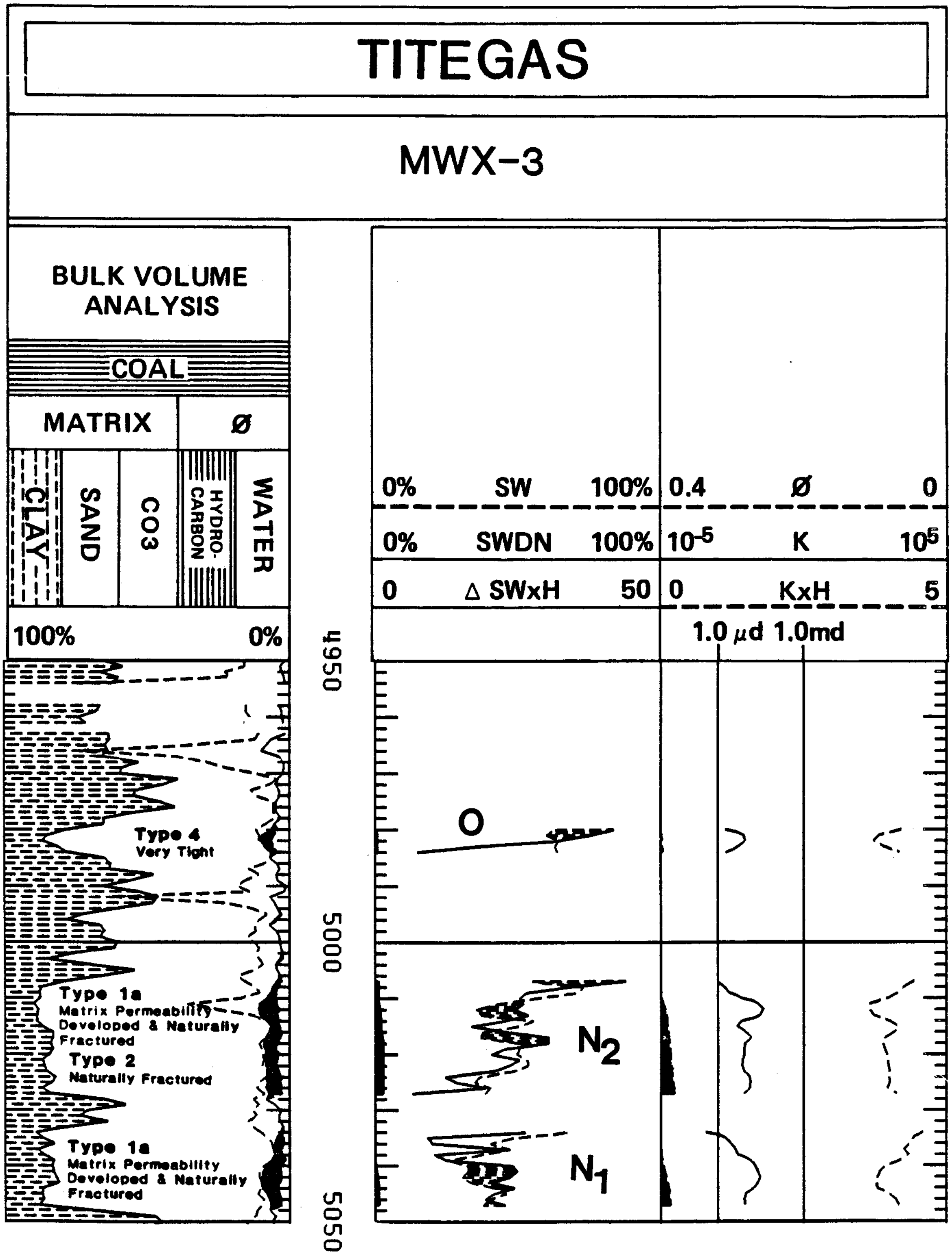

Figure 4.37, Continued

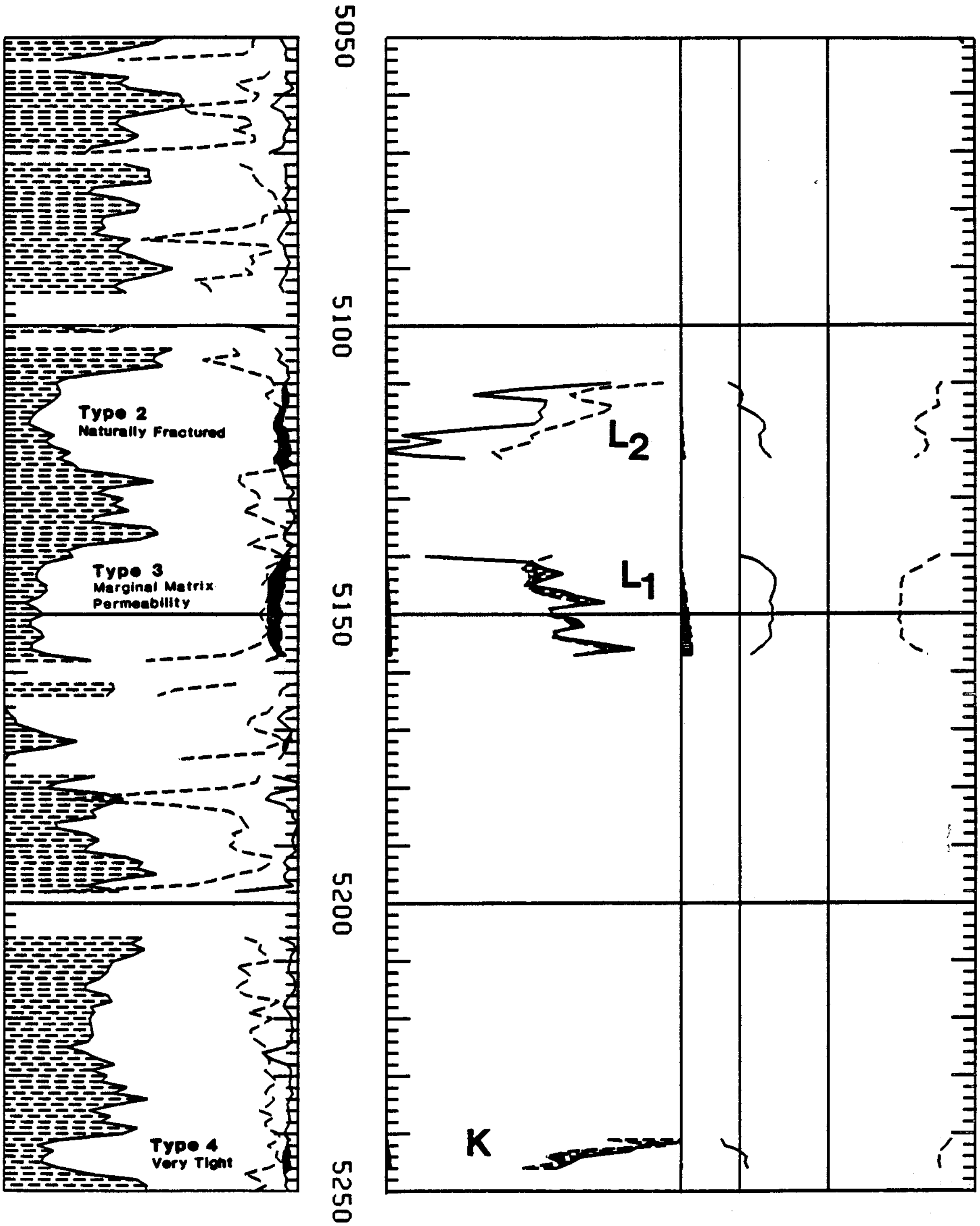

Figure 4.37, Continued

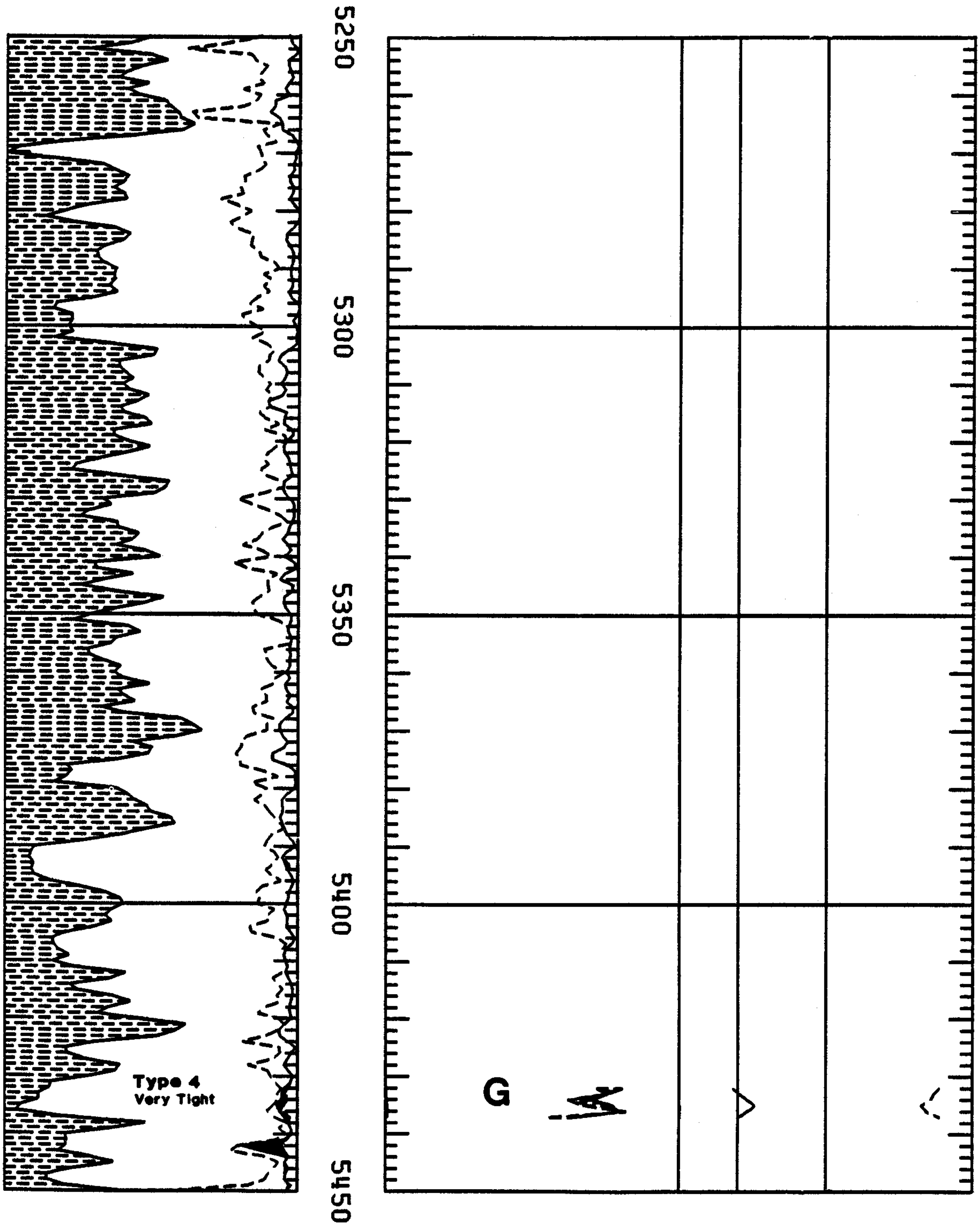

Figure 4.37, Continued

CER COMPUTER PROCESSED ANALYSIS

CER TIGHT GAS SANDSTONE ANALYSIS

A COMPREHENSIVE MODEL FOR THE LOG INTERPRETATION OF LOW-PERMEABILITY GAS RESERVOIRS

CER Corp. Post Office Box 15090 Las Vegas, Nevada 89114 Phone (702) 735-7136

COMPANY CER Corporation

WELL MWX-3

FIELD Rulison

COUNTY Garfield STATE CO

DATE 1/22/86	LOCATION SW/NW	ELEVATION 5379.0 KB 5378.0 DF
ANALYST E.R. Monson	SEC. 34 TWP. 6S RGE. 94W	5359.5 GL

Figure 4.38 MWX-3 Low Fluvial Interpretation of Fracture Logs

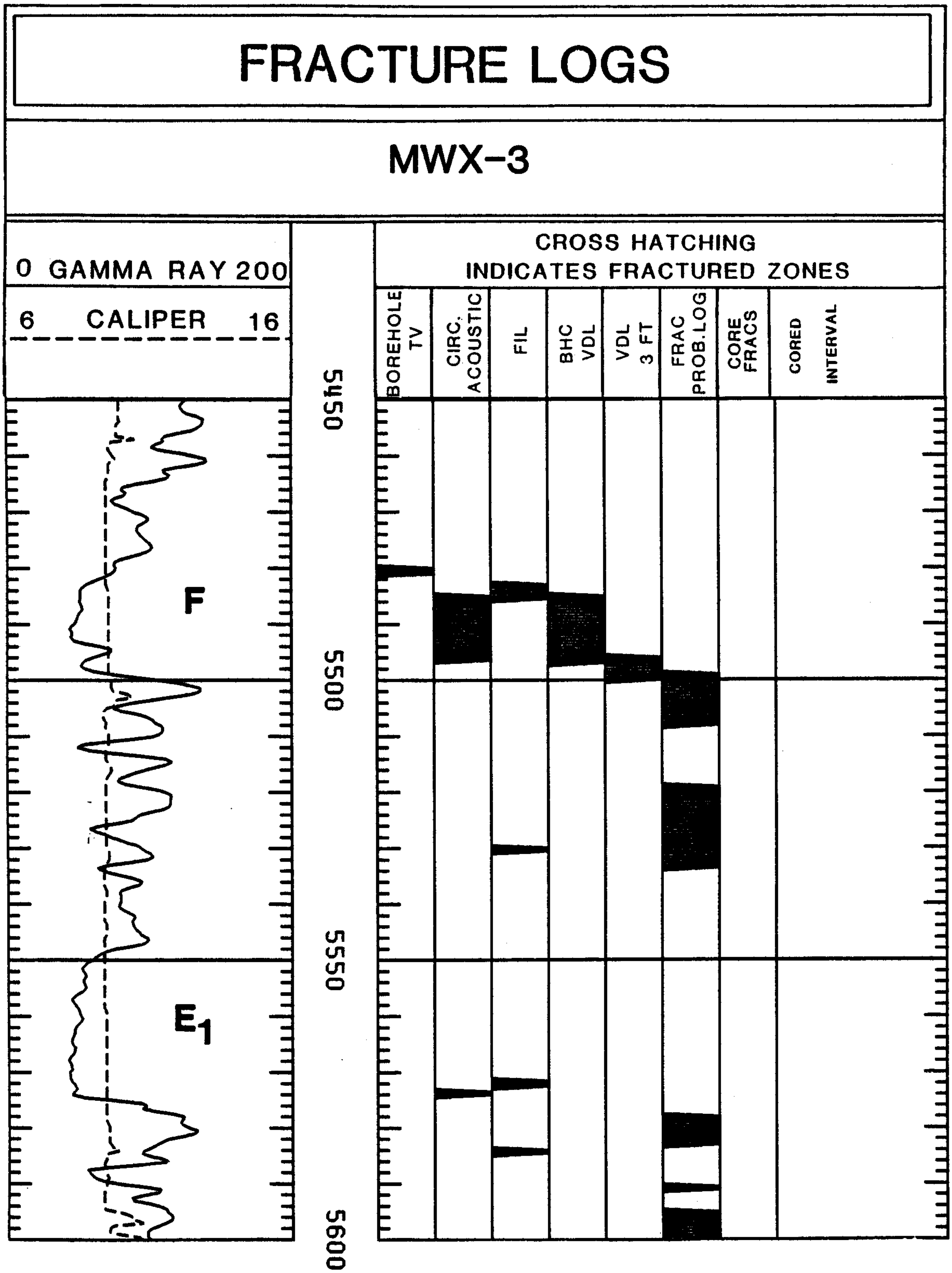

Figure 4.38, Continued

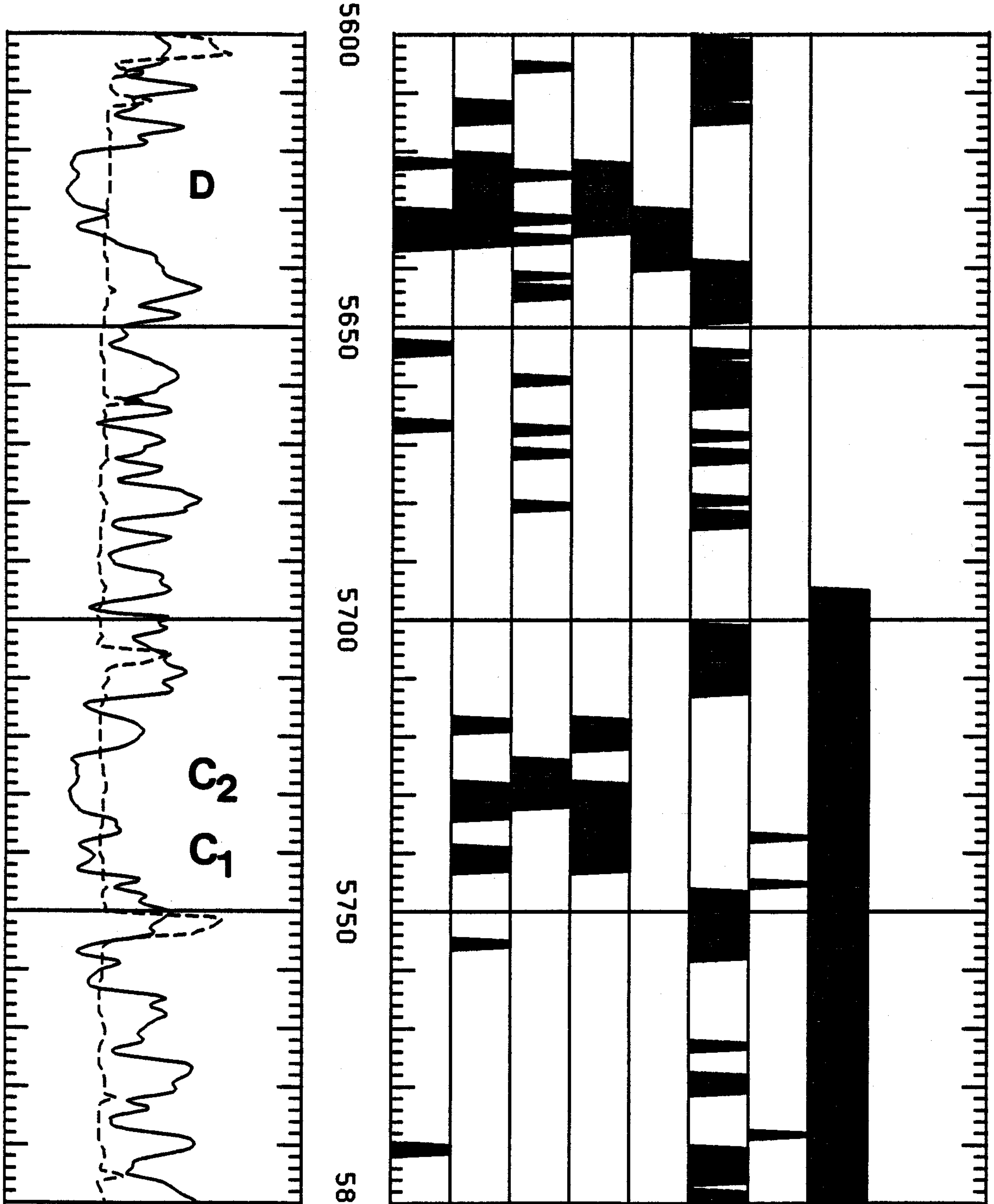

Figure 4.38, Continued

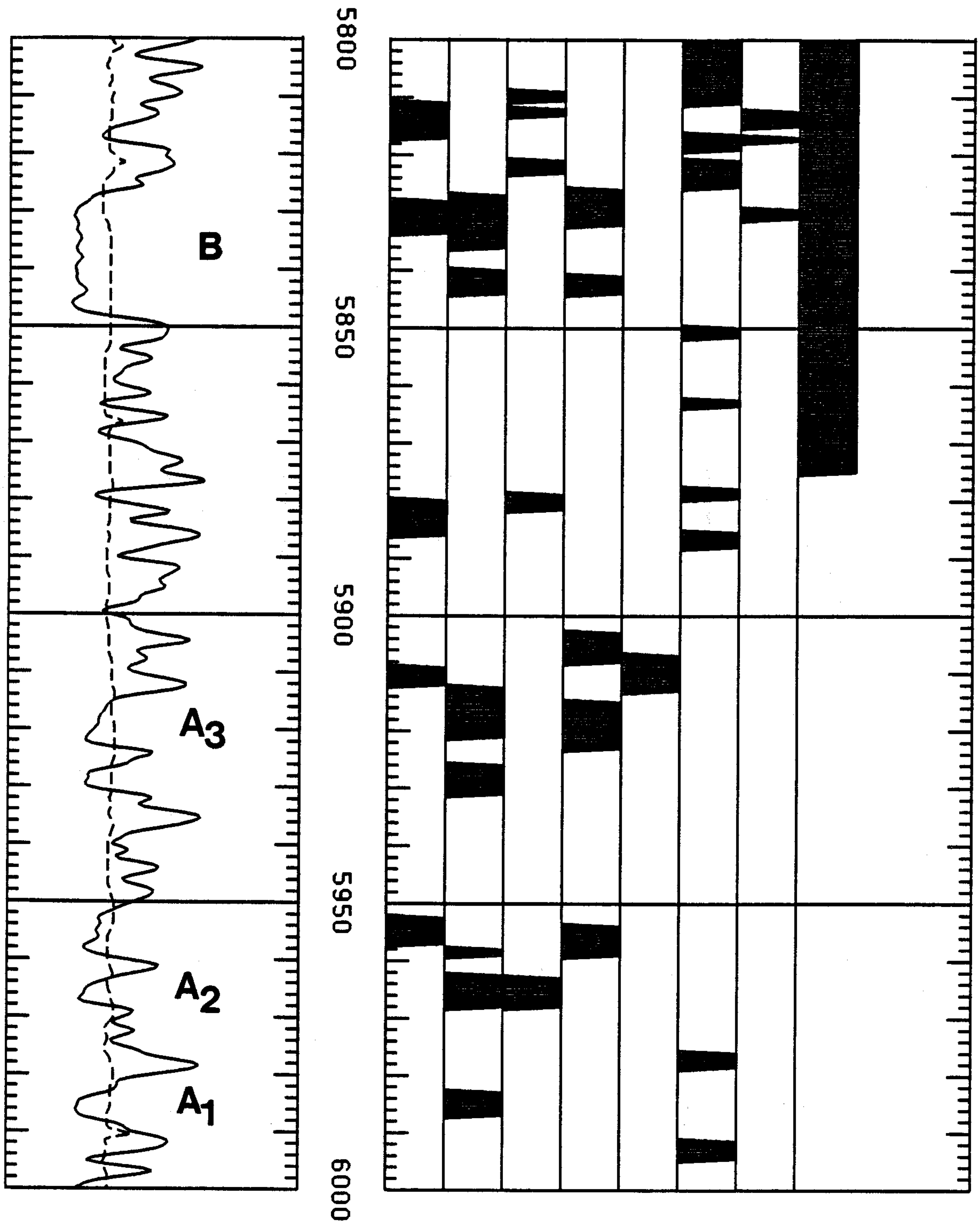

Figure 4.38, Continued

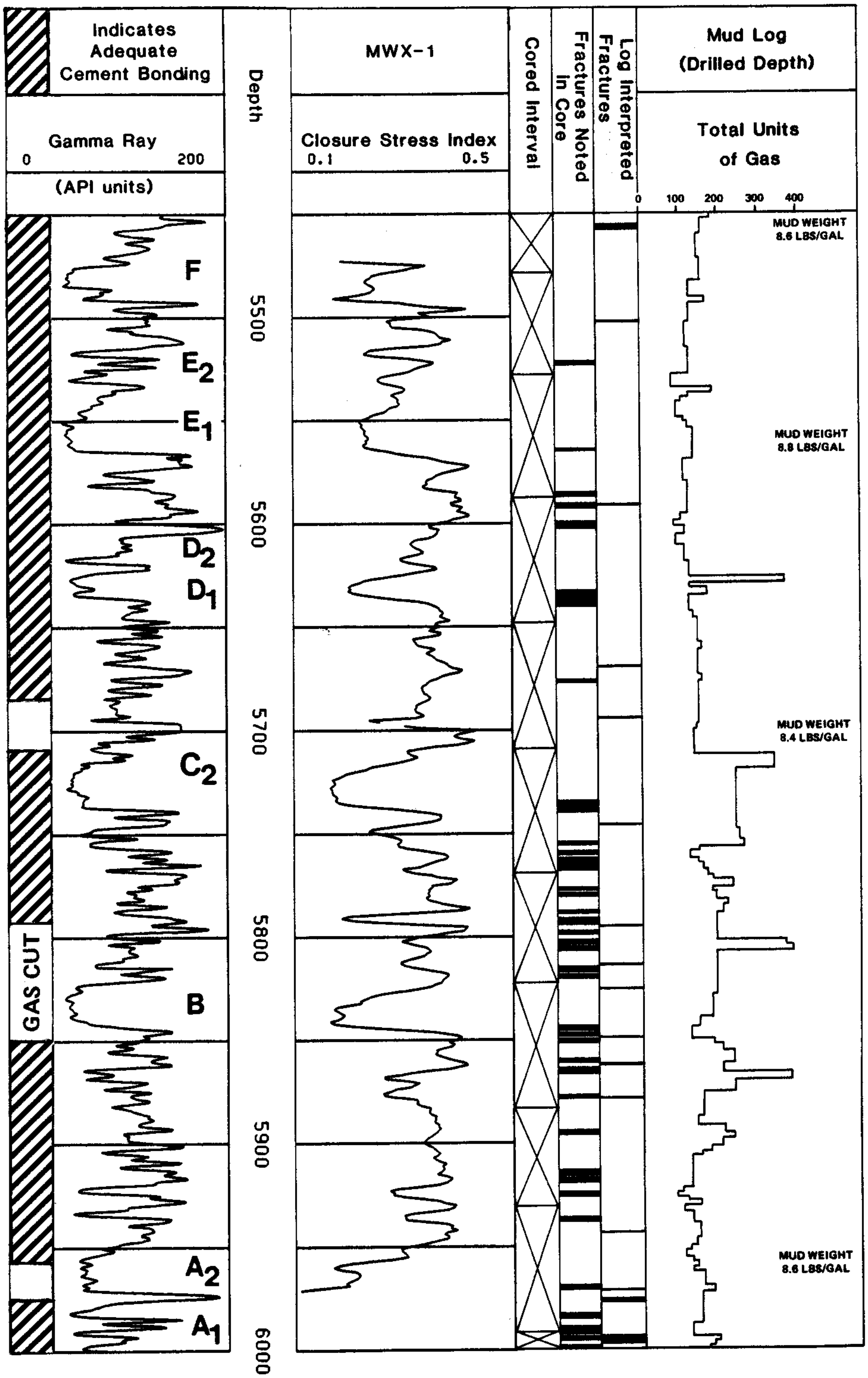

Figure 4.39 Composite Mud Log Including Natural Fracture Data, MWX-1 Low Fluvial Interval

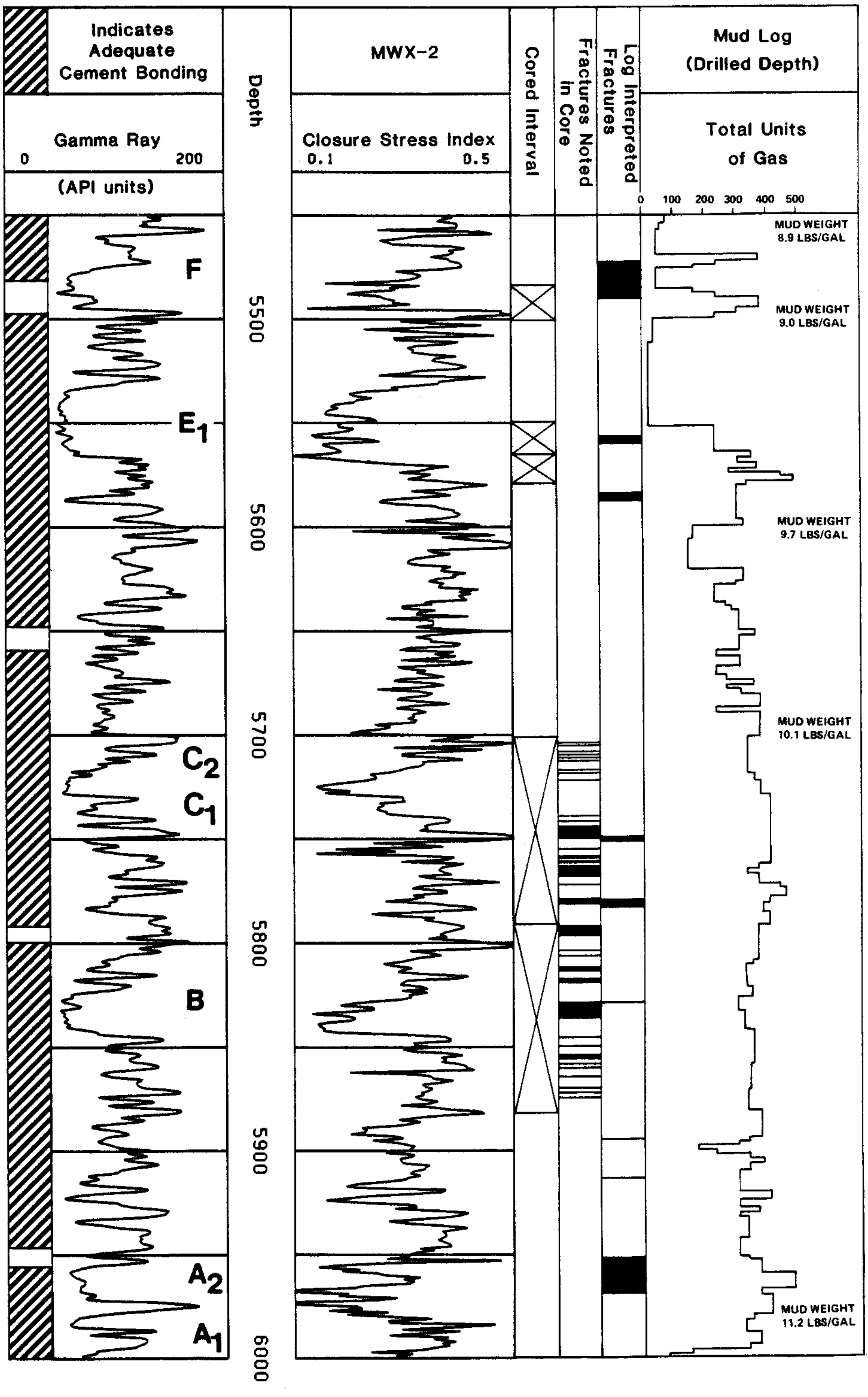

Figure 4.40 Composite Mud Log Including Natural Fracture Data, MWX-2 Low Fluvial Interval

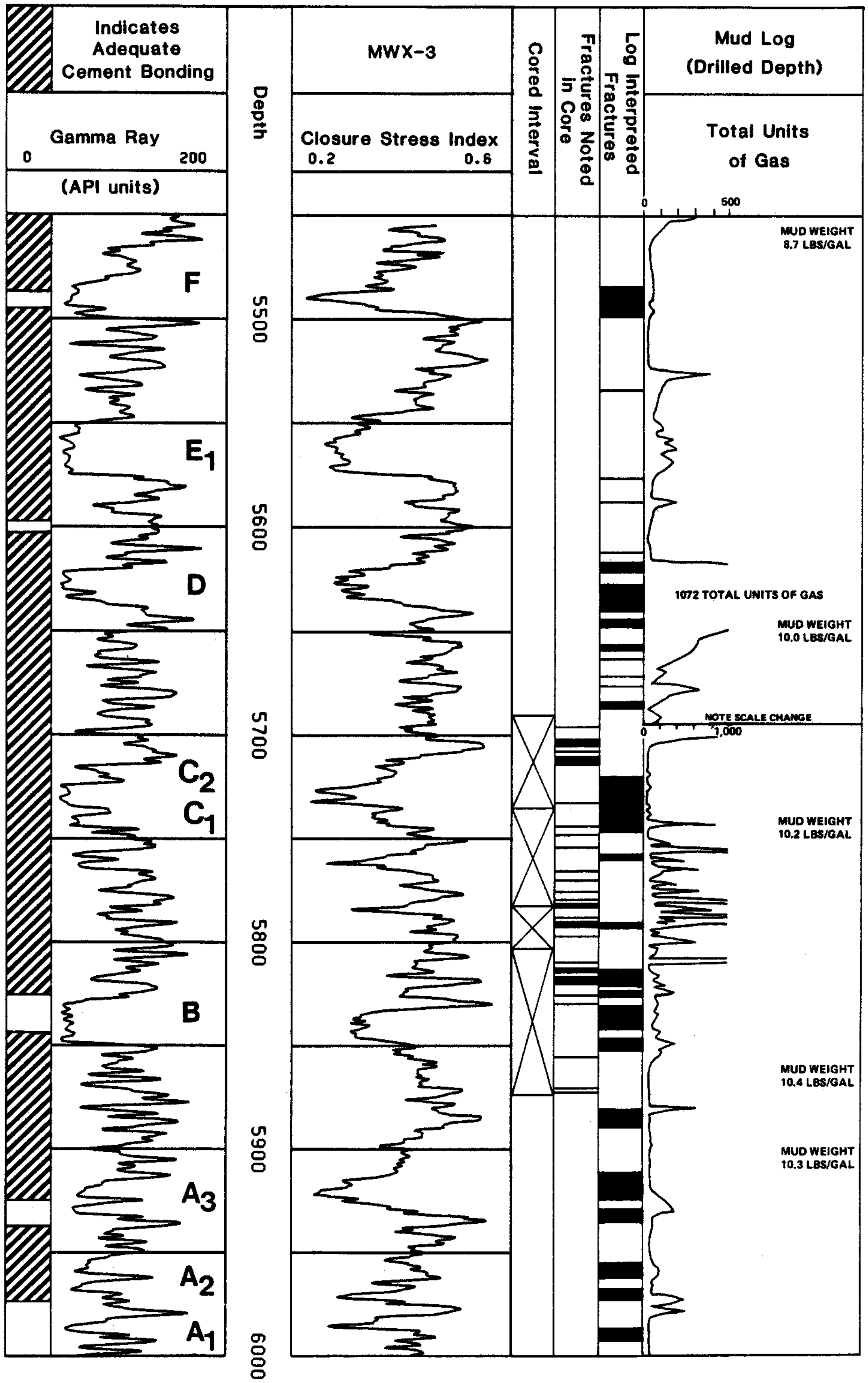

Figure 4.41 Composite Mud Log Including Natural Fracture Data, MWX-3 Low Fluvial Interval

CER COMPUTER PROCESSED ANALYSIS

CER TIGHT GAS SANDSTONE ANALYSIS

A COMPREHENSIVE MODEL FOR THE LOG INTERPRETATION
OF LOW-PERMEABILITY GAS RESERVOIRS

CER Corp. Post Office Box 15090 Las Vegas, Nevada 89114 Phone (702) 735-7136

COMPANY CER Corporation

WELL MWX-3

FIELD Rulison

COUNTY Garfield STATE CO

DATE 1/22/86	LOCATION SW/NW	ELEVATION 5379.0 KB 5378.0 DF
ANALYST R.E. Hill	SEC. 34 TWP. 6S RGE. 94W	5359.5 GL

Figure 4.42 MWX-3 Low Fluvial Interval NATUFRAC Computed Log

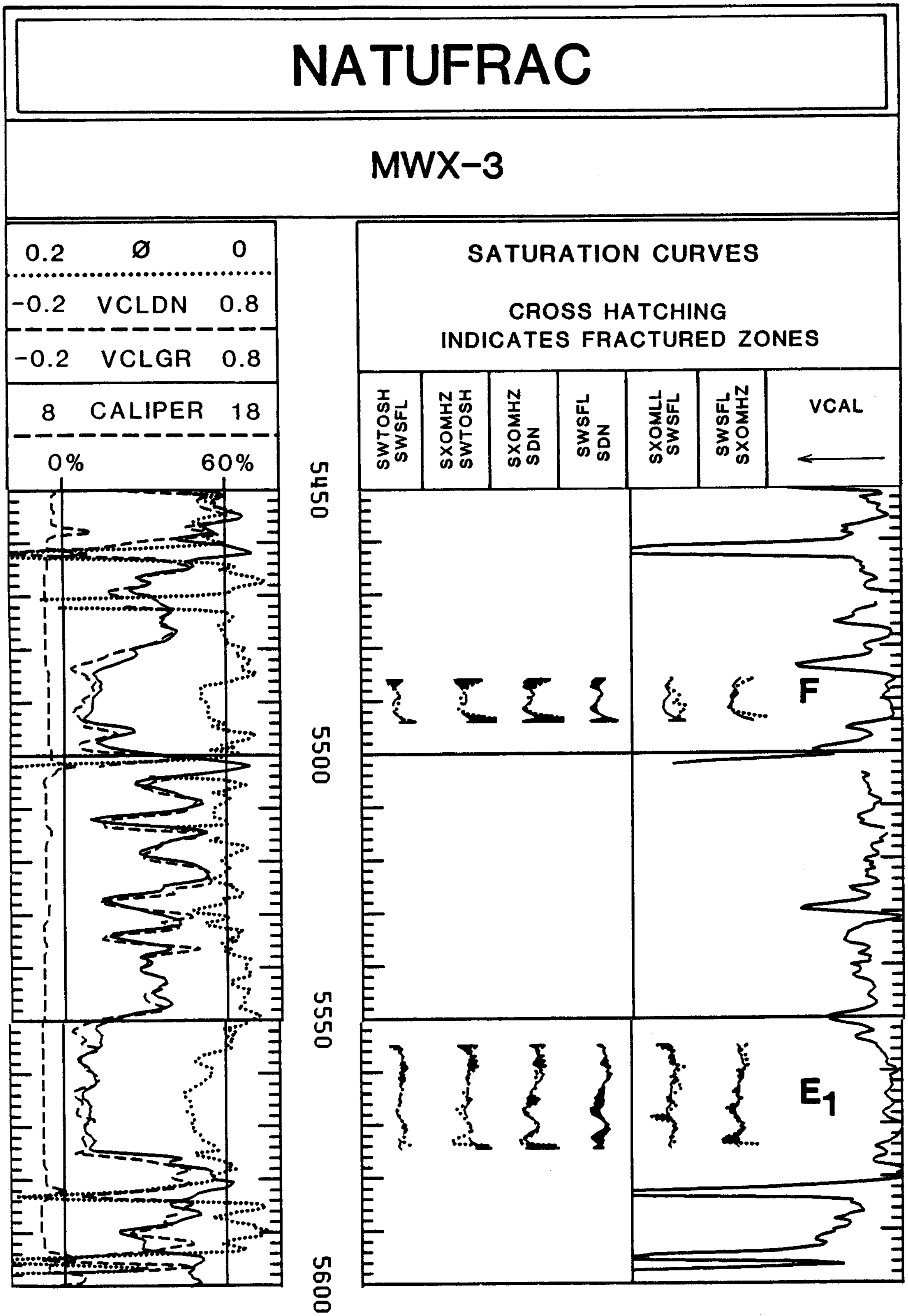

Figure 4.42, Continued

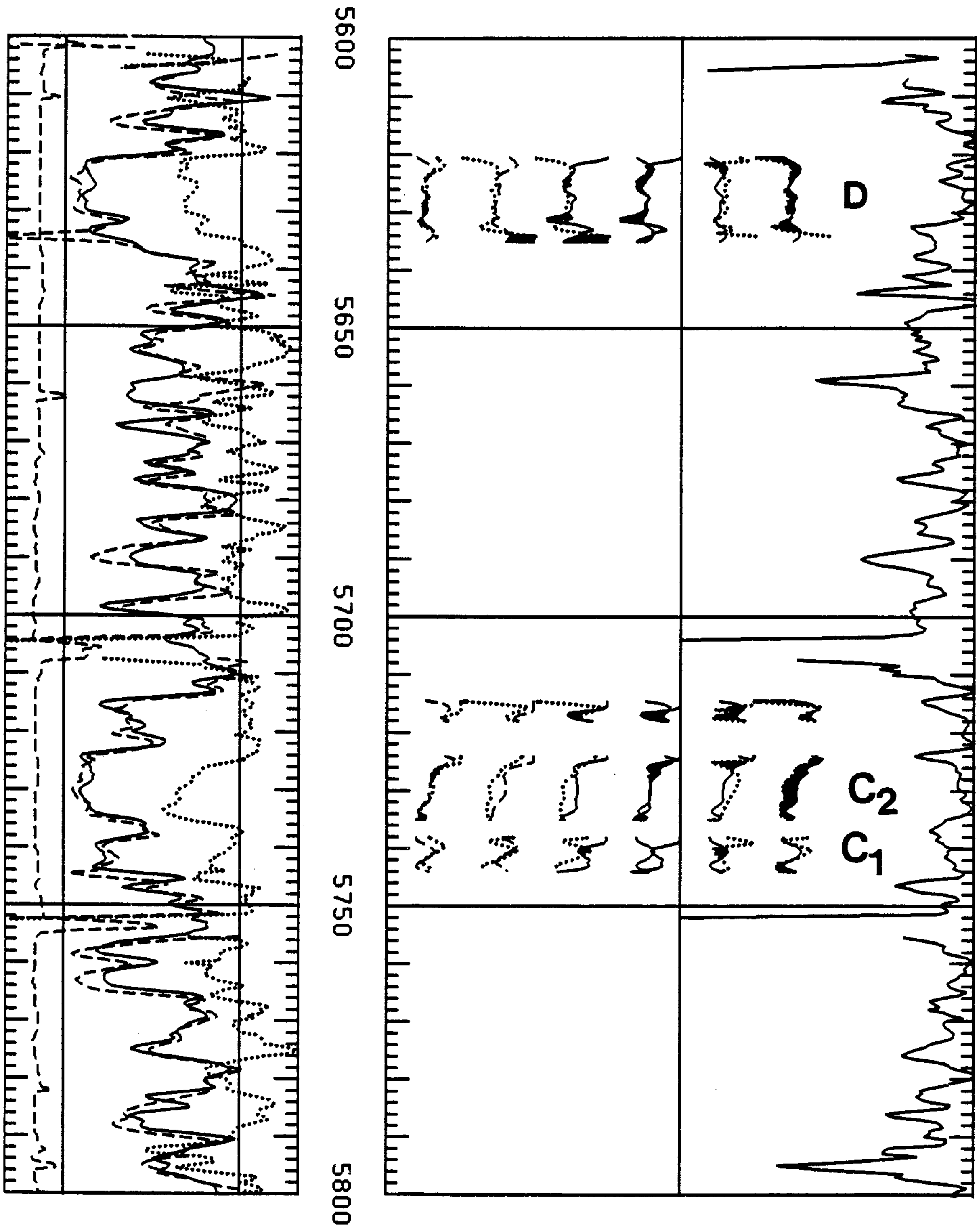

Figure 4.42, Continued

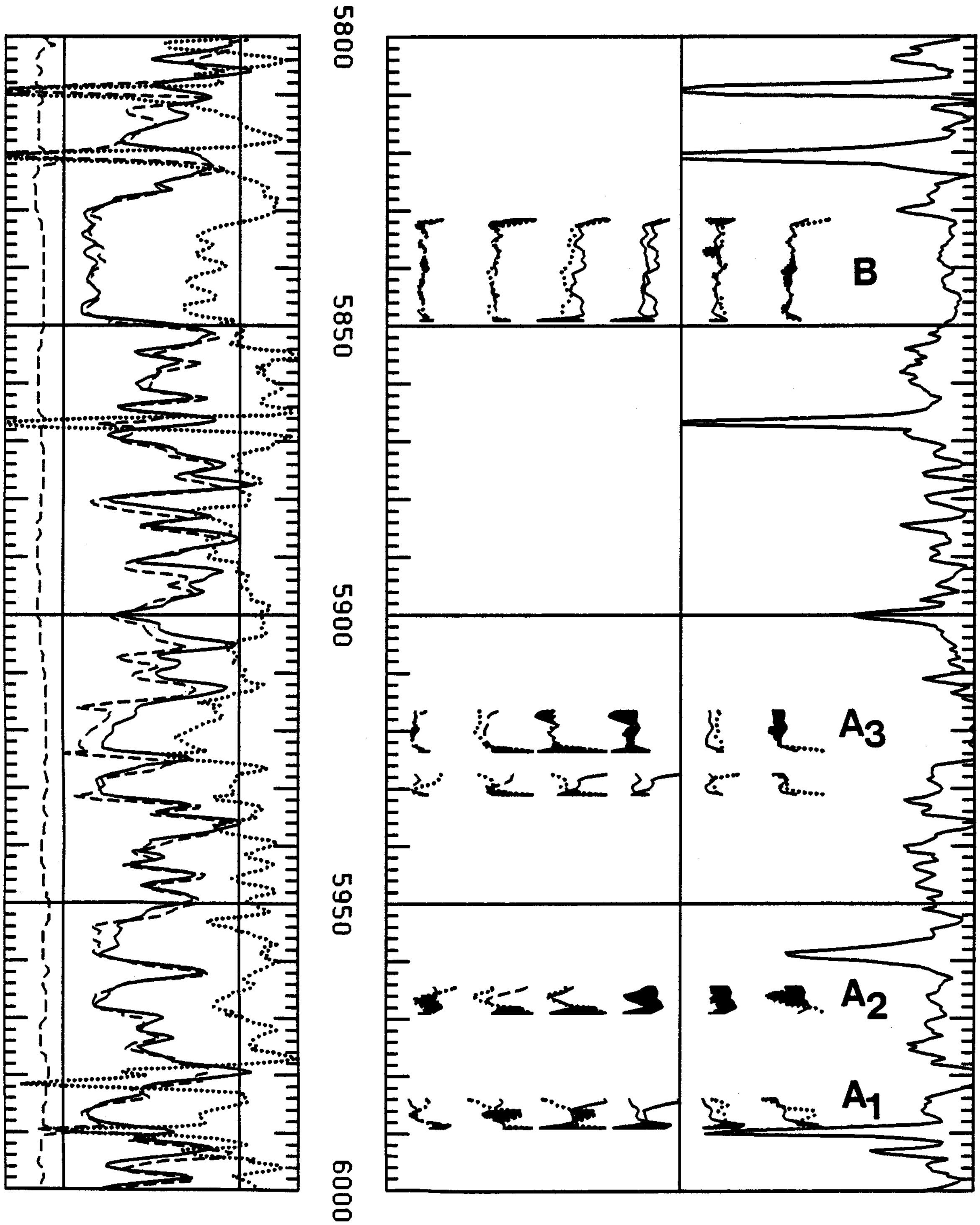

Figure 4.42, Continued

CER COMPUTER PROCESSED ANALYSIS

CER TIGHT GAS SANDSTONE ANALYSIS

A COMPREHENSIVE MODEL FOR THE LOG INTERPRETATION OF LOW-PERMEABILITY GAS RESERVOIRS

CER Corp. Post Office Box 15090 Las Vegas, Nevada 89114 Phone (702) 735-7136

COMPANY CER Corporation

WELL MWX-1

FIELD Rulison

COUNTY Garfield **STATE** CO

DATE 2/24/86	**LOCATION** SW/NW	**ELEVATION** 5374.0 **KB**
		– **DF**
ANALYST R.E. Hill	**SEC.** 34 **TWP.** 6S **RGE.** 94W	5355.0 **GL**

Figure 4.43 MWX-1 Low Fluvial Interval Multiple Density Pass Log

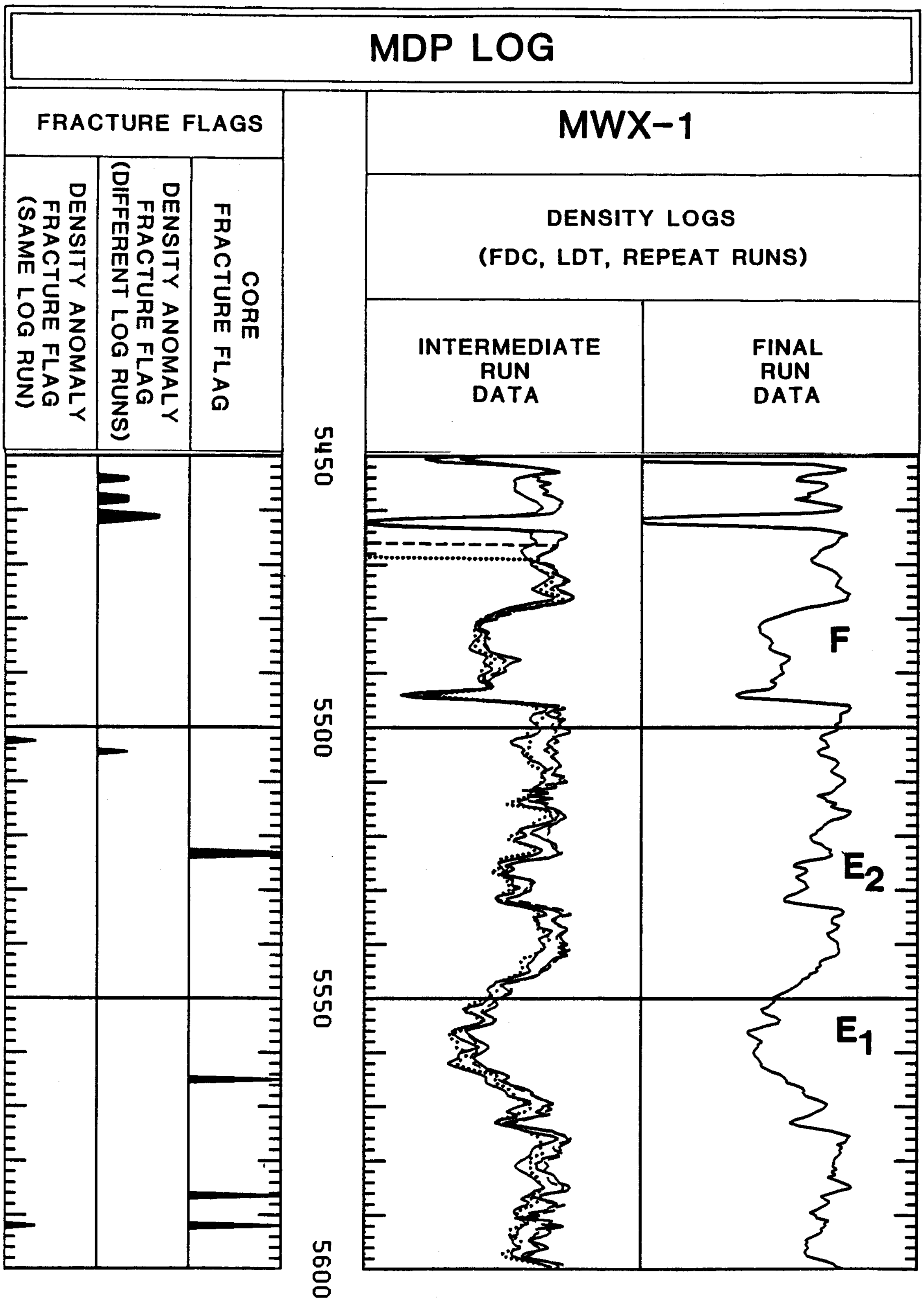

Figure 4.43, Continued

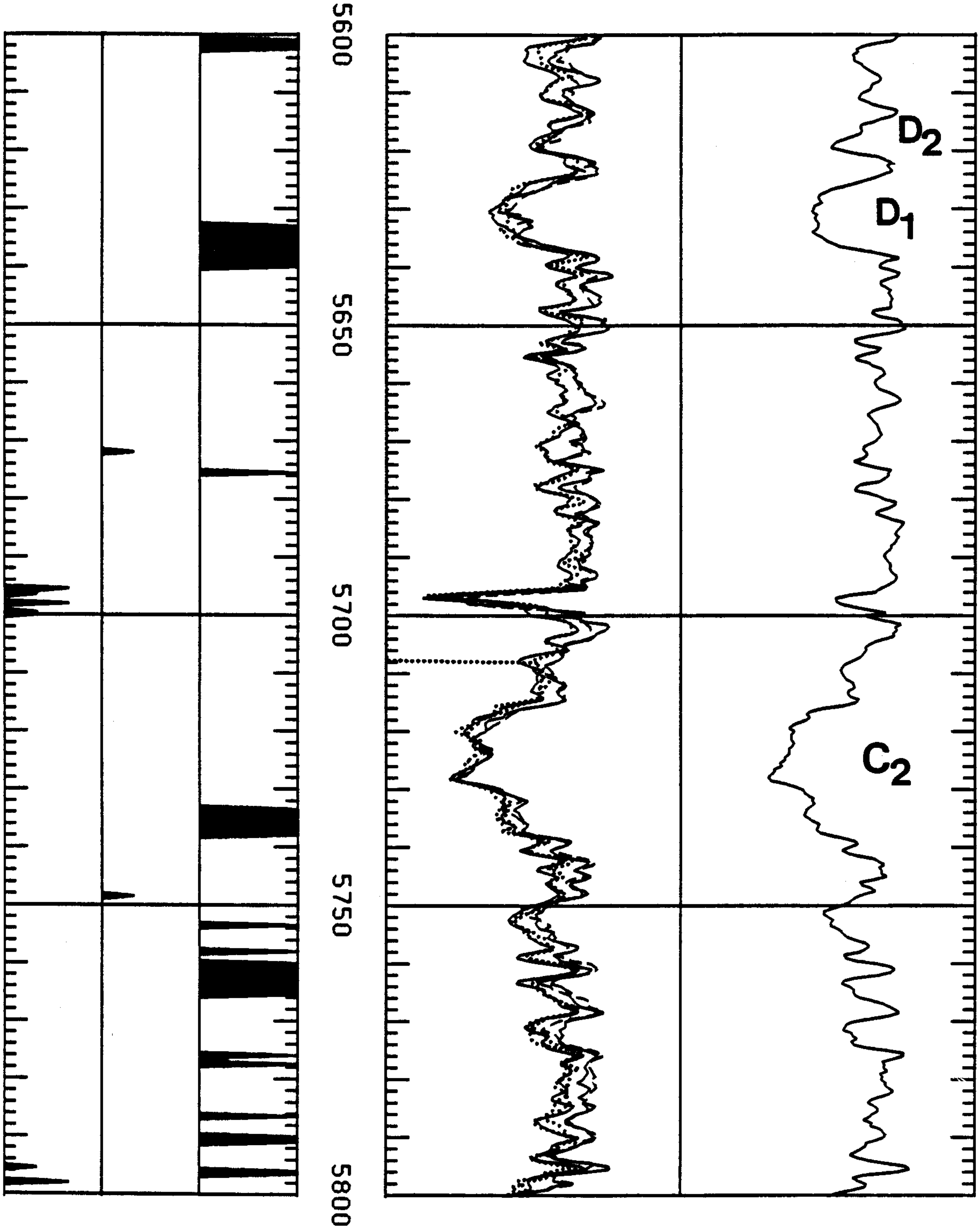

Figure 4.43, Continued

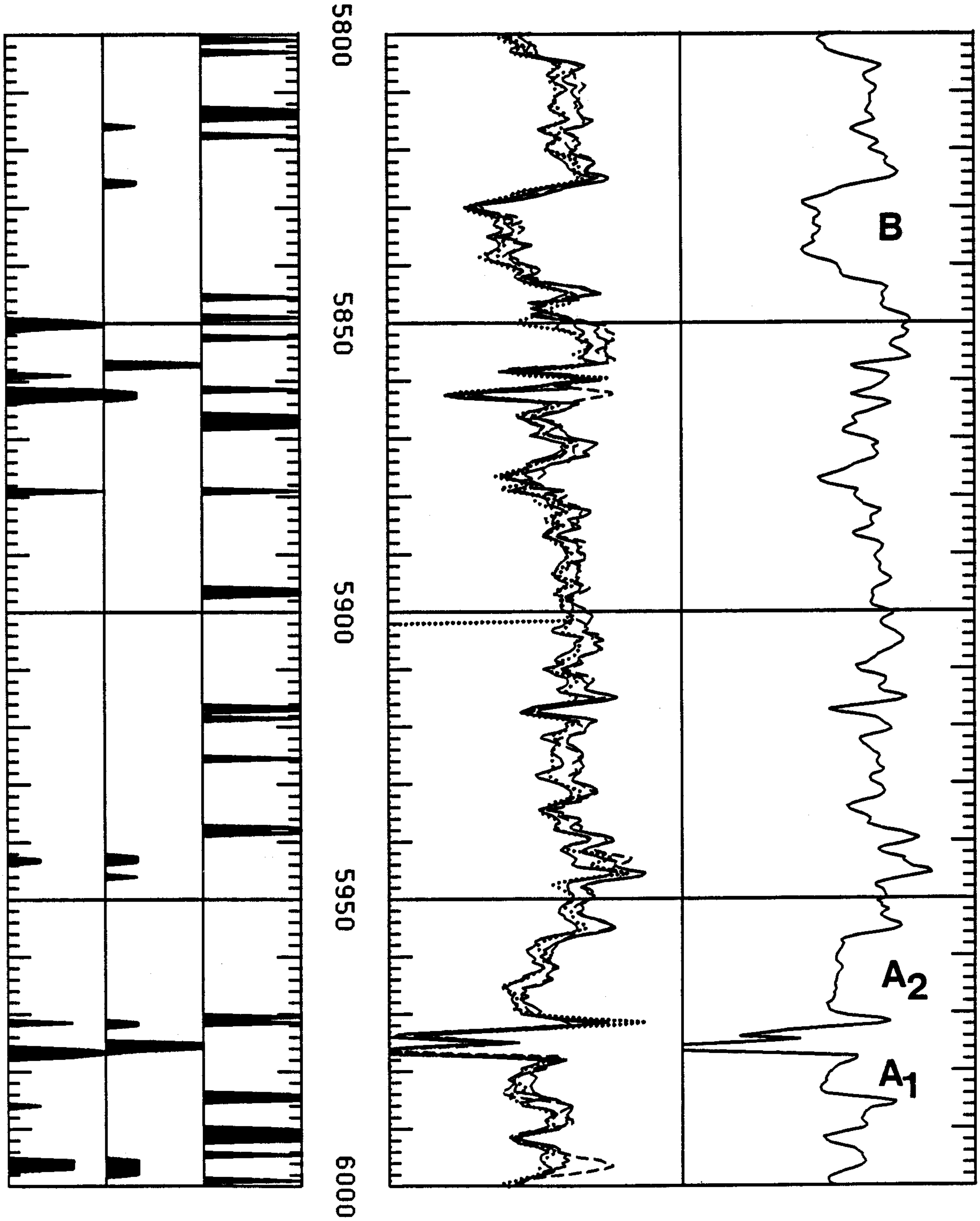

Figure 4.43, Continued

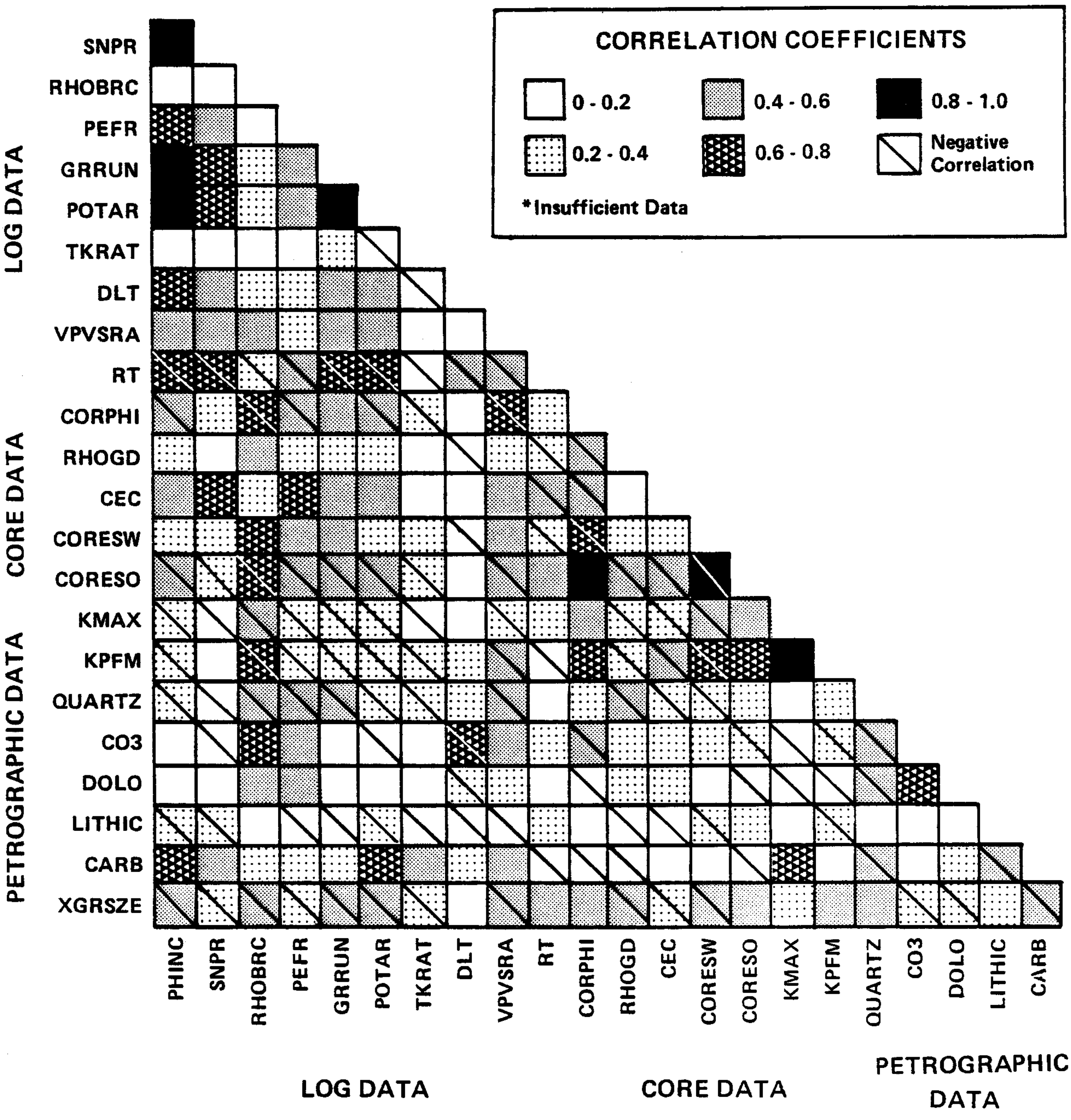

Figure 4.44 Correlation Coefficient Matrix, MWX-1 Low Fluvial Interval

5.0 CORE ANALYSIS

A. R. SATTLER
SANDIA NATIONAL LABORATORIES

5.1 INTRODUCTION

The fluvial zone occurs at a depth of 4400 to 6000 ft at the MWX site. The core data help describe the formations and the reservoir, and they provide input data to all MWX activities. In this section examples of the core data are presented and discussed to put them in perspective. Specifically these remarks indicate:

- what core was taken and what analyses were made;
- typical values of reservoir parameters, rock properties and other measurements;
- implications of the core data; and
- some comparisons of the core data with that of other geologic sections of interest in the Mesaverde.

Rocks from the fluvial zone were deposited in an environment of meandering fluvial systems. Most of the systems at MWX were relatively small and probably originated on the alluvial plane rather than in the contemporaneous fold and thrust belt further west. Study of outcrops indicate that fluvial sandstones were laid down as arcuate point bars on the inside of river beds during lateral migration of the river. A sandstone deposited as a point bar is often partially eroded and replaced as subsequent point bars migrated over the same area, constructing complex composite meander belt reservoirs.

The sandstones in this zone contain an estimated 35 BCF/mi^2 of gas vs an estimated 156 BCF/mi^2 for all Mesaverde sandstones. The pore pressure is about 3400 psi in the lower fluvial zone and the net confining stress is in the neighborhood of 2000 psi for an unperturbed reservoir in that part of the fluvial zone.

After the continuous drilling/coring of MWX-1, the fluvial B and C sandstones were chosen for coring in MWX-2, and MWX-3 in order to study the lateral variability of properties of the fluvial zone. A pair of mid-fluvial sandstones around 4900 ft were chosen for the same reason; these sandstones seemed to have reasonably promising reservoir properties based on log and routine core analyses data and were relatively thick (for lenticular fluvial sandstones). The E and F sandstones in MWX-2 were selected as targets for pressure coring in an effort to obtain unambiguous water saturation data for tight sandstone. The E and F sandstones were deep enough in the Mesaverde column to have reasonable reservoir properties but high enough in the column as not to be greatly overpressured. (The pressure core assembly could only be pressurized to 5000 psi at that time.) Most of the fluvial sandstone core analyses is concentrated in the lower fluvial zone, the A-F sandstones (shown in Figure 5.1), although some data is also presented on the above mentioned mid-fluvial sandstones. The B, C, and E sandstones were eventually stimulated.

A total of 2010 ft of 4-inch diameter core was cut from the three wells in the fluvial interval as follows:

- MWX-1: Continuous core was taken through the fluvial interval, from 4400 to 6000 ft. The core from 4645 to 4822 ft and from 5425 to 5535 ft was oriented.

- MWX-2: Core was taken from 4870 to 4956 ft and from 5676 to 5780 ft. The lower interval included the B and C sandstones. The upper interval was oriented.

- MWX-3: Core was taken from 4887 to 4927 ft and from 5690 to 5870 ft. The lower interval included the B and C sandstones. All core was oriented.

- In addition 36 ft of 2 1/2 in-diameter pressure core were taken in the MWX-2 from 5485 to 5500 ft, from 5551 to 5566 ft and from 5566 to 5581 ft. This covered much of the E and F sandstones.

5.2 CORE PROGRAM

The MWX core analysis program is described in detail elsewhere.[1-2] The results of analyses presented in this section have been taken from the reports submitted by the participants. These reports are specifically referenced where used in this section, and more comprehensive listings are found in Section 11.0 and Appendix Q. This section presents reservoir, mechanical, and organic properties obtained from core. Other core-derived properties are reported in other sections: lithology (3.2), mineralogy/petrology (3.2.3), sedimentology (3.3), natural fractures (3.4), and estimates of in situ stresses from core (6.0). Core-log correlations are displayed with the log analyses formalisms in Section 4.0, although correlations made with respect to the televiewer and caliper logs are in Section 5.5.

There were over 25 participants in the core program. The major ones involved in fluvial zone core analysis were Core Laboratories, Institute of Gas Technology (IGT), and New Mexico Petroleum Recovery Research Center (PRRC) (reservoir and electrical properties, caprock analysis); RE/SPEC (mechanical rock properties); Bendix Field Engineering Corp. and the US Geological Survey (mineralogy/petrology); Colorado Geological Survey and Amoco (organic maturation); and National Institute of Petroleum and Energy Research (NIPER) and Dowell Schlumberger (laboratory work supporting completion, Section 10.0). Much of the fluvial core analysis date from Core Laboratories, IGT, and RE/SPEC are given as Appendices C, D, and E, respectively.

In many core studies, analyses are confined to the reservoir rock only. In MWX, however, the material abutting the sandstones was studied to obtain properties useful for hydraulic fracture design and analyses of stress test data; for example, mechanical property measurements were made on both sandstone and confining rock samples. In addition, caprock analyses and cation exchange capacity (CEC) measurements were often made to help determine the extent of the reservoir.

5.3 CORE HANDLING AND PREPARATION

The special core processing facility was established in a building at the Department of Energy's Anvil Points Facility across the Colorado River and about 15 miles from the MWX site. When the core come to the surface, it was removed from the core barrel by project geologists and placed in trays. After a quick preliminary inspection and removal of samples for special measurements, such as anelastic strain recovery (ASR), the core was first covered with plastic to prevent evaporation, and then with thick canvas to protect it from the elements. The core was then transported to Anvil Points for processing. Field processing of the core entailed many procedures such as the following:

- Construction and use of a six-detector core gamma assembly. The core gamma assembly provided for well control during drilling and for core-log depth correlations after logging. The core gamma assembly also had better spatial resolution than the open-hole gamma ray log.

- Marking the positions and magnitude of scribe line deviation and locations of connections and other breaks in core.

- Photographing the entire amount of core in color.

- Taking core plugs and sealing and preserving selected sections.

- Making a visual core log (which was subsequently followed by a detailed lithology/sedimentology log from slabbed core).

- A special no-freeze freight service was used in the winter to ship samples selected for measurements of reservoir parameter or mechanical rock properties.

Because there were so many conflicting requirements for the MWX core, many of the routine and special core analyses were performed on plugs. This allowed most of the whole core to be available for studies of sedimentology and depositional environment, mechanical rock properties, and organic maturation. Thin sections were taken by facing off the ends of the same core plugs. Preference for thin section analyses was given to the plug ends corresponding to the plugs selected for the restored-pressure-state permeability measurements. This allowed correlations of sandstone reservoir properties with mineralogy/petrology. Since properties can often vary rapidly in a lenticular sequence, it was necessary to make the correlations from the same sample.

5.4 CORE ANALYSES, RESULTS, AND DISCUSSION

Reservoir properties (water saturation, capillary pressure, permeability and porosity) are used in production testing. Caprock analyses can help define the limit of the reservoir and give an idea of the ability of abutting materials to contain gas. Mineralogy/petrology data provide checks of the frac fluid/formation compatibility (Section 10.0), information on the paragenesis of the formation, and details on the formation of the pore structure. Electrical data (formation factor, resistivity index, and cation exchange capacity (CEC) are used in the Archie/Waxman Smits formalisms of log analysis. Mechanical rock properties provide inputs to the analysis of hydraulic fracture length, width, azimuth, and frac containment. Stress-related mechanical property measurements are used for predicting hydraulic fracture azimuth and for modeling the existing in situ stresses (Section 6.0). Organic maturation data are necessary to determine origin and migration of the gas and provide inputs to burial history hypotheses and paleostress information through paleo-pore-pressure estimates. The televiewer and oriented caliper logs can also be used to predict hydraulic fracture azimuth. Fractures from the televiewer can be compared with those from oriented core.

5.4.1 Reservoir Parameters

Many reservoir parameter measurements were made at frequent intervals in the sandstones. For example, routine core analyses providing porosity and water saturation information were taken every foot in the sandstones and at every other foot for four to six feet into the material abutting the sandstones.[3-5] Routine core analyses across the lower fluvial A-F sandstones and across mid-fluvial sandstones around 4900 ft are displayed in Figures 5.2 to 5.10.

Water saturations are very important in tight sandstone. The drilling/coring was actually done "at or near balanced" conditions (i.e., weight of the column of drilling fluid is made about the same as formation gas pressure) to minimize invasion of core and formation by drilling fluid. (It was later determined that the mud weights were about 500 psi less than the measured reservoir pressures.) Oil-base drilling fluid was used in drilling MWX-1 and MWX-2, in part to further prevent invasion of core and formation by water-base drilling fluids. These steps would result in more accurate water saturation measurements. Water-base drilling fluid was used in MWX-3 so that a more thorough suite of electrical logs could be run. An ammonium nitrate tag was used in the drilling of MWX-3 in an attempt to correct the water saturations from invasion. Differences in nitrate concentration reported by the mud logger and Core Laboratories, plus the rapid variation of properties in these lenticular sandstone lenses over short distances, made an accurate assessment of these correction factors impossible.[6] As a result, each saturation value for MWX-3 may be from 5 to 15 percent high due to invasion.

The water saturation values were determined by the Dean Stark distillation method in MWX-1 and MWX-2, and by the summation of fluids method in MWX-3 because results from the MWX pressure core data suggested that the Dean Stark method may not be the water extraction method of choice.[7] Water saturations average around 40 to 50 percent in the B and C sandstones, around 60 percent in the E sandstone, and about 55 to 65 percent in the mid-fluvial sandstones around 4900 ft.

Porosities were determined by Boyle's Law method. There had been questions whether the pressure of the helium entering the tight whole core would equilibrate during these routine measurements; plugs had an advantage of equlibrating in a shorter time. Because this core was so tight, additional time was allowed for pressure equilibration in determining the porosity of these tight plugs.

Porosity average around 6.5 to 8 percent in the B and C sandstones, 5 percent in the E sandstone and 7 to 8 percent in the mid-fluvial sandstones around 4900 ft. Porosity as a function of confining pressure was measured by Core Laboratories[8] (Table 5.1) and IGT[9-11]. There appears to be little change of porosity with confining pressure.

Core Laboratories used the non-steady state, pulsed method to determine Klinkenberg (gas slippage corrected) permeabilities. IGT used the steady state method to determine their Klinkenberg permeabilities and they performed all of their restored pressure state permeabilities without cleaning. Before measuring their Klinkenberg permeabilities, Core Laboratories subjected each of the core plugs to toluene extraction to remove any residue from oil-base drilling fluid and they leached precipitated salts out of the pores with hot methyl alcohol.

Selection of plugs for dry, restored-pressure state, Klinkenberg permeability measurements were made after inspection of the routine core analysis data and re-examination of the core plugs. Core Laboratories provided restored-pressure-state permeability date for the A-F sandstones[3,12-18] and the mid-fluvial sandstones around 4900 ft.[12] Core Laboratories also provided a few vertical permeability measurements in these sandstones[12,19,20] (Figures 5.2 to 5.10). IGT[9-11] and PRRC[21] were provided some of the cleanest sandstones in these lower fluvial and mid-fluvial sandstones (Tables 5.2 and 5.3).

The dry Klinkenberg permeabilities of the fluvial sandstones are rather small, comparable with those found in the coastal zone[22] or the marine sandstones[23] but smaller than those found in the paludal sandstones[24]. The average permeability at 2000 psi confining pressure of the B sandstone is ≈5 microdarcies and that of the E sandstone is ≈2 microdarcies. The estimated net confining stress in the lower fluvial zone, through the A-F sandstones is in the neighborhood of 2000 psi. The majority of the permeability samples in these sandstones were measured at 1000, 2000, and 3000 psi confining pressure. Most of the remaining permeability samples were measured at 1000, 3000, and 4000 psi confining pressure. Vertical permeabilities are about the same as the horizontal permeabilities. The permeabilities of the fluvial sandstones depend on net confining stress. This dependence on confining stress is greater in the fluvial zone than it is for other zones of the Mesaverde. Figure 5.11 contrasts this dependence for paludal zone core (the least sensitive) and for fluvial zone core (the most sensitive). There is as yet no completely satisfactory mineralogical explanation of this phenomena.

The dry permeabilities over these sandstone lenses are not uniform. They peak in the interior of the lens and decrease at the edges. There are permeability streaks here in the fluvial zone. Permeability streaks (Figure 5.12) are defined as thin regions in sandstone where the matrix permeability of the core samples is substantially higher than in most other portions of the sandstone lens. The Bendix mineralogy data (Appendix B)[25] suggest some open porosity in these more permeable samples, but it is very difficult to make any quantitative correlations with the mineralogical properties. Often the total clay content of the higher permeability samples is low.

These horizontal permeability streaks would create conduits to a vertical fracture system occurring at the MWX site. The permeability streaks might recharge the natural fracture system during gas production (Figure 5.13). There appear to be permeability streaks in both the B and E sandstones.

Often the most permeable of the core plugs were selected for additional analyses such as specific permeability to brine, permeability vs. water saturation, capillary pressure, formation factor, and resistivity index measurements (Figure 5.14) as well as parametric studies permeability vs. net stress vs. water saturation (Figures 5.15 and 5.16).[26,27] Core Laboratories performed specific permeability to brine measurements (Table 5.3).[8] PRRC performed permeability to brine[28] and relative permeability measurements on preserved core (Figures 5.17 and 5.18).

Correction for realistic water saturations would result in permeabilities of ≈0.2 microdarcy for the B sandstone and ≈0.1 microdarcy for the E sandstone. These permeabilities are one-twentieth or less than that of the dry values, making effective permeabilities of these two sandstone lenses among the lowest in the Mesaverde.

Recent measurements made on sealed fluvial zone core show that permeabilities of preserved core are significantly less than those obtained from resaturated oven-dried core.[28] Such measurements made by PRRC showed the following:

- Much of the preserved core retained its water content for over five years.

- The permeability difference between the preserved core and oven-dried core is significant. For example, at 2000 psi confining pressure, the permeability of the preserved core is about 1/2 that of resaturated oven-dried core.

- Permeabilities of the preserved core are less than the corresponding oven-dried core at all water saturations, and the differences become quite small below 30 percent water saturation.

The capillary pressures of the fluvial zone core to brine are fairly high, of the order of a few hundred psi at realistic saturations. Capillary pressure curves to brine were generated by Core Laboratories[16,17] and PRRC[29] which extended the curves at very low water saturations by adsorption measurements. The capillary pressure curves have about the same shape as those of the other zones that were studied in the Mesaverde. The capillary pressures to brine appear in some instances to be somewhat less than the other zones of the Mesaverde because the water saturations are somewhat higher on the average. Capillary pressure data for some fluvial zone core are shown in Table 5.5.

5.4.2 Pressure Core Measurements

A pressure core operation was performed in the E and F fluvial sandstones, at 5485 to 5500 and 5551 to 5581 ft, during the drilling of MWX-2. The goals of this operations were (1) to obtain accurate water saturation data, (2) to measure the amount and composition of gas on a foot-by-foot basis, and (3) to recover fluids for water-chemistry analyses. This was felt to be a novel approach for accurate water saturation measurements in tight sandstone core.

Several changes in usual pressure coring procedures were adopted, including the development of an organic, noninvasive coring fluid to help preserve the water saturation. The pressure core barrel was modified so that gas, not trapped during the freezing process, would not be lost. During the operation, three 15-ft-long pressure core barrels were taken; they were filled with reservoir rock.

Water saturation data were obtained on the pressure core first by Dean Stark distillation and later by vacuum oven-drying. The Dean Stark distillation lasted 8 days, and the vacuum oven-drying (at 240°F) lasted three more weeks. Not only was there core weight loss from the Dean Stark distillation but additional weight loss occurred from the vacuum oven-drying. Analyses of the data suggests the added weight loss is due mainly to removal of additional connate water from tight core.[7] The additional weight loss (Figure 5.19) was not considered to be due to water from invasion of core, to clay-bound water, or to water from decomposition of some of the organic matter in the rock during the vacuum oven-drying. The analysis suggests that water extraction should be carried on for a long time, and that the Dean Stark procedure may not be the most efficient way to extract water from tight sandstone core.

No water was recovered during the thawing of the pressure core prior to the Dean Stark analyses, probably because permeabilities of the samples were too low. Gas was recovered during the thawing process and the gas was analyzed on a foot-by-foot basis (Table 5.6).

The failure of one pressure core barrel, coring from 5551 to 5566 ft, to hold pressure during retrieval of the core was a bonus. It allowed identical analyses to be made on both pressurized and unpressurized core from the same sandstone lens. These analyses showed no water saturation differences on rock with the same porosities. It appears that pressure core and the more routine water extraction methods can give the same results if the extraction methods are carried on long enough.

5.4.3 Caprock Analyses

The caprock analyses includes permeability to brine and minimum gas threshold pressures necessary to displace water. IGT[30-32] and Core Laboratories[33] performed caprock analyses (Tables 5.7 to 5.8). A combination of very low permeability plus a high threshold pressure for gas displacement would indicate a good caprock and stratigraphic barrier.

The caprock analyses on the rock abutting the B and C sandstones and the mid-fluvial sandstones indicates, for the most part, that the permeabilities to brine are quite low, often in the subnanodarcy range. However, the caprock testers could only go to a maximum of about 1000 psi for the threshold pressures, well below the pore pressures seen in the lower and mid-fluvial sandstones. (What pore pressures actually exist in these siltstones/mudstones/ shales can not really be defined.) Thus these caprock tests and especially the threshold pressure tests should only be considered the qualitative indicator of the worth of the caprock.

5.4.4 Permeabilities of Core Samples Containing Natural Fractures

The frequency of all natural fractures vs. depth is given in Figure 5.20. The (vertical) extension fractures vs. depth are shown in

Figure 5.21. The reservoir permeabilities derived from production testing are compared with the matrix rock in Figure 5.22. Measurement of permeabilities of fluvial zone core samples along the primarily calcite filled natural fractures[16,17,28,34-36] (Table 5.9) and carbonaceous stringers (Table 5.10) were made.[37]

In all regions of the Mesaverde, natural fractures dominate production: the resulting formation production is at least one, and more often two or more orders of magnitude higher than can be accounted for by matrix rock alone (Figure 5.22).[38,39] The overall fracture frequency and the frequency of the extension fractures is the highest in the fluvial zone. Within the fluvial zone the fractures seem most numerous in the vicinity of the E and F with fewer fractures found in the vicinity of the A sandstone or about 5000 ft.

5.4.5 Mechanical Rock Properties

The mechanical rock property measurements were made by RE/SPEC.[40-44] (Figure 5.23 to 5.25) and Dowell Schlumberger[45] (Table 5.11) in the lower and mid-fluvial sandstones and in the rock abutting these sandstones. These properties include Young's modulus, compressive and tensile strength, Poisson's Ratio and fracture toughness. In both MWX-2 and MWX-3 these measurements were made on the cleanest, least shaly sandstones and on the most shaly (highest gamma ray signature) material abutting these sandstones. The plugs cut by RE/SPEC were vertical, while the plugs cut by Dowell Schlumberger were both horizontal and vertical.

Young's Moduli range from 25 to 49 GPa for the fluvial sandstones measured and from 17 to 54 GPa for rock abutting the sandstones (siltstone/ mudstones), compressive strengths in the sandstones from 146 to 311 MPa and from 98 to 146 MPa in the rock abutting the sandstones. In the fluvial zone it appears that the moduli, compressive strengths and tensile strengths, and fracture toughnesses are highest for siltstones, intermediate for the sandstones and are lowest for the mudstones (Figure 5.26). The moduli and the compressive strengths for the sandstones of the fluvial zone are about the same as those found in the other lenticular regions, but are somewhat lower than those seen in the Corcoran and Cozzette marine sandstones. It is difficult to make more precise correlations of the mechanical rock properties with lithology, but there are some fundamental differences in the behavior of both the stress strain curves and fracture toughness curves between the sandstones and the abutting materials.[46] In the fluvial zone there appears to be no systematic difference between the properties measured with vertical and horizontal plugs.[45]

5.4.6 Electrical Properties

CEC analyses were performed by means of the adsorbed water and chemistry methods[8,12,33,47] (Figures 5.3 to 5.6). Formation factor and resistivity index measurements were made (Table 5.12, Figures 5.27 and 5.28).[16,48] The CEC values in the fluvial zone sandstones are higher than the values in the marine sandstones and are among the higher CEC values in the Mesaverde. CEC values average slightly over two in the B and E sandstones and around 2.4 in the mid-fluvial sandstones around 4900 ft. CEC values in the materials abutting some of the fluvial sandstones are about the highest measured in the Mesaverde and approach 15 meq/100 gram.[33]

Cementation exponent values were derived from the porosity dependence of the formation factor measurements. The cementation exponent values, m and m* (clay corrected), are about 1.9 and 2.1 at 3000 psi confining pressure (Table 5.12). These values do not seem to depend strongly on depositional environment. A cementation exponent calculated from the PRRC data is about 20 percent higher than the Core Laboratories data.[28] Saturation exponent values were derived from the saturation dependence of resistivity index measurements. Saturation exponent values, n and n* (clay corrected), were about 1.4 and 1.8 (Table 5.12). Resistivity index values appear to vary with depositional environment. These values were obtained with the aid of a centrifuge and removal of such small amounts of water from a plug are difficult. Moreover, the distribution of the brine remaining after centrifugation may not be the same as would be found in situ resulting in different measured electrical characteristics. Therefore, it is difficult to assess the reliability of the resistivity index data.

5.4.7 Organic Content and Maturation

Vitrinite reflectance measurements were made on some fluvial samples by Amoco (Figure 5.29).[49] These measurements were performed not only on the coal, but on rock containing any organic material (Table 5.13). The vitrinite reflectance curve vs. depth has the same general shape as is seen from other data in this part of the basin. The Colorado Geological Survey (CGS) performed analyses on carbonaceous rock through the Mesaverde column and the data for the fluvial is given in Table 5.14.[50] Total organic carbon, rock evaluation pyrolysis, and C1-C5+ gas analyses were performed on coastal zone samples by Core Laboratories (Tables 5.15 and 5.16).[51-53]

5.4.8 Directional Permeabilities of Oriented Core

Permeability measurements were made on oriented fluvial core and core from other zones at N80°W and N10°E (Table 5.17).[54] These directions are close to the maximum and minimum horizontal stress existing in the fluvial zone (Section 6.0). The following observations are made:

- In all cases, the permeabilities in the direction of minimum principal, horizontal stress (N10°E) are greater than those in the direction of maximum principal horizontal stress (N80°W). Microcracks resulting from stress relaxation would be aligned along the minimum rather than along the maximum horizontal stress, and thus, the permeability would be higher in the direction of the microcracks.

- Using the reasoning above, the vertical permeabilities would be expected to be the smallest because the vertical stresses are the predominant ones in these zones. While this is true for the paludal and coastal sandstones, the effects of bedding on vertical permeability may be important, especially in the composite fluvial sandstones.

- The difference in the horizontal anisotropy may be the greatest in the fluid zone.

5.4.9 Permeability as a Function of Net Confining Stress

The permeabilities of one coastal and fluvial core plug were measured as a function of pore pressure and confining stress such that the net confining stress was constant at 2900 psi.[55-57] At the time these measurements were made, the net confining stress in the coastal/fluvial region was estimated to be around 2900 psi and was based on: (1) the measured pore pressure, (2) the measured minimum horizontal stress from in situ stress tests (Section 6.0),[58] (3) the maximum horizontal stress, which was estimated as about 800 psi higher than the minimum horizontal stress from open-hole stress measurement[59] and the modeling of ASR data,[60] and (4) an estimate of 1 psi/ft for vertical, overburden stress. Five pore pressures were chosen, with the initial pore pressure chosen to be close to that existing in the coastal interval (4400 psi). The results are given in Figure 5.30. For both samples it appears that gas permeability is constant at a pore pressure of 1500 psi and above. Presumably, the increase in gas permeability at low pore pressures is due to reduction in Klinkenberg slippage effects. This curve suggests that permeability in these tight sandstones depends more on the value of the net stress rather than on the individual values of pore or confining pressure.

5.5 CORRELATIONS OF STRESS RELATED CORE AND LOG MEASUREMENTS

MWX ASR/DSCA core data, the MWX-3 televiewer log, and the MWX-3 oriented caliper log all provide predictions of the maximum horizontal stress azimuth with depth. It is assumed that the breakouts identified in the nearly vertical MWX-3 well are orthogonal to the maximum principal stress.[61] Predictions of the maximum principle horizontal stress azimuth from the three methods for the fluvial zone are given below.

- The ASR/DSCA data gives a prediction between 60° and 115° (Section 6.0).[59] These measurements were taken in the B, C, and F sandstones, the mid-fluvial sandstones around 4900 ft, and sandstones between 4650 and 4820 ft.

- The breakouts from the borehole televiewer give an appropriate prediction between 80° and 115° from 4650 to 5800 ft. (Figure 5.31). It is very easy to discern a preferred stress direction in the fluvial zone on the televiewer log (perhaps to greater horizontal anisotropy) except in the region of the A, B, E, and F sandstones. (The region of the E and F sandstones is where cross fractures have been seen in MWX core.)

- The breakouts from the oriented caliper log (Figure 5.32) give a prediction for the maximum horizontal stress roughly between 80° to 120°. A preferred stress direction is seen in the fluvial zone except in the regions of the A and B sandstones.

While oriented caliper can be read within 4 to 5°, the oriented caliper log may not seat squarely along the direction of maximum elongation. Furthermore, in some regions, washouts and stress breakouts may coincide making interpretations from this log difficult. By way of comparison it is difficult to read breakouts from the televiewer log better than 15° and the ASR/DSCA data was accurate within 10° due to inherent inaccuracies in orienting. Within the spread and uncertainties of the data (≈40° for each method at any depth) the correlation of the three types of measurements is considered fair.

The fluorescence microscopy and directional sonic velocity techniques for orienting relaxation microcracks were applied to a sample from the F sandstone in MWX-1 at 5490 ft.[62-63] The data suggest the following:

- The strikes of relaxation microfractures (Figure 5.33) are roughly oriented east-west which suggests a maximum principle stress orientation of around 0°.

- The strike of the natural microfractures (Figure 5.34) has a general east-west direction, but the statistics are poor.

- The maximum directional velocity occurs around 80° (Figure 5.35). If it is assumed that this corresponds to the strike of the relaxation microcracks, then the principle stress direction would be north-south.

These fluorescence microscopy and directional sonic velocity results appear to differ from the ASR results (Section 6.4). The televiewer (Figure 5.31) and oriented caliper log suggest anomalous behavior in this region. The reason for this anomaly is not known, but may be related to the presence of the second set of natural fractures observed in this region. These samples have some type of "intrinsic" velocity anisotropy even at 4000 psi confining pressure, about twice the estimated net confining stress.

The ratio of the minor to major wellbore axis was obtained from the oriented caliper logs for the fluvial and other lenticular zones (Figure 5.36). There is a greater deviation from unity in the fluvial zone suggesting that the fluvial zone may generally have a somewhat greater degree of anisotropy. This is consistent with the directional permeability data (Table 5.17) and the general appearance of the televiewer and caliper logs run in the MWX wells.

5.6 REFERENCES

1. Sattler, A. R., ""Core Analysis in a Low Permeability Sandstone Reservoir: Results from the Multiwell Experiment," Sandia National Laboratories Report, SAND89-0701, April, 1989.

2. Sattler, A. R., "The Multiwell Experiment Core Program, II," SPE 11763, Proceedings of the 1984 SPE/DOE Unconventional Gas Recovery Symposium, Pittsburgh, PA, May 16-18, 1984.

3. Core Laboratories, Report RP-2-6714, November 1981.

4. Core Laboratories, Report RP-2-6806, March 1982.

5. Core Laboratories, Report 3806-7119, July 1983.

6. Core Laboratories, Report P83012, January 1984.

7. Sattler, A. R., A. A. Heckes and J. A. Clark, "Pressure Core Measurements in Tight Sandstone Lenses During the Multiwell Experiment," SPE/DOE/GRI 12853, Proceedings of the SPE/DOE/GRI Unconventional Gas Recovery Symposium, Pittsburgh, PA, May 1984.

8. Core Laboratories, SCAL report 203-830024, March 15, 1984.

9-11. Institute of Gas Technology, Project 6506 Reports, "Sandstone Permeability and Porosity Measurements," July 1982, August 1982, and October 1982.

12. Core Laboratories, SCAL Report 203-820027, September 14, 1982.

13. Core Laboratories, SCAL Report 203-830070, November 1983.

14. Core Laboratories, SCAL Report 203-830024, March 15, 1984.

15. Core Laboratories, SCAL Report 203-840026, August 20, 1984.

16. Core Laboratories, SCAL Report 203-860019, May 1986.

17. Core Laboratories, SCAL Report 203-860024, June 1986.

18. Core Laboratories, SCAL Report 203-860053, September 1986.

19. Core Laboratories, SCAL Report 203-820108, February 9, 1983.

20. Core Laboratories, SCAL Report 203-830108, November 1984.

21. Wei, K. K., N. R. Morrow and K. R. Brower, "Effect of Fluid, Confining Pressure, and Temperature on Absolute Permeabilities of Low Permeability Sandstone," SPE Formation Evaluation, August 1986.

22. Multiwell Experiment Final Report III, the Coastal Interval of the Mesaverde Formation, SAND88-3284, March 1989.

23. Multiwell Experiment Final Report I, the Marine Interval, SAND87-0327, April 1987.

24. Multiwell Experiment Final Report II, the Paludal Interval, SAND88-1008, May 1988.

25. Bendix Field Engineering, Series of Contractor Reports on Mineralogic and Petrographic Analyses of Multiwell Experiment Samples, 1982-1984 (given in Appendix B for all fluvial related reports).

26,27. Institute of Gas Technology, Project 65056 Reports, "Sandstone Permeability and Porosity Measurements: Relative Permeability Data," October 1982 and November 1982.

28. New Mexico Petroleum Research Recovery Center, New Mexico Institute of Mining and Technology, Project 2-75-7339, Reports for Morgantown Energy Technology Center, 1987, 1988.

29. Ward, J. S. and N. R. Morrow, "Capillary Pressures and Gas Relative Permeabilities of Low Permeability Sandstones," SPE Formation Evaluation, pp. 345-346, September 1987.

30,31. Institute of Gas Technology, Project 65056 Reports, "Caprock Analysis," June 1982 and September 1982.

32. Institute of Gas Technology, Project 61071 Report, "Analysis of Stratigraphic Barriers (Caprock) between Sands in the Cretaceous Mesaverde Formation--US DOE Multiwell Experiment, Garfield County, Colorado," June 1984.

33. Core Laboratories, SCAL Report 203-840055, March 27, 1984.

34. Core Laboratories, SCAL Report 203-840026, August 1984.

35. Core Laboratories, SCAL Report 203-850062, December 1985.

36. Core Laboratories, SCAL Report 203-860053, September 1986.

37. Core Laboratories, SCAL Report 203-87005, April 1986.

38. Lorenz, J. C., P. T. Branagan, N. R. Warpinski and A. R. Sattler, "Fracture Characteristics and Reservoir Behavior of Stress-Sensitive Fracture Systems in Flat-Lying Lenticular Formations," SPE 15244, Proceedings of the SPE Unconventional Gas Technology Symposium, Louisville, KY, May 18-21, 1986, pp. 423-436.

39. Northrop, D. A., "Insights into Natural Gas Production from Low Permeability Reservoirs," SPE 17706, Proceedings of the 1988 Gas Technology Symposium, Dallas, TX, June 13-15, 1988.

40. RE/SPEC Inc., Data Report RSI-0226, September 1983.

41. RE/SPEC Inc., Data Report RSI-0234, October 1983.

42. RE/SPEC Inc., Data Report RSI-0238, November 1983.

43. RE/SPEC Inc., Progress Report, RSI(RCO)-046/7-84/214, July 1984.

44. RE/SPEC Inc., Progress Report RSI(RCO)-046/5-85/200, May 1985.

45. Dowell Schlumberger Formation Analysis Laboratory (Tulsa) Reports, "Formation Evaluation of MWX-1, MWX-2, MWX-3 (Fluvial Interval)," October 1986.

46. Senseny, P. E. and T. W. Pfeirfle, "Fracture Toughness of Sandstones and Shales," Proceedings of the 25th Symposium in Rock Mechanics, Evanston, IL, June 1984.

47. Core Laboratories, SCAL Report 203-840016, May 1984.

48. Core Laboratories, SCAL Report 203-870050, November 1987.

49. Hemmler, T., "MWX-1 and MWX-2 Cores; Vitrinite Reflectance Data," Letter Report to A. R. Sattler, Sandia National Laboratories, November 1982.

50. Tremain, C. L., Colorado Geological Survey Letter Reports to A. R. Sattler, Sandia National Laboratories; January 1982, March 1982, July 1982, November 1982, February 1983, March 1983, and January 1984.

51. Core Laboratories, Geochemical Services Report 84012, March 1984.

52. Core Laboratories, Geochemical Services Report 84109, June 1984.

53. Core Laboratories, Geochemical Services Report 84137, August 1984.

54. Institute of Gas Technology, Project 61071 Report, "Directional Core Analysis of the Mesaverde Formation, US DOE Multiwell Experiment, Garfield County, Colorado," September 1984.

55. Walls, J. D., "Tight Gas Sands-Permeability, Pore Structure and Clay," JPT, November 1982.

56. Litton Core Research (Petrophysical Services/Core Laboratories) Report, "Gas Permeability of Sandstone Samples," Contract No. 04-4594, July 1986.

57. Litton Core Research (Petrophysical Services/Core Laboratories) Report 38B, "Gas Permeability of Fractured Whole Core and Matrix Plugs at Reservoir Pressures," April 1987.

58. Warpinski, N. R., P. Branagan and R. Wilmer, "In Situ Stress Measurements at DOE's Multiwell Experiment Site, Mesaverde Group, Rifle, Colorado," JPT, March 1985.

59. Warpinski, N. R., "Determining the Minimum In Situ Stresses from Hydraulic Fracturing Through Perforations," Proceedings of the 2nd International Workshop on Hydraulic Fracture Stress Measurements, Minneapolis, Minnesota, June 1988.

60. Warpinski, N. R. and L. W. Teufel, "In Situ Stresses in Low Permeability, Nonmarine Rocks," Proceedings of the 1987 SPE/DOE Joint Symposium on Low Permeability Reservoirs, Denver, CO, SPE/DOE 16402, May 1987. Also JPT, April 1989.

61. Bell, J. S. and D. T. Gaugh, "The Use of Borehole Breakouts in the Study of Crustal Stress," Proceedings of Hydraulic Fracturing Stress Measurements, USGS Open File Report 82-1075, 1982.

62. Western Atlas (Core Laboratories, Dallas) Report 88118, July 1988.

63. Western Atlas (Core Laboratories, Dallas) Report 88044, July 13, 1988.

TABLE 5.1

POROSITY AS A FUNCTION OF OVERBURDEN PRESSURE (MWX-2, CORE LABS)

Depth (ft)	Porosity (%) at Overburden Pressure of (psi)				
	200	1000	2000	3000	200
5034.4-34.8	3.9	3.8	3.7	3.7	3.9
5034.4-34.8	4.2	4.1	4.0	3.7	4.1
5132.8-33.0	9.1	9.0	8.9	8.8	9.0
5132.8-33.0	9.1	9.0	9.0	8.9	9.1
5730.0-30.3	6.1	6.0	5.9	5.9	6.1
5730.0-30.3	5.5	5.3	5.3	5.2	5.3

TABLE 5.2

RESULTS FROM ANALYSIS OF DRY FLUVIAL CORE (IGT)

			Values at Net Confining Stress*					
Depth (ft)	Well No.	Lab Net Confining Stress* (psi)	Porosity (percent)	As Received Water Sat. (percent)	Klinkenberg Permeability (μd)	Klinkenberg "B" (psi/μd)	Pore Volume** Compressibility (microsips)	H_g Capillary Entry Pressure (psia)
4910.8	MWX-2	3460	10.77	42	3.79	58.3	11.0	180
4911.5	MWX-1	3520	5.56	20	1.25	73.5	23.6	230
4940.3	MWX-2	3480	9.40	55	2.70	57.3	12.6	210
4949.5	MWX-1	3550	4.56	59	4.89	33.9	28.8	90
5718.9	MWX-2	3790	4.88	51	.10	1,440.0	14.2	-
5720.5	MWX-1	4040	7.13	48	1.67	79.9	14.3	150
5725.4	MWX-2	3790	4.49	70	.69	89.9	24.3	270
5734.3	MWX-2	3800	8.68	43	4.49	63.2	17.2	140
5737.0	MWX-2	3800	8.88	25	3.20	63.9	14.9	170
5834.9	MWX-1	4110	8.52	37	2.08	83.7	8.7	-
5842.0	MWX-2	3870	7.65	75	3.81	49.6	13.0	130
5847.3	MWX-2	3870	7.69	46	2.31	65.8	13.9	210

*Calculated using (0.925) (sample depth) - (0.5) (pore pressure estimated from mud weight).

**Pore volume compressibility ($\Delta V/V\Delta P$) determined by fractional changes in pore volume per psi of stepwise increase in confining pressure on the first compression of the rock from about 2,000 psi net stress to the net stress used for testing. Lower values would probably result from cycling of net stress to the maximum that would be experienced in reservoir depletion.

TABLE 5.3

SUMMARY OF MWX FLUVIAL CORE (IGT)

Well	MWX-3	MWX-3	MWX-3
Core	60-11	61-13	63-12
Depth (ft)	5719	5737	5830
<u>Documentation</u>			
Lithology	Med to CS SS	Med SS	Med to CS SS
Color (Wet Surface)	N7	N7	N6
Bedding	TK BD	TK BD	TN-TK BD
Degree of Size Sorting	moderate	moderate	poor
Grain Roundness	subangular	subrounded	subangular
Grain Mineralogy (Primary)	quartz	quartz, feld	quartz, feld
Secondary Minerals/Cement	calcite	calc, dol, clay	calc, dol, cla
Dominant Pore Geometry	GSP & SOLN	SLOTS, SOLN	SLOTS, SOLN
Horiz. Orientation Plug Axis	N 80° W	N 80° W	N 80° W
As-Received Sw (%)	72	69	70
Bulk Density of Plug (g/cm^3)	2.46	2.49	2.46
Grain Density of Plug (g/cm^3)	2.64	2.65	2.65
<u>CORAL Analysis</u>[1]			
Dry Porosity to Gas (0%)	6.06	5.49	6.44
Dry Permeability: K_∞ (microdarcy)	1.69	1.23	2.51
Klinkenberg "b" (psi)	86.0	97	81
Slot Width (microns)	0.106	0.094	0.113
Flow Path Tortuosity (plug lengths)	5.80	5.74	5.21
Compressibility (10^{-6} psi^{-1})	14	15	13
CORAL Run Number[2]	43-2	43-3	43-4
<u>Mercury Porosimeter Data</u>[3]			
Hg Entry Pressure (psia)	245	325	167
Mean Pore Radius (microns)	0.119	0.080	0.158

[1]At 3800 psia net confining stress on core dried at 60°C under 45% relative humidity.
[2]Number to left of hyphen designates run; number to right designates coreholder.
[3]Data obtained with conventional mercury porosimeter on <u>unconfined</u> samples.

TABLE 5.4

SPECIFIC PERMEABILITY TO WATER (CORE LABS)

Depth, (feet)	Porosity (%)	Confining Pressure (psi)	Specific Permeability To Water (μd)
4850.3	2.7	1000	- - -
4853.1	4.8	1000	0.025
		2000	0.009
4983.4	2.7	1000	0.010
		2000	0.006
5064.5	7.2	1000	0.088
		2000	0.0060
		3000	0.0054

TABLE 5.5

SUMMARY OF CAPILLARY PRESSURE TEST RESULTS (CORE LABS)

			Brine Saturation (% Pore Space) at Pressures (psi) of:									
Well	Depth, (ft)	Porosity (%)	1	2	5	10	25	50	100	200	500	1000
MWX-1	5717.5	9.9	100.0	100.0	100.0	100.0	99.3	92.9	71.0	59.6	47.7	34.0
	5723.4	10.3	100.0	100.0	100.0	100.0	90.0	75.1	64.0	53.6	44.5	37.2
	5725.5	11.0	100.0	100.0	100.0	100.0	90.0	74.0	63.5	53.6	42.7	32.9
	5732.0-32.6	7.8	100.0	100.0	100.0	100.0	100.0	100.0	88.5	72.9	55.9	40.6
	5732.0-32.6	6.4	100.0	100.0	100.0	100.0	100.0	100.0	94.6	86.3	68.7	56.8
	5734.1-34.7	6.7	100.0	100.0	100.0	100.0	100.0	100.0	94.2	86.9	74.3	64.9
	5829.6	10.7	100.0	100.0	100.0	100.0	82.4	66.4	55.2	47.1	35.8	25.9
	5837.6	8.0	100.0	100.0	100.0	100.0	100.0	99.7	89.5	77.3	62.0	44.9
MWX-2	5726.2	6.9	100.0	100.0	100.0	100.0	96.6	90.8	83.3	74.0	57.7	53.2
	5733.1	8.6	100.0	100.0	100.0	91.9	86.2	80.3	72.7	63.2	49.9	46.1

TABLE 5.6

ANALYSIS OF LIBERATED GAS BY GAS CHROMATOGRAPHY (MWX-2, CORE LABS)

Depth (ft)	Component Analysis, Mole Percent H_2S	CO_2	N_2	C_1	C_2	C_3	IC_4	NC_4	IC_5	NC_5	C_6	C_7+	Calc. Gas Gravity (Air=1.0)	Gas Volume cc @ STP
5485.0-5486.0	0.00	35.39	9.43	50.99	0.38	3.81	0.00	0.00	0.00	0.00	0.00	0.00	0.973	33
5486.0-5487.0	0.00	30.70	14.03	52.58	1.73	0.96	0.00	0.00	0.00	0.00	0.00	0.00	0.926	74
5487.0-5488.0	0.00	1.90	59.73	36.09	0.76	1.52	0.00	0.00	0.00	0.00	0.00	0.00	0.838	30
5488.0-5489.0	0.00	12.73	48.34	35.65	2.55	0.73	0.00	0.00	0.00	0.00	0.00	0.00	0.896	53
5489.0-5490.0	0.00	3.82	1.39	88.12	4.96	1.30	0.22	0.19	0.00	0.00	0.00	0.00	0.639	522
5490.0-5491.0	0.00	3.99	5.77	83.38	4.94	1.40	0.30	0.22	0.00	0.00	0.00	0.00	0.661	705
5491.0-5492.0	0.00	4.25	3.24	85.82	4.97	1.31	0.24	0.17	0.00	0.00	0.00	0.00	0.651	509
5492.0-5493.0	0.00	3.48	4.05	85.99	4.91	1.23	0.20	0.14	0.00	0.00	0.00	0.00	0.645	503
5493.0-5494.0	0.00	5.31	8.49	82.70	3.50	0.00	0.00	0.00	0.00	0.00	0.00	0.00	0.657	96
5494.0-5495.0	0.00	1.98	0.82	89.70	5.77	1.73	0.00	0.00	0.00	0.00	0.00	0.00	0.621	749
5495.0-5496.0	0.00	5.26	0.09	86.76	5.26	2.63	0.08	0.00	0.00	0.00	0.00	0.00	0.656	1306
	0.00	1.90	0.00	92.40	5.72	1.49	0.00	0.00	0.00	0.00	0.00	0.00	0.611	
5496.0-5496.6	0.00	4.85	18.81	70.69	4.24	1.41	0.00	0.00	0.00	0.00	0.00	0.00	0.713	995
	0.00	2.79	2.35	86.66	6.22	1.98	0.00	0.00	0.00	0.00	0.00	0.00	0.640	
5566.0-5567.0	0.00	3.08	0.07	84.72	7.15	2.92	0.77	0.69	0.36	0.23	0.00	0.00	0.680	3008
	0.00	2.58	0.33	87.75	6.83	2.21	0.68	0.28	0.00	0.00	0.00	0.00	0.646	
5567.0-5568.0	0.00	3.32	0.66	85.98	6.60	2.36	0.54	0.54	0.00	0.00	0.00	0.00	0.659	2757
	0.00	3.16	0.15	87.92	6.40	1.98	0.39	0.30	0.00	0.00	0.00	0.00	0.644	
5568.0-5569.0	0.00	2.41	2.33	85.89	6.35	2.17	0.46	0.40	0.00	0.00	0.00	0.00	0.651	2028
	0.00	2.08	0.37	89.11	6.15	1.73	0.30	0.25	0.00	0.00	0.00	0.00	0.630	
5569.0-5570.0	0.00	2.33	1.31	87.47	6.32	1.89	0.38	0.29	0.00	0.00	0.00	0.00	0.641	1793
5570.0-5571.0	0.00	2.66	1.01	81.82	8.88	3.85	0.88	0.90	0.00	0.00	0.00	0.00	0.690	2146
5571.0-5572.0	0.00	2.19	0.83	87.37	6.59	2.19	0.45	0.37	0.00	0.00	0.00	0.00	0.644	2483
	0.00	1.95	0.08	89.40	6.26	1.76	0.29	0.25	0.00	0.00	0.00	0.00	0.628	
5572.0-5573.0	0.00	2.17	4.53	83.68	6.57	2.20	0.47	0.38	0.00	0.00	0.00	0.00	0.659	2366
	0.00	1.84	0.75	88.51	6.49	1.84	0.32	0.24	0.00	0.00	0.00	0.00	0.632	
5573.0-5574.0	0.00	6.29	2.28	84.84	5.32	0.99	0.20	0.08	0.00	0.00	0.00	0.00	0.664	905
5574.0-5575.0	0.00	3.64	2.08	86.70	5.60	1.58	0.27	0.23	0.00	0.00	0.00	0.00	0.648	848
5575.0-5576.0	0.00	2.15	1.53	88.34	5.85	1.61	0.30	0.22	0.00	0.00	0.00	0.00	0.633	1620
5576.0-5578.0	0.00	6.61	3.07	86.01	3.85	0.46	0.00	0.00	0.00	0.00	0.00	0.00	0.654	707

TABLE 5.7

CAPROCK ANALYSIS (IGT)

Well	Depth (ft)	Lithology	Vertical Permeability to Water (nanodarcies)	Threshold Pressure (psi)
MWX-1	4901	Silty Mudstone	<0.1	250
MWX-1	4920	Siltstone	0.3	795
MWX-1	4921	Mudstone/Shale	<0.1	760
MWX-1	4952	Silty Shale	<0.1	600
MWX-1	5739	Mudstone	10^3	720
MWX-1	5755	Siltstone	1.3	780
MWX-1	5817	Siltstone/Shale	<0.1	525
MWX-1	5844	Siltstone/Shale	0.5	790
MWX-2	4889	Silty Shale	0.5	770
MWX-2	4903	Siltstone/Mudstone	<0.1	600
MWX-2	4950	Shale	9.3	225
MWX-3	4898	Silty Shale	0.3	765
MWX-3	5849	Siltstone/Shale	0.9	760

TABLE 5.8

CAPROCK ANALYSES (CORE LABS)

Depth (ft)	Vertical Permeability to Water (nanodarcies)	Threshold Pressure (psi)
4897.4-97.8	65	>1000 psi
4927.0-27.3	Sample Failure	---------
5696.4-97.6	<10	>1000 psi
5770.4-70.9	<10	>1000 psi
5802.5-02.9	<10	>1000 psi
5849.5-49.9	Sample Failure	---------

TABLE 5.9

PERMEABILITIES ALONG MINERALIZED FRACTURES
AND OF MATRIX ROCK IN CORE PLUGS (CORE LABS)

			Klinkenberg Permeability (md) at Effective Overburden Pressure (psi) of:		
Sample Identification*	Sample Depth (ft)	Porosity (%)	1000	2000	3000
VF	5454.0-54.9	2.8	0.00004	0.00003	0.00001
VM		2.3	0.00012	0.00008	0.00006
HF		1.7	0.00003	0.00001	0.00001
HM		2.6	0.00006	0.00004	0.00002
VF	5454.9-55.65	0.5	2.13072	0.60850	0.29099
VM		0.3	-	-	-
HF		3.1	0.00003	0.00001	0.00001
HM		1.8	-	-	-
VF	5732.0-32.6	6.1	0.00056	0.00047	0.00034
VM		6.1	0.00045	0.00032	0.00024
HF		8.1	0.21192	0.03337	0.00425
HM		7.3	0.00814	0.00649	0.00271
VF	5734.1-34.7	7.2	0.07155	0.00113	0.00095
VM		6.2	0.00070	0.00053	0.00037
HF		5.3	0.00535	0.00279	0.00134
HM		5.3	0.00320	0.00089	0.00071
VF	5739.9-41.0	1.9	-	-	-
VM		1.8	0.00002	-	-
HF		1.3	-	-	-
HM		1.3	0.00002	-	-
VF	5798.5-99.2	6.5	0.00037	0.00031	0.00027
VM		9.8	0.00057	0.00044	0.00040
HF		5.8	0.01567	0.00213	0.00037
HM		4.8	0.00109	0.00061	0.00051
HF	5723.4	10.3	0.15512	0.06552	0.03513
HF	5735.7	6.1	0.01915	0.00867	0.00388
HF	5740.5	1.3	0.01064	0.00598	0.00491
HF	5870.4	2.4	0.00035	0.00024	0.00014

*VF - Vertical Perm Along Fracture HF - Horizontal Perm Along Fracture.
VM - Vertical Perm Matrix Only HM - Horizontal Perm Matrix Only.

TABLE 5.10

CORE PLUGS WITH CARBONACEOUS STRINGERS

Depth (ft)	Porosity (%)	Klinkenberg Permeability (md) at Overburden Pressure (psi) of: 1000	3000
4323.2	3.0	0.00616	0.00124
4685.5	4.2	0.00277	0.00095
4781.6	4.1	0.00348	0.00049
4975.2	2.4	0.23400	0.02160
5003.8	5.2	0.00390	0.00070
5005.5	7.0	0.00445	0.00291
5052.3	8.8	**	0.39221
5081.3	0.9	0.00024	0.00009
5133.7	3.1	0.00024	0.00010
5142.6	3.4	0.01740	0.00047
5189.1	0.5	0.00009	*
5240.4	4.1	0.00079	0.00028
5616.5	3.9	0.01704	0.00342
5870.4	4.0	0.00012	0.00006

*Below lower permeability range of equipment; did not produce data.
**Above upper permeability range of equipment; did not produce data.

TABLE 5.11

MECHANICAL ROCK PROPERTIES (DOWELL SCHUMBERGER)

Well No.	Depth* (ft)	Zone	Confining Pressure (MPa)	Young's Modulus (GPa)	Poisson's Ratio	Compressive Strength (MPa)
MWX-1	5948.8 V	Mudstone Above	24.1	21.0	0.14	
		A Sandstone	37.9	25.2	0.18	173.2
	5984.7 H	A Sandstone	24.1	30.8	0.18	
			37.9	34.6	0.19	260.8
MWX-2	4949 H	Mudstone	24.1	40.8	0.18	
			37.9	41.4	0.22	--
	5735 H	C Sandstone	24.1	29.0	0.18	
			37.9	33.1	0.18	250.9
	5735 V	C Sandstone	24.1	26.3	0.17	
			37.9	30.3	0.18	231.0
	5838 H	B Sandstone	24.1	35.9	0.14	
			37.9	42.5	0.16	298.7
	5838 V	B Sandstone	24.1	35.4	0.17	
			37.9	41.85	0.18	278.8
	5857 H	Mudstone Below	24.1	47.9	0.12	
		B Sandstone	37.9	55.6	0.16	398.2
	5857 V	Mudstone Below	24.1	46.2	0.20	
		B Sandstone	37.9	51.7	0.15	342.5

TABLE 5.11

MECHANICAL ROCK PROPERTIES (DOWELL SCHUMBERGER) (CONTINUED)

Well No.	Depth* (ft)	Zone	Confining Pressure (MPa)	Young's Modulus (GPa)	Poisson's Ratio	Compressive Strength (MPa)
MWX-3	5695 H	Mudstone	24.1	43.4	0.22	
			37.9	50.6	0.26	198.9
	5802 H	Mudstone Above	24.1	18.5	0.39N	
		B Sandstone			0.13P	
			37.9	19.4	0.33N	111.4
					0.14P	
	5816 H	Mudstone Above	24.1	17.4	0.35N	
		B Sandstone			0.16P	
			37.9	21.4	0.25N	131.4
					0.11P	
	5840 H	B Sandstone	24.1	31.2	0.14	
			37.9	35.6	0.14	263.9
	5840 V	B Sandstone	24.1	31.3	0.17	
			37.9	36.5	0.18	255.1
	5853 H	Mudstone Below	24.1	42.3	0.18	
		B Sandstone	37.9	45.9	0.19	292.7
	5853 V	Mudstone Below	24.1	46.4	0.17	
		B Sandstone	37.9	52.6	0.19	326.5

TABLE 5.11

MECHANICAL ROCK PROPERTIES (DOWELL SCHUMBERGER) (CONCLUDED)

Well No.	Depth* (ft)	Zone	Confining Pressure (MPa)	Young's Modulus (GPa)	Poisson's Ratio	Compressive Strength (MPa)
			DYNAMIC MECHANICAL PROPERTIES			
MWX-1	5828 H	B Sandstone	20.7	34.0	0.26	--
MWX-2	5805 H	Mudstone	20.7	40.1	0.26	--
	5837 H	B Sandstone	20.7	35.5	0.17	--
	5857 H	Mudstone Below B Sandstone	20.7	57.5	0.20	--

* Indicates Depth and V-Vertical; H-Horizontal.
N Value measured normal to bedding plane.
P Value measured parallel to bedding plane.

TABLE 5.12

DERIVED COMPOSITE, CLAY-CORRECTED CEMENTATION AND SATURATION EXPONENTS

Interval	Well	Effective Overburden Pressure (psi)	Cementation Exponent m	Cementation Exponent m*	Saturation Exponent n	Saturation Exponent n*
Fluvial	MWX-1	0	1.72	1.92	1.37	1.83
		200	1.79	2.00		
		3000	1.89	2.08		
Coastal	MWX-1	0	1.74	1.96	1.85	2.55
		200	1.79	1.98		
		3200	1.88	2.09		
Paludal	MWX-2	0	1.82	2.03	1.08	1.47
		200	1.92	2.12		
		3600	1.95	2.17		

TABLE 5.13

LITHOLOGY OF ORGANIC-RICH CORE (AMOCO)

MWX-1 Depth (ft)	Sample Description
5460.5 - 5466	Coal; coal laminations included in siltstone
5580.0 - 5592.5	Shale; dark gray
5650.8 - 5652	Shale; dark gray
5736.5 - 5744	Shale; dark gray, abundant coal
5887.6 - 5888	Lignite; black to dark gray, greasy to waxy texture
5995.4 - 5997.8	Mudstone; carbonaceous, medium-dark gray, abundant coaly fragments

TABLE 5.14

LITHOLOGY OF ORGANIC-RICH CORE (COLORADO GS)

Depth (ft)	Sample Description
5432.9 - 5433.1	Coal, part fusinite (?), some vitrain
5460.6 - 5461	Gray siltstone with lenses of coal and carbonaceous shale at top and bottom
5768.8 - 5769.0	Dark gray carbonaceous shale with minor coal stringers
5887.8 chips	Dark gray to black carbonaceous shale with very thin coaly stringers
5975.7 - 5975.8	Brown to gray mudstone to siltstone with thick coal lenses on top and bottom

TABLE 5.15

CONCENTRATION (VOLUME PPM OF TOTAL SOLIDS) OF C1-C5+ HYDROCARGONS

	MWX-1			MWX-2			MWX-3	
Depth (ft):	5584.2	5585.0	5953.5	5707.0	5708.9	5854.1	5694.0	5849.5
Methane C1	3308	2133	2221	662	491	1135	2060	697
Ethane C2	2578	1820	174	1794	1982	93	1245	852
Propane C3	1934	1288	63	1265	1026	339	681	508
Isobutane iC4	232	183	31	220	112	135	68	82
Butane nC4	257	163	20	220	169	163	92	89
- C5+	258	115	457	415	182	325	91	70

TABLE 5.16

ROCK EVALUATION PYROLYSIS DATA FROM THE FLUVIAL INTERVAL

Depth (ft)	Total Organic Carbon (%)	Gas Evolved* (mg/gm rock) S_1	S_2	S_3	T(max) (°C)
MWX-1					
5584.2	0.46	0.01	-	0.34	-
5585.0	0.43	0.01	-	0.34	-
5953.5	0.86	0.27	0.32	0.33	471
5570.5	0.43	0.04	0.14	0.09	472
5585.0	0.41	0.03	0.10	0.06	471
5697.0	0.25	0.01	0.01	0.10	359
5744.0	0.88	0.09	0.34	0.08	471
5771.0	0.50	0.06	0.24	0.09	389
5974.5	0.39	0.01	0.05	0.09	405
MWX-2					
5707.0	0.45	0.06	-	0.29	-
5741.0	0.71	0.20	0.23	0.23	469
5776.0	0.90	0.16	0.41	0.21	475
5825.0	0.33	0.05	-	0.14	-
5854.0	0.51	0.06	-	0.20	-
5854.1	0.54	0.12	-	0.19	-
MWX-3					
5817.2	0.33	0.09	0.06	0.08	436
5847.5	0.77	0.24	0.22	0.15	479
5849.5	0.24	0.05	0.03	0.11	423
5863.2	0.39	0.04	0.05	0.08	412

*S_1 Free hydrocarbons present
S_2 Hydrocarbons produced by thermal conversion of kerogen
S_3 Organic carbon dioxide produced by pyralysis of kerogen

TABLE 5.17

DIRECTIONAL PERMEABILITIES (MWX-3)

Interval	Depth (ft)	Net Confining Stress (psi)	Dry Klinkenberg Permeability to Air (μd) N80°W	N10°E	Vertical	N10°E / N80°W
Fluvial	5737	3800	1.22	2.16	1.88	1.77
	5830	3800	2.51	3.75	4.93	1.49
Coastal	6446	4000	1.77	1.88	1.16	1.06
	6514	4000	0.89	1.20	0.74	1.35
Paludal	7090	4200	1.40	1.95	0.56	1.39
	7131	4200	9.2	11.3	7.0	1.23

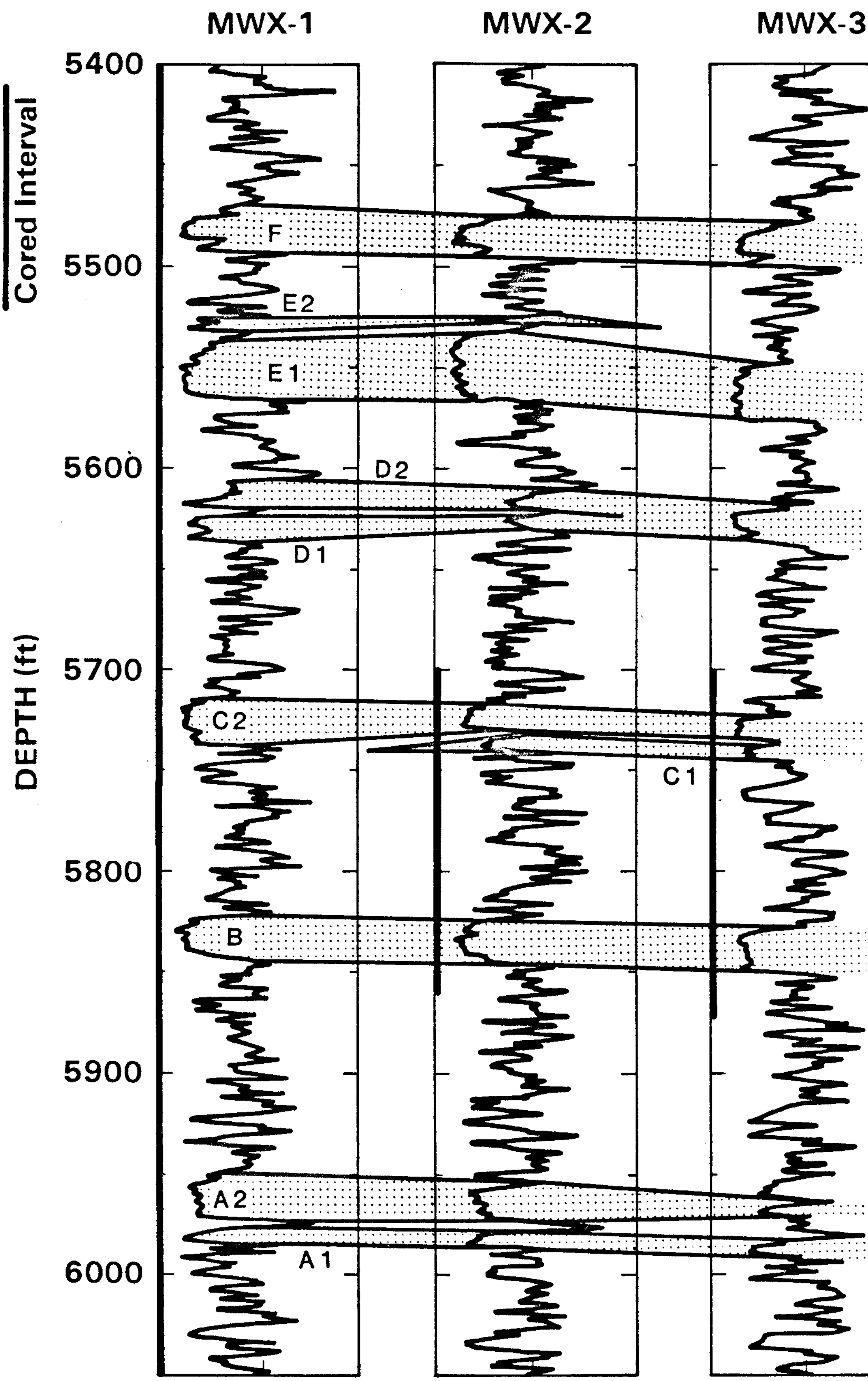

Figure 5.1. Lower Fluvial Zone, A-F Sandstones

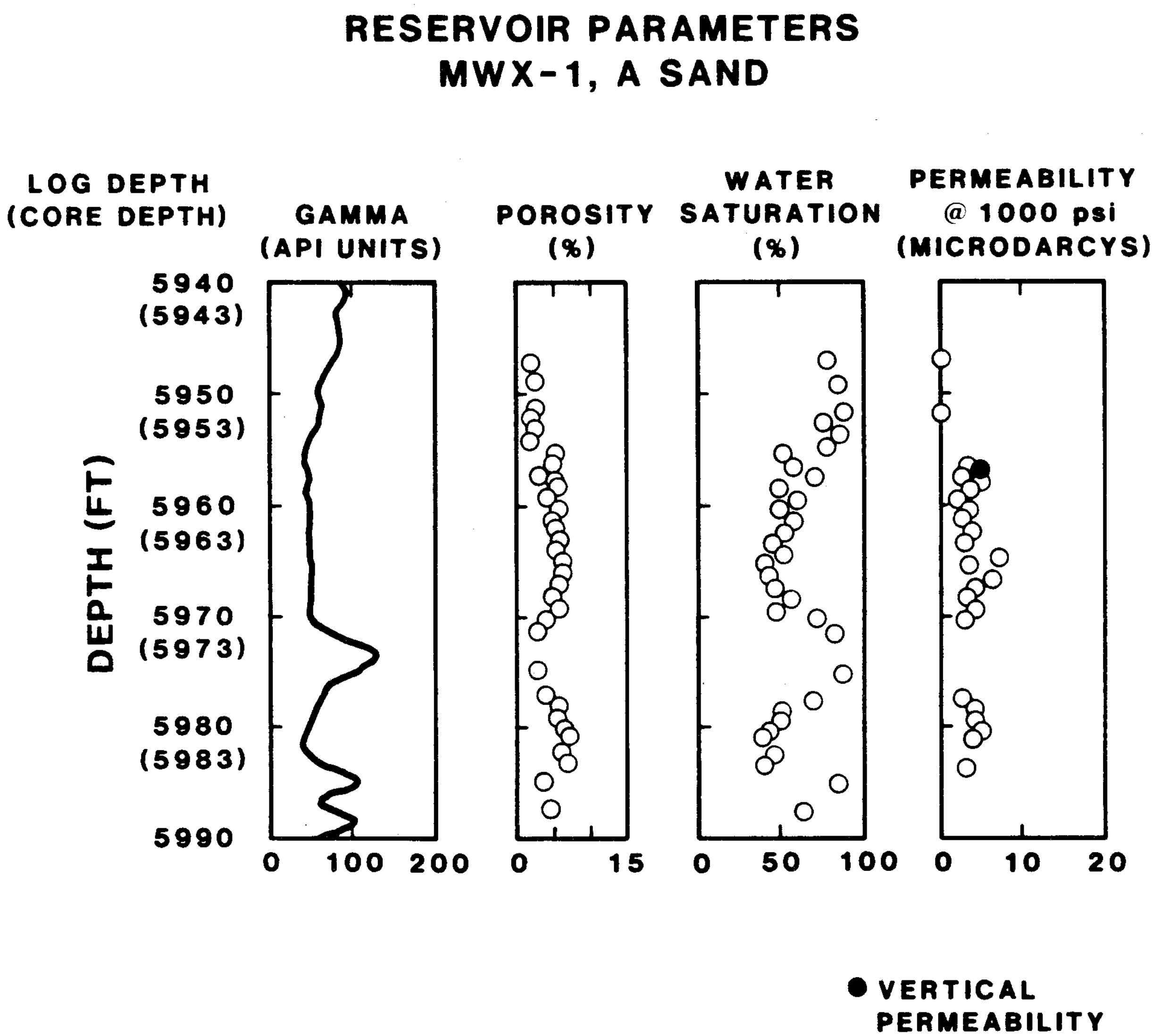

Figure 5.2. Reservoir Properties, A Sandstone, MWX-1

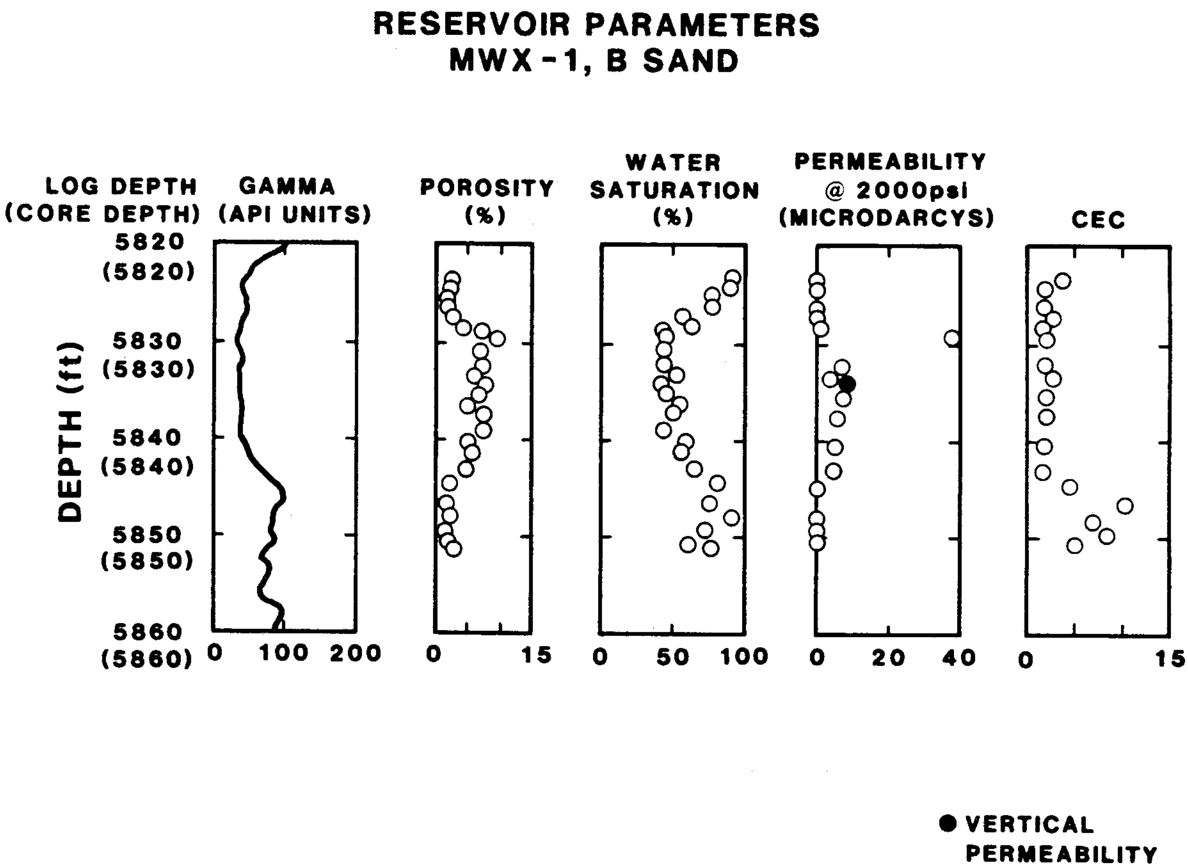

Figure 5.3. Reservoir Properties, B Sandstone, MWX-1

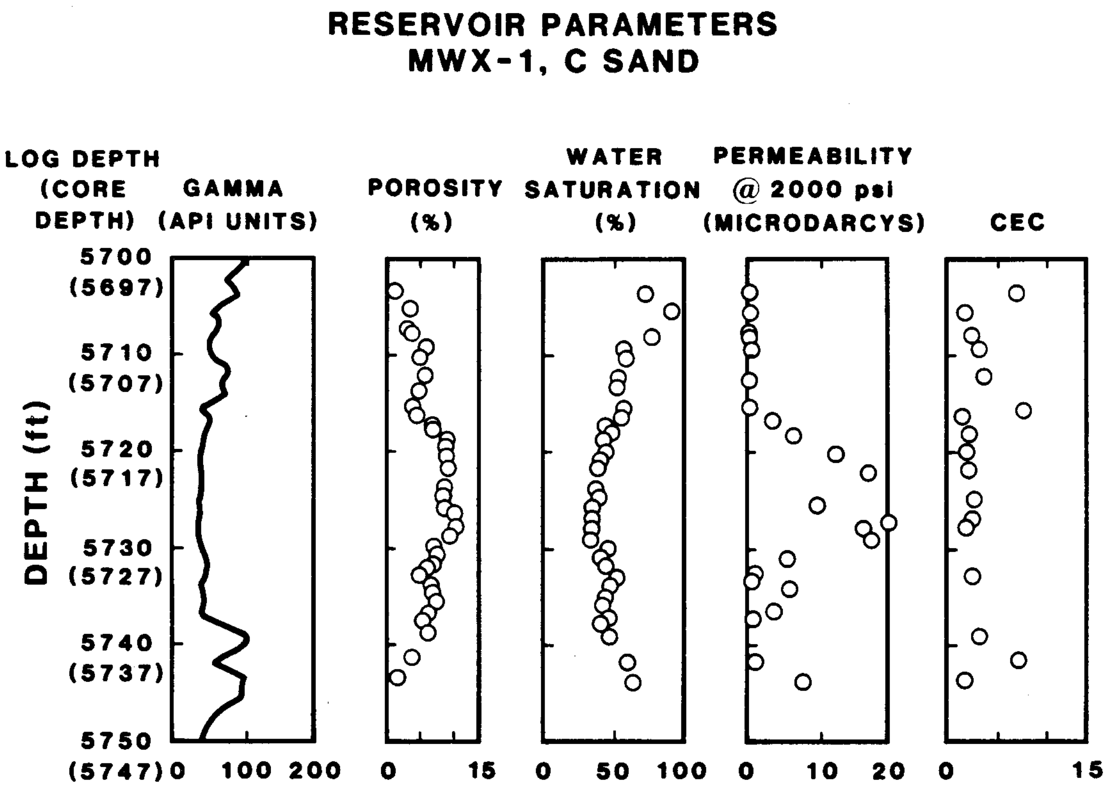

Figure 5.4. Reservoir Properties, C Sandstone, MWX-1

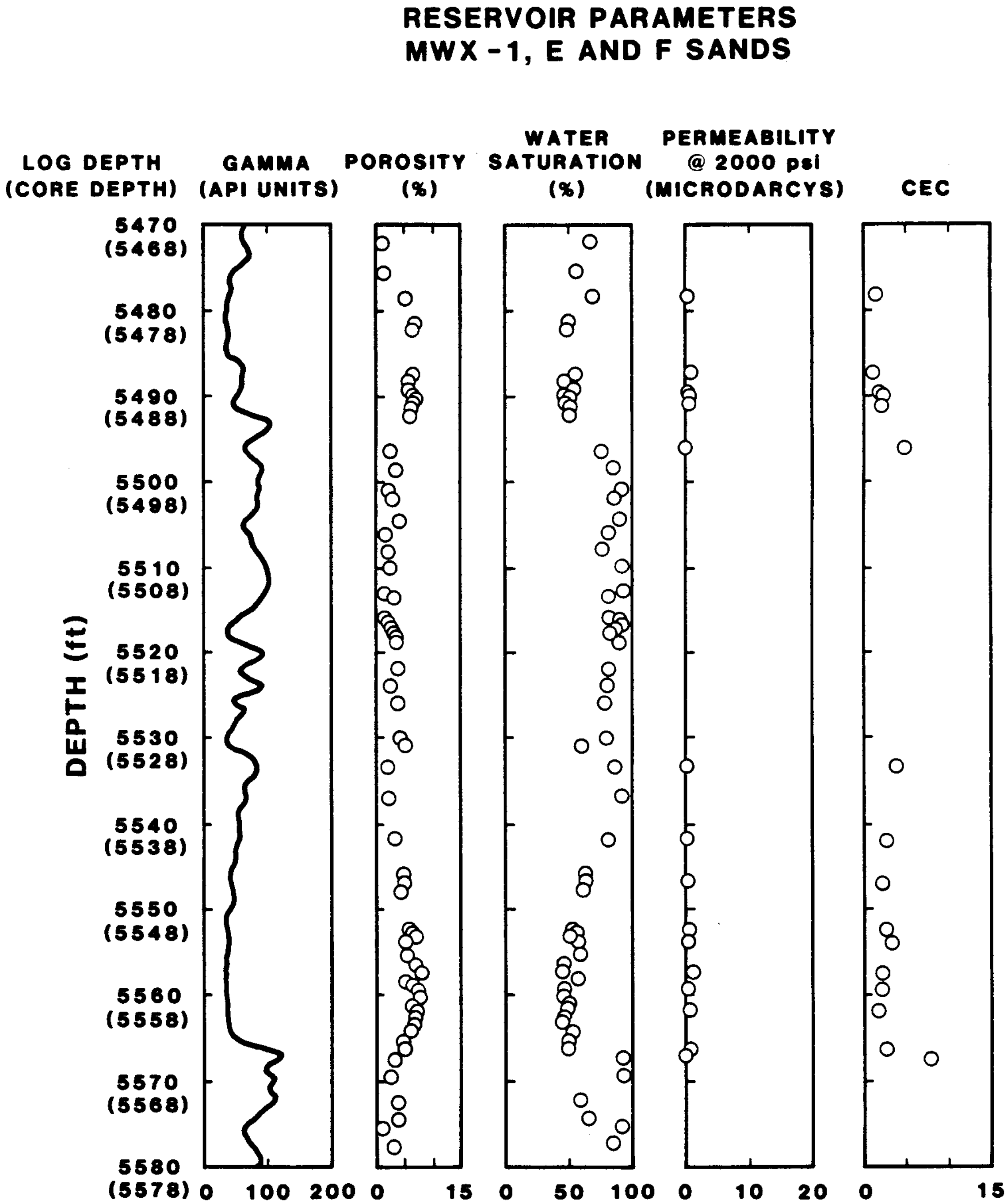

Figure 5.5. Reservoir Properties, E and F Sandstones, MWX-1

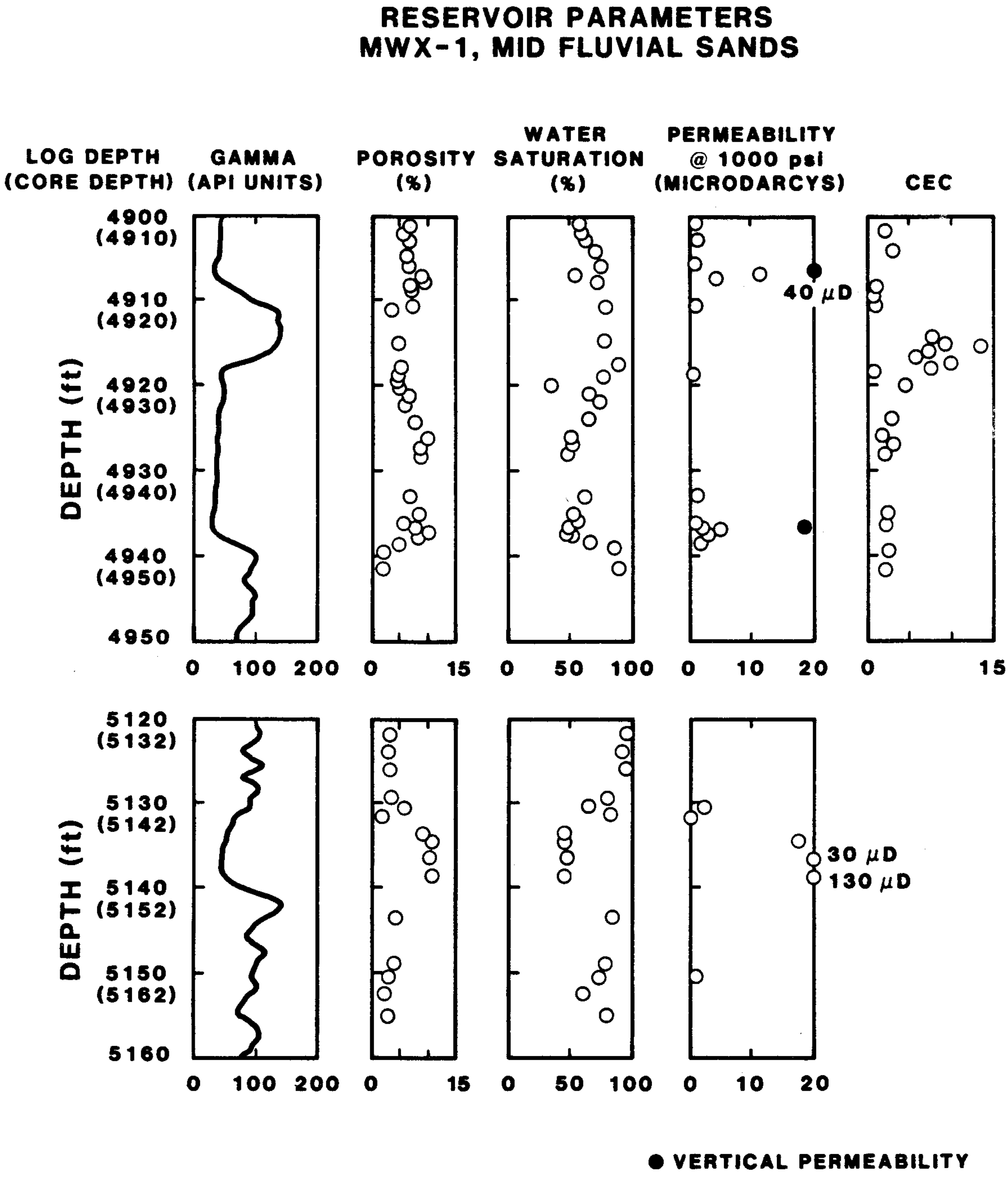

Figure 5.6. Reservoir Properties, Mid Fluvial Sandstones, MWX-1

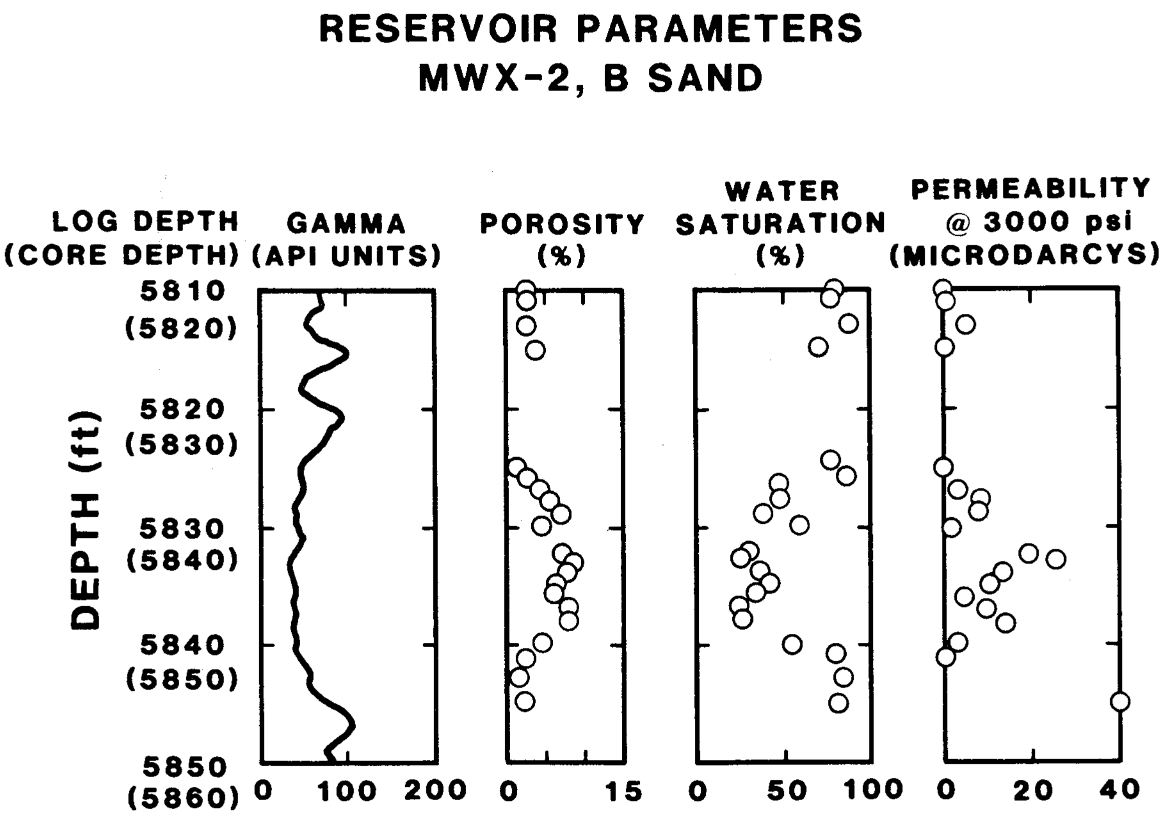

Figure 5.7. Reservoir Properties, B Sandstone, MWX-2

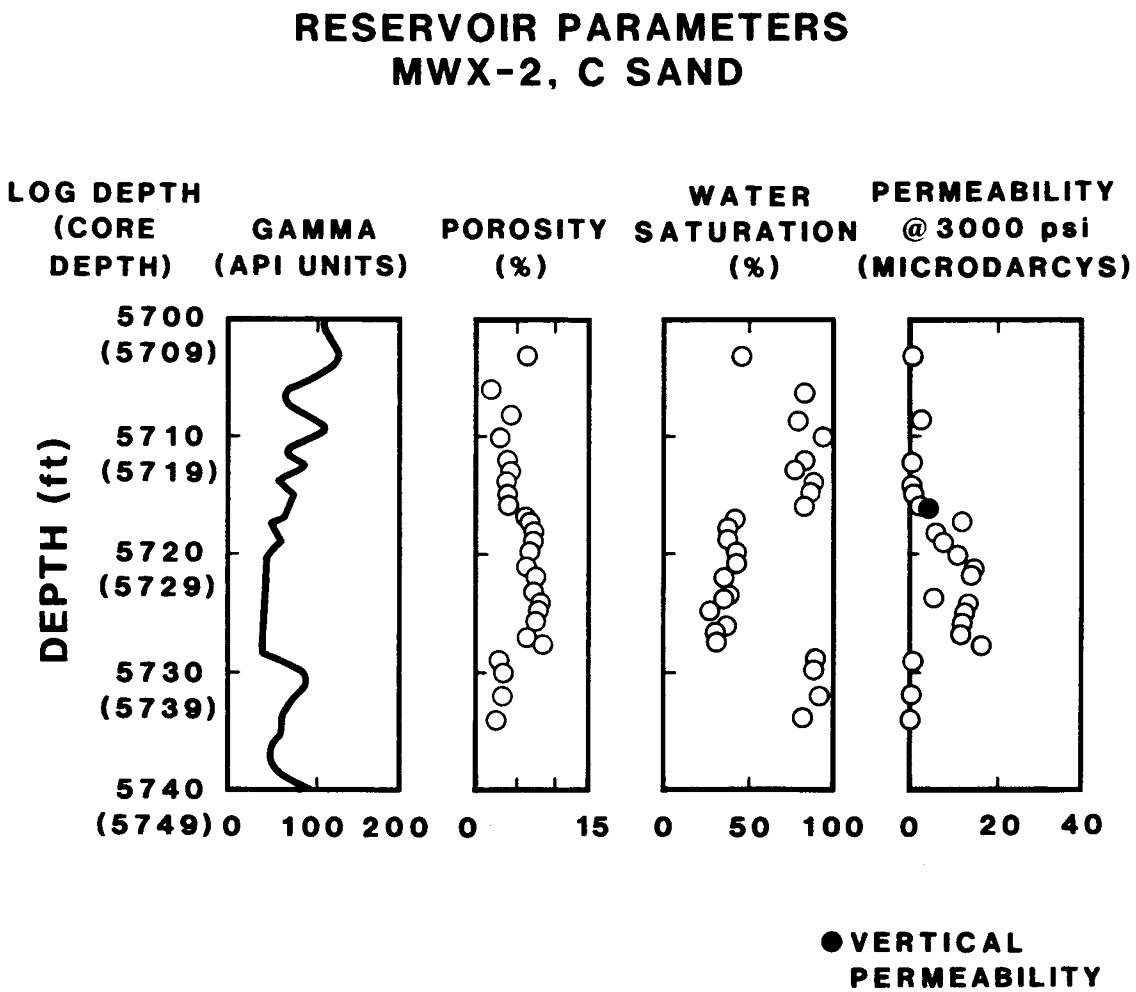

Figure 5.8. Reservoir Properties, C Sandstone, MWX-2

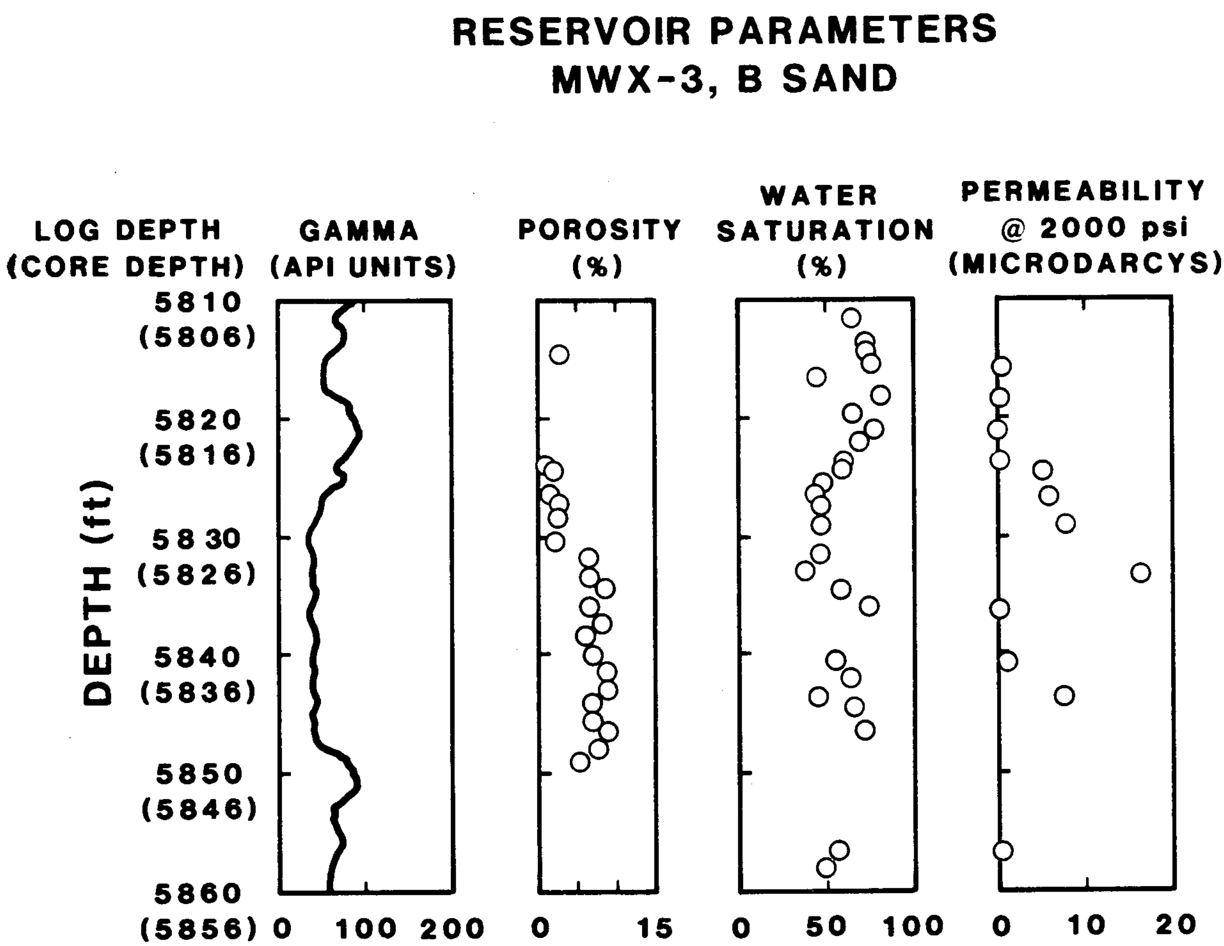

Figure 5.9. Reservoir Properties, B Sandstone, MWX-3

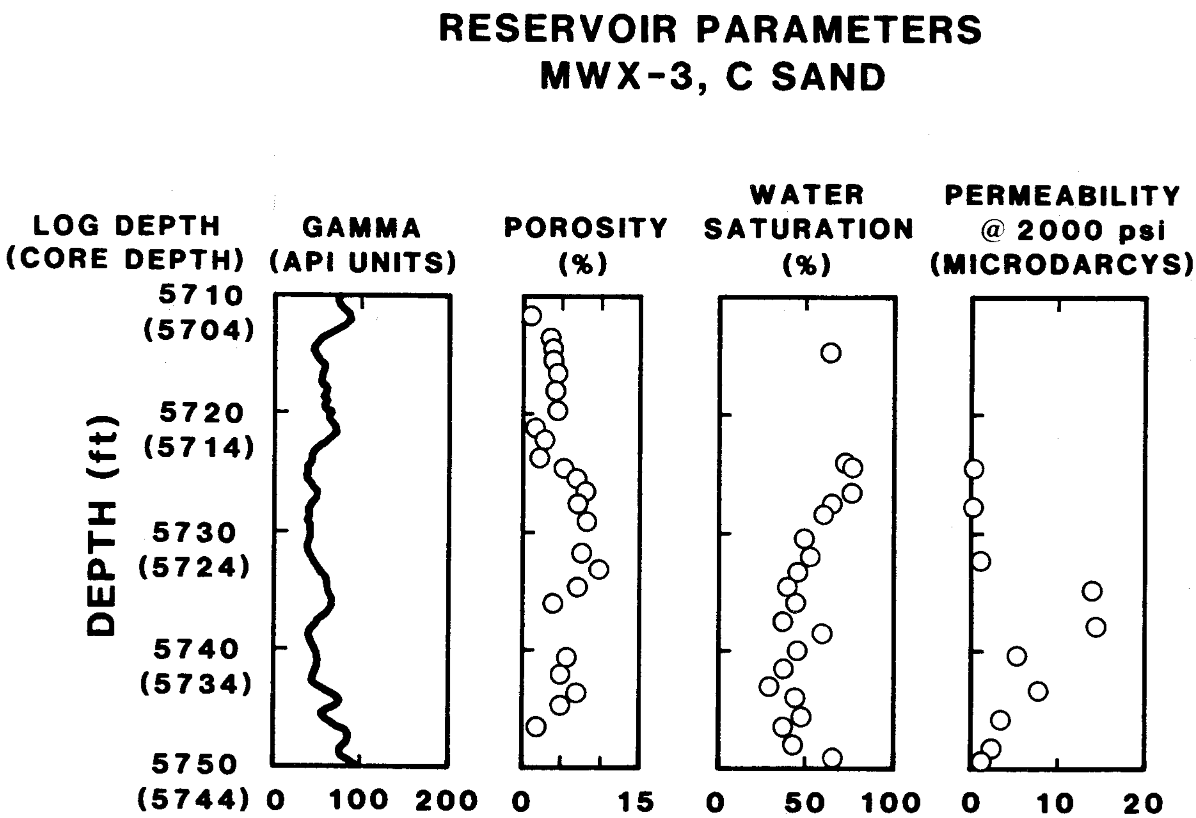

Figure 5.10. Reservoir Properties, C Sandstone, MWX-3

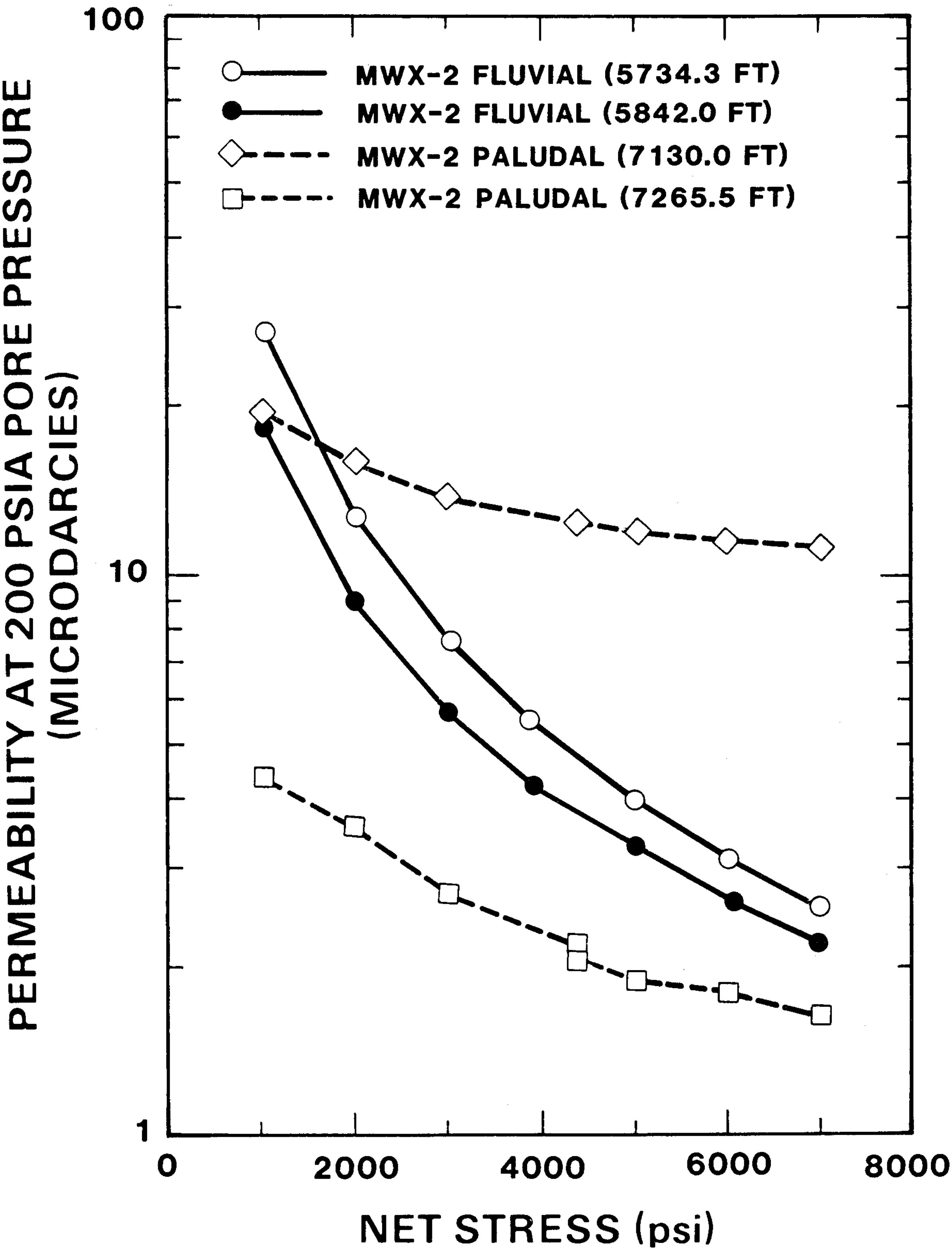

Figure 5.11. Permeability as a Function of Net Confining Stress

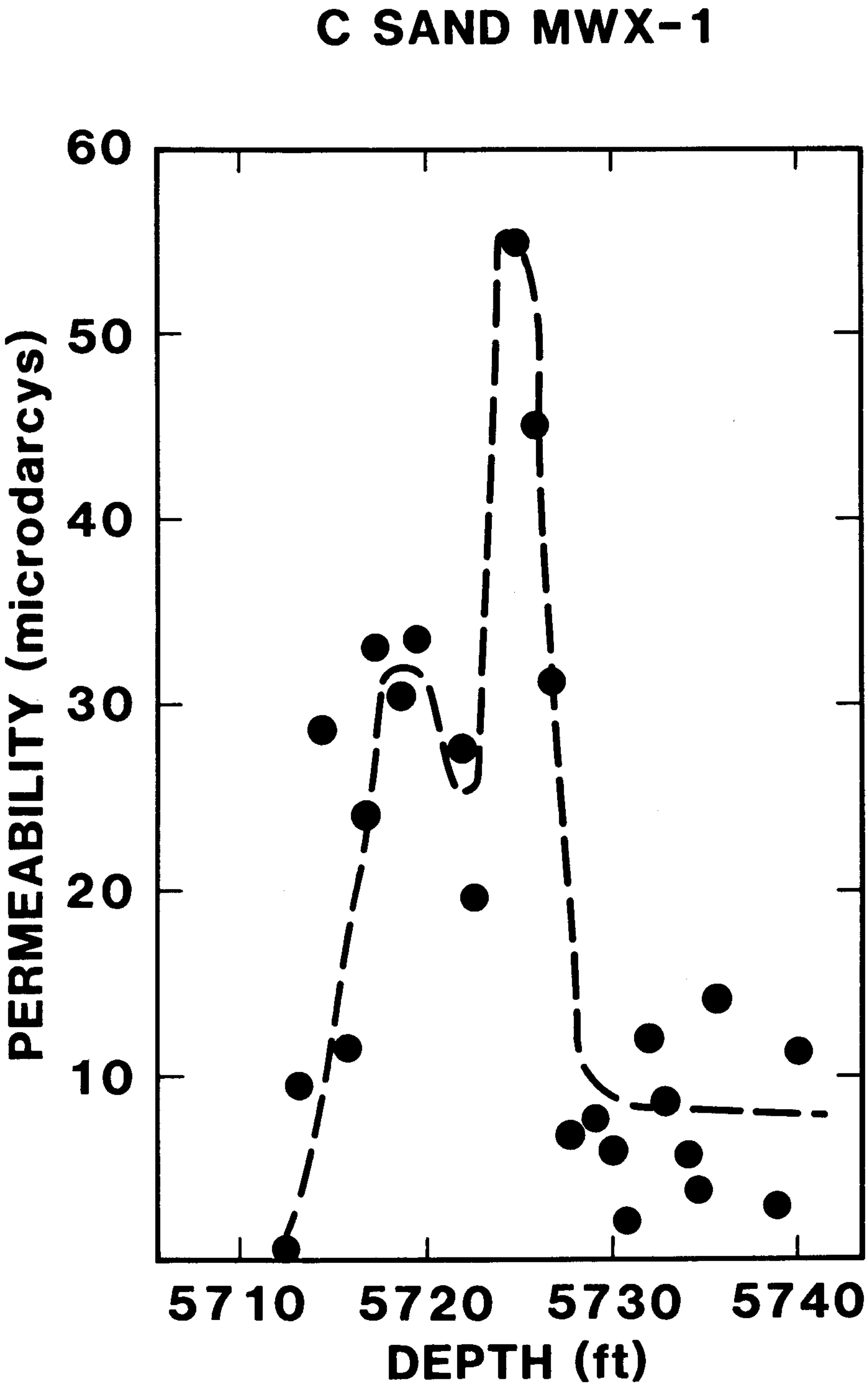

Figure 5.12. Permeability Streak in Lower Fluvial Zone

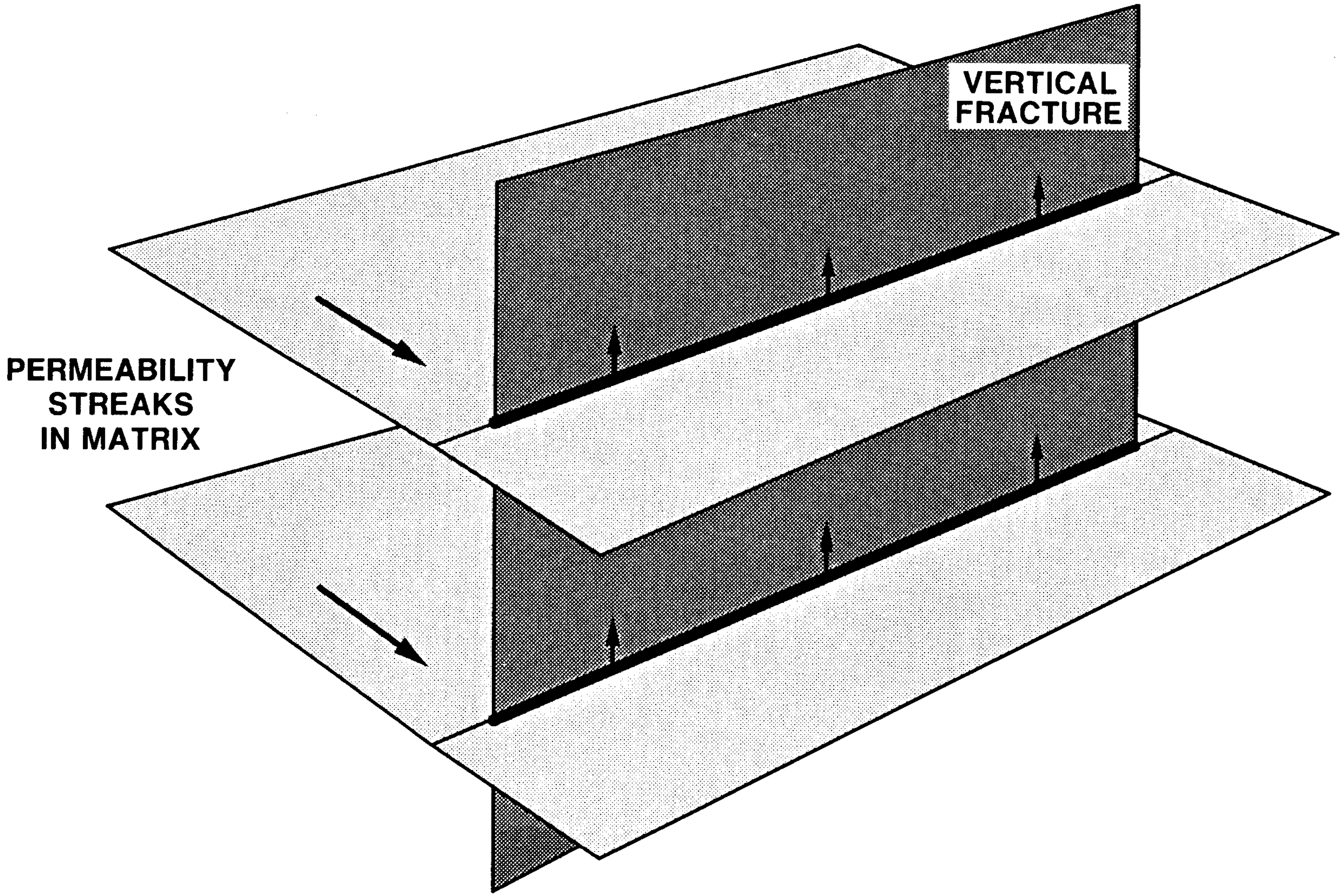

Figure 5.13. Schematic of Interaction Between Permeability Streaks and Vertical Fractures

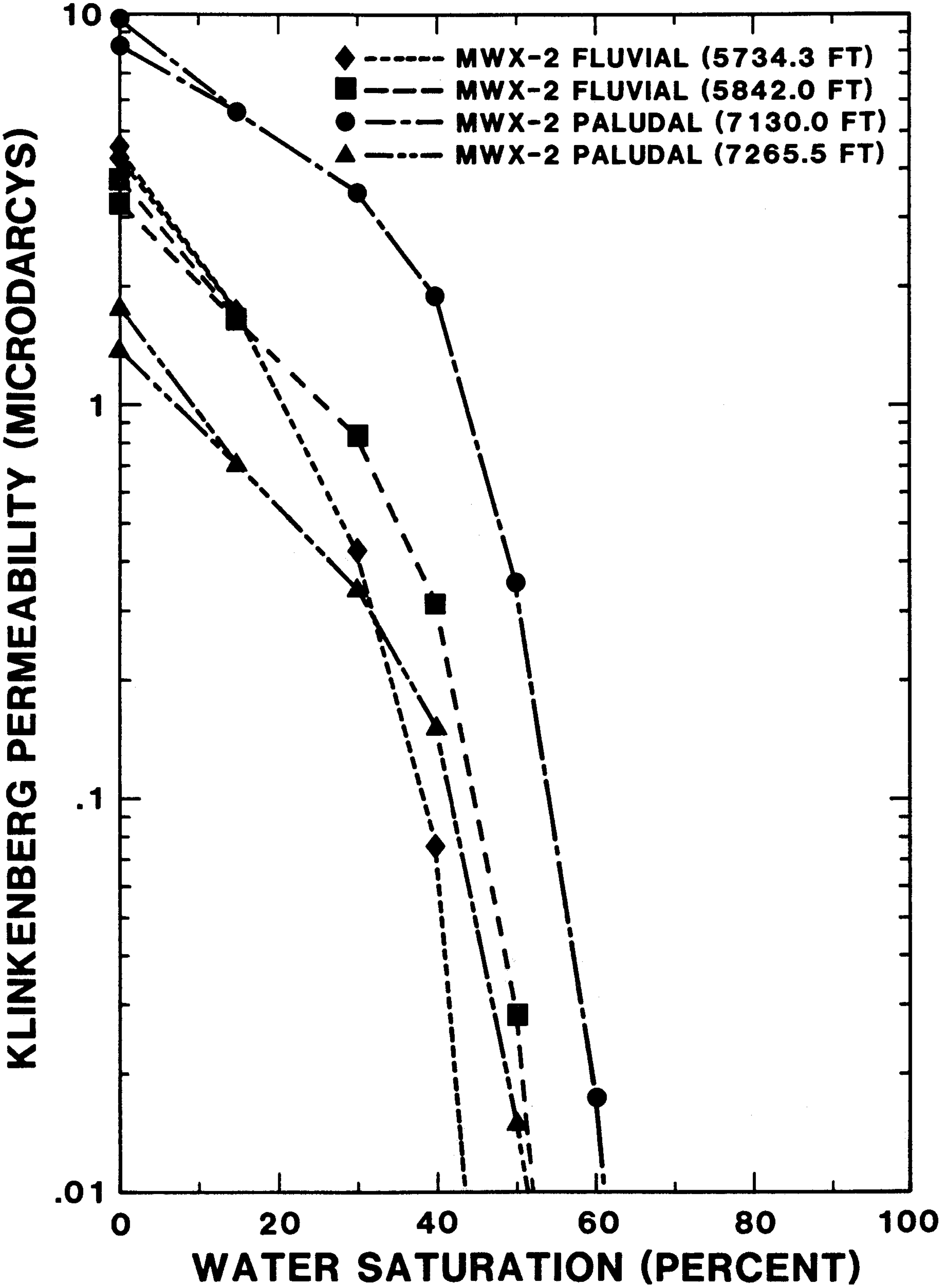

Figure 5.14. Permeability as a Function of Water Saturation

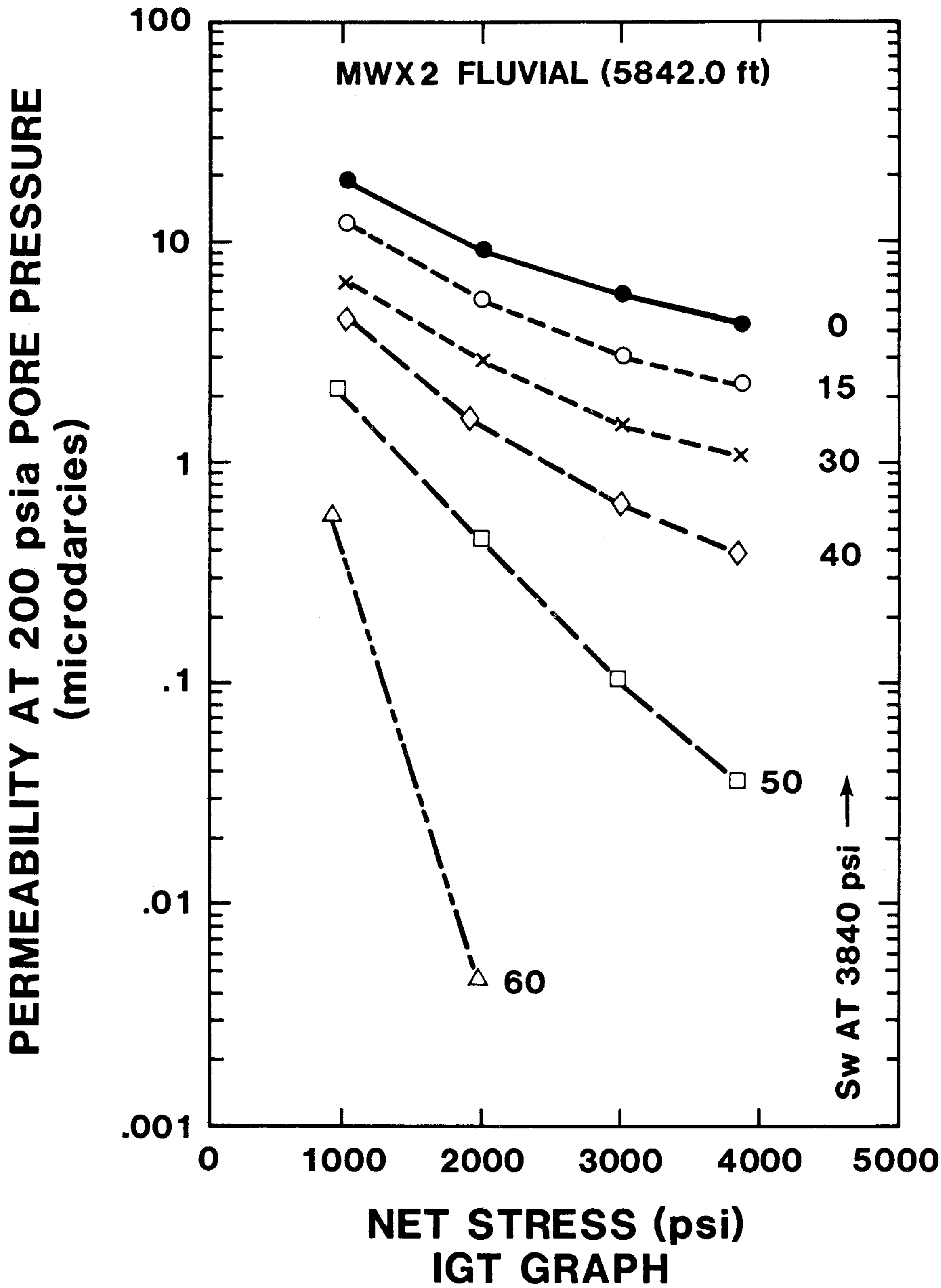

Figure 5.15. Permeability as a Function of Net Stress for Different Water Saturations

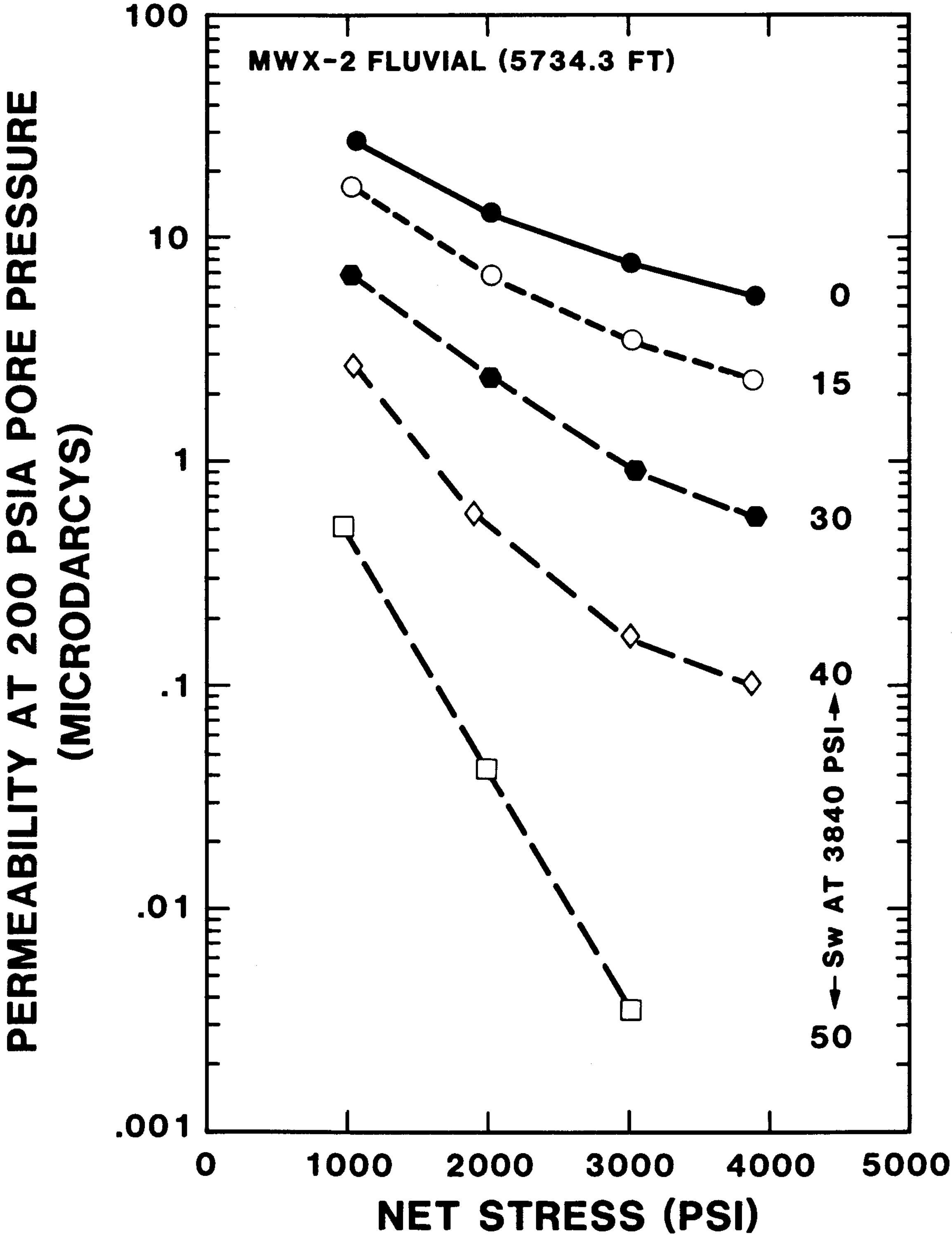

Figure 5.16. Permeability as a Function of Net Stress for Different Water Saturations

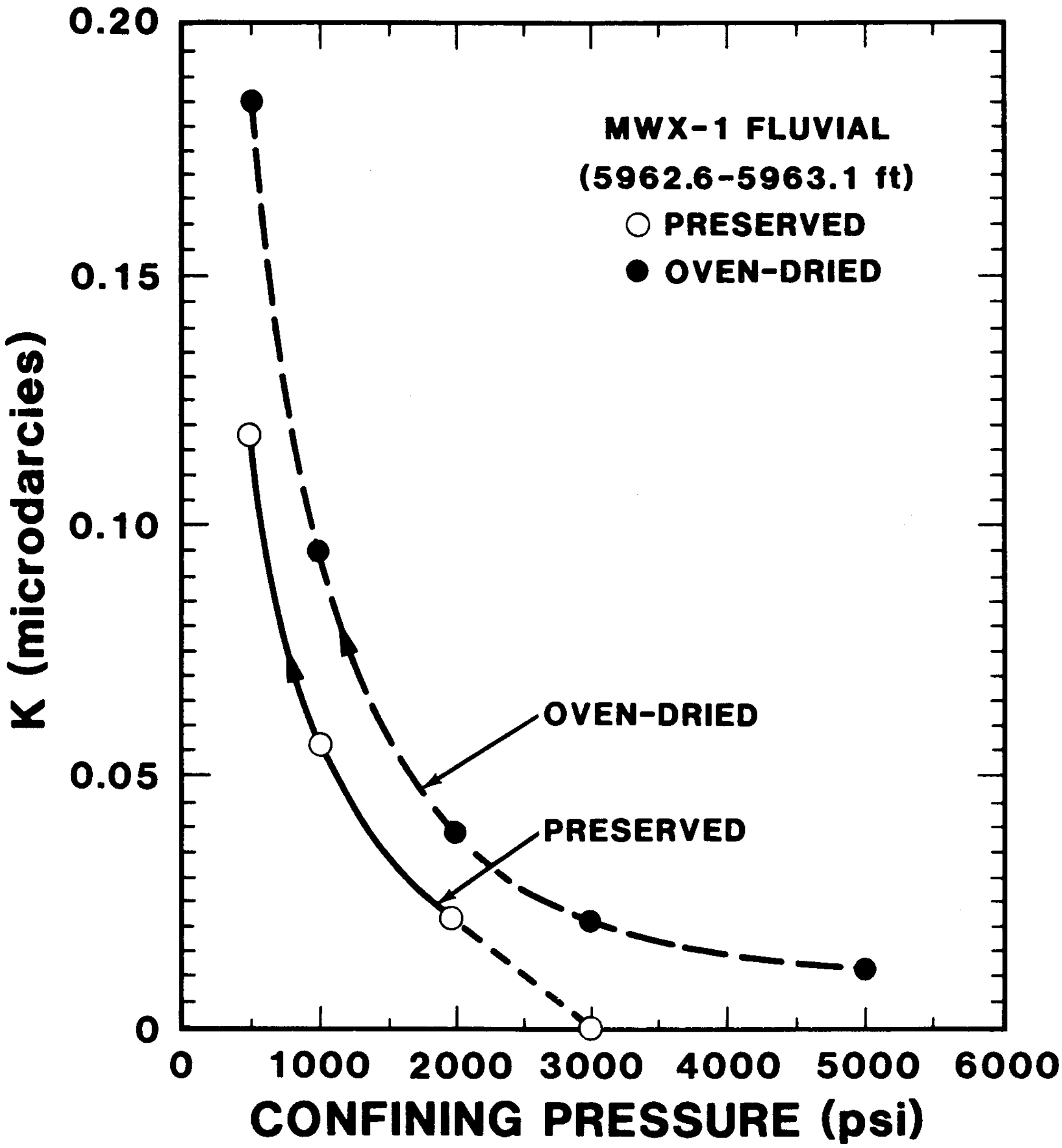

Figure 5.17. Increase in Permeability Caused by Oven Drying

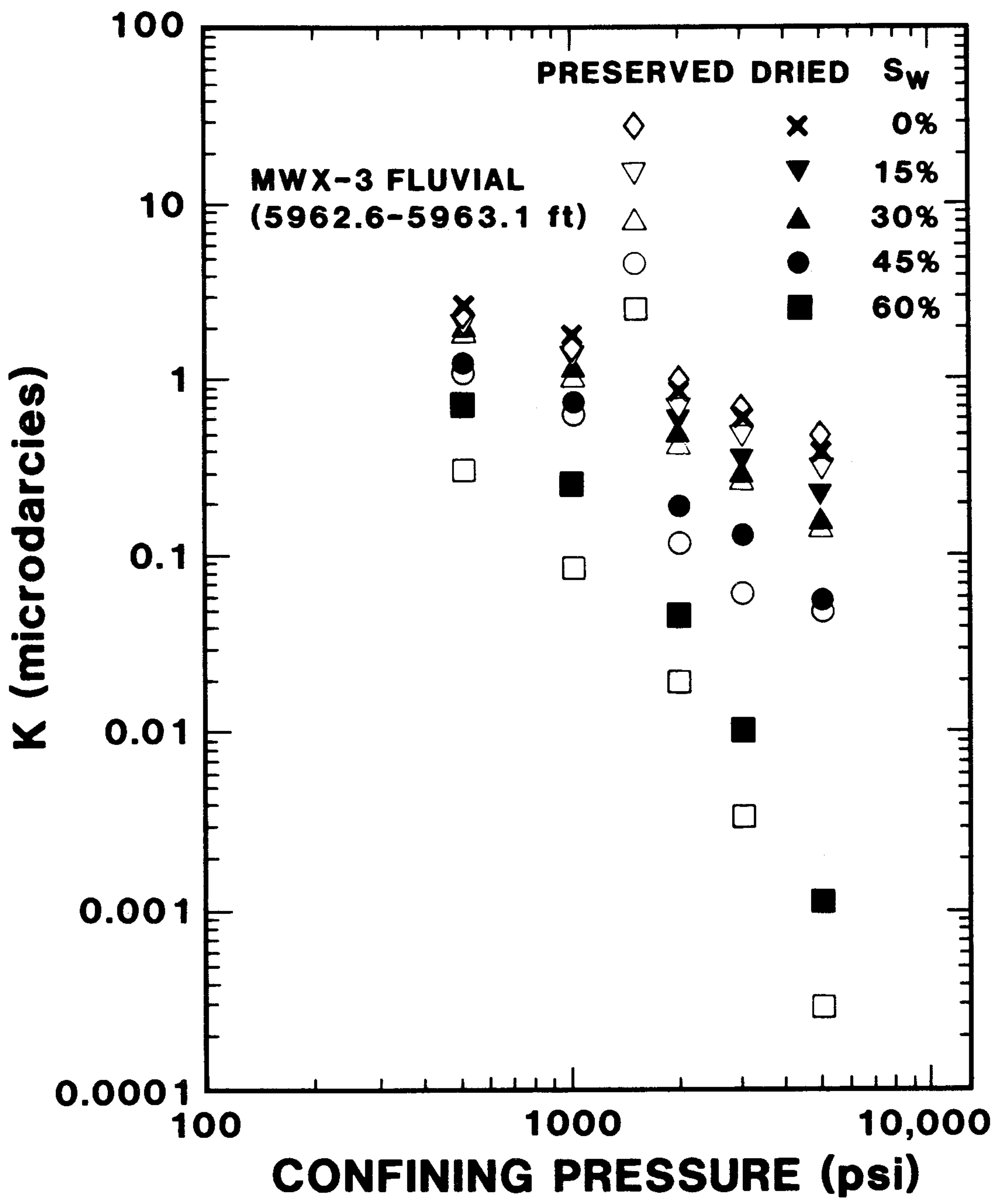

Figure 5.18. Relative Permeabilities to Gas for Preserved vs. Oven-Dried Core

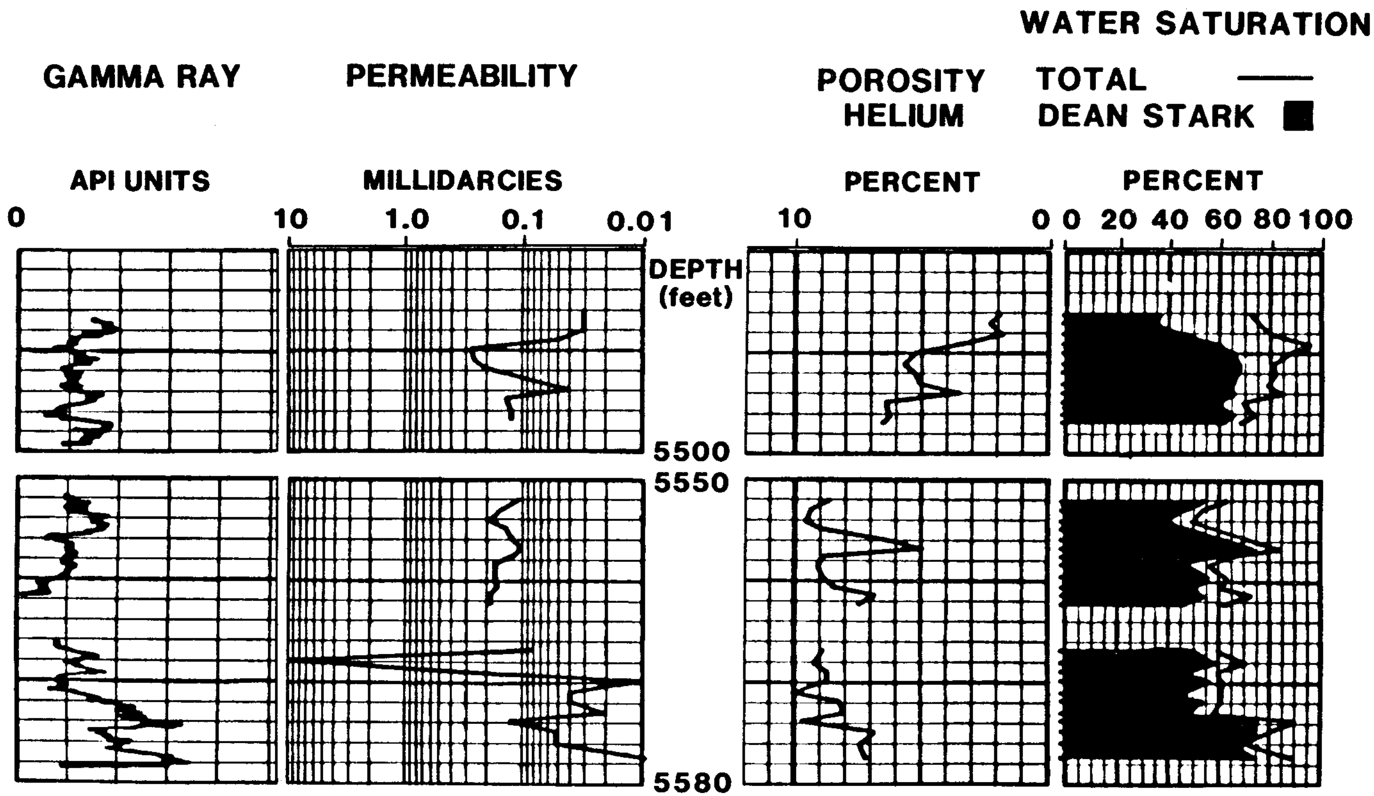

Figure 5.19. Pressure Core Results, E and F Sandstones MWX-2

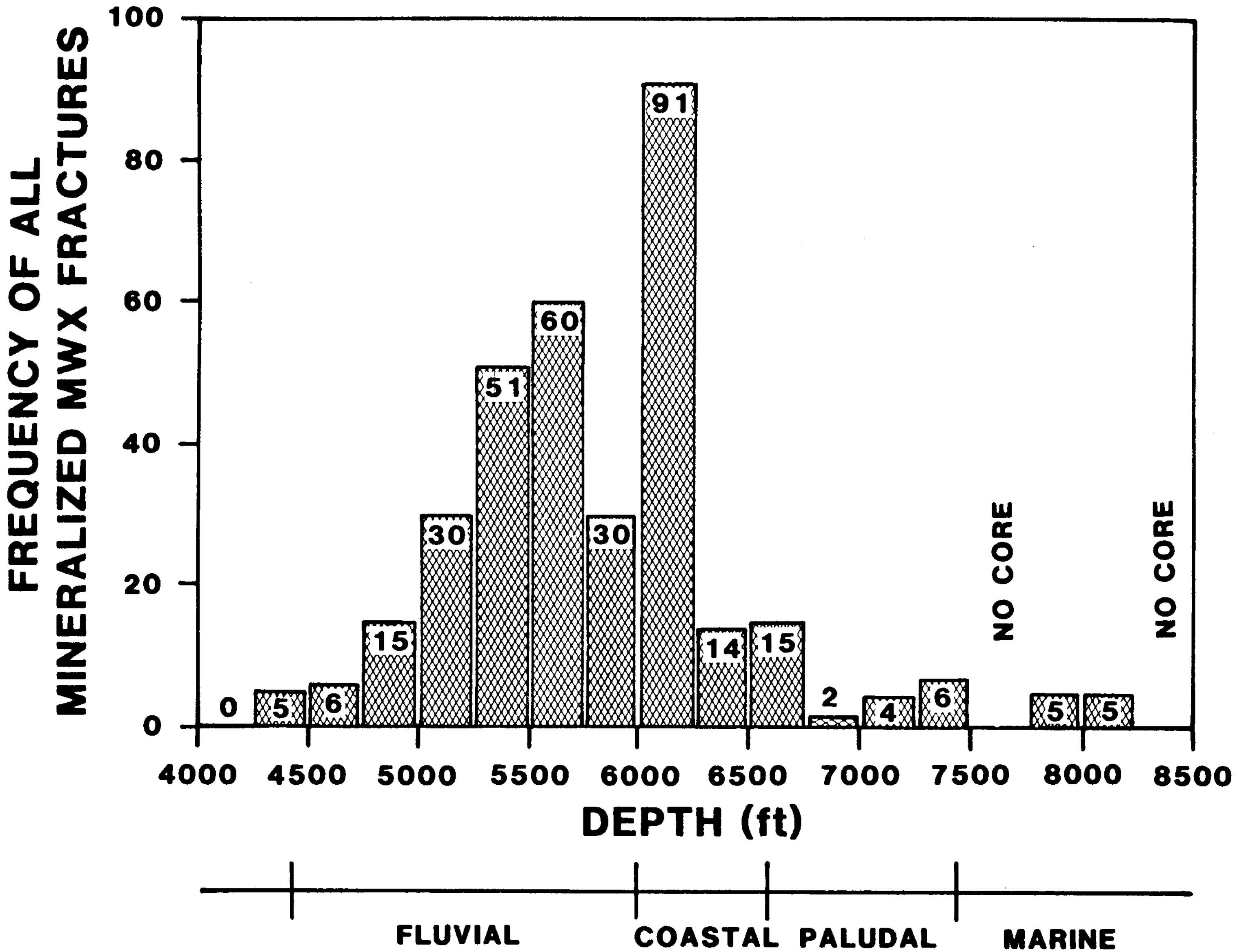

Figure 5.20. Histogram of all Natural Fractures vs. Depth at MWX

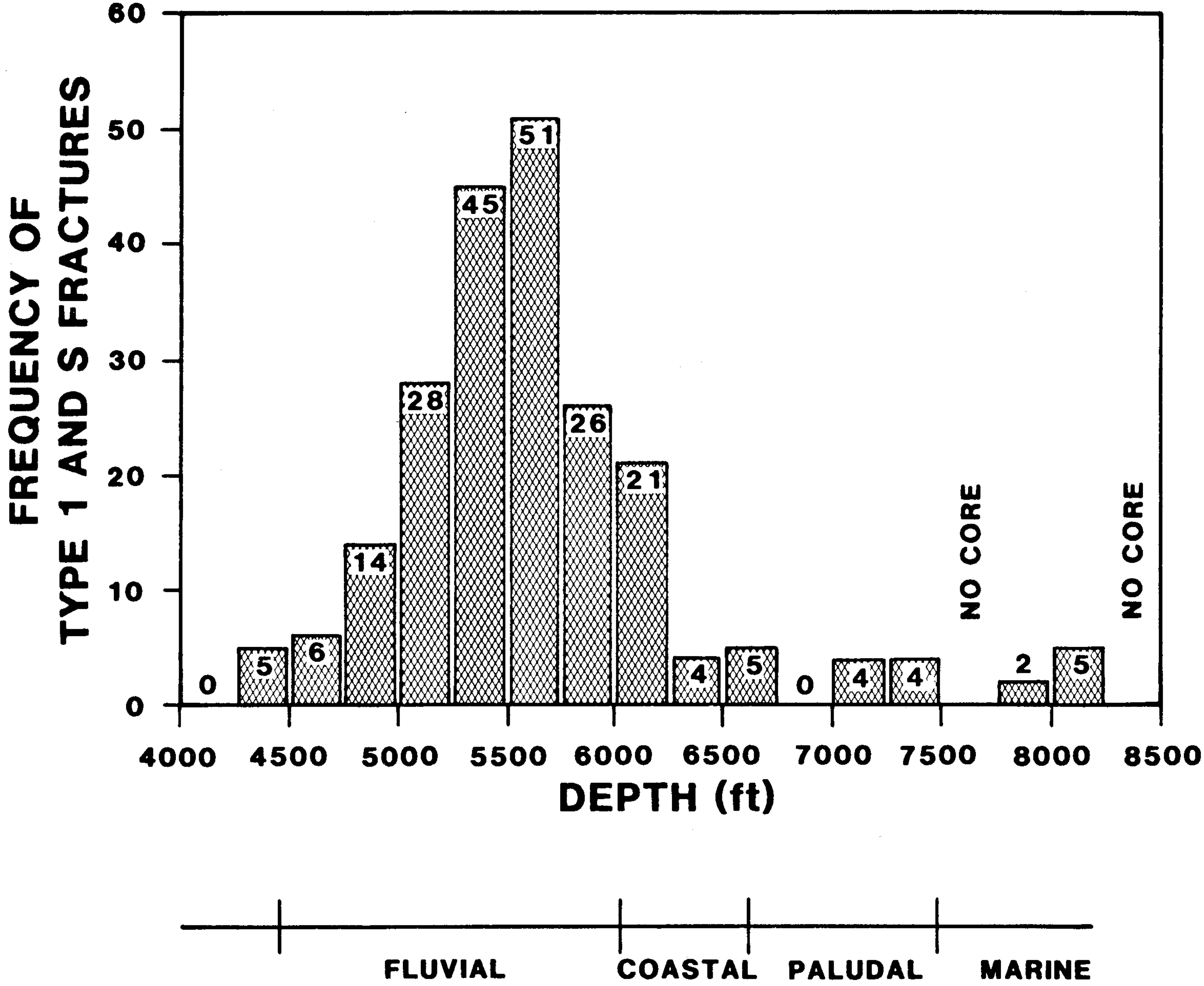

Figure 5.21. Histogram of all Extension Fractures vs. Depth at MWX

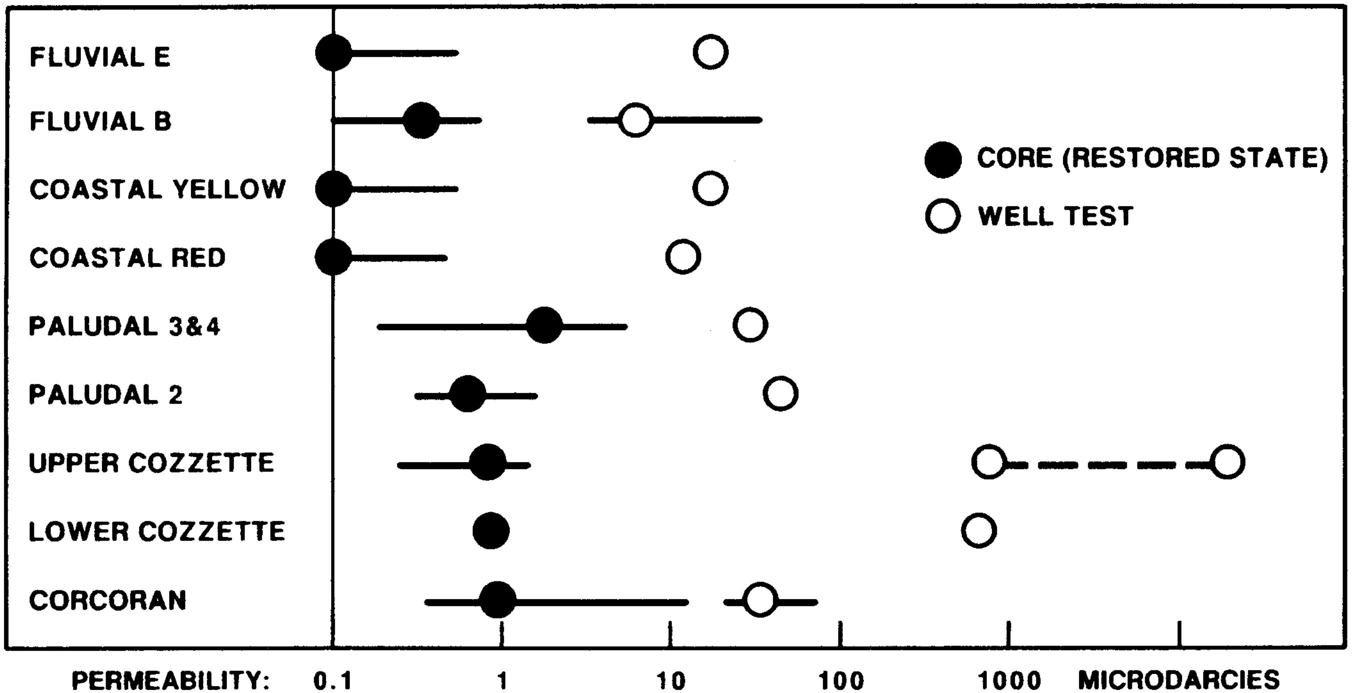

Figure 5.22. Matrix vs. Well Test Permeability for MWX-1 Sandstones

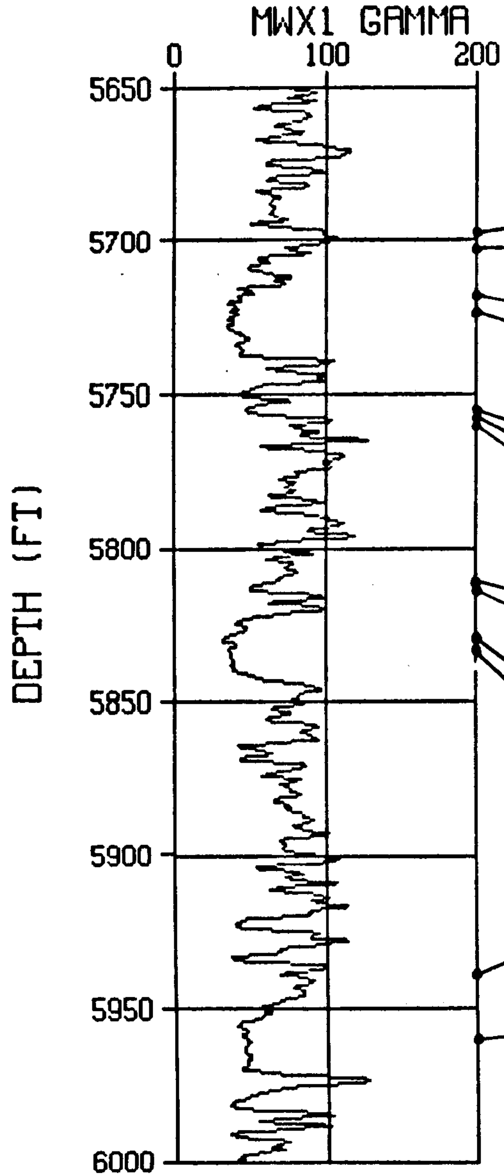

Lithology	Core Interval (Feet) [~Log Depth]	Brazilian Tests: Tensile Strength (MPa)	Triaxial Tests: Confining Pressure (MPa)	Triaxial Tests: Compressive Strength^a (MPa)	Triaxial Tests: E^b (GPa)	Triaxial Tests: ν^b	Fracture Toughness K_{IC} (MPa·m$^{-1/2}$)
(1) Siltst/Mudst	(1) 5693.6-5694.1* [5697.6-5698.1]	-10.85±2.13(2)	0	-	-	-	1.17±0.05(1)
(2) Siltst/Mudst	(2) 5699.9-5700.8] [5703.9-5704.8]		10(2)	312.1	51.2	.17	
			20(2)	347.7	54.5	.16	
			30	-	-	-	
(1) Sandst	(1) 5716.5-5717.3 [5717.5-5718.3]	-7.68±0.67(1)	0	-	-	-	1.10±0.08(1&2)
(2) Sandst	(2) 5722.2-5723.5 [5723.2-5724.5]		10(2)	149.6	25.0	.19	
			20(2)	199.6	28.3	.23	
			30(2)	213.4	28.9	.18	
			50	-	-	-	
(1) Siltst/Mudst	(1) 5755.6-5756.7 [5756.6-5757.7]	-7.00±0.19(2)	0	-	-	-	1.18 (3)
(2) Mudst	(2) 5757.0-5757.6 [5758.0-5758.6]		10(2)	180.7	25.4	.19	
(3) Mudst	(3) 5757.6-5758.4 [5758.6-5759.4]		20(1)	202.4	24.6	.20	
			30(1)	224.8	25.5	.24	
			50(1)	-	-	-	
(1) Sandst	(1) 5814.2-5815.4* [5812.2-5813.4]	-16.30±1.70(1)	0(2)	59.6	15.3	.31	1.97±0.04(1)
(2) Mudst	(2) 5815.4-5816.0* [5813.4-5814.0]		10(2)	81.8	13.9	.25	
			20(2)	100.4	12.4	.22	
			30(2)	108.4	12.8	.23	
			50	-	-	-	
(1) Sandst	(1) 5831.5-5832.5 [5829.5-5830.5]	-6.62±0.50(2)	0(2)	92.5	17.7	.22	1.25±0.08(1)
(2) Sandst	(2) 5835.2.5836.3* [5833.2-5834.3]		10(2)	153.8	26.7	.20	
			20(2)	182.3	29.0	.21	
			30(2)	201.6	30.2	.20	
			50(2)	286.2	32.8	.20	
Siltst	5940.6-5941.2 [5938.6-5939.2]	-	0	-	-	-	
			10	191.5	43.9	.09	
			20	202.1	31.8	.08	
			30	279.5	42.5	.15	
			50	-	-	-	
Sandst	5963.1-5964.0 [5961.1-5962.0]	-	0	-	-	-	
			10	194.2	35.0	.18	
			20	233.3	34.7	.15	
			30	261.0	34.5	.15	
			50	-	-	-	

* Sealed at Well
a Ultimate Axial Stress Difference
b Calculated for Stresses Between 20 and 60 Percent of Ultimate Axial Stress Difference

Figure 5.23. Rock Property Data for MWX-1

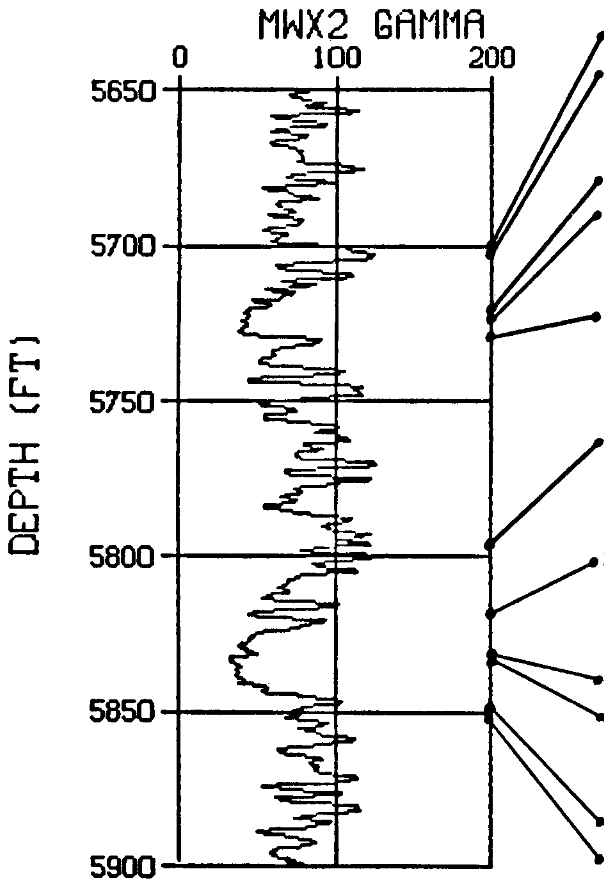

Lithology	Core Interval (Feet) [~Log Depth]	Brazilian Tests: Tensile Strength (MPa)	Triaxial Tests: Confining Pressure (MPa)	Triaxial Tests: Compressive Strength[a] (MPa)	Triaxial Tests: B^b (GPa)	Triaxial Tests: ν^n	Fracture Toughness K_{IC} ($MPa \cdot m^{-1/2}$)
(1) Mudst	(1) 5710.4-5711.0*	-16.01±4.54(2)	0	-	-	-	2.38±0.55(2)
	[5700.4-5701.0]						
(2) Siltst	(2) 5712.7-5713.7*		10(1)	50.7	13.2	.23	
	[5702.7-5703.7)		20(1)	61.0	13.2	.42	
			30(2)	332.8	43.3	.20	
			50	-	-	-	
(1) Sandst	(1) 5730.2-5731.0	-8.62±0.11(1)	0(1)	103.3	19.8	.18	1.28±0.20(2)
	[5720.2-5721.0]						
(2) Sandst	(2) 5733.0-5734.0*		10(2)	146.4	26.4	.18	
	[5723.0-5724.0]		20(1)	206.4	30.8	.18	
			30(2)	211.8	29.7	.22	
			50(1)	309.9	33.2	.28	
Silty Mudst	5738.0-5739.0*	-6.13±1.04	0	-	-	-	0.74±0.07
	[5729.0-5730.0]		10	95.2	22.6	.24	
			20	119.9	21.5	.20	
			30	137.3	21.2	.24	
			50	-	-	-	
Siltst	5806.4-5807.5*	-15.63±5.43	0	119.9	48.1	.17	0.80±0.11
	[5796.4-5797.5]		10	268.0	55.4	.16	
			20	269.6	53.6	.17	
			30	343.1	57.0	.21	
			50	-	-	-	
Muddy Siltst	5829.0-5830.1*	-11.75±2.81	0	-	-	-	1.03±0.20
	[5819.0-5820.1]		10	87.6	20.6	.28	
			20	-	19.2	.21	
			30	164.8	26.4	.18	
			50	-	-	-	
(1) Sandst	(1) 5842.2-5843.1*	-6.38±0.13(2)	0(2)	47.3	8.7	.18	1.24±0.11(1)
	[5832.2-5833.1]						
(2) Sandst	(2) 5843.1-5843.9		10(1)	157.1	30.5	.22	
	[5833.1-5833.9]		20(1)	207.8	41.0	.24	
			30(1)	230.1	33.5	.17	
			50	-	-	-	
(1) Siltst	(1) 5858.4-5859.4*	-9.27±1.16(2)	0(2)	72.7	19.9	.15	2.34±0.32(1)
	[5848.4-5849.4]						
(2) Silty Mudst	(2) 5861.8-5862.7*		10(1)	168.7	38.9	.15	
	[5851.8-5852.7]		20(1)	175.4	38.9	.14	
			30(1)	196.0	38.2	.15	
			50(2)	204.0	19.6	.22	

* Sealed at Well
a Ultimate Axial Stress Difference
b Calculated for Stresses Between 20 and 60 Percent of Ultimate Axial Stress Difference

Figure 5.24. Rock Property Data for MWX-2

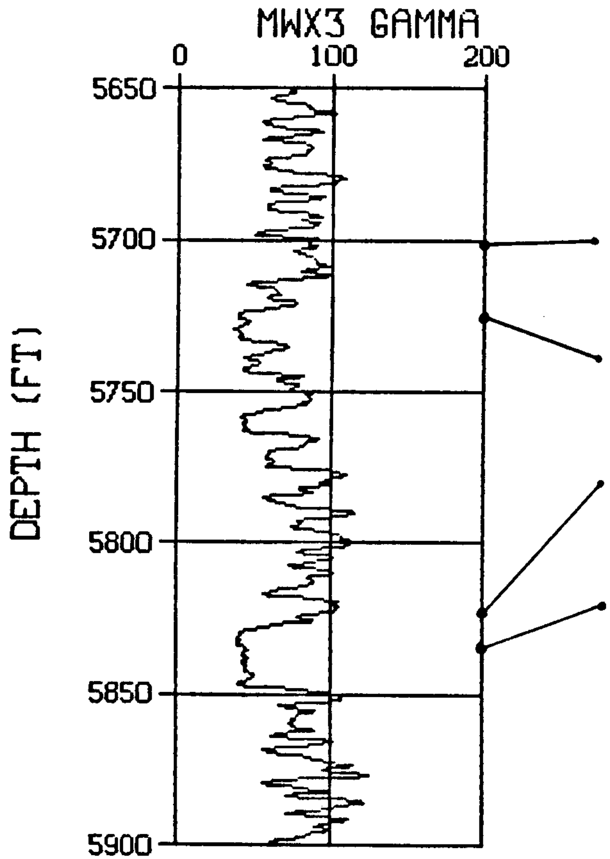

Lithology	Core Interval (Feet) [~Log Depth]	Brazilian Tests: Tensile Strength (MPa)	Triaxial Tests: Confining Pressure (MPa)	Compressive Strength[a] (MPa)	E^b (GPa)	ν^a	Fracture Toughness K_{IC} ($MPa \cdot m^{-1/2}$)
Mudstone	5697.6-5698.3* [5702.6-5703.3]	-	0	-	-	-	1.68
			10	150.5	26.8	.17	
			20	173.6	28.8	.14	
			30	-	-	-	
			50	-	-	-	
Sandstone	5720.5-5721.4* [5725.5-5726.4]	-6.4±0.5	0	-	-	-	1.37±0.11
			10	127.2	21.7	.22	
			20	167.3	25.8	.17	
			30	-	-	-	
			50	-	-	-	
Mudstone	5818.7-5819.3* [5823.7-5824.3]	-3.0±1.3	0	-	-	-	-
			10	-	-	-	
			20	81.7	13.1	.25	
			30	-	-	-	
			50	-	-	-	
Sandstone	5830.8-5831.9* [5835.8-5836.9]	-5.2±0.4	0	73.9	12.5	.21	1.54±0.14
			10	137.6	22.1	.21	
			20	176.6	26.2	.21	
			30	197.9	27.2	.23	
			50	-	-	-	

* Sealed at Well
a Ultimate Axial Stress Difference
b Calculated for Stresses Between 20 and 60 Percent of Ultimate Axial Stress Difference

Figure 5.25. Rock Property Data for MWX-3

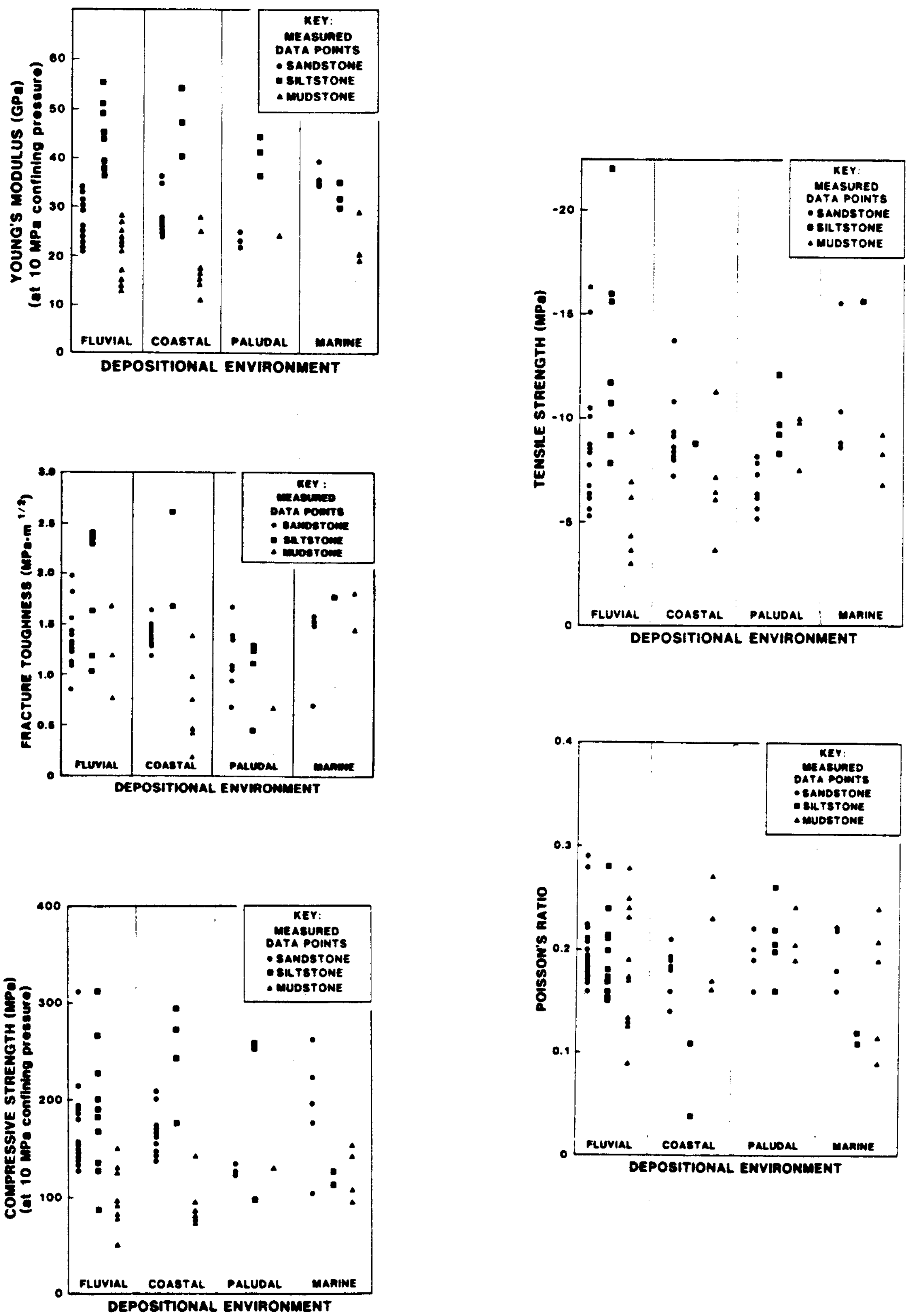

Figure 5.26. Summary of Rock Property Data for Each Depositional Environment

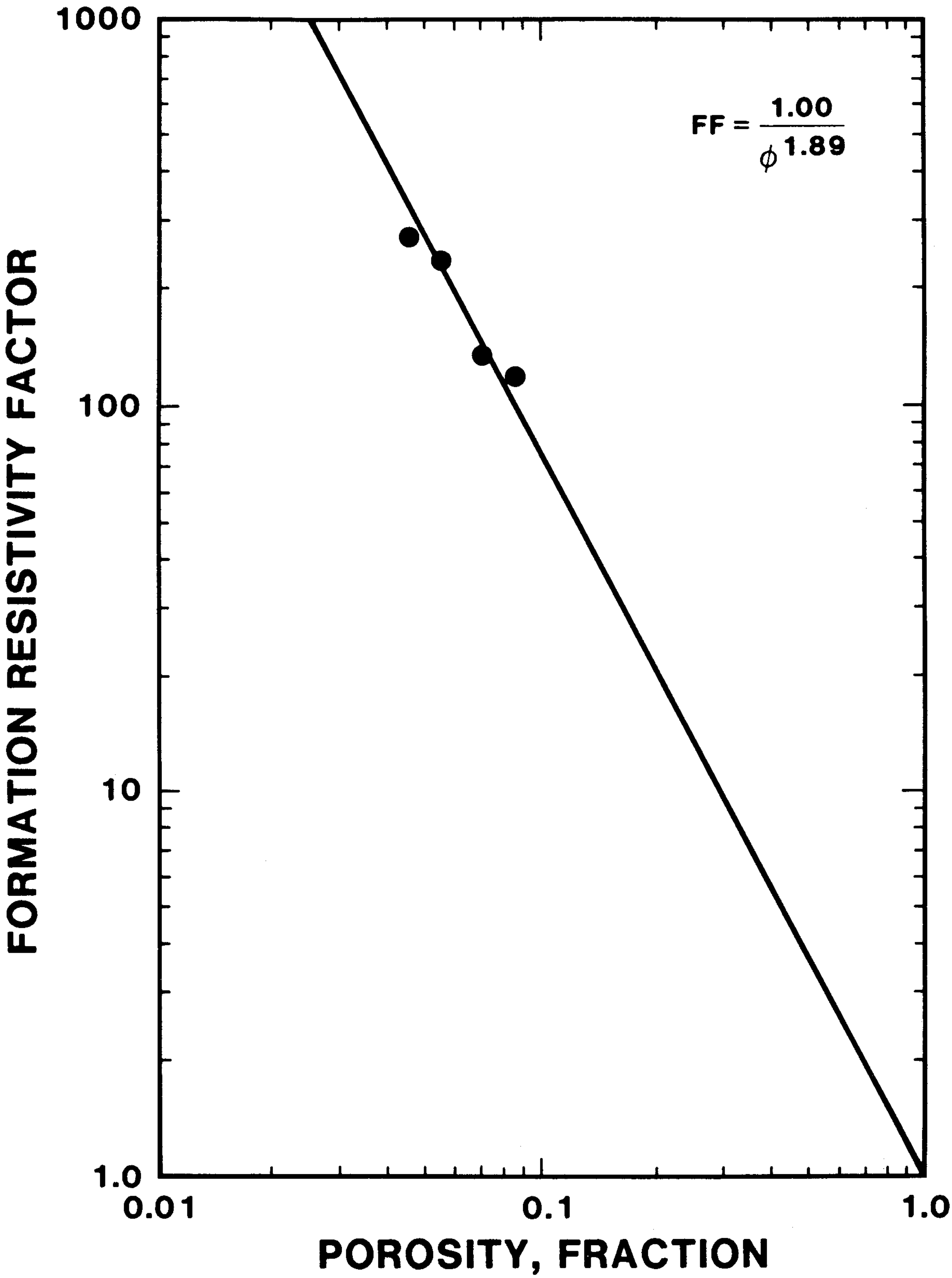

Figure 5.27. Formation Factor Data, Fluvial Zone

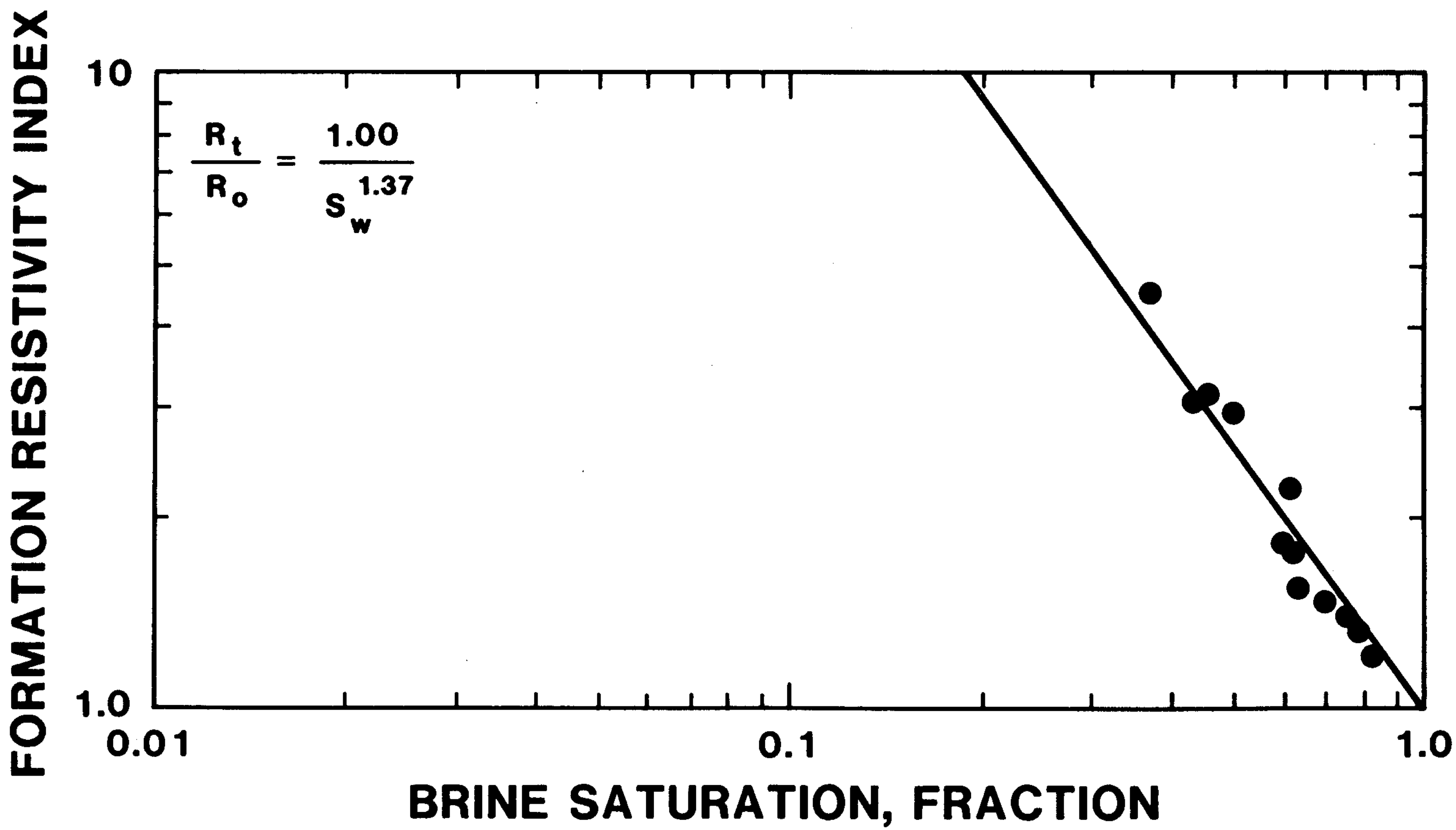

Figure 5.28. Resistivity Index Data, Fluvial Zone

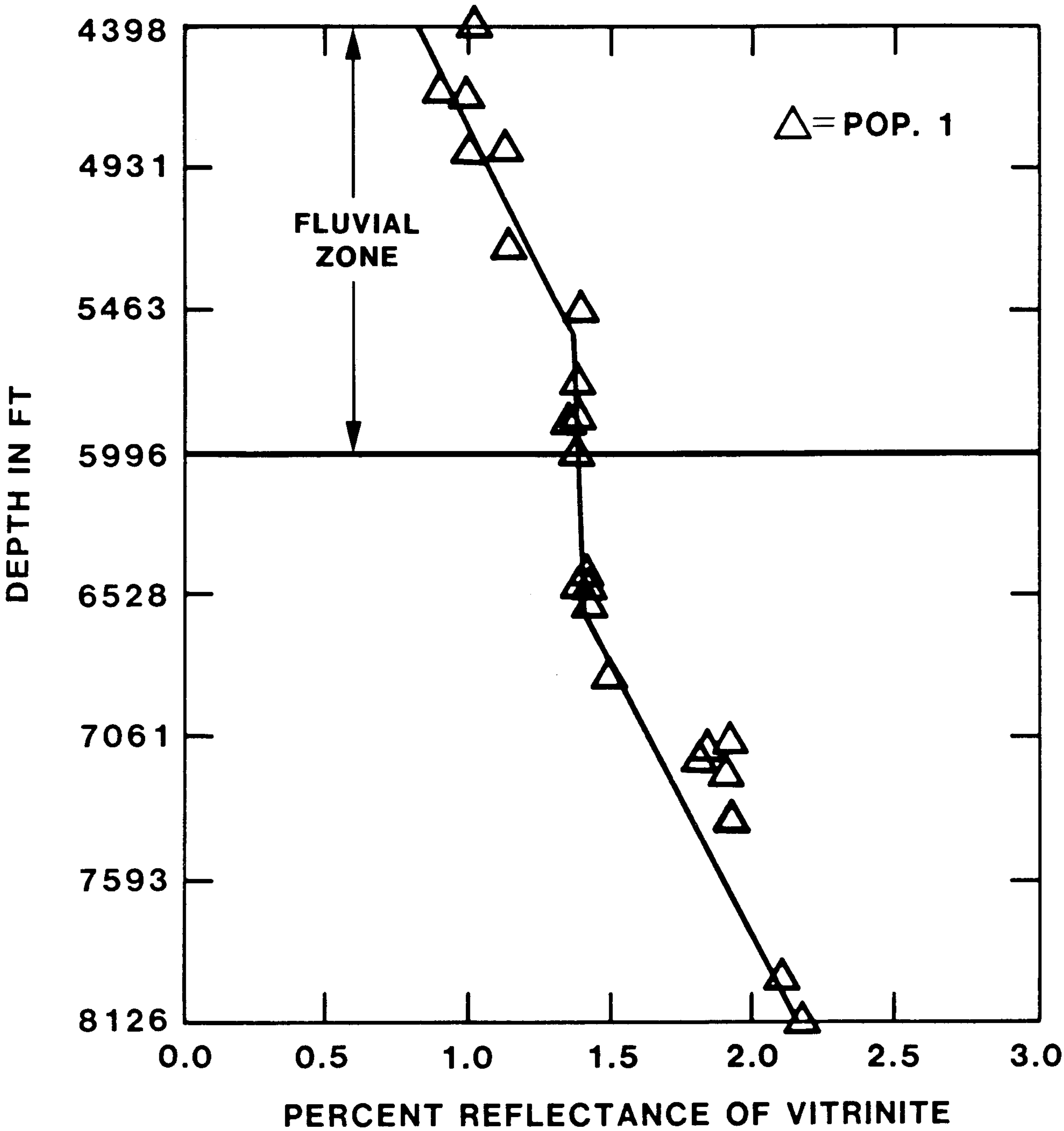

Figure 5.29. Vitrinite Reflectance Data

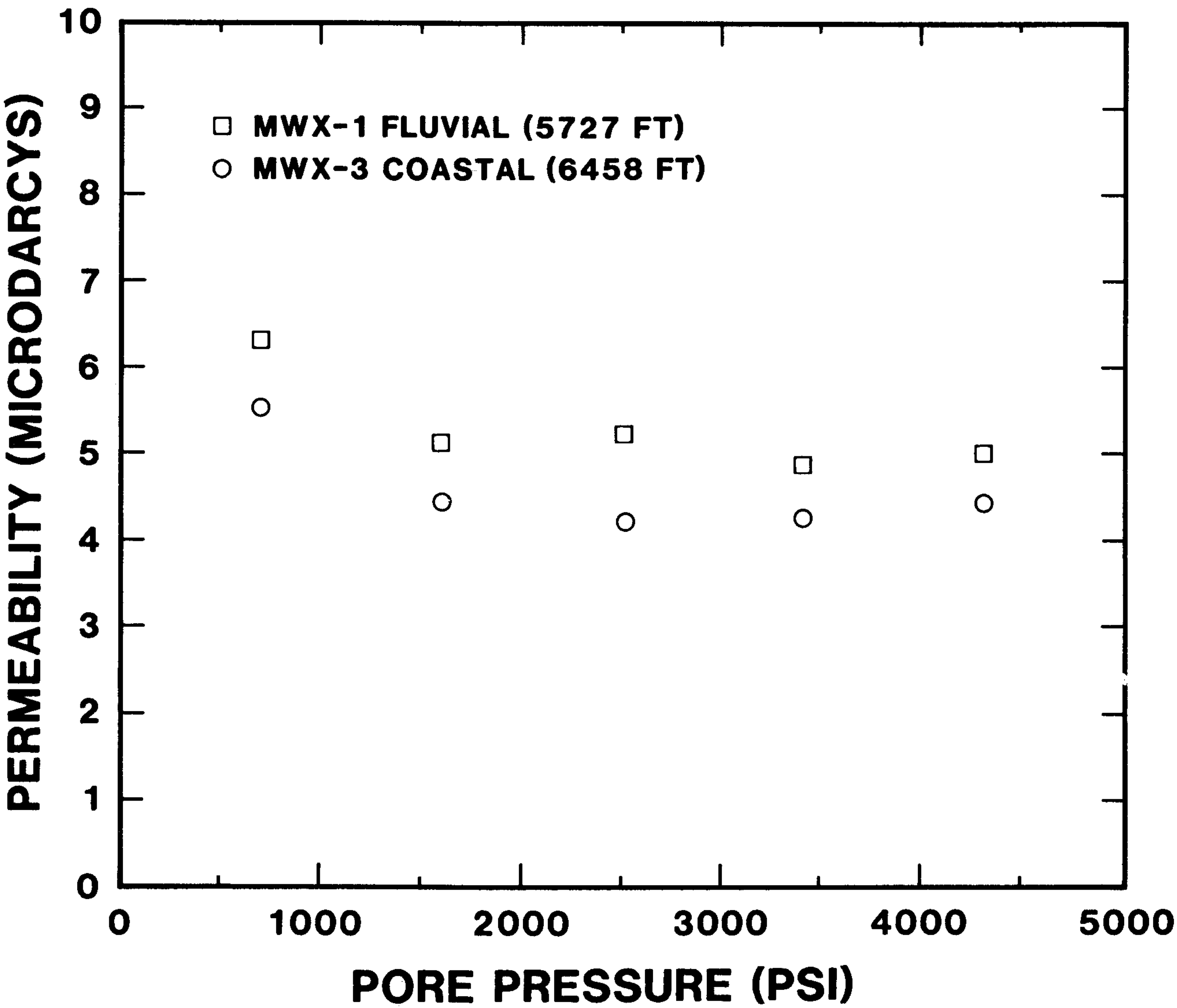

Figure 5.30. Permeability vs. Pore Pressure at Constant Net Confining Stress

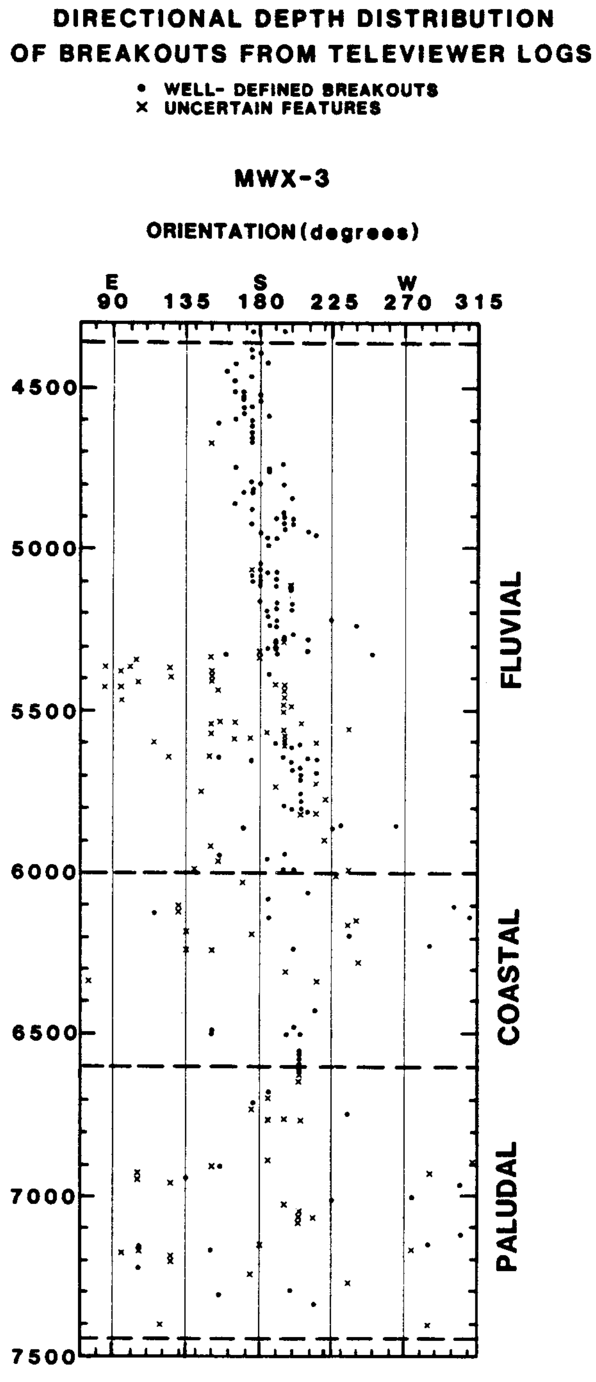

Figure 5.31. Directional Breakouts from Televiewer Logs

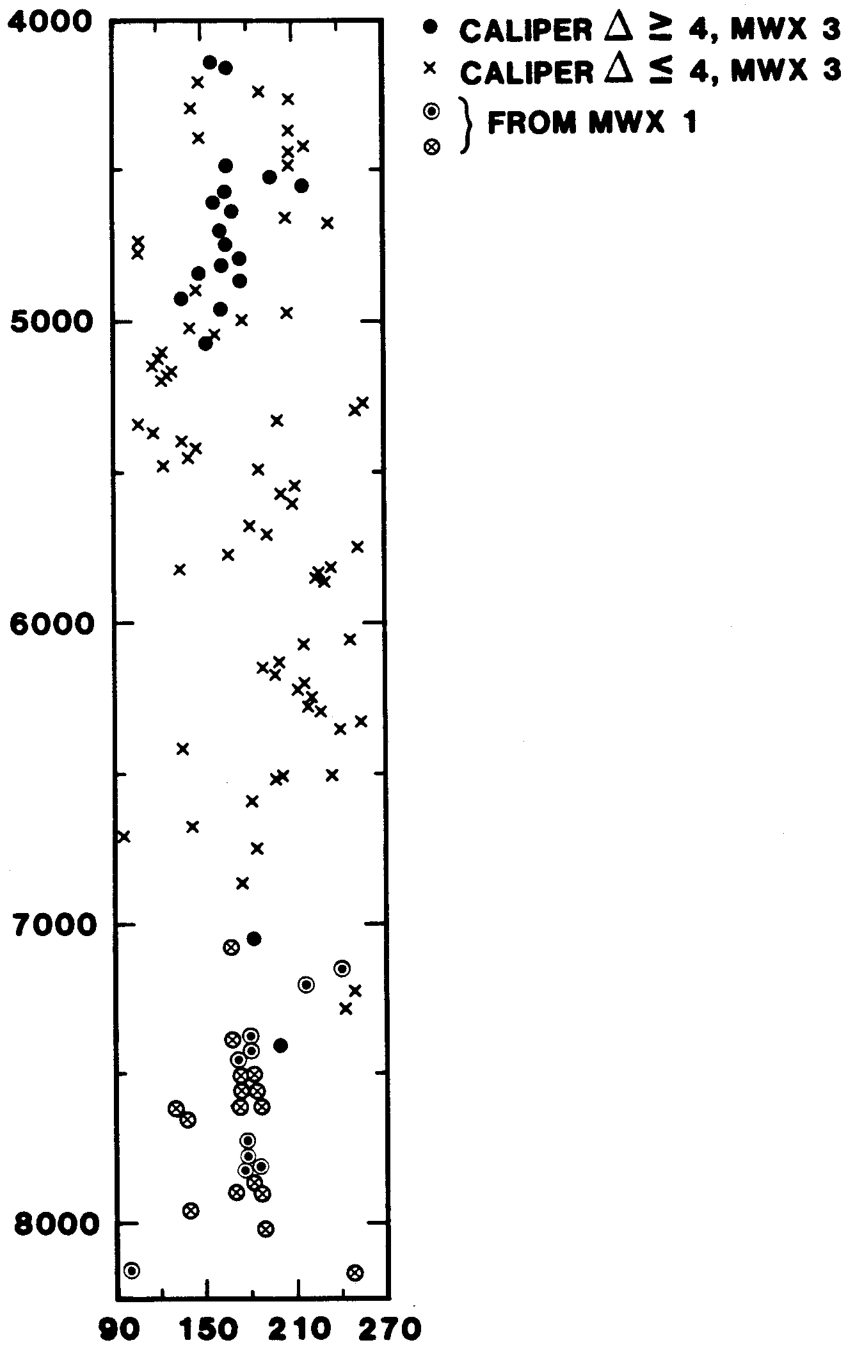

Figure 5.32. Wellbore Breakouts vs. Depth, MWX-3 Oriented Caliper Log

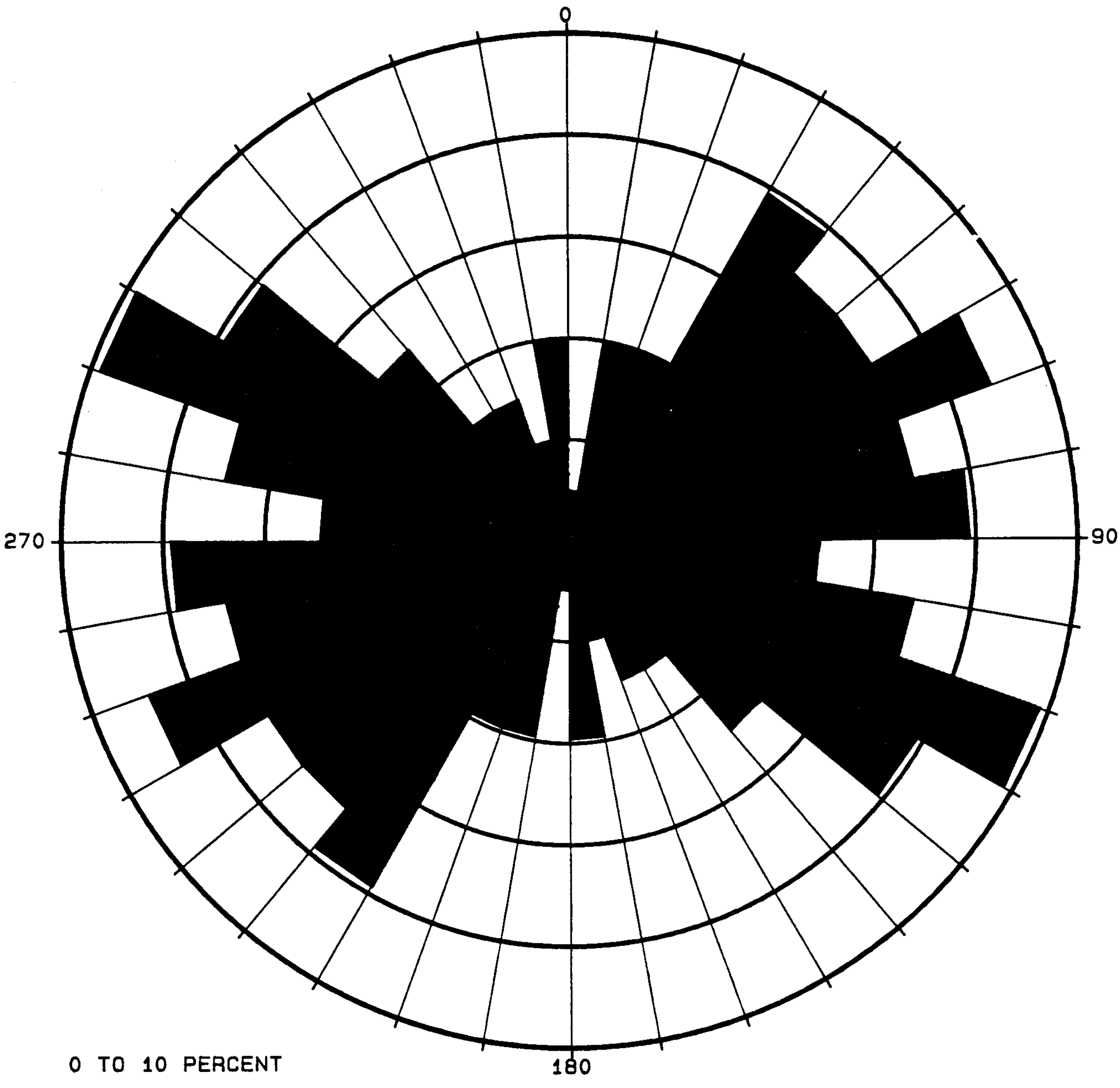

5.33. Histogram of Relaxation Microfractures, MWX-1 Sample, 5490 ft

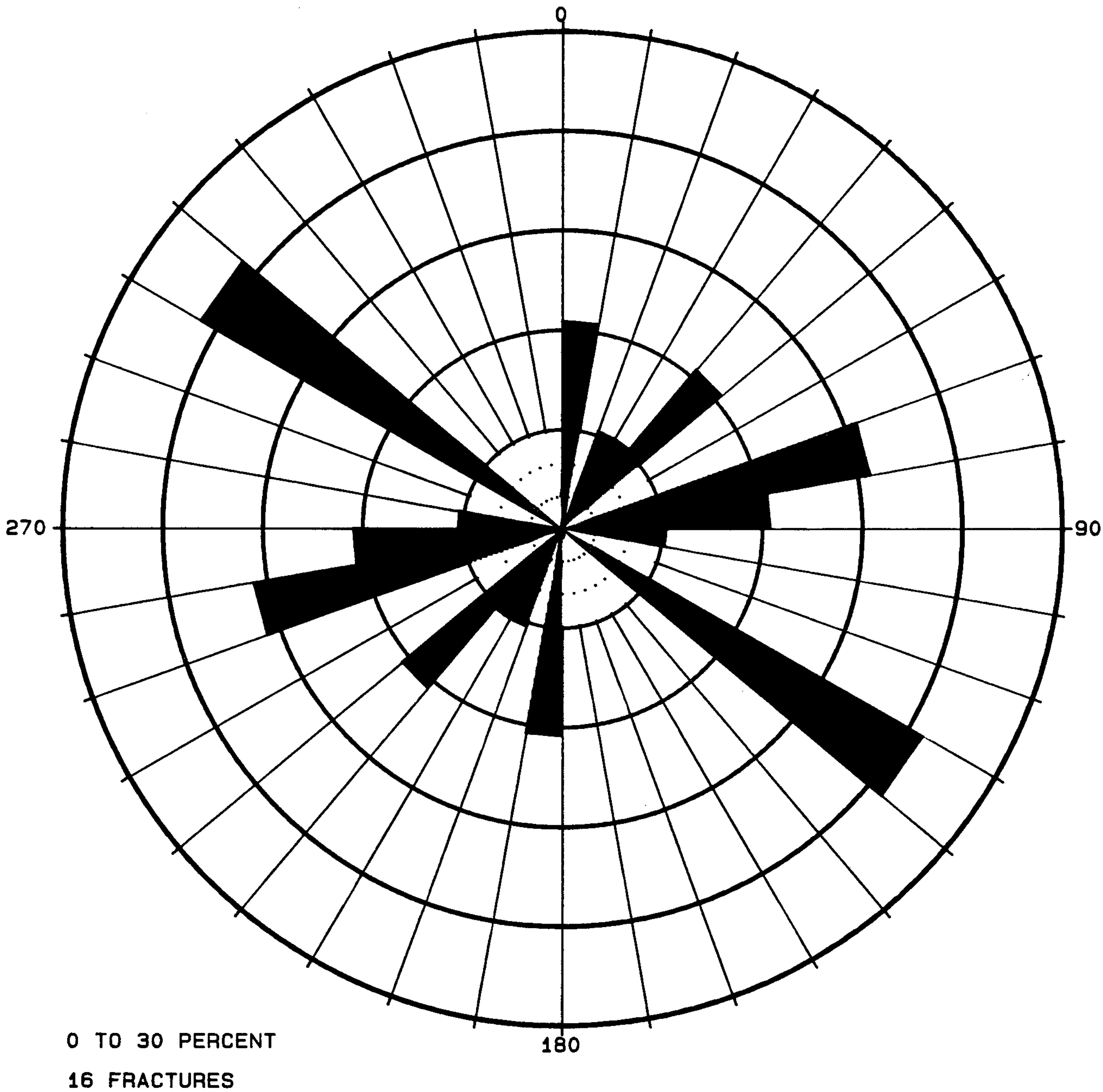

Figure 5.34. Histogram of Natural Microfractures, MWX-1 Sample, 5490 ft

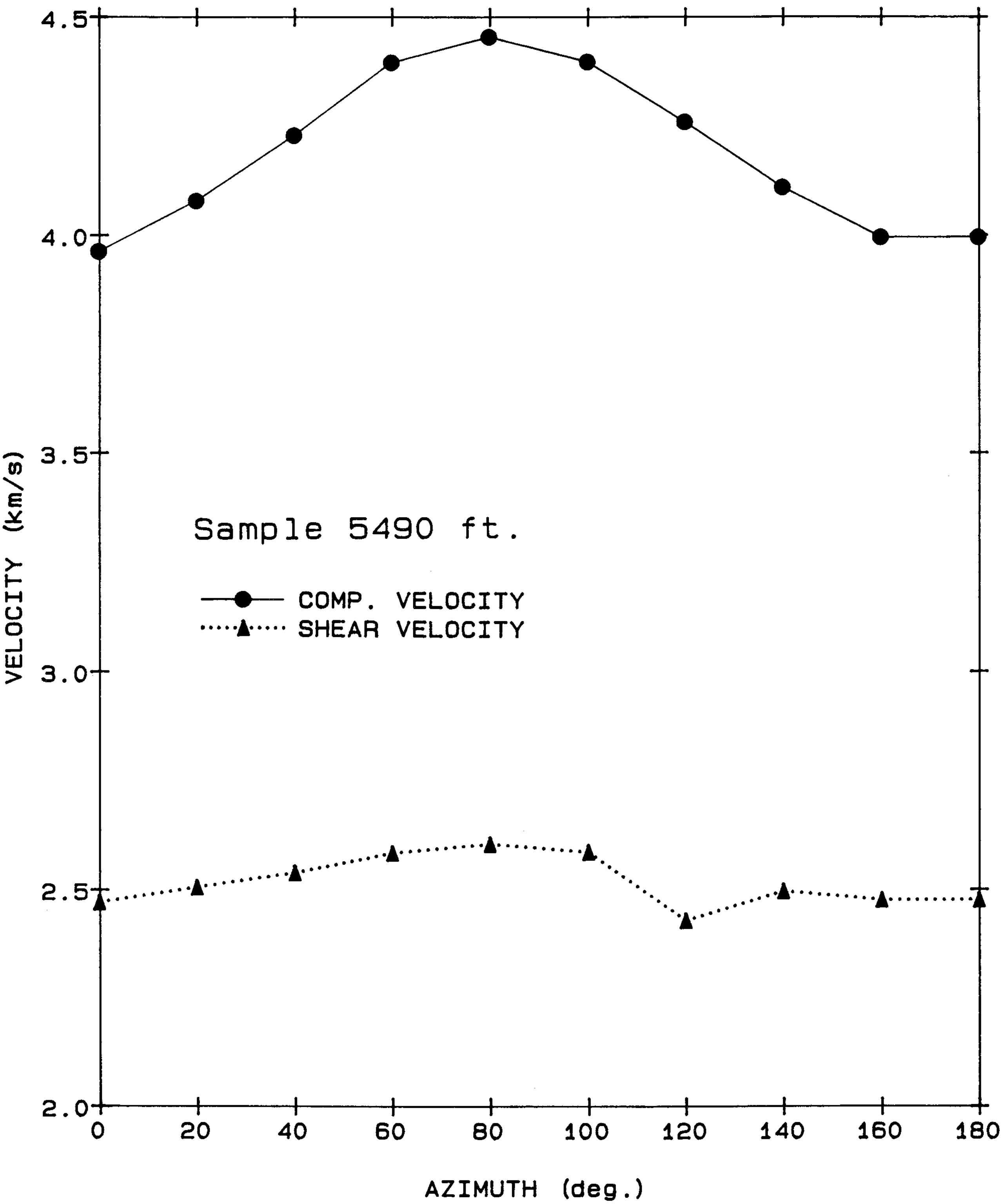

Figure 5.35. Directional Sonic Velocities, MWX-1 Sample

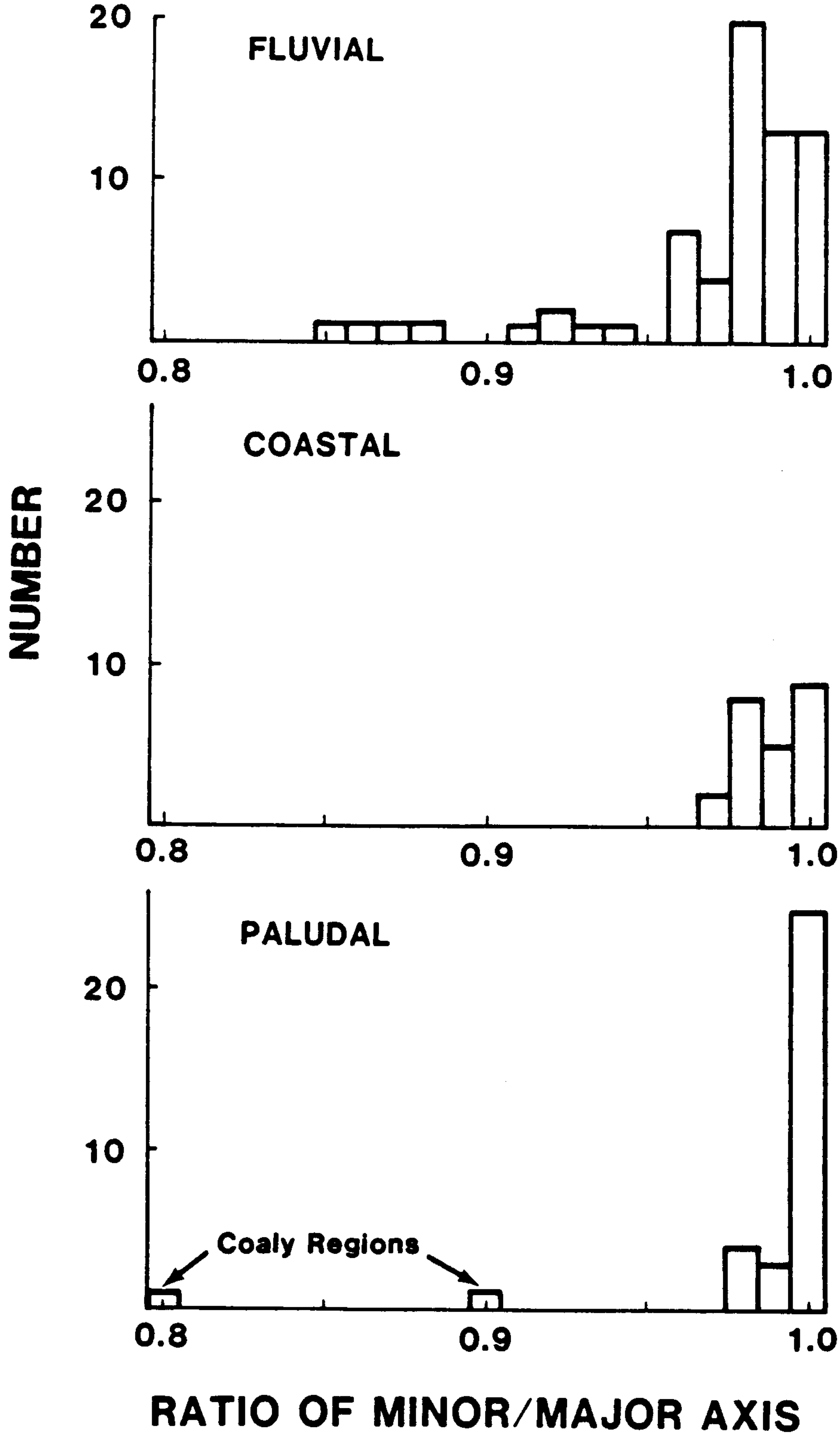

5.36. Borehole Eccentricity from Four-Arm Oriented Caliper Log

6.0 IN SITU STRESS

N. R. Warpinski
Sandia National Laboratories

6.1 OBJECTIVE

The objectives of the in situ stress testing program are to (1) determine the vertical distribution of the minimum, principal, horizontal, in situ stress, (2) to determine the orientation of the horizontal stress field, (3) to estimate the maximum, principal, horizontal, in situ stress, and (4) to estimate the net stress on the reservoir and abutting rocks (for property measurements). These stress results are important for analyses of containment of hydraulic fractures, for estimating the behavior of natural fractures during stimulations, for determination of accurate rock/reservoir properties, and for many other factors.

6.2 IN SITU STRESS MEASUREMENTS

The in situ stresses are now recognized to be important for many completion and production activities, including containment of hydraulic fractures,[1-6] interaction of natural and hydraulic fractures,[7] property measurements such as permeability,[8] and others. Previous results[9-14] have shown that large stress contrasts exist between sandstones and the abutting mudstone or shale material. These high stresses have apparently kept hydraulic fractures well-contained, but have also resulted in relatively high treatment pressures. Detailed measurements of the stress distribution are essential for understanding hydraulic fracture behavior in this environment.

Additionally, the magnitude of the maximum horizontal in situ stress may be significant for fluvial treatments because of the possibility of interactions with the natural fracture system during hydraulic fracture treatments. In such cases, the orientation of the stress field with respect to the natural fractures is also important.

Hydraulic fracturing stress measurements are used to determine the vertical distribution of the minimum principal in situ stress. Anelastic strain recovery (ASR) techniques provide the stress orientation and, when calibrated using measured minimum stress data and log-derived overburden stresses, provide an estimate of the maximum horizontal principal in situ stress. A number of differential strain curve analysis (DSCA) tests were also provided by Dowell-Schlumberger.

6.2.1 Hydraulic Fracturing Measurements

The stress test technique was our usual small-volume hydraulic fracture method.[10] A two foot perforated interval (4 shots/ft) is isolated with packers and fractured with KCl water at rates of 3-16 gpm. A bottom-hole, HP pressure gage measures the pressure and a bottom-hole closure tool is used to provide fast shut-ins without tube waves or wellbore storage problems that may mask the instantaneous shut-in pressure (ISIP). Total volumes injected are usually 10-50 gal, so the fracture can equilibrate and close rapidly at shut-in. Data sampling rates are typically 5-10 per second so the ISIP can be resolved. The ISIP is taken to be equivalent to the minimum in situ stress, although it is recognized that the ISIP will always be slightly greater because of fracture toughness, asperity mismatches at closure and the resultant residual width. We do not believe the discrepancy is more than a few tens of psi for the crack size generated with these tests. In these tests, no information can be obtained about the maximum, principal, horizontal, in situ stress. The stress tests were all conducted in MWX-2.

6.2.2 Anelastic Strain Recovery Measurements (ASR)

The ASR technique used in these experiments is described in references 15-17. Briefly, it consists of mounting clip-on displacement gages on a piece of sealed, oriented core and recording the time-dependent relaxation of that core. In vertical holes in flat-lying beds, as we have in these experiments, only four gages are used (one vertical, three horizontal). Determination of the orientation of the stress field has been shown to be straightforward[18,19] for many sedimentary rocks and is readily calculated by determining the principal strain orientations. If there is no rock fabric to distort the results, the maximum strain direction is found to be coincident with the maximum stress direction, as determined by an independent method.

The determination of the stress magnitudes is more complicated and requires a model for the ASR process. Blanton[20] and Warpinski and Teufel[21] have developed different types of viscoelastic models to explain the behavior. Both models will be used in the analyses of these data.

Blanton's[20] solution, referred to as the direct model, is the easiest to apply and yields a direct calculation of the stresses from the principal strains as

$$\sigma_1 = (\sigma_v - \alpha P) \frac{(1-\nu)\Delta\varepsilon_1 + \nu(\Delta\varepsilon_2 + \Delta\varepsilon_v)}{(1-\nu)\Delta\varepsilon_v + \nu(\Delta\varepsilon_1 + \Delta\varepsilon_2)} + \alpha P \tag{2}$$

and

$$\sigma_2 = (\sigma_v - \alpha P) \frac{(1-\nu)\Delta\varepsilon_2 + \nu(\Delta\varepsilon_1 + \Delta\varepsilon_v)}{(1-\nu)\Delta\varepsilon_v + \nu(\Delta\varepsilon_2 + \Delta\varepsilon_1)} + \alpha P \tag{3}$$

where the $\Delta\varepsilon$ are the change in the principal strains between any two times, ν is Poisson's ratio, P is the pore pressure, α is a poroelastic constant (approximately unity for Mesaverde rocks at the MWX site) and the subscripts 1 and 2 refer to the maximum horizontal and minimum horizontal directions, respectively, while v refers to the overburden. Important assumptions for the direct model include (1) linearly viscoelastic behavior, (2) constant Poisson's ratio throughout the relaxation process, (3) step unloading of the in situ stresses at the moment of coring, (4) a constant α throughout the process, (5) a vertical overburden stress and wellbore, and (6) isotropic behavior.

Warpinski and Teufel's model,[21] referred to as the strain-history model (because to apply the model, the measured strain history must be fit to a theoretical model), requires a least-squares fit of the entire strain data set to an expected relaxation behavior of the form

$$\varepsilon_r(t) = (2\sigma_1\cos^2\theta + 2\sigma_2\sin^2\theta - \sigma_1\sin^2\theta - \sigma_2\cos^2\theta - \sigma_v)\ J_1\ (1 - e^{-t/t_1})$$
$$+ (\sigma_1 + \sigma_2 + \sigma_v - 3P)\ J_2\ (1 - e^{-t/t_2}) \tag{4}$$

and

$$\varepsilon_v(t) = (2\sigma_v - \sigma_1 - \sigma_2)\ J_1\ (1 - e^{-t/t_1})$$
$$+ (\sigma_1 + \sigma_2 + \sigma_v - 3P)\ J_2\ (1 - e^{-t/t_2}) \tag{5}$$

where θ is the gage angle orientation with respect to the maximum stress, J_1 and J_2 are distortional and dilatational creep compliance arguments (i.e., equilibrium values of the creep compliance), t is the time, t_1 and t_2 are deviatoric and dilatational time constants, respectively, and the subscript r refers to radial direction in the horizontal plane. Important assumptions for this model are (1) the rock behaves as if it is linearly viscoelastic, (2) the behavior is exponential and can be described using standard models, (3) the overburden stress and wellbore are vertical, (4) the rock is isotropic, (5) the bulk modulus of the grain material is not a viscoelastic parameter (since the process appears to be a fracturing phenomenon), and (6) step unloading of the in situ stresses at the moment of coring.

Once the data are least-squares fit, estimates of the stresses can be made if J_1 is known. Alternately, a minifrac in tandem with the ASR data (so σ_2 is known) allows J_1 to be determined. In this study, we are still acquiring data on J_1 and thus cannot use these data to determine σ_2. We currently use the minifrac data to calculate σ_1 and J_1.

The primary problems with ASR are (1) to ascertain that rock fabric is not distorting the results and (2) obtaining sufficient data to use either viscoelastic model to calculate stress magnitudes.

6.2.3 Differential Strain Curve Analysis (DSCA)

Dowell-Schlumberger has performed DSCA measurements[22-24] on several MWX cores from the fluvial zone, as well as the variant, differential wave velocity analysis[25] (DWVA). Using DSCA, DWVA and suitable estimates of important rock properties and reservoir parameters, the magnitudes of the horizontal in situ stresses can be estimated. The orientation of the stress field also proceeds directly from the measurement process (as in ASR).

6.3 HYDRAULIC FRACTURE STRESS MEASUREMENT RESULTS

The stress results are given in Table 6.1 and Figure 6.1 for the entire fluvial interval. The sandstones are solid symbols to distinguish them from the clay-rich lithologies. These results are considerably different than what we observed in the marine, paludal and coastal intervals. It is remarkable that from 5000-6000 ft, the stresses in the fluvial sandstones hardly change. Above 5000 ft, we see a more normal stress gradient in the two upper sands.

Below 5800 ft, we measured high stresses in the clay-rich rocks with stress contrasts of about 1500 psi between sands and mudstones. This is similar to all of our previous results. From 5400-5800 ft, the stress contrasts are about 600-800 psi and from 5000-5400 ft we only measured contrasts of 100-300 psi. However, the two highest pairs of stress tests, at 4300 and 4700 ft, showed large stress contrasts again. There is no obvious change in lithology or rock properties that can explain these sudden changes of stress properties.

The mudstone data from 5400-5800 ft are also good examples of the variability of the stresses in these nonmarine rocks. In this complex lithology, every layer with different mineralogy has somewhat different stresses, probably in response to elastic properties, clay content, permeability, degree of fracturing, and possibly many other parameters. Stress measurements in some of these zones are very difficult because of the lithologic complexity.

Many of the mudstone intervals in the fluvial were difficult to break down and showed a large rate sensitivity, as if there was a restriction at the entrance to the fracture. We tried both 19 and 22 gm shaped charges and

15/32 in bullets to try to enhance the perforation entrance condition, but there was no significant difference between the bullets and shaped charges.

The first test that was performed in the fluvial zone was a mudstone at 6006-08 ft. Figure 6.2 shows the second pump at a rate of 12 gpm. The pressure drop at shut-in is very large (1200-1600 psi) for all tests in this zone and the accuracy of the ISIP (6200 psi) is only $\pm$100 psi. On the next pump, the rate was decreased, but little pressure change was induced by the rate change. We might expect these large pressures to be induced by some sort of a fracture entrance restriction, but the relative insensitivity to rate suggests that something else is causing the high injection pressures.

Figure 6.3 shows the second injection into the A sand at 5962-64 ft. The rate in this test is 7.5 gpm. While the ISIP at 4600 psi is fairly clear, the 900 psi pressure drop at shut-in is much larger than we usually have in sandstones.

The third pump of the stress test in a mudstone at 5940-42 ft is shown in Figure 6.4. The pressure drop at shut-in is about 600 psi and the ISIP is about 5750 psi; however the ISIP is not well-defined (particularly on this scale) and the uncertainty in the ISIP is about $\pm$100 psi. The flow rate was 7.5 gpm.

A stress test was conducted at 5896-98 ft, but the data were not understandable and no results are given. Pressure drops at shut-in were about 2500 psi and we were not certain that we ever fractured the interval.

The breakdown pump for a mudstone at 5850-52 ft is shown in Figure 6.5. This test was conducted at 13 gpm and shows a clear ISIP at 5925 psi and a small pressure drop at shut-in. This is a good test for a mudstone. (Note that the breakdown peak pressure is not as sharp as is shown in Figure 6.5; we were only taking data at once every 10 sec during the injection phase, resulting in the sharp appearance.)

Figure 6.6 shows the breakdown pump into a mudstone at 5778-80 ft at a rate of 12 gpm. This test shows a large breakdown peak and a well-defined ISIP at 5315 psi. This is also a good test for a mudstone.

Another mudstone at 5757-59 ft was tested at 13.5 gpm. Figure 6.7 shows the fourth injection into this zone, resulting in an ISIP just below 5500 psi. The pressure drop at shut-in was quite large, but reduced flow rates on other pumps helped to reduce the pressure.

Figure 6.8 shows a mudstone at 5744-46 ft that had similar behavior to that seen in Figure 6.7. This record is for the third injection where the pressure was decreased from 15 gpm to about 6 gpm. The pressure drops almost 700 psi in response to this rate change and the pressure drop at shut-in is reduced from about 2500 psi on the preceding pump to about 1300 psi on this injection. The ISIP is about 5050 psi in this zone.

The second injection into the C sand at 5721-23 ft is shown in Figure 6.9. This zone did not show a clear ISIP on most pumps. The first injection showed the best ISIP (about 4574 psi) but most subsequent pumps had a similar pressure response to Figure 6.9. The reason for this unusual behavior is not known, but we suspect that the hydraulic fracture broke into a natural fracture that may be oriented at some small angle from the hydraulic-fracture azimuth. The natural fracture may also begin to dilate during pumping and the closure would be complicated by ISIP values associated with the natural fracture as well as the hydraulic fracture. The ISIP is taken to be 4575 psi, but it may be as low as 4525 psi.

A pressure record for the second injection into a mudstone interval at 5700-02 ft is shown in Figure 6.10. This zone also had high injection pressures and a rate test was used to achieve a reasonable shut-in. In this zone, the ISIP was about 5150 psi with an uncertainty of ± 100 psi because of varying ISIP values on each of several tests.

Figure 6.11 shows the fourth injection into a mudstone interval at 5680-82 ft. This test also had an apparent entrance restriction and the drop in rate to about 5 gpm reduced the injection pressure by about 900 psi so that the drop at shut-in was only 600 psi and the ISIP was well-defined at 5275 psi.

The mudstone interval at 5649-51 ft had a similar response to a stress-test injection as the previous zone. As shown in Figure 6.12, the second pump into this interval had fairly high injection pressures until the rate was reduced. The corresponding ISIP for this injection is well-defined at 5210 psi.

Figure 6.13 shows a mudstone test at 5620-22 ft that also was similar to the two previous tests. A rate reduction lowers the injection pressure of this fourth pump by about 900 psi and the ISIP is clear at 5320 psi. Although a restriction is causing the injection pressure to be high, it is not interfering with the ISIP and well-defined values are obtained. This suggests that the restriction is right at the fracture entrance and does not extend any distance into the rock mass, or the ISIP would be more smeared.

Another mudstone test at 5600-02 ft shows similar behavior to the previous few tests. The second injection is shown in Figure 6.14 and a rate test is again used to obtain better ISIP values. In this test, the ISIP is about 5480 psi with an accuracy of about $\pm$50 psi.

The first injection into at mudstone at 5575-77 ft has a little different behavior. Figure 6.15 shows the breakdown pump at a rate of 15.5 gpm and the injection pressure indicates that the fracture is breaking through some restriction in small increments, as seen by the fluctuating pressure behavior. The pressure drop at shut-in on this test is about 1500 psi and the ISIP is about 5125 psi. Rate changes on subsequent tests helped to clearly define the ISIP value.

Figure 6.16 shows the second pump into a mudstone at 5506-08 ft. In this pump, the fracture breaks through a restriction with an 1800 psi drop in pressure. Subsequent pumps all had injection pressures of about 6400 psi and well-defined ISIP values. The ISIP in this zone is 5230 psi with an uncertainty of $\pm$20 psi. The flow rate in this test was 11 gpm.

The second injection into the F sandstone at 5480-82 ft is shown in Figure 6.17. The rate on this pump was 12 gpm. This test also shows a fluctuating pressure behavior, but without any significant change in the average pressure level. The restriction, whatever it may be, appears to act like a variable choke, possibly in response to pressure in the fracture. The pressure in all tests showed some degree of fluctuation and rate tests in subsequent injections lowered the pressure considerably. In all tests, the ISIP was well-defined at 4520 psi.

A mudstone at 5450-52 ft was tested at 13 gpm and the fourth pump is shown in Figure 6.18. This zone consistently showed unclear ISIP values on all injections, even those where the rate was decreased. This type of test is difficult to pick an ISIP from, but techniques such as log-log, semilog, square-root-of-time and other functions are often tried. None of those techniques has a well-developed theoretical backing that proves that they can accurately determine an appropriate ISIP from a test such as that shown in Figure 6.18, and, most of the time, each of those techniques will give different results. A technique that does not presume to determine the ISIP from this data, but does help to estimate it's range and the uncertainty, is to examine the curvature of the shut-in pressure record.[26] In tests with a well-defined ISIP, the radius of curvature becomes very small at the point of the ISIP. In a test such as shown in Figure 6.18, there is only a broad minimum band, but it should be safe to assume that the ISIP is embedded somewhere in that band. Figure 6.19 shows a normalized radius of curvature plot from these results; the minimum extends from 0.05 min after shut-in to 0.8 min after shut-in, corresponding to pressures of 4850 and 4580 psi respectively. This is the logical range of the ISIP and the average value is probably as good a pick as any other technique for the ISIP value. The average is 4715 psi with an uncertainty of 135 psi (one half the width of the minimum band).

Figure 6.20 shows the fourth pump into a mudstone at 5414-16 ft. This test also has fairly high injection pressures that are reduced considerably by lowering the rate. The ISIP is about 4450 psi with an uncertainty of ±100 psi. The pressure drop at shut-in is about 700 psi.

The fourth pump into a mudstone at 5320-22 ft is shown in Figure 6.21. A rate test was used in this zone to reduce the injection pressure, but the pressure drop associated with the rate decrease was relatively small. In addition, we observed indications of a dual shut-in behavior in all of the shut-in pressure records. The ISIP is about 4800 psi with an uncertainty of ±100 psi. We often find that tests with this dual closure behavior do not have well-defined ISIP values. Possibly, the multiple closure pressures smear the closure process.

A test in a sandstone at 5294-96 ft is shown in Figure 6.22. This is the fourth injection at a rate of 12 gpm. There is a large reopening pressure, which is typical of sandstone tests, a small pressure drop at shut-in (about 300 psi) and a well-defined shut-in at 4530 psi.

Figure 6.23 shows the third injection into a mudstone at 5074-76 ft, which was pumped at 12 gpm. This zone had a clear ISIP at 4650 psi, although the expanded scale does not show the ISIP adequately. This zone had small pressure drops at shut-in and reproducible ISIP values in all tests.

The fifth pump into a sandstone at 5044-46 ft is shown in Figure 6.24. The initial pumps into this zone showed no clear ISIP, but with continued testing, the ISIP values became reasonably well-defined, with a value of about 4460 psi. The rate in this example was 16 gpm.

Figure 6.25 shows the pressure record for the fourth injection into a mudstone at 4714-16 ft. This test had a well-defined ISIP, although the expanded scale reduces the definition somewhat, with a value of 5250 psi. This test was conducted at 12 gpm.

A sandstone at 4692-94 ft was tested and showed relatively high injection pressures. As shown in Figure 6.26 for the sixth injection, a rate test decreased the injection pressures and gave a clear ISIP at 3730 psi.

A good test was conducted in a mudstone at 4376-78 ft. The third injection, at a rate of 12 gpm, is shown in Figure 6.27. The pressure drop at shut-in is about 600 psi and the ISIP is about 4050 psi.

The shallowest test conducted at MWX was a sandstone at 4330-32 ft. The fourth pump into this zone was performed at 6 gpm and the pressure record is shown in Figure 6.28. The ISIP is somewhat unclear, with a value of about 3350 psi and an uncertainty of about 75 psi.

The preceding examples may not exactly match the data in Table 6.1 since Table 6.1 gives average stress values over all of the valid tests for each zone. A valid test is one in which there is a reasonably clear ISIP and no strange behavior during or after fracturing.

6.4 ASR STRESS MEASUREMENT RESULTS

In the Multiwell Experiment, there are ASR data from core in all three wells, but only the MWX-3 data were obtained with the latest improved gages. These MWX-3 data are more accurate and reliable than earlier data. Hence, only the MWX-3 data are used for these analyses. Additionally, any data where the rock showed a pre-existing fabric were not included.

The ASR strain and orientation data are given in Table 6.2. In the sandstones, the maximum compressive horizontal stress direction, the hydraulic fracture azimuth, varies from N67°E to N103°E with an average of about N84°E. This is consistent with other data in the well.[9] In the single mudstone test in this interval, there is no preferred stress orientation.

The magnitudes of the stresses, determined from both the direct and strain history models, are given in Table 6.3. Maximum stresses in the sandstones are greater than the measured minimum stresses by 500-1200 psi, depending on the depth. This is different than lower intervals where the ASR and DSCA data indicated that the maximum stress was 600-800 psi above the minimum stress in most intervals. An open-hole, hydraulic-fracture measurement[14] of the maximum stress in the Rollins sandstone at 7550 ft yielded a maximum stress that was about 400 psi above the minimum stress. In the mudstone, the horizontal stresses are nearly identical, as they must be if there is no preferred stress orientation.

Some limited DSCA and DWVA data were also obtained in the fluvial interval and these results are shown in Table 6.4. The orientation of the stresses in the sandstones is similar to the ASR orientation results.

Figures 6.29 through 6.37 show the ASR data for these fluvial tests including both the actual ASR data for the four gages taken at hour intervals and the calculated strain-history fits of the data using our strain-history model. Using this model, the total strain which the piece of core has undergone is estimated. The format for these Figures does not imply that the rock has experienced negative strains in early times. For convenience, the original form of the data is preserved, i.e., all strains start at zero at the time the core is first instrumented, and the early negative strains represent the anelastic strains that the core experienced before being instrumented.

The data quality is excellent for these Mesaverde sandstones and the theoretical viscoelastic strain-history model[21] matches the measured response very well. It is clear in all of these tests that the vertical strain relaxation is considerably greater than the horizontal strain relaxation, implying that the maximum principal stress is the overburden stress. A comparison of these Figures shows that the total anelastic strain undergone by the rock in any gage direction, as determined by the strain-history model, is fairly constant throughout the fluvial interval at the MWX site.

6.5 DISCUSSION

6.5.1 Large Stress Contrasts

One of the important, as well as perplexing, results of these studies is the high stress in many of the mudstones compared to the sandstones. These large stress contrasts are useful for hydraulic fracture containment, but it is difficult to theorize how the stresses in some of the mudstones are isotropic at nearly the lithostatic value while the stresses in the sands are much lower and show a strong preferred orientation. It is hard to explain these contrasts in terms of rock properties, particularly when some of the high-stress mudstones have higher moduli and lower Poisson's ratios than the sands. Yet some of the stress must be transmitted through a solid mechanics mechanism (as opposed to pore pressure) because the sands show preferred stress orientations (from anelastic strain recovery, differential strain curve analysis, and fracture diagnostics). Creep can help but it requires large differential relaxation times between sands and mudstones and relatively recent tectonic perturbations. The stress in the sandstones must have a residual component that has been locked in from an earlier period. Most likely, an acceptable stress model will need to invoke all of these factors--material property contrasts, differences in pore pressure between sands and mudstones, creep, tectonics, residual stresses--to effectively model the current stresses.

A change in trend in the fluvial section, compared to lower intervals, is the decrease in mudstone stresses in the interval between about 5000 and 5800 ft. In the upper half of this interval (5000-5400 ft), there is very little difference between the minimum stress in the sandstones and the minimum stress in the mudstones. This interval has also shown other anomalous features, such as a high density of natural fractures, the presence of small thrust faults, a cross-natural-fracture set, and others.

6.5.2 Hydraulic Fracturing

These stress data were used in the design and analysis of hydraulic fracture treatments in these sandstones. The minimum stress in the mudstones around the fluvial B sandstone are 5925 psi below and about 5400 psi above the reservoir. The initial stress in the B sandstone was not measured (so that the KCl water from the stress tests would not cause any near-wellbore damage before the interference test), but based on surrounding sandstone tests it should be about 4550-4600 psi. However, as will be discussed later, several weeks of drawdown for the pre-frac well testing appeared to reduce the pore pressure sufficiently that the minimum stress appeared to be about 4400 psi at the time of the fracture experiments. This yields stress contrasts of 1525 psi below and 1000 psi above the reservoir. Height growth should be predominantly upward in the B sandstone tests. Containment calculations will be given in a later section.

Around the C sandstone, the stresses in the mudstones are 5000-5400 psi below and 5200 psi above the reservoir. The stress in the C sandstone is 4575 psi, so the stress contrasts are only 400-800 psi below and 600 psi above the reservoir interval. Significant height growth should be expected in the C sandstone fracture experiments.

The stresses in the mudstone around the E sandstone are 5125 psi below and 5230 psi above the reservoir rocks, while the stresses in the sandstone are about 4550 psi, based on pump-in/shut-in tests (described later). This gives stress contrasts of only 575 psi for downward growth and 655 psi for upward growth. Again, significant height growth should be expected in this interval. However, other factors, such as the reduced width in the higher stress mudstones and inefficiently fracture growth due to bedding, may aid the overall containment of the fracture.

6.5.3 Shaped-Charge Vs Bullet Perforations

In this interval, both shaped-charge and bullet perforators were used to try and improve the clarity of the ISIP. The expectation was that bullet perforators would probably induce a different type of damage to the rock (microcracking) than shaped-charges (compaction and stressing), and the difficulty in breaking down some of the mudstone intervals might be alleviated. Bullets were used in tests from 6006-08 ft to 5850-52 ft and also from 5480-82 ft to 5294-96 ft, but no significant differences in the test results were observed. This suggests that the difficulties were not so much with perforation damage to the rock, but rather with the cement annulus or the formation, particularly with respect to fracture initiation and orientation. There is probably no single mechanism, as evidenced by the diversity of pressure records, and it is not clear if any perforation technique will improve the data.

6.5.4 Value of Diagnostic Tests

As seen in the stress test pressure records, determining the ISIP is not always a simple matter and many tests exhibit unusual behavior that add to the complexity. We have found that simple diagnostic tests, such as (1) changing rate (both higher and lower), (2) pumping variable volumes, and (3) conducting long bleed tests to remove any residual fluid from the fractures, can significantly aid in improving the definition of the ISIP. These tests can also help diagnose the source of the problem.

6.6 CONCLUSIONS

These stress results in the fluvial zone show that large stress contrasts exist between the sandstones and mudstones only in the vicinity of the B sandstone. Moderate stress contrasts are present around the C and E intervals and some height growth should be expected in the latter two intervals.

Stress gradients for the sandstones vary from 0.77 to 0.88 psi/ft while they range from 0.82 to 1.11 psi/ft for the mudstones. The mudstones are approximately lithostatic at the bottom of the fluvial interval and possibly near the top, but mudstone stresses between 5000 and 5800 ft are much less than the lithostatic value. The only ASR mudstone test, at 5701 ft, showed that the horizontal stresses are also isotropic. This is expected if the magnitudes of the horizontal stresses in the mudstones are lithostatic, but in this zone the stresses are considerably reduced.

There is good agreement between ASR, DSCA and hydraulic fracture stress measurements. ASR and DSCA results suggest that the difference in horizontal stresses varies from 500-1200 psi and the maximum stress orientation is about N84°E.

These stress results, although similar to the coastal interval tests[13], are still not as reproducible and accurate as the marine data.[10,11] This is probably due to the lithology; marine rocks tend to be massive and stress test fractures propagate over a fairly uniform zone. The complex layering in nonmarine sequences makes interpretation much more difficult.

6.7 REFERENCES

1. Perkins, T. K., and L. R. Kern, "Widths of Hydraulic Fractures," Journal of Petroleum Technology, Vol. 13, September 1961, p. 937.

2. Simonson, E. R., A. S. Abou-Sayed, and R. J. Clifton, "Containment of Massive Hydraulic Fractures," Society of Petroleum Engineers Journal, Vol. 18, February 1978, p. 27.

3. Warpinski, N. R., J. A. Clark, R. A. Schmidt, and C. W. Huddle, "Laboratory Investigation on the Effect of In Situ Stresses on Hydraulic Fractures Containment," Society of Petroleum Engineers Journal, Vol. 22, No. 3, June 1982, p. 333.

4. Teufel, L. W. and J. A. Clark, "Hydraulic Fracture Propagation in Layered Rock: Experimental Studies of Fracture Containment," SPE/DOE 9878, Proceedings, 1981 SPE/DOE Symposium on Low Permeability Gas Reservoirs, May 1981, Denver, Colorado, p. 449.

5. Hanson, M. E., G. D. Anderson, R. J. Shaffer, and L. D. Thorson, "Some Effects of Stress Friction, and Fluid Flow on Hydraulic Fracturing," Society of Petroleum Engineers Journal, Vol. 22, No. 3, June 1982, p. 321.

6. Warpinski, N. R., R. A. Schmidt, and D. A. Northrop, "In Situ Stresses: The Predominant Influence on Hydraulic Fracture Containment," Journal of Petroleum Technology, Vol. 34, March 1982, pp. 653-664.

7. Warpinski, N. R. and Teufel, L. W., "Influence of Geologic Discontinuities on Hydraulic Fracture Propagation," Journal of Petroleum Technology, Vol. 39, No. 2, February 1987, pp. 209-220.

8. Randolph, P. L., "Porosity and Permeability of Mesaverde Sandstone Core from the U.S. DOE Multiwell Experiment, Garfield County, Colorado," SPE 11765, proceedings 1983 SPE/DOE Joint Symposium on Low Permeability Gas Reservoirs, Denver, CO, March 13-16, 1983, pp. 449-460.

9. Warpinski, N. R. and L. W. Teufel, "In Situ Stresses in Low-Permeability, Nonmarine Rocks," SPE 16402, Proceedings 1987 SPE/DOE Joint Symposium on Low Permeability Reservoirs, Denver, CO, pp. 125-138, May 1987.

10. Warpinski, N. R., P. T. Branagan, and R. Wilmer, "In Situ Measurements at U.S. DOE's Multiwell Experiment Site, Mesaverde Group, Rifle, Colorado," JPT, Vol. 37, March 1985.

11. Northrop, D. A., ed., "Multiwell Experiment Final Report: 1. The Marine Interval of the Mesaverde Formation," Sandia National Laboratories Report, SAND87-0327, April 1987.

12. Northrop, D. A., ed., "Multiwell Experiment Final Report: 2. The Paludal Interval of the Mesaverde Formation," Sandia National Laboratories Report, SAND88-1008, May 1988.

13. Northrop, D. A., ed., "Multiwell Experiment Final Report: 3. The Coastal Interval of the Mesaverde Formation," Sandia National Laboratories Report, SAND88-3284, March 1989.

14. Warpinski, N. R., P. T. Branagan, A. R. Sattler, J. C. Lorenz, D. A. Northrop, R. L. Mann, and K. H. Frohne, "Fracturing and Testing Case Study of Paludal, Tight, Lenticular, Gas Sands," SPE Formation Evaluation, Vol. 2, No. 4, pp. 535-545, December 1987.

15. Teufel, L. W., "Prediction of Hydraulic Fracture Azimuth from Anelastic Strain Recovery Measurements of Oriented Core," in 23rd U.S. National Rock Mechanics Symposium, Berkeley, CA, ed. R. Goodman and F. Heuze, pp. 238-246, 1982.

16. Teufel, L. W., "Determination of In Situ Stress from Anelastic Strain Recovery Measurement of Oriented Core," SPE 11649, Proceedings, SPE/DOE Symposium on Low Permeability, pp. 421-430, Denver, CO, March 1983.

17. Teufel, L. W., and N. R. Warpinski, "Determination of In Situ Stress from Anelastic Strain Recovery Measurements of Oriented Core: Comparison to Hydraulic Fracture Stress Measurements," Proceedings 25th U.S. Symposium on Rock Mechanics, Northwestern University, Evanston, IL, pp. 176-185, June 1984.

18. Teufel, L. W. C. Hart, A. R. Sattler, and J. A. Clark, "Determination of Hydraulic Fracture Azimuth by Geophysical, Geological and Oriented-Core Methods at the Multiwell Experiment Site, Rifle, CO," SPE 13226, presented at 59th Annual SPE Technical Conference, Houston, TX, September 16-19, 1984.

19. Lacy, L. L., "Comparison of Hydraulic Fracture Azimuth by Geophysical, Geological and Oriented-Core Methods at the Multiwell Experiment Site, Rifle, CO," SPE 13226, presented at 59th Annual SPE Technical Conference, Houston, TX, September 16-19, 1984.

20. Blanton, T. L., "The Relation Between Recovery Deformation and In Situ Stress Magnitudes," SPE 11624, Proceedings, 1983 SPE/DOE Symposium on Low Permeability Gas Reservoirs, Denver, CO, pp. 213-218, March 14-16, 1983.

21. Warpinski, N. R. and L. W. Teufel, "A Viscoelastic Constitutive Model for Determining In Situ Stress Magnitudes from Anelastic Strain Recovery of Core," SPE 15368, presented at 61st Annual SPE Technical Conference, New Orleans, LA, October 5-8, 1986.

22. Strickland, F. and N. Ren, "Predicting the In Situ Stress for Deep Wells Using the Differential Strain Curve Analysis," SPE 8954, Proceedings, SPE/DOE Symposium on Unconventional Gas Recovery, Pittsburgh, PA, pp. 251-258, May 1980.

23. Strickland, F. G. and N. K. Ren, "Predicting the In Situ Stress State for Deep Wells Using Differential Strain Curve Analysis," presented at the 31st Ann. Tech. Meeting of the Pet. Soc. of CIM: Calgary, paper no. 80-31-33, May 1980.

24. Ren, N. K. and J. C. Roegiers, "Differential Strain Curve Analysis--A New Method for Determining the Preexisting In Situ Stress State from Rock Core Measurements," presented at the 5th ISRM Congress, Melbourne, April 1983.

25. Ren, N. K. and P. J. Hudson, "Predicting the In Situ Stress State Using Differential Wave Velocity Analysis," Proceedings, 26th U.S. Symposium on Rock Mechanics, pp. 1235-1246, E. Ashworth, ed., Rapid City, SD, June 26-28, 1985.

26. Warpinski, N. R., "Determining the Minimum In Situ Stress from Hydraulic Fracturing through Perforations," proceedings, Second International Workshop on Hydraulic Fracturing Stress Measurements, Minneapolis, MN, June 16-18, 1988.

Table 6.1

Stress Data and Rock Properties

MWX-2

Depth (ft)	Lithology	σ_{min} (psi)	Estimated Uncertainty (psi)	ν_{log}	E_{lab} (10^6 psi)	Gradient
6006-08	Mudstone	6200	100	0.27	--	1.03
5962-64	Sandstone	4600	30	0.20	--	0.771
5940-42	Mudstone	5750	75	0.27	--	0.968
5850-52	Mudstone	5925	20	0.26	5.7	1.01
5778-80	Mudstone	5315	20	0.30	--	0.920
5757-59	Mudstone	5440	50	0.29	--	0.945
5744-46	Mudstone	5050	100	0.32	3.2	0.879
5721-23	Sandstone	4575	50	0.16	4.2	0.800
5700-02	Mudstone	5150	100	0.28	--	0.903
5680-82	Mudstone	5275	50	0.24	--	0.929
5649-51	Mudstone	5210	20	0.25	--	0.922
5620-22	Mudstone	5320	50	0.27	--	0.946
5600-02	Mudstone	5480	50	0.28	--	0.978
5575-77	Mudstone	5125	50	0.28	--	0.919
5506-08	Mudstone	5230	20	0.24	--	0.950
5480-82	Sandstone	4520	20	0.21	--	0.825
5450-52	Mudstone	4715	135	0.27	--	0.865
5414-16	Mudstone	4450	100	0.28	--	0.822
5320-22	Mudstone	4800	100	0.27	--	0.902
5294-96	Sandstone	4530	20	0.22	--	0.856
5074-76	Mudstone	4650	20	0.25	--	0.916
5044-46	Sandstone	4460	30	0.22	--	0.884
4714-16	Mudstone	5250	30	0.29	--	1.110
4692-94	Sandstone	3730	50	0.22	--	0.795
4376-78	Mudstone	4050	30	--	--	0.925
4330-32	Sandstone	3350	75	--	--	0.773

Table 6.2

ASR Strain and Orientation Data

Depth (ft)	Lithology	Core Age* (hrs)	$t\varepsilon_1$	ε_2	ε_v	θ	Maximum Horizontal Stress Direction
4906	Sandstone	4-43	152	44	212	-31.3	N67°E
4909	Sandstone	4-43	210	84	292	71.3	N78°E
4910	Sandstone	4-43	173	73	268	73.3	N80°E
5701	Mudstone	5-48	150	136	212	-	-
5724	Sandstone	5-48	217	43	248	41.0	N81°E
5725	Sandstone	5-48	167	53	196	35.2	N75°E
5766	Sandstone	5-48	281	111	422	65.1	N88°E
5781	Sandstone	5-48	163	58	266	-52.1	N103°E
5782	Sandstone	5-48	219	77	328	-56.0	N97°E

*Core age is the elapsed time interval (to within 1 hour) from when the core was cut and strain relief monitoring began to when monitoring ended.

Table 6.3

ASR Stress Data

		Input Parameters			Direct Model		Strain-History Model	
Depth (ft)	Lithology	σ_v (psi)	σ_{2meas} (psi)	P (psi)	σ_1 (psi)	σ_2 (psi)	σ_1 (psi)	J_1 (10^{-6} psi^{-1})
4906	Sandstone	5150	4300	2800*	4743	4017	4821	0.086
4909	Sandstone	5155	4300	2800*	4757	4151	4810	0.046
4910	Sandstone	5155	4300	2800*	4647	4108	4742	0.105
5701	Mudstone	5985	5150	3300	5360	5259	5315	0.044
5724	Sandstone	6010	4575	3300	5807	4680	5790	0.073
5725	Sandstone	6010	4575	3300	5774	4852	5705	0.054
5766	Sandstone	6055	4575	3360	5508	4845	5360	0.090
5781	Sandstone	6070	4575	3370	5417	4754	5290	0.074
5782	Sandstone	6070	4575	3370	5520	4806	5402	0.090

* Estimated from nearest interval where the pressure was measured with a well test.

Table 6.4

Summary of MWX DSCA/DWVA Results

Sample	Azimuth	Total $\sigma_1:\sigma_2:\sigma_3$	Fracture Gradient	Type
MWX-2 4949.1 ft	N77E;45S	1.975:1.389:1.0	0.70	DSCA
MWX-3 5694.5 ft	N67W;45SW	1.955:1.610:1.0	0.75	DSCA
MWX-3 5727.5 ft	N74E;V	2.001:1.211:1.0	0.69	DSCA
MWX-2 4949.3 ft	N55E;80SE	---	--	DWVA

Explanation: Azimuth is with respect to the (σ_2 - σ_3) plane (and thus the fracture), while "V" denotes a vertical inclination. Fracture gradients are listed in psi/foot of depth.

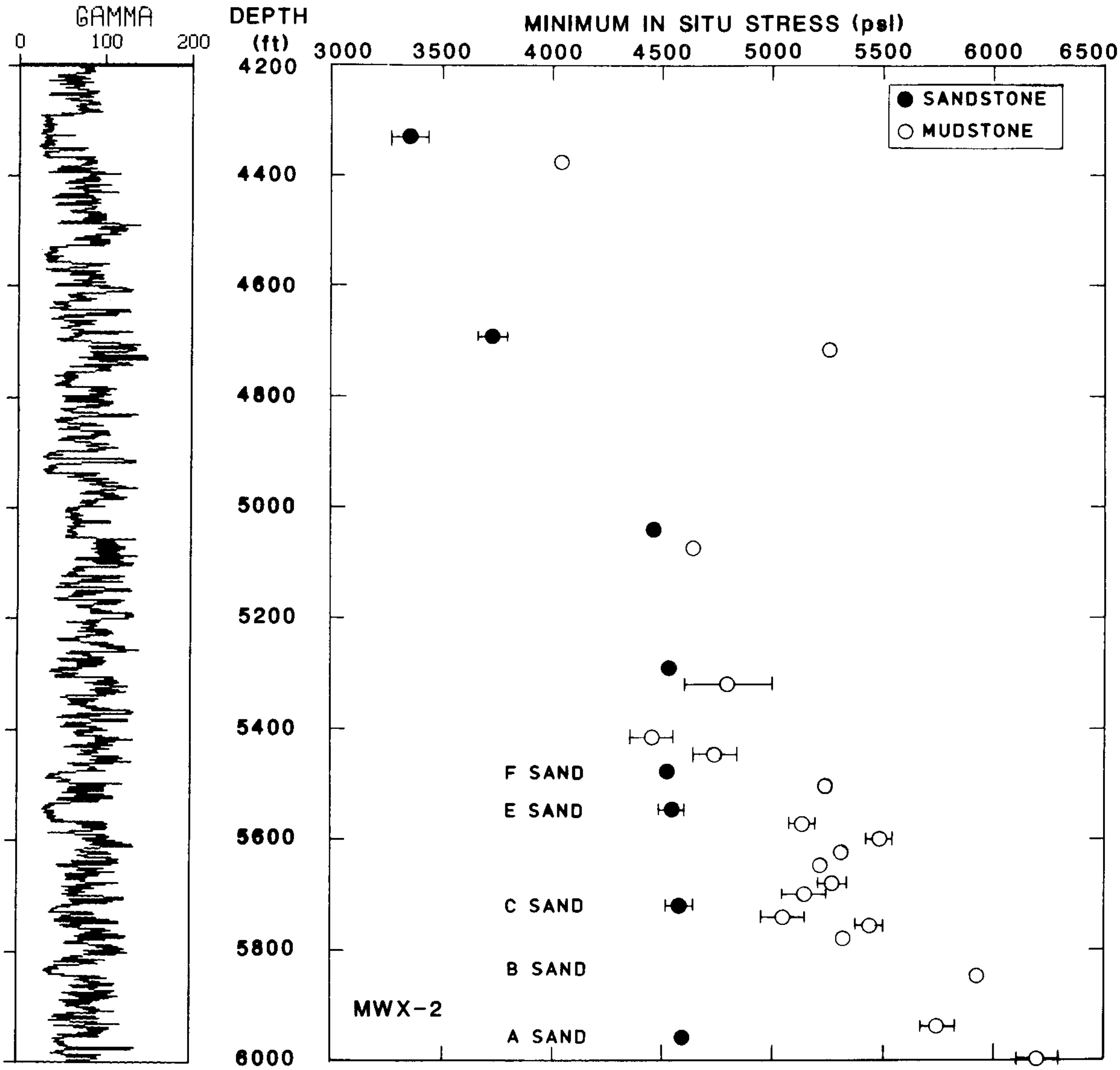

Figure 6.1 Stress Test Results

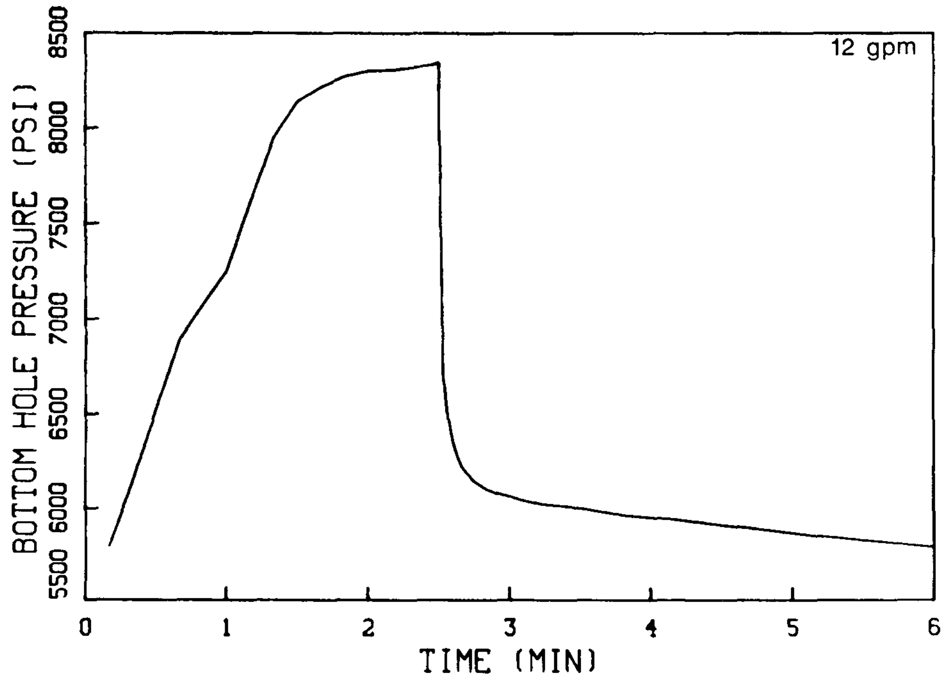

Figure 6.2 Example Stress Data, 6006-08 ft, 2nd Injection

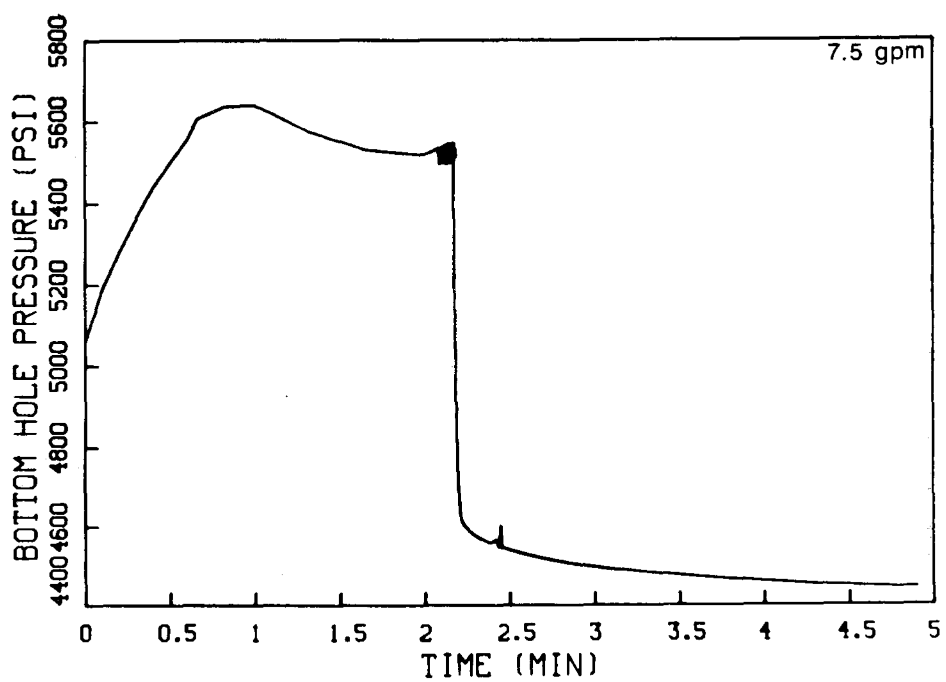

Figure 6.3 Example Stress Data, 5962-64 ft, 2nd Injection

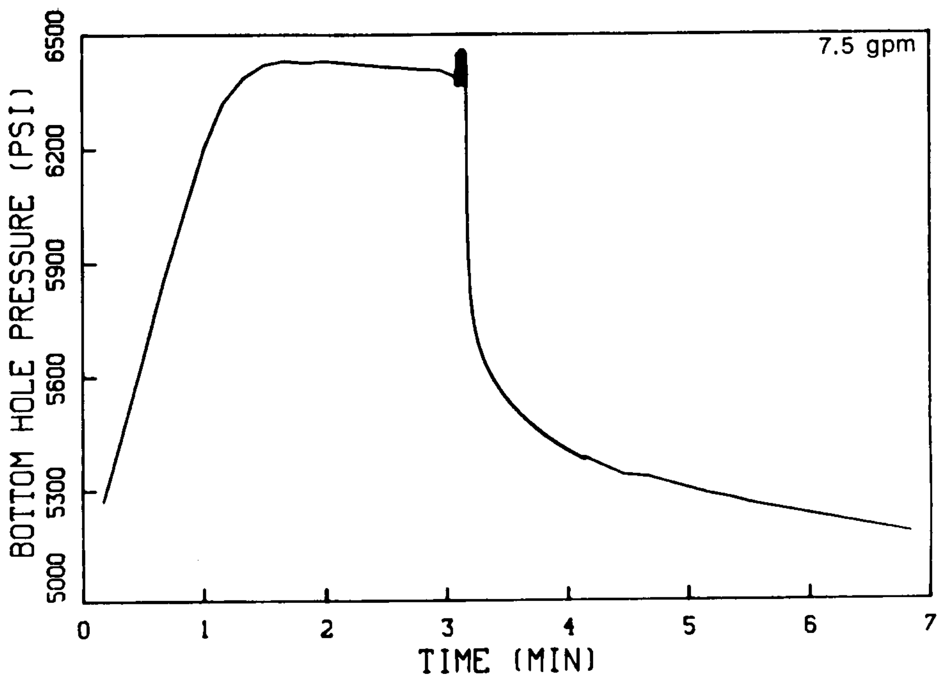

Figure 6.4 Example Stress Data, 5940-42 ft, 3rd Injection

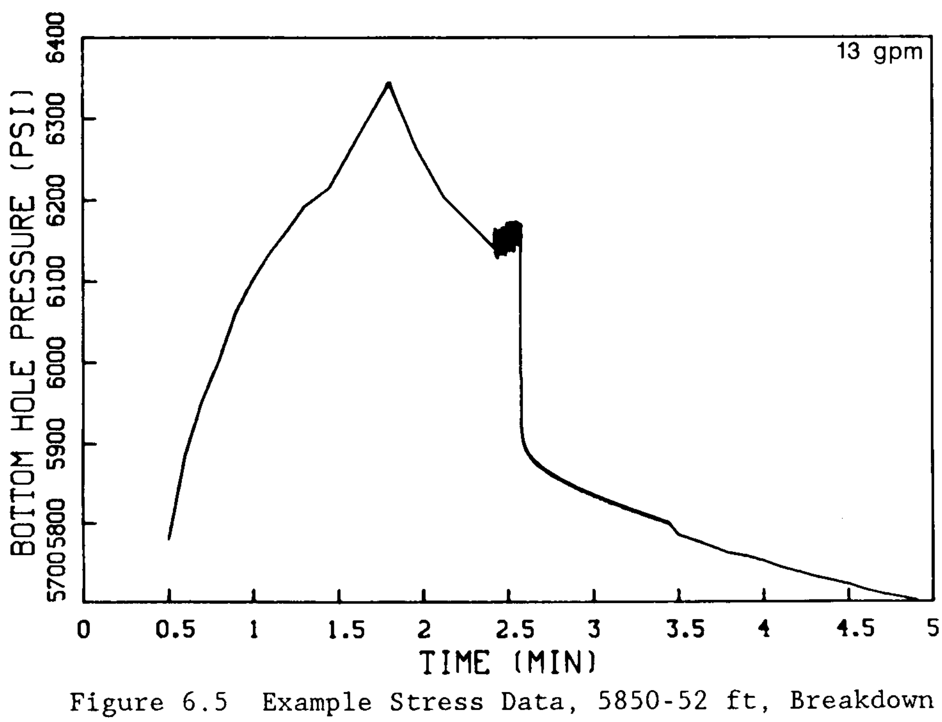

Figure 6.5 Example Stress Data, 5850-52 ft, Breakdown

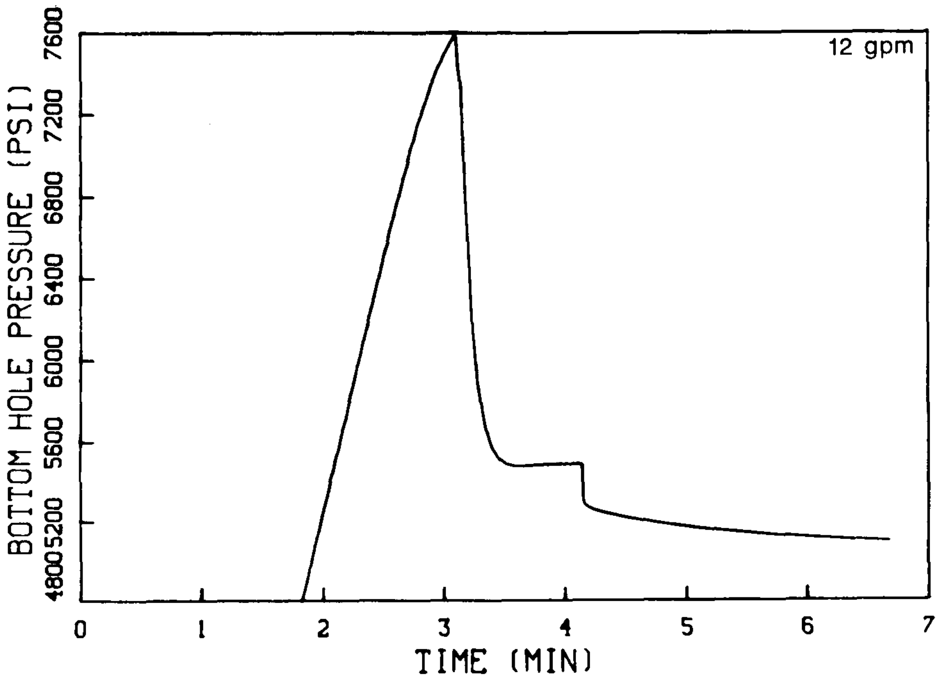

Figure 6.6 Example Stress Data, 5778-80 ft, Breakdown

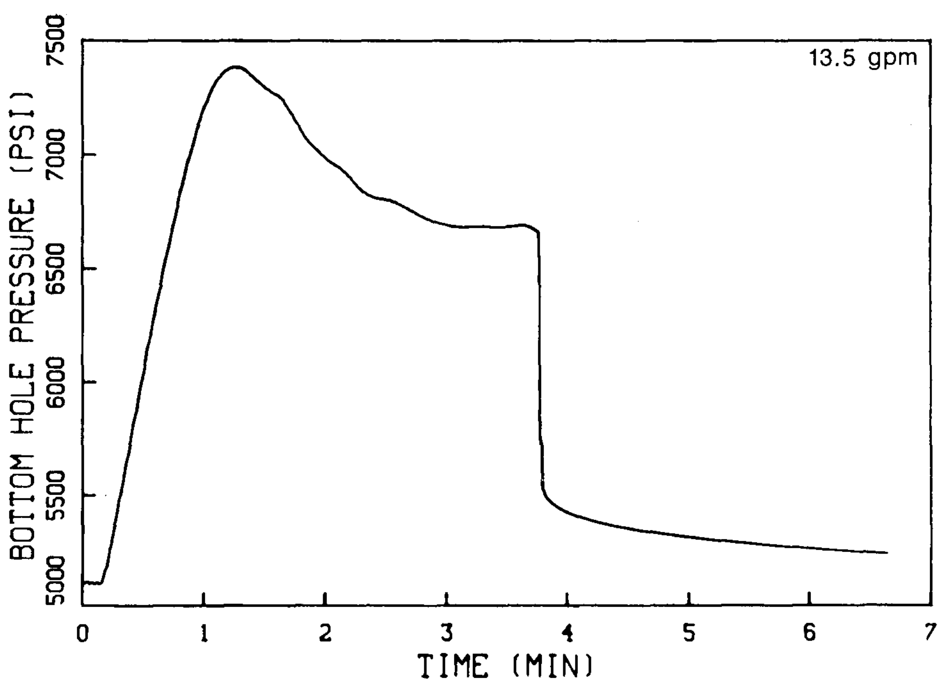

Figure 6.7 Example Stress Data, 5757-59 ft, 4th Injection

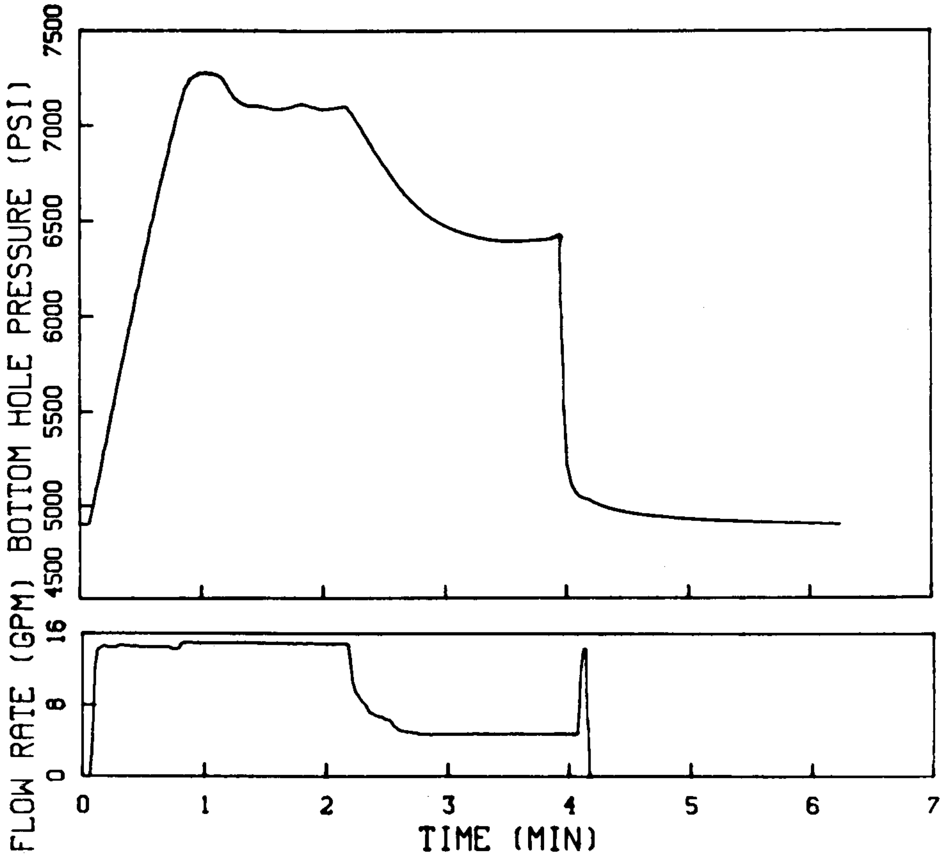

Figure 6.8 Example Stress Data, 5744-46 ft, 3rd Injection

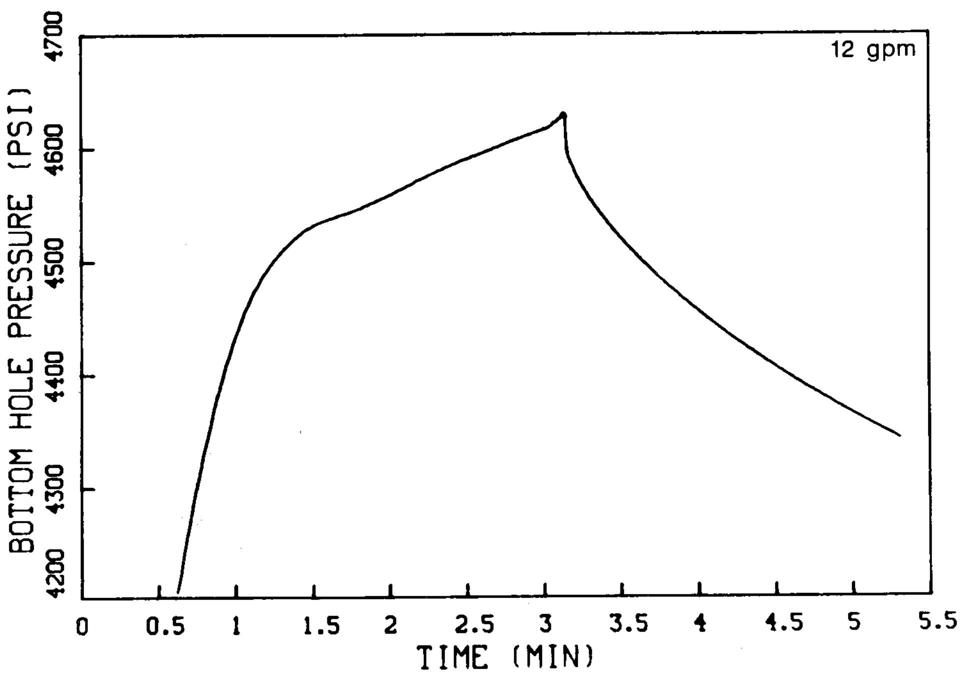

Figure 6.9 Example Stress Data, 5721-23 ft, 2nd Injection

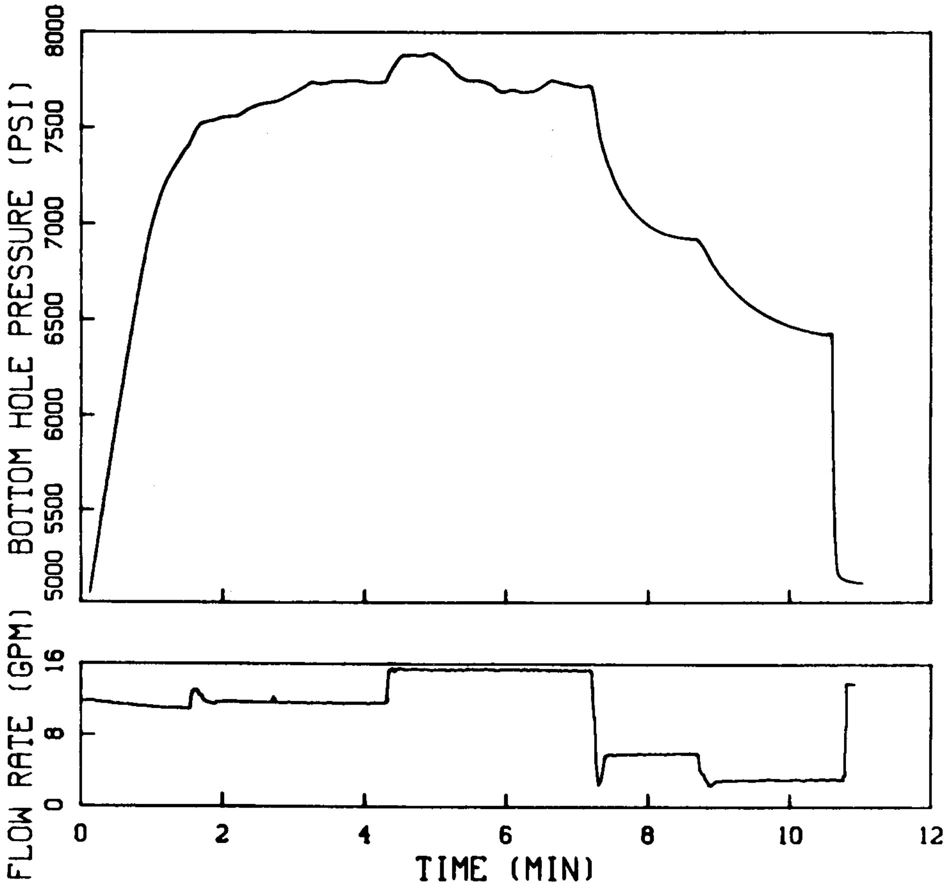

Figure 6.10 Example Stress Data, 5700-02 ft, 2nd Injection

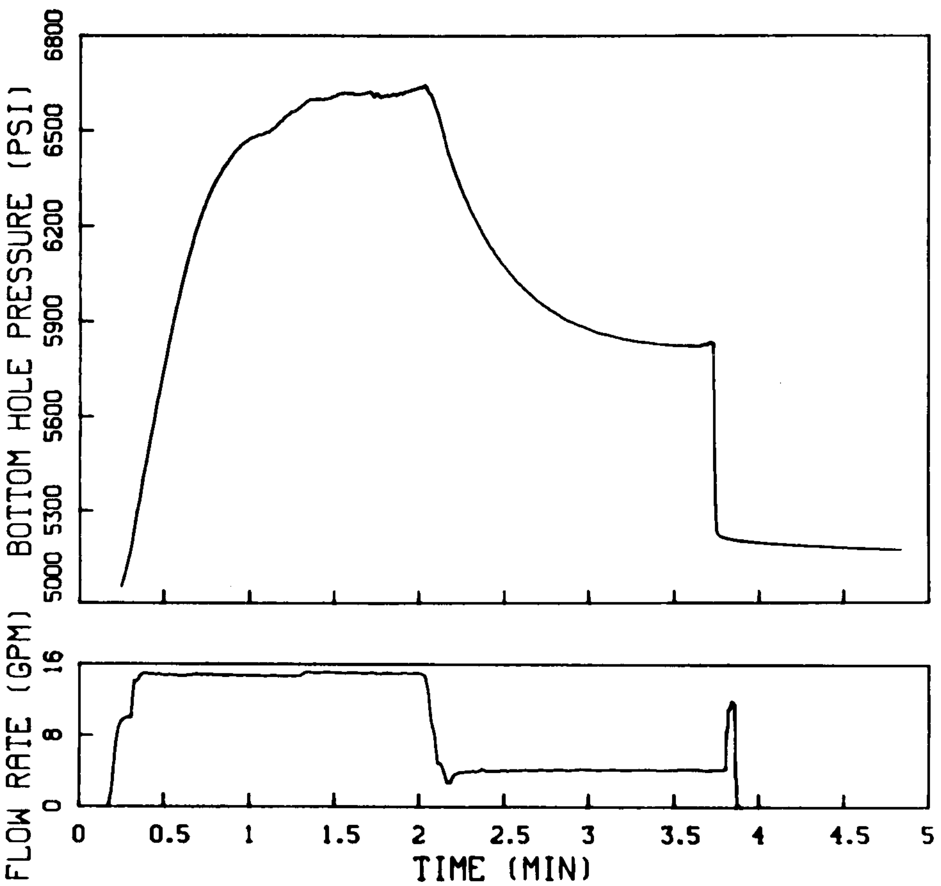

Figure 6.11 Example Stress Data, 5680-82 ft, 4th Injection

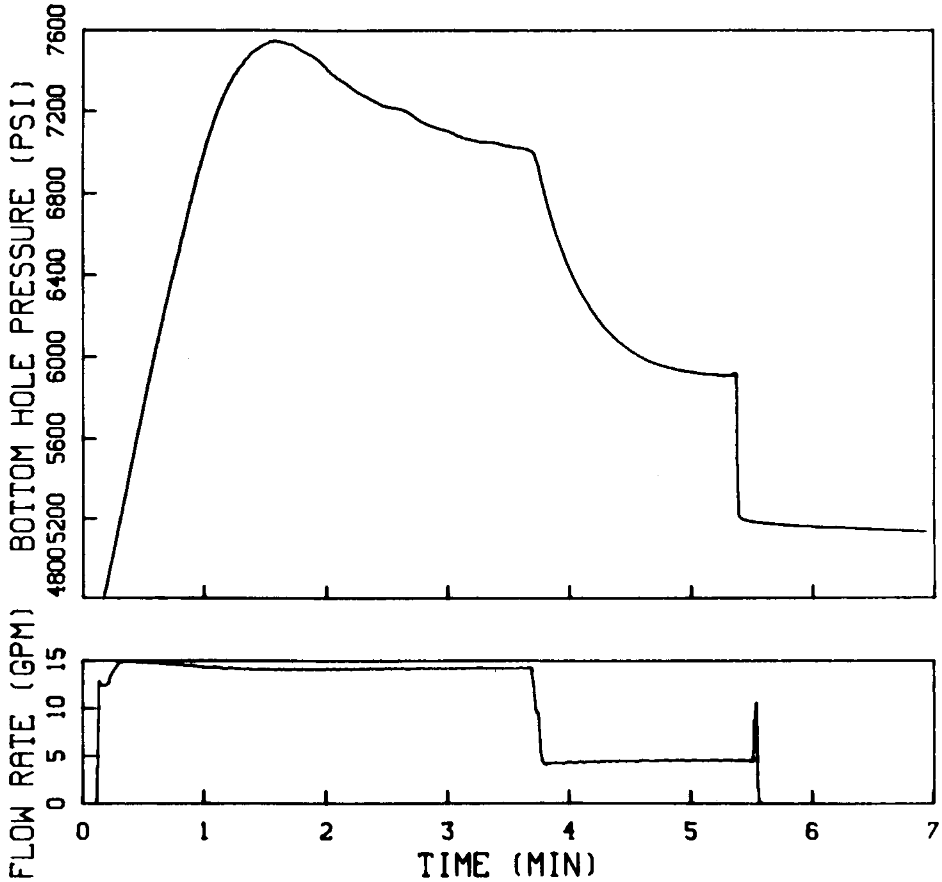

Figure 6.12 Example Stress Data, 5649-51 ft, 2nd Injection

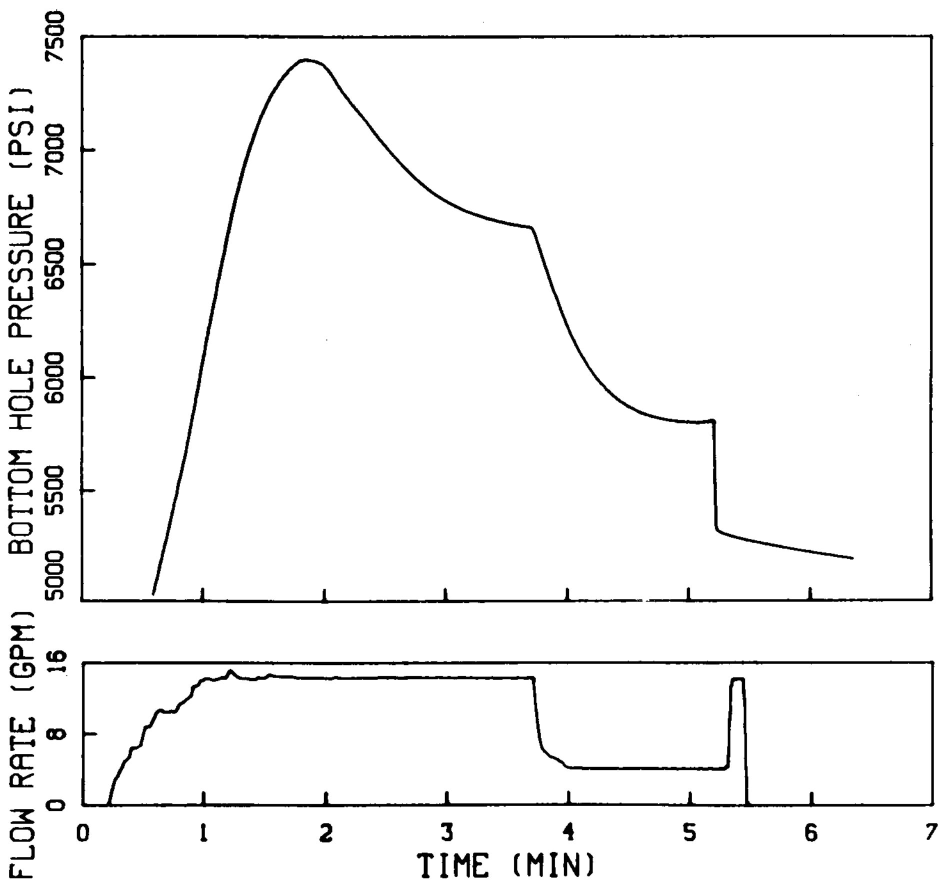

Figure 6.13 Example Stress Data, 5620-22 ft, 4th Injection

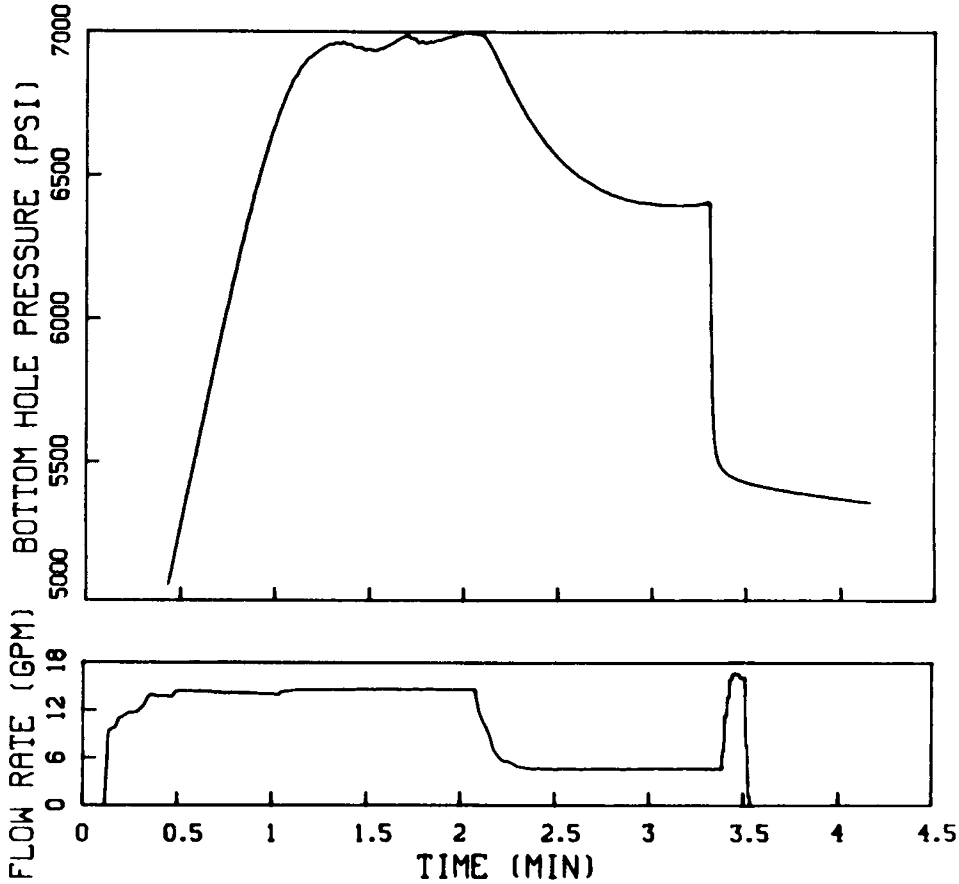

Figure 6.14 Stress Test Results, 5600-02 ft, 2nd Injection

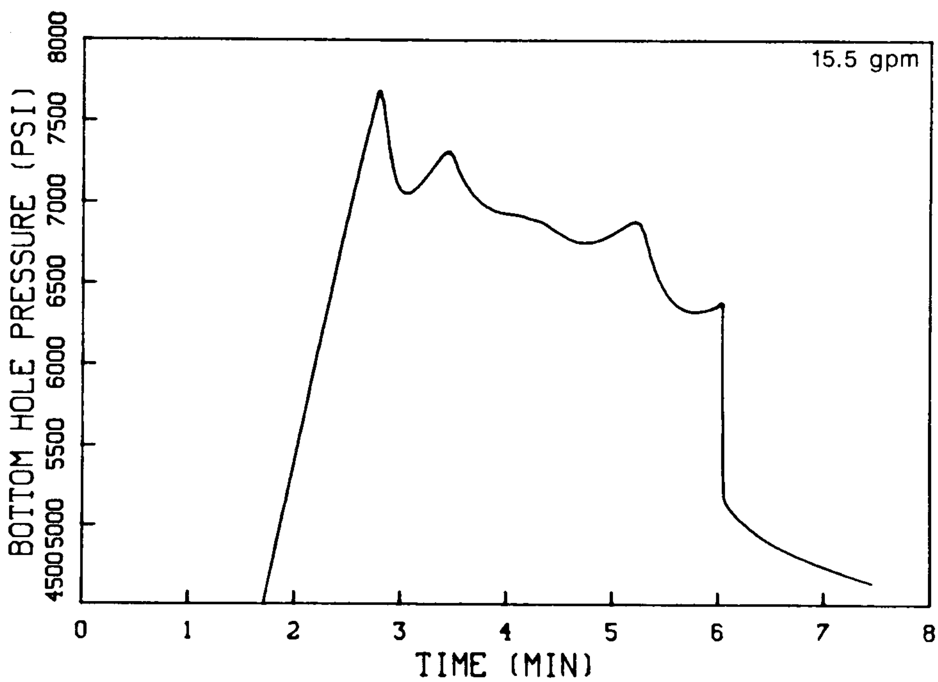

Figure 6.15 Example Stress Data, 5575-77 ft, Breakdown

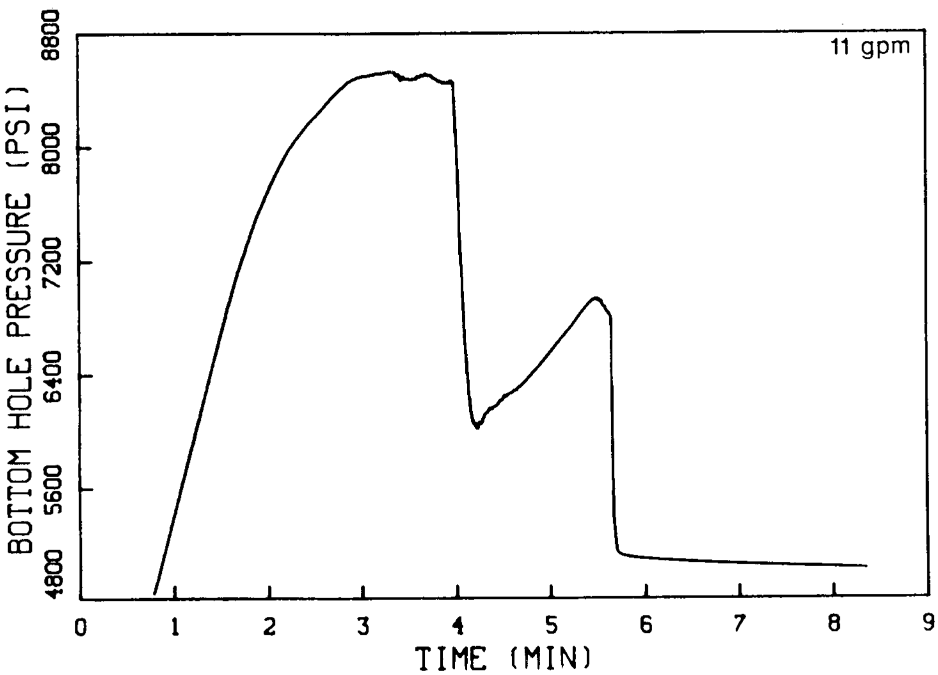

Figure 6.16 Example Stress Data, 5506-08 ft, 2nd Injection

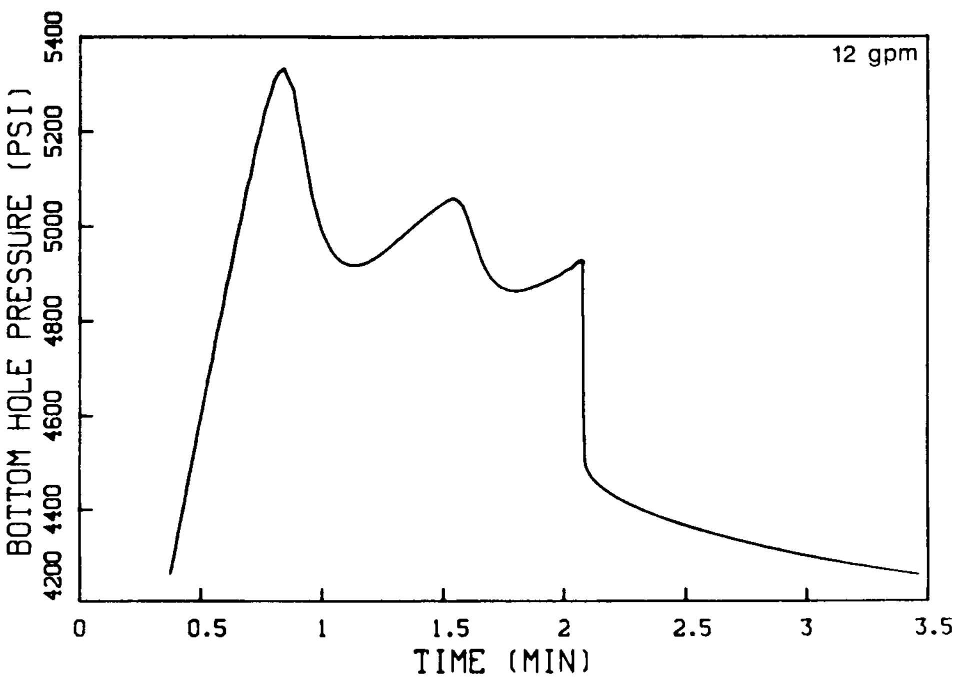

Figure 6.17 Example Stress Data, 5480-82 ft, 2nd Injection

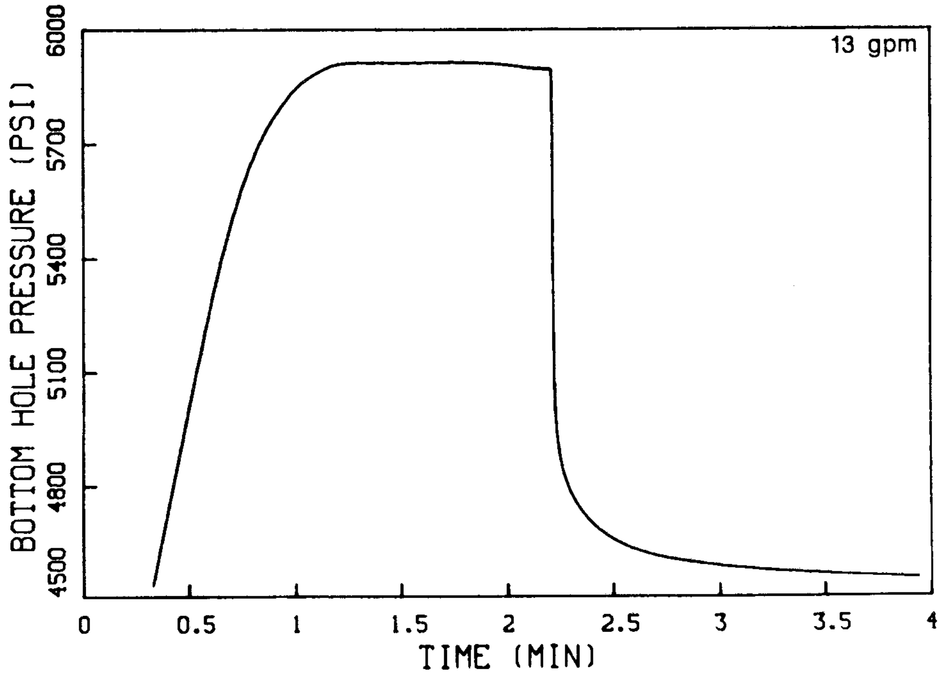

Figure 6.18 Example Stress Data, 5450-52 ft, 4th Injection

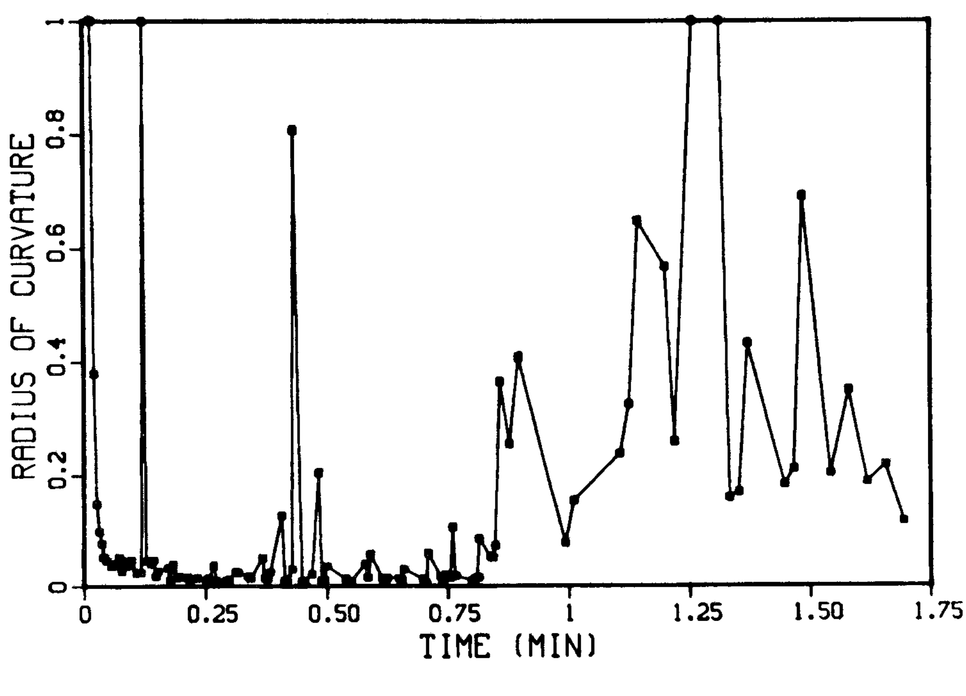

Figure 6.19 Radius of Curvature Plot of Data in Figure 6.18

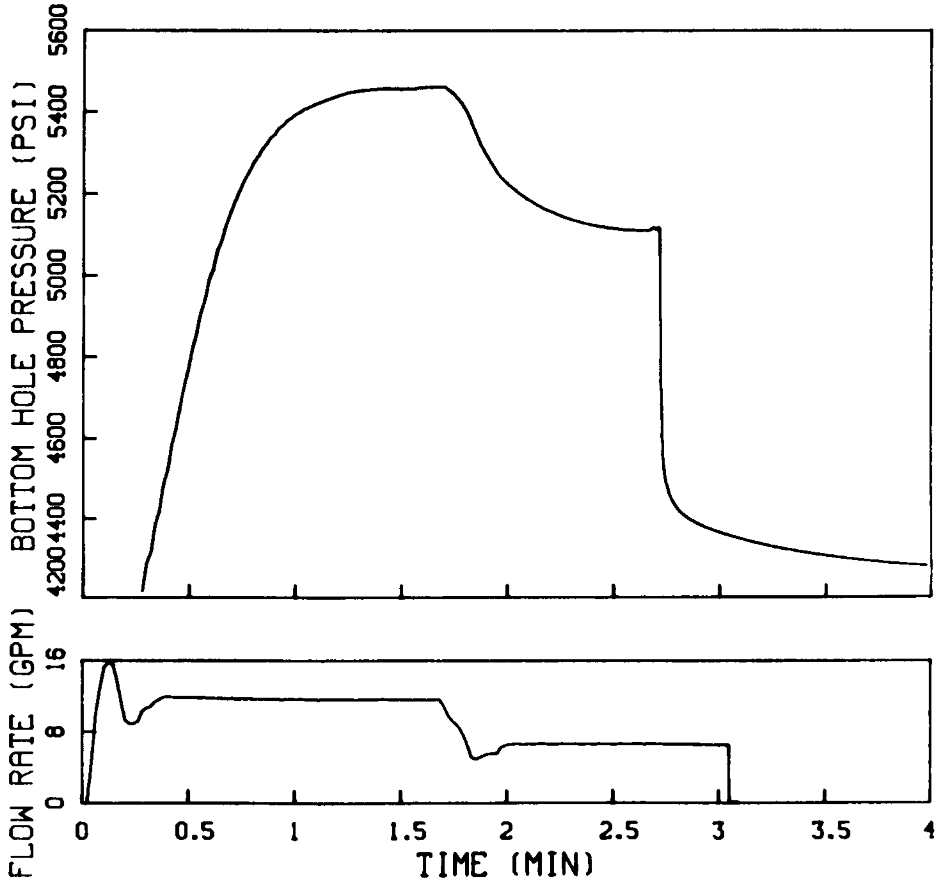

Figure 6.20 Example Stress Data, 5414-16 ft, 4th Injection

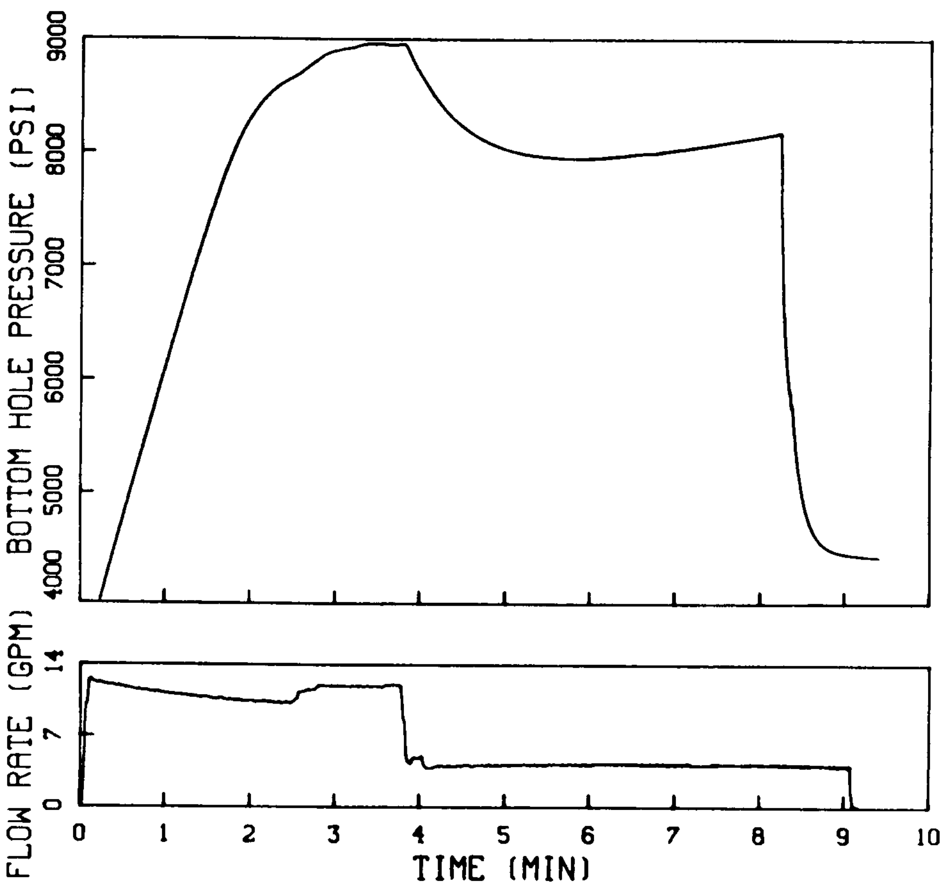

Figure 6.21 Example Stress Data, 5320-22 ft, 4th Injection

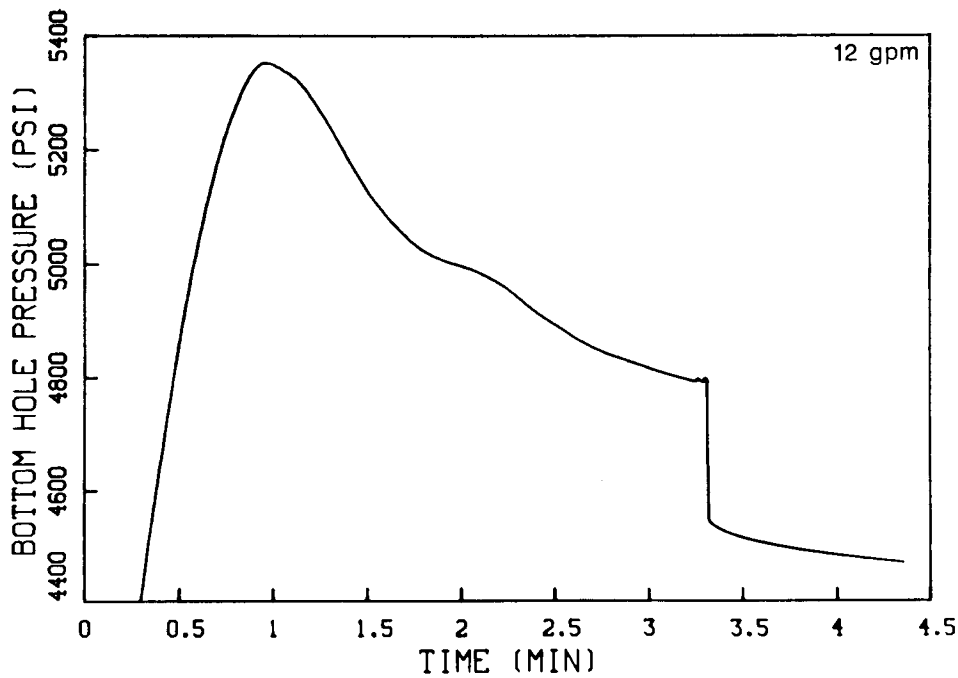

Figure 6.22 Example Stress Data, 5294-96 ft, 4th Injection

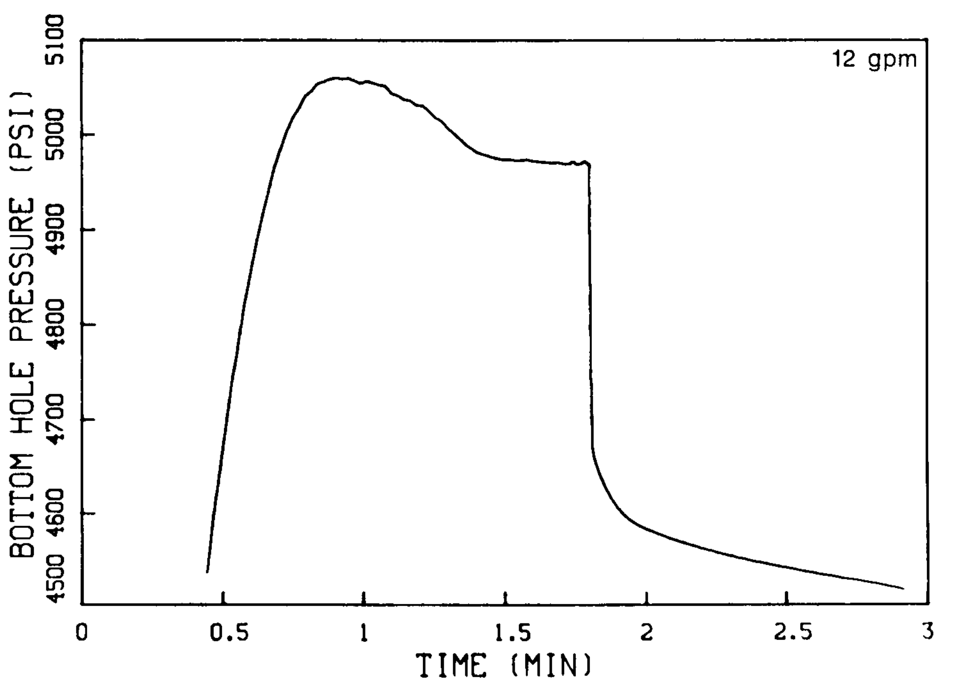

Figure 6.23 Example Stress Data, 5074-76 ft, 3rd Injection

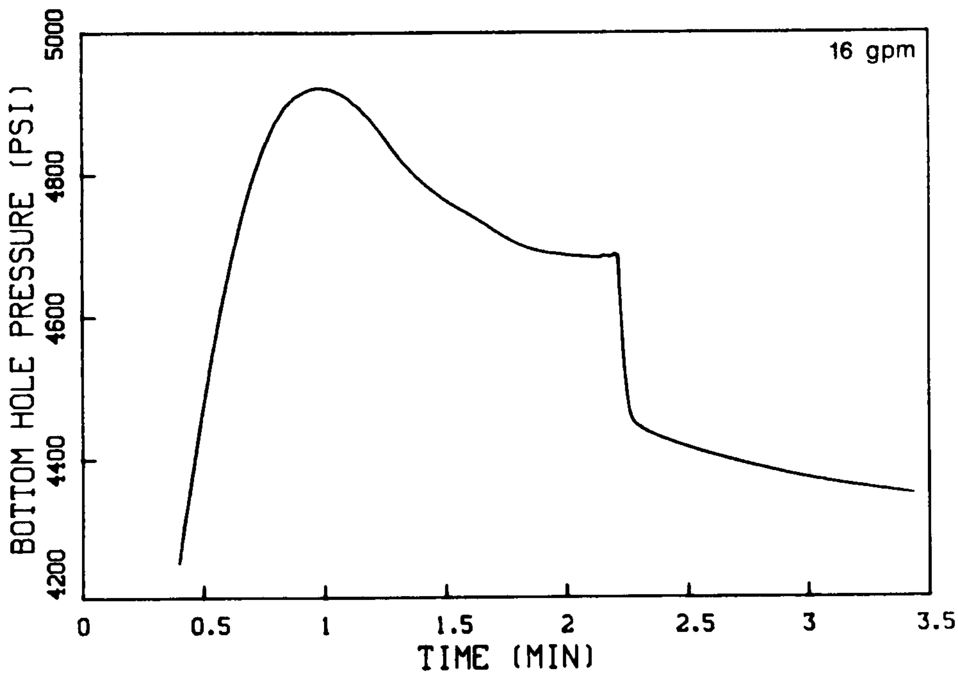

Figure 6.24 Example Stress Data, 5044-46 ft, 5th Injection

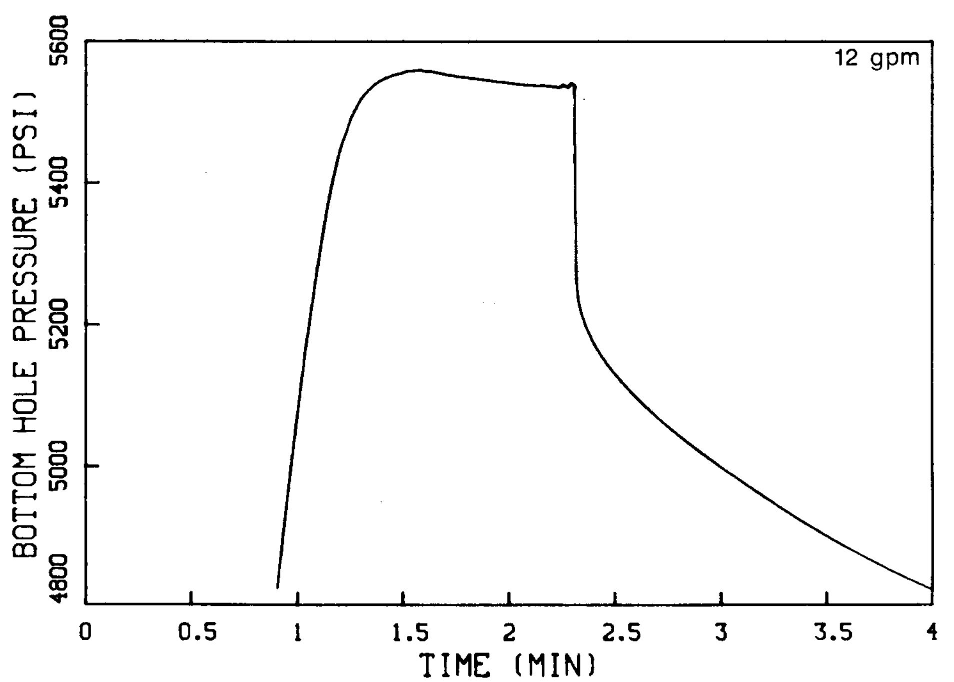

Figure 6.25 Example Stress Data, 4714-16 ft, 4th Injection

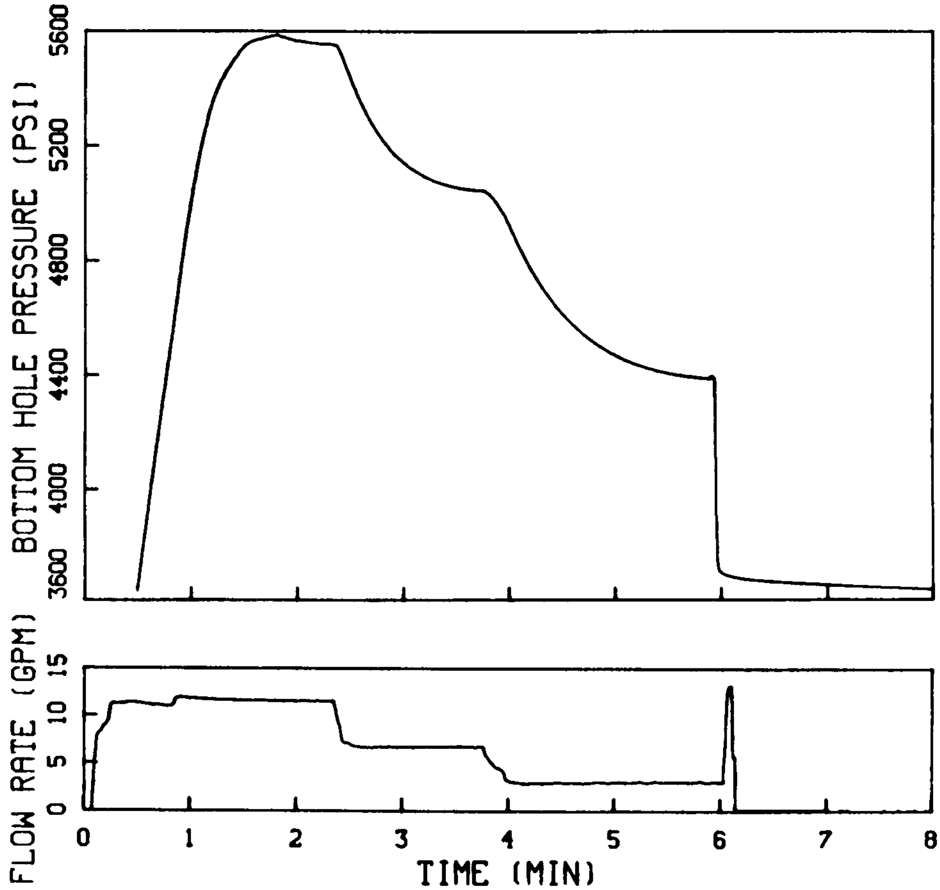

Figure 6.26 Example Stress Data, 4692-94 ft, 6th Injection

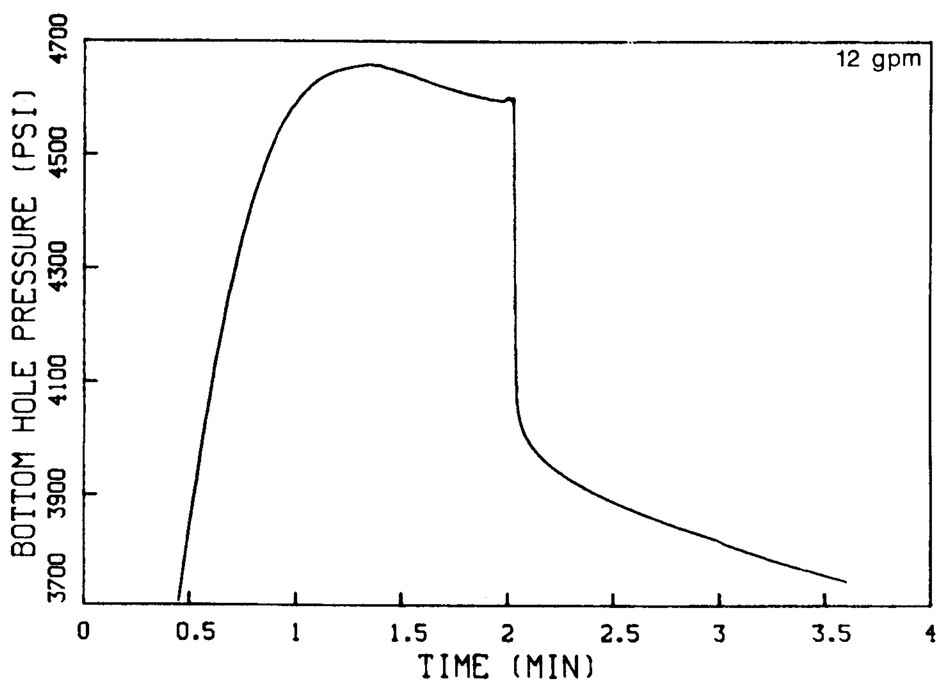

Figure 6.27 Example Stress Data, 4376-78 ft, 3rd Injection

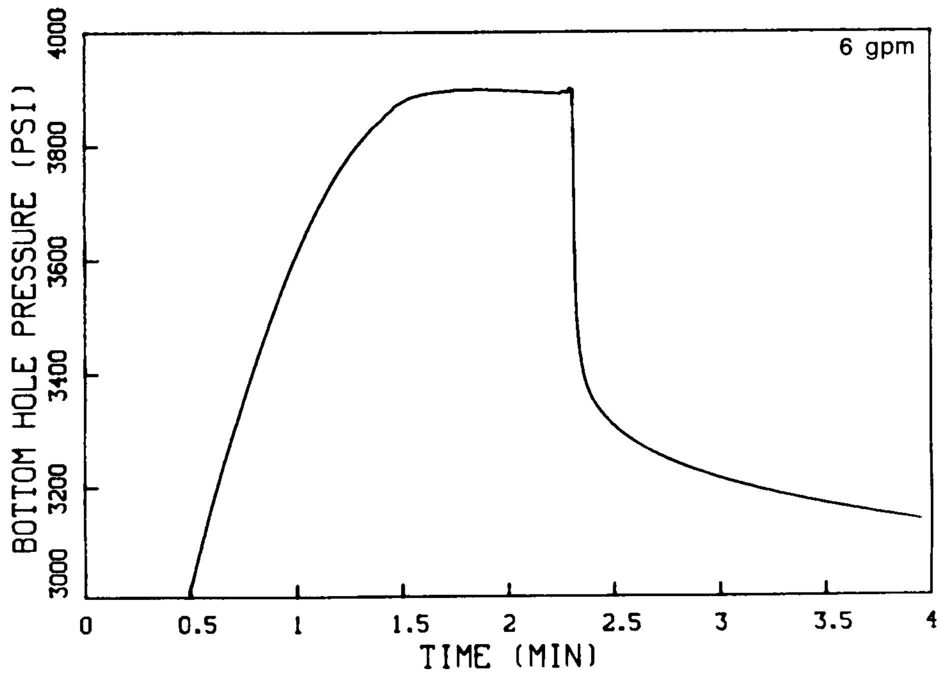

Figure 6.28 Example Stress Data, 4330-32 ft, 4th Injection

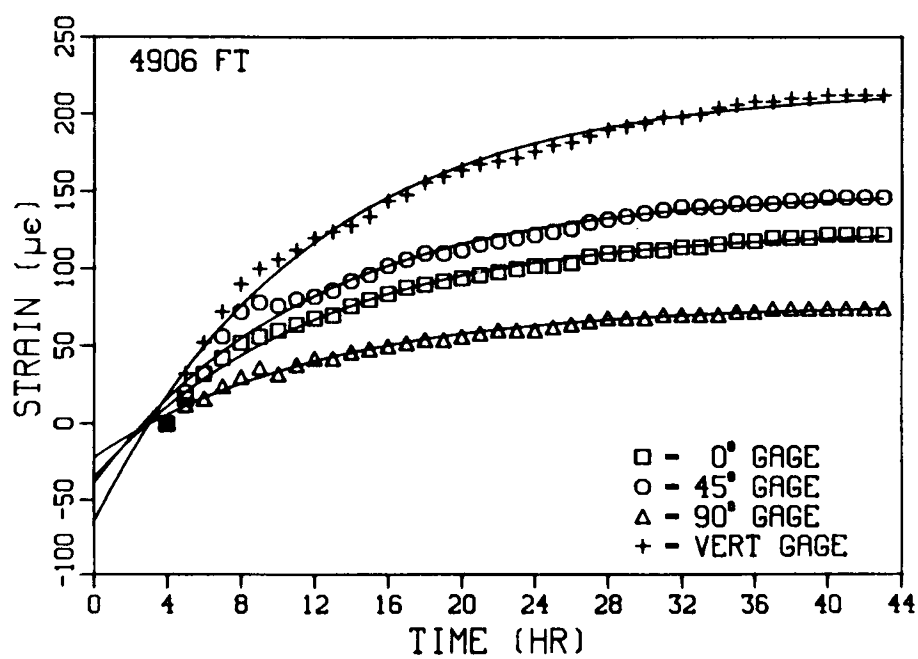

Figure 6.29 ASR Data, Sandstone at 4906 ft

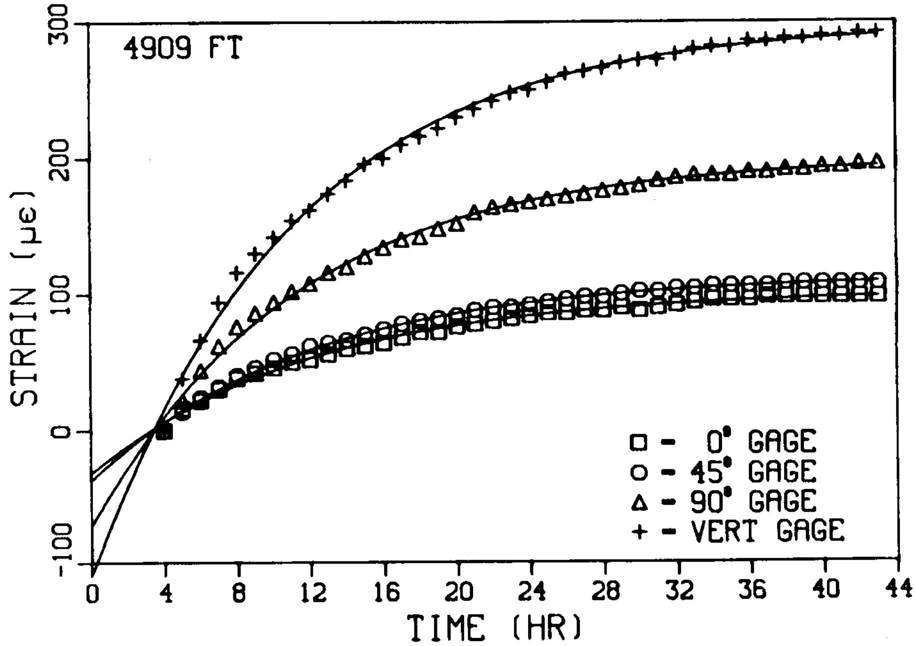

Figure 6.30 ASR Data, Sandstone at 4909 ft

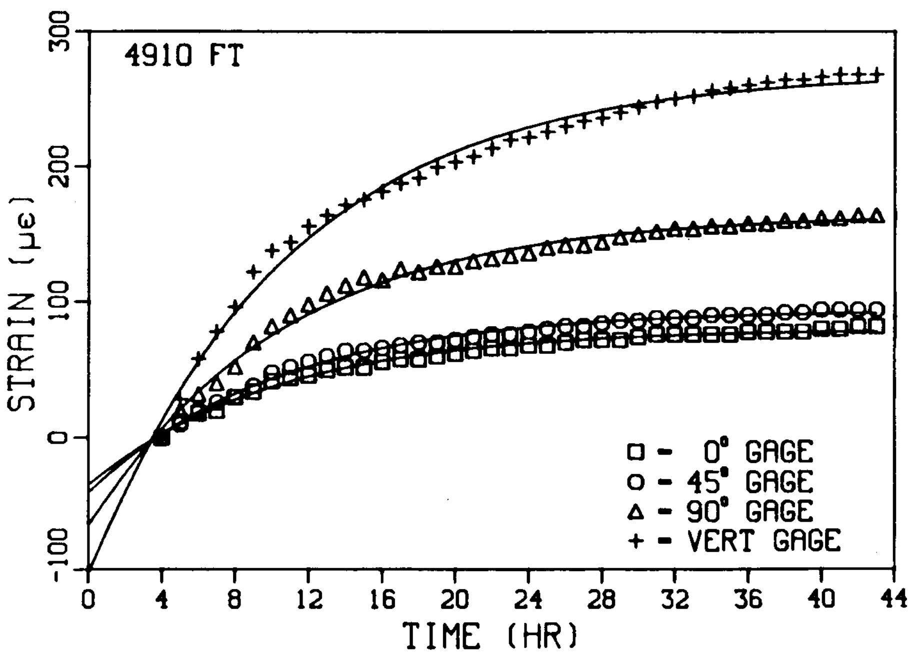

Figure 6.31 ASR Data, Sandstone at 4910 ft

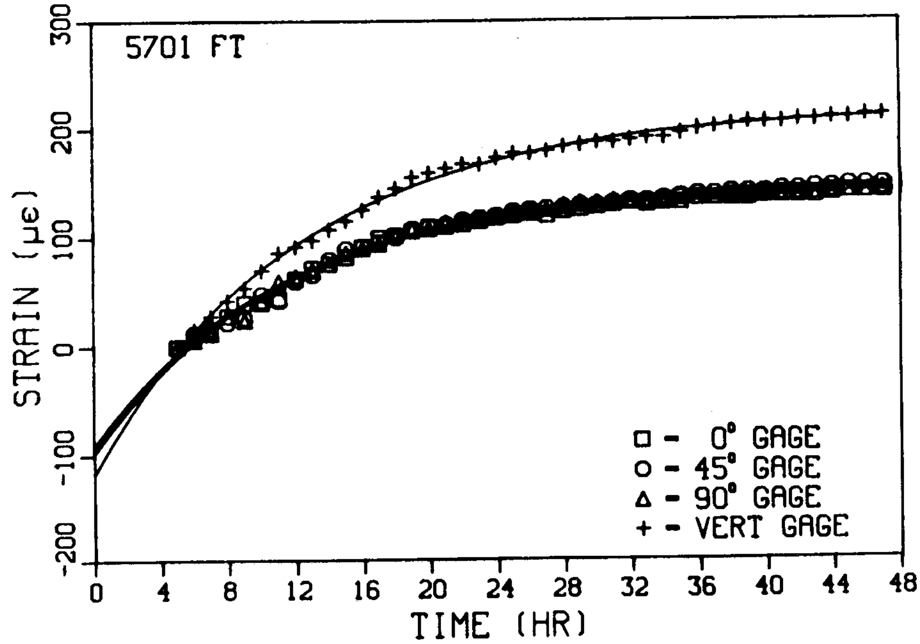

Figure 6.32 ASR Data, Mudstone at 5701 ft

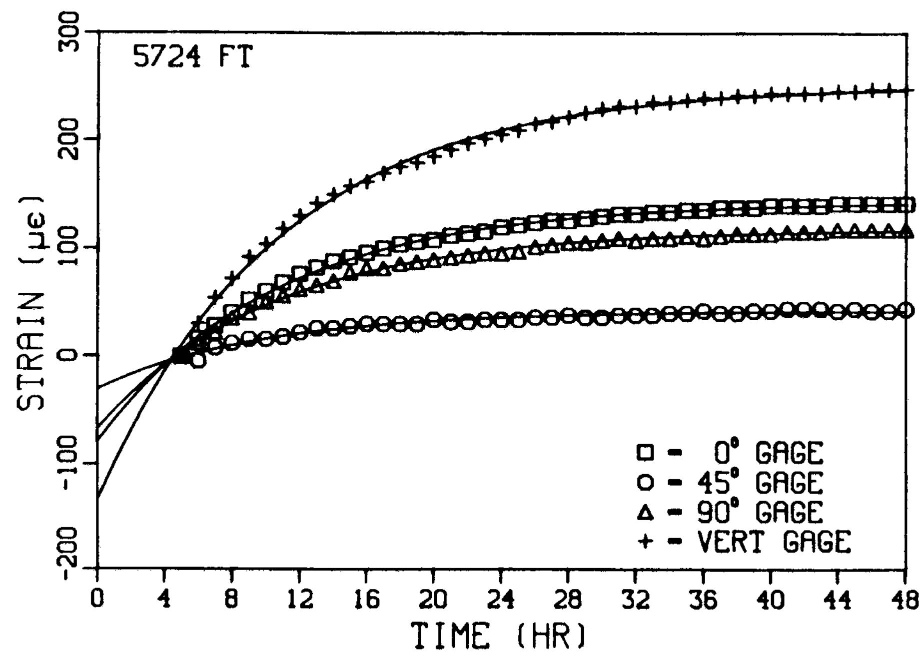

Figure 6.33 ASR Data, Sandstone at 5724 ft

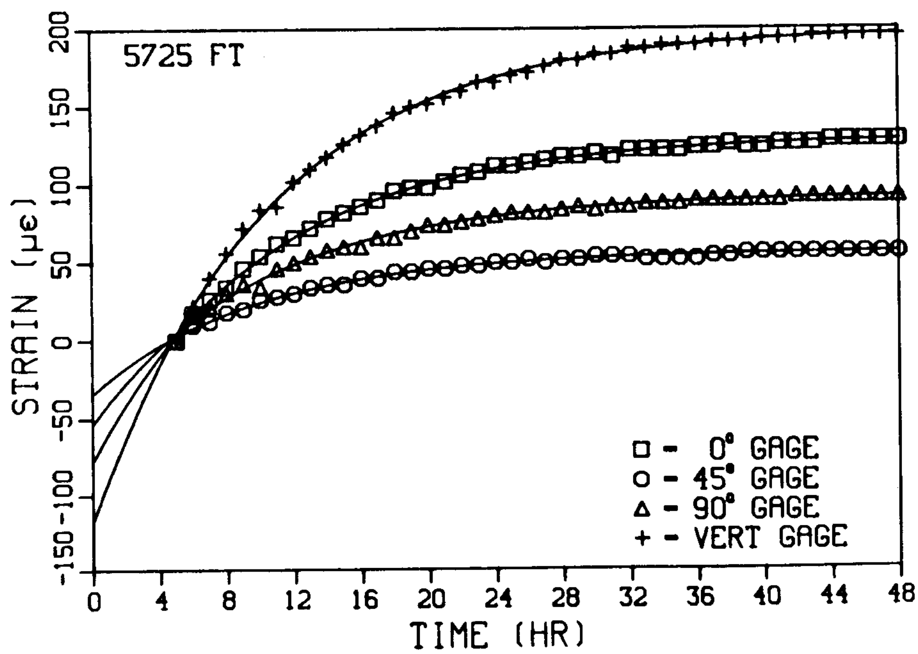

Figure 6.34 ASR Data, Sandstone at 5725 ft

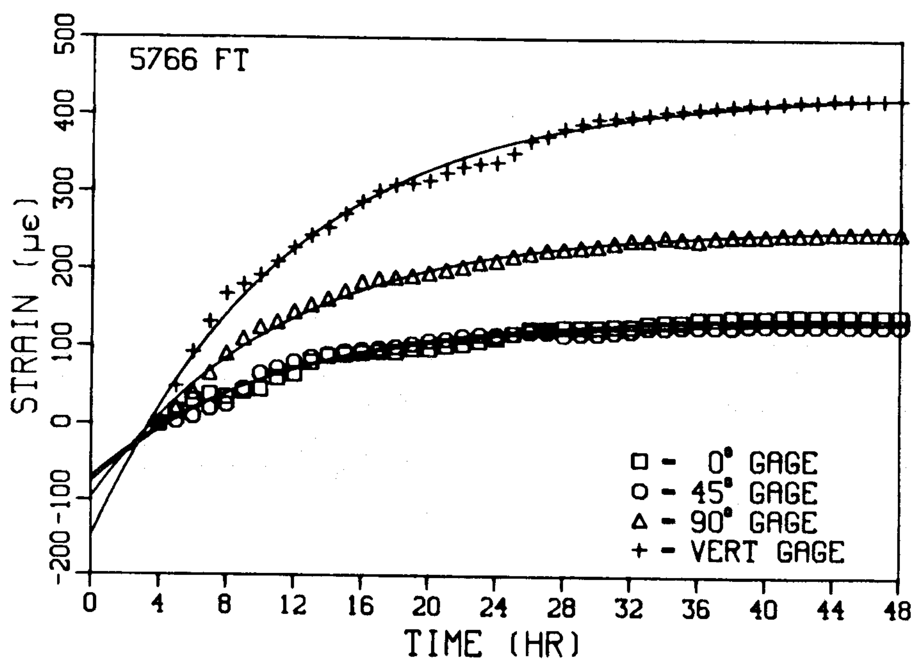

Figure 6.35 ASR Data, Sandstone at 5766 ft

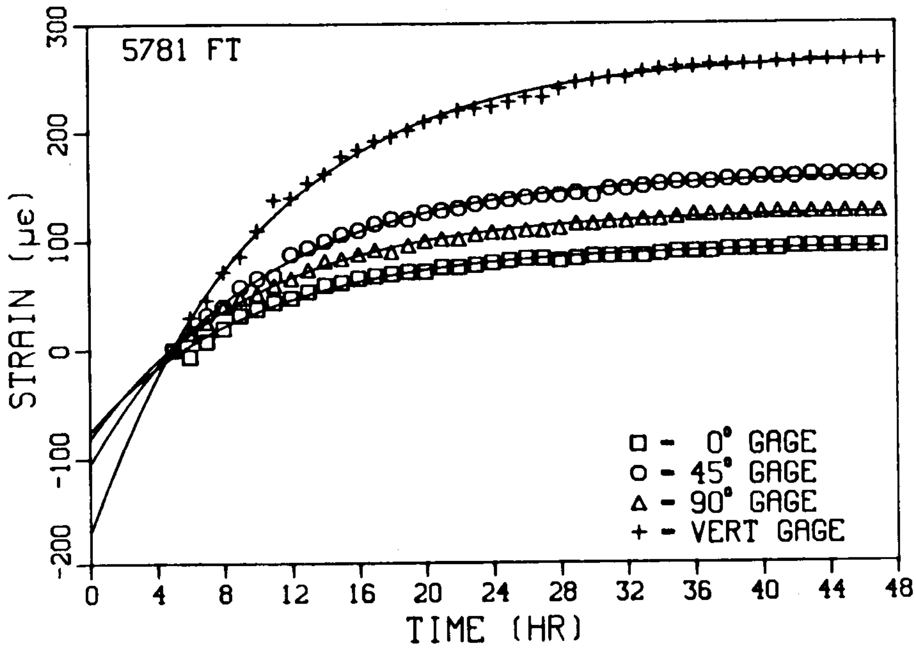

Figure 6.36 ASR Data, Sandstone at 5781 ft

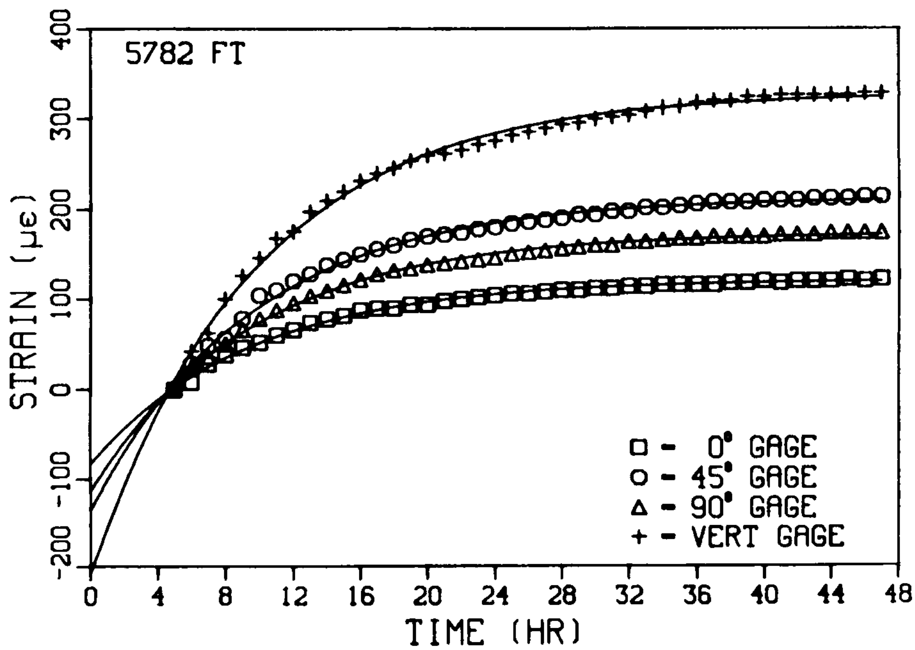

Figure 6.37 ASR Data, Sandstone at 5782 ft

DISTRIBUTION:

M. J. Singer
Deputy Assistant Secretary for Oil, Gas, Shale, and Special Technologies
US Department of Energy
FE-30 Forrestal Bldg.
Washington, DC 20585

J. D. Batchelor
Office of Oil, Gas, and Shale Technologies
US Department of Energy
FE-33 Germantown
Washington, DC 20545

J. R. White
Office of Oil, Gas and Shale Technologies
US Department of Energy
FE-33 Germantown
Washington, DC 20545

D. A. Juckett
Office of Geoscience Research
US Department of Energy
FE-3 Forrestal Bldg.
Washington, DC 20585

US Department of Energy (10)
Morgantown Energy Technology Center
Box 880 Collins Ferry Road
Morgantown, WV 26505
Attn: A. A. Pitrolo
H. D. Guthrie
C. A. Komar
K-H. Frohne (3)
G. Latham
A. Layne
J. K. Westhusing
J. Duda

US Department of Energy (2)
Bartlesville Project Office
PO Box 1398
Bartlesville, OK 74005
Attn: T. C. Wesson
A. B. Crawley

F. Heuze
Lawrence Livermore National Laboratory
MS L200
Livermore, CA 94550

Los Alamos National Laboratory (3)
Earth and Space Science Division
Los Alamos, NM 87545
Attn: C. W. Myers
R. J. Hanold
J. A. Albright

US Geological Survey (4)
Box 25046
Denver Federal Center
Denver, CO 80225
Attn: B. E. Law, MS 971
C. W. Spencer, MS 940
R. Johnson, MS 971
T. Fouch, MS 951

CER Corporation (30)
PO Box 94977
Las Vegas, NV 89193-4977
Attn: R. L. Mann (25)
F. R. Myal
P. T. Branagan
G. C. Kukal
W. H. Mathis
C. Cipolla

L. F. Elkins
2615 Oak Drive, #28
Lakewood, CO 80215

T. C. Vogt
Mobil Oil Corp.
1225 17th Street
Denver, CO, 80202

F. G. Martin
907 Glendell Drive
Irving, TX 75061

D. E. Nierode
Exxon Production Research Co.
PO Box 2189
Houston, TX 77001

R. J. Saucier
Shell Offshore Incorporated
PO Box 60149
New Orleans, LA 70160

Mobil Research and Development
Corp. (4)
PO Box 819047
Dallas, TX 75381
Attn: M. Strubhar
L. Medlin
E. Sprunt
I. Abou-Sayed

R. W. Veatch
Amoco Production Co.
Research Department
PO Box 3385
Tulsa, OK 74102

Chandler & Associates
Suite 1400
1860 Lincoln Street
Denver, CO 80203

National Institute for Petroleum and
Energy Research (3)
PO Box 2128
Bartlesville, OK 74005
Attn: H. B. Carroll
C. J. Raible
B. L. Gall

Smith Energy Services (2)
R. D. Timberline Building
Junction Hwys 58 & 93
Golden, CO 80403
Attn: D. Holcomb
W. Holcomb

L. Harrington
The Western Company
PO Box 186
Fort Worth, TX 76101

Dowell Schlumberger
Research Center (4)
PO Box 2710
Tulsa, OK 74101
Attn: J. Elbel
K. Nolte
B. Ainley
K. Nimerick

P. Warembourg
Dowell Schlumberger
PO Box 5818
Denver, CO 80217

M. Brugler
Western Atlas International
Core Laboratories
7304 E 38th Street
Tulsa, OK 74145

S. Leeds
Western Atlas International
Core Laboratories
10703 E. Bethany Drive
Aurora, CO 80014

Western Atlas International (4)
Core Laboratories
1300 East Rochelle Blvd.
Irving, TX 75062
Attn: J. Walls
L. Hall
D. Malek
E. York

T. Zeller
RE/SPEC, INC.
PO Box 725
Rapid City, SD 57701

UNC Geotech (2)
PO Box 14000
Grand Junction, CO 81502
Attn: L. Fukui
R. Dayvault

Institute of Gas Technology (2)
3424 S. State Street
Chicago, IL 60616
Attn: P. L. Randolph
D. J. Soeder

Petroleum Recovery Research Center
(2)
NM Institute of Mining and
Technology
Socorro, NM 87801
Attn: F. D. Martin
N. R. Morrow

Gas Research Institute (4)
8600 West Bryn Mawr Avenue
Chicago, IL 60631
Attn: C. F. Brandenberg
W. F. Perry
T. Wooten
I. A. Salehi

S. A. Holditch
S. A. Holditch and Assoc. Inc.
900 Southwest Parkway East
Suite 200
College Station, TX 77840

ARCO Oil & Gas Company (3)
2300 West Plano Parkway
Plano, TX 75075
Attn: R. L. Hirsch
F. H. Hsu
C. Ossian

B. McGlothlin
Chevron Geosciences Co.
PO Box 42832
Houston, TX 77242

T. L. Reeves
CNG Producing Co.
PO Box 2115
Tulsa, OK 74101-2115

CNG Producing Company (2)
Canal Place 1
Suite 3100
New Orleans, LA 70130-9990
Attn: B. Coffin
T. L. Reeves

D. Pellatz
Conoco Inc.
907 N. Poplar
Casper, WY 82601

D. Munson
David Munson Inc.
1525 Elm Street, Suite 1900
Dallas, TX 75201

M. Smith
NSI Technologies, Inc.
7030 Yale, Suite 502
Tulsa, OK 74136

J. Schwoebel
Resource Enterprises, Inc.
400 Wakara Way
Salt Lake City, UT 84108

T. Juranek
Mobil Exploration and Producing U.S.
Inc.
12450 Greenspoint Drive
Houston, TX 77060-1991

D. L. Luffel
ResTech Houston
14411 Cornerstone Village Drive
Houston, TX 77014

R. E. Barba
Schlumberger
1031 Andrews Highway
Midland, TX 79701

R. A. Plumb
Schlumberger-Doll Research
Old Quarry Road
PO Box 307
Ridgefield, CT 06877

Shell Development Co. (3)
Bellaire Research Center
PO Box 481
Houston, TX 77001
Attn: D. C. Schultze
K. Hansen
J. Shlyapobersky

M. Conway
Stim-Lab, Inc.
3445 N. Hwy 81
Duncan, OK 73534

G. R. Coulter
Oryx Energy Company
PO Box 830936
Richardson, TX 75083

Terra Tek Inc. (2)
420 Wakara Way
Salt Lake City, UT 84108
Attn: A. Jones
J. McClennan

H. A. Illich
Oryx Energy Co.
Campbell Center II
PO Box 2880
Dallas, TX 75221

Union Oil Co. of California (4)
Research Department
PO Box 76
Brea, CA 92621
Attn: C. Allen
J. Smith
J. Cameron
W. Minner

W. Stoner
Universal Well Services, Inc.
159 Northwood Dr.
Box 1456
Meadville, PA 16335

Canadian Hunter Exploration, Ltd. (2)
435 4th Avenue SW
Calgary, Alberta T2P 3A8
Canada
Attn: R. E. Wyman
R. A. Clark

R. Kry
Esso Resources Canada Limited
Research Department
339 50th Avenue SE
Calgary, Alberta T2G 2B3
Canada

L. Roodhart
Shell Canada Ltd.
PO Box 2506
Calgary, Alberta T2P 3S6
Canada

W. Hansen
Amoco Production Co.
1670 Broadway
Denver, CO 80202

S. Stone
Amoco Production Company
PO Box 800
Denver, CO 80201

D. O. Cox
Angus Petroleum
350 Indiana, Ste #600
Golden, CO 80401-5050

Barrett Energy Company (2)
1125 17th Street, Suite 2100
Denver, CO 80202
Attn: W. J. Barrett
K. Reinecke

J. N. Burkhalter
Burkhalter Engineering Inc.
715 Horizon Drive
Suite 330
Grand Junction, CO 81506

R. Martin
Coors Energy Company
PO Box 467
Golden, CO 80402

E. L. Sampson
Coseka Resources (USA) Ltd.
200 Writer Square
1512 Larimer Street
Denver, CO 80202-1602

Exxon Company USA (2)
PO Box 120
Denver, CO 80201
Attn: R. Moore
S. Barker

F. M. Moore
Pancanadian Petroleum Co.
600 17th Street, Suite 1800
Denver, CO 80202

W. H. Pease, Jr.
Willard Pease Oil and Gas Company
PO Box 1874
Grand Junction, CO 81502

R. Poppe
Poppe Engineering
6066 E. Long Place
Englewood, CO 80112

T. Logan
Resource Enterprises
2516 Foresight Circle #7
Grand Junction, CO 81505

R. E. Chancellor
Rio Blanco Natural Gas Company
621 17th Street, Suite 1255
Denver, CO 80293

S. M. Struna
Tenneco Oil Company
PO Box 3249
Englewood, CO 80293

T. Barrett
Terred Oil Company
3631 Parfet
Wheatridge, CO 80033

J. D. Haley
Van Pollen and Haley, Inc.
5601 S. Broadway, Suite 400
Littleton, CO 80121

M. Krey
133 N. 8th Street
Grand Junction, CO 81505

J. A. Morel
Consultant
2792 S. Fillmore Street
Denver, CO 80210

L. Fivas
John Brown E and C Inc.
PO Box 90159
Casper, WY 82604

Chief Geologist
Bureau of Land Management
Horizon Drive
Grand Junction, CO 81505

Chief Geologist
Colorado Geological Survey
Department of Natural Resources
1313 Sherman Street Rm 715
Denver, CO 80203

Colorado Oil & Gas Commission
1580 Logan Street, Suite 380
Denver, CO 80203

Petroleum Information Services
PO Box 2610
Denver, CO 80201-2612

J. W. Crafton
Petroleum Engineering Dept.
Colorado School of Mines
Golden, CO 80401

J. Johnson
Department of Geology
Mesa College
Grand Junction, CO 81501

A. H. Harvey
Petroleum Engineering Dept.
University of Missouri at Rolla
Rolla, MO 65401

R. Desbrandes
Petroleum Engineering Department
Louisiana State University
Baton Rouge, LA 70803-6417

L. Crossey
Department of Geology
University of New Mexico
Albuquerque, NM 87131

C. T. Luiskutty
Engineering and Physics Dept.
Oral Roberts University
Tulsa, OK 74171

N. Tyler
Bureau of Economic Geology
University of Texas at Austin
Austin, TX 78713

C. G. Guffey
Texas Tech University
PO Box 4099
Lubbock, TX 79409

E. Rybicki
Mechanical Engineering Dept.
University of Tulsa
Tulsa, OK 74104

K. Aminian
West Virginia University
PO Box 6070, 213 White Hall
Morgantown, WV 26506

D. Hambley
Argonne National Laboratory
EES-362, 9700 S. Cass Avenue
Argonne, IL 60439

P. L. Archer
Battelle
505 King Avenue
Columbus, OH 43201

W. K. Overby
BDM Corporation
1199 Van Voorhis Road, Suite 4
Morgantown, WV 26505

ICF-Lewin Energy Division (2)
9300 Lee Highway
Fairfax, VA 22031-1207
Attn: V. A. Kuuskraa
K. McFall

David D. Blackwell
Dept. of Geological Sciences
Southern Methodist University
Dallas, TX 75275-0395

H. Siriwardane
Dept. of Civil Engineering
West Virginia University
Morgantown, WV 26506

0410	D. E. Arvizu
6000	D. L. Hartley
6200	V. L. Dugan
6201	D. Engi
6210	B. W. Marshall
6230	V. L. Dugan, Acting
6232	W. R. Wawersik
6232	L. W. Teufel
6250	R. K. Traeger
6252	J. C. Dunn
6253	D. A. Northrop (30)
6253	J. C. Lorenz (5)
6253	A. R. Sattler (5)
6253	N. R. Warpinski (5)
6253	MWX File
6257	J. K. Linn
6258	P. J. Hommert
6258	B. J. Thorne
6258	H. E. Morris
6344	S. J. Finley
9114	C. A. Searls
3141	S. A. Landenberger (5)
3151	W. I. Klein (3)
3154-1	C. L. Ward (8) for DOE/OSTI
8524	J. R. Wackerly

☆ U.S. GOVERNMENT PRINTING OFFICE: 1990—773-118/20029